Complexity

Open Challenges on the Stability of Complex Systems: Insights of Nonlinear Phenomena with or without Delay 2020

Lead Guest Editor: Baltazar Aguirre-Hernández
Guest Editors: Raúl Villafuerte-Segura, Carlos Arturo Loredo Villalobos, Edgar Cristian Díaz González, and Alberto Luviano Juárez

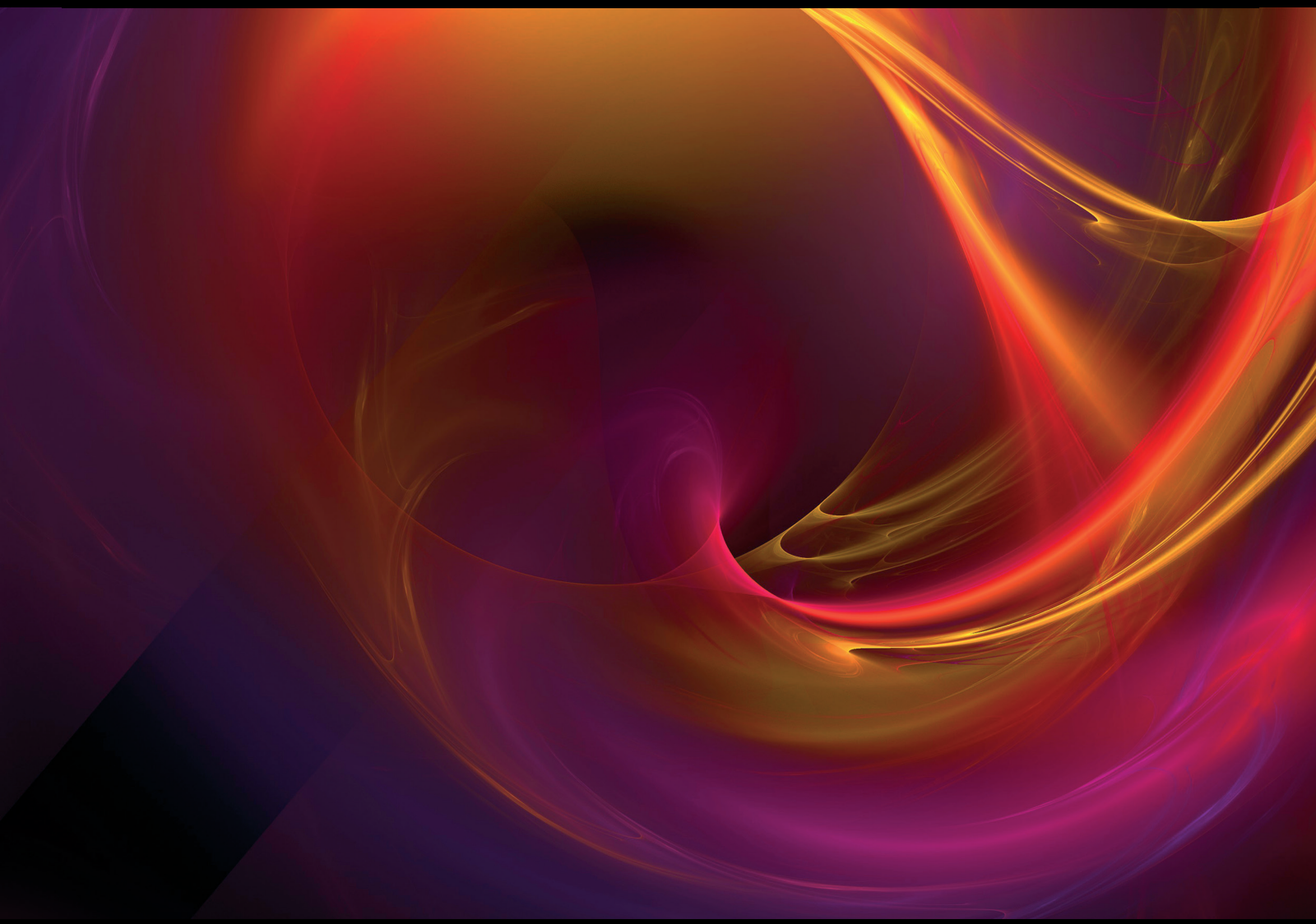

Open Challenges on the Stability of Complex Systems: Insights of Nonlinear Phenomena with or without Delay 2020

Complexity

Open Challenges on the Stability of Complex Systems: Insights of Nonlinear Phenomena with or without Delay 2020

Lead Guest Editor: Baltazar Aguirre-Hernández
Guest Editors: Raúl Villafuerte-Segura, Carlos Arturo Loredo Villalobos, Edgar Cristian Díaz González, and Alberto Luviano Juárez

Copyright © 2020 Hindawi Limited. All rights reserved.

This is a special issue published in “Complexity.” All articles are open access articles distributed under the Creative Commons Attribution License, which permits unrestricted use, distribution, and reproduction in any medium, provided the original work is properly cited.

Chief Editor

Hiroki Sayama, USA

Associate Editors

Albert Diaz-Guilera, Spain
Carlos Gershenson, Mexico
Sergio Gómez, Spain
Sing Kiong Nguang, New Zealand
Yongping Pan, Singapore
Dimitrios Stamovlasis, Greece
Christos Volos, Greece
Yong Xu, China
Xinggang Yan, United Kingdom

Academic Editors

Andrew Adamatzky, United Kingdom
Marcus Aguiar, Brazil
Tarek Ahmed-Ali, France
Maia Angelova, Australia
David Arroyo, Spain
Tomaso Aste, United Kingdom
Shonak Bansal, India
George Bassel, United Kingdom
Mohamed Boutayeb, France
Dirk Brockmann, Germany
Seth Bullock, United Kingdom
Diyi Chen, China
Alan Dorin, Australia
Guilherme Ferraz de Arruda, Italy
Harish Garg, India
Sarangapani Jagannathan, USA
Mahdi Jalili, Australia
Jeffrey H. Johnson, United Kingdom
Jurgen Kurths, Germany
C. H. Lai, Singapore
Fredrik Liljeros, Sweden
Naoki Masuda, USA
Jose F. Mendes, Portugal
Christopher P. Monterola, Philippines
Marcin Mrugalski, Poland
Vincenzo Nicosia, United Kingdom
Nicola Perra, United Kingdom
Andrea Rapisarda, Italy
Céline Rozenblat, Switzerland
M. San Miguel, Spain
Enzo Pasquale Scilingo, Italy
Ana Teixeira de Melo, Portugal
Shahadat Uddin, Australia
Jose C. Valverde, Spain
Massimiliano Zanin, Spain

Contents

Finite-Time Current Tracking in Boost Converters by Using a Saturated Super-Twisting Algorithm
Juan-Eduardo Velázquez-Velázquez, Rosalba Galván-Guerra, José-Antonio Ortega-Pérez, Yair Lozano-Hernández, and Raúl Villafuerte-Segura
Research Article (16 pages), Article ID 7326157, Volume 2020 (2020)

Hybrid Deep-Learning Framework Based on Gaussian Fusion of Multiple Spatiotemporal Networks for Walking Gait Phase Recognition
Tao Zhen, Jian-lei Kong, and Lei Yan
Research Article (17 pages), Article ID 8672431, Volume 2020 (2020)

Solving Interval Quadratic Programming Problems by Using the Numerical Method and Swarm Algorithms
M. A. Elsisy, D. A. Hammad, and M. A. El-Shorbagy
Research Article (11 pages), Article ID 6105952, Volume 2020 (2020)

Simulation and Analysis of the Complex Dynamic Behavior of Supply Chain Inventory System from Different Decision Perspectives
Zusheng Zhang, Xu Wang, Shanshan Yang, Yingbo Wu, and Jianhui Du
Research Article (20 pages), Article ID 7393848, Volume 2020 (2020)

Control of Coexisting Attractors with Preselection of the Survived Attractor in Multistable Chua's System: A Case Study
Zeric Tabekoueng Njitacke, Theophile Fonzin Fozin, Christian Tchito Tchapga, Gervais Dolvis Leutcho, K. Marcel Wouapi, and Jacques Kengne
Research Article (16 pages), Article ID 5191085, Volume 2020 (2020)

A Panoramic Sketch about the Robust Stability of Time-Delay Systems and Its Applications
Baltazar Aguirre-Hernández, Raúl Villafuerte-Segura, Alberto Luviano-Juárez, Carlos Arturo Loredo-Villalobos, and Edgar Cristian Díaz-González
Research Article (26 pages), Article ID 9410315, Volume 2020 (2020)

Using Interval Operations in the Hungarian Method to Solve the Fuzzy Assignment Problem and Its Application in the Rehabilitation Problem of Valuable Buildings in Egypt
M. A. Elsisy, A. S. Elsaadany, and M. A. El Sayed
Research Article (11 pages), Article ID 9207650, Volume 2020 (2020)

Attitude Control with Auxiliary Structure Based on Adaptive Dynamic Programming for Reentry Vehicles
Xu Li, Zhongtao Cheng, Bo Wang, Yongji Wang, and Lei Liu
Research Article (19 pages), Article ID 2837916, Volume 2020 (2020)

A Robust Control Scheme for a PVTOL System Subject to Wind Disturbances
Carlos Alejandro Merlo-Zapata, Carlos Aguilar-Ibanez, Octavio Gutiérrez-Frías, Mayra Antonio-Cruz, Celso Márquez-Sánchez, and Miguel S. Suarez-Castanon
Research Article (11 pages), Article ID 3510396, Volume 2020 (2020)

Cascade Delayed Controller Design for a Class of Underactuated Systems
G. Ochoa-Ortega, R. Villafuerte-Segura, A. Luviano-Juárez, M. Ramírez-Neria, and N. Lozada-Castillo
Research Article (18 pages), Article ID 2160743, Volume 2020 (2020)

Input-to-State Stabilization of a Class of Uncertain Nonlinear Systems via Observer-Based Event-Triggered Impulsive Control
Xiangru Xing and Jin-E Zhang
Research Article (19 pages), Article ID 3951381, Volume 2020 (2020)

Constrained Uncertain System Stabilization with Enlargement of Invariant Sets
Walid Hamdi, Wissal Bey, and Naceur Benhadj Braiek
Research Article (11 pages), Article ID 1468109, Volume 2020 (2020)

Dynamic Complexity in a Prey-Predator Model with State-Dependent Impulsive Control Strategy
Chuanjun Dai
Research Article (12 pages), Article ID 1614894, Volume 2020 (2020)

Stability of a Nonlinear Stochastic Epidemic Model with Transfer from Infectious to Susceptible
Yanmei Wang and Guirong Liu
Research Article (12 pages), Article ID 9614670, Volume 2020 (2020)

Position Control of a Maglev System Fed by a DC/DC Buck Power Electronic Converter
Victor Manuel Hernández-Guzmán, Ramón Silva-Ortigoza, and Magdalena Marciano-Melchor
Research Article (16 pages), Article ID 8236060, Volume 2020 (2020)

Analysis of Stochastic Nicholson-Type Delay System under Markovian Switching on Patches
Xin Yi and Guirong Liu
Research Article (13 pages), Article ID 9078471, Volume 2020 (2020)

Hindawi
Complexity
Volume 2020, Article ID 7326157, 16 pages
https://doi.org/10.1155/2020/7326157

Research Article

Finite-Time Current Tracking in Boost Converters by Using a Saturated Super-Twisting Algorithm

Juan-Eduardo Velázquez-Velázquez,[1] **Rosalba Galván-Guerra**,[1] **José-Antonio Ortega-Pérez**,[2] **Yair Lozano-Hernández**,[3] **and Raúl Villafuerte-Segura**[4]

[1]*Instituto Politécnico Nacional, Unidad Profesional Interdisciplinaria de Ingeniería Campus Hidalgo, San Agustin Tlaxiaca, Hidalgo 42162, Mexico*
[2]*Instituto Politécnico Nacional, Centro de Investigación y Desarrollo de Tecnología Digital, Tijuana, Baja California 22435, Mexico*
[3]*Instituto Politécnico Nacional, Escuela Superior de Ingeniería Mecánica y Eléctrica Unidad Zacatenco, Mexico, CDMX 07738, Mexico*
[4]*Universidad Autónoma del Estado de Hidalgo, Centro de Investigación en Tecnologías de Información y Sistemas, Pachuca, Hidalgo 42184, Mexico*

Correspondence should be addressed to Rosalba Galván-Guerra; rgalvang@ipn.mx

Received 27 May 2020; Revised 29 August 2020; Accepted 24 September 2020; Published 30 October 2020

Academic Editor: Ning Cai

Copyright © 2020 Juan-Eduardo Velázquez-Velázquez et al. This is an open access article distributed under the Creative Commons Attribution License, which permits unrestricted use, distribution, and reproduction in any medium, provided the original work is properly cited.

The power converters are widely used in several industrial applications where it is necessary to obtain from a fixed voltage another one higher or lower than the original. In this paper, we focus on the DC-DC (direct current) boost converters, where to guarantee the desired voltage, an internal current tracking loop is usually used. However, this tracking cannot be assured in the presence of unknown load changes and external perturbations when traditional controller strategies are implemented. In this paper, an advanced control strategy is proposed to ensure the current tracking using a saturated super-twisting controller on the power converter. The finite-time current tracking of a DC-DC boost converter is assured in the presence of bounded Lipschitz perturbations composed by unknown load changes and exogenous signals. The proposed approach generates a continuous bounded control signal applied to the converter by using a sigma-delta modulator ($\Sigma\Delta M$). The controller gains are tuned to obtain finite-time stabilization of the tracking error, while the control signal remains bounded. To illustrate the effectiveness of the proposed results, the controller is applied to a physical boost converter using the hardware implemented ($\Sigma\Delta M$) and an STM32 Discovery development card. Besides, the controller is compared with a first-order sliding mode controller showing that for small sample times, the energy of the error signal is reduced.

1. Introduction

The DC-DC power converters are used in contemporary applications and have been widely investigated in the last three decades. They are the ideal candidates in several applications such as electric and hybrid vehicles, fuel cells, microgrids, and photovoltaic and renewable energy storage systems [1–7]. The natural operation of power converters requires that the control variable takes values from a discrete set. Several efforts to control power converters involving discrete components, integrated circuits, and/or pulse width modulation (PWM) have been reported in the literature [8–16], where schemes based on PI, passivity, adaptive backstepping, fuzzy logic, deadbeat, H-infinity, or model predictive control are used.

In general, the main control objective of power converters is the voltage regulation. According to [17–20], this control problem can be solved by using a cascaded control structure with two loops: an inner current loop and an outer voltage loop. Traditionally, a simple PI compensator is applied to regulate the voltage and generate the current reference signal. Moreover, several applications require that

the current follows a specific current profile [21–24]. It is worth to mention that the rate of the current is faster than the one of the output voltage, making necessary the design of fast strategies that guarantee the exact tracking of the current profile. Moreover, in practice, the load may vary depending on external factors affecting the tracking of the desired current [17, 25–27].

The effects of the unknown load changes can be seen as perturbations. The sliding mode controllers are well known by its ability to compensate theoretically exactly the matched uncertainties/perturbations [18, 28]. The accuracy and structure of these controllers depend on the uncertainties/disturbances considered and the relative degree of the sliding variable.

In the sliding mode framework, the first-order sliding mode (FOSM) control is widely used in the current control loop implementation [17, 29]. This controller works in the on-off mode and allows compensating in finite-time bounded matched uncertainties/perturbations. However, if the commuting frequency is not high enough, it generates high-level chattering or ripple [20, 29]. An alternative to this controller type is a super-twisting algorithm (STA) based controller [30, 31]. This controller compensates Lipschitz uncertainties/perturbations by using continuous control signals, and the generated chattering is diminished in comparison with a FOSM [32, 33]. However, it cannot guarantee that the generated control signal remains bounded, preventing its use in power converters. Recently, a saturated STA (SSTA) has been proposed in [34, 35], and it generates a bounded control signal, while it compensates in finite-time bounded Lipschitz uncertainties/perturbations.

Among the power converters, the boost converter is a nonminimum phase highly nonlinear system. This difficult the control design for the regulation or tracking of a reference voltage. The voltage tracking problem can be reformulated in terms of the current one, which makes the design of the inner current control loop crucial. In the literature, several strategies based on the FOSM have been designed for the boost converter. For example, [36] uses an adaptive controller guaranteeing asymptotic stability of the closed-loop system, while [27] proposes an adaptive backstepping control strategy considering the presence of a constant power load (CPL) and bounded external perturbations and parameter uncertainties. The closed-loop system's sensitivity function amplitude is reduced in [37] by using an optimized feedback control scheme. In [20], a control design procedure is given for DC-DC power converters with different control objectives, and the chattering is attenuated by using a harmonic cancellation method approach.

The aim of this paper is the design of the inner current control loop for boost converters. A tracking control strategy based on the SSTA is proposed to guarantee in finite-time a desired inductor current profile in the presence of Lipschitz and bounded uncertainties/perturbations conformed by unknown changes in the load, model uncertainties, and external perturbations. To illustrate the benefits of the proposed approach, the SSTA controller is compared with a FOSM controller using a chattering analysis via simulation. This comparison shows that the use of a continuous sliding mode control strategy attenuates the energy of the error signal. An efficiency analysis is also performed in simulation, and the SSTA controller is compared in terms of power efficiency with a conventional LQ controller and a FOSM one. This analysis reveals that the use of a variable structure controller improves considerably the efficiency of the boost converter. In addition, the obtained results are implemented in a boost converter prototype to illustrate the applicability of the proposed methodology.

This paper is organized as follows. Some preliminaries results, the test setup, and the problem formulation are described in Section 2. The controller design that stabilize in finite-time the tracking inductor current error is given in Section 3. Section 4 gives the simulation results and the performed analysis. The implementation is detailed in Section 5. Finally, Section 6 concludes the paper.

2. Preliminaries and Problem Formulation

2.1. Ideal Boost Converter. The boost power converter [38] was selected as the test setup. This converter is a voltage elevator capable to increase the capacitor voltage v over the input voltage E of the converter. In Figure 1, a schematic of this converter is shown, assuming ideal elements.

Due to the transistor Q, the converter commutes between two states $u(t) = 1$ and $u(t) = 0$, that denotes the on-off state of the transistor. The two subsystems are depicted in Figures 2 and 3.

Let i be the inductor current and v the capacitor voltage, and the mathematical model of the converter [38] is given below.

(i) If $u(t) = 1$

$$\begin{aligned} L\dot{i}(t) &= E, \\ C\dot{v}(t) &= -\frac{v(t)}{R}. \end{aligned} \tag{1}$$

(ii) If $u(t) = 0$

$$\begin{aligned} L\dot{i}(t) &= -v(t) + E, \\ C\dot{v}(t) &= i(t) - \frac{v(t)}{R}. \end{aligned} \tag{2}$$

Observe that this switched system can be expressed in the bilinear form as

$$\begin{aligned} \dot{i}(t) &= -(1 - u(t))\frac{v(t)}{L} + \frac{E}{L}, \\ \dot{v}(t) &= (1 - u(t))\frac{i(t)}{C} - \frac{v(t)}{CR}, \end{aligned} \tag{3}$$

where the control input $u(t) \in \{0, 1\}$. To implement a continuous control signal in this converter, a $\Sigma\Delta M$ circuit [17, 38] is used.

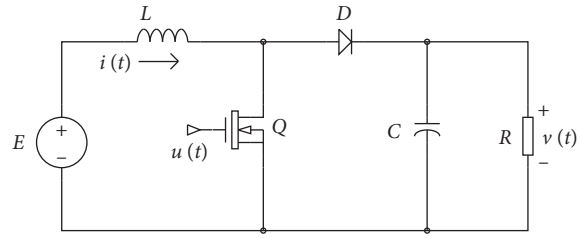

Figure 1: Electronic circuit of a boost power converter.

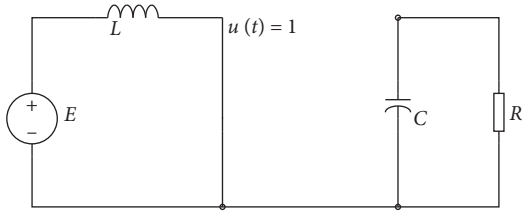

Figure 2: On mode.

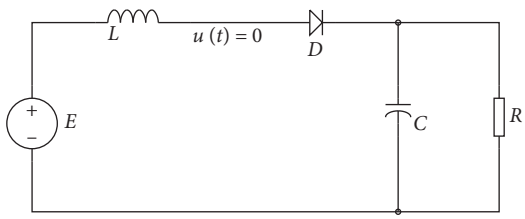

Figure 3: Off mode.

2.2. Boost Converter with Perturbations. When nonideal elements and unknown changes in the nominal load R are considered, the boost converter model (3) can be seen as a perturbed system of the form

$$\begin{aligned} \dot{i}(t) &= -(1-u(t))\frac{v(t)}{L} + \frac{E}{L} + \phi_1(t), \\ \dot{v}(t) &= (1-u(t))\frac{i(t)}{C} - \frac{v(t)}{CR} + \phi_2(t), \end{aligned} \tag{4}$$

where $\phi_1 \colon \mathbb{R} \longrightarrow \mathbb{R}$ and $\phi_2 \colon \mathbb{R} \longrightarrow \mathbb{R}$ denote unknown matched uncertainties/perturbations, composed by unknown load changes, differences in the nominal input voltage E, uncertainties in the system parameters, and exogenous signals.

2.3. ΣΔ Modulator. To convert a continuous signal to a digital one, a $\Sigma\Delta M$ [17, 39, 40] may be utilized, allowing the switched synthesis of any feedback controller designed following an average viewpoint. This modulator can be used to translate a continuous average design into a discontinuous one with the property that the equivalent output signal of the modulator matches the input signal generated by the continuous average feedback controller. In this paper, the following $\Sigma\Delta M$ is used (for more details about the modeling of this modulator see [17]).

$$\begin{aligned} \dot{z}(t) &= \zeta(t), \\ \dot{x}(t) = u(t) &= \frac{1}{2}(1 + \operatorname{sign}(\sigma(t))), \\ \sigma(t) &= z(t) - x(t); \end{aligned} \tag{5}$$

where $\zeta(t)$ is the analogue input signal, and $u(t) \in \{0, 1\}$ is the output of the modulator. This modulator is only capable to modulate the input if $\zeta(t) \in [0, 1]$. The block diagram of the $\Sigma\Delta M$ is shown in Figure 4.

2.4. Super-Twisting Algorithm. Consider a relative degree one scalar system:

$$\dot{s}(t) = u(t) + \psi(t), \tag{6}$$

where $\psi(t)$ is a Lipschitz uncertainty/perturbation. The STA [28] is a second-order sliding mode control that drives the sliding variable s and its derivatives to zero in finite-time. It generates a continuous control and attenuate the chattering effect by hiding the switching term under an integral. In general, the STA controller is given as

$$\begin{aligned} u(t) &= -k_1 \lfloor s(t) \rceil^{(1/2)} + w(t), \\ \dot{w}(t) &= -k_2 \lfloor s(t) \rceil^{0}, \end{aligned} \tag{7}$$

where $\lfloor \cdot \rceil^p = |\cdot|^p \operatorname{sign}(\cdot)$, and k_1 and k_2 are designed to guarantee the finite-time convergence of s and $\dot{s}$ to the origin in finite-time. This controller compensates in finite-time Lipschitz uncertainties/perturbations. However, the generated continuous control signal is unbounded.

To produce a bounded continuous control signal with the characteristics of the STA, in [35], a SSTA is proposed. This controller assures finite-time convergence to the origin of the sliding variable s and its time derivatives while compensating bounded Lipschitz uncertainties/perturbations. The design conditions of such a controller are given in the following theorem.

Theorem 1. *[35] Let the scalar system (6) with $\psi(t)$, a bounded Lipschitz perturbation, i.e., $\dot{\psi}(t) \leq \overline{\psi}_1$, and $\psi \leq \overline{\psi}_0 \leq M$. Consider the SSTA controller:*

$$\begin{aligned} u(t) &= \operatorname{sat}_U\left(-k_1 \lfloor s(t) \rceil^{(1/2)} + w(t)\right), \\ \dot{w}(t) &= -k_2 \lfloor s(t) \rceil^{0}, \\ w(0) &= 0, \end{aligned} \tag{8}$$

where $\lfloor \cdot \rceil^p = |\cdot|^p sign(\cdot)$, and

$$\operatorname{sat}_U(y) = \begin{cases} y, & \text{if} \quad |y| \leq M, \\ M \lfloor y \rceil^0, & \text{if} \quad |y| > M, \end{cases} \tag{9}$$

with SSTA gains, such that

$$\begin{aligned} k_1 &> \sqrt{k_2 + \overline{\psi}_1}, \\ k_2 &> \overline{\psi}_1. \end{aligned} \tag{10}$$

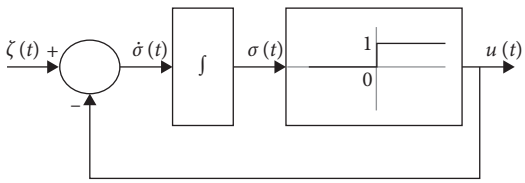

Figure 4: $\Sigma\Delta M$ block diagram.

Then, the control law (8) globally stabilizes the plant (6) in finite-time with a control input u that is continuous with respect to time and satisfies $|u(t)| \leq M$, for all $t \geq 0$.

Note that in comparison with the conventional FOSM, the SSTA generates a bounded continuous control signal and reduces the chattering effect in the system.

2.5. Problem Formulation. Consider the perturbed boost system (4) and define the inductor current error:

$$e_i(t) = i(t) - i^*(t), \tag{11}$$

where $i^*: \mathbb{R} \longrightarrow \mathbb{R}$ is the desired inductor current bounded C^2 function. The current error dynamics takes the form

$$\dot{e}_i(t) = -(1 - u(t))\frac{v(t)}{L} + \frac{E}{L} + \phi_1(t) - \dot{i}^*(t). \tag{12}$$

It can be seen that the current error dynamics are not directly affected by $\phi_2(t)$. Also, along this paper, the following assumptions are necessary.

Assumption 1. The uncertainties/perturbations $\phi_1(t)$ are bounded and Lipschitz, i.e.,

$$\begin{aligned} \overline{\phi}_0 \leq \phi_1(t) \leq \overline{\phi}_1, \\ \left|\dot{\phi}_1(t)\right| \leq \overline{\phi}_2, \end{aligned} \tag{13}$$

where $\overline{\phi}_0, \overline{\phi}_1 \in \mathbb{R}$, and $\overline{\phi}_2 \in \mathbb{R}_+$.

Assumption 2. The uncertainties/perturbations $\phi_2(t)$ are continuous and bounded, such that

$$\left|\phi_3(t)\right| \leq \overline{\phi}_3, \quad \overline{\phi}_3 \in \mathbb{R}_+. \tag{14}$$

Under Assumptions 1 and 2, the task is to ensure that the inductor current i tracks the desired inductor current i^* exactly by using a SSTA controller after a finite transient, i.e., the problem resides on to stabilize in finite-time the current error (12), $i(t) \longrightarrow i^*(t)$ for all $t \geq t_r$, where t_r is the reaching time, by using a continuous control law $u(t)$.

Note that as it is mentioned in [17, 29], to track a desired voltage, two control loops are needed. An inner current control loop and an outer voltage control loop. The objective of this paper is the design of a controller that guarantees the finite-time tracking of a desired current in the presence of bounded Lipschitz uncertainties/perturbations.

3. Control Design

Consider the perturbed boost converter (4) and define $e_i(t)$ as the sliding variable. To guarantee $i(t) \longrightarrow i^*(t)$ in finite-time, it is necessary to select a suitable controller capable to achieve such a task. Observe that e_i has relative degree one, and it is assumed that ϕ_1 is a bounded Lipschitz perturbation. Hence, it is possible to use an SSTA controller [34, 35]. The next theorem gives sufficient condition to the design of the SSTA controller for the internal current control loop of the boost converter.

Theorem 2. *Consider the error dynamics of the inductor current in the boost converter (12), with a bounded Lipschitz perturbation $\phi_1(t)$, such that*

$$\overline{\phi}_0 < -\frac{E}{L} + \dot{i}^*(t) \leq \phi_1(t) \leq \frac{v(t)}{L} - \frac{E}{L} + \dot{i}^*(t) < \overline{\phi}_1, \tag{15}$$

and $|\dot{\phi}_1(t)| \leq \overline{\phi}_2$. By using the controller,

$$\begin{aligned} u(t) &= \frac{1}{2} + \mathrm{sat}_U\left(\frac{L}{v(t)}\left(u_{\mathrm{neq}}(t) + \overline{u}(t)\right)\right), \\ u_{\mathrm{neq}}(t) &= \frac{v(t)}{2L} - \frac{E}{L} + \dot{i}^*(t), \\ \overline{u}(t) &= -k_1 \lfloor e_i(t) \rceil^{(1/2)} + w(t), \\ \dot{w}(t) &= -k_2 \lfloor e_i(t) \rceil^0, \end{aligned} \tag{16}$$

where $\lfloor \cdot \rceil^p = |\cdot|^p sign(\cdot)$, and

$$\mathrm{sat}_U(y) = \begin{cases} y, & \text{if} \quad |y| \leq \dfrac{1}{2}, \\ \dfrac{1}{2}\lfloor y \rceil^0, & \text{if} \quad |y| > \dfrac{1}{2}; \end{cases} \tag{17}$$

with the SSTA gain designed, such that

$$\begin{aligned} k_1 &> \sqrt{k_2 + \overline{\phi}_2}, \\ k_2 &> \overline{\phi}_2. \end{aligned} \tag{18}$$

Then, the tracking error converges to the origin after a finite transient, i.e., $e_i(t) = \dot{e}_i(t) = \ddot{e}_i(t) = 0$ for all $t > t_r$, where t_r is the reaching time, and the control effort remains in the inherent bounds, i.e., $u(t) \in [0, 1]$ for all $t \geq 0$.

Proof. To analyze the dynamics of the tracking error in the sliding mode, let

$$u(t) = \frac{1}{2} + \frac{L}{v(t)}\left(u_{\mathrm{neq}}(t) + \overline{u}(t)\right). \tag{19}$$

By substituting this controller in the tracking error dynamics (12), it can be seen that

$$\dot{e}_i(t) = \overline{u}(t) + \phi_1(t). \tag{20}$$

Assume that for $t > t_r$, the sliding mode is achieved, i.e., $e_i(t) = \dot{e}_i(t) = \ddot{e}_i(t) = 0$; then,

$$\overline{u}(t) = -\phi_1(t). \tag{21}$$

Hence, if the sliding mode is achieved, the proposed controller is capable to compensate exactly the matched uncertainties/perturbations ϕ_1. Note that if ϕ_1 satisfies the

inequality (15), the control signal satisfies the inequality $0 \leq u(t) \leq 1$ for all $t > t_r$.

Now, observe that the tracking error dynamics (20) resemble the system of Theorem 1, and the conditions of such theorem are satisfied. Hence, the finite-time convergence of the tracking error dynamics is guaranteed.

Note that the proposed controller has a symmetric structure, but it contains an offset that keeps the control signal in the interval $[0, 1]$. □

Remark 1. Once the sliding variable $e_i(t)$ has converged to the origin, the controller $\overline{u}(t) = -\phi_1(t)$ for $t > t_r$. Hence, the control signal $\overline{u}(t)$ reconstructs the negative of the perturbation and compensates the perturbation in finite-time. In comparison with a FOSM, the continuity of the SSTA allows to know exactly the value of the perturbation without filtering [28].

Observe also that u_{neq} in (9) is the nominal equivalent control signal that eliminates the known dynamic of the sliding variable. However, it is possible to consider $u_{\text{neq}}(t) = 0$ and let the SSTA to reconstruct all the tracking error dynamics. The next lemma states this result.

Lemma 1. *Under the conditions of Theorem 1 and Assumption 2, by using the controller,*

$$\begin{aligned} u(t) &= \frac{1}{2} + \text{sat}_U\left(\frac{L}{v(t)}\overline{u}(t)\right), \\ \overline{u}(t) &= -k_1 \lfloor e_i(t) \rceil^{(1/2)} + w(t), \\ \dot{w}(t) &= -k_2 \lfloor e_i(t) \rceil^0, \end{aligned} \tag{22}$$

where $\lfloor \cdot \rceil^p = |\cdot|^p sign(\cdot)$, *and*

$$\text{sat}_U(y) = \begin{cases} y, & \text{if} \quad |y| \leq \dfrac{1}{2}, \\ \dfrac{1}{2}\lfloor y \rceil^0, & \text{if} \quad |y| > \dfrac{1}{2}. \end{cases} \tag{23}$$

If SSTA gains are designed such that

$$\begin{aligned} k_1 &> \sqrt{k_2 + \overline{\psi}(t)}, \\ k_2 &> \overline{\psi}(t), \end{aligned} \tag{24}$$

with

$$\overline{\psi}(t) \geq \left|\frac{v(t)}{2\text{LCR}} - \dddot{i}^*(t)\right| + \frac{\overline{\phi}_3}{2L} + \overline{\phi}_2. \tag{25}$$

Then, the tracking error converges to the origin after a finite transient, i.e., $e_i(t) = \dot{e}_i(t) = \ddot{e}_i(t) = 0$ *for all* $t > t_r$, *where* t_r *is the reaching time, and the control effort remains in the inherent bounds, i.e.,* $u(t) \in [0, 1]$ *for all* $t \geq 0$.

Proof. The proof is obtained following a similar procedure as in Theorem 2 and a straightforward computation of the bound $\overline{\psi}(t)$.

If the controller is designed satisfying the above results, the bound of the control signal is guaranteed, and it can be fed to $\Sigma\Delta M$ to generate a suitable control signal for the boost converter assuring the tracking in finite-time of the desired current in the presence of the uncertainties/perturbations.

4. Simulation Results

To validate the above results, some MATLAB simulations are presented. Consider a boost converter with $L = 10\,\text{mH}$, $C = 2.2\,\mu\text{F}$, and $E = 12\,\text{V}$. The desired current is

$$i^*(t) = 0.8\sin(t) + 1. \tag{26}$$

The considered unknown perturbation is

$$\phi_1(t) = 3\sin(16\cos(\pi t)) + 500, \tag{27}$$

and $\phi_2(t)$ is constructed by changes in the nominal load $R = 500\Omega$, such that the real load $\overline{R}$ has the form

$$\overline{R}(t) = \begin{cases} 560\,\Omega, & \text{if} \quad 0 \leq t \leq 10 \vee t \geq 30, \\ 200\sin(10\pi t) + 300, & \text{if} \quad 10 < t \leq 20, \\ 150\,\Omega, & \text{if} \quad 20 < t \leq 30. \end{cases} \tag{28}$$

Note that the proposed load is a continuous function that is bounded. In the simulation, it is considered $\overline{\phi}_2 = 15000$ as the bound of the perturbation ϕ_1, and the controller is designed as given in Theorem 2.

The results obtained by applying the designed SSTA to the boost converter in a time window $T = 40$ s with a sample step of $\Delta t = 1 \times 10^{-6}$ s are shown in Figure 5. It can be seen that the current converges to the desired trajectory in finite-time despite the presence of the perturbation.

It is worth to mention the effect of the perturbation in the voltage of the load, and this state is not controlled, so this behavior is expected. To guarantee that the voltage is not affected by the perturbation, an external control loop that modified the desired current needs to be designed. However, observe that the tracking error (Figure 6) converge to the origin in finite-time, showing that $i(t) \longrightarrow i^*(t)$ in the same manner. The designed control signal is retrieved in Figure 7. Observe that the control signal is continuous and remains in the interval $[0, 1]$ in the time interval.

4.1. Chattering Analysis. According to Levant [32], in the sliding mode control, the chattering is caused by the high, theoretically infinite, frequency of control switching and reveals itself as high-frequency dangerous vibrations of the whole system. In power systems, this phenomenon is known as ripple.

Definition 1. [32] Consider an absolutely continuous scalar signal $\xi(t) \in \mathbb{R}$ and $t \in [0, T]$. Also, let $\overline{\xi}(t) \in \mathbb{R}$ be an absolutely continuous nominal signal, such that $\xi(t)$ is considered as its disturbance. Let $\Delta\xi(t) = \xi(t) - \overline{\xi}(t)$. Define the L_2 chattering of the signal as

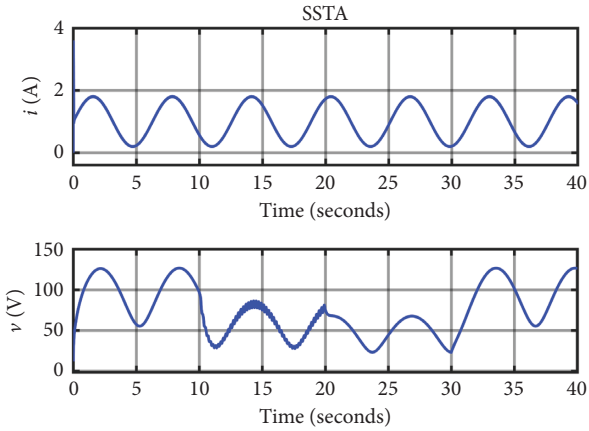

Figure 5: Boost current and voltage with the SSTA controller.

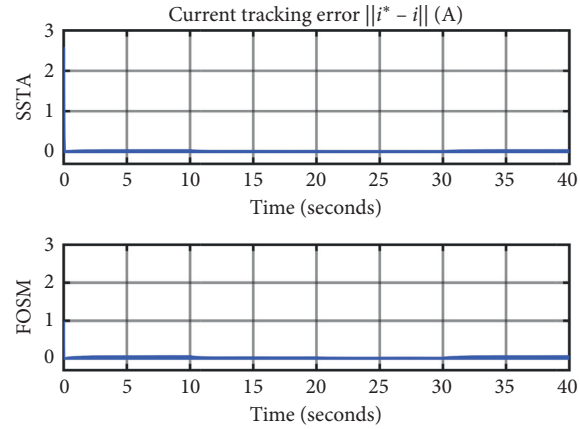

Figure 6: Tracking error for both controllers.

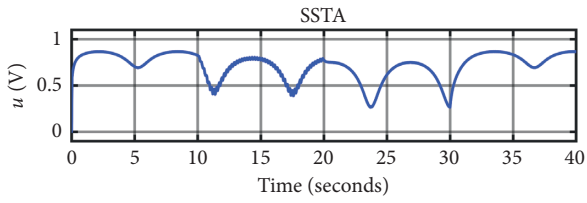

Figure 7: SSTA control signal.

$$\text{chat}_{L_2} = \left(\int_0^T \Delta\dot{\xi}^2(t)\mathrm{d}t \right)^{(1/2)}. \tag{29}$$

In power systems, to evaluate the performance of the power converter, the ripple is normally measured by computing the energy contained in the error signal [29].

For comparison purposes, a FOSM controller [20, 29] is applied to the boost converter considering the load change in the same manner as in the SSTA case. The considered controller is

$$u(t) = \frac{1}{2}\left(1 - \text{sign}\left(e_i(t)\right)\right). \tag{30}$$

The inductor current behavior is shown in Figure 8 and its respective error in Figure 6. Observe that the tracking task

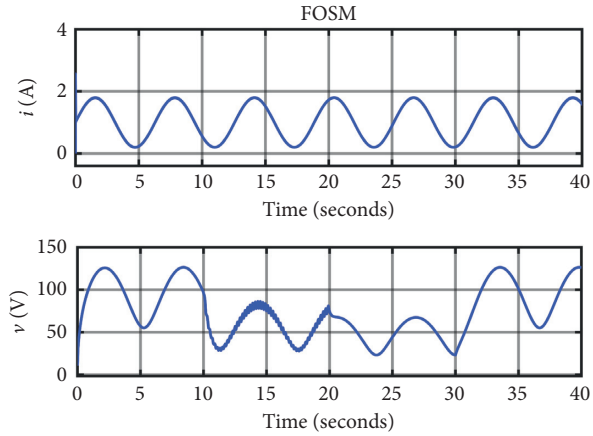

Figure 8: Boost current and voltage with the FOSM controller.

is also achieved, i.e., $i(t) \longrightarrow i^*(t)$ in finite-time despite the perturbation. The controller is not continuous, but it can be applied to the boost converter without needing $\Sigma\Delta M$.

In the performed simulations, it can be seen that the difference in the performance of the two controllers is basically in the size of the chattering, depicted in Figure 6. However, by only seeing the picture, it is very hard to decide if any of the two controllers gives any advantage.

To visualize in a better way the differences between the two control strategies, an energy and chattering analysis has been performed. First, the energy of the tracking error signal [41] is obtained as

$$\text{Energy} = \int_{t_r}^{T} e_i^2(t)\mathrm{d}t. \tag{31}$$

Afterwards, a chattering analysis [32, 42] is performed by computing the level of chattering in the L_2 space of the tracking error signal:

$$\text{chat}_{L_2} = \left(\int_{t_r}^{T} \dot{e}_i^2(t)\mathrm{d}t \right)^{(1/2)}. \tag{32}$$

The analyses are performed for different sample times assuming that the error signal has passed the reaching phase, i.e., the analysis is performed for $t \in [t_r, T]$, with $t_r = 0.2$ s. The result is summarized in Tables 1 and 2.

By analyzing the energy signal of both controllers, it is evident that the use of a SSTA diminishes the energy of the error signal. However, the chattering measurement remains more or less the same. It was proved in [32, 33] that the chattering of a continuous sliding mode controller is infinitesimal while one of a FOSM controller is bounded. It seems that the use of $\Sigma\Delta M$ changes the chattering type of the SSTA to a bounded one. Hence, the only advantage that can be seen by the performed analysis is the decrement in the energy of the error signal by the use of the SSTA.

4.2. Power Efficiency. In several applications as hybrid electric vehicles or fuel cell vehicles, energy storage is employed to reduce the cost and to improve the performance of the system [1]. In these applications, the voltage

Table 1: Energy and chattering analysis for the SSTA controller.

Sample step	Energy	Chattering
1×10^{-3}	3678	43611.1
1×10^{-4}	3.01	21857.51
1×10^{-5}	0.02	19892.86
1×10^{-6}	2.16×10^{-4}	19710.9
1×10^{-7}	2.15×10^{-6}	19692.87

Table 2: Energy and chattering analysis for the FOSM controller.

Sample step	Energy	Chattering
1×10^{-3}	974.8	24175.92
1×10^{-4}	5.17	21275.37
1×10^{-5}	0.05	19743.29
1×10^{-6}	4.72×10^{-4}	19687.46
1×10^{-7}	4.711×10^{-6}	19681.85

level is normally lower than the required, and power converters are widely used. These systems require good efficiency in the energy consumption, since they are working constantly over transient states. This makes it necessary to analyze how the efficiency of the boost converter is affected by the controller. The power efficiency is defined by the ratio of the output power P_o to the input power P_i.

$$\eta = \frac{P_o}{P_i} = \frac{\left(v_{\text{RMS}}^2/R\right)}{Ei_{\text{RMS}}}, \tag{33}$$

where v_{RMS} and i_{RMS} denote the root mean square value of the load voltage and the inductor current, respectively, over the time interval $[0, t_f]$. Assume that the boost converter is performing a current regulation task over the range 0.03 A–3 A and that there are not any uncertainties/perturbations that affect the behavior of the system, i.e., $\phi_1(t) = \phi_2(t) = 0$. Three controllers are considered for comparison purposes: (1) a saturated linear quadratic (LQ) controller designed for the linearized system around the equilibrium point defined by the desired current i^*, (2) a FOSM controller defined in the previous section, and (3) the proposed SSTA. In Figure 9, the power efficiency of the boost converter with the considered controllers, obtained by simulation with a sample step $\Delta t = 1 \times 10^{-6}$, is depicted. Note that the use of a sliding mode control technique improves considerably the efficiency in comparison with the LQ controller. Observe also that the performed analysis is very simple, and more complex analysis can be performed for the proposed controller as the one given in [43].

4.3. Discussion. The presented result is focused on the design of the inner current control loop of the boost converter. As mentioned previously, the objective of the power converters is to deliver a desired voltage that can be constant or time varying depending on the application. There are several control methodologies that can be used to design the outer loop. In [17], a frequency-based approach is used, in [29], the desired current is designed by using a SMC approach, while in [26], an MPC approach is used. The chosen approach will depend on the conditions of the converter and the control objective.

In this paper, the considered load does not have a specific form, and it is seen as a perturbation. The form of the load depends on the specific application, and the only restriction is that it must be bounded and Lipschitz. In the microgrid applications [25, 26], the load can be modeled as the connection of several CPLs. This type of load has the characteristic that its model is a first-order vectorial dynamic equation and can be considered as a Lipschitz-bounded perturbation.

To show the applicability of the proposed approach, a voltage regulation scenario is presented with a CPL. For simulation purposes, the parameters of the considered CPL were taken from [26]. The desired voltage v^* is assumed as constant, and the error $e_v(t) = v(t) - v^*$ is taken as the sliding variable. The desired current that guarantees the voltage regulation is constructed by an asymptotic sliding mode (ASM) controller [28]. This controller provides asymptotic regulation of the desired voltage by using a differentiable desired current i^*. Once more, three controllers are compared: (1) the saturated LQ, (2) the FOSM, and (3) the SSTA. The simulation was performed with a sample step $\Delta t = 1 \times 10^{-6}$ s, $v^* = 100$ V, and a nominal load resistor $R = 500\Omega$. The used perturbation $\phi_1(t)$ is defined in (24), and $\phi_2(t)$ is composed by a parallel arrangement of a resistor load of 60 Ω and the CPL. The obtained results are shown in Figure 10. The LQ controller is uncapable to deal with the perturbations as it is shown in Figure 10(c). In general, the used controller in the outer loop shapes the convergence to the desired voltage. In the considered case, the ASM guarantees asymptotic convergence of $e_v(t)$ to the origin once $i(t) = i^*(t)$ (Figures 10(a) and 10(b)). The proposed inner current control loop guarantees the tracking in finite-time. Note that the desired current $i^*(t)$ generated by the ASM controller is time varying for both the FOSM and the SSTA, and it guarantees the compensation of the perturbations. The error tracking for the voltage and the current are shown in Figures 11 and 12, respectively.

5. Implementation

The boost converter prototype is designed to work with a 12 V input source and a maximum of 3 A. The PCB layout of the converter is shown in Figure 13. Table 3 indicates the technical specifications of the converter, obtained with a duty cycle of 70% that gives the highest efficiency of the converter (Figure 14).

The inductor current i is measured by an ACS723 sensor and the capacitor voltage v by a potential divider. The data acquisition is made through a STM32 Discovery development card. The SSTA is embedded in the STM32 Discovery development card. The control signal generated by the controller is feed to $\Sigma\Delta M$. In Figure 15, the constructed prototype is shown. The voltage is given by a commuted source, and an oscilloscope was used to verify the signals in the prototype. To eliminate external magnetic perturbations, the current sensor is in a Faraday cage. The measurements are processed by the STM32 Discovery development card that is connected to a personal computer that displays the

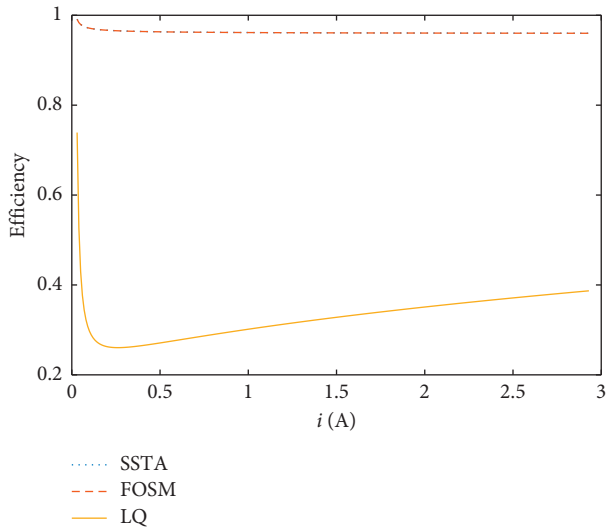

Figure 9: Efficiency of the boost converter for different desired current values.

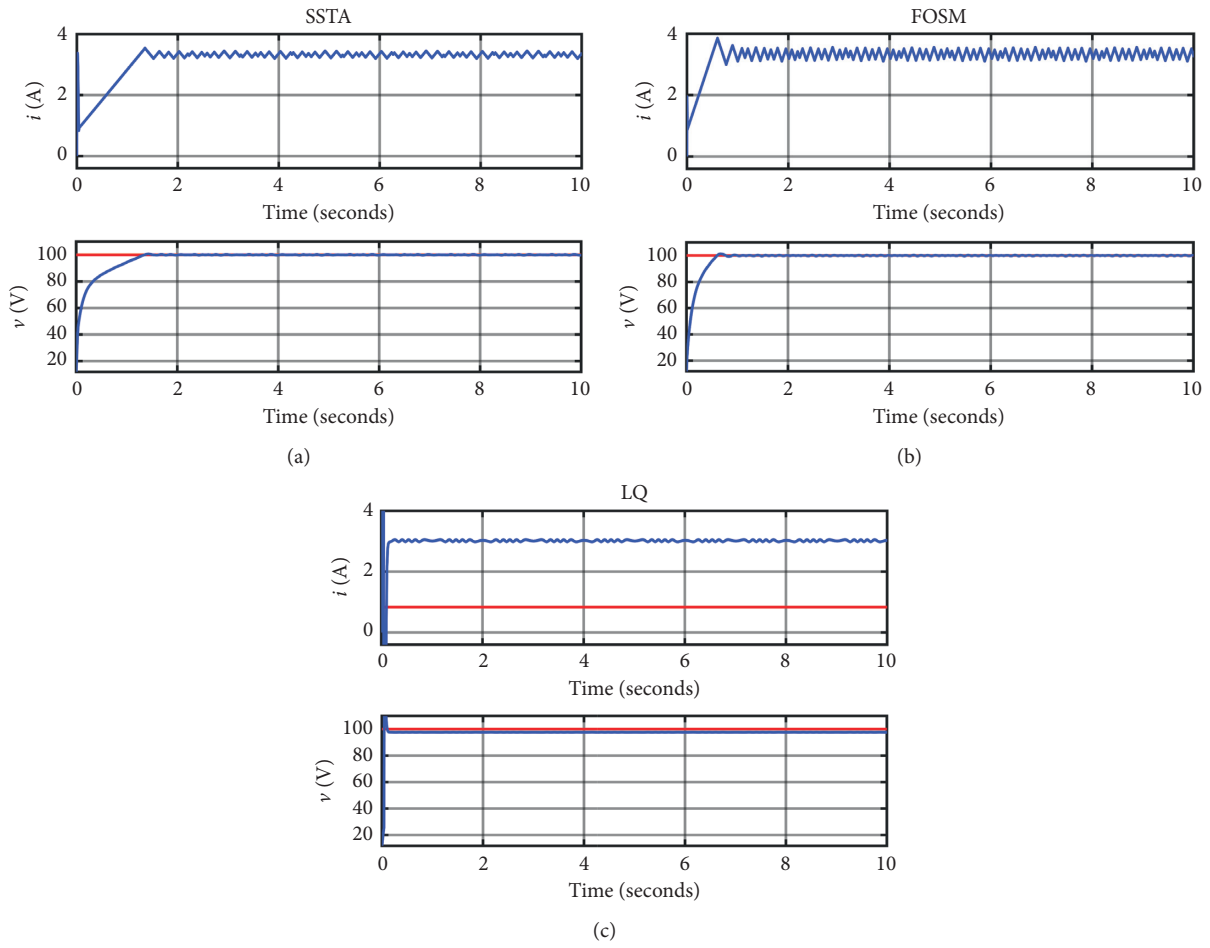

Figure 10: Voltage tracking (reference, red line and boost converter behavior, blue line). (a) SSTA controller. (b) FOSM controller. (c) LQ controller.

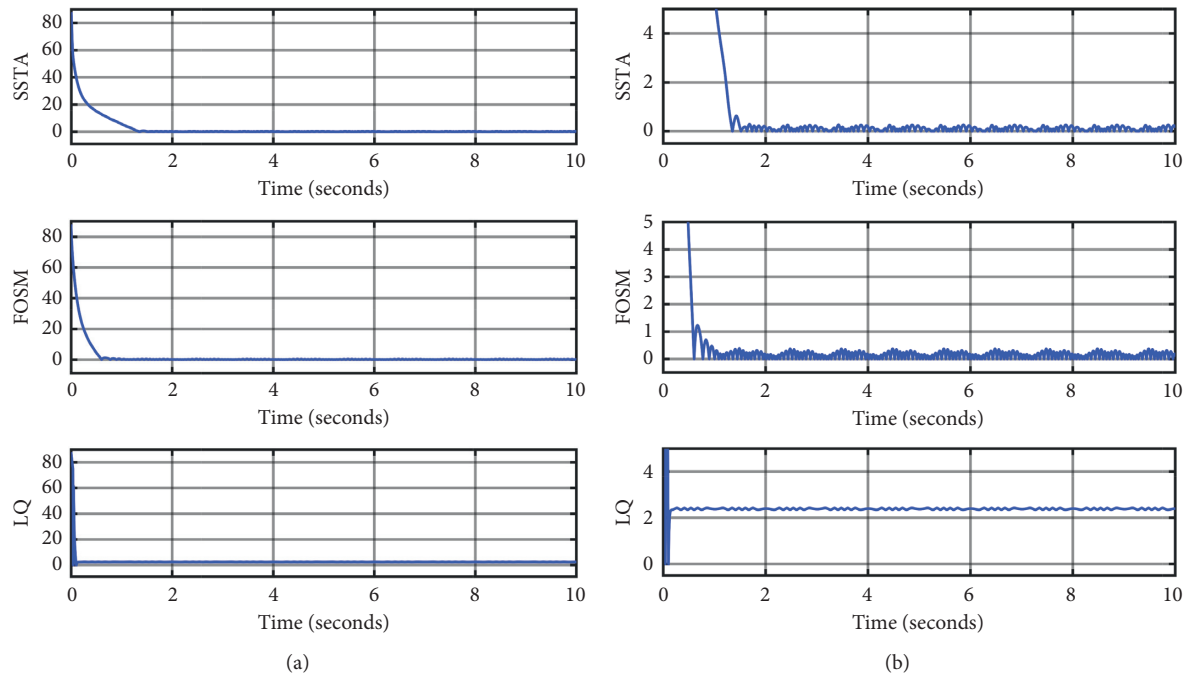

Figure 11: Voltage error tracking. (a) Voltage tracking error $\|v^* - v\|[V]$. (b) Zoom.

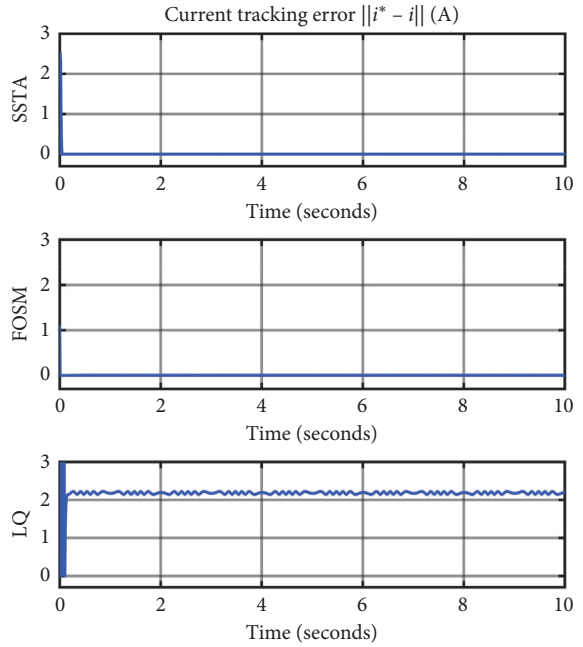

Figure 12: Current error tracking.

necessary graphs for the experiments. The scheme of the proposed approach is illustrated in Figure 16.

Two experiments are developed in the prototype using the proposed SSTA approach. First, a regulation test is performed, assuming $i^* = 0.5$ A. An unknown change in the load is considered. In the experiment, a 47 Ω resistor is connected in parallel to the nominal one around $t = 7$ s (Figure 17). The results obtained with the oscilloscope are shown in Figures 18 and 19. Observe that the current converges to the desired value in finite-time, and as in the simulation, the voltage is affected by the perturbation. Note that the SSTA reconverge after the load change. This is an expected behavior in the experiment, since the Lipschitz condition is not fulfilled, and the controller loses its convergence. However, after perturbation is applied, the tracking error reconverges to the origin

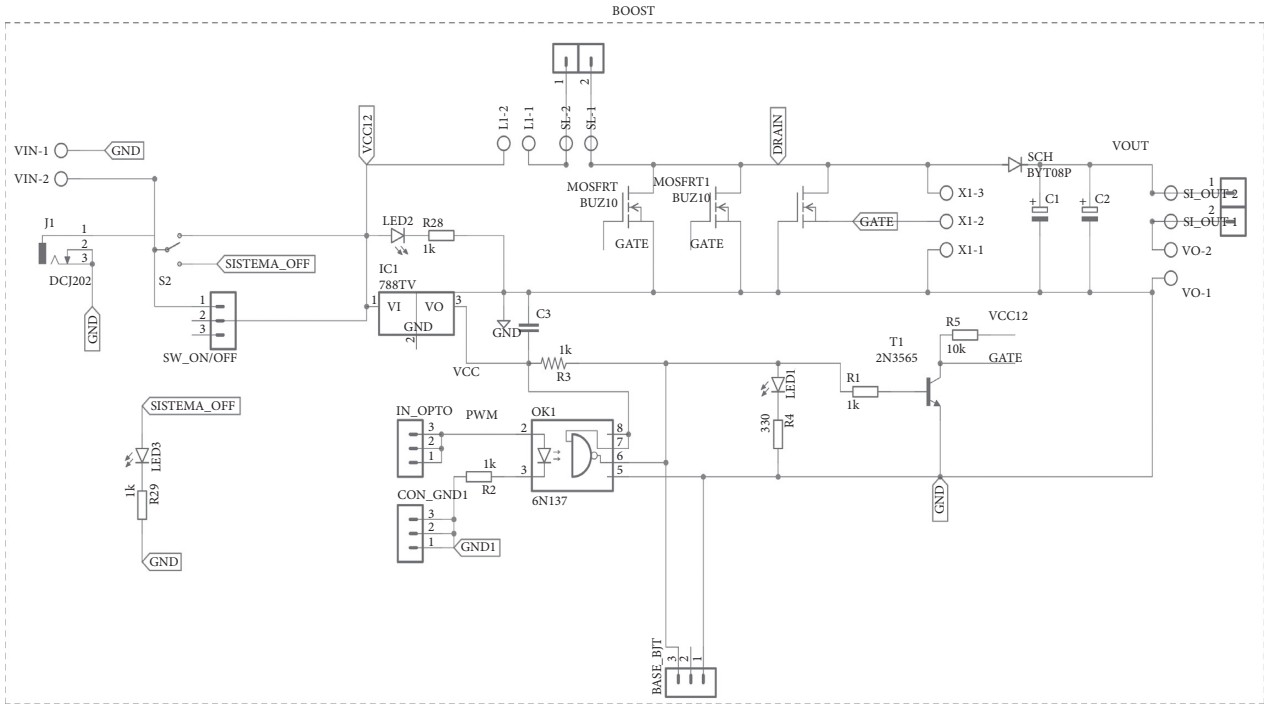

Figure 13: Boost converter PCB.

Table 3: Boost converter specifications.

Specification	Value	Units
Load resistance, R	560	Ω
Inductor, L	10	mH
Capacitor, C	2200	μF
Output power, P_o	1.8	W
Input power, P_i	3.09	W
Frequency	5	kHz
Input supply voltage, E	12	V
Ripple	0.02	%
Output voltage, v_o	31.65	V
Duty cycle, D	70	%
Efficiency, η	58.16	%
Load resistor current, i_o	56.51	mA
Inductor current, i	252	mA

(Figure 17(b)). The applied control signal is continuous and remains in the set $[0, 3.3]$ V that is equivalent to the logic set $[0, 1]$.

Now, for comparison purposes, a FOSM controller is also implemented. The controller is constructed in a PCB following the scheme proposed in [17]. The scheme of the FOSM strategy is shown in Figure 20. This strategy was implemented completely in hardware, and the development card was used only for data acquisition. The results obtained for this controller are shown in Figures 21–23. Observe that this controller is capable to guarantee in finite-time the control objective, and it is not affected by the use of non-Lipschitz perturbations. But it generates more chattering than the SSTA.

Finally, a tracking experiment was performed. The desired current has a sinusoidal profile, a SSTA controller is implemented, and the same source of perturbation is applied. The results obtained with the oscilloscope are shown in Figures 24 and 25. Observe that the current follows the desired sinusoidal signal in finite-time, and the control signal is bounded. But, as in the regulation experiment, the SSTA loses convergence around $t = 7$ s due to non-Lipschitz perturbations (Figure 26).

Figure 27 shows the efficiency of the implemented controllers. The experiments were carried out with an initial condition of 0.3 A, and the desired current was modified in a range from 0.3 to 0.9 A. The efficiency is computed considering the transient and steady state behavior of the boost converter. However, it is well known that the efficiency is affected by the frequency characteristic of the control input and the elements used in the implementation of the controller.

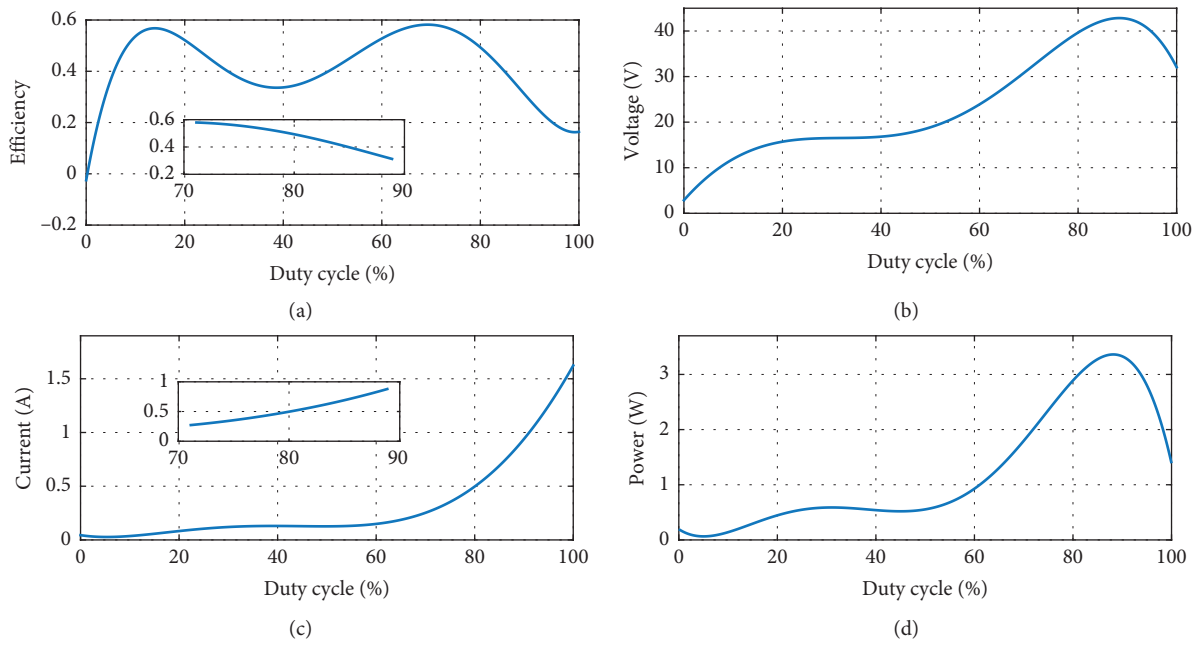

FIGURE 14: $\eta - D$, $v_o - D$, $i - D$, and $P_o - D$ characteristic curves of the boost converter. (a) Efficiency vs duty cycle. (b) Output voltage vs duty cycle. (c) Inductor current vs duty cycle. (d) Output power vs duty cycle.

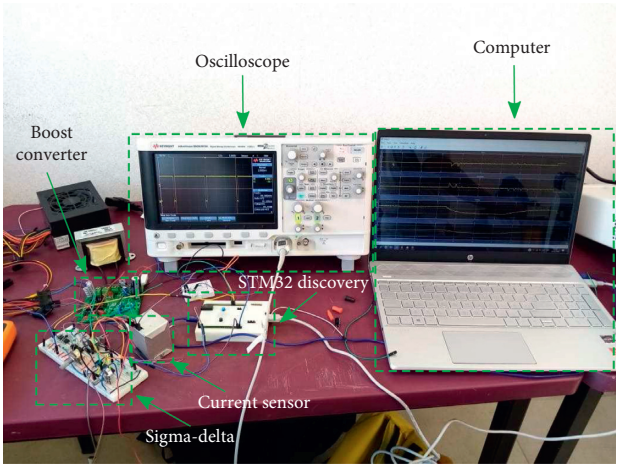

FIGURE 15: Photograph of the prototype.

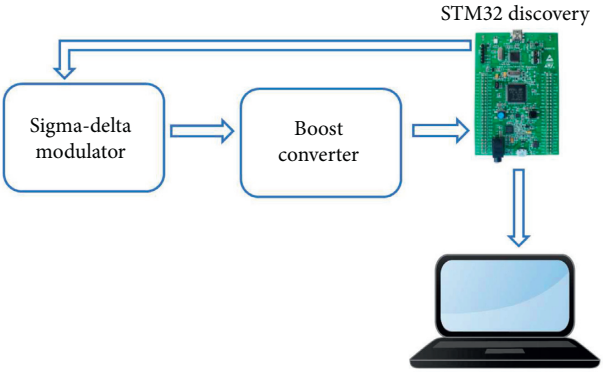

FIGURE 16: Boost converter prototype scheme for the SSTA controller.

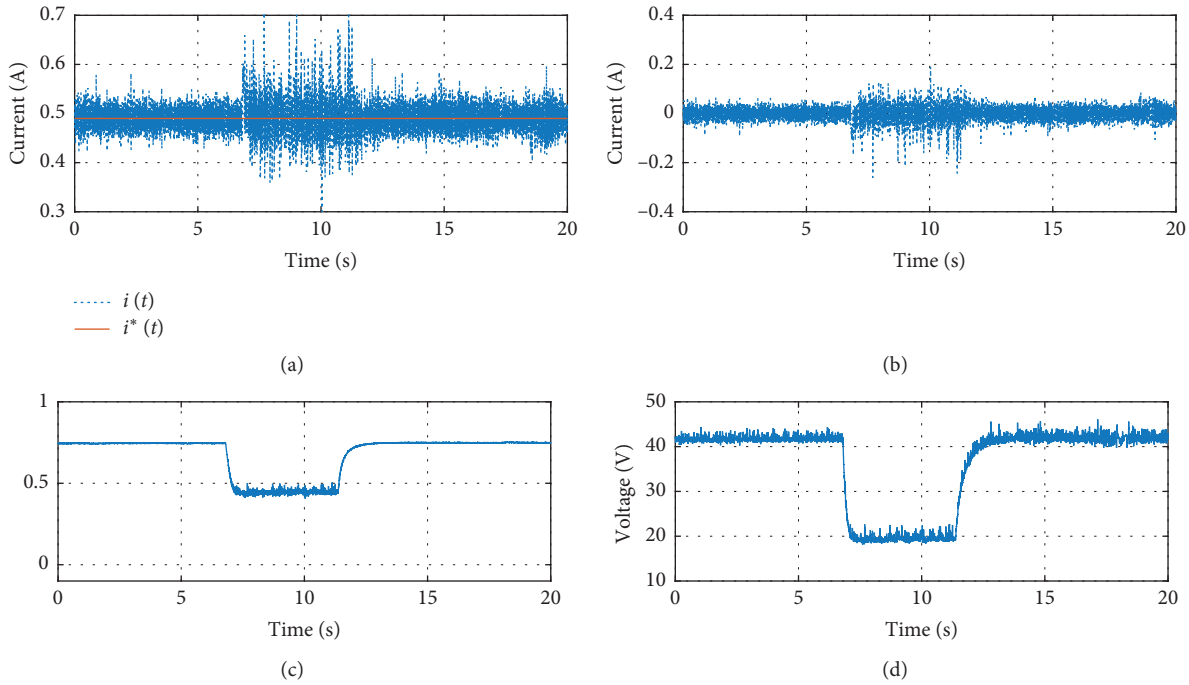

Figure 17: Boost converter response to disturbances, SSTA controller. (a) Desired current and measured current. (b) Error. (c) Control action. (d) Output voltage.

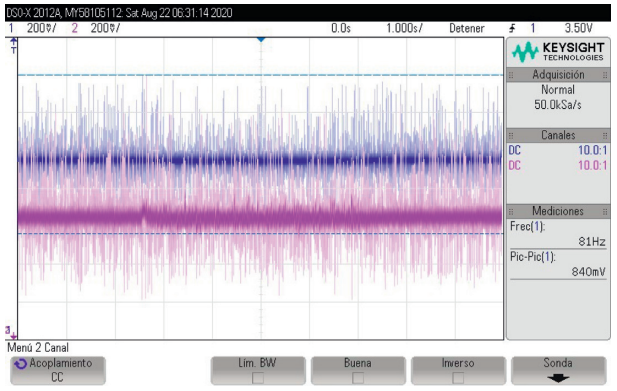

Figure 18: Desired current (blue) and measured current (magenta) for the SSTA controller.

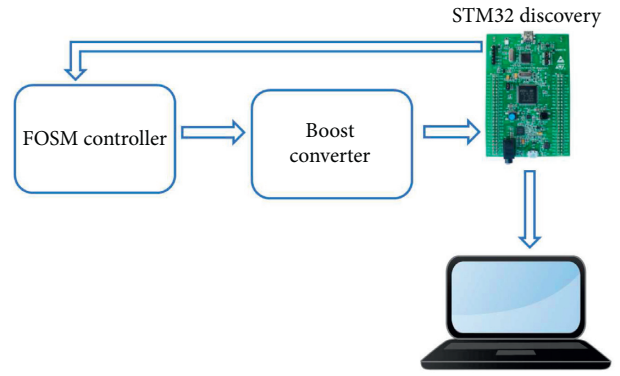

Figure 20: Boost converter prototype scheme for the FOSM controller.

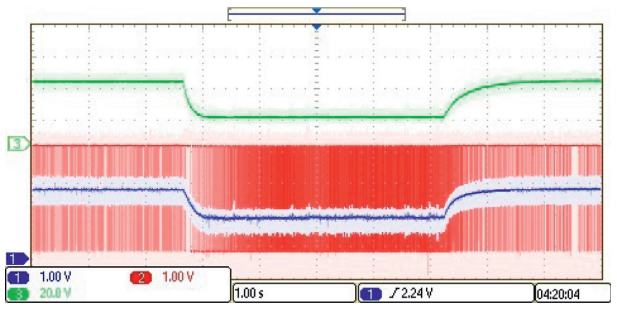

Figure 19: Output voltage (green), SSTA controller signal (blue), and $\Sigma\Delta M$ output (red).

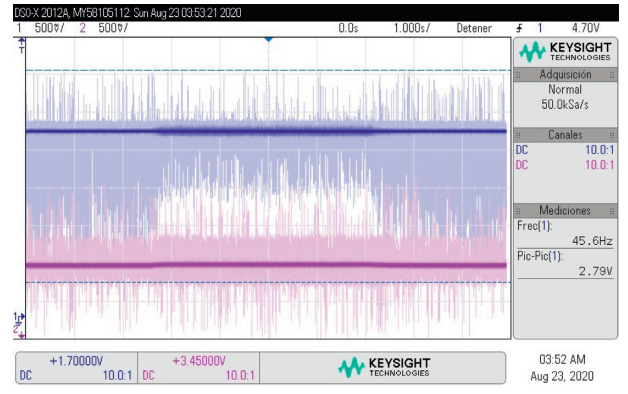

Figure 21: Desired current (magenta) and measured current (blue) for the FOSM controller.

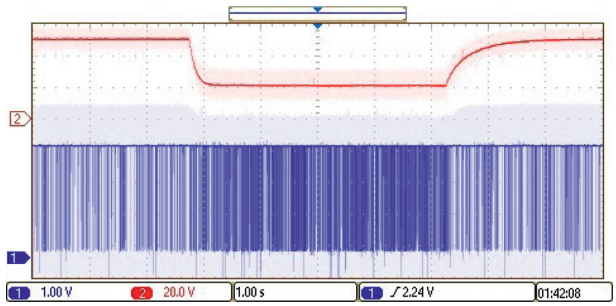

Figure 22: Output voltage (red) and FOSM controller signal (blue).

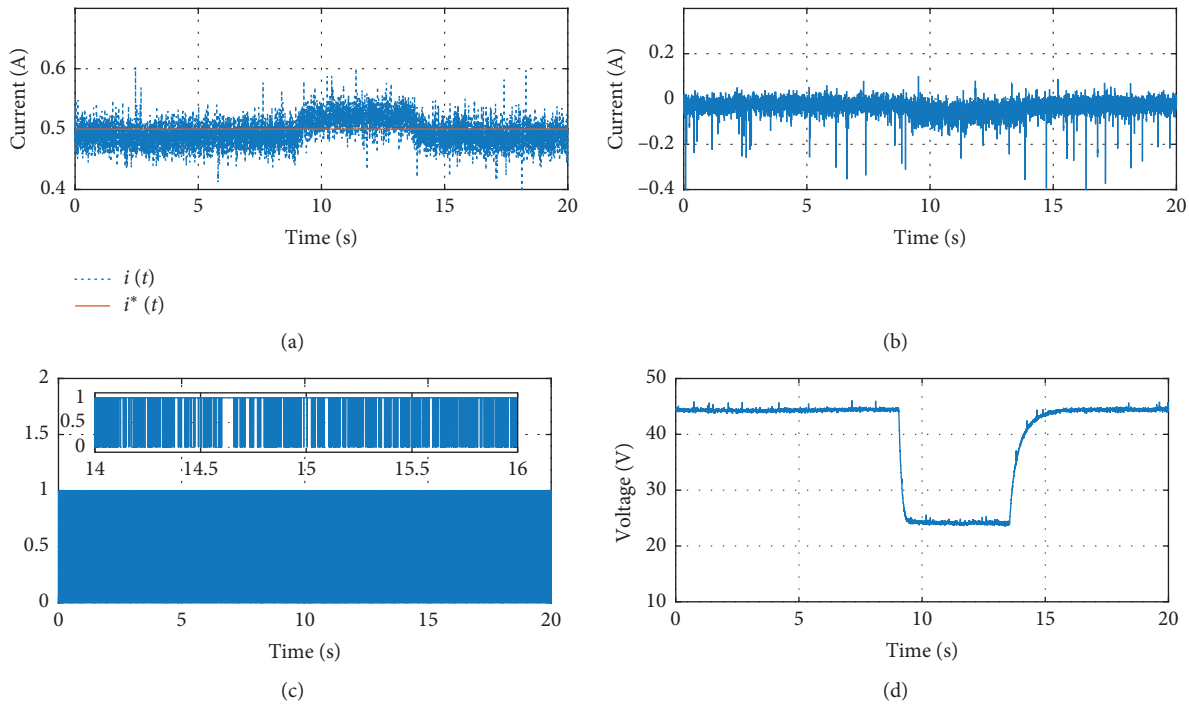

Figure 23: Boost converter response to disturbances, FOSM controller. (a) Desired current and measured current. (b) Error. (c) Control action. (d) Output voltage.

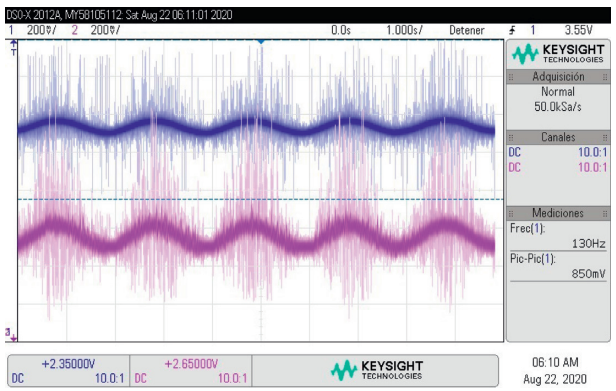

Figure 24: Desired current path (blue) and measured current (magenta).

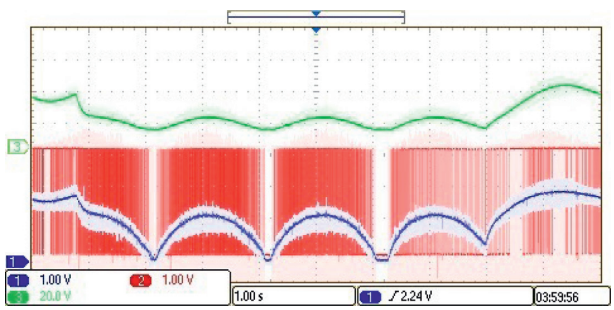

Figure 25: Output voltage (green), SSTA controller signal (blue), and $\Sigma\Delta M$ output (red) for trajectory tracking.

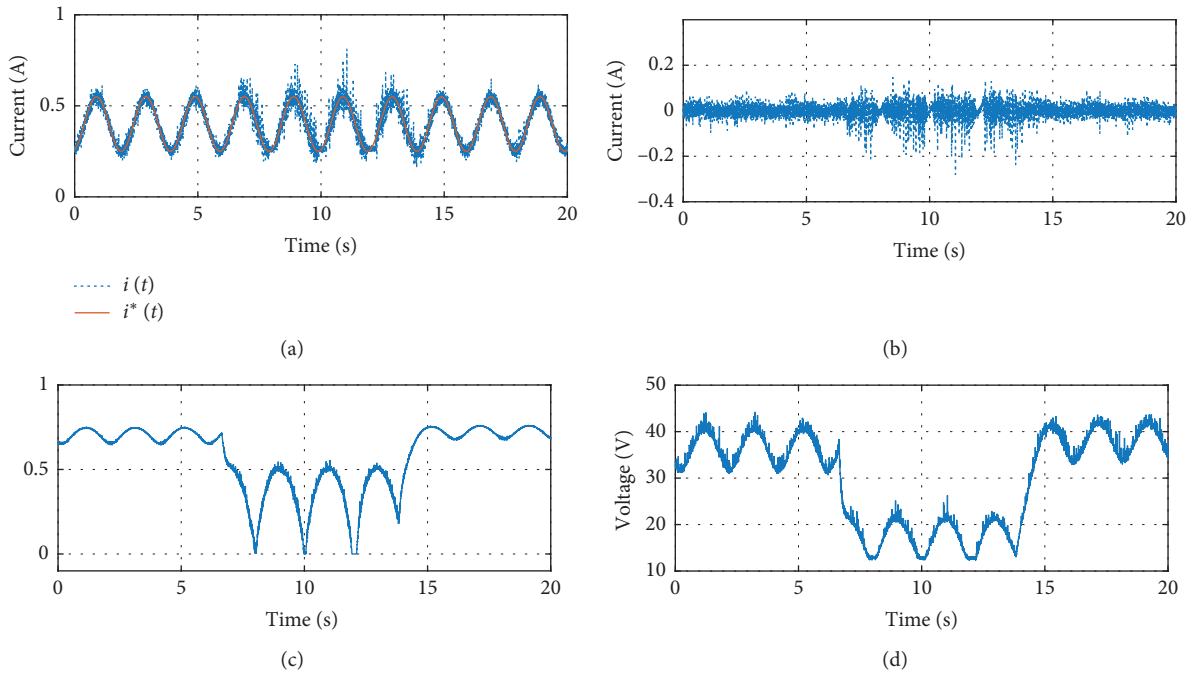

Figure 26: Boost converter response to path following with the SSTA controller. (a) Desired current and measured current. (b) Error. (c) Control action. (d) Output voltage.

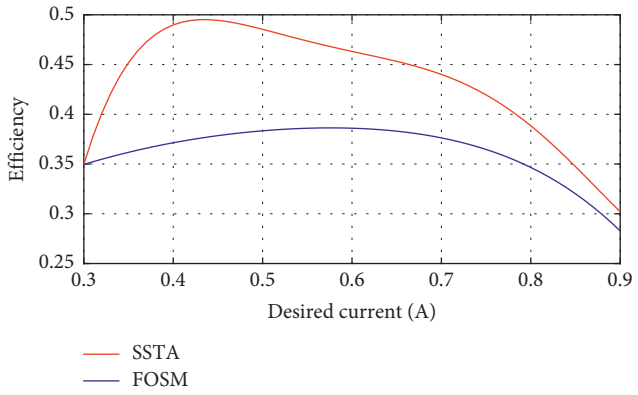

Figure 27: $\eta - i^*$ characteristic curves of the SSTA and FOSM controllers.

6. Conclusion

An SSTA controller is designed for a boost converter. This methodology can be applied to other power converters. The controller is capable to track in finite-time a desired current profile, while it compensates, in the same manner, bounded Lipschitz uncertainties/perturbations by generating a bounded continuous control signal. The continuous control signal is applied to the boost converter by using $\Sigma\Delta M$. The application of a continuous sliding mode controller in a power converter diminishes the energy of the error signal in comparison with the one presented with a FOSM controller. The proposed controller is embedded in a development card and applied to a real boost converter, showing the applicability of the proposed approach.

Data Availability

The data used to support this study are included within this article.

Conflicts of Interest

The authors declare that there are no conflicts of interest regarding the publication of this paper.

Acknowledgments

In memory of Oscar Villafuerte-Segura, my brother, my partner, and unconditional friend. I will never forget you, Andrés A. Galván-Navarro, my beloved father, teacher, guide, and dearest friend; you will always be in my heart. This work was supported in part by the Secretaría de Investigación y Posgrado of the Instituto Politécnico Nacional (20200687, 20202256, and 20200143) and the CONACyT scholarship (no. 958158).

References

[1] J.-S. Lai and D. J. Nelson, "Energy management power converters in hybrid electric and fuel cell vehicles," *Proceedings of the IEEE*, vol. 95, no. 4, pp. 766–777, 2007.

[2] B. Ge, Q. Lei, F. Z. Peng, D. Song, Y. Liu, and A. R. Haitham, "An effective PV power generation control system using Quasi-*Z* source inverter with battery," in *Proceedings of the 2011 IEEE Energy Conversion Congress and Exposition*, Phoenix, AZ, USA, September 2011.

[3] M. Habib, A. A. Ladjici, and E. Bollin, "Finite set MPC control of two level inverter for PV/battery grid-connected system," in

Proceedings of the 2017 6th International Conference on Systems and Control (ICSC), Batna, Algeria, May 2017.

[4] A. Sahli, F. Krim, A. Laib, and B. Talbi, "Energy management and power quality enhancement in grid-tied single-phase PV system using modified PUC converter," *IET Renewable Power Generation*, vol. 13, no. 14, pp. 2512–2521, 2019.

[5] Y. Zhou, H. Obeid, S. Laghrouche, M. Hilairet, and A. Djerdir, "Disturbance rejection control strategy of hybrid battery/super capacitors power system based on a single converter," in *Proceedings of the 2019 8th International Conference on Renewable Energy Research and Applications (ICRERA)*, Brasov, Romania, November 2019.

[6] S. A. Gorji, H. G. Sahebi, M. Ektesabi, and A. B. Rad, "Topologies and control schemes of bidirectional DC-DC power converters: an overview," *IEEE Access*, vol. 7, no. 1, pp. 117997–118019, 2019.

[7] S. Hajiaghasi, A. Salemnia, and M. Hamzeh, "Hybrid energy storage system for microgrids applications: a review," *Journal of Energy Storage*, vol. 21, no. 1, pp. 543–570, 2019.

[8] H. El Fadil and F. Giri, "Backstepping based control of PWM DC-DC boost power converters," in *Proceedings of the 2007 IEEE International Symposium on Industrial Electronics*, Vigo, Spain, June 2007.

[9] M.-G. Kim, "Proportional-integral (PI) compensator design of duty-cycle-controlled buck LED driver," *IEEE Transactions on Power Electronics*, vol. 30, no. 7, pp. 3852–3859, 2015.

[10] A. Kuperman, "Proportional-resonant current controllers design based on desired transient performance," *IEEE Transactions on Power Electronics*, vol. 30, no. 10, pp. 5341–5345, 2015.

[11] S. Padmanaban, G. Grandi, F. Blaabjerg, P. Wheeler, P. Siano, and M. Hammami, "A comprehensive analysis and hardware implementation of control strategies for high output voltage DC-DC boost power converter," *International Journal of Computational Intelligence Systems*, vol. 10, no. 1, pp. 140–152, 2017.

[12] A. Mushi, S. Nagai, H. Obara, and A. Kawamura, "Fast and robust nonlinear deadbeat current control for boost converter," *IEEJ Journal of Industry Applications*, vol. 6, no. 5, pp. 311–319, 2017.

[13] K. Shen, J. Feng, and J. Zhang, "Finite control set model predictive control with feedback correction for power converters," *CES Transactions on Electrical Machines and Systems*, vol. 2, no. 3, pp. 312–319, 2018.

[14] S. Pang, B. Nahid-Mobarakeh, S. Pierfederici et al., "Interconnection and damping assignment passivity-based control applied to on-board DC-DC power converter system supplying constant power load," *IEEE Transactions on Industry Applications*, vol. 55, no. 6, pp. 6476–6485, 2019.

[15] H. W. Choi, S. M. Kim, J. Kim, Y. Cho, and K. B. Lee, "Deadbeat predictive direct power control of interleaved buck converter-based fast battery chargers for electric vehicles," *Journal of Power Electronics*, vol. 20, no. 1, pp. 1162–1171, 2020.

[16] G. Rigatos, P. Siano, and M. Sayed-Mouchaweh, "Adaptive neurofuzzy *H*-infinity control of DC–DC voltage converters," *Neural Computing and Applications*, vol. 32, no. 1, pp. 2507–2520, 2020.

[17] H. Sira-Ramírez and R. Silva-Ortigoza, *Control Design Techniques in Power Electronics Devices*, Springer-Verlag London, London, UK, 1 edition, 2006.

[18] V. I. Utkin, J. Guldner, and J. Shi, *Sliding Mode Control in Electro-Mechanical Systems*, CRC Press, Boca Raton, FL, USA, 2009.

[19] Z. Chen, "Double loop control of buck-boost converters for wide range of load resistance and reference voltage," *IET Control Theory & Applications*, vol. 6, no. 7, pp. 900–910, 2012.

[20] Y. M. Alsmadi, V. Utkin, M. A. Haj-ahmed, and L. Xu, "Sliding mode control of power converters: DC/DC converters," *International Journal of Control*, vol. 91, no. 11, pp. 2472–2493, 2018.

[21] J. A. V. Formenti and G. R. Elder, "Method and apparatus for controlling charge balance among cells while charging a battery array," US. Patent 6700350B2, 2004.

[22] C. W. Tan, T. C. Green, and C. A. Hernandez-Aramburo, "An improved maximum power point tracking algorithm with current-mode control for photovoltaic applications," in *Proceedings of the 2005 International Conference on Power Electronics and Drives Systems*, Kuala Lumpur, Malaysia, November 2005.

[23] M. Aime, G. Gateau, and T. A. Meynard, "Implementation of a peak-current-control algorithm within a field-programmable gate array," *IEEE Transactions on Industrial Electronics*, vol. 54, no. 1, pp. 406–418, 2007.

[24] Q. Huang, X. Zou, D. Zhu, and Y. Kang, "Scaled current tracking control for doubly fed induction generator to ride-through serious grid faults," *IEEE Transactions on Power Electronics*, vol. 31, no. 3, pp. 2150–2165, 2016.

[25] N. Vafamand, A. Khayatian, and M. H. Khooban, "Stabilisation and transient performance improvement of DC MGs with CPLs: non-linear reset control approach," *IET Generation, Transmission & Distribution*, vol. 13, no. 14, pp. 3169–3176, 2019.

[26] N. Vafamand, S. Yousefizadeh, M. H. Khooban, J. D. Bendtsen, and T. Dragicevic, "Adaptive TS fuzzy-based MPC for DC microgrids with dynamic CPLs: nonlinear power observer approach," *IEEE Systems Journal*, vol. 13, no. 3, pp. 3203–3210, 2019.

[27] J. Wu and Y. Lu, "Adaptive backstepping sliding mode control for boost converter with constant power load," *IEEE Access*, vol. 7, no. 1, pp. 50797–50807, 2019.

[28] Y. Shtessel, C. Edwards, L. Fridman, and A. Levant, *Sliding Mode Control and Observation*, Birkhäuser, New York, NY, USA, 1 edition, 2014.

[29] V. Utkin, "Sliding mode control of DC/DC converters," *Journal of the Franklin Institute*, vol. 350, no. 8, pp. 2146–2165, 2013.

[30] A. Levant, "Sliding order and sliding accuracy in sliding mode control," *International Journal of Control*, vol. 58, no. 6, pp. 1247–1263, 1993.

[31] R. Seeber and M. Horn, "Stability proof for a well-established super-twisting parameter setting," *Automatica*, vol. 84, no. 1, pp. 241–243, 2017.

[32] A. Levant, "Chattering analysis," *IEEE Transactions on Automatic Control*, vol. 55, no. 6, pp. 1380–1389, 2010.

[33] U. P. Ventura and L. Fridman, "Chattering measurement in SMC and HOSMC," in *Proceedings of the 2016 14th International Workshop on Variable Structure Systems (VSS)*, Nanjing, China, June 2016.

[34] I. Castillo, M. Steinberger, L. Fridman, J. Moreno, and M. Horn, "Saturated super-twisting algorithm based on perturbation estimator," in *Proceedings of the 2016 IEEE 55th Conference on Decision and Control (CDC)*, Las Vegas, NV, USA, December 2016.

[35] R. Seeber and M. Horn, "Guaranteeing disturbance rejection and control signal continuity for the saturated super-twisting algorithm," *IEEE Control Systems Letters*, vol. 3, no. 3, pp. 715–720, 2019.

[36] S. Oucheriah, L. Guo, "PWM-Based adaptive sliding-mode control for boost DC-DC convertersy," *IEEE Transactions on Industrial Electronics*, vol. 60, no. 8, pp. 3291–3294, 2013.

[37] A. Goudarzian, A. Khosravi, and H. A. Raeisi, "Optimized sliding mode current controller for power converters with non-minimum phase nature," *Journal of the Franklin Institute*, vol. 356, no. 15, pp. 8569–8594, 2019.

[38] H. Sira-Ramírez, *Sliding Mode Control: The Delta-Sigma Modulation Approach*, Birkhäuser Basel, Basel, Switzerland, 1 edition, 2015.

[39] J. D. Reiss, "Understanding sigma-delta modulation: the solved and unsolved issues," *Journal of the Audio Engineering Society*, vol. 56, no. 1/2, pp. 49–64, 2008.

[40] J. M. De La Rosa, "Sigma-delta modulators: tutorial overview, design guide, and state-of-the-art survey," *IEEE Transactions on Circuits and Systems I: Regular Papers*, vol. 58, no. 1, pp. 1–21, 2011.

[41] O. Alkin, *Signals and Systems: A MATLAB Integrated Approach*, CRC Press, Inc., Boca Raton, FL, USA, 2014.

[42] B. Lehman and Z. Mihajlovic, "Output ripple analysis of switching DC-DC converters," in *Proceedings of the PESC97. Record 28th Annual IEEE Power Electronics Specialists Conference. Formerly Power Conditioning Specialists Conference 1970-71. Power Processing and Electronic Specialists Conference 1972*, Saint Louis, MO, USA, June 1997.

[43] O. López-Santos, H. Valderrama-Blavi, G. García, D. O. Mercuri, and L. Martínez-Salamero, "Efficiency analysis of a sliding-mode controlled quadratic boost converter," *IET Power Electronics*, vol. 6, no. 2, pp. 364–373, 2013.

Hindawi
Complexity
Volume 2020, Article ID 8672431, 17 pages
https://doi.org/10.1155/2020/8672431

Research Article

Hybrid Deep-Learning Framework Based on Gaussian Fusion of Multiple Spatiotemporal Networks for Walking Gait Phase Recognition

Tao Zhen,[1,2] Jian-lei Kong,[1,3,4] and Lei Yan[2]

[1]*School of Artificial Intelligence, Beijing Technology and Business University, Beijing 100048, China*
[2]*School of Engineering, Beijing Forestry University, Beijing 100083, China*
[3]*National Key Laboratory of Environmental Protection Food Chain Pollution Prevention, Beijing 100048, China*
[4]*China Light Key Laboratory of Industry Internet and Big Data, Beijing 100048, China*

Correspondence should be addressed to Jian-lei Kong; kongjianlei@btbu.edu.cn and Lei Yan; mark_yanlei@bjfu.edu.cn

Received 22 May 2020; Revised 15 August 2020; Accepted 28 August 2020; Published 9 October 2020

Academic Editor: Carlos-Arturo Loredo-Villalobos

Copyright © 2020 Tao Zhen et al. This is an open access article distributed under the Creative Commons Attribution License, which permits unrestricted use, distribution, and reproduction in any medium, provided the original work is properly cited.

Human gait phase detection is a significance technology for robotics exoskeletons control and exercise rehabilitation therapy. Inertial Measurement Units (IMUs) with accelerometer and gyroscope are convenient and inexpensive to collect gait data, which are often used to analyze gait dynamics for personal daily applications. However, current deep-learning methods that extract spatial and the isolated temporal features can easily ignore the correlation that may exist in the high-dimensional space, which limits the recognition effect of a single model. In this study, an effective hybrid deep-learning framework based on Gaussian probability fusion of multiple spatiotemporal networks (GFM-Net) is proposed to detect different gait phases from multisource IMU signals. Furthermore, it first employs the gait information acquisition system to collect IMU data fixed on lower limb. With the data preprocessing, the framework constructs a spatial feature extractor with AutoEncoder and CNN modules and a multistream temporal feature extractor with three collateral modules combining RNN, LSTM, and GRU modules. Finally, the novel Gaussian probability fusion module optimized by the Expectation-Maximum (EM) algorithm is developed to integrate the different feature maps output by the three submodels and continues to realize gait recognition. The framework proposed in this paper implements the inner loop that also contains the EM algorithm in the outer loop and optimizes the reverse gradient in the entire network. Experiments show that this method has better performance in gait classification with accuracy reaching more than 96.7%.

1. Introduction

Robotics exoskeletons has become a burgeoning technology in continuous development in the field of medical, architectural, and military applications. Focusing on the medical domain, lower limb exoskeletons are mainly designed to enhance the patient's mobility in the rehabilitation therapy and strengthen physical performance after undergoing treatment with great expectations of improving his/her living quality as much as possible. This robot should own an intelligent gait phase recognition method to provide cogent means to deal with large amounts of momentary or sequential data and identify different walking styles, one of the most important features displaying posture and phase of each particular patient [1]. Therefore, accurate classification of changing walking style of human lower limbs' status is urgently required to achieve consistency and coordination of human-machine interaction [2]. An effective analysis of walking style is performed well in athletic performance improvement or disease diagnosis and rehabilitation research, which have been applied in clinical treatment plan with multiple sclerosis, Parkinson, brain trauma, and other diseases [3, 4]. Note that traditional walking analysis is represented by detecting the different gait phase based on motion information (e.g., angles, speed, or acceleration) of the knees, ankles, and hips when walking or running. For

example, Buckley et al. [3] used gait phase detection to diagnose stroke patients, and Achanta et al. [5] used a novel hidden-Markov-based adaptive dynamic time warping to analysis gait for identifying physically challenged persons and providing them with appropriate alerts by monitoring walking. In order to make exoskeleton robots have better human-machine coordination, some researchers have begun to try program human robots, generate gait trajectories of wearers through gait phase recognition technology, and control the movement of wearable auxiliary devices, such as robotic prostheses and orthotics [6, 7]. Berger et al. [8] reported that robot-assisted gait training has proven to be a promising treatment for restoring and improving walking ability. Similarly, Luo et al. [9] also mentioned that the high-quality gait-subphase recognition plays an important role in the synergetic control of lower limb powered exoskeletons.

In recent years, walking gait phase detection has been one of the most important research problems. Many scholars have studied the relevant sensor technologies and methods to distinguish attributes for gait phase recognition. Jin et al. [10] realized the recognition of the frontal gait phase by using deep-learning models to obtain information from multiple cameras. Although the optical gait analysis technology has obtained the accurate enough performance, the full cost of multicamera system is very high for simple walking gait identification. Moreover, the operation process captures spatial trajectory of marking points related to body positions in the indoor infrastructure, which make the identification accuracy easily affected by the instable light intensity and limit the generic application of gait phase detection. To better adapt to environmental factors, the measuring technology of biological signals such as electromyography (EMG) is introduced to evaluate the continuous movement status of the human body. With EMG sensors fixed on the skin surface, the action potential changes are observed after being amplified to reflect muscle activity information when the central nervous system controls lower limb motion. Since the muscle contraction process has a time effect of electromechanical delay, those EMG signals are generated about 40 ms to 100 ms faster than lower limb motion, which is conducive for understanding motion pattern and recognizing gait phases in advance, also making it possible for the real-time control system of exoskeletons. Fei et al. [11] took the multisource EMG signals on the hip joint angle and the skin surface of thigh muscles to realize prediction of the human lower limb motion. To further improve the prediction effect of the model on the gait phase, some studies have also added the plantar pressure signal to the input of the neural network model. Si et al. [12] propose a support vector machine model optimized by fractal analysis algorithm to cope with synchronized information of EMG and foot pressure sensors for gait phase recognition. However, such an acquisition approach of EMG data asks participants wearing a special cumbersome cloth with expensive cost, which is subject to observers' intra- and external variability including weight, muscle content, or load, making it difficult to design progressive therapeutic strategies to improve automatic control performance of lower limb exoskeletons.

At present, many researchers have paid attention to more flexible wearable sensors, typically as IMUs, to handle with the relative issues of gait phase detection. These sensors are relatively lightweight, cheap, easy to use, and unobtrusive compared with aforementioned motion capture systems consisting of RGB-D cameras, EMG, or force plates sensors. With some simple constrained equipment fixed on waist, thigh, calf, or foot, IMUs sensors can provide continuous and high-resolution inertial data, which can well quantify gait phase recognition performance, which is basically unaffected by various human body factors. It is not surprising that there exist the developing trends of human motion analysis using IMUs, for instance, gait phase detection by statistical analysis or machine learning and exoskeleton decision-making control by postural stability metrics. For instance, Kang et al. [13] used inertial information obtained from the IMU on the calf to study whether cognitive impairment increases the fall risk of patients. Gohar et al. [14] used inertia information on the chest to realize ID identification of personnel. However, the local information provided by a single IMU sensor is limited to descript the complexity exercise process of human body. More and more scholars have begun to explore the combined use of inertial and acceleration information from multiple body parts to enhance the reliability and accuracy of gait event detection. For example, Zhou et al. [15] used the inertial information obtained by the IMU on the legs and feet to achieve gait assistance. Yeo and Park [16] used the inertial information of the shin and leg surface through the IMU to provide gait measurements and enable accurate analysis. In another example, Yan et al. [1] used the inertial information on the feet, thighs, and calves to accurately identify the gait phase. The above researches have exhibited that only using a small number of IMU sensors located on the lower limb can provide extremely cost-effective and efficient signals to characterize the periodic cycle of the gait phase and to discriminate different levels of walking ability. Importantly, this sensor application is harmless, comfort, and convenient to the personal activities and daily work, which will help clinicians make more accurate judgments about the early intervention of lower extremity diseases, the treatment plan, and the assessment of the rehabilitation progress of patients.

Although researchers have always been interested in IMU technology, there is still a lack of realistic research that implements multiple wearable sensors validators to monitor walking status and gait stability in actual clinical practice. In the context of multi-IMU-based approaches, the intelligent enough pattern recognition model of diversity gait phases with multisensor data preprocessing analysis and information fusion technology is the most critical issue that needs to be solved for lower limb gait phase detection of various wearable exercise systems or rehabilitation exoskeletons. To achieve this, some statistical learning or machine learning methods are carried to calculate spatial-temporal and biomechanical parameters of the walking gait patterns, achieving a complete assessment of lower limb motion, and providing the potential for rehabilitation training of abnormal body activities. Many researchers have studied the integrated strategy of traditional intelligent algorithms from

different perspectives. The mainstream solution is constructing various shallow-structure models including artificial neural networks (ANN), hidden-Markov model (HMM), AdaBoosting, and support vector machines (SVMs), which carefully select the threshold parameters based on physical and statistical analysis of raw or processed data to divide the gait phases. These methods build feature engineering to adaptively learn model parameters and obtain hidden relationships between historical data and then perform operations based on preset rules and algorithms to identify the subsequent patterns of gait phases. However, the gait phase detecting is still a challenging problem because the high-sampling frequency data collected from sensors always contain complex nonlinear relationships with multiple components, which makes it impossible to apply the traditional models to analyze sensory data and distinguish walking information in real time.

Different from the aforementioned algorithms, the deep-learning neural networks (DNNs) had shown the outstanding ability of handling with the complex temporal relation of gait phase detection. Thanks to the breakthroughs in the design and training of model architecture with complex structures consisting of multiple processing layers or nonlinear transformations, the improved network structure has penetrated into many smart devices including large scale visual classification, natural language processing, and time series predicting. Such fast-pacing progresses in research have also drawn attention of the related researchers and corporations to build software and hardware to recognize walking gait phases snapshotted in real life. Particularly, the convolutional neural network (CNN) and the recurrent neural network (RNN) have been used for extracting the motion features of sequential temporal data obtained by accelerometers and gyroscopes in IMU. For example, Chao et al. [17] Yan use a multitask framework to extract features and perform gait, perspective, and scene recognition. They use the output of gait energy image descriptors as input data for a CNN to detect gait phases in the complete walking cycles. Similarly, Omid et al. [18] use time-frequency expansion in order to capture joint two-dimensional spectral and temporal patterns of gait cycles, which are inserted to train an ensemble CNNs-based classifier, a typical multilayer perceptron consisting of convolutional and full-connection based on multisensor fusion. In addition, the authors in [19] propose a different voting-weighted integrated neural network for training a model for gait recognition, obtaining state-of-the-art results.

Due to the talent in handling two-dimensional signals such as the images, the most CNNs have to translate the time series inertial data as energy image or visual segmentation data. This does help to exploit the characteristics of spatial relationships in gait phase recognition, yet obviously ignoring temporal rule and periodic change when processing sequential time series data captured by IMU sensors, which is often hard to measure continuous motion trajectory and extract quality features of lower limb in unconstrained scenarios. Therefore, RNN and its improved models including long short-term memory (LSTM) network and gated recurrent unit (GRU) network pass time recording order and parameters of previous hidden layer thought the current output layer to capture the high nonlinearity and sequential relationship of time-serial IMU data, which have attracted extensive attention from researchers [20]. Neverova et al. [21] build a temporal RNN network for active biometric authentication and walking motion analysis with multisource data provided by accelerometers and gyroscope sensors in smartphone. As an improved version of the RNN, the LSTM is gradually replacing it as a new popular time series data analysis technology for gait phase recognition. For example, Hu et al. [22] trained a deep-learning network with LSTM units to process IMU data segmented by sliding windows and implement gait phase detection. Similar, Zhen et al. [23] proposed an LSTM-based recognition algorithm to perform real-time gait phase detection using absolute heading and angular velocity of IMU sensor mounted on the shank and foot. Although related researches have increased significantly in recent years, it is still difficult to accurately predict the current phase with LSTM alone through long-term sensor data. To this end, there have only been a small number of studies attempting to combine LSTM and CNN to assist patients with severe gait abnormalities and related ethical issues. Jin et al. [24] proposed a deep-learning algorithm based on a LSTM and CNN fusion framework for diagnosis and classification of abnormal gait patterns using Euler angle information of IMU sensor on the patient's legs. In this way, CNN is usually used as a spatial feature extractor and then LSTM is used to further mine the temporal features for ultima gait phases detection. In addition, the GRU unit inherits the advantages of LSTM and can automatically learn features and is an effective model [25], and the AutoEncoder unit also exhibits a significant increase in computational speed and model size compared to the existing deep-learning models [26]. Both of them are introduced as alternative patterns parts of various hybrid models based on deep-learning in many application scenarios, which have been proven effective at improving prediction performance of gait phase recognition for nonlinear time series IMU data.

In the previous studies mentioned above, it can be found that, with the development of wearable IMU biotechnology, the human motion status can be estimated by a comprehensive combination of signal processing approaches and intelligent pattern recognition algorithms to extract quantitative features of walking gait and distinguish the categories of different gait phases. For a realistic implementation of exercise rehabilitation therapy in the clinical setting, various machine learning algorithms have been developed to handle with a mass of time series data offered by multisource IMU sensors on the lower limb for quantifying gait phase and balance. Particularly, because of the excellent ability in high-dimensional feature representation of spatial and temporal characteristics, many sorts of deep-learning neural network are selected for their relevance to the sensor data types and used together in a parallel or serial structure adaptive to data structures, which have been proven effective at improving the performance for walking gait phase detection. However, the combination framework of these networks still needs to be developed to obtain better prediction effect and recognition for the nonlinear time series IMU data in order to

meet the requirement of effective rehabilitation therapy and real-time exoskeleton control.

Researchers agree that one of the reasons for the decline in recognition performance is that the data from different IMU sensors always contain multiple component signals, which is complex nonlinearity to a single deep-learning model or simple combination of different networks [27]. On the one hand, each single network is likely to focus on the constant feature of specific domain, such as spatial feature related to CNN and temporal feature associated with RNN, which lacks the capability of distinguishing small variances between similar gait phases in a global perspective. On the other hand, the simple combination solution of multiple networks lacks the guidance of effective fusion strategy and fails in leverage information complementation and comprehensive decision-making, which will reduce the overall classification accuracy especially when low-quality interference noise occurs. To augment algorithm performance currently used in the IMU-based gait phase recognition, we propose an effective hybrid deep-learning framework based on Gaussian probability fusion of multiple spatiotemporal networks (named as GFM-Net) for recognizing discriminative parts of various walking gait phases. In detail, the framework consisted of three components: a spatial feature extractor with AutoEncoder and CNN modules and temporal feature extractor with three collateral modules combining RNN, LSTM, and GRU modules. In addition, a novel classifier equipped with Gaussian probability fusion module optimized by Expectation-Maximum (EM) algorithm is developed to integrate different feature maps of components model for the ultimate gait phase recognition [28]. Different from the previous studies, the end-to-end network adaptively selects spatiotemporal feature vectors from different IMU sensors and absorbs the vast quantities of hybrid complementary knowledge available in the training corpora, which show the better promotion effect in terms of gait phase recognition accuracy in sequential walking cycle. Such an approach would likely help exoskeletons make informed control decisions about patients' treatment efficacy and recovery progress.

The remainder of this study is organized as follows. Section 2 introduces the data source and preprocess technology and then describes each part of the hybrid framework. Section 3 presents experimental results of the proposed model evaluated with correlation comparison methods. Section 4 discusses the advantages and disadvantages of our work, and finally Section 5 presents our conclusion.

2. Materials and Methods

2.1. Data Collection. In terms of experimental data, 16 volunteers with body weight ranging from 46 kg to 70 kg and height ranging from 158 cm to 177 cm were selected to collect IMU data. The height and weight distribution of the subjects is shown in Figure 1. The subjects are all healthy participants and have no physical or nerve injury to their legs or feet, which may affect walking gait phase detection. In addition, it should be noted that the participants are between 20 and 26 years old.

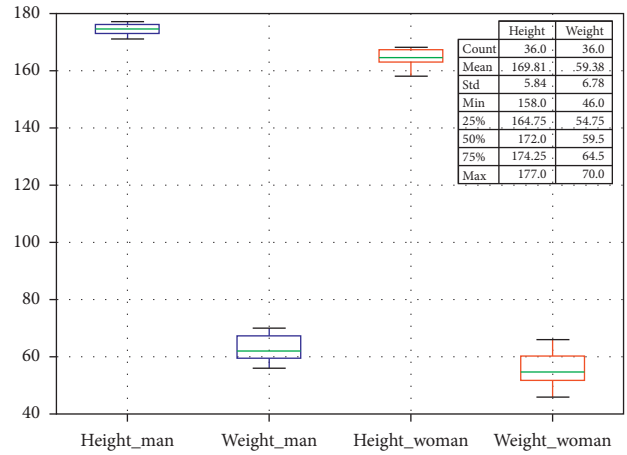

Figure 1: Weight and height information about volunteers participating.

With the advancement of sensor processing technology and algorithms, this study used three IMU modules to collect the corresponding inertial information. Input data in this work only include lower leg calf acceleration signals. To collect lower limb calf acceleration signals, the JY901 nine-axis angle sensor (Uxin Electronics Co., Ltd., Gansu, China) with Kalman filtering algorithm is used in this paper. We can choose two modes of serial communication and I2C communication. In order to cooperate with the microprocessor, we chose the serial communication mode when the system was built. Connect the TX, RX, VCC, and GND pins on the JY901 sensor to the corresponding pins on the microcontroller. The microcontroller selected is STM32C8T6, which is a 32-bit microcontroller based on the ARM Cortex-M core STM32 series, the program memory capacity is 64 KB, the required voltage is 2V~3.6 V, the operating temperature is −40°C~85°C, and the operating frequency is 72 MHz.

The inertial sensor module is placed outside the lower leg. The arrangement of acceleration sensors for calf monitoring lower limb movement is shown in Figure 2 that shows the system flow of the entire experimental data collection, processing, and application. The acceleration resolution of the nine-axis inertial sensor module (MPU9250) used in the experiment is 0.0005 g, the stability of the attitude measurement is 0.05°, and the transmission baud rate in the experiment is set to 115200 bps.

During the experiment, all participants were required to walk normally on the same treadmill at a speed of 0.78 m/s, 1.0 m/s, and 1.25 m/s for at least 120 s. All participants were asked to walk normally 3 times at each speed. All participants have the same sports environment in the same state. In order to prevent participants from affecting the later movement gait due to continuous exercise, the experiment requires all participants to rest for 2 minutes after completing the designated walking test each time to alleviate the possible impact of exercise fatigue on walking gait. In addition, when collecting data, it should be noted that we only

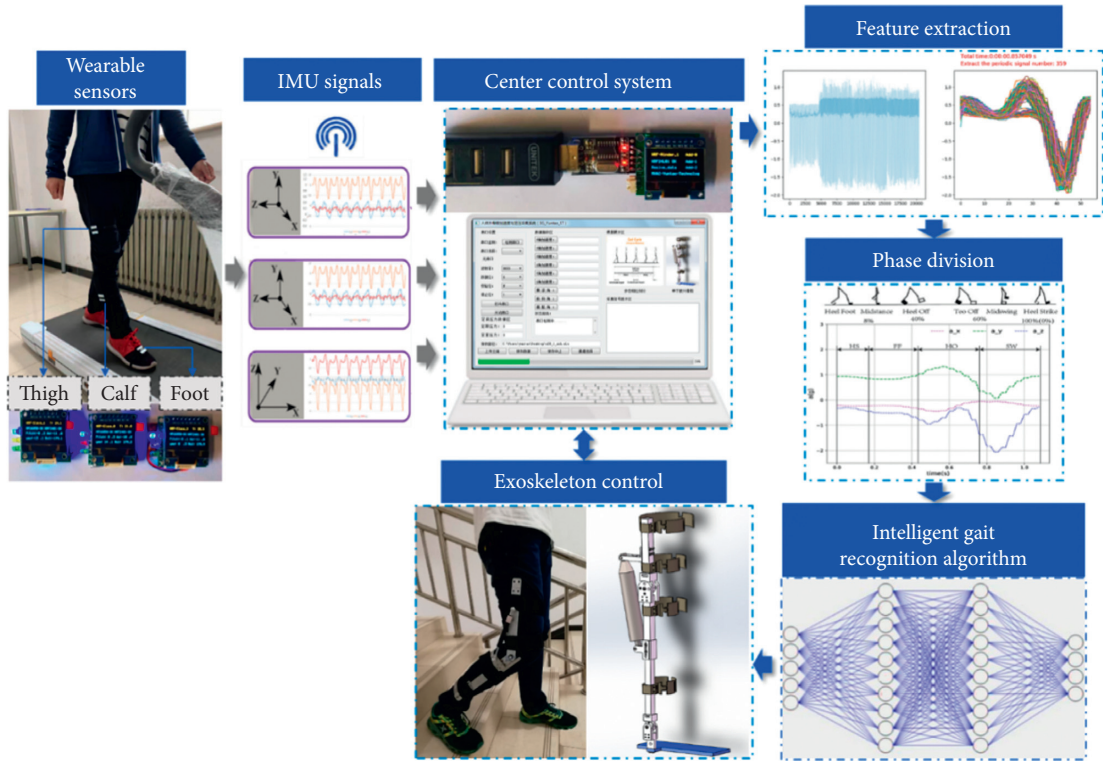

Figure 2: Human gait information acquisition system.

start saving data after the running speed of the treadmill reaches the set speed. When the treadmill starts to slow down, we stop collecting data and complete the data collection process. The information acquisition process of human gait is shown in Figure 3.

2.2. Data Preprocessing. Each data sample contains multiple features from three sensors and each data includes acceleration and angular velocity data in X, Y, and Z directions. Let two sequences of gait data be the input of the network, which is expressed as

$$\vec{x} = \left(a_x, a_y, a_z, g_x, g_y, g_z\right), \tag{1}$$

where a_x , a_y, and a_Z represent the acceleration signals in the X, Y , and Z directions, respectively, and g_x, g_y, and g_z represent the angular velocity in the three-dimensional space, respectively. Based on the above operation, we can get the combined curve of the acceleration and angular velocity in the X, Y, and Z directions obtained by three IMU sensors as shown in Figure 2.

Then, the second preprocess step is to extract the periodic feature by splitting the data. The data collected by the inertial sensors is a data stream distributed over time. Features cannot be directly extracted and classified, so the data needs to be segmented. At present, the data segmentation method is a multidimensional sliding window segmentation method. The acceleration signal is cut into periodic signals by using a sliding window segmentation method [29]. However, this signal extraction method requires a lot of tentative experiments to try different sizes of sliding windows on the extraction of gait signals, which is difficult for us to guarantee the quality of the extracted signals. In order to improve the adaptivity and efficiency of sliding window, this paper uses Pearson's correlation coefficient and significance level P [30] value to extract gait periodic signals. Since the significance level is the P value, the sliding window is associated with significance without being affected by the high correlation coefficients. However, relevance may be caused by accident. So, how much is significant; generally P value is less than 0.05 which is significant; if it is less than 0.01, it is more significant. In addition, according to Pearson's correspondence, the relationship between the correlation coefficient value and the degree of correlation is defined as follows: the correlation coefficient range of 0.0–0.2 means "very weakly correlated or uncorrelated" in degree of relevance, the range of 0.2–0.4 means "weak correlation," the range of 0.4–0.6 means "moderately relevant," the range of 0.6–0.8 means "strong correlation," and the range of 0.8–1.0 means "very strong correlation." In this work, Pearson's correlation coefficient is chosen as 0.87 and P value is set as 0.01 according to actual condition and repeated tests. Based on the selected parameters, a partial signal extraction diagram is shown in Figure 4.

Next, we need to perform phase division. The human walking process is a rhythmic movement, and a complete gait cycle definition is from one-sided heel landing to the same-sided heel landing again. Two phase model recognition systems are sufficient to control active knee orthosis [31].

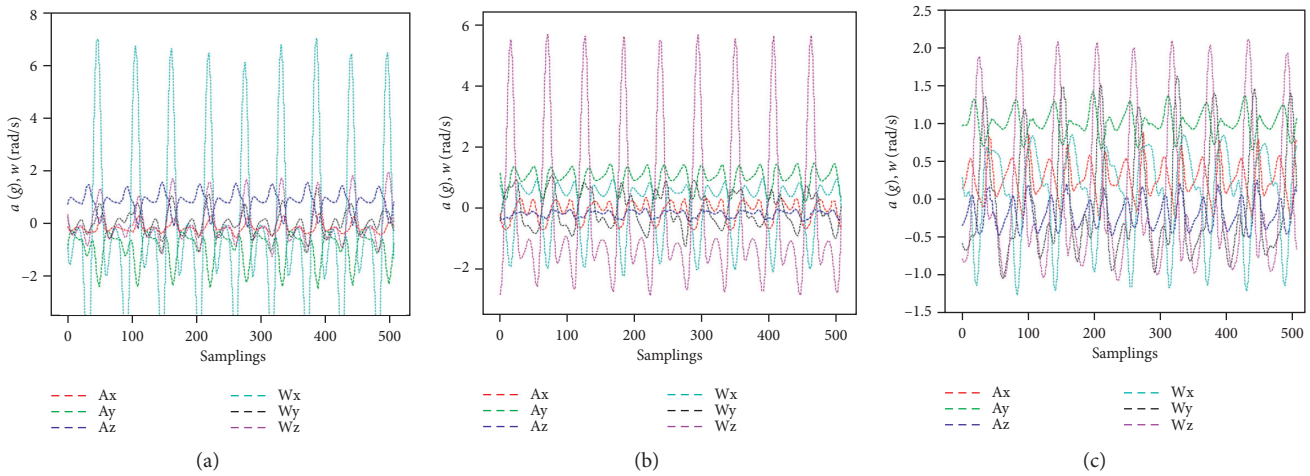

FIGURE 3: Acceleration and angular velocity data collected under three body parts covering foot (left), calf (center), and thigh (right). In the figures, Ax, Ay, Az, Wx, Wy, and Wz represent the curves of acceleration and angular velocity in the X, Y, and Z directions over time during the acquisition process, respectively.

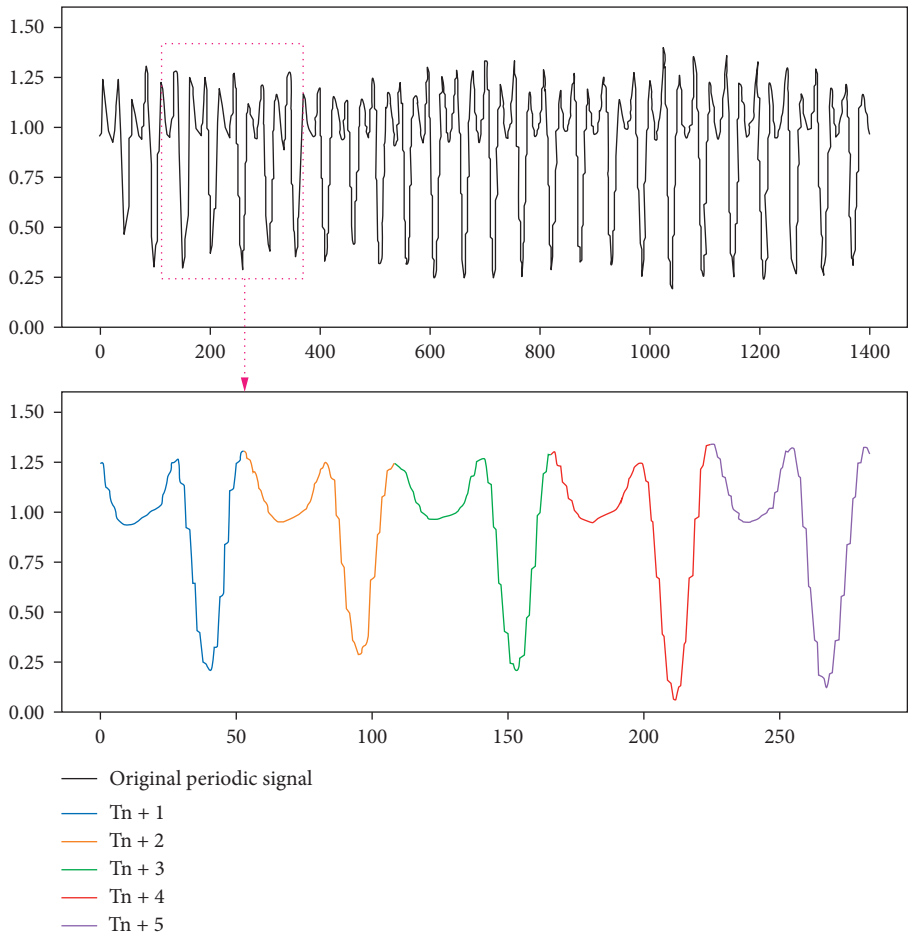

FIGURE 4: Example of periodic signal extraction results. Periodic signals Tn + 1, Tn + 2, Tn + 3, Tn + 4, and Tn + 5 are extracted from the pink box of original periodic signal using Pearson's correlation coefficient and P value.

However, the most widespread method currently relies on four-phase identification technology [32], which is represented as heel strike (HS), load response phase or flat foot (FF), heel lift or heel disengagement (HO), and initial swing phase (SW). This four-phase gait partition model has been used to drive multiple robotic ankle-foot orthosis robots

[33]. Referring to previous studies, this study also divides the gait cycle into HS, FF, HO, and SW phases. During normal walking, the acceleration signals and angle signals on the feet, thighs, and lower legs are strongly periodic. Studies have shown that the swing phase accounts for 40% of the entire gait cycle, while the standing phase accounts for 60% of the entire gait cycle [34]. According to the previous analysis, the schematic diagram of the gait cycle division is shown in Figure 5.

2.3. GFM-Net Gait Phase Detection. As the analysis of the ability differences of individual models for different categories and the fusion advantage of multiple models, we find that the reasonable integration way will fuse the different feature extraction capabilities of various models for better gait phase recognition. Therefore, we design a hybrid deep-learning framework to converge the spatiotemporal feature vectors of the multistream networks through the Gaussian probability layer output, so that the submodels complement each other and improve the whole accuracy. The architecture of the hybrid framework is shown in Figure 6.

2.3.1. AutoEncoder-CNN Spatial Feature Extractor. The spatial feature extractor is composed of an automatic encoder and CNN. In order to enhance the adaptive ability of the model, we adjusted the parameters such as the stride of the convolution layer or the size of the convolution kernel. This adjustment usually hardly increases the complexity of the network model, but the prediction accuracy of the model is improved. First, we briefly introduce the AutoEncoder architecture as a coarse feature extractor to study model adjustment, which covers an encoding layer, an intermediate layer, and a decoding layer with the Leaky-ReLU activation function. The input channel of this article is 60 and the output channel is 72. Then, the feature vector f extracted by AutoEncoder is input to the "sub-CNN" structure, which consists of four convolutional layers. In this paper, we select the 3*3 kernels convolution layer with the stride 1 and padding 0 to build the first conv1 pipeline. Then, a 2×2 max pooling layer with a stride of 2 is followed as the conv2 stage, where the input stem begins with a downsampling block. And the conv3 and conv4 layers are, respectively, selected as a 2×2 convolution kernel and 1×1 convolution kernel with the same stride 1. The activation function of each convolution layer is set as the ReLU function in this network. To reduce the risk of the gradient disappearing, we introduce the batch-normalization module right after conv3 and conv4 layers. The period operation process is shown as follows:

$$\begin{aligned} f &= H_{\text{auto}}\left(\overrightarrow{x}, \left\{W_1, B_1, \delta_{\text{leaky-relu}}\right\}\right), \\ F &= H_{\text{cnn}}\left(f, \overrightarrow{y}, \{W_2, B_2, \delta_{\text{relu}}\}\right), \end{aligned} \tag{2}$$

where the function H_{auto} can represent the encoding and decoding layers of the AutoEncoder architecture with the inputs $\overrightarrow{x}$ denoted to the raw IMU data. W_1 denotes the weight matrix of the network convolution kernel. B_1 is the bias of the network convolution kernel. And $\delta_{\text{leaky-relu}}$ denotes the nonlinear activation functions. Then, the feature map f and the related gait phase division result $\overrightarrow{y}$ are combined as the input of H_{cnn} function, which indicated the multiple convolutional layers with the weight matrix W_2 and the bias vector B_2 under the inspiration of the ReLU activation function δ_{relu}. We randomly initialize the weights and start training all networks with a momentum of 0.9. With the learning rate 0.05, the spatial feature vector F with 300 channels is obtained to extract the further temporal features.

2.3.2. Multisteams Temporal Feature Extractor. $x_t \in F(f_1, f_2, \ldots, f_n)$ is the input of the three subnetworks; P_t, S_t, and Q_t $(t = 1, 2, \ldots, n)$ are the relevant outputs of sub-GRU, sub-LSTM, and sub-RNN models, respectively. The GRU uses an update gate to control the degree to which the previous state affects the current state. The reset gate is equivalent to the forget gate in LSTM for controlling the degree of the previous moment. The forward propagation of each submodel is as follows:

$$\begin{aligned} P &= R_{\text{gru}}\left\{\sum_{t=1}^{n}\left[x_t, h_t, z_t, r_t, \left(w_1, b_1, \delta_{\text{tanh}}\right)\right]\right\}, \\ S &= R_{\text{lstm}}\left\{\sum_{t=1}^{n}\left[x_t, h_t', g_t, \left(w_2, b_2, \delta_{\text{tanh}}\right)\right]\right\}, \\ P &= R_{\text{rnn}}\left\{\sum_{t=1}^{n}\left[x_t, a_t, \left(w_3, b_3, \delta_{\text{tanh}}\right)\right]\right\}, \end{aligned} \tag{3}$$

where x_t is the input vector to each submodel. h_t, z_t, and r_t stand for the active state, update gate, and reset gate of the current hidden node in GRU cells at time t; w_1 and b_1 are, respectively, the weight matrices and bias vectors to be learned during model training; and δ_{tanh} are the tanh activation functions. Similarly, h_t' and g_t represent the active state and the forget gate in LSTM cells at time t with the weight matrices w_2 and the related bias vectors b_2. In addition, a_t, w_3, and b_3 indicate the network parameters of the RNN models. Finally, the model is trained by gradient descent algorithm and the parameters such as weight and bias are constantly updated.

2.3.3. Gaussian Probability Fusion Module. Next, we further propose a probabilistic fusion module that uses the multistream spatiotemporal feature maps generated by the submodules for the final fusion decision of the model. In the fusion module, the output is the fused classification probability, and the input is the various features of sub-RNN, sub-GRU, and sub-LSTM models. In order to further improve the disappearance of the gradient, this paper adds a convolutional layer and a batch-normalization layer to follow the results of three submodel outputs. This operation is to unify the output vector of different models into the same dimensional space layer, which facilitates subsequent fusion operations. The entire operation process is described as follows:

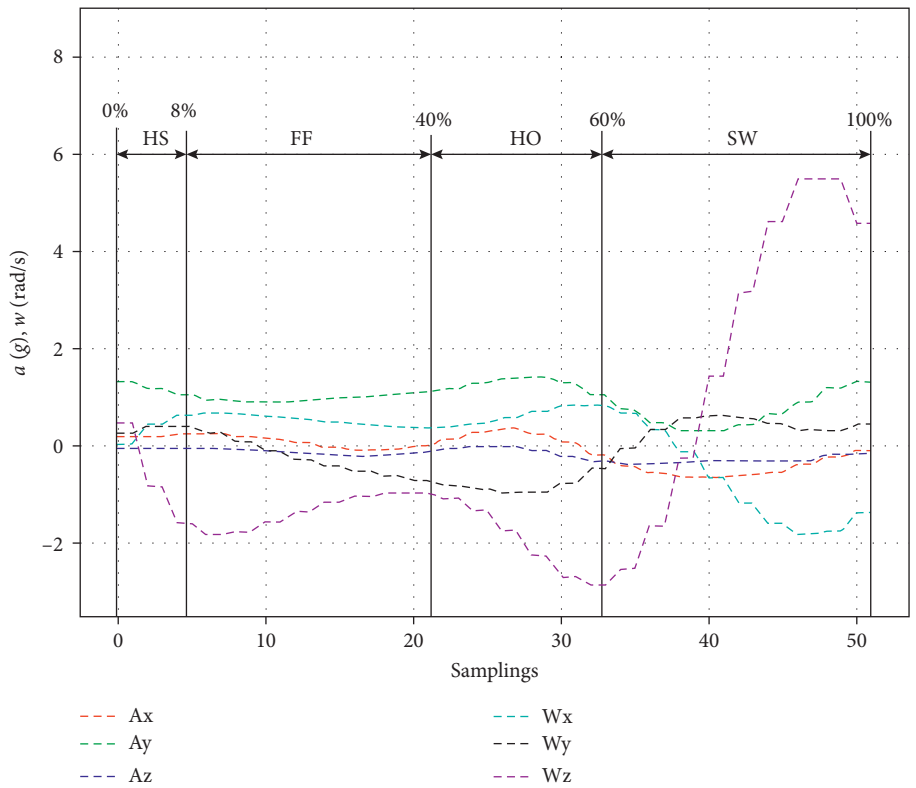

Figure 5: Phase division diagram of gait.

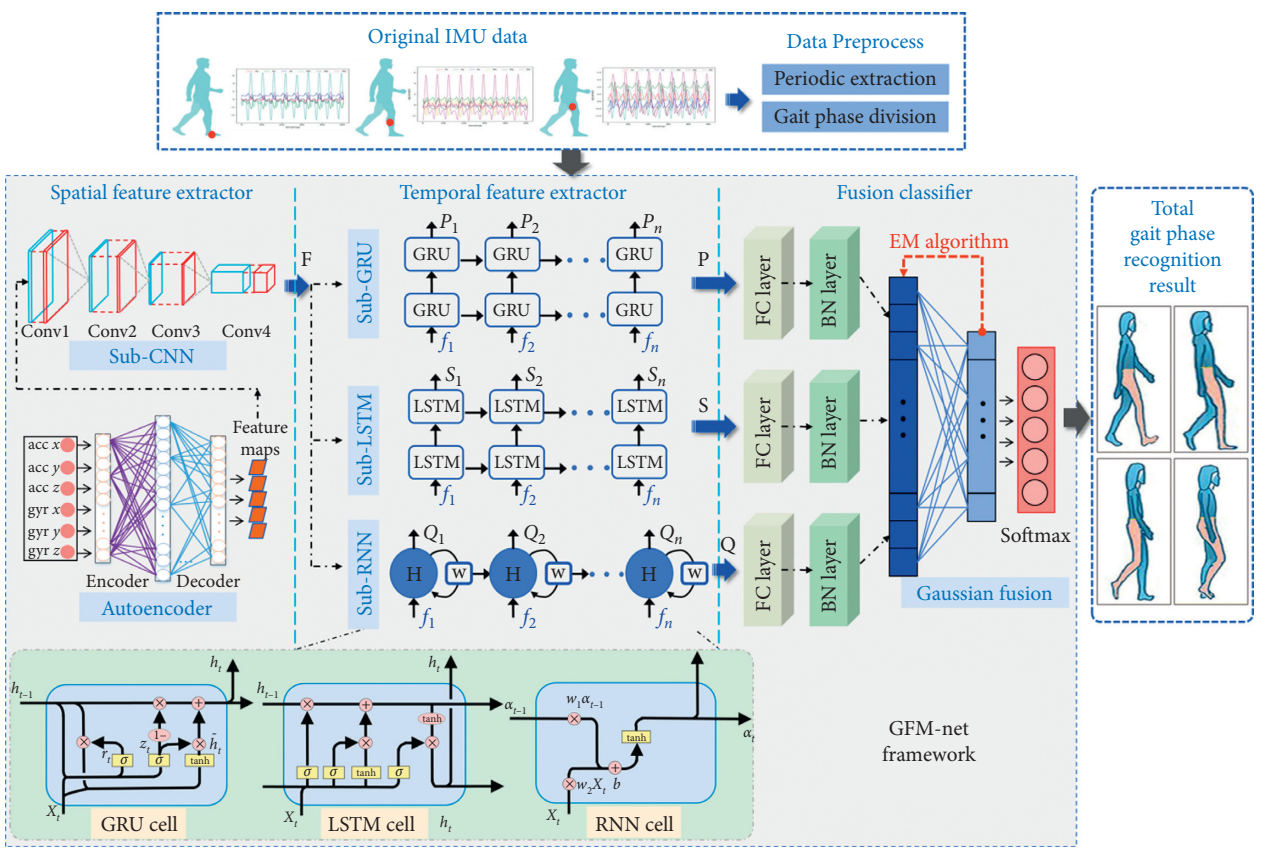

Figure 6: The proposed architecture of GFM-Net framework for gait phase recognition.

$$F' = \sum_{i=1}^{3} H_{BN}^{i} * \delta_{\text{relu}}\left(W_{\text{full}}^{i}[P, S, Q] + b_{\text{full}}^{i}\right). \tag{4}$$

The function H_{BN}^{i} can represent i-th batch-normalization layer, and the vectors P, S, Q denote the output feature maps of three submodels. W_{full}^{i} denotes i-th square weight matrix asymptotically approximating complicated combination of the full-connection layer. b_{full}^{i} can perform i-th biases of the convolution kernel parameters. And δ_{relu} denotes the nonlinear activation functions, which was selected as Leak-ReLU. With initializing a weight decay of 0.0001 and a momentum of 0.9, we obtain the prediction score vector F' representing the probability that the input of i-th extractor belongs to the corresponding category. After normal distribution analysis, we choose the Gaussian distribution functions to fit multimodal distributions E_{ij} of each submodel. The Gaussian distribution of i-th component model is defined as follows:

$$E_{ij}(\tilde{y} \mid \theta_i) = \frac{1}{\sqrt{2\pi}\sigma_i} \exp\left(-\frac{(F' - \mu_i)^2}{2\sigma_i^2}\right), \tag{5}$$

where $\theta_i = (\mu_i, \sigma_i^2)$ is the estimated parameter, which consists of the mean vector μ_i and covariance matrix σ_i^2, respectively. $F' = \{F_{\text{gru}}, F_{\text{lstm}}, F_{\text{rnn}}\}$ is the output label vector corresponding to each submodel, which reflects the essential characteristics of the original IMU data. Then, the Gaussian mixture method is used to construct a connection layer based on probabilistic fusion. Its purpose is to cluster similar features adaptively at different submodel clustering centers and further combine the probability sizes of the three submodels to determine the final recognition estimate. S denotes the final output probability, which is calculated as follows:

$$S\left(F' \mid \theta\right) = \sum_{i=1}^{3} S_i = \prod_{j=1}^{N} \prod_{i=1}^{3} E_{ij}\left(F' \mid \theta_i\right), \tag{6}$$

where $\theta = (\theta_1, \theta_2, \theta_3)$ represents the Gaussian mixture parameters of the fusion layer. γ_{ji} represent implicit variables. By integrating the joint probabilities between F' and γ_{ij}, the fusion score S in (6) is redefined to solve the log-likelihood expression as follows:

$$\log S(F', \gamma \mid \theta) = \sum_{i=1}^{3} \sum_{j=1}^{N} \gamma_{ji} \left[\log\left(\frac{1}{\sqrt{2\pi}}\right) - \log \sigma_i - \frac{1}{2\sigma_i^2}\left(F_j' - \mu_i\right)^2\right]. \tag{7}$$

Then, we choose the EM algorithm to estimate the hyperparameters of the fusion layer. Each iteration of the EM algorithm is divided into two steps: the expected step (E-step) and the maximum step (M-step). The E-step calculates the expectation of implicit variables γ_{ji} defined as $\hat{\gamma}_{ji} = E(\gamma_{ji} \mid \tilde{y}, \theta)$, which denotes the responsivity of i-th component model to the label y_j. Subsequently, step M updates the corresponding parameters by maximizing the expected value of the given log-likelihood function in (7). After several iterations of the EM algorithm, the parameters gradually converge. The detailed process is shown as the following (Algorithm 1).

Note that the internal EM algorithm iteration loop is used for corresponding parameter estimation and the EM algorithm iteration loop is performed inside the external network loop. Specifically, when the network is in training, each external loop will be accompanied by a lot of internal EM algorithm iteration loops. Through the above network structure, our proposed GFM-Net obtains a better prediction effect from the perspective of decision fusion. Finally, we add a softmax layer after the fusion layer to normalize the output result into a probability classification result and output the final classification result through the argmax function.

We use the cross entropy (CE) loss function to evaluate the degree of inconsistency between the predicted probability obtained by softmax and the true label. Then, the gradient descent method is used to update the model parameters so that the two probability distributions are similar to each other. The loss expression is shown as

$$\begin{aligned} \text{softmax}(\text{q})_i &= \frac{e^{q_i'}}{\sum_{i=1}^{n} e^{q_i'}}, \\ l &= -\sum_{i=1}^{4} y_i \log\left((q)_i\right), \\ o &= \max(q), \end{aligned} \tag{8}$$

where y_i denotes the indicative variable (0 or 1); if the category is the same as the sample category, it is 1; otherwise it is 0; q_i denotes the predicted probability that the observation sample belongs to category i. For each input sample x, the predicted output of the network is $q = (q_0, q_1, q_2, q_3)$. Then, the value of q_i is between 0 and 1, and the larger the value, the greater the probability that x belongs to the real label. Based on the output q_i, we can get the class label as O. Then, we can construct the training loss with cross entropy, as formulated by (8); the cross entropy is a positive number. When the probability value of the true label q_i in the vector q is smaller, larger difference between q_i and y_i will result in a larger cross entropy value. This property will help the convergence of the network in the training. In order to avoid overfitting, we chose 70% of the sample set for training and 30% of the samples for testing. After using the same training set to train different models 10,000 times, use the same test set to test the trained model and record the classification accuracy and macro-F value of each classifier after testing the classification model with the test machine. Then, evaluate the performance of all models based on these three indicators.

3. Results and Discussion

3.1. Evaluation Methods. In this paper, we propose the GFM-Net network. In order to prove its performance in classification, we need to draw the corresponding conclusion through corresponding indicators. As we all know, accuracy is a good comprehensive indicator, which is widely used in evaluation indicators. However, in the classification, it is difficult to characterize the performance of a certain model simply by relying on accuracy, and we have to choose other

Initialize $\gamma_{ji} = 1$ and **set** estimation parameter θ
For T iterations do
Procedure M-step:
Calculate the expectations of (7):

$$M(\theta, \theta^{(t)}) = E[\log S(F', \gamma \mid \theta) \mid y_j, \theta^{(t)}] = \sum_{i=1}^{3} \sum_{j=1}^{N} \widehat{\gamma}_{ji} [\log(1/\sqrt{2\pi}) - \log \sigma_i - 1/2\sigma_i^2 (y_j - \mu_i)^2],$$

Calculate partial derivatives of $\theta(\mu_i, \sigma_i^2)$:

$$(\partial M(\theta, \theta^{(t)})/\partial \mu_i) \longrightarrow \widehat{\mu}_i = \sum_{j=1}^{N} \widehat{\gamma}_{ji} y_j / \sum_{j=1}^{N} \widehat{\gamma}_{ji},$$

$$(\partial M(\theta, \theta^{(t)})/\partial \sigma_i^2) \longrightarrow \widehat{\sigma}_i^2 = \sum_{j=1}^{N} \widehat{\gamma}_{ji} (y_j - \mu_i)^2 / \sum_{j=1}^{N} \widehat{\gamma}_{ji},$$

Return $\widehat{\mu}_i$, $\widehat{\sigma}_i^2$
Procedure E-step:
Calculate i-th submodel responsivity:

$$\widehat{\gamma}_{ji} = S(\gamma_{ji} = 1, \widetilde{y}_j \mid \theta) / \sum_{i=1}^{3} S(\gamma_{ji} = 1, \widetilde{y}_j \mid \theta) = E_{ij}(y_j \mid \theta_i) / \sum_{i=1}^{3} E_{ij}(y_j \mid \theta_i),$$

Return $\widehat{\gamma}_{ji}$
Update the estimation parameter:
$\theta^{(t)}(\widehat{\mu}_i, \widehat{\sigma}_i^2)$,
$\theta^{(t+1)} = \arg\max_{\theta} M(\theta, \theta^{(t)})$,
End For till the parameter threshold:
$\theta^{(t+1)} > \theta_{\text{th}}$ or $T > T_{\text{th}}$
End Procedure **M-step** and **E-step**
Return $\theta^{(t+1)}$ **and the fusion score S**

Algorithm 1: Training process of the Gaussian fusion layer based on EM-Algorithm.

indicators to comprehensively characterize the classification performance of a certain model. In classification problems, commonly used classification performance indicators also include precision (P), recall (R), and F1. Among them, P and *R* are widely used to evaluate the quality of the model results. P is used to measure the accuracy of the retrieval system. *R* is used to measure the recall of the retrieval system. Of course, we hope that P and *R* results are as high as possible. Generally speaking, if both P and *R* are high, we can conclude that this model performs well in this classification task. Hence, the F1 indicator is chosen since it can represent the performance of the model by combining the results of both P and R. When F1 performs well, it means that both P and *R* will perform well. However, this paper studies a multiclassification task and cannot directly use F1. The most direct method is to calculate macro-F1 [35]. Accuracy reflects the ratio of correctly classified samples to total samples. The definition equation of the above evaluation factors can be seen in [1]; we can easily calculate the accuracy, macro-P, macro-R, and macro-F1 evaluation factors.

In multiclassification tasks, we also often use the area AUC under the ROC curve to measure the classification effect. The ROC curve was first publicly proposed to verify machine learning in model evaluation [36]. In recent years, it has been widely used in the fields of machine learning and deep-learning. The larger the AUC, the more reliable the model's recognition of the target.

3.2. Results. The confusion matrix (Figures 7–9) provides the performance of visual gait-subphase recognition. The vertical axis of the matrix represents the actual classification category of the test, and the horizontal axis represents the corresponding predicted classification category. In addition, in the confusion matrix diagram, "0.0" represents the "HS" stage, "1.0" represents the "FF" stage, "2.0" represents the "HO" stage, and "3.0" represents the "SW" stage. These nine matrices are the average recognition results of all subjects under different walking steps. The value in the main diagonal is the proportion of correctly classified samples. As shown in Figure 7, except for the HS stage, all confusion matrices perform well. The HS stage is mostly erroneously classified as FF and SW stages. In order to verify the effectiveness of the proposed recognition model, we compared two other integrated algorithms to identify gait phases, namely, AdaBoosting and Bagging. The corresponding confusion matrix is shown in Figures 8 and 9. As can be seen from Figures 8 and 9, the Bagging model cannot identify the HS phase, and most HS phases are erroneously directly classified as adjacent FF phases. The AdaBoosting algorithm can identify most of the HS phase. The AdaBoosting and Bagging models have achieved good recognition results in other stages.

From the confusion matrix, we can get Table 1. As shown in Table 1, the F1 of the four groups (HS, FF, HO, and SW) of the GFM-Net model differ greatly. When the walking speed is 0.78 m/s, F1 is 65.9%, 96.4%, 97.6%, and 98.8%, respectively; when the walking speed is 1.0 m/s, F1 is 70.8%, 97.0%, 98.1%, and 98.9%, respectively; when the walking speed is 1.25 m/s, F1 is 53.6%, 96.8%, 97.4%, and 98.1%. As can be seen from the above data, FF, HO, and SW have the best effect and obtain better recognition effect (over 96%). The

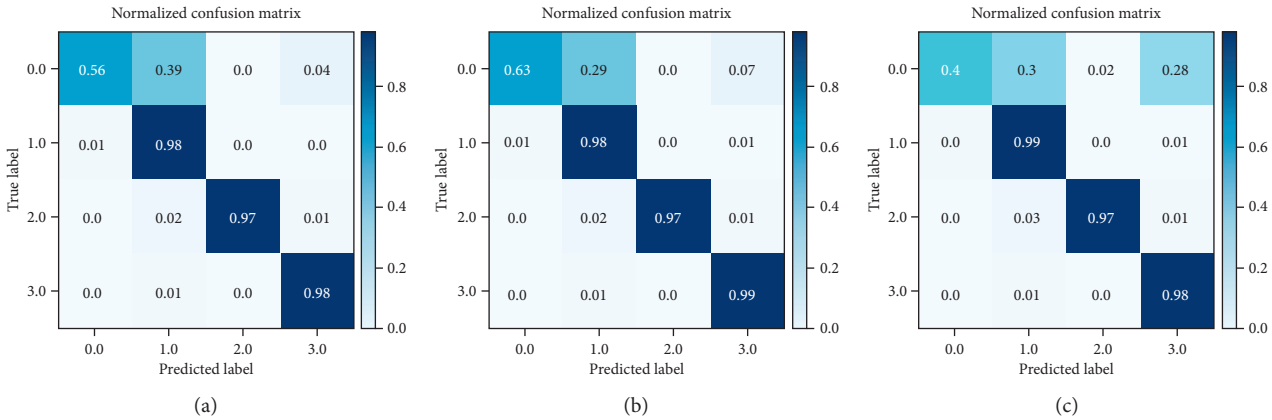

FIGURE 7: Confusion matrix of three gait patterns derived from Bagging classification under three paces. Settings: 0.78 m/s (a), 1.0 m/s (b), and 1.25 m/s (c).

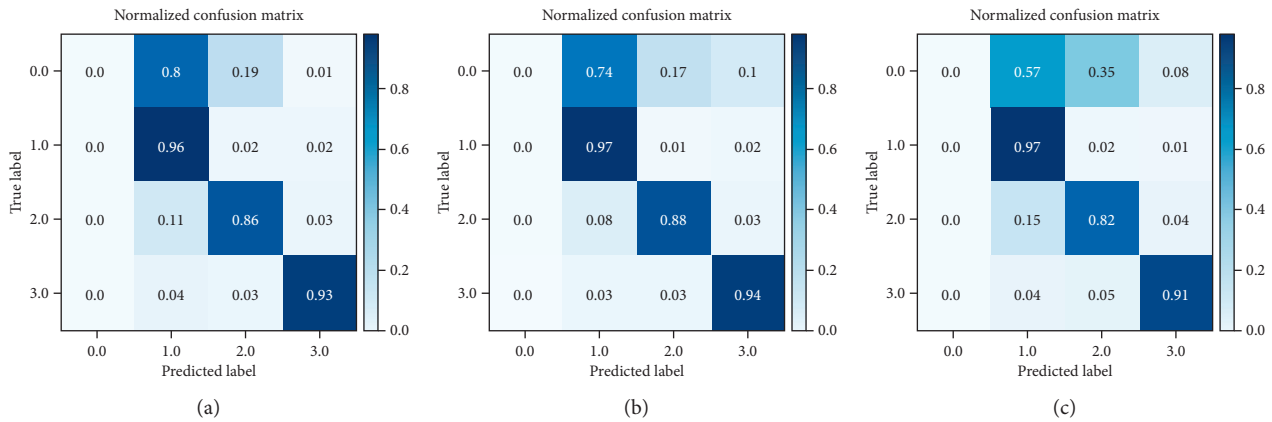

FIGURE 8: Confusion matrix of three gait patterns derived from AdaBoosting classification under three paces. Settings: 0.78 m/s (a), 1.0 m/s (b), and 1.25 m/s (c).

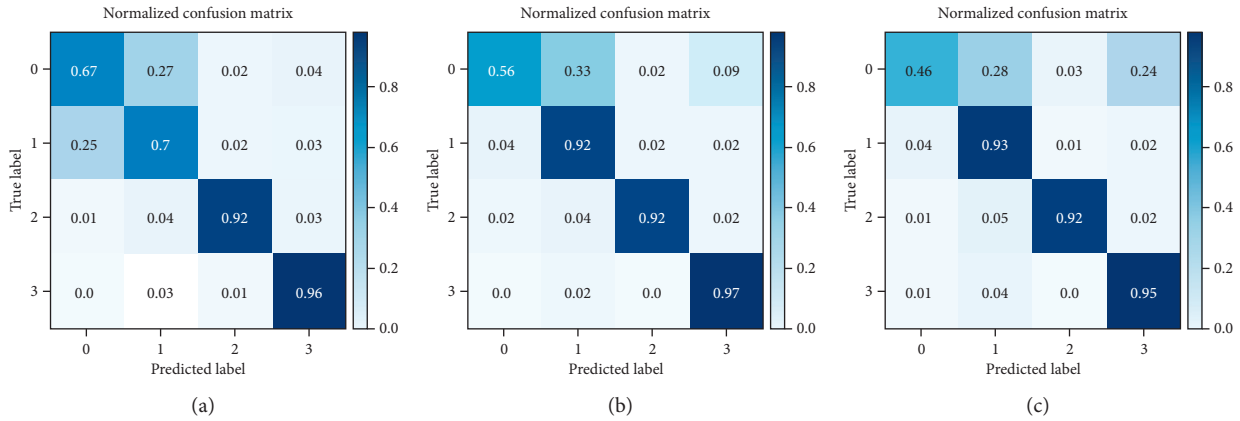

FIGURE 9: Confusion matrix of three gait patterns derived from GFM-Net classification under three paces. Settings: 0.78 m/s (a), 1.0 m/s (b), and 1.25 m/s (c).

performance of HS phase recognition is the worst. As for the recognition accuracy of each substage, the swing stage (SW) performed best, with a maximum value of 1.0 m/s (98.9%). The recognition effect of FF phase and HO phase is also very good. Obviously, the performance of the HS phase recognition effect is the worst, the F1 value has not reached 71%,

Table 1: Summary of classification performance of different models at unsynchronized speed.

Model	Speed	0.78 m/s				1.0 m/s				1.25 m/s			
	Phase	HS	FF	HO	SW	HS	FF	HO	SW	HS	FF	HO	SW
Bagging	Precision (%)	0	84.7	85.9	98.1	0	86.5	87.5	97.2	0	84.3	80.4	97.3
	Recall (%)	0	96.2	85.1	94.6	0	97.5	88.4	93.4	0	97.6	81.0	91.3
	F1 (%)	0	90.1	85.5	96.3	0	91.7	88.0	95.3	0	90.5	80.7	94.2
AdaBoosting	Precision (%)	48.8	91.8	92.2	96.9	42.1	90.8	94.2	97.2	40.7	90.4	96.0	96.3
	Recall (%)	52.6	90.4	93.4	97.0	53.7	91.7	91.9	94.7	54.5	92.1	93.8	94.0
	F1 (%)	50.7	91.1	92.8	97.0	50.7	91.3	93.0	95.9	46.6	91.3	94.9	95.1
GFM-Net	Precision (%)	79.1	94.5	98.2	99.2	80.6	95.8	99.0	98.9	80.9	95.0	97.9	97.9
	Recall (%)	56.4	98.3	97.0	98.4	63.1	98.4	97.1	98.9	40.1	98.6	96.8	98.4
	F1 (%)	65.9	96.4	97.6	98.8	70.8	97.0	98.1	98.9	53.6	96.8	97.3	98.1

and the F1 with the lowest HS phase recognition is only 53.6%. For the Bagging and AdaBoosting models, at three paces, the average value of F1 in the HS stage is 0 and 49.3%, respectively, indicating that the recognition effect of the HS stage is relatively poor; for SW phase recognition, the minimum value of F1 is 94.2% and 95.1%, showing strong recognition performance for SW phase.

In order to verify the effectiveness of the proposed GFM-Net, this paper also compares the existing deep-learning algorithm model and obtains Table 2. According to Table 2, the recognition accuracy of the GFM-Net algorithm is as high as 96% or higher, while the recognition accuracy of the other two integrated algorithm models is lower. In particular, the accuracy of Bagging's phase recognition in three steps is lower than 92%. In addition, we can also see that the GFM-Net algorithm is also better than the existing CNN + LSTM model. The CNN + GRU model and CNN + RNN model are superior in recognition accuracy and macro-F1, although the gap between them is not counted. In addition, we can easily conclude that the GFM-Net model has the highest AUC at asynchronous speed, which is higher than the other two models. It can be clearly seen from Figures 10 and 11 that, at any step, the accuracy and macro-F1 of the GFM-Net algorithm are higher than those of the other five algorithms. Finally, in order to show that the proposed method not only has better performance, but also has significant differences compared with other methods, we tested the significance of the results of each model and the GFM-Net results and got the results shown in Table 3. As shown, P value of the GFM-Net result and any other model result is less than 0.01, which is "very significant."

4. Discussion

This study proves that the proposed system can effectively detect the corresponding gait phase based on a single IMU sensor. In order to support this hypothesis, this paper proposes using the GFM-Net algorithm to detect the gait phase and comparing it with other timing algorithms to verify the effectiveness of the algorithm. The core technology of gait phase recognition system is the design of recognition algorithm model. The predecessors generally used machine learning or deep-learning methods to detect HS, FF, HO, and SW from IMU signals. This paper proposes the GFM-Net model and uses it to identify HS, FF, HO, and SW phases by the collected acceleration and angle data. The data obtained by the JY901 sensor shows that when pedestrians walk normally on flat ground, the acceleration signals and angle signals on the thighs, calves, and feet have low variability and stability. Moreover, this study can obtain a better recognition effect, and this study also proposes a more complex neural network model to achieve this effect, so the possible result is that it takes longer training time. Some portable gait event detection devices require accurate gait biofeedback information and dynamic gait monitoring devices, but there are currently no wearable sensors to meet these requirements.

The GFM-Net algorithm is an integrated algorithm, and its result depends on the fusion of three subneural networks. The three subneural networks in this paper are RNN, GRU, and LSTM. However, whether the three subnetworks are the best choice needs further research. The recognition performance of the three subnetworks should not be too different to avoid the fact that the final classification result of the model only depends on the classification result of one of the subnetworks. In terms of fusion, this paper uses fully connected layers to connect the obtained results with the model input values and then performs Gaussian fusion. In order to avoid the problem that the gradient of the model becomes smaller because the network is too deep, this paper uses the BN network. In terms of feature extraction, AutoEncoder is first used to implement the GFM-Net algorithm with denoising and functional improvements. Then, we use CNN network to extract spatial scale features. It can be seen from Table 1 that neither Bagging nor AdaBoosting algorithms can identify the HS phase, but the GFM-Net algorithm can identify most HS phases. The GFM-Net algorithm has an HS phase recognition rate of 63.4% at three paces. Although the GFM-Net algorithm has greatly improved compared with the other two algorithms, the algorithm still needs further optimization and improvement. But the three models showed better recognition performance for the other three phases. As can be seen from Figures 12 to 14 the macro-AUC of the GFM-Net algorithm is also the best performing of the three algorithms. The GFM-Net algorithm based on the voting fusion mechanism can effectively detect the HS, FF, HO, and SW phases, has high recognition accuracy, and is also macro-F1 and

Table 2: Summary of classification performance for different training functions.

Speed (m/s)	Training function	Classification result		
		Accuracy (%)	Macro-F1 (%)	Macro-AUC
0.78	Bagging	90.5	67.7	0.97
	AdaBoosting	93.1	82.9	0.92
	CNN + LSTM	95.2	87.8	0.98
	CNN + GRU	94.7	87.3	0.97
	CNN + RNN	93.6	86.6	0.95
	GFM-Net	97.0	89.7	0.99
1.0	Bagging	91.4	68.7	0.95
	AdaBoosting	92.4	82.7	0.91
	CNN + LSTM	97.2	90.6	0.99
	CNN + GRU	96.6	89.3	0.98
	CNN + RNN	95.6	88.5	0.97
	GFM-Net	97.5	91.2	0.99
1.25	Bagging	89.2	66.3	0.95
	AdaBoosting	92.3	82.0	0.92
	CNN + LSTM	95.7	85.2	0.99
	CNN + GRU	95.3	84.6	0.99
	CNN + RNN	94.2	83.2	0.98
	GFM-Net	96.7	86.5	1.0

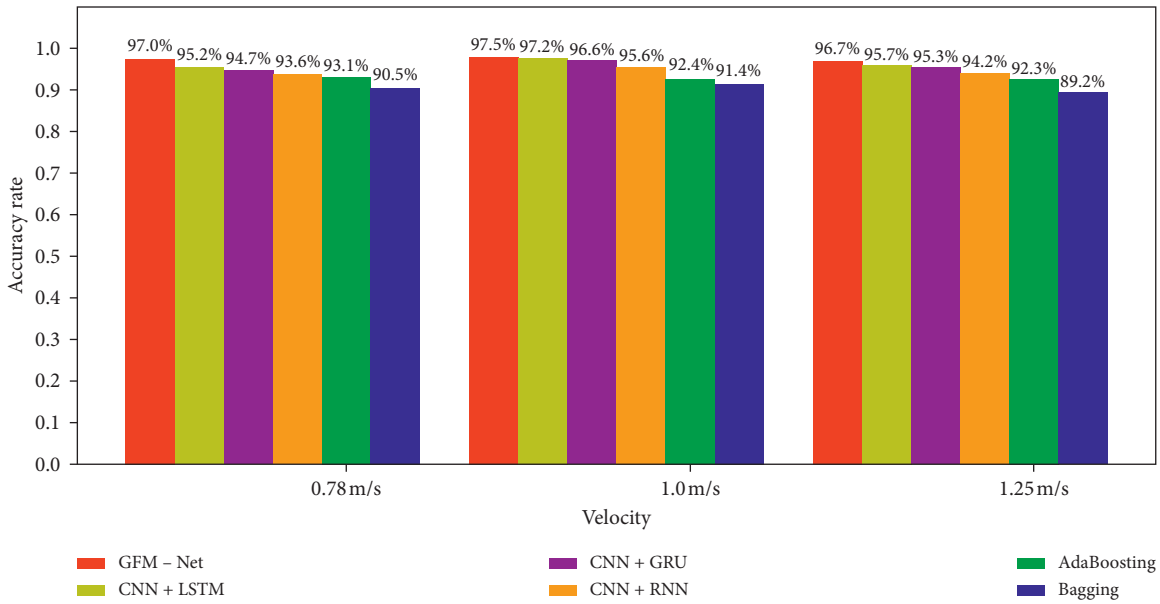

Figure 10: More tag set classifier accuracy distribution at three paces.

macro-AUC compared to the existing Bagging and AdaBoosting, being the best performer. We can get from Table 2 that the GFM-Net algorithm has the best recognition accuracy, followed by AdaBoosting, and Bagging is the worst. And we can clearly find that the GFM-Net algorithm improves the recognition accuracy by almost 5 percentage points compared with AdaBoosting. In order to propose an acceleration data acquisition system suitable for the general public, we tested the recognition effect of the FGFM-Net algorithm proposed in this paper on unlearned acceleration signals and angular velocity data. This study found that the proposed system can successfully predict the gait events of unlearned data, and the phase recognition accuracy of HS, FF, HO, and SW is as high as 97.1%, so the result is relatively reliable but still needs to be optimized.

At the same time, in order to verify the effectiveness of the model proposed in this paper, this paper still compares our model with CNN + LSTM, CNN + GRU, and CNN + RNN. According to Table 2, we can still see that the GFM-Net model has the best performance in terms of accuracy, macro-F1, and macro-AUC. Through Figure 14, we can see the recognition accuracy of the FMS-Net algorithm. Macro-F1 and AUC basically remain stable as the pace increases. But we can also find that the macro-F1 has been

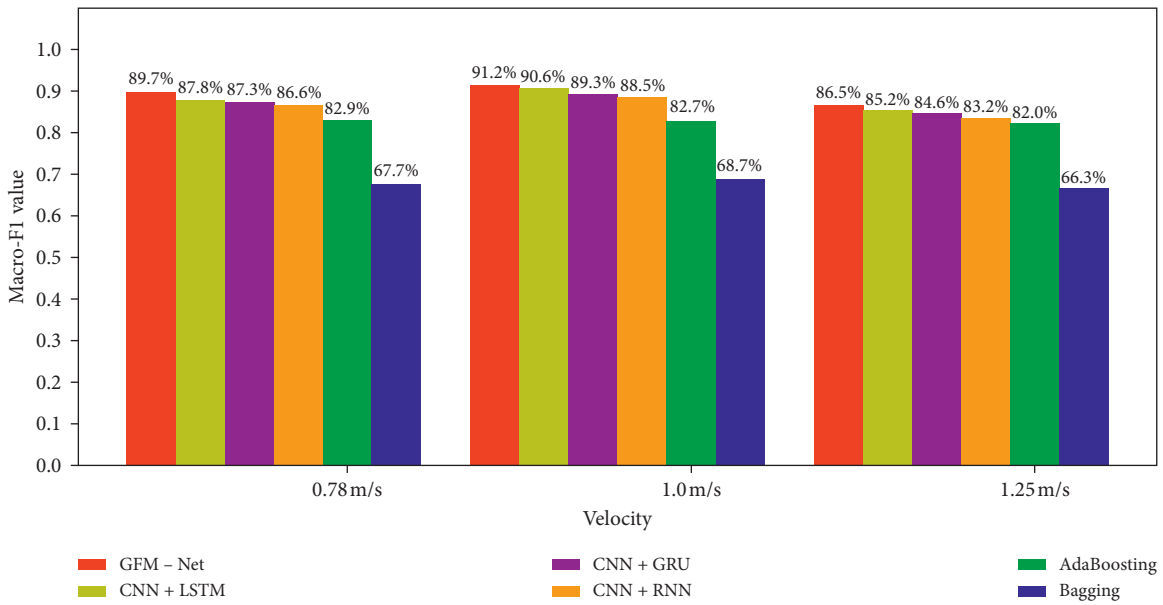

Figure 11: More tag data set classifier macro-F1 distribution under sync speed.

Table 3: The difference between GFM-Net results and other model results is significant P value.

Model	P value
(GFM-Net, Bagging)	$1.37e-6$
(GFM-Net, AdaBoosting)	$1.61e-11$
(GFM-Net, CNN + LSTM)	$7.40e-15$
(GFM-Net, CNN + GRU)	$4.67e-15$
(GFM-Net, CNN + RNN)	$7.59e-15$

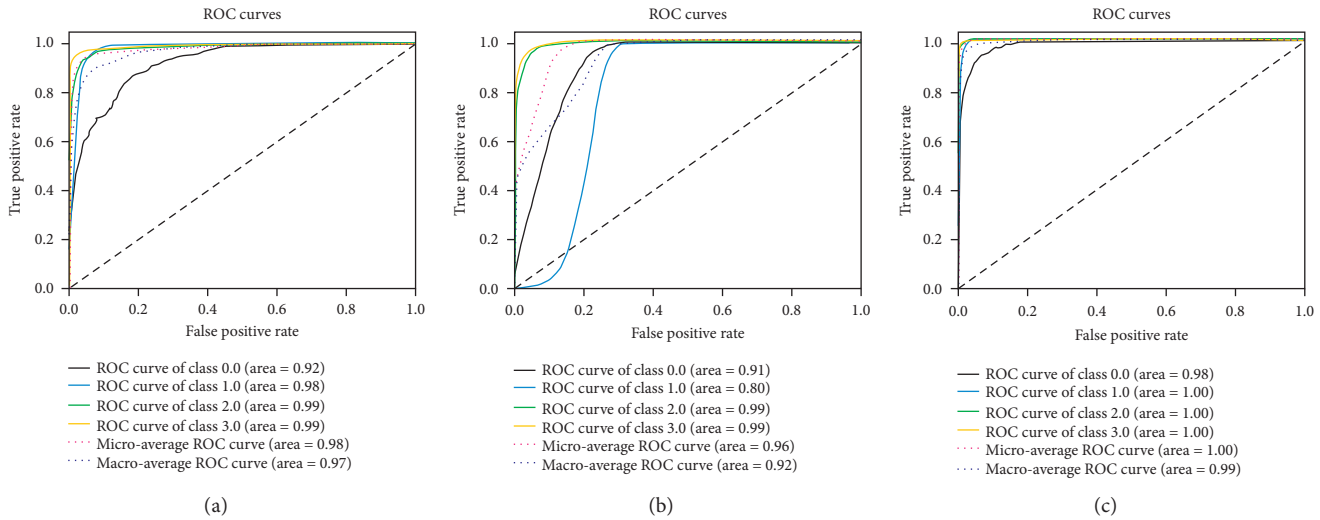

Figure 12: ROC curve performance in three models: Bagging (a), AdaBoosting (b), and GFM-Net. (c) The treadmill speed is set to 0.78 m/s.

declining as the pace increases, which needs our attention. In addition, we need to add more pace control experimental groups for further exploration and draw more reliable conclusions. Even though GFM-Net has shown its usefulness in classifying acceleration and angular velocity signals detected by gait events, other machine learning methods are needed for further evaluation. Future work should improve classification accuracy by improving feature

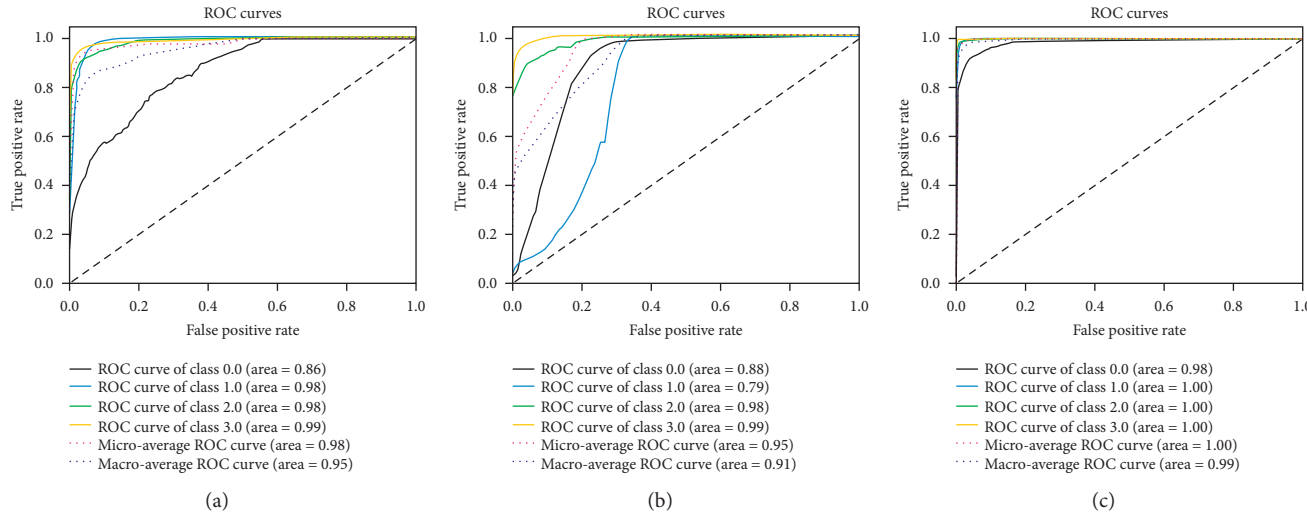

Figure 13: ROC curve performance in three models: Bagging (a), AdaBoosting (b), and GFM-Net (c) The treadmill speed is set to 1.0 m/s.

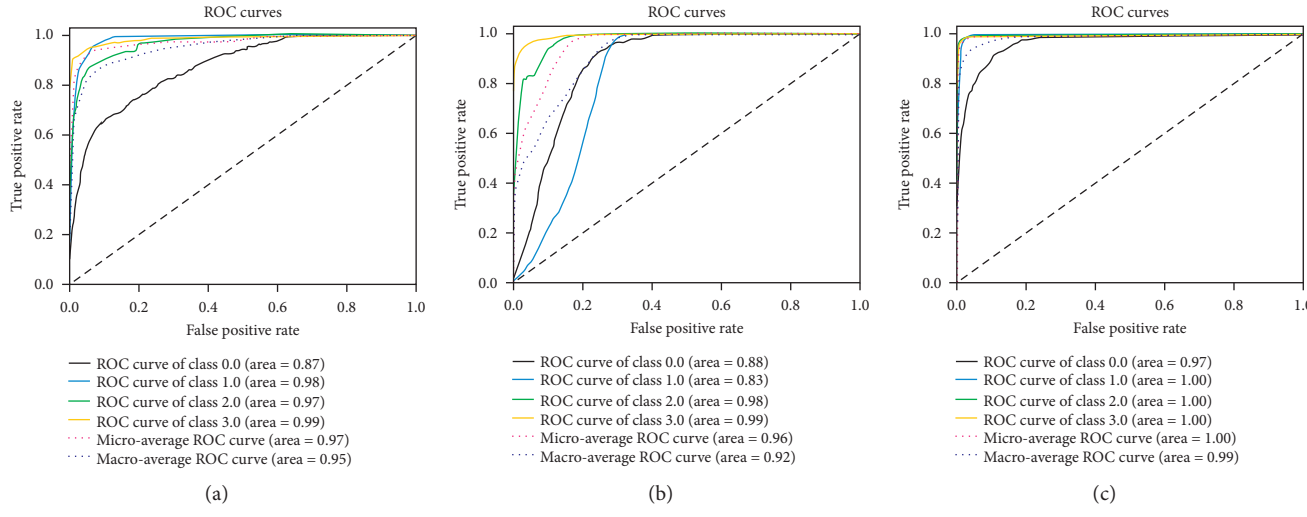

Figure 14: ROC curve performance in three models: Bagging (a), AdaBoosting (b), and GFM-Net (c). The treadmill speed is set to 1.25 m/s.

extraction and gait phase recognition algorithms. In this study, the three inertial sensors are transmitted to the host computer wirelessly, so we think that the three wearable inertial sensor modules are acceptable wearable sensors and will not have obvious impact on the subject's walking gait influences. However, in practice, the wearing of sensors may have a potential impact on the gait of people who have not yet been investigated. In the future, we will explore the use of fewer inertial units to identify gait phases and minimize the impact on the human body.

5. Conclusion

This paper studies the method of gait recognition using three inertial sensors on the treadmill. A hybrid deep fusion learning method is proposed, which seamlessly combines GRU, LSTM, and RNN to achieve a robust representation of spatiotemporal features of inertial gait. In order to accurately identify walking gait, this paper proposes an effective hybrid deep-learning framework GFM-Net based on Gaussian probability fusion of multiple spatiotemporal networks to analyze multidimensional acceleration signals and detect out-of-sync events including HS, FF, HO, and SW. It consists of three main parts: data preprocessing, multistream integrated neural network, and fusion model. Data preprocessing uses automatic encoders to select key features, while CNN extracts more spatial information. In addition, we use three parallel modules RNN, LSTM, and GRU as multistream time feature extractor. The network uses mixed particle information to form high-dimensional time-scale features. Finally, a Gaussian fusion module was developed to fuse different submodels. It uses the EM algorithm to optimize Gaussian probability fusion of different submodels and proves that it is a practical method to increase model

capacity on a large scale. Experiments and discussions prove that GFM-Net has higher accuracy up to 96.7% and the effectiveness of macro-F1 is up to 86.5%, which is superior to that of other integrated algorithm models.

There are a lot of variables and hyperparameters in the network structure proposed in this paper, which will undoubtedly cause a lot of time for the model to be trained. Therefore, this paper strongly recommends training the model on the GPU, which will improve the model training efficiency. Our future work is to try to design a lightweight network to recognize human gait phases and achieve online gait phase recognition with high efficiency, which is of great significance for medical rehabilitation training robots and gait disease diagnosis.

Data Availability

In terms of experimental data, 16 volunteers between 20 and 26 years old with body weight ranging from 46 kg to 70 kg and height ranging from 158 cm to 177 cm were selected to collect IMU data. All data can be obtained by sending e-mail to the first author (Tao Zhen).

Conflicts of Interest

The authors declare that there are no conflicts of interest regarding the publication of this paper.

Authors' Contributions

Tao Zhen and Jian-lei Kong proposed the conception and design of this research, acquired the data, and drafted this article. Lei Yan helped with the data analysis and model optimization. All authors have read and agreed to the published version of the manuscript.

Acknowledgments

This work was supported financially by National Natural Science Foundation of China (no. 61903009), Beijing Municipal Education Commission (no. KM201910011010), Beijing Excellent Talent Training Support Project for Young Top-Notch Teams (2018000026833TD01), and Fundamental Research Funds for the Central Universities (no. 2015ZCQ-GX-03).

References

[1] L. Yan, T. Zhen, J.-L. Kong, L.-M. Wang, and X.-L. Zhou, "Walking gait phase detection based on acceleration signals using voting-weighted integrated neural network," *Complexity*, vol. 2020, no. 1, 14 pages, Article ID 4760297, 2020.

[2] L. Rong, D. Zhiguo, Z. Jianzhong, and L. Ming, "Identification of individual walking patterns using gait acceleration," *International Conference on Bioinformatics and Biomedical Engineering*, vol. 142, pp. 543–546, 2007.

[3] C. Buckley, M. Encarna Micó-Amigo, M. Dunne-Willow et al., "Gait Asymmetry Post-Stroke: determining valid and reliable methods using a single accelerometer located on the trunk," *Sensors*, vol. 20, no. 1, p. 37, 2020.

[4] A. Picelli, C. Melotti, F. Origano et al., "Robot-assisted gait training in patients with Parkinson disease," *Neurorehabilitation and Neural Repair*, vol. 26, no. 4, pp. 353–361, 2012.

[5] S. D. M. Achanta, T. Karthikeyan, and R. Vinothkanna, "A novel hidden Markov model-based adaptive dynamic time warping (HMDTW) gait analysis for identifying physically challenged persons," *Soft Computing*, vol. 23, no. 18, pp. 8359–8366, 2019.

[6] H. Vu, F. Gomez, P. Cherelle, D. Lefeber, A. Nowé, and B. Vanderborght, "ED-FNN: a new deep learning algorithm to detect percentage of the gait cycle for powered prostheses," *Sensors*, vol. 18, no. 7, p. 2389, 2018.

[7] S. Murray and M. Goldfarb, "Towards the use of a lower limb exoskeleton for locomotion assistance in individuals with neuromuscular locomotor deficits," in *Proceedings of the 2012 Annual International Conference of the IEEE Engineering in Medicine and Biology Society*, pp. 1912–1915, San Diego, CA, USA, August-September 2012.

[8] A. Berger, F. Horst, F. Steinberg et al., "Increased gait variability during robot-assisted walking is accompanied by increased sensorimotor brain activity in healthy people," *Journal of NeuroEngineering and Rehabilitation*, vol. 16, no. 1, pp. 1–13, 2019.

[9] R. Luo, S. Sun, X. Zhang, Z. Tang, and W. Wang, "A low-cost end-to-end sEMG-based gait sub-phase recognition system," *IEEE Transactions on Neural Systems and Rehabilitation Engineering*, vol. 28, no. 1, pp. 267–276, 2019.

[10] X. Jin, H. Sun, and F. Yang, "Advances in multi-sensor information fusion: theory and applications," *Sensors*, vol. 18, no. 4, p. 1162, 2018.

[11] W. Fei, T. Yin, C. Lei, Y. Zhang, Y. Wang, and J. Liu, "Prediction of lower limb joint angle using sEMG based on GA-GRNN," in *Proceedings of the 2015 IEEE International Conference on Cyber Technology in Automation, Control, and Intelligent Systems (CYBER)*, Shenyang, China, June 2015.

[12] W. Si, G. Yang, X. Chen, and J. Jia, "Gait identification using fractal analysis and support vector machine," *Soft Computing*, vol. 23, no. 19, pp. 9287–9297, 2019.

[13] G. E. Kang, J. Yang, and B. Najafi, "Does the presence of cognitive impairment exacerbate the risk of falls in people with peripheral neuropathy? An application of body-worn inertial sensors to measure gait variability," *Sensors*, vol. 20, no. 5, p. 1328, 2020.

[14] I. Gohar, Q. Riaz, M. Shahzad, M. Zeeshan Ul Hasnain Hashmi, H. Tahir, and M. Ehsan Ul Haq, "Person re-identification using deep modeling of temporally correlated inertial motion patterns," *Sensors*, vol. 20, no. 3, p. 949, 2020.

[15] Z. Zhou, S. Yang, Z. Ni, W. Qian, C. Gu, and Z. Cao, "Pedestrian navigation method based on machine learning and gait feature assistance," *Sensors*, vol. 20, no. 5, p. 1530, 2020.

[16] S. S. Yeo and G. Y. Park, "Accuracy verification of spatio-temporal and kinematic parameters for gait using inertial measurement unit system," *Sensors*, vol. 20, no. 5, p. 1343, 2020.

[17] Y. Chao, F. Coenen, and B. Zhang, "Multi-attributes gait identification by convolutional neural networks," in *Proceedings of the 2015 8th International Congress on Image and Signal Processing (CISP)*, Shenyang, China, October 2015.

[18] D. Omid, T. Mojtaba, and C. V. Raghvendar, "IMU-based gait recognition using convolutional neural networks and multi-sensor fusion," *Sensors*, vol. 17, no. 12, p. 2735, 2017.

[19] T. Zhen, L. Yan, and J.-L. Kong, "An acceleration based fusion of multiple spatiotemporal networks for gait phase detection,"

International Journal of Environmental Research and Public Health, vol. 17, no. 16, p. 5633, 2020.

[20] X.-B. Jin, T.-L. Su, J.-L. Kong, Y.-T. Bai, B.-B. Miao, and C. Dou, "State-of-the-art mobile intelligence: enabling robots to move like humans by estimating mobility with artificial intelligence," *Applied Sciences*, vol. 8, no. 3, p. 379, 2018.

[21] N. Neverova, C. Wolf, G. Lacey et al., "Learning human identity from motion patterns," *IEEE Access*, vol. 4, pp. 1810–1820, 2016.

[22] B. Hu, P. C. Dixon, J. V. Jacobs, J. T. Dennerlein, and J. M. Schiffman, "Machine learning algorithms based on signals from a single wearable inertial sensor can detect surface- and age-related differences in walking," *Journal of Biomechanics*, vol. 71, pp. 37–42, 2018.

[23] D. Zhen, C. Yang, K. Xing et al., "The real time gait phase detection based on long short-term memory," in *Proceedings of the 2018 IEEE Third International Conference on Data Science in Cyberspace (DSC)*, Guangzhou, China, June 2018.

[24] X.-B. Jin, X.-H. Yu, X.-Y. Wang, Y.-T. Bai, T.-L. Su, and J.-L. Kong, "Deep learning predictor for sustainable precision agriculture based on internet of things system," *Sustainability*, vol. 12, no. 4, p. 1433, 2020.

[25] Y.-T. Bai, X.-Y. Wang, X.-b. Jin, Z.-y. Zhao, and B.-h. Zhang, "A neuron-based kalman filter with nonlinear autoregressive model," *Sensors*, vol. 20, no. 1, p. 299, 2020.

[26] Y. Bai, X. Wang, X. Jin, T. Su, J. Kong, and B. Zhang, "Adaptive filtering for MEMS gyroscope with dynamic noise model," *ISA Transactions*, vol. 101, pp. 430–441, 2020.

[27] Y.-T. Bai, X.-B. Jin, X.-Y. Wang, X.-k. Wang, and J.-p. Xu, "Dynamic correlation analysis method of air pollutants in spatio-temporal analysis," *International Journal of Environmental Research and Public Health*, vol. 17, no. 1, p. 360, 2020.

[28] Y.-Y. Zheng, J.-L. Kong, X.-B. Jin, X.-Y. Wang, T.-L. Su, and J.-L. Wang, "Probability fusion decision framework of multiple deep neural networks for fine-grained visual classification," *IEEE Access*, vol. 7, pp. 122740–122757, 2019.

[29] S. Qiu, H. Wang, J. Li et al., "Towards wearable-inertial-sensor-based gait posture evaluation for subjects with unbalanced gaits," *Sensors*, vol. 20, no. 4, p. 1193, 2020.

[30] Coefficient PSC, "Pearson's correlation coefficient," *The New Zealand Medical Journal*, vol. 109, no. 1015, p. 38, 1996.

[31] S. Rosati, V. Agostini, M. Knaflitz, and G. Balestra, "Muscle activation patterns during gait: a hierarchical clustering analysis," *Biomedical Signal Processing and Control*, vol. 31, pp. 463–469, 2017.

[32] C. Mummolo, L. Mangialardi, and J. H. Kim, "Quantifying dynamic characteristics of human walking for comprehensive gait cycle," *Journal of Biomechanical Engineering*, vol. 135, no. 9, 2013.

[33] X. Su, H. Tong, and P. Ji, "Activity recognition with smartphone sensors," *Tsinghua Science and Technology*, vol. 19, no. 3, pp. 235–249, 2014.

[34] Q. Zou, Y. Wang, Q. Wang, Y. Zhao, and Q. Li, "Deep learning based gait recognition using smartphones in the wild," 2018, https://arxiv.org/abs/1811.00338.

[35] Y.-Y. Zheng, J.-L. Kong, X.-B. Jin, X.-Y. Wang, and M. Zuo, "CropDeep: the crop vision dataset for deep-learning-based classification and detection in precision agriculture," *Sensors*, vol. 19, no. 5, p. 1058, 2019.

[36] X.-B. Jin, N.-X. Yang, X.-Y. Wang, Y.-T. Bai, T.-L. Su, and J.-L. Kong, "Deep hybrid model based on emd with classification by frequency characteristics for long-term air quality prediction," *Mathematics*, vol. 8, no. 2, p. 214, 2020.

Hindawi
Complexity
Volume 2020, Article ID 6105952, 11 pages
https://doi.org/10.1155/2020/6105952

Research Article

Solving Interval Quadratic Programming Problems by Using the Numerical Method and Swarm Algorithms

M. A. Elsisy,[1] **D. A. Hammad**,[1] **and M. A. El-Shorbagy**[2,3]

[1]*Basic Engineering Sciences Department, Benha Faculty of Engineering, Benha University, Benha 13512, Egypt*
[2]*Department of Mathematics, College of Science and Humanities in Al-Kharj, Prince Sattam Bin Abdulaziz University, Al-Kharj 11942, Saudi Arabia*
[3]*Department of Basic Engineering Science, Faculty of Engineering, Menoufia University, Shebin El-Kom, Egypt*

Correspondence should be addressed to M. A. Elsisy; mohamedelsisy2@gmail.com

Received 20 May 2020; Revised 21 July 2020; Accepted 5 August 2020; Published 30 September 2020

Guest Editor: Edgar Cristian Díaz González

Copyright © 2020 M. A. Elsisy et al. This is an open access article distributed under the Creative Commons Attribution License, which permits unrestricted use, distribution, and reproduction in any medium, provided the original work is properly cited.

In this paper, we present a new approach which is based on using numerical solutions and swarm algorithms (SAs) to solve the interval quadratic programming problem (IQPP). We use numerical solutions for SA to improve its performance. Our approach replaced all intervals in IQPP by additional variables. This new form is called the modified quadratic programming problem (MQPP). The Karush–Kuhn–Tucker (KKT) conditions for MQPP are obtained and solved by the numerical method to get solutions. These solutions are functions in the additional variables. Also, they provide the boundaries of the basic variables which are used as a start point for SAs. Chaotic particle swarm optimization (CPSO) and chaotic firefly algorithm (CFA) are presented. In addition, we use the solution of dual MQPP to improve the behavior and as a stopping criterion for SAs. Finally, the comparison and relations between numerical solutions and SAs are shown in some well-known examples.

1. Introduction

Nonlinear programming has been appeared in solving many real-world problems. Solving interval programming problems is a hot issue in the research area. Interval programming problems are divided into interval linear programming and interval nonlinear programming [1–12].

Interval nonlinear programming problems are used in modeling and solving many real applications such as planning of waste management activities [13]. The mathematical model and the proofs of interval analysis can be found easily in [14]. Many researchers and authors solve the interval nonlinear programming problems by different methods [15–18], but all these methods try to get the optimal solution under some specific conditions. For example, in [8, 9], Hladík divided the problem into subclasses which can be reduced to easy problems. He put a condition for solving these problems that they must be convex quadratic programming. Jiang et al. [11] suggested a method to solve the nonlinear interval number programming problem with uncertain coefficients both in nonlinear objective function and nonlinear constraints. Liu and Wang [17] presented a numerical method to interval quadratic programming. Li and Tian [18] generalized Liu and Wang's method [17] to solve interval quadratic programming. Their proposed method requires less computing compared with Liu and Wang's method.

As mentioned above, there are many approaches for solving IQPP, but the most common one is dividing the interval problem into two problems. In the first problem, the optimal solution of the lower objective function on the largest feasible region is found, while in the second one, the optimal solution of the upper objective function on the lowest feasible region is obtained. So, the solution value of the interval problem is between values of the lower objective function and the upper objective function. As is known, this process is very difficult in many applications which lead to the difficultly in reaching the lowest value of the objective function of the problem.

KKT conditions are first-order necessary conditions for solving quadratic programming problems. KKT conditions

are optimality conditions for the optimization problems with interval-valued objective functions and real-valued constraint functions investigated and discussed in [19–22]. Wolfe's duality theorems, strong duality theorems, and duality gap in interval-valued optimization problems are discussed in a good mathematical view in [12]. Chalco-Cano et al. [19] introduced a new concept of a stationary point for an interval-valued function based on the *gH* derivative.

SAs are an important concept in computer science [23, 24]. SAs can be described as a population of agents or individuals interacting with each other and with their environment and working under very few rules. The inspiration often comes from nature, especially biological systems. They are successfully applied in real-life applications. Examples of SAs are ant colony optimization [24, 25], particle swarm optimization (PSO) [26, 27], firefly algorithm (FA) [28], glowworm algorithm [29], krill herd algorithm [30], monkey algorithm [31], and grasshopper optimization algorithm [32].

On the other hand, most of the researchers proposed hybrid algorithms to improve the solution quality, to benefit from their advantages, and to overcome any deficiencies. For example, a gaining sharing knowledge-based algorithm for solving optimization problems over the continuous space was proposed in [33]. Yulian Cao et al. presented a comprehensive learning particle swarm optimizer (CLPSO) embedded with local search (LS) which has the strong global search capability of CLPSO and fast convergence ability of LS [34]. In [35], the authors presented an adaptive particle swarm optimization with supervised learning and control (APSO-SLC) for the parameter settings and diversity maintenance of particle swarm optimization (PSO) to adaptively choose parameters, while improving its exploration competence. A new hybrid PSO algorithm that introduces opposition-based learning (OBL) into PSO variants for improving the latter's performance is proposed in [36]. In [37], a surrogate-assisted PSO with Pareto active learning was proposed to solve the multiobjective optimization problem with high computational cost. Finally, the historical memory-based PSO (HMPSO) is proposed in [38] which used an estimation of distribution algorithm to estimate and preserve the distribution information of particles' historical promising p bests.

In this paper, a new approach is suggested to solve the interval quadratic programming problem (IQPP). IQPP is converted into the modified quadratic programming problem (MQPP) by replacing all intervals by additional variables. KKT conditions of MQPP are derived and solved by a numerical method. The numerical method provides the boundaries of the basic variables which are used as starting points in SAs. The solutions of KKT conditions are obtained by using the Mathematica program. CPSO and CFA are used to solve these problems to give the decision maker (DM) a fast view about the position of the optimal solution in the intervals. The dual of MQPP is discussed. The solutions of this problem are used to improve the behavior of the proposed approach and as a stopping criterion for this approach.

2. Interval Quadratic Programming Problem (IQPP)

The interval quadratic programming problem (IQPP) is an interval nonlinear programming problem [9–11]. The objective function is the quadratic function, and the constraints are linear functions. IQPP can be defined as

$$\begin{aligned} &\min \sum_{i=1}^{k} y_i^f f_i(x) \\ &\text{subject to: } \sum_{i=1}^{l} y_{ij}^c g_{ij}(x) \le y_j^R, \quad j = 1, 2, \ldots, m, \end{aligned} \tag{1}$$

where $\sum_{i=1}^{k} y_i^f f_i(x)$ is an interval-valued function, $y_i^f = [y_i^{fL}, y_i^{fU}] \forall i$, $f_i(x)$ is a quadratic function, $g_{ij}(x), i = 1, \ldots, l$, $j = 1, \ldots, m$ are the linear functions, $y_{ij}^c = [y_{ij}^{cL}, y_{ij}^{cU}]$, and $y_j^R = [y_j^{RL}, y_j^{RU}]$. The feasible region is supposed to be nonempty and fixed.

The optimal solution of the interval programming problem cannot be defined exactly because at each value belonging to interval coefficients in the objective function and/or the constraints, there may be a new optimal solution. So, no one can define the exact optimal solution. Many researchers descried the optimal solution of IQPP by the objective function values. In [4, 15], the authors defined the optimal solution for the interval linear programming problem. For example, Garajová and Hladík [4] defined the optimal set of the interval linear programming problem and examined sufficient conditions for its closedness, boundedness, connectedness, and convexity. So, we defined the optimal solution as the union of all optimal solutions of IQPP. We explored the whole feasible region to get all possible optimal solutions of IQPP. In our approach, by numerical methods, we tried to get all optimal solutions in the feasible region, while by SAs, we found the best objective value in the whole interval.

3. The Solution of IQPP

The idea of our new vision to solve IQPP starts by replacing all intervals by additional variables and converting IQPP to the modified interval nonlinear problem (MQPP). KKT conditions of MQPP are obtained and solved by a numerical method. The solutions of the numerical method are functions in the additional variables. These solutions are providing the boundaries of the basic variables which are used as start points for SA. The dual of MQPP is presented and solved. CPSO and CFA are used to solve MQPP and its dual form. Furthermore, the solution of dual MQPP is used as a stopping criterion for our approach and to improve its performance. The proposed approach leads to explore the whole feasible region to get the optimal solution anywhere in the intervals.

3.1. Numerical Methodology. KKT conditions are a system of equations solved by two methods, with additional variables and with interval coefficients. Mathematica is used to solve this system program. In the first method, the equations are solved as algebraic equations where the solutions can be expressed as a

function of the additional variables. These solutions are very helpful for DM if the optimal solution at certain values of interval coefficients is required. We use the Newton method in the second method if we want to know the boundary of the variables. The solution of this method is used as an initial stage of CPSO, and CFA improved their ability to find the solution in short time than using the whole space of the variables.

The following theorems are used for solving the system of nonlinear equations with interval coefficients. Let MQPP have a continuous function G: $A_0 \subseteq \mathrm{IR}^n \longrightarrow \mathrm{IR}^n$ which has a zero y^* in a given subset A of A_0, i.e., a vector $y^* \in A \subseteq A_0$ exists such that $G(y^*) = 0$, where IR^n is the set of real intervals' n vectors. Let R^n be the set of real n vectors, $R^{n\times n}$ be the set of $n \times n$ matrices, $\tilde{y}$ be an element of an interval vector y, B^H be a hull inverse of the $n \times n$ interval matrix B, $\mathrm{int}(A)$ be an interior of the $m \times n$ interval matrix A, IA be the set $\{y \in IR^n \mid y \subseteq A\}$, $\mathrm{int}(y) \equiv \,]\underline{y}, \overline{y}[$ be the interior of an interval y, and $\mathrm{vol}(y)$ be a volume-reducing property of the Newton iteration.

Theorem 1 (see [38]). *Let G: $A_0 \subseteq R^n \longrightarrow R^n$ be Lipschitz continuous on $A \subseteq A_0$ and let B be a regular Lipschitz set on A, then*

(i) For every $a^* \in R^n$, the equation $G(y^*) = a^*$ has at most one solution $y^* \in A$

(ii) The inverse function G^{-1}: $G^*(A) \longrightarrow R^n$ defined on the range $G^*(A) \coloneqq \{G(\tilde{y}) \mid \tilde{y} \subseteq A\}$ by $G^{-1}(\tilde{a}) = \tilde{y} :\Longleftrightarrow G(\tilde{y}) = \tilde{a}$ is Lipschitz continuous, and B^{-1} is a Lipschitz matrix for G^{-1} on $G^*(A)$

(iii) If $a^* \in G^*(A)$, then for every $\tilde{y}^0 \in A$, $G^{-1}(a^*) \in y^0 + B^H(a^* - G(\tilde{y}^0))$

(iv) If A is compact and there is a point $\tilde{y}^0 \in \mathrm{int}(A)$ such that $G(\tilde{y}) \neq \lambda G(\tilde{y}^0) + (1-\lambda)a^*$ for all $\tilde{y} \in \partial A$ $\lambda \in (0,1]$, then $a^* \in G^*(A)$, i.e., the equation $G(y^*) = a^*$ has a unique solution $y^* \in A$

Theorem 2 (see [38]). *Under the assumption of Theorem 1 above, if $\tilde{y} \in y \in IA$, then every $y' \in IR^n$ satisfying $N(y, \tilde{y}) \coloneqq \tilde{y} - B^H G(\tilde{y}) \subseteq y'$ has the following three properties:*

(i) Every zero $y^* \in y$ of G satisfies $y^* \in y'$

(ii) If $y' \cap y = 0$, then G contains no zero in y

(iii) If $y^* \in \mathrm{int}(y)$ and $y' \subseteq y$, then G contains a unique zero in y (and hence in y')

Since $\tilde{y}$, $y^* \in y$ implies $y^* \in N(y, \tilde{y})$, it is natural to consider the general Newton iteration [38]:

$$y^0 \coloneqq y, y^{l+1} \coloneqq N_I\left(y^l, \tilde{y}^l\right) \cap y^l, \quad \text{for } l = 0, 1, 2, \ldots. \tag{2}$$

With the general Newton operator:

$$N_I(y, \tilde{y}) \coloneqq \tilde{y} - (\mathrm{CB})^I(\mathrm{CG}(\tilde{y})). \tag{3}$$

Theorem 3 (see [38]). *Let B be a strongly regular Lipschitz matrix on $y \in IA_0$ for G: $A_0 \subseteq R^n \longrightarrow R^n$. Let $C \in R^{n\times n}$ be such that CB is regular and let $(CB)^I$ be an inverse of CB. If $(CB)^I$ is regular, then the Newton iteration (6) is strongly convergent for every choice of $\tilde{y}^l \in y^l$. Moreover, for all $l \geq 0$, we have either*

$$\tilde{y}^l \notin y^{l+1} \text{ or } y^{l+1} = \tilde{y}^l \text{ and } G\left(y^l\right) = 0. \tag{4}$$

Corollary 1 (see [38]). *If, for some $C \in R^{n\times n}$, CB is an M-matrix or $I - CB < (1/2)$, then the optimal Newton iteration (6) is strongly convergent for every choice of $\tilde{y}^l \in y^l$ and the relations (8) and $\mathrm{vol}(y^{l+1}) \leq (1/2)\mathrm{vol}(y^l)$ hold.*

$\mathrm{vol}(y)$ is defined as

$$\mathrm{vol}(y) \coloneqq \left(\overline{y}_1 - \underline{y}_1\right)\left(\overline{y}_2 - \underline{y}_2\right)\cdots\left(\overline{y}_n - \underline{y}_n\right), \quad y \in \mathrm{IR}^n. \tag{5}$$

3.2. Swarm Algorithm (SA). Chaos theory (CT) is used to improve the performance of many SAs [39], where the high randomness of the chaotic sequence improves the convergence and diversity of the solutions. CT is considered as irregular behavior in nonlinear systems due to using the chaotic maps. These maps are worked as particles which move in a small range of nonlinear dynamic systems without knowing the traveling path of these particles. Many researchers proposed combinations between CT and meta-heuristic algorithms to improve the solution quality such as hybrid chaos-PSO [40], chaotic genetic algorithm [41], combined evolutionary algorithm with chaos [42], chaotic whale optimization algorithm [43], and chaotic artificial neural networks [44].

3.2.1. Chaotic Firefly Algorithm (CFA). FA is an evolutionary computation technique [28]. The main advantages of FA are exploitation and exploration. The improved FA with CT which is called the chaotic firefly algorithm (CFA) is applied to solve IQPP. The details of the main steps of CFA are described as follows:

Step 1. Initialization. A population of random N fireflies (solutions) is initialized $t = 0$, where T is the total number of iterations. The position of the i-th firefly in an n–dimensional space is denoted as x_i and represented as $x_i^t = (x_{i1}, x_{i2}, \ldots, x_{\mathrm{in}})$.

Step 2. Evaluation. Evaluating the fitness value (the light intensity $I(X_i^K)\,\forall i = 1, 2, \ldots, N$ of each firefly in the population or simply $I(x_i^t) = f(x_i^t)\,\forall i = 1, 2, \ldots, N$.

Step 3. Determination of Best Solution. For minimization problems, the firefly that has minimum light intensity is the best solution x_b.

Step 4. Updating Positions of Fireflies. For every firefly $i = 1, 2, \ldots, N$ and for every firefly $j = 1, 2, \ldots, N$ do the following: if $I(x_j^t) < I(x_i^t)$, the i-th firefly is attracted to the firefly j, and its position X_i^K is updated according to the following equation:

$$x_i^{t+1} = x_i^t + \beta_0 e^{-\gamma r_{ij}^2}\left(x_j^t - x_i^t\right) + \alpha\varepsilon_G, \tag{6}$$

$$r_{ij=}\left|x_i^t - x_j^t\right| = \sqrt{\sum_{d=1}^{d}\left(x_{id}^t - x_{jd}^t\right)^2}, \tag{7}$$

where β_0 the attractiveness at r_{ij} is 0, γ is the light absorption coefficient, r_{ij} is the Cartesian distance between the two fireflies i and j, α is a step size factor controlling the step size, and ε_G is a vector drawn from a Gaussian or other distribution. If $I(x_j^{t+1}) < I(x_i^t)$, then $x_i^{t+1} = x_i^{t+1}$ otherwise $x_i^{t+1} = x_i^t$.

Step 4-1. Chaotic repairing of the new position x_i^{t+1}.

Step 4-2. Updating the best solution x_b: if the new position of the i-th firefly x_i^{t+1} is better than the best solution x_b, i.e., $I(x_j^{t+1}) < I(x_b)$, then $x_b = x_i^{K+1}$.

Step 5. Stopping Condition. If a prespecified stopping criterion is satisfied, stop the run; otherwise, go to *Step 4*.

3.2.2. Chaotic Particle Swarm Optimization Algorithm (CPSO). PSO can solve many difficult optimization problems. It has a faster convergence on some problems in comparison [45]. The idea of PSO is that several random particles are placed in the search domain of the optimization problem. At its current location, each particle evaluates the objective function. After that, each particle determines the direction of movement in the search domain by combining some aspects of the history of its own current and best locations with particles located nearby in the swarm, but with some random disturbance. The next iteration takes place after all particles have been moved. Eventually the swarm, like a flock of birds collectively foraging for food, is likely to move close to an optimum of the fitness function. The i-th particle is described by an n-dimensional vector as $x_i = (x_{i1}, x_{i2}, \ldots, x_{\text{in}})$, while its velocity is represented as $v_i = (v_{i1}, v_{i2}, \ldots, v_{\text{in}})$. The best position of the particle in its memory that it visited is denoted as $p_i^{\text{best}} = (p_{i1}, p_{i2}, \ldots, p_{\text{in}})$. The best position in the swarm is denoted as $g^{\text{best}} = (g_1, g_2, \ldots, g_n)$. The steps of the CPSO algorithm are described as follows:

Step 1. Initialization.

(a) Initializing randomly the positions of all particles
(b) Initializing randomly the velocities of all particles
(c) Setting $t = 1$, where t is the increment of time and T is the total number of iterations

Step 2. Optimization.

(a) Evaluating the objective function value f_i^t
(b) If $f_i^t \le f_i^{\text{best}}$, then $f_i^{\text{best}} = f_i^t$ and $p_i^{\text{best}} = x_i^t$
(c) If $f_i^t \le f_g^{\text{best}}$, then $f_g^{\text{best}} = f_i^t$ and $g_i^{\text{best}} = x_i^t$
(d) If the stopping criterion is satisfied go to Step 3
(e) All velocities ($v_i^t \forall i$ the particle) are updated according to the following equation:

$$v_i^{t+1} = wv_i^t + c_1 \times r_1 \times\left(p_i^{\text{best}} - x_i^t\right) + c_2 \times r_2 \times\left(g_i^{\text{best}} - x_i^t\right), \tag{8}$$

where w is an inertia term, c_1 and c_2 are the positive constants, and r_1 and r_2 are the random numbers belonging to (0, 1).

(f) All positions ($x_i^t \forall i$ the particle) are updated according to the following equation:

$$x_i^{t+1} = x_i^t + v_i^{t+1}. \tag{9}$$

(g) Chaotic repairing of the new position x_i^{t+1}
(h) $t = t + 1$
(i) Go to Step 2(a)

Step 3. Termination. If a prespecified stopping criterion is satisfied, stop the run; otherwise, go to Step 2.

3.2.3. Chaotic Repairing of Infeasible Solution. If the new position x_i^{t+1} is infeasible, it is repaired according to the following equation:

$$x_i^{t+1} = \phi \times x_i^{t+1} + (1 - \phi) \times \text{FS}. \tag{10}$$

If x_i^{t+1} is still infeasible, x_i^{t+1} is repaired according to the following equation:

$$x_i^{t+1} = \phi \times \text{FS} + (1 - \phi) \times x_i^{t+1}, \tag{11}$$

where FS is any feasible solution in the search space and ϕ is a chaotic number generated by the following logistic map:

$$\phi_{m+1} = c\phi_m(1 - \phi_m), \tag{12}$$

where m is the age of the infeasible solution, $c = 4$, $\phi_0 \in (0, 1)$, and $\phi_0 \notin \{0, 0.25, 0.5, 0.75, 1\}$.

3.3. The Proposed Approach. In this section, we discuss the proposed approach. The following steps describe the proposed approach clearly:

Step 1. Replacing all intervals in IQPP by additional variables which is called MQPP and obtaining the dual form of MQPP.

Step 2. Constructing KKT for MQPP, and solving KKT equations by the numerical algorithm.

Step 3. Using the solutions of the numerical algorithm as a start point of CPSO and CFA.

Step 4. Solving MQPP and its dual form by CPSO and CFA.

Step 5. The values of the objective function which are obtained from solving the problem by SA and its dual form are compared. If their values are the same, the global optimal solution of our problem is found. If there is a difference between the outputs from the problem and its dual, we solve the problem and its dual form again until the difference between them is ε, where ε can be computed as

$$\varepsilon = \frac{\delta}{\text{the optimal value of the problem}}, \tag{13}$$

where δ is the difference between the optimal value of the problem and the optimal value of its dual problem. This solution is a local optimal solution. This comparison is used as a new stopping criterion.

The suggested method is suitable for convex and nonconvex problems. The steps of the proposed approach are illustrated in Figure 1.

4. Results and Discussion

The proposed algorithm is tested by solving three problems taken from the literature. Each problem was independently run 30 times. The proposed algorithm was programmed in MATLAB (R2016b) and implemented on the PC with P4 CPU 3.00 GHz, 1 GB RAM with an i5 processor, Windows 7 operating system. The proposed algorithm, as any nontraditional optimization algorithms, involves a number of parameters that affect the performance of the algorithm. The parameters adopted in the implementation of CFA and CPSO are listed in Table 1.

4.1. Problem 1. This problem is formulated as follows [10]:

$$\begin{aligned} &\min\ x_1^2 + x_2^2 + [1,2] \\ &\text{subject to: } [1,6]x_1 + [1,2]x_2 \geq [1,12], \quad x_1, x_2 \geq 0. \end{aligned} \tag{14}$$

By replacing all intervals by additional parameters, the problem becomes

$$\begin{aligned} &\min\ x_1^2 + x_2^2 + a \\ &\text{subject to: } b_1 x_1 + b_2 x_2 \geq b_3, \quad x_1, x_2 \geq 0, \end{aligned} \tag{15}$$

where $a = [1,2], b_1 = [1,6], b_2 = [1,2]$, and $b_3 = [1,12]$.

The dual form of problem (15) is

$$\begin{aligned} \max\ & x_1^2 + x_2^2 + a - u_1(b_1 x_1 + b_2 x_2 - b_3) - u_2 x_1 - u_3 x_2, \\ & u_1 \geq 0, u_2 \geq 0, u_3 \geq 0. \end{aligned} \tag{16}$$

KKT conditions of problem (15) are

$$\begin{aligned} 2x_1 - u_1 b_1 - u_2 &= 0, \\ 2x_2 - u_1 b_2 - u_3 &= 0, \\ u_1(b_1 x_1 + b_2 x_2 - b_3) &= 0, \\ u_2 x_1 &= 0, \\ u_3 x_2 &= 0, \\ b_1 x_1 + b_2 x_2 &\geq b_3, \\ x_1, x_2 &\geq 0, \\ u_1 &\geq 0, \\ u_2 &\geq 0, \\ u_3 &\geq 0. \end{aligned} \tag{17}$$

In [8, 9], problem (14) can be divided into two problems. The first problem is

$$\begin{aligned} &\min\ x_1^2 + x_2^2 + 1 \\ &\text{subject to: } 6x_1 + 2x_2 \geq 1, \quad x_1, x_2 \geq 0. \end{aligned} \tag{18}$$

Its solution is $(x_1, x_2) = (0.15, 0.05)$ and $f(x) = 1.025$. The second problem is

$$\begin{aligned} &\min\ x_1^2 + x_2^2 + 2 \\ &\text{subject to: } x_1 + x_2 \geq 12, \quad x_1, x_2 \geq 0. \end{aligned} \tag{19}$$

Its solution is $(x_1, x_2) = (6, 6)$ and $f(x) = 74$. The solutions of KKT conditions in (18) can be expressed as

$$\text{solutions set} = \left\{\left(\frac{b_1 b_3}{b_1^2 + b_2^2}, \frac{b_2 b_3}{b_1^2 + b_2^2}\right)\right\}. \tag{20}$$

In addition, the numerical solution provides the boundaries of the basic variables as $x_1 = [0.025, 36]$ and $x_2 = [0.025, 12]$. The comparison between different types of SAs in solving problem (1) is shown in Table 2.

4.2. Problem 2. This problem is formulated as follows [1]:

$$\begin{aligned} &\min\ [2,3]x_1^2 + 2x_2^2 - 2x_1 x_2 + [-5,-3]x_1 + [1,2]x_2, \\ &\text{subject to: } [1,2]x_1 + x_2 \leq [2,4], [2,3]x_1 + [-1,-0.5]x_2 \\ &\qquad \leq [3,4], \quad x_1, x_2 \geq 0. \end{aligned} \tag{21}$$

By replacing all intervals by additional parameters, the problem becomes

$$\begin{aligned} &\min\ a_1 x_1^2 + 2x_2^2 - 2x_1 x_2 + a_2 x_1 + a_3 x_2 \\ &\text{subject to: } b_1 x_1 + x_2 \leq b_2 b_3 x_1 + b_4 x_2 \leq b_5, \quad x_1, x_2 \geq 0, \end{aligned} \tag{22}$$

where $a_1 = [2,3], a_2 = [-5,-3], a_3 = [1,2], b_1 = [1,2]$, $b_2 = [2,4], b_3 = [2,3]$, $b_4 = [-1,-0.5]$, and $b_5 = [3,4]$.

The dual form of problem (22) is

$$\begin{aligned} \max\ & a_1 x_1^2 + 2x_2^2 - 2x_1 x_2 + a_2 x_1 + a_3 x_2 + u_1(b_1 x_1 + x_2 - b_2) \\ & + u_2(b_3 x_1 + b_4 x_2 - b_5) - u_3 x_1 - u_4 x_2 \\ \text{subject to: } & u_1 \geq 0, u_2 \geq 0, u_3 \geq 0, u_4 \geq 0. \end{aligned} \tag{23}$$

The KKT conditions of problem (22) are

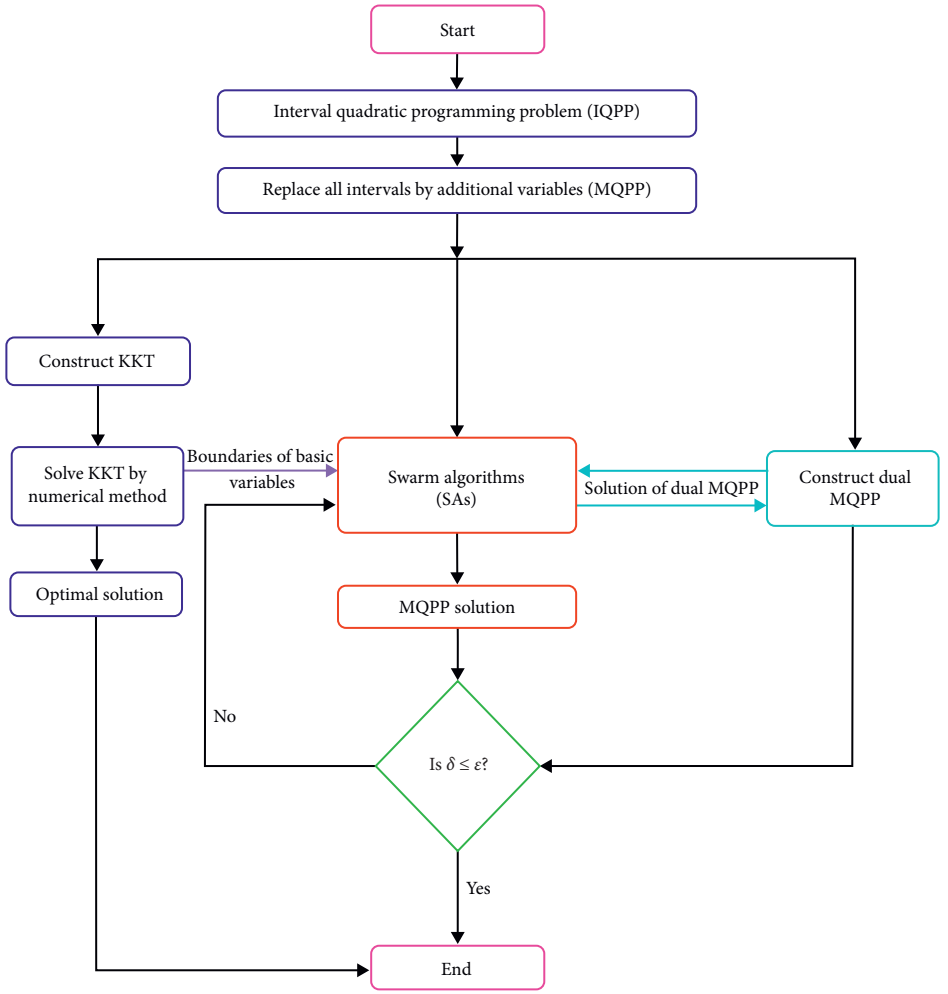

Figure 1: The flowchart of the proposed approach.

Table 1: The proposed algorithm parameters.

CFA parameters		CPSO parameters		
The swarm size (m)	20	The swarm size		20
Number of iteration (T)	200	Number of iteration (T)		200
Initial attractiveness (β_0)	1	Acceleration coefficients	c_1	2.8
The light absorption coefficient (γ)	1		c_2	1.3
The step size factor (α)	0.95	The inertia weight (w)		0.6
Chaos search repairing iteration (m)		1E02		
ε		1E-6		

Table 2: The results of problem (1) by using SAs.

	PSO	FA	CPSO	CFA
(x_1, x_2)	(0.37931, 0.21558)	(0.20087, 0.12304)	(0.1504, 0.0489)	(0.149462, 0.0516)
$f(x)$	1.6209	1.5252	1.0250	1.0250

$$
\begin{aligned}
2a_1x_1 - 2x_2 + a_2 + u_1b_1 + u_2b_3 - u_3 &= 0,\\
4x_2 - 2x_1 + a_3 + u_1 + u_2b_4 - u_4 &= 0,\\
u_1\left(b_1x_1 + x_2 - b_2\right) &= 0,\\
u_2\left(b_3x_1 + b_4x_2 - b_5\right) &= 0,\\
u_3x_1 &= 0,\\
u_4x_2 &= 0,\\
b_1x_1 + x_2 &\le b_2\\
b_3x_1 + b_4x_2 &\le b_5x_1,\\
x_2 &\ge 0,\\
u_1 &\ge 0,\\
u_2 &\ge 0,\\
u_3 &\ge 0,\\
u_4 &\ge 0.
\end{aligned}
\tag{24}
$$

In [8, 9], problem (21) is divided into two problems. The first problem is

$$
\begin{aligned}
&\min\ 2x_1^2 + 2x_2^2 - 2x_1x_2 - 5x_1 + x_2,\\
&\text{subject to: } x_1 + x_2 \le 4, 2x_1 - x_2 \le 4, \quad x_1, x_2 \ge 0.
\end{aligned}
\tag{25}
$$

Its solution is $(x_1, x_2) = (1.5, 0.5)$ and $f(x) = -3.5$. The second problem is

$$
\begin{aligned}
&\min\ 3x_1^2 + 2x_2^2 - 2x_1x_2 - 3x_1 + 2x_2\\
&\text{subject to: } 2x_1 + x_2 \le 2, 3x_1 - 0.5x_2 \le 3, \quad x_1, x_2 \ge 0.
\end{aligned}
\tag{26}
$$

Its solution is $(x_1, x_2) = (0.5, 0)$ and $f(x) = -0.75$. The solutions of KKT conditions in (24) can be expressed as

$$
= \left\{ \begin{array}{c} \left(\dfrac{2a_2 + a_3}{2 - 4a_1}, \dfrac{a_2 + a_1a_3}{2 - 4a_1}\right), \left(-\dfrac{a_2}{2a_1}, 0\right), \left(\dfrac{-b_2b_4 + b_5}{b_3 - b_1b_4}, \dfrac{b_2b_3 - b_1b_5}{b_3 - b_1b_4}\right), \left(\dfrac{b_5}{b_3}, 0\right), \left(\dfrac{b_2}{b_1}, 0\right), \\ \left(\dfrac{2b_2\left(2b_1 + 1\right) - a_2 + a_3b_1}{2a_1 + 4b_1\left(b_1 + 1\right)}, \dfrac{a_2b_1 - a_3b_1^2 + 2b_2\left(a_1 + b_1\right)}{2a_1 + 4b_1\left(b_1 + 1\right)}\right) \end{array} \right\}. \tag{27}
$$

In addition, the numerical solution provides the boundaries of the basic variables as $x_1 = [0.4, 4.08333]$ and $x_2 = [-1.6, 3.6]$. The results of problem (2) by using SAs are shown in Table 3.

4.3. Problem 3. This problem is formulated as follows [46]:

$$
\begin{aligned}
&\min\ [2,3]x_1^2 + 2x_2^2 - 2x_1x_2 + [-5,-3]x_1 + [1,2]x_2\\
&\text{subject to: } [1,2]x_1 + x_2 \le [2,4], [2,3]x_1 + [-1,-0.5]x_2\\
&\qquad \le [3,4], [4,5]x_1 + [-8,-7]x_2 = [1,1.5], \quad x_1, x_2 \ge 0.
\end{aligned}
\tag{28}
$$

By replacing all intervals by additional parameters, the problem becomes

$$
\begin{aligned}
&\min\ a_1x_1^2 + 2x_2^2 - 2x_1x_2 + a_2x_1 + a_3x_2\\
&\text{subject to: } b_1x_1 + x_2 \le b_2, b_3x_1 + b_4x_2\\
&\qquad \le b_5, b_6x_1 + b_7x_2 = b_8, \quad x_1, x_2 \ge 0,
\end{aligned}
\tag{29}
$$

where $a_1 = [2,3], a_2 = [-5,-3], a_3 = [1,2], b_1 = [1,2]$, $b_2 = [2,4], b_3 = [2,3], b_4 = [-1,-0.5]$, $b_5 = [3,4], b_6 = [4,5]$, $b_7 = [-8,-7]$, and $b_8 = [1,1.5]$.

The dual form of problem (29) is

$$
\begin{aligned}
&\max\ a_1x_1^2 + 2x_2^2 - 2x_1x_2 + a_2x_1 + a_3x_2 + u_1\left(b_1x_1 + x_2 - b_2\right)\\
&\qquad + u_2\left(b_3x_1 + b_4x_2 - b_5\right) + \lambda\left(b_6x_1 + b_7x_2 - b_8\right)\\
&\qquad - u_3x_1 - u_4x_2,\\
&u_1 \ge 0,\ u_2 \ge 0, u_3 \ge 0, u_4 \ge 0.
\end{aligned}
\tag{30}
$$

The KKT conditions of problem (28) are

$$
\begin{aligned}
2a_1x_1 - 2x_2 + a_2 + u_1 + u_1b_1 + u_2b_3 + \lambda b_6 - u_3 &= 0,\\
4x_2 - 2x_1 + a_3 + u_1 + u_2b_4 + \lambda b_7 - u_4 &= 0,\\
u_1\left(b_1x_1 + x_2 - b_2\right) &= 0,\\
u_2\left(b_3x_1 + b_4x_2 - b_5\right) &= 0,\\
\lambda\left(b_6x_1 + b_7x_2 - b_8\right) &= 0,\\
u_3x_1 &= 0,\\
u_4x_2 &= 0,\\
b_1x_1 + x_2 &\le b_2,\\
b_3x_1 + b_4x_2 &\le b_5,\\
b_6x_1 + b_7x_2 &= b_8,\\
x_1, x_2 &\ge 0,\\
u_1 &\ge 0,\\
u_2 &\ge 0,\\
u_3 &\ge 0,\\
u_4 &\ge 0.
\end{aligned}
\tag{31}
$$

Table 3: The results of problem (2) by using SAs.

	PSO	FA	CPSO	CFA
(x_1, x_2)	(1.217548, 0.42732)	(1.23733, 0.39811)	(0.1504, 0.0489)	(1.4964, 0.4970)
$f(x)$	−3.2759	−3.3355	−3.3355	−3.5

Table 4: The results of problem (2) by using SAs.

	PSO	FA	CPSO	CFA
(x_1, x_2)	(1.07113, 0.41978)	(1.07116, 0.41973)	(0.7754, 0.2002)	(1.4998, 0.5624)
$f(x)$	−1.9297	−3.1872	−2.7046	−3.4922

Table 5: The statistical results of SAs over the 30 runs.

			Algorithm	CPU time(s)	Mean	SD	Worst	Best
Problem 1	Range of $f(x)$	[1.025, 74]	PSO	5.45	1.6783	0.0419	1.7024	1.6209
			FA	4.56	1.5337	0.0065	1.5379	1.5252
			CPSO	3.76E−002	1.0250	0	1.0250	1.0250
			CFA	2.95E−002	1.0250	0	1.0250	1.0250
Problem 2	Range of $f(x)$	[−3.5, −0.75]	PSO	12.05	−3.2244	0.0458	−3.1846	−3.2759
			FA	7.96	−3.3230	0.0066	−3.3257	−3.3355
			CPSO	2.54E−002	−3.4999	0	−3.4999	−3.4999
			CFA	1.51E−002	−3.5	0	−3.5	−3.5
Problem 3	Range of $f(x)$	[−3.4922, 0.5217]	PSO	22.45	−1.8795	0.0304	−1.8750	−1.9297
			FA	10.38	−3.1498	0.0487	−3.0907	−3.1872
			CPSO	9.41E−002	2.7037	0.0013	−2.7005	−2.7046
			CFA	8.95E−002	−3.4922	0	−3.4922	−3.4922

In [8, 9], problem (28) is divided into two problems. The first problem is

$$\begin{aligned} &\min\ 2x_1^2 + 2x_2^2 - 2x_1x_2 - 5x_1 + x_2 \\ &\text{subject to: } x_1 + x_2 \le 4, 2x_1 - x_2 \le 4, 4x_1 - 8x_2 = 1.5, \quad x_1, x_2 \ge 0. \end{aligned} \tag{32}$$

Its solution is $(x_1, x_2) = (1.5, 0.5625)$ and $f(x) = -3.4922$. The second problem is

$$\begin{aligned} &\min\ 3x_1^2 + 2x_2^2 - 2x_1x_2 - 3x_1 + 2x_2 \\ &\text{subject to: } 2x_1 + x_2 \le 2, 3x_1 - 0.5x_2 \le 3, 5x_1 + -7x_2 = 1, \quad x_1, x_2 \ge 0. \end{aligned} \tag{33}$$

Its solution is $(x_1, x_2) = (0.3268, 0.0906)$ and $f(x) = -0.5217$.

The solutions of KKT conditions in (31) can be expressed as

$$\text{solutions set} = \left\{ \begin{array}{c} \left(\frac{2a_2 + a_3}{2 - 4a_1}, \frac{a_2 + a_1a_3}{2 - 4a_1}\right), \left(-\frac{a_2}{2a_1}, 0\right), \left(\frac{b_4b_8 + b_5b_7}{b_4b_6 - b_3b_7}, \frac{b_5b_6 + b_3b_8}{b_4b_6 - b_3b_7}\right), \left(\frac{b_5}{b_3}, 0\right), \left(\frac{b_8 + b_2b_7}{b_6 - b_1b_7}, \frac{b_2b_6 + b_1b_8}{b_6 - b_1b_7}\right), \\ \left(\frac{b_5 - b_2b_4}{b_3 - b_1b_4}, \frac{b_2b_3 - b_1b_5}{b_3 - b_1b_4}\right), \left(\frac{b_5}{b_3}, 0\right), \left(\frac{2b_2(2b_1 + 1) - a_2 + a_3b_1}{2a_1 + 4b_1(b_1 + 1)}, \frac{a_2b_1 - a_3b_1^2 + 2b_2(a_1 + b_1)}{2a_1 + 4b_1(b_1 + 1)}\right), \left(\frac{b_2}{b_1}, 0\right) \\ \left(\frac{a_3b_6b_7 - a_2b_7^2 + 2b_8(2b_6b_7)}{4b_6^2 + 4b_6b_7 + 2a_1b_7^2}, \frac{-a_3b_6^2 + a_2b_6b_7 + 2b_8(b_6 + a_1b_7)}{4b_6^2 + 4b_6b_7 + 2a_1b_7^2}\right), \left(\frac{b_2}{b_1}, 0\right) \end{array} \right\}. \tag{34}$$

In addition, the numerical solution provides the boundaries of the basic variables $x_1 = [0.28289, 9.8]$ and $x_2 = [-5.4, 5.8]$. In Table 4, the results of problem (2) by using SAs are listed.

In addition, the statistical results obtained, by original PSO, original FA, CPSO, and CFA, over the 30 runs are summarized in terms of CPU time, mean value, standard deviation, and worst and best values in Table 5.

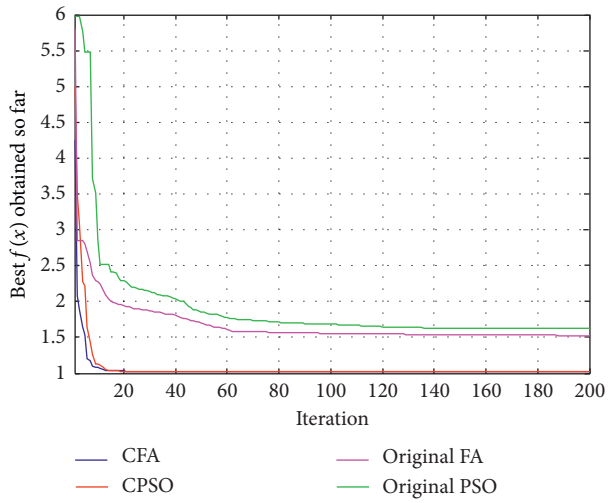

Figure 2: The convergence curve of the best $f(x)$ obtained so far by original PSO, original FA, CPSO, and CFA for problem 1.

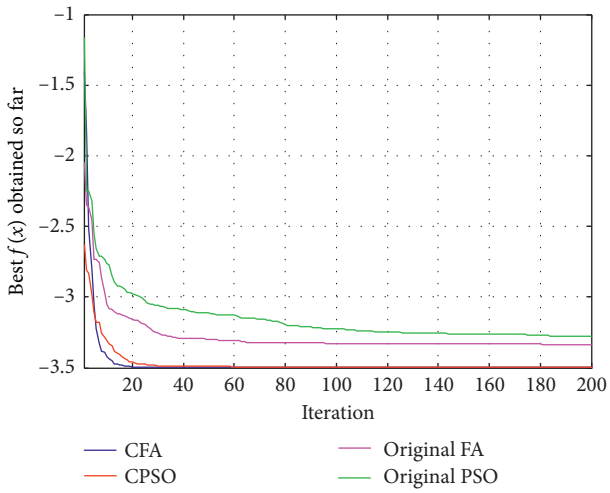

Figure 3: The convergence curve of the best $f(x)$ obtained so far by original PSO, original FA, CPSO, and CFA for problem 2.

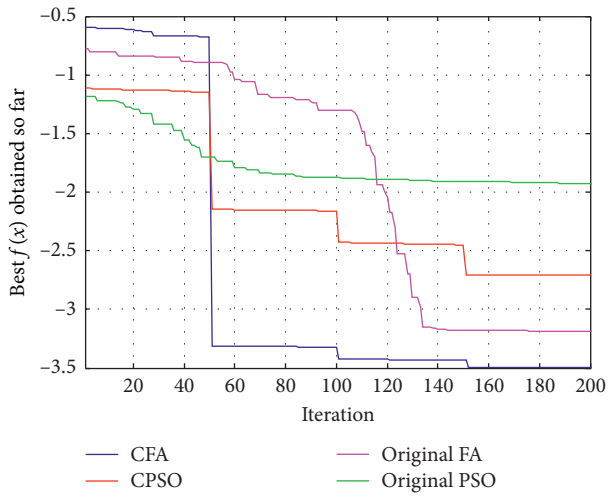

Figure 4: The convergence curve of the best $f(x)$ obtained so far by original PSO, original FA, CPSO, and CFA for problem 3.

Furthermore, Figures 2–4 show the convergence curve of the best $f(x)$ obtained so far by original PSO, original FA, CPSO, and CFA for the 3 problems.

Results show that the proposed SAs (CFA and CPSO) outperform the other original algorithms in terms of the optimality. In addition, these results prove that the proposed SAs can solve IQPP effectively with low computational cost where the CPU time is less than the other original algorithms as shown in Table 5. In other words, the solutions, of the test problems, of CPSO and CFA are the same as the solutions of previous methods, but they are very fast without any effort of computation. On the other hand, the numerical approach gives the solution as a general formula in the additional variables, where we can obtain, by this formula, the solution at any values inside the intervals. In addition, the numerical solution provides the boundaries of the basic variables which are used in the step of initialization in SAs. Finally, we can say that our approach, as any SAs, is more generalized and suitable for real applications than traditional methods.

5. Conclusion

This paper deals with a new approach to solve IQPP. We aim to explore the feasible region to get the optimal solution anywhere. All intervals were replaced by additional variables. The new form with additional variables is MQPP. KKT conditions for MQPP were solved numerically to get the solutions as a function in the additional variables and provide the boundaries of the basic variables. The solutions are used as start points for SAs. CPSO and CFA are used to solve MQPP and its dual form. The advantages of our procedure are (1) the solution of the numerical method is more general than previous methods, (2) giving the decision maker a very fast view of the optimal solution inside the intervals, (3) using the optimal solution of the dual problem as a stopping criterion for SAs is more suitable than other criteria, and (4) its effectiveness is verified as compared with other studies. Also, we compare PSO, FA, CPSO, and CFA with each other. Real applications of interval nonlinear programming problems should be conducted in the future. In addition, we are planning to use this vision to solve multiobjective linear programming with interval coefficients. Also, we aim to discuss the GSK algorithm to solve IQPP.

Data Availability

All data used to support the findings of this study are included within the article.

Conflicts of Interest

The authors declare that this article content has no conflicts of interest.

References

[1] A. K. Bhurjee and G. Panda, "Efficient solution of interval optimization problem," *Mathematical Methods of Operations Research*, vol. 76, no. 3, pp. 273–288, 2012.

[2] M. Chen, S.-G. Wang, P. P. Wang, and X. Ye, "A new equivalent transformation for interval inequality constraints of interval linear programming," *Fuzzy Optimization and Decision Making*, vol. 15, no. 2, pp. 155–175, 2016.

[3] J. W. Chinneck and K. Ramadan, "Linear programming with interval coefficients," *The Journal of the Operational Research Society*, vol. 51, no. 2, pp. 209–220, 2000.

[4] E. Garajová and M. Hladík, "On the optimal solution set in interval linear programming," *Computational Optimization and Applications*, vol. 72, no. 1, pp. 269–292, 2019.

[5] M. Hladík, "Robust optimal solutions in interval linear programming with forall-exists quantifiers," *European Journal of Operational Research*, vol. 254, no. 3, pp. 705–714, 2016.

[6] M. Hladík, "How to determine basis stability in interval linear programming," *Optimization Letters*, vol. 8, no. 1, pp. 375–389, 2014.

[7] M. Hladík, "Weak and strong solvability of interval linear systems of equations and inequalities," *Linear Algebra and Its Applications*, vol. 438, no. 11, pp. 4156–4165, 2013.

[8] M. Hladík, "Optimal value bounds in nonlinear programming with interval data," *TOP*, vol. 19, no. 1, pp. 93–106, 2011.

[9] M. Hladík, "Optimal value range in interval linear programming," *Fuzzy Optimization and Decision Making*, vol. 8, no. 3, pp. 283–294, 2009.

[10] C. Jiang, Z. G. Zhang, Q. F. Zhang, X. Han, H. C. Xie, and J. Liu, "A new nonlinear interval programming method for uncertain problems with dependent interval variables," *European Journal of Operational Research*, vol. 238, no. 1, pp. 245–253, 2014.

[11] C. Jiang, X. Han, G. R. Liu, and G. P. Liu, "A nonlinear interval number programming method for uncertain optimization problems," *European Journal of Operational Research*, vol. 188, no. 1, pp. 1–13, 2008.

[12] H.-C. Wu, "On interval-valued nonlinear programming problems," *Journal of Mathematical Analysis and Applications*, vol. 338, no. 1, pp. 299–316, 2008.

[13] X. Y. Wu, G. H. Huang, L. Liu, and J. B. Li, "An interval nonlinear program for the planning of waste management systems with economies-of-scale effects-A case study for the region of Hamilton, Ontario, Canada," *European Journal of Operational Research*, vol. 171, no. 2, pp. 349–372, 2006.

[14] R. E. Moore, *Methods and Applications of Interval Analysis*, Society for Industrial and Applied Mathematics, Philadelphia, PA, USA, 1979.

[15] M. Allahdadi and H. Mishmast Nehi, "The optimal solution set of the interval linear programming problems," *Optimization Letters*, vol. 7, no. 8, pp. 1893–1911, 2013.

[16] H. Ishibuchi and H. Tanaka, "Multiobjective programming in optimization of the interval objective function," *European Journal of Operational Research*, vol. 48, no. 2, pp. 219–225, 1990.

[17] S.-T. Liu and R.-T. Wang, "A numerical solution method to interval quadratic programming," *Applied Mathematics and Computation*, vol. 189, no. 2, pp. 1274–1281, 2007.

[18] W. Li and X. Tian, "Numerical solution method for general interval quadratic programming," *Applied Mathematics and Computation*, vol. 202, no. 2, pp. 589–595, 2008.

[19] Y. Chalco-Cano, R. Osuna-Gómez, B. Hernández-Jiménez, and H. Román-Flores, *A Note on Optimality Conditions to Interval Optimization Problems*, Atlantis Press, Paris, France, 2015.

[20] L. Stefanini and B. Bede, "Generalized Hukuhara differentiability of interval-valued functions and interval differential equations," *Nonlinear Analysis: Theory, Methods & Applications*, vol. 71, no. 3-4, pp. 1311–1328, 2009.

[21] H.-C. Wu, "The Karush-Kuhn-Tucker optimality conditions in an optimization problem with interval-valued objective function," *European Journal of Operational Research*, vol. 176, no. 1, pp. 46–59, 2007.

[22] J. Zhang, S. Liu, L. Li, and Q. Feng, "The KKT optimality conditions in a class of generalized convex optimization problems with an interval-valued objective function," *Optimization Letters*, vol. 8, no. 2, pp. 607–631, 2014.

[23] K. G. Dhal, S. Ray, A. Das, and S. Das, "A survey on nature-inspired optimization algorithms and their application in image enhancement domain," *Archives of Computational Methods in Engineering*, vol. 26, pp. 1607–1638, 2018.

[24] M. Dorigo and M. Birattari, "Ant colony optimization," in *Encyclopedia of Machine Learning*, C. Sammut and G. I. Webb, Eds., pp. 36–39, Springer, Boston, MA, USA, 2010.

[25] Abd el-wahed, F. Waiel, A. A. Mousa, and M. A. Elsisy, "Solving economic emissions load dispatch problem by using hybrid ACO-MSM approach," *The Online Journal on Power and Energy Engineering (OJPEE)*, vol. 1, no. 1, pp. 31–35, 2009.

[26] M. A. El-Shorbagy and A. E. Hassanien, "Particle swarm optimization from theory to applications," *International Journal of Rough Sets and Data Analysis*, vol. 5, no. 2, pp. 1–24, 2018.

[27] M. A. El-Shorbagy, "*Hybrid particle swarm algorithm for multi-objective optimization*," M.S. thesis, Menoufiya University, Al Minufya, Egypt, 2010.

[28] S. Verma and V. Mukherjee, "Firefly algorithm for congestion management in deregulated environment," *Engineering Science and Technology, an International Journal*, vol. 19, no. 3, pp. 1254–1265, 2016.

[29] M. Marinaki and Y. Marinakis, "A glowworm swarm optimization algorithm for the vehicle routing problem with stochastic demands," *Expert Systems with Applications*, vol. 46, pp. 145–163, 2016.

[30] A. L. a. Bolaji, M. A. Al-Betar, M. A. Awadallah, A. T. Khader, and L. M. Abualigah, "A comprehensive review: krill Herd algorithm (KH) and its applications," *Applied Soft Computing*, vol. 49, pp. 437–446, 2016.

[31] Y. Zhou, X. Chen, and G. Zhou, "An improved monkey algorithm for a 0-1 knapsack problem," *Applied Soft Computing*, vol. 38, pp. 817–830, 2016.

[32] S. Saremi, S. Mirjalili, and A. Lewis, "Grasshopper optimisation algorithm: theory and application," *Advances in Engineering Software*, vol. 105, pp. 30–47, 2017.

[33] A. W. Mohamed, A. A. Hadi, and A. K. Mohamed, "Gaining-sharing knowledge based algorithm for solving optimization problems: a novel nature-inspired algorithm," *International Journal of Machine Learning and Cybernetics*, vol. 11, no. 7, pp. 1501–1529, 2020.

[34] Y. Cao, H. Zhang, W. Li, M. Zhou, Y. Zhang, and W. A. Chaovalitwongse, "Comprehensive learning particle swarm optimization algorithm with local search for multimodal functions," *IEEE Transactions on Evolutionary Computation*, vol. 23, no. 4, pp. 718–731, 2018.

[35] W. Dong and M. Zhou, "A supervised learning and control method to improve particle swarm optimization algorithms," *IEEE Transactions on Systems, Man, and Cybernetics: Systems*, vol. 47, no. 7, pp. 1135–1148, 2016.

[36] Q. Kang, C. Xiong, M. Zhou, and L. Meng, "Opposition-based hybrid strategy for particle swarm optimization in noisy environments," *IEEE Access*, vol. 6, pp. 21888–21900, 2018.

[37] Z. Lv, L. Wang, Z. Han, J. Zhao, and W. Wang, "Surrogate-assisted particle swarm optimization algorithm with Pareto active learning for expensive multi-objective optimization," *IEEE/CAA Journal of Automatica Sinica*, vol. 6, no. 3, pp. 838–849, 2019, þ.

[38] A. Neumaier, *Interval Methods for Systems of Equations*, Vol. 37, Cambridge University Press, Cambridge, UK, 1990.

[39] D. Yang, G. Li, and G. Cheng, "On the efficiency of chaos optimization algorithms for global optimization," *Chaos, Solitons & Fractals*, vol. 34, no. 4, pp. 1366–1375, 2007.

[40] M. A. E. Shorbagy and A. A. Mousa, "Chaotic particle swarm optimization for imprecise combined economic and emission dispatch problem," *Review of Information Engineering and Applications*, vol. 4, no. 1, pp. 20–35, 2017.

[41] M. A. El-Shorbagy, A. A. Mousa, and S. M. Nasr, "A chaos-based evolutionary algorithm for general nonlinear programming problems," *Chaos, Solitons & Fractals*, vol. 85, pp. 8–21, 2016.

[42] J. Xiao, *Improved Quantum Evolutionary Algorithm Combined with Chaos and its Application*, Springer, Berlin, Germany, 2009.

[43] D. Oliva, M. Abd El Aziz, and A. Ella Hassanien, "Parameter estimation of photovoltaic cells using an improved chaotic whale optimization algorithm," *Applied Energy*, vol. 200, pp. 141–154, 2017.

[44] Z. Aram, S. Jafari, J. Ma, J. C. Sprott, S. Zendehrouh, and V.-T. Pham, "Using chaotic artificial neural networks to model memory in the brain," *Communications in Nonlinear Science and Numerical Simulation*, vol. 44, pp. 449–459, 2017.

[45] M. A. El-Shorbagy, M. Elhoseny, A. E. Hassanien, and S. H. Ahmed, "A novel PSO algorithm for dynamic wireless sensor network multiobjective optimization problem," *Transactions on Emerging Telecommunications Technologies*, vol. 30, no. 11, 2018.

[46] D. Ghosh, D. Ghosh, S. K. Bhuiya, and L. K. Patra, "A saddle point characterization of efficient solutions for interval optimization problems," *Journal of Applied Mathematics and Computing*, vol. 58, no. 1-2, pp. 193–217, 2018.

Hindawi
Complexity
Volume 2020, Article ID 7393848, 20 pages
https://doi.org/10.1155/2020/7393848

Research Article

Simulation and Analysis of the Complex Dynamic Behavior of Supply Chain Inventory System from Different Decision Perspectives

Zusheng Zhang[1,2], **Xu Wang**[1,2], **Shanshan Yang**[3], **Yingbo Wu**[4] and **Jianhui Du**[1,2]

[1]*College of Mechanical Engineering, Chongqing University, Chongqing, China*
[2]*Chongqing Key Laboratory of Logistics, Chongqing University, Chongqing, China*
[3]*School of Economics and Business Administration, Chongqing University, Chongqing, China*
[4]*School of Big Data & Software Engineering, Chongqing University, Chongqing, China*

Correspondence should be addressed to Xu Wang; wx921@163.com

Received 27 May 2020; Revised 18 July 2020; Accepted 3 August 2020; Published 30 September 2020

Guest Editor: Baltazar Aguirre-Hernández

Copyright © 2020 Zusheng Zhang et al. This is an open access article distributed under the Creative Commons Attribution License, which permits unrestricted use, distribution, and reproduction in any medium, provided the original work is properly cited.

Based on the local decision perspective and the global decision perspective, considering the limitation of supply capacity and prohibiting returns, the system dynamics method is used to establish a nonlinear supply chain system model. We use the *Z*-transform theory to transform the dynamic transfer equation into a block diagram, build a supply chain system simulation model, and use it to conduct simulation experiments. The Wolf reconstruction method is used to calculate the largest Lyapunov exponent (LLE) value of each node or combined system to judge the stability of the system. Based on different decision-making perspectives, under different combinations of safety stock factors and demand scenarios, the adjustment coefficients' decision-making schemes that keep each node in a stable state are obtained. Then, we comparatively analyze the inventory changes of each node and combined system in a stable state under different decision-making schemes.

1. Introduction

Supply chain management has always been a concern of enterprises. To help enterprises better implement effective supply chains, Pittiglio, Rabin, Todd & McGrath (PRTM) and AMR Research (AMR) led the establishment of the Supply Chain Council (SCC) in 1996 and released supply chain operations reference (SCOR) model, realized the transformation from function-based management to process-based management, and improved the performance of the supply chain. With the emergence of cloud computing, Internet of things (IoT), artificial intelligence (AI), and other new information technologies (IT), supply chain management has a new background and requirements. New technologies can change the way of communication among the supply chain members. Before the 1960s and 1970s, due to technical limitations, the rapid flow and sharing of information cannot be achieved. In the early traditional SC model, each node enterprise is responsible for its inventory control, production, or distribution ordering activities, and each echelon only has its immediate customer information [1]. The application of new information technology makes it possible to easily share the main information on the supply chain (SC) nodes.

Gradually, some new supply chain models are formed and applied in practice. Among them, the more commonly used are the vendor-managed inventory (VMI) model and the third-party logistics management inventory (TMI) model [2] so that the problems faced by the traditional SC have undergone some changes. For example, the bullwhip effect can be improved. The bullwhip effect is a description of the image of demand information distorted in the SC [3].

The development of science and technology has promoted the vertical integration of the supply chain, and the

management concept has also changed. More and more decision makers have magnified the decision perspective, and supply chain management presents the trend of vertical integration. More and more decisions are made based on local alliances and the whole supply chain. Also, there are many different types of uncertainties in the SC, such as changes in market demand, limited production capacity, the delay of transportation time, and so on [4]. Even, the level of decision makers also has a huge impact on the SC. All of the above factors will lead to the supply chain system (SCS) in an unstable state, which will increase the difficulty and cost of management. So, it makes great sense to study the complex dynamic behavior of the SC closely related to these factors from different perspectives.

2. Literature Review

The research on the dynamic behavior of supply chain systems started in the early 1960s. It first appeared in the classic work "Industrial Dynamics" by Forrester, which is the simplest manifestation of the dynamic complexity of supply chain systems [5] and was later named "bullwhip effect." Since then, the research literature on the dynamic behavior of the supply chain keeps emerging. These studies can be divided into two parts, including the dynamic behavior analysis of the linear system model and dynamic behavior analysis of the nonlinear system model.

In the early days of the concept of dynamic behavior emergence, many research studies were based on the inventory and order based production control system (IOBPCS) and analyzed as a linear system. Towill [6] analyzed a reasonable industrial dynamics model of an inventory control system, which is IOBPCS, by using transfer function techniques. A general rule for parameter settings which can then be used for "local" tuning in a large-scale industrial dynamics simulation is proposed. Disney et al. [7] outlined a method of developing a fitness measure for use in a genetic algorithm for assessing the performance of a generic production control system. Disney et al. [8] described a genetic algorithm for optimizing system performance, via five vectors including inventory recovery to "shock" demands, inbuilt filtering capability, robustness to production lead time variations, robustness to pipeline level information fidelity, and systems selectivity. In a vendor-managed inventory (VMI) supply chain, Disney and Towill [9] considered a well-established production and distribution scheduling algorithm termed automatic pipeline, inventory, and order based production control system (APIOBPCS). Simulation and analysis demonstrate that poor design can cause instability and the recommended parameter can avoid it. Dejonckheere et al. [10] introduced a general decision rule that avoids variance amplification and succeeds in generating smooth ordering patterns, even when the demand has to be forecasted. Lin and Wang [11] analyzed the stability of the system using the characteristic equation. It is proved that the intuitive operation of a supply system with demand forecasting will cause bullwhip and lead time alone would not cause bullwhip. Nagatani and Helbing [12] studied several feasible production strategies for stabilizing the supply chain in the linear supply chain. Disney [13] analyzed the quasiperiodicity, bullwhip effect, and stability of the supply chain inventory system. In these studies of a linear systems model, most assume that orders at all levels of the supply chain are satisfied, regardless of inventory constraints, mainly used to study and analyze the dynamic behavior of the supply chain, the bullwhip effect.

With the deepening of research, it is found that based on various assumptions, for example, orders at all levels of the supply chain are satisfied, regardless of inventory constraints, and the supply chain system is regarded as a simple linear system model. It leads to the inconsistency between the research results and the actual situation and fails to reveal the nonlinear phenomena except the bullwhip effect. Therefore, more and more research studies have been conducted to construct nonlinear system models to study the supply chain. Mosekilde and Laugesen [14] established a nonlinear inventory model under the nonnegative constraint of order quantity and found chaos in the system. Wang et al. [15] studied the stability of a constrained production and inventory system with a forbidden returns constraint. The results show that accurate lead time information is the key to eliminating inventory drift and instability, and ordering strategies must be reasonably designed according to actual lead times to avoid these fluctuations and differences. Garcia et al. [16] designed a supply chain switching control system to improve the stability of the supply chain through internal mode control technology. Wang et al. [17] assumed that the system input was a certain step demand model and return was forbidden, obtaining the stability, period, quasiperiod, and chaotic boundary of the system by solving the system characteristic values. Ma and Si [18] investigated the influence of delay and weight on the complex dynamic characteristics of the system. Si and Ma [19] established a triopoly output game model with multiple delays in the competition of green products. By analyzing the existence of equilibrium points and local asymptotic stability, the influence of parameters on system stability and complexity is studied. Zhan et al. [20] established the model of VMI-APIOBPCS in apparel supply chain and used the Routh–Hurwitz stability criterion to analyze the stability. Jin and Song [21] established a nonlinear system model to study the effects of two strategies of the nonlinear supply chain with and without a shortage on the dynamic behavior of the remanufacturing supply chain system. Lin and Naim [22] developed a hybrid ATO system dynamics model based on the well-established inventory and order based production control systems and analytically studied the impact of nonlinearities on its dynamic performance. Xu and Lee [23] presented A multiechelon supply chain system having parametric perturbations and disturbances to demonstrate chaotic nonlinear dynamical behaviors.

In the existing research on the complex dynamic behavior of the supply chain, many scholars used hypotheses to simplify the research objects and used the linear model to analyze the bullwhip effect in the supply chain. At the same time, many scholars consider practical factors such as prohibiting returns and limited supply capacity, constructing nonlinear dynamic models, and studying the

impact of different demand scenarios, production models, and decision parameters on the stability of the supply chain, which has achieved rich results.

The analysis found that most studies can be divided into the category of local decision-making perspectives. However, in the existing research, no research mentions the decision-making perspective, nor does it study and analyze the complex behavior of the supply chain under different decision-making perspectives. In this paper, the idea of a decision perspective is introduced. Based on the local decision perspective and the global decision perspective, the difference equations and simulation models of the system are established, respectively, and the simulation experiments are carried out to compare and analyze the complex dynamic behavior of the supply chain inventory system from different perspectives. At the same time, the effect of safety stock parameters on the complex dynamic behavior of the supply chain is analyzed.

3. Supply Chain System Dynamic Model

3.1. System Description. The supply chain is based on a third-party logistics management inventory model (TMI) and includes a supplier, a retailer, and a third-party logistics service provider (3PLP). The operation process of the supply chain is shown in Figure 1. The inventory system of the supply chain includes three nodes: the production warehouse, the distribution center, and the retailer. The supplier purchases or produces its own raw materials and produces the raw materials as finished products. The retailer buys finished products from the supplier and sells them to end consumers. The supplier performs production according to the replenishment order issued by the warehouse to the production system. The warehouse is adjacent to the production workshop, and the finished products can be quickly delivered to the warehouse. Suppose the transportation cycle is 0. In order to immediately respond to the retailer's ordering needs, build a distribution center near the retailer, assuming that the transportation cycle from the distribution center to the retailer is 0. The inventory information of each node is transmitted to the decision system in real-time. The decision-making system will provide decision-making services for each node. When the inventory is lower than the safety stock, it will send a replenishment notification to the node, and then each node will send an order notification to the superior node. For the decision-making system, it can make decisions based on two decision-making perspectives. One is based on the perspective of local decision making, taking the production system and the warehouse-distribution system as a whole. The other is based on the perspective of global decision making, taking the entire supply chain as a whole. The local decision-making perspective does not include the retailer, regardless of the difference in the status of the node inventory goods and the goods in transit.

3.2. Model Parameters and Variables. To facilitate model description, the following relevant notations of model variables and parameters are introduced (Table 1).

3.3. Systematic Difference Equations

3.3.1. Demand Forecast. For the superior node of the supply chain, the demand forecast is based on the actual demand of terminal consumers. This forecasting method can reduce the amplification effect of orders in the supply chain, which is more reasonable than the demand forecasting based on the orders of subordinate nodes. The simple exponential smoothing method is often used in demand forecasting and has achieved good results. Therefore, this paper uses this method to forecast the demand. The prediction expression is shown in equation (1). In this study, two kinds of customer demand are considered, including random demand obeying normal distribution and random demand obeying uniform distribution. Assume that the mean of two kinds of customer demand is μ.

$$F(t) = \theta F(t-1) + (1-\theta)D(t), \tag{1}$$

where θ is the exponential smoothing constant. Existing studies have shown that $0 \le \theta < 2$ is required for stability of the forecasting system. In the paper, let $\theta = 0.5$.

3.3.2. Production Strategy. The study uses automated pipeline, inventory, and order based production control system (APIOBPCS), a commonly used method of production control. The specific meaning of APIOBPCS is that the order quantity (or production plan) is equal to the sum of the predicted demand quantity, the adjustment quantity to the actual inventory level, and the adjustment quantity to the inventory in transit (or work-in-process (WIP) inventory). Most of the existing literature on the complex behavior of the supply chain has adopted this strategy [9, 24].

Based on the local decision perspective of the supply chain, the actual inventory of the warehouse-distribution system is considered as the supplier's finished product inventory. The production strategy is expressed as follows:

$$O_1(t) = \max\left(0, F(t) + \alpha_S\left(I_1^0 - I_1(t)\right) + \alpha_{SL}\left(Y^0 - Y(t)\right)\right). \tag{2}$$

Based on the global decision perspective of the supply chain, the actual inventory of the entire supply chain is considered as the supplier's finished product inventory. The production strategy is expressed as follows:

$$O_2(t) = \max\left(0, F(t) + \alpha_S\left(I_2^0 - I_2(t)\right) + \alpha_{SL}\left(Y^0 - Y(t)\right)\right). \tag{3}$$

3.3.3. Inventory Strategy. The supplier, the retailer, and the distribution center adopt periodic inventory strategy. The strategy is to replenish at regular intervals, each time to the target inventory level.

From the local decision perspective, the initial inventory $B_1(t)$ and the end-of-cycle inventory $I_1(t)$ of the warehouse-distribution system are expressed as follows:

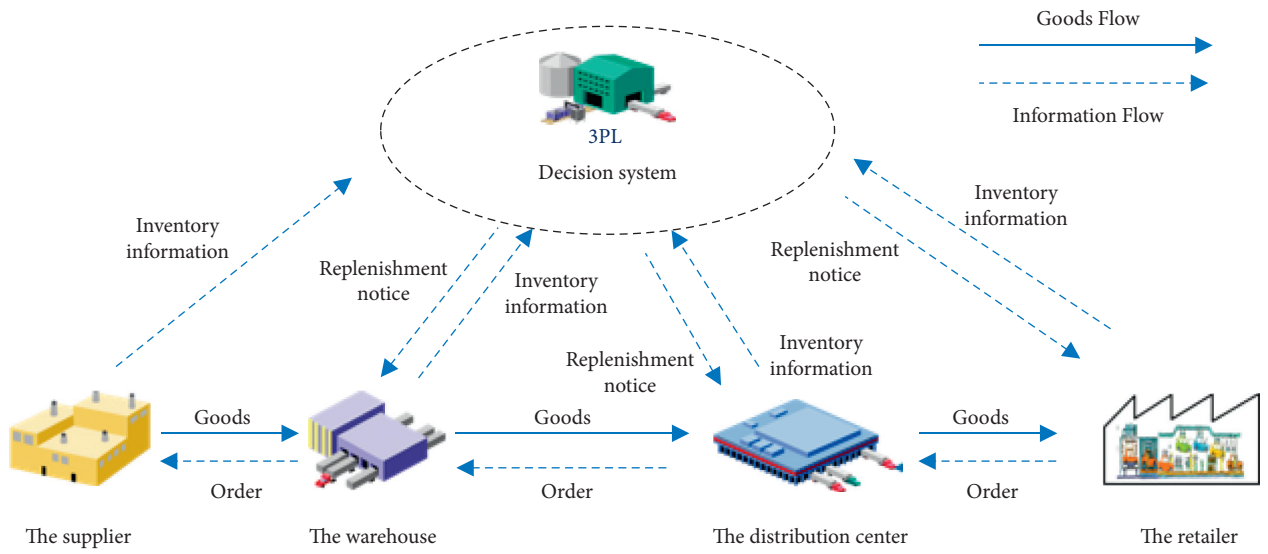

Figure 1: The TMI-SC operation flowchart.

Table 1: Model variables and parameters.

	Notation	Description
Variables	$D(t)$	The actual demand of consumers in period t
	$F(t)$	The forecast demand in period t
	$I_r(t)$	Retailer's initial inventory in period t
	$B_r(t)$	Retailer's end-of-cycle inventory in period t
	$R_r(t)$	Retailer's arrivals in period t
	$S_r(t)$	Retailer's sales in period t
	$O_r(t)$	Retailer's order quantity in period t
	$S_d(t)$	Distribution center's shipments in period t
	$I_d(t)$	Distribution center's initial inventory in period t
	$B_d(t)$	Distribution center's end-of-cycle inventory in period t
	$R_d(t)$	Distribution center arrivals in period t
	$W_d(t)$	The in-transit inventory of the distribution center in period t
	$O_d(t)$	The replenishment volume of the distribution center in period t
	$S_w(t)$	Warehouse shipments in period t
	$I_w(t)$	Warehouse's initial inventory in period t
	$B_w(t)$	Warehouse's end-of-cycle inventory in period t
	$R_w(t)$	Warehouse arrivals in period t
	$I_i(t)$	The initial inventory of system from the perspective of decision making in period t. When $i = 1$, it is local decision perspective. When $i = 2$, it is global decision perspective.
	$B(t)$	The end-of-cycle inventory of system in period t
	$O_i(t)$	The replenishment of the system of system from the perspective of decision making in period t. When $i = 1$, it is local decision perspective. When $i = 2$, it is global decision perspective.
	$Y(t)$	Supplier's WIP inventory in period t
Parameters	Y^0	The expected WIP inventory level of the supplier
	α_S	The adjustment coefficient of inventory
	α_{SL}	The adjustment coefficient of WIP inventory
	T_P	Transport lead time
	T_C	Production lead time
	G_r	Safety inventory coefficient of the retailer
	G_d	Safety inventory coefficient of the distribution center
	G_i	Safety inventory coefficient of the system from the perspective of decision making. When $i = 1$, it is local decision perspective. When $i = 2$, it is global decision perspective.
	I_r^0	Retailer's expected inventory level
	I_d^0	Distribution center's expected inventory level
	I_i^0	The expected inventory level of system from the perspective of decision making. When $i = 1$, it is local decision perspective. When $i = 2$, it is global decision perspective.

$$\begin{aligned} B_1(t) &= B_1(t-1) - S_d(t-1) + R_w(t), \\ I_1(t) &= I_1(t-1) + R_w(t) - S_d(t), \\ I_1(t) &= B_1(t) - S_d(t), \\ I_1^0 &= \mu G_1. \end{aligned} \tag{4}$$

From the global decision perspective, the inventory of the entire supply chain system is expressed as follows:

$$\begin{aligned} B_2(t) &= B_2(t-1) - S_r(t-1) + R_w(t), \\ I_2(t) &= I_2(t-1) + R_w(t) - S_r(t), \\ I_2(t) &= B_2(t) - S_r(t), \\ I_2^0 &= \mu G_2. \end{aligned} \tag{5}$$

Due to the production delay, the following formula can be obtained:

$$R_w(t) = O\left(t - T_C - 1\right). \tag{6}$$

The expression of the supplier's WIP inventory is given by

$$Y(t) = Y(t-1) + O(t-1) - R_w(t). \tag{7}$$

The expression of the replenishment quantity of the distribution center is shown in the following equation:

$$O_d(t) = \max\left(0, F(t) + \alpha_S\left(I_d^0 - I_d(t)\right) + \alpha_{SL}\left(W^0 - W_d(t)\right)\right). \tag{8}$$

The expression of the distribution center's inventory is given by equations (9)–(11). Moreover, the distribution center's expected inventory level is obtained by equation (12).

$$B_d(t) = B_d(t-1) - S_d(t-1) + R_d(t), \tag{9}$$

$$I_d(t) = I_d(t-1) + R_d(t) - S_d(t), \tag{10}$$

$$I_d(t) = B_d(t) - S_d(t), \tag{11}$$

$$I_d^0 = \mu G_d. \tag{12}$$

Among them, the distribution center's shipments in period t are given by

$$S_d(t) = \begin{cases} I_d(t-1) + R_d(t), & I_d(t-1) + R_d(t) \le O_r(t-1), \\ O_r(t-1), & I_d(t-1) + R_d(t) > O_r(t-1). \end{cases} \tag{13}$$

Due to transportation delay, the following formula can be obtained:

$$R_d(t) = O_d\left(t - T_P - 1\right). \tag{14}$$

The retailer is prohibited from returning goods, so the retailer's order quantity is expressed as follows:

$$O_r(t) = \max\left(0, I_r^0 - I_r(t)\right). \tag{15}$$

The expression of the retailer's inventory is given by

$$\begin{aligned} B_r(t) &= B_r(t-1) - S_r(t-1) + R_r(t), \\ I_r(t) &= I_r(t-1) + R_r(t) - S_r(t), \\ I_r(t) &= B_r(t) - S_r(t), \\ I_r^0(t) &= \mu G_r. \end{aligned} \tag{16}$$

The replenishment of the retailer can be quickly obtained from the distribution center. That is, the replenishment notice is issued at the end of the period, and the replenishment can be received at the beginning of the next period. So, the following expression can be obtained:

$$R_r(t) = \min\left(O_r(t-1), I_d(t-1) + R_d(t)\right). \tag{17}$$

At the same time, the retailer's sales and consumer demand satisfied the following formula:

$$S_r(t) = \begin{cases} I_r(t-1) + R_r(t), & I_r(t-1) + R_r(t) \le D(t), \\ D(t), & I_d(t-1) + R_d(t) > D(t). \end{cases} \tag{18}$$

4. The Block Diagram from Different Perspectives

Using the discrete system Z-transform theory, according to the difference equation in the previous chapter, the block diagram of each supply chain node can be drawn.

4.1. The Block Diagram of the Supply Chain

4.1.1. The Block Diagram of Supply Chain Nodes from the Local Decision Perspective. For retailers, the information input of the inventory system is customer demand, and the information output is order quantity. For the distribution center, the information input of the inventory system is customer demand, retailer's order quantity, and inventory in transit, and the output information is the replenishment quantity. The block diagrams of the retailer and the distribution center are shown in Figures 2 and 3, respectively.

Based on the perspective of local decision making, for the production-warehouse system, the production-warehouse system and the distribution center are regarded as a combined system, and retailer inventory is not taken into account. The block diagram of the production-warehouse system is shown in Figure 4.

4.1.2. The Block Diagram of Supply Chain Nodes from the Global Decision Perspective. Based on the perspective of global decision-making, for retailers and distribution centers, the operation process, information input, and output of the inventory system are unchanged, so the block diagram is the same as that based on the local decision-making perspective. For the production-inventory system, the inventory of the entire supply chain including the retailer's inventory is used as the basis for decision making, and the input information is customer demand, distribution center replenishment volume, distribution center inventory, and retailer inventory. The block

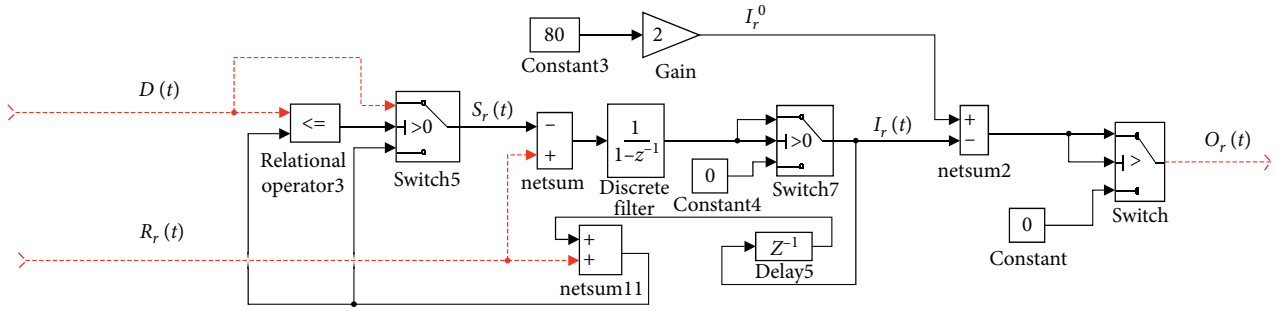

Figure 2: The block diagram of the retailer from the local decision perspective.

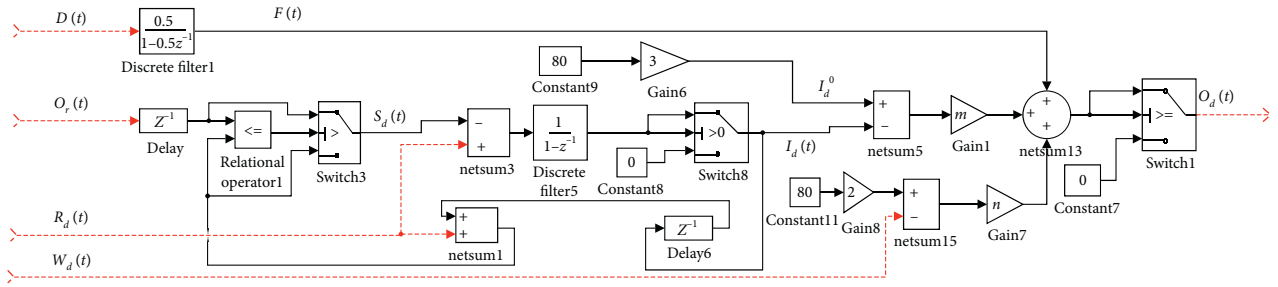

Figure 3: The block diagram of the distribution center from the local decision perspective.

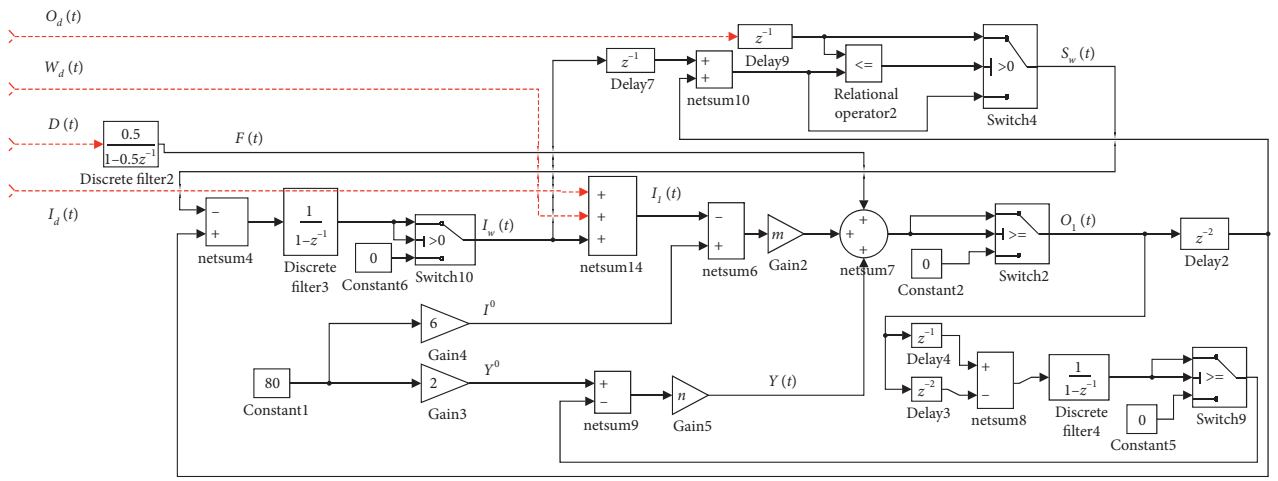

Figure 4: The block diagram of production and warehouse systems from the local decision perspective.

diagram of production and warehouse systems from the global decision perspective is shown in Figure 5.

4.2. The Block Diagram of the Whole Supply Chain. According to the models established above based on the local perspective and the global perspective, combined with the unitary transformation theory, the block diagrams of the system under the two models are shown in Figures 6 and 7.

5. System Simulation and Data Analysis

The largest Lyapunov exponent (LLE) is a standard to measure the stability of the system. Many studies use it to judge the stability of the system. When LLE is less than or equal to 0, it indicates that the system is in a stable, periodic, or quasiperiodic state. It is an ideal state for ordering decisions. When LLE is greater than 0, the system is in a chaotic or quasichaotic state. In the paper, the Wolf reconstruction method is used to calculate the largest Lyapunov exponent (LLE) value of each node or combined system to judge the stability of the system. The calculation principle of this method is as follows.

Suppose the time series is $X_1, X_2, \ldots, X_n$. Reconstruct the phase space and get $Y(t_i) = (X(t_i), X(t_{i+T}), \ldots, X(t_{i+(m-1)T}))$ $(i = 1, 2, \ldots, N)$, where m is the embedding dimension and T is the time delay. Take the initial point $Y(t_0)$, and let its distance from the nearest neighboring point $Y_0(t_0)$ be L_0. The time evolution of the two

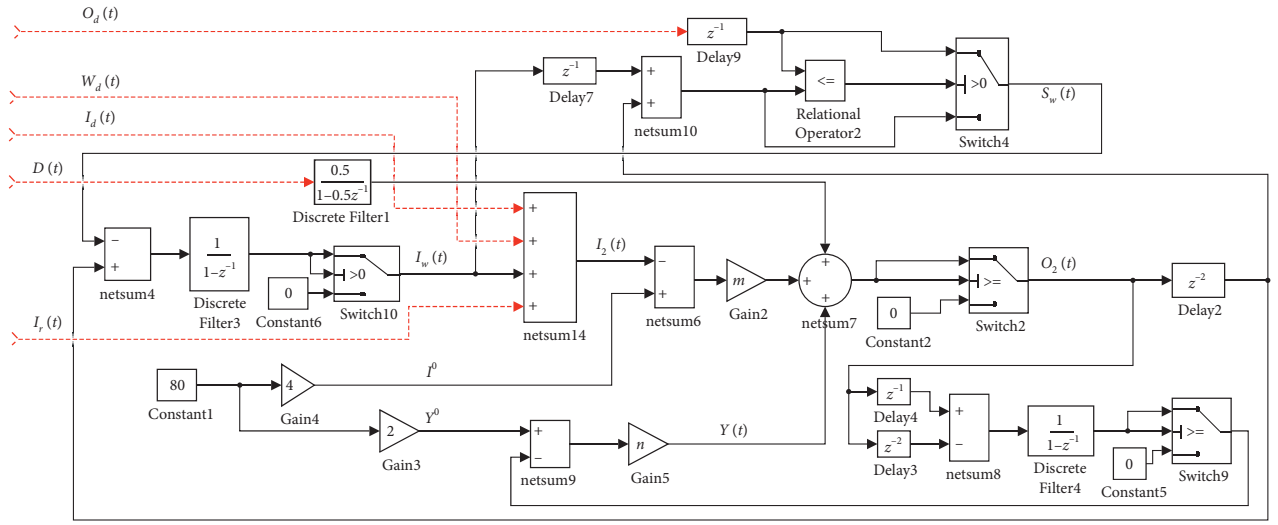

FIGURE 5: The block diagram of production and warehouse systems from the global decision perspective.

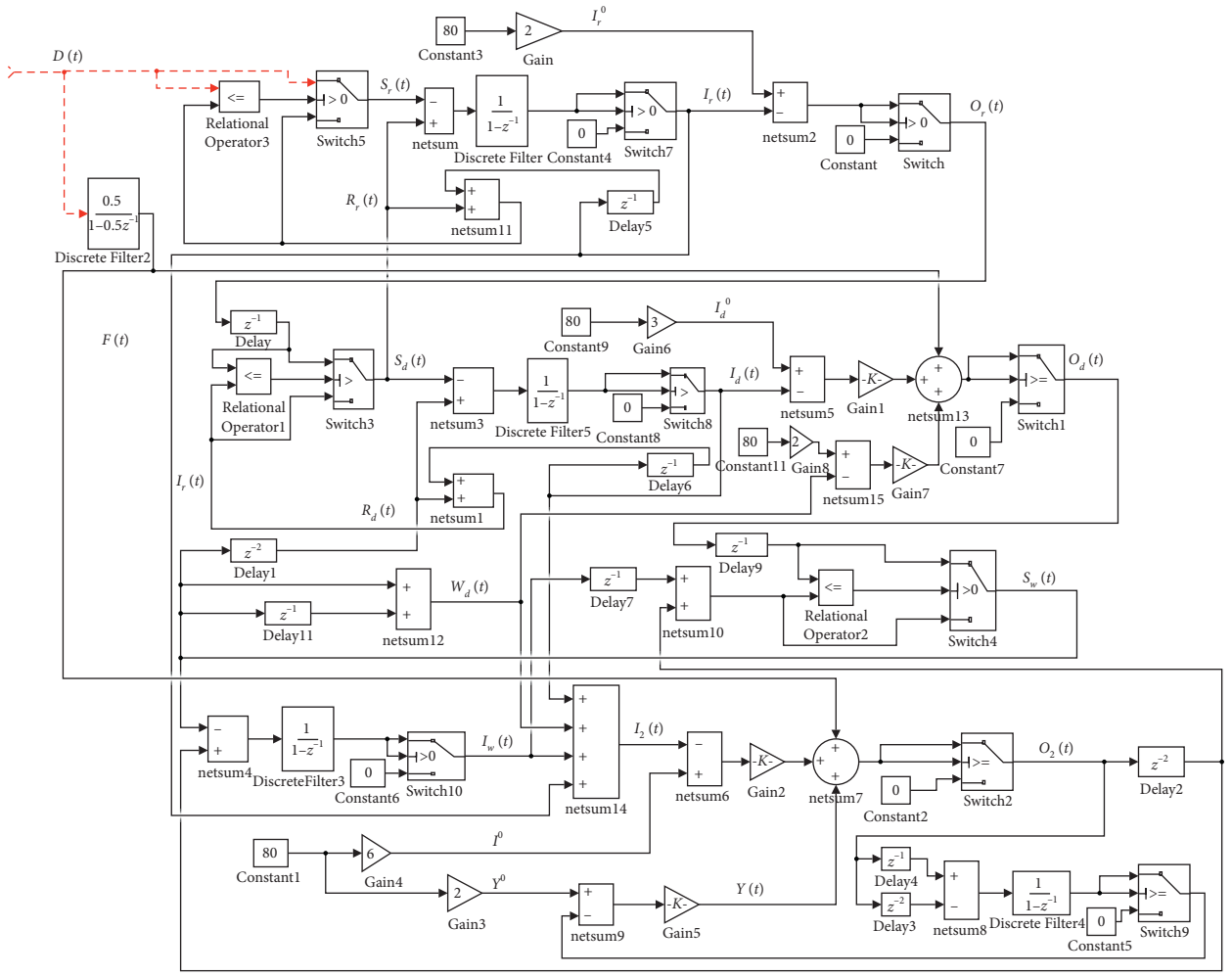

FIGURE 6: The block diagrams of the system under the global decision perspective.

points is traced until t_i, two points $Y(t_1)$ and $Y_0(t_1)$ are obtained, and the distance L_0^1 between them exceeds a specified value ε. Keep $Y(t_1)$ and find a point $Y_1(t_1)$ near it. The distance L_1 between the two points should be less than ε, and the angle formed should be as small as possible. The evolution process is continued until $Y(t)$ reaches the end N of the time

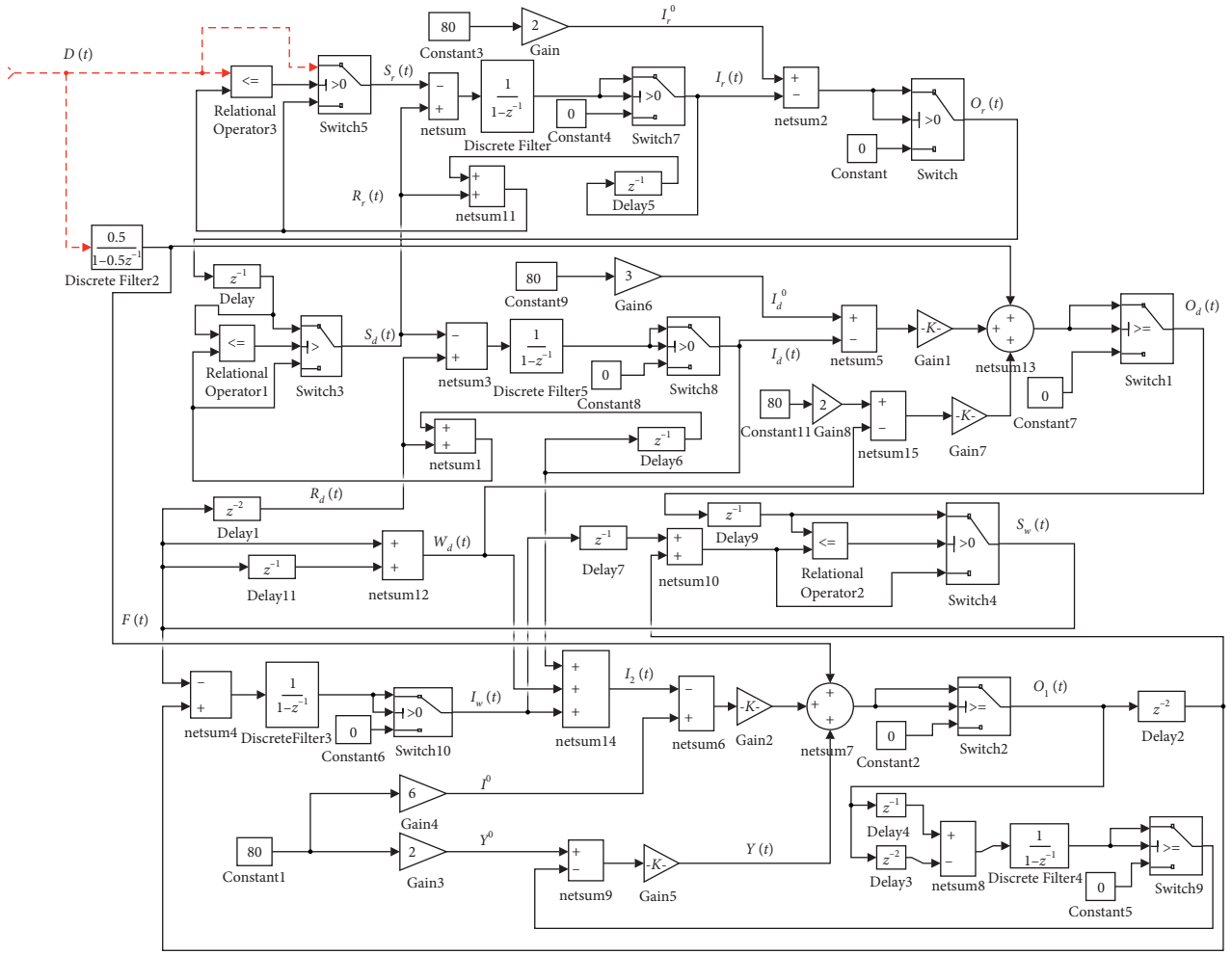

Figure 7: The block diagrams of the system under the local decision perspective.

series. The total number of iterations is M. The formula for calculating the LLE is as follows:

$$\lambda = \frac{1}{t_M - t_0} \sum_{i=0}^{M} \ln \frac{L_i^1}{L_i}. \tag{19}$$

5.1. Decision Parameters. Based on the constructed model and block diagrams, we plan to further study the impact of different ordering strategies and inventory management strategies on the nonlinear supply chain system with restrictions on the prohibition of returns and limited inventory from different perspectives. Previous studies have shown that relevant order decision parameters such as inventory adjustment parameters have an important impact on the dynamic characteristics of the system.

We designed a simulation experiment under various order parameter combinations in the decision space $[\alpha_S, \alpha_{SL}]$, and $[G_d, G_i]$. Then, using the simulation data, the LLE is calculated to analyze the impact of the different demand types, inventory adjustment coefficients, and safety inventory coefficients on system stability from different perspectives.

In general, the decision makers pay more attention to inventory adjustment, and the adjustment parameters are less than 1; this article assumes the value range of these two inventory adjustment coefficients is $0 < \alpha_{SL} \le \alpha_S$ to $0.02 \le \alpha_S \le 1$. Both α_S and α_{SL} have changed by 0.02 steps [2, 25]. And three combinations of safety stock factors $[G_d, G_i]$ are selected, including [1, 4], [2, 5], and [3, 6].

5.2. Simulation Analysis. According to the selection of the aforementioned decision parameter range, use Matlab to carry on the simulation experiment. Suppose that in this research supply chain, the production delay is 1, the transportation delay is 2, and the safety inventory coefficient of the retailer is 2. That is, $T_P = 2$, $T_C = 1$, and $G_r = 2$. At the same time, in order to ensure the effectiveness of the simulation experiment, the setting of the simulation period should not be too short. In this paper, the simulation period is set to 1000. If the period is calculated in days, then it is the amount of data for nearly 3 years. In the actual problem, to analyze the company's inventory system, the three-year operation data are completely sufficient.

This article combines practical issues and considers two demand scenarios including the random demand that meets the normal distribution and the random demand that meets the uniform distribution. Both of these demand scenarios

are more commonly used in real-world problems. The latter are more stringent and have higher requirements for supply chain response.

Firstly, based on a global perspective, under the scenario of random demand obeying normal distribution, we use the model shown in Figure 6 for simulation, calculate the index of each node of the supply chain according to the obtained data, and obtain the contour map under different combinations of safety stock factors, as shown in Figures 8–10.

By comparing and analyzing Figures 8–10, we can find that, based on the global decision perspective, with the increase of the safety stock factor, the decision area in the stable state for each node of the supply chain and the system under the perspective gradually increases. As can be seen from Figure 8, based on the global perspective for decision making, when $G_d = 1$ and $G_1 = 4$, under the scenario of random demand obeying normal distribution, the stability of the supply chain nodes under different inventory adjustment parameters is very different. Figure 8(a) shows that the LLE value of the retailer's inventory system is less than 0 in the entire decision area of adjustment coefficients. However, Figure 8(b) shows that the value of the LLE is greater than zero in most decision areas. Figure 8(c) shows that in most areas, the LLE value of the whole supply chain inventory is less than zero. That is to say, based on the perspective of global decision making, when $G_d = 1$ and $G_1 = 4$, under the scenario of random demand obeying normal distribution, the retailer inventory system can be in a stable state regardless of any value of adjustment parameters. Under the same conditions, the distribution center inventory system is in an unstable state in most decision-making areas. For the entire supply chain from the perspective of decision making, if the state of the item is not considered, only the quantity is considered, and the system is stable in most decision-making areas. The research on the system from the perspective of decision making is based on the total quantity of goods in the system, and the nodes where the goods are located in the system may be different, and the state may be different. So, there will be a phenomenon where the system is in a stable state and the nodes in it are in an unstable state. As can be seen from Figures 9 and 10, regardless of whether $G_d = 2$ and $G_1 = 5$ or $G_d = 3$ and $G_1 = 6$, for retailers, the values of LLE are all less than zero in the entire decision area.

In addition, based on the global decision perspective, under the setting of different demand scenarios and the combination of safety stock parameters, the LLE of each node and combination system under 1275 adjustment parameter combinations was calculated separately. It is found that, based on the perspective of global decision making, there are 374 adjustment parameter combinations that can keep each node and combination system of the supply chain in a stable state in the case of positive distribution demand and $G_d = 1$ and $G_1 = 4$. For the other two settings of safety stock parameters, there are 746 and 1109 different adjustment parameter decision schemes that can make the supply chain local and overall stable. At the same time, based on the calculation of the LLE for the entire decision area, we can find the adjustment coefficients that can keep the inventory system of each node of the supply chain and the entire supply chain inventory system in a stable state and the average value is the smallest. When $G_d = 1$ and $G_1 = 4$, $\alpha_S = 0.38$ and $\alpha_{SL} = 0.3$. When $G_d = 2$ and $G_1 = 5$, $\alpha_S = 0.24$ and $\alpha_{SL} = 0.14$. When $G_d = 3$ and $G_1 = 6$, $\alpha_S = 0.16$ and $\alpha_{SL} = 0.14$. Under different combinations of safety stock parameters, the number and optimal combination of adjustment parameter combinations that can keep the supply chain nodes and the combined system in a stable state are shown in Table 2.

Then, we change the demand scenario and perform simulation under the scenario of random demand obeying uniform distribution to obtain the contour map of each node under different combinations of safety stock coefficients, as shown in Figures 11–13.

As can be seen from Figures 11–13, under the scenario of random demand obeying uniform distribution, as the safety stock factor increases, the area where the LLE value of the entire supply chain inventory system and the inventory system of each node of the supply chain is less than zero gradually increases. The order of the area with the LLE value less than zero is the retailer, the whole supply chain, and the distribution center under certain safety stock factors. And it can be seen that for the distribution center and the entire supply chain, the area where the LLE value is less than zero exhibits a band distribution, which is immediately below $\alpha_{SL} = \alpha_S$. For retailer, in almost all regions, the LLE value is less than zero. However, the part with the smallest LLE value exhibits a dot-like and linear distribution, as shown in the dark parts of Figures 11(a), 12(a), and 13(a).

In addition, among the 1,275 kinds of adjustment parameter combinations, for different safety stock parameters, the number of parameter combinations that can keep each node of the supply chain and the combined system in a stable state is 146, 334, and 532 in order. Among these parameters, when $G_d = 1$ and $G_1 = 4$, if $\alpha_S = 0.18$ and $\alpha_{SL} = 0.06$, the LLE value of the inventory system of each node of the supply chain and the entire supply chain inventory system are less than zero and the average value is the smallest. Similarly, when $G_d = 2$ and $G_1 = 5$, $\alpha_S = 0.32$ and $\alpha_{SL} = 0.26$. When $G_d = 3$ and $G_1 = 6$, $\alpha_S = 0.24$ and $\alpha_{SL} = 0.22$. Under different combinations of safety stock parameters, the number and optimal combination of adjustment parameter combinations that can keep the supply chain nodes and the combined system in a stable state are shown in Table 3.

Based on the local perspective, under the scenario of random demand obeying normal distribution, using the model shown in Figure 7 for simulation, we can get the contour map of each supply chain node under different combinations of safety stock factors, as shown in Figures 14–16.

It can be seen from Figures 14–16 that based on a local perspective, under the scenario of random demand obeying normal distribution, as the safety stock factors increases, the area where the LLE value of the inventory system of the production-warehouse-distribution system and some node of the supply chain is less than zero gradually increases. Under certain safety stock factors, the regional distribution of the LLE value does not show obvious characteristics. Especially when $G_d = 2$ and $G_2 = 5$ and $G_d = 3$ and $G_2 = 6$, the distribution of the LLE value in the decision area shows

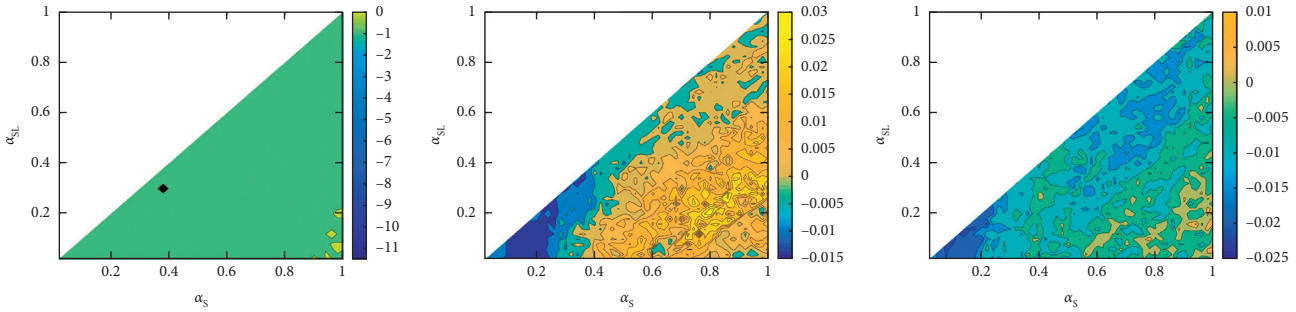

Figure 8: LLE diagram of supply chain nodes under the scenario of random demand obeying normal distribution from the global decision perspective when $G_d = 1$ and $G_2 = 4$. (a) The retailer's LLE chart. (b) The LLE chart of the distribution center. (c) The LLE chart of the combined system from the decision perspective.

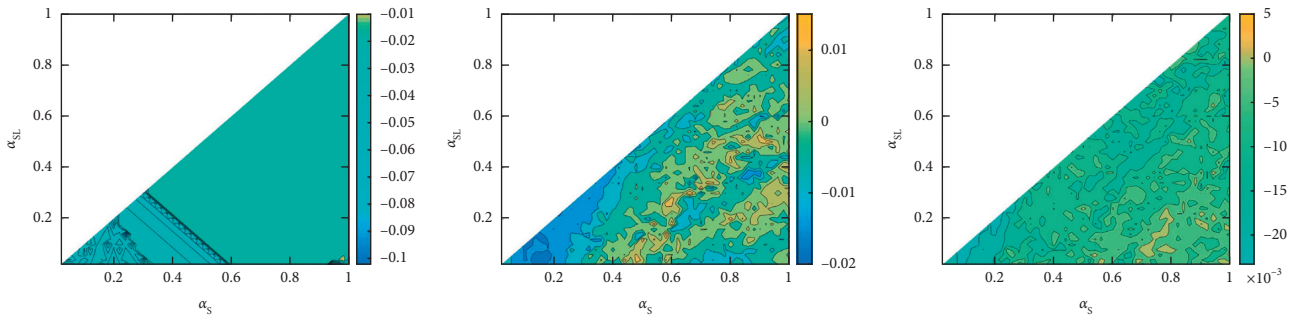

Figure 9: LLE diagram of supply chain nodes under the scenario of random demand obeying normal distribution from the global perspective when $G_d = 2$ and $G_2 = 5$. (a) The retailer's LLE chart. (b) The LLE chart of the distribution center. (c) The LLE chart of the combined system from the decision perspective.

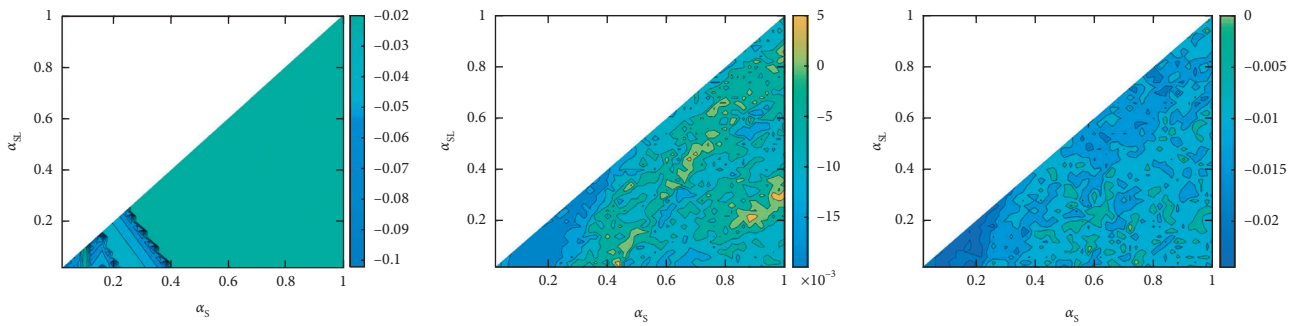

Figure 10: LLE diagram of supply chain nodes under the scenario of random demand obeying normal distribution from the global perspective when $G_d = 3$ and $G_2 = 6$. (a) The retailer's LLE chart. (b) The LLE chart of the distribution center. (c) The LLE chart of the combined system from the decision perspective.

Table 2: The number and optimal combination of reasonable adjustment parameter combinations under the scenario of random demand obeying normal distribution from the global decision perspective.

Combination of safety stock parameters $[G_d, G_i]$	Number of reasonable adjustment parameter combinations	Optimal combination $[\alpha_S, \alpha_{SL}]$
[1, 4]	374	[0.38, 0.3]
[2, 5]	746	[0.24, 0.14]
[3, 6]	1109	[0.16, 0.14]

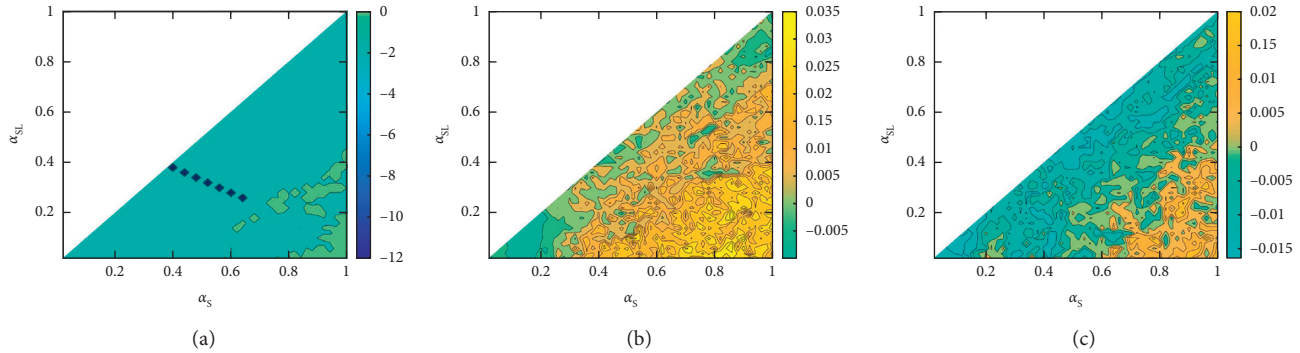

Figure 11: LLE diagram of supply chain nodes under the scenario of random demand obeying uniform distribution from the global perspective when $G_d = 1$ and $G_2 = 4$. (a) The retailer's LLE chart. (b) The LLE chart of the distribution center. (c) The LLE chart of the combined system from the decision perspective.

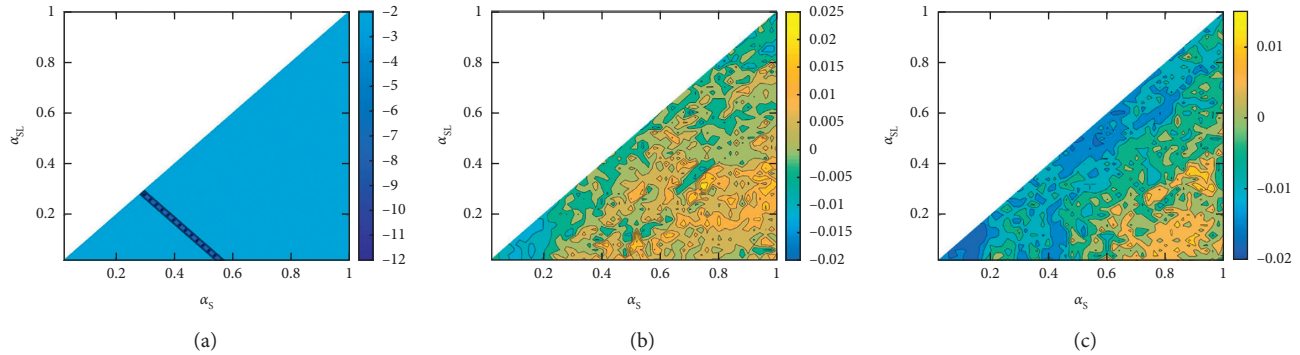

Figure 12: LLE diagram of supply chain nodes under the scenario of random demand obeying uniform distribution from the global perspective when $G_d = 2$ and $G_2 = 5$. (a) The retailer's LLE chart. (b) The LLE chart of the distribution center. (c) The LLE chart of the combined system from the decision perspective.

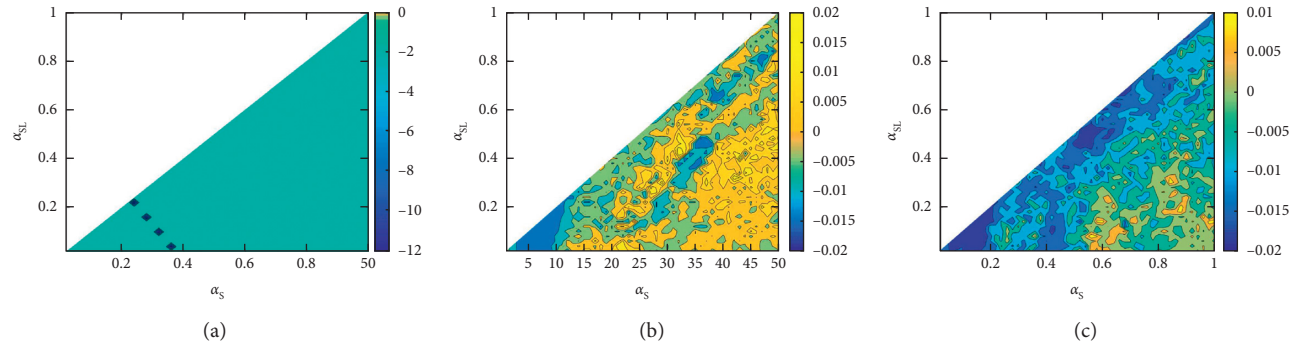

Figure 13: LLE diagram of supply chain nodes under the scenario of random demand obeying uniform distribution from the global perspective when $G_d = 3$ and $G_2 = 6$. (a) The retailer's LLE chart. (b) The LLE chart of the distribution center. (c) The LLE chart of the combined system from the decision perspective.

an irregular state. From Figure 14, it can be seen that from the local perspective, when $G_d = 1$ and $G_2 = 4$, for the retailer and the production-warehouse systems, the distribution of the larger part of the LLE value is relatively similar. The LLE value of distribution center is greater than zero in most decision-making areas. However, as can be seen from Figure 15, when $G_d = 2$ and $G_2 = 5$, there are decision parameters that can keep the retailer's inventory system in an unstable state.

In addition, based on the local decision perspective, under the scenario of random demand obeying normal distribution, for different safety stock parameters, there are different numbers of reasonable decision-making schemes in the entire decision-making area. When $G_d = 1$ and $G_2 = 4$, there are 380 reasonable adjustment parameter combinations. When $G_d = 2$ and $G_2 = 5$, there are 775 reasonable adjustment parameter combinations. When $G_d = 3$ and $G_2 = 6$, there are 1156 reasonable adjustment parameter

Table 3: The number and optimal combination of reasonable adjustment parameter combinations under the scenario of random demand obeying uniform distribution from the global perspective.

Combination of safety stock parameters $[G_d, G_i]$	Number of reasonable adjustment parameter combinations	Optimal combination $[\alpha_S, \alpha_{SL}]$
[1, 4]	146	[0.18, 0.06]
[2, 5]	334	[0.32, 0.26]
[3, 6]	532	[0.24, 0.22]

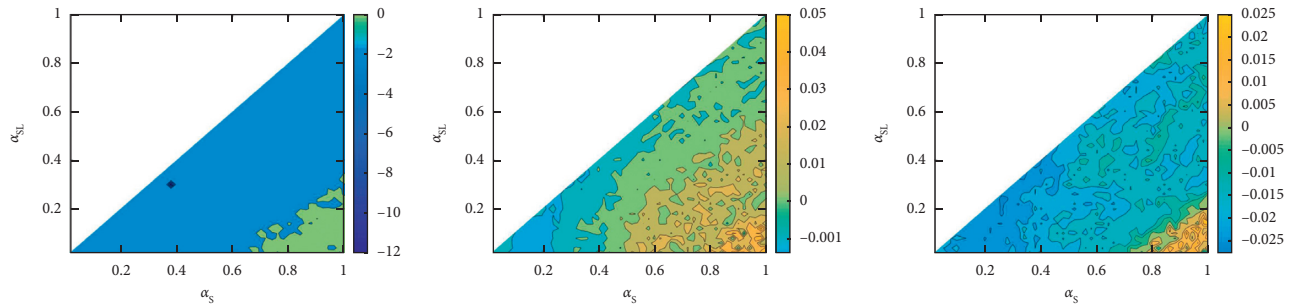

(a) (b) (c)

Figure 14: LLE diagram of supply chain nodes under the scenario of random demand obeying normal distribution from local perspective when $G_d = 1$ and $G_1 = 4$. (a) The retailer's LLE chart. (b) The LLE chart of the distribution center. (c) The LLE chart of the combined system from the decision perspective.

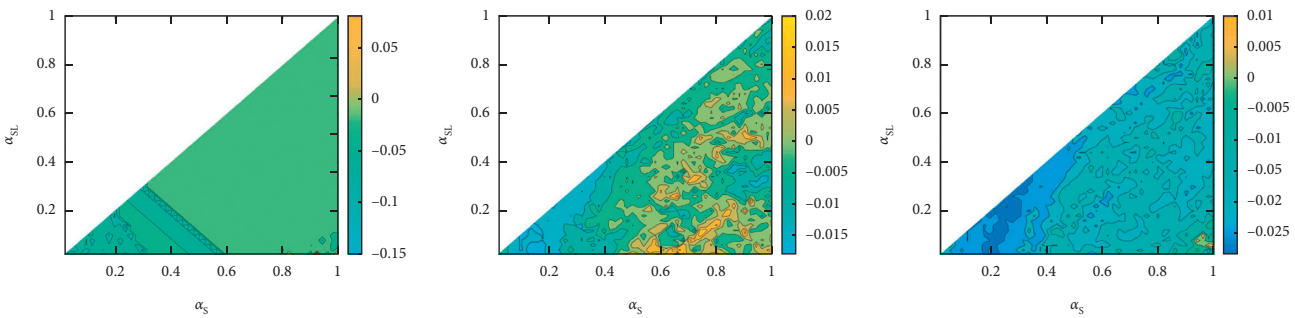

(a) (b) (c)

Figure 15: LLE diagram of supply chain nodes under the scenario of random demand obeying normal distribution from local perspective when $G_d = 2$ and $G_1 = 5$. (a) The retailer's LLE chart. (b) The LLE chart of the distribution center. (c) The LLE chart of the combined system from the decision perspective.

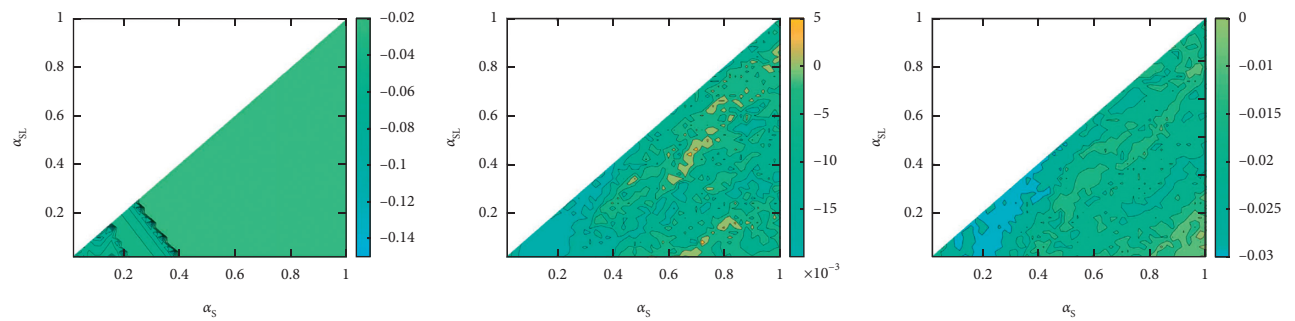

(a) (b) (c)

Figure 16: LLE diagram of supply chain nodes under the scenario of random demand obeying normal distribution from local perspective when $G_d = 3$ and $G_1 = 6$. (a) The retailer's LLE chart. (b) The LLE chart of the distribution center. (c) The LLE chart of the combined system from the decision perspective.

combinations. Among these parameter combinations that can stabilize the system, when $G_d = 1$ and $G_2 = 4$, if $\alpha_S = 0.38$ and $\alpha_{SL} = 0.3$, the LLE value of the inventory system of the production-warehouse-distribution system and each node of the supply chain are less than zero and the average value is the smallest. Similarly, when $G_d = 2$ and $G_2 = 5$, $\alpha_S = 0.18$ and $\alpha_{SL} = 0.06$. When $G_d = 3$ and $G_2 = 6$, $\alpha_S = 0.16$ and $\alpha_{SL} = 0.14$. Under different combinations of safety stock parameters, the number and optimal combination of adjustment parameter combinations that can keep the supply chain nodes and the combined system in a stable state are shown in Table 4.

Then, based on the local perspective, we change the demand scenario and perform simulation under the scenario of random demand obeying uniform distribution to obtain the contour map of each node under different combinations of safety stock coefficients, as shown in Figures 17–19.

As can be seen from Figures 17–19, under the scenario of random demand obeying uniform distribution, as the safety stock factor increases, the area where the LLE value of the inventory system of the production-warehouse-distribution system and each node of the supply chain is less than zero gradually increases. From Figure 17, it can be seen that for retailers, when $G_d = 1$ and $G_2 = 4$, the smallest part of the LLE value presents a point-line distribution. In the same decision area, no other nodes present this feature. It can be seen from Figures 18 and 19 that as the safety stock parameter increases, for retailers, the area distribution of the smaller part of the LLE value shifts to the lower left in the entire decision area.

In addition, for the three combinations of safety stock parameters considered, there are 174, 361, and 542 reasonable adjustment parameter combinations that can keep the supply chain nodes and combination system in a stable state. In these reasonable decisions, when $G_d = 1$ and $G_2 = 4$, if $\alpha_S = 0.2$ and $\alpha_{SL} = 0.12$, the LLE value of the inventory system of the production-warehouse-distribution system and each node of the supply chain are less than zero and the average value is the smallest. Similarly, when $G_d = 2$ and $G_1 = 5$, $\alpha_S = 0.16$ and $\alpha_{SL} = 0.14$. When $G_d = 3$ and $G_1 = 6$, $\alpha_S = 0.24$ and $\alpha_{SL} = 0.22$. Under different combinations of safety stock parameters, the number and optimal combination of adjustment parameter combinations that can keep the supply chain nodes and the combined system in a stable state are shown in Table 5.

According to the above analysis, it can be found that, on the whole, regardless of the local decision perspective or the global decision perspective, as the safety stock factors increase, the stability of each node of the supply chain gradually increases, and the requirements for adjustment parameters gradually decrease, that is, more adjusting parameters can keep the supply chain inventory system in a stable state. Regardless of the safety stock factors and the decision perspective, in the entire supply chain, the distribution center has the highest requirements for adjustment parameters, that is, the decision area of adjustment parameter where the distribution center is unstable is the largest. At the same time, based on the perspective of global decision making, a lower overall inventory of the supply chain can also keep the nodes in the supply chain and the system under the perspective of a stable state. At the same time, an interesting phenomenon can be found. When only considering the quantity of goods, when the system composed of multiple nodes is in a stable state, the nodes in it may be in an unstable state. This is also a manifestation of the complexity of the system's dynamic behavior.

Table 4: The number and optimal combination of reasonable adjustment parameter combinations under the scenario of random demand obeying normal distribution from local perspective.

Combination of safety stock parameters $[G_d, G_i]$	Number of reasonable adjustment parameter combinations	Optimal combination $[\alpha_S, \alpha_{SL}]$
[1, 4]	380	[0.38, 0.3]
[2, 5]	775	[0.18, 0.06]
[3, 6]	1156	[0.16, 0.14]

In order to more intuitively analyze the changes in inventory and the impact of demand types, adjustment parameters, and safety stock factors on the ability of each node of the supply chain and the system from different decision perspectives, a reasonable combination of adjustment parameters is selected for simulation experiments under different demand types and safety stock factors. This adjustment parameter combination can make the supply chain node and system in a stable state, and its average value is minimum.

In order to analyze the influence of different decision-making perspectives on the complex behavior of the supply chain, the inventory change chart of the nodes in the supply chain and the system under the perspective from the local perspective and the global perspective is drawn, as shown in Figures 20–25.

It can be seen from Figure 20 that under the scenario of random demand obeying normal distribution, when the retailer's inventory changes in a stable state, the performance of the retailer' inventory is basically the same under different decision-making perspectives. Inventory quickly increased from zero to safety stock level and then remained stable at 160. This is a very good change feature, which verifies the effectiveness of the simulation model. At the same time, for different safety stock parameters, the retailer's stock changes are basically the same when they are in a stable state. As shown in Figure 21, under the scenario of random demand obeying uniform distribution, when it is stable, the retailer's inventory changes are basically the same as in the scenario of random demand obeying normal distribution. It shows that reasonable parameter settings can keep the supply chain in a stable state when the demand fluctuates greatly.

It can be seen from Figures 22 and 23 that under the scenario of random demand obeying normal distribution, when it is in a stable state, for the same safety stock factor, whether it is based on a local decision perspective or a global decision perspective, the distribution center inventory changes are basically the same. When $G_d = 1$ and $G_2 = 4$, the distribution center inventory increases from zero to about 160 and then fluctuates around 160. When $G_d = 2$ and $G_2 = 5$, the inventory of the distribution center increases

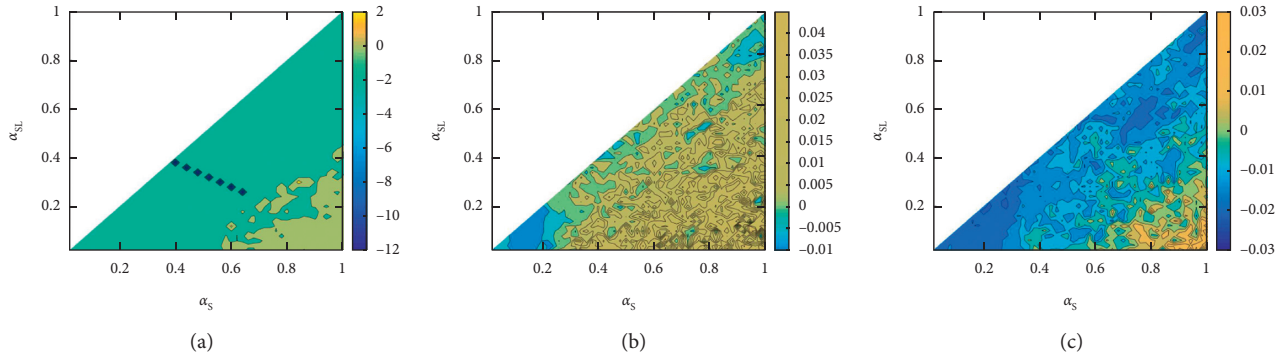

Figure 17: LLE diagram of supply chain nodes under the scenario of random demand obeying uniform distribution from local perspective when $G_d = 1$ and $G_1 = 4$. (a) The retailer's LLE chart. (b) The LLE chart of the distribution center. (c) The LLE chart of the combined system from the decision perspective.

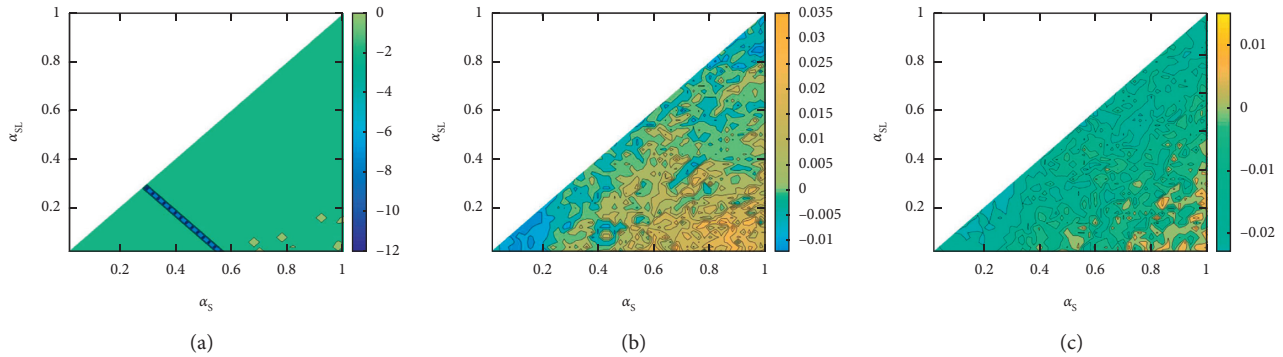

Figure 18: LLE diagram of supply chain nodes under the scenario of random demand obeying uniform distribution from local perspective when $G_d = 2$ and $G_1 = 5$. (a) The retailer's LLE chart. (b) The LLE chart of the distribution center. (c) The LLE chart of the combined system from the decision perspective.

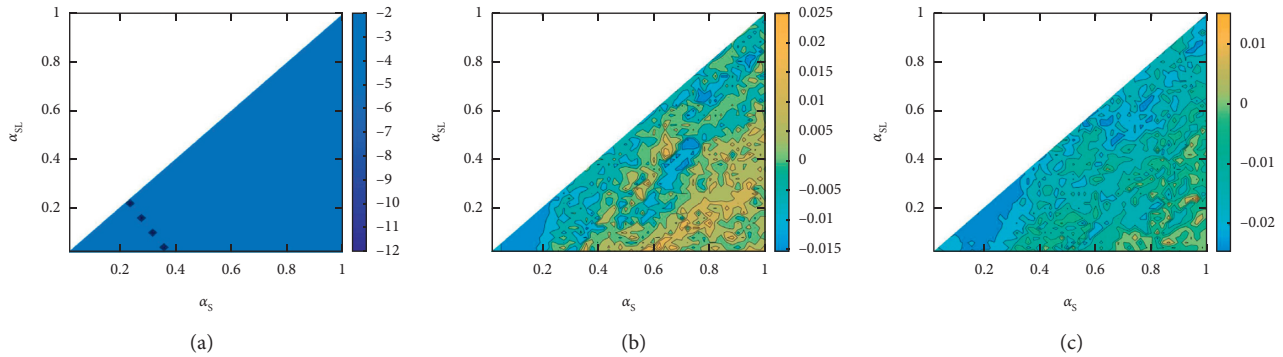

Figure 19: LLE diagram of supply chain nodes under the scenario of random demand obeying uniform distribution from local perspective when $G_d = 3$ and $G_1 = 6$. (a) The retailer's LLE chart. (b) The LLE chart of the distribution center. (c) The LLE chart of the combined system from the decision perspective.

from zero to about 240 and then fluctuates around 240. When $G_d = 3$ and $G_2 = 6$, the distribution center inventory increases from zero to about 320 and then fluctuates around 320. The fluctuation ranges under the three safety stock factor combinations are basically the same. As shown in Figure 23, under the scenario of random demand obeying uniform distribution, when in a stable state, the fluctuation range of the distribution center inventory change becomes significantly larger. It is verified that demand changes can

Table 5: The number and optimal combination of reasonable adjustment parameter combinations under the scenario of random demand obeying uniform distribution from local perspective.

Combination of safety stock parameters $[G_d, G_i]$	Number of reasonable adjustment parameter combinations	Optimal combination $[\alpha_S, \alpha_{SL}]$
[1, 4]	174	[0.2, 0.12]
[2, 5]	361	[0.16, 0.14]
[3, 6]	542	[0.24, 0.22]

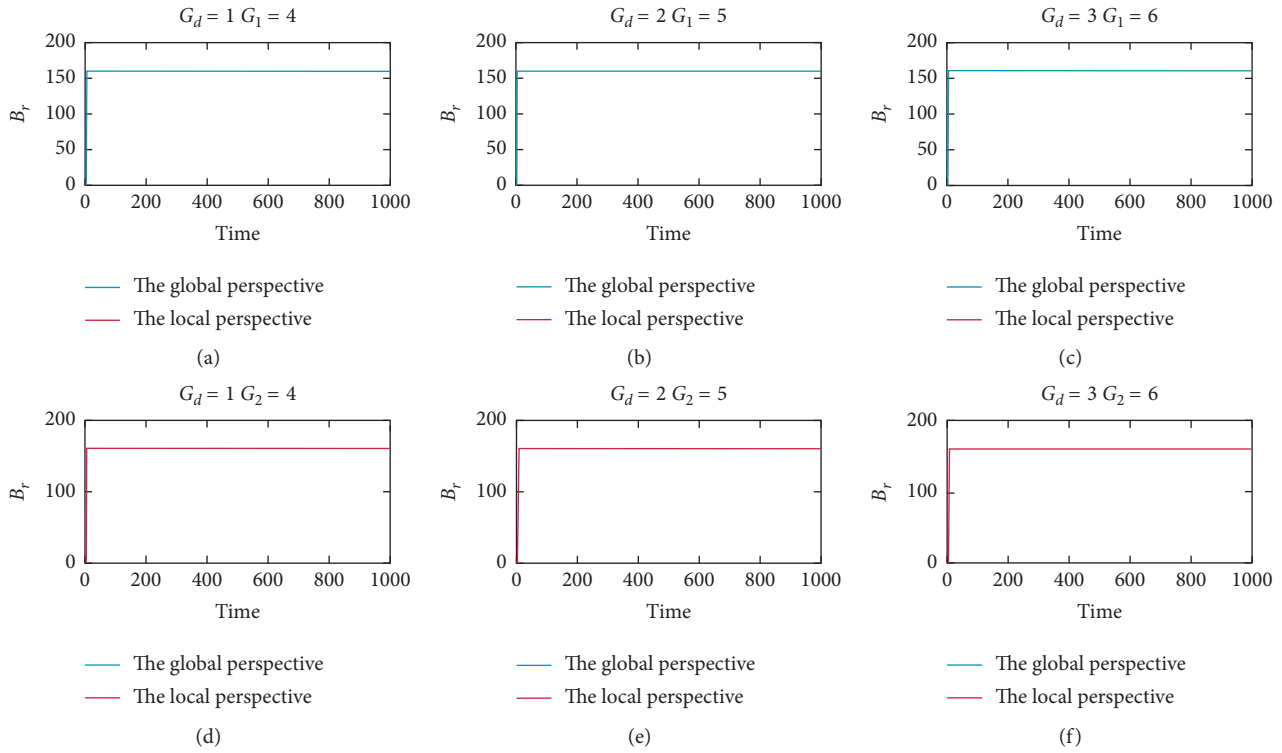

Figure 20: The initial inventory changes of the retailer in a stable state under the scenario of random demand obeying normal distribution from different perspectives.

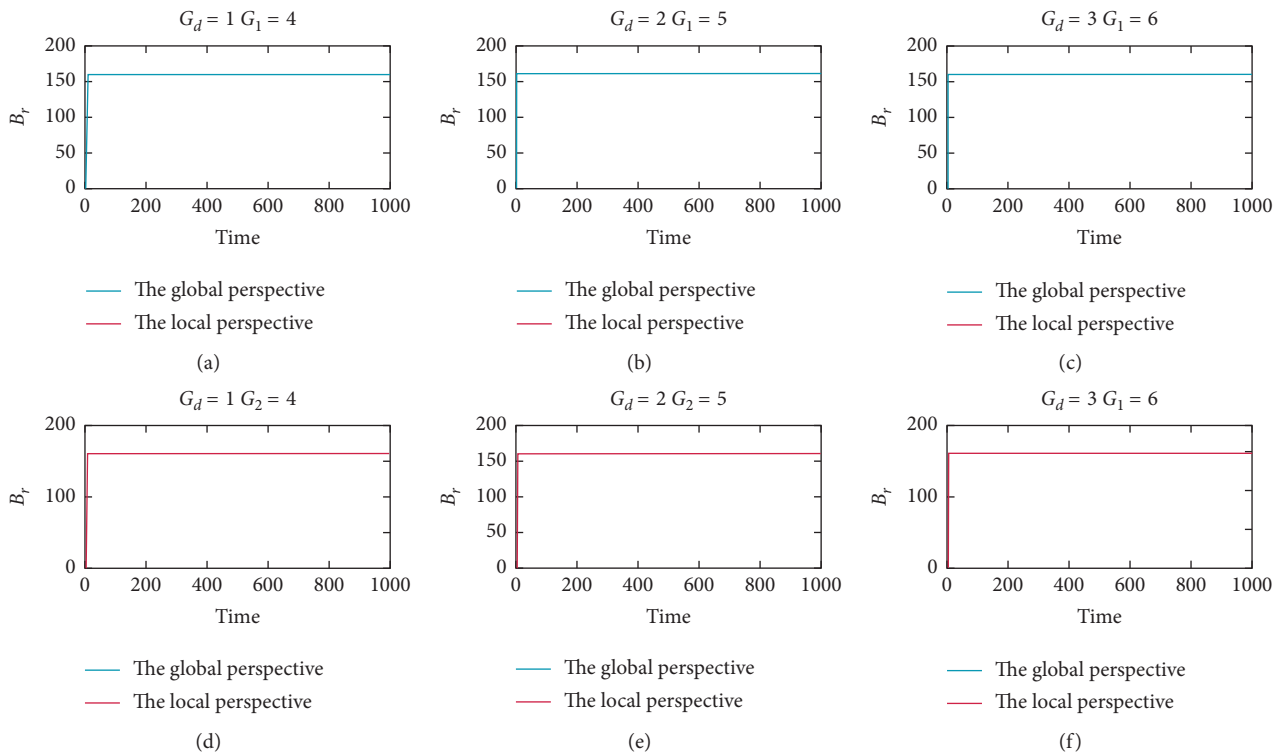

Figure 21: The initial inventory changes of the retailer in a stable state under the scenario of random demand obeying uniform distribution from different perspectives.

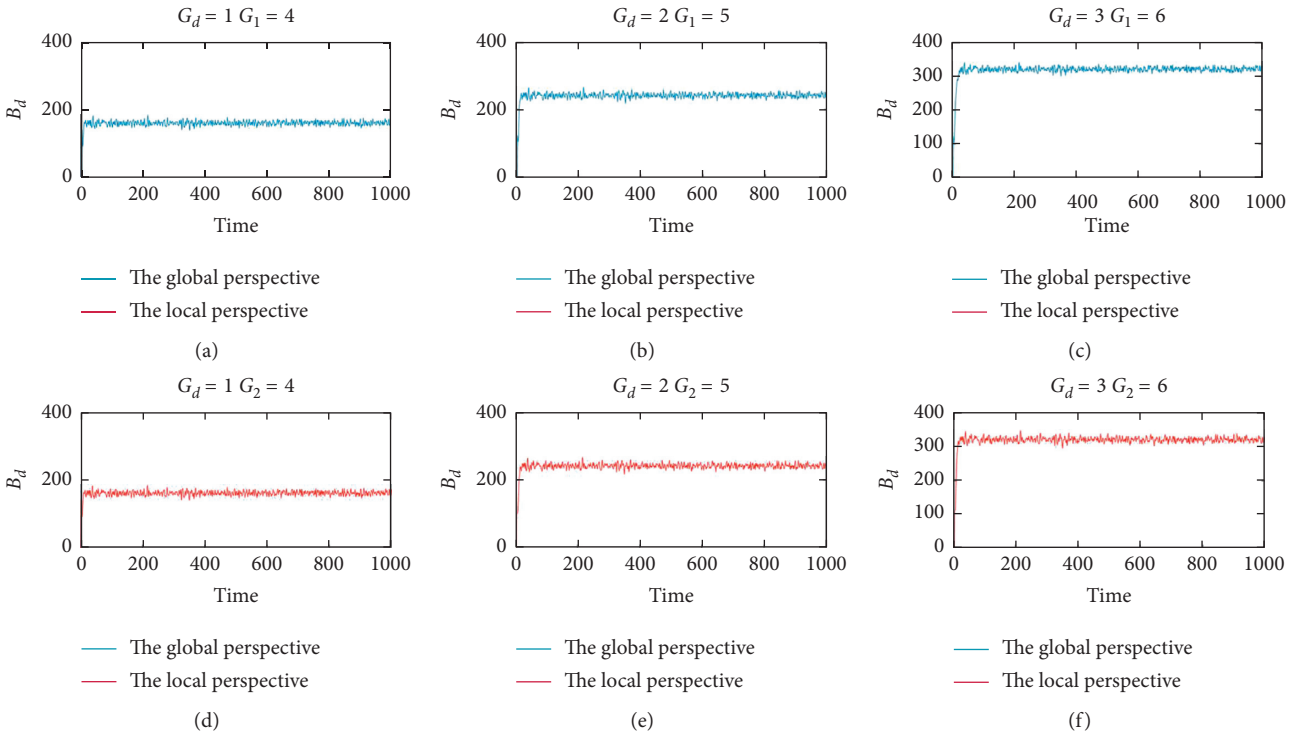

Figure 22: The initial inventory changes of the distribution center in a stable state under the scenario of random demand obeying normal distribution from different perspectives.

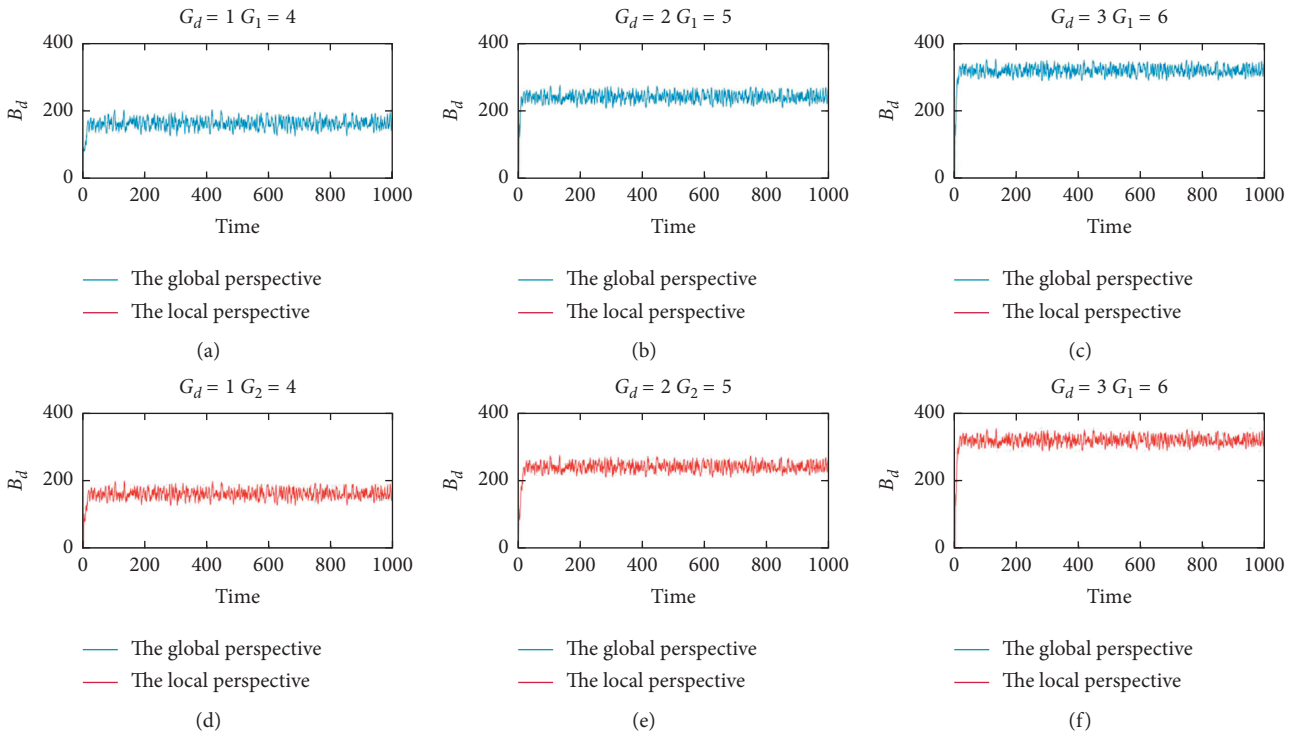

Figure 23: The initial inventory changes of the distribution center in a stable state under the scenario of random demand obeying uniform distribution from different perspectives.

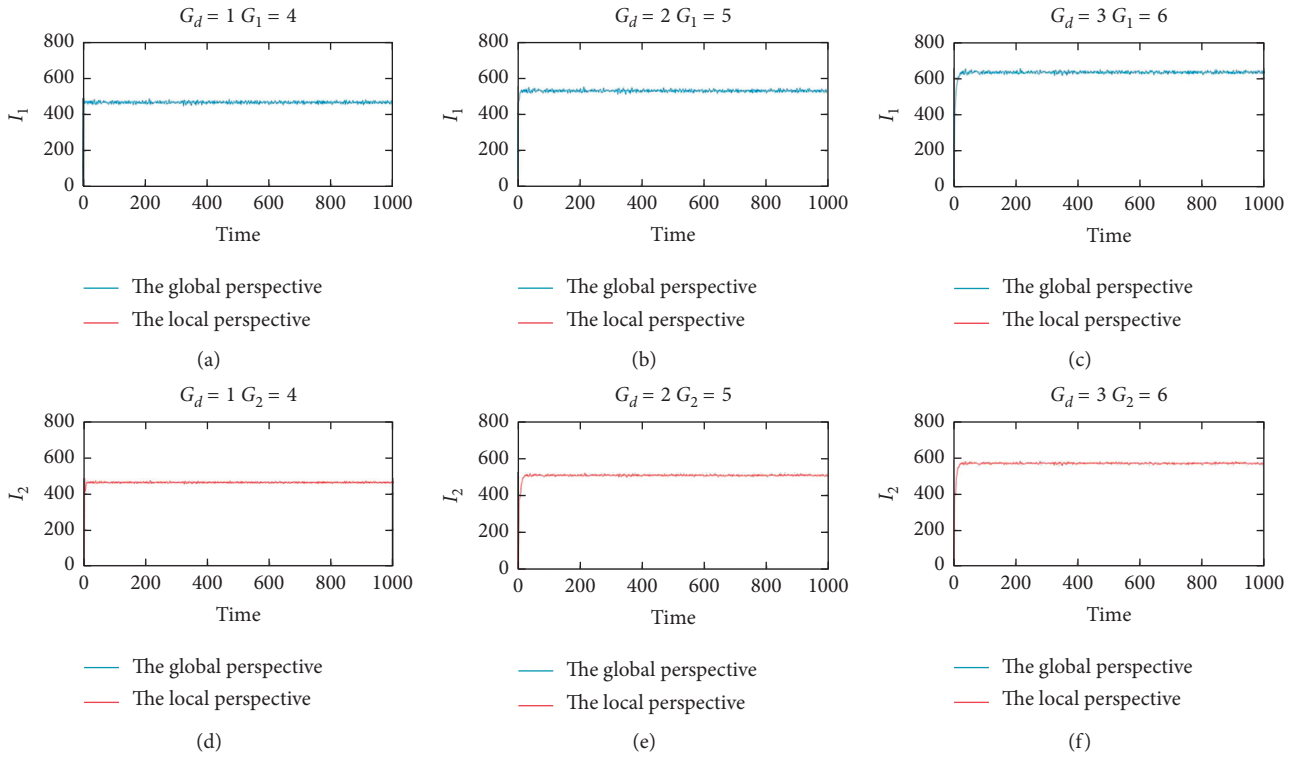

Figure 24: The initial inventory changes of the system from the perspective of decision under the scenario of random demand obeying normal distribution from different perspectives.

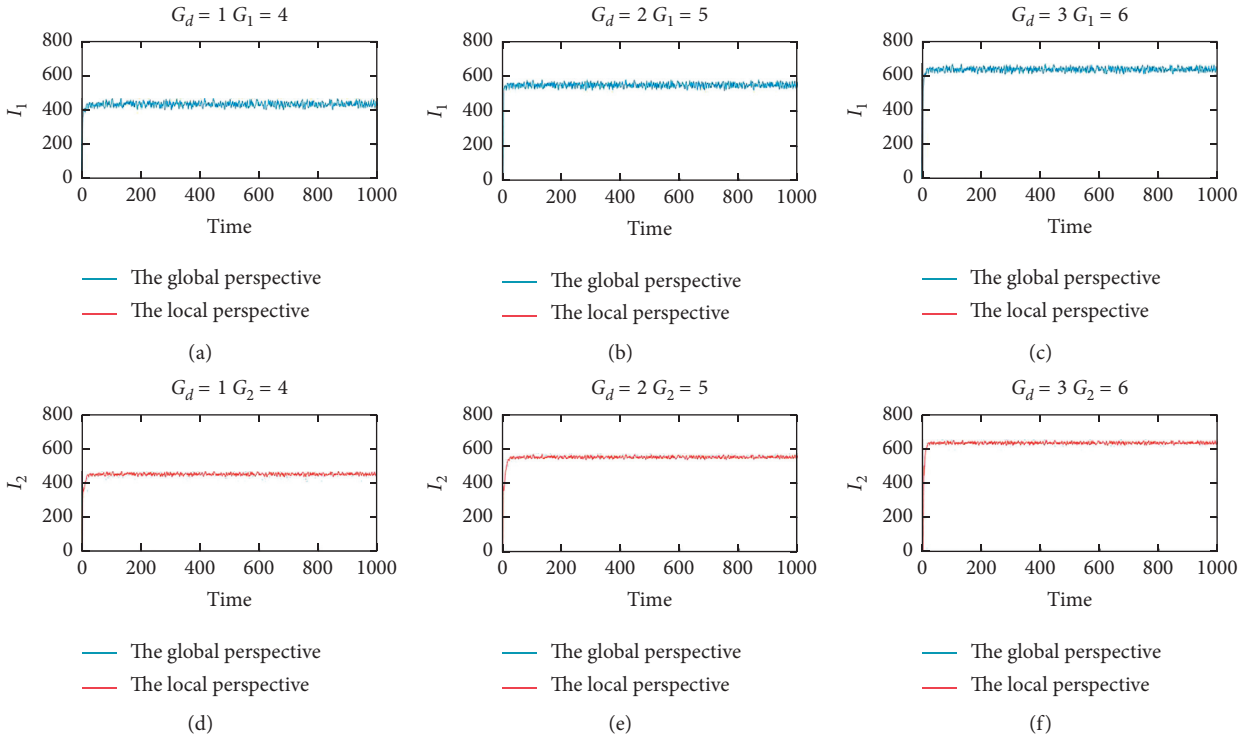

Figure 25: The initial inventory changes of the system from the perspective of decision under the scenario of random demand obeying uniform distribution from different perspectives.

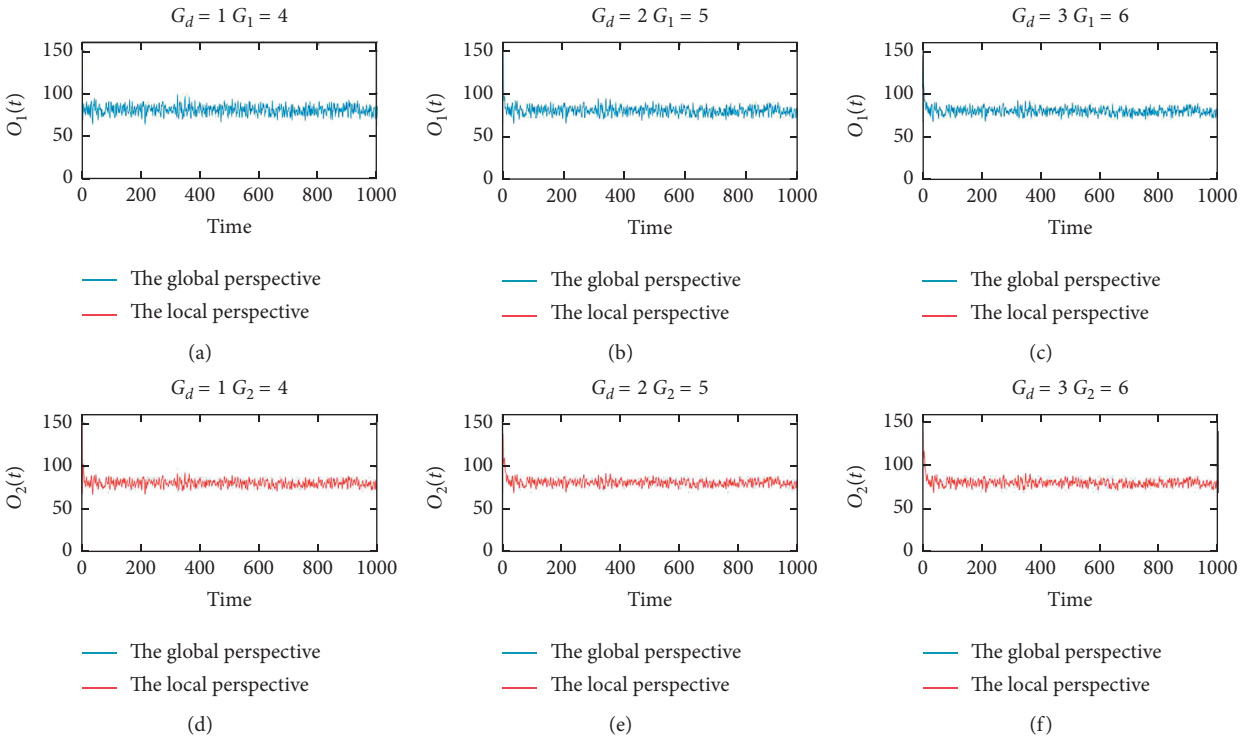

Figure 26: The production fluctuation under the scenario of random demand obeying normal distribution from different perspectives.

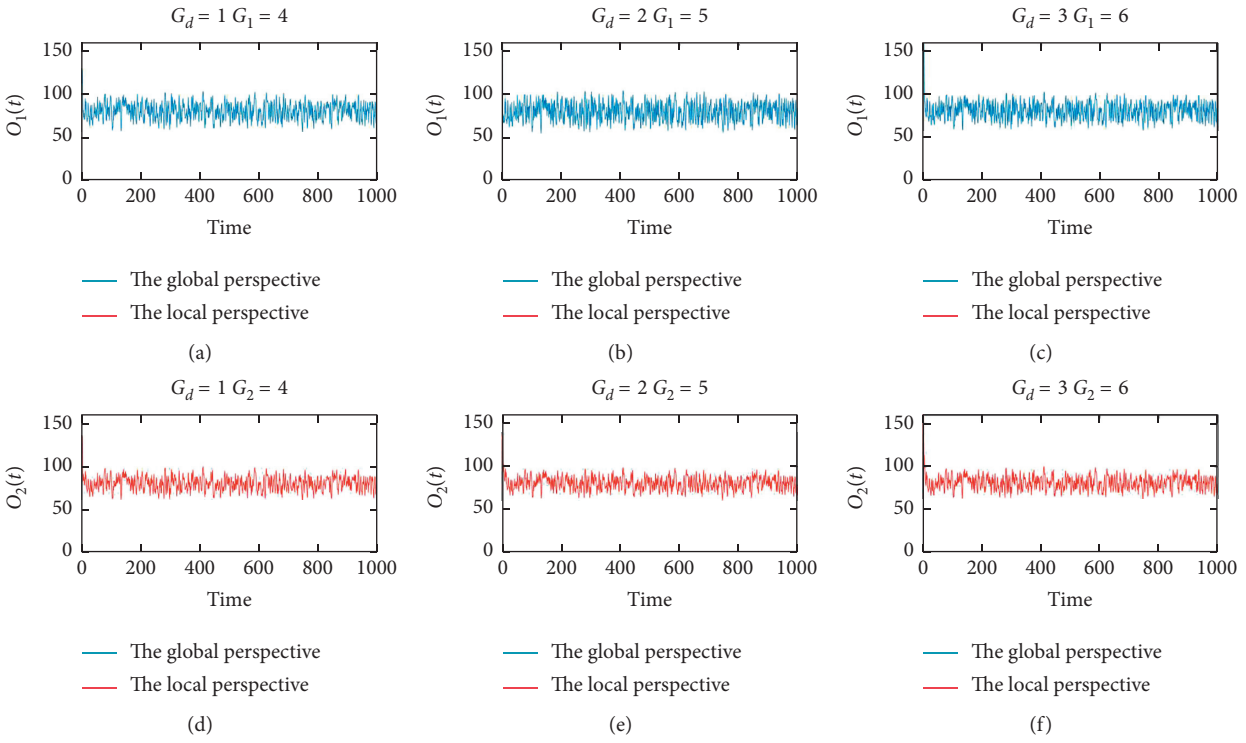

Figure 27: The production fluctuation under the scenario of random demand obeying uniform distribution from different perspectives.

have an impact on the dynamic behavior of supply chain systems. However, the inventory levels are basically equal in the two demand scenarios.

For the combined system under the decision perspective, regardless of the state of the goods, as can be seen from Figures 24 and 25, under specific demand scenarios and safety stock parameters, the combined system under different decision perspectives has a very similar inventory change at steady state. At the same time, it was found that for the distribution center and the combined system, when it is in a stable state, the inventory level in the scenario of random demand obeying normal distribution is lower than the inventory level in the scenario of random demand obeying uniform distribution. As can be seen from Figure 24, under the scenario of random demand obeying normal distribution, when the safety stock parameter combination is [1, 4], based on the global decision perspective, when the supply chain system is in a stable state, the overall stock level is about 460. Under the same demand scenario and safety stock parameter combination, based on the perspective of local decision making, the combined system inventory level under the perspective is 460. In other words, the entire supply chain system does not include the retailer, and the inventory of other parts has reached 460. Similarly, when the safety stock parameter combination is [2, 5], the overall stock level is about 520 based on the global decision perspective. Based on the local decision perspective, the combined system inventory level under the perspective is about 505. When the safety stock parameter combination is [3, 6], the overall stock level is about 627 based on the global decision perspective. Based on the local decision perspective, the combined system inventory level under the perspective is about 567.

Under the scenario of random demand obeying uniform distribution, when the supply chain system is in a stable state, Figure 25 shows the inventory level and fluctuation status under different safety stock parameter combinations and decision perspectives. When the safety stock parameter combination is [1, 4], the overall stock level is about 425 based on the global decision perspective. Based on the local decision-making perspective, the combined system inventory level under the perspective is 446. When the safety stock parameter combination is [2, 5], the overall stock level is about 547 based on the global decision perspective. Based on the local decision perspective, the combined system inventory level under the perspective is about 505. When the safety stock parameter combination is [3, 6], based on the global decision perspective, the overall stock level is about 632. Based on the local decision perspective, the inventory level of the combined system under the perspective is about 631. Therefore, for any combination of safety inventory parameters and any demand scenarios, based on a global decision perspective, choosing a reasonable adjustment parameter scheme can reduce the overall inventory level of the supply chain. The overall inventory volatility has increased slightly, but it does not affect the stability of the overall inventory.

In the supply chain, the stability of production has a great influence on the cost, and the production system produces according to the order quantity of the warehouse. In order to analyze the fluctuation of production in a stable state more intuitively, we draw the production fluctuation chart, as shown in Figures 26 and 27.

As can be seen from Figures 26 and 27, under steady conditions, the volatility of production appears to be stable at the desired level of demand, with slight fluctuations. Compared with demand, it is found that the volatility of production is basically the same as the fluctuation of demand, and the fluctuation of production is smaller than that of demand. It shows that the system can smoothen the change of demand very well.

6. Conclusion

Based on the needs of practical problems, this paper introduces the global decision-making thoughts in order to adapt to the trend of supply chain integration and puts forward different decision-making perspectives of supply chain inventory system management. Based on the proposed local decision perspective and global decision perspective, the complex dynamic behavior of the supply chain inventory system is studied. At the same time, the influence of the safety inventory setting on the dynamic behavior of the supply chain inventory system is studied.

The study found that, based on the perspective of global decision making, choosing a reasonable adjustment parameter scheme can reduce the overall inventory level of the supply chain. The overall inventory volatility has increased slightly, but it does not affect the stability of the overall inventory. When the safety stock parameter combination is [1, 4], based on the global decision perspective, the overall stock level is about 425. Based on the local decision-making perspective, the combined system inventory level under the perspective is 446. Based on a global decision perspective, the overall inventory can be reduced by about 180. When the safety stock parameter combination is [2, 5], the overall stock can be reduced by about 118. When the safety stock parameter combination is [3, 6], the overall stock can be reduced by about 159. At the same time, based on different decision-making perspectives, the status distribution maps of each node or combination system under different demand scenarios and the most reasonable parameter settings are obtained.

On the whole, regardless of the local decision perspective or the global decision perspective, as the safety stock parameters increase, the stability of each node of the supply chain gradually increases, and the requirements for adjustment parameters gradually decrease. The analysis also found that each node has a different sensitivity to the adjustment parameters. Changes in adjustment parameters have little effect on the retailer. Under different scenarios and decision parameters, the retailer is in a stable state in almost the entire decision area. However, changes in adjustment parameters have a significant impact on the distribution center. In addition, the study also found that, whether based on a local decision perspective or a global decision perspective, the overall inventory level is in a stable

state and maybe in an unstable state for internal nodes. This has important guiding significance for actual operation.

Although this paper selects three safety stock parameter combinations for research and obtains some effective conclusions, it does not study the entire safety stock parameter decision area. In the follow-up, we hope that interested scholars will conduct further research on the impact mechanism of safety stock parameters on the complex dynamic behavior of the supply chain.

Data Availability

The data used are the data obtained by simulation.

Conflicts of Interest

The authors declare that they have no conflicts of interest.

Acknowledgments

This study was supported by the National Key Research and Development Program of China (grant no. 2019YFB1706101) and Chongqing Technology Innovation and Application Demonstration Project (grant no. cstc2018jszx-cyzdX0143).

References

[1] A. R. Nia, M. H. Far, and S. T. A. Niaki, "A fuzzy vendor managed inventory of multi-item economic order quantity model under shortage: an ant colony optimization algorithm," *International Journal of Production Economics*, vol. 155, pp. 259–271, 2014.

[2] Z. Zhang, Xu Wang, Q. Guo, Z. Li, and Y. Wu, "Simulation and analysis of the complex behavior of supply chain inventory system based on third-party logistics management inventory model with no accumulating of unsatisfid demand," *Complexity*, vol. 2019, Article ID 3194093, 18 pages, 2019.

[3] H. L. Lee, V. Padmanabhan, and S. Whang, "Bullwhip effect in a supply chain," *Sloan Management Review*, vol. 38, pp. 93–102, 1997.

[4] K. P. Lin, P.-T. Chang, K.-C. Hung, and P.-F. Pai, "A simulation of vendor managed inventory dynamics using fuzzy arithmetic operations with genetic algorithms," *Expert Systems with Applications*, vol. 37, no. 3, pp. 2571–2579, 2010.

[5] J. W. Forrester, *Industrial Dynamics*, MIT Press, Cambridge, MA, USA, 1961.

[6] D. R. Towill, "Dynamic analysis of an inventory and order based production control system," *International Journal of Production Research*, vol. 20, no. 6, pp. 71–687, 1982.

[7] S. M. Disney, M. M. Naim, and D. R. Towill, "Development of a fitness measure for an inventory and production control system," in *Proceedings of the 2nd International Conference on Genetic Algorithms in Engineering Systems: Innovations and Applications*, Glasgow, UK, 1997.

[8] S. M. Disney, M. M. Naim, and D. R. Towill, "Genetic algorithm optimisation of a class of inventory control systems," *International Journal of Production Economics*, vol. 68, no. 3, pp. 259–278, 2000.

[9] S. M. Disney and D. R. Towill, "A discrete transfer function model to determine the dynamic stability of a vendor managed inventory supply chain," *International Journal of Production Research*, vol. 40, no. 1, pp. 179–204, 2002.

[10] J. Dejonckheere, S. M. Disney, M. R. Lambrecht, and D. R. Towill, "Measuring and avoiding the bullwhip effect: a control theoretic approach," *European Journal of Operational Research*, vol. 147, no. 3, pp. 567–590, 2003.

[11] P. Lin and D. S.-H. Wong, "Controller design and reduction of bullwhip for a model supply chain system using z-transform analysis," *Journal of Process Control*, vol. 14, pp. 487–499, 2004.

[12] T. Nagatani and D. Helbing, "Stability analysis and stabilization strategies for linear supply chains," *Physica A: Statistical Mechanics and Its Applications*, vol. 335, no. 3-4, pp. 644–660, 2004.

[13] S. M. Disney, "Supply chain aperiodicity, bullwhip and stability analysis with Jury's inners," *IMA Journal of Management Mathematics*, vol. 19, no. 2, pp. 101–116, 2008.

[14] E. Mosekilde and J. L. Laugesen, "Nonlinear dynamic phenomena in the beer model," *System Dynamics Review*, vol. 23, no. 2-3, pp. 229–252, 2007.

[15] X. Wang, S. M. Disney, and J. Wang, "Stability analysis of constrained inventory systems with transportation delay," *European Journal of Operational Research*, vol. 223, no. 1, pp. 86–95, 2012.

[16] C. A. Garcia, A. Ibeas, and R. Vilanova, "A switched control strategy for inventory control of the supply chain," *Journal of Process Control*, vol. 23, no. 6, pp. 868–880, 2013.

[17] X. Wang, S. M. Disney, and J. Wang, "Exploring the oscillatory dynamics of a forbidden returns inventory system," *International Journal of Production Economics*, vol. 147, pp. 3–12, 2014.

[18] J. Ma and F. Si, "Complex dynamics of a continuous bertrand duopoly game model with two-stage delay," *Entropy*, vol. 18, no. 7, p. 266, 2016.

[19] F. Si and J. Ma, "Complex dynamics in a triopoly game with multiple delays in the competition of green product level," *International Journal of Bifurcation and Chaos*, vol. 28, no. 2, Article ID 1850027, 2018.

[20] X. Zhan, Q. Zhang, and W. F. Xie, "Dynamic performance and stability research of VMI-APIOBPCS in apparel industry based on control theory," *International Journal of Enterprise Information Systems*, vol. 14, no. 2, pp. 56–76, 2018.

[21] M. Z. Jin and L. J. Song, "Simulation analysis of production decision optimization of supply chain system based on nonlinear system and fractional differential operator," *CHAOS*, vol. 29, no. 1, Article ID 013129, 2019.

[22] J. Lin and M. M. Naim, "Why do nonlinearities matter? The repercussions of linear assumptions on the dynamic behaviour of assemble-to-order systems," *International Journal of Production Research*, vol. 57, p. 6824, 2019.

[23] X. Xu and S. D. Lee, "Management and optimization of chaotic supply chain system using adaptive sliding mode control algorithm," *International Journal of Production Research*, 2020.

[24] S. John, M. M. Naim, and D. R. Towill, "Dynamic analysis of a WIP compensated decision support system," *International Journal of Manufacturing System Design*, vol. 1, no. 4, pp. 283–297, 1994.

[25] Z. Li and G. Yan, "Analysis of complex dynamics behaviors in constrained supply chain system under uncertain demand process," *Control and Decision*, vol. 31, no. 1, pp. 173–179, 2016.

Hindawi
Complexity
Volume 2020, Article ID 5191085, 16 pages
https://doi.org/10.1155/2020/5191085

Research Article

Control of Coexisting Attractors with Preselection of the Survived Attractor in Multistable Chua's System: A Case Study

Zeric Tabekoueng Njitacke,[1,2] **Theophile Fonzin Fozin**,[3,4] **Christian Tchito Tchapga**,[1] **Gervais Dolvis Leutcho**,[2,5] **K. Marcel Wouapi**,[6] **and Jacques Kengne**[2]

[1]*Department of Electrical and Electronic Engineering, College of Technology (COT), University of Buea, P.O. Box 63, Buea, Cameroon*
[2]*Research Unit of Automation and Applied Computer (URAIA), Electrical Engineering Department of IUT-FV, University of Dschang, P.O. Box 134, Bandjoun, Cameroon*
[3]*Department of Research, Development, Innovation and Training, Inchtech's, Yaoundé, Cameroon*
[4]*Department of Electrical and Electronic Engineering, Faculty of Engineering and Technology (FET), University of Buea, P.O. Box 63, Buea, Cameroon*
[5]*Department of Physics, Faculty of Sciences, University of Mons, P.O. Box 7000, Mons, Belgium*
[6]*Research Unit of Condensed Matter, Electronics and Signal Processing (UR-MACETS) Department of Physics, Faculty of Sciences, University of Dschang, P.O. Box 67, Dschang, Cameroon*

Correspondence should be addressed to Zeric Tabekoueng Njitacke; zerictabekoueng@yahoo.fr

Received 26 May 2020; Revised 23 August 2020; Accepted 30 August 2020; Published 29 September 2020

Academic Editor: Carlos-Arturo Loredo-Villalobos

Copyright © 2020 Zeric Tabekoueng Njitacke et al. This is an open access article distributed under the Creative Commons Attribution License, which permits unrestricted use, distribution, and reproduction in any medium, provided the original work is properly cited.

Although the control of multistability has already been reported, the one with preselection of the desired attractor is still uncovered in systems with more than two coexisting attractors. This work reports the control of coexisting attractors with preselection of the survived attractors in paradigmatic Chua's system with smooth cubic nonlinearity. Techniques of linear augmentation combined to system invariant parameters like equilibrium points are used to choose the desired surviving attractors among the coexisting ones. Nonlinear dynamical tools including bifurcation diagrams, standard Lyapunov exponents, phase portraits, and cross section of initial conditions are exploited to reveal the selection scenarios of the survived attractor in the multistability control process of Chua's system. The main crisis towards annihilation of multistability in Chua's system when varying the coupling strength is interior crisis and border collision. Theoretical and numerical results obtained are further validated with PSpice analysis.

1. Introduction

In the study of nonlinear dynamic systems, the simultaneous existence of attractors (finite or infinite), also known as multistability [1–13], extreme multistability [14–16], or megastability [17], is now in the forefront. Recall that the famous Chua's circuit is among the widely studied electronic circuits capable to display chaos [18]. When Professor Leon Chua introduced that circuit, it was intentionally built in such a way that three equilibria of the model were unstable. Based on the local stability of each point, the circuit was able to exhibit a double-scroll chaotic attractor [18]. During the investigation of this oscillator, the main challenge was to design the nonlinear part called Chua's diode. Using op-amps [19], diodes [20], transistors [21], current feedback op-amps [22], and inductor free CNN (cellular neural network) cells [23], many experimental results were reported on the realization of Chua's diode. Finally, by exploiting two-stage op-amp-based negative impedance converters (NICs) in parallel, a usual implementation of Chua's diode was proposed and accepted as a standard [19]. Also in [24], Bao and collaborators, during their investigation, found that, with an unstable zero saddle point and two symmetric stable non-zero node-foci, improved Chua's circuit can also generate a

self-excited chaotic attractor. Very recently, exponential sampled-data control for T-S fuzzy systems with application to Chua's circuit has been explored [25]. Of particular interest, Chua had also presented the ability to display the coexistence of multiple attractors for the same set of system parameters but using different initial conditions [24]. This coexistence of attractors is sometimes undesirable and needs to be avoided; hence, the investigation was carried out in this work.

Remark that these coexisting solutions in a given nonlinear dynamics system can be self-excited or hidden. Recall that an attractor is called a self-excited attractor if its basin of attraction intersects with any open neighborhood of an unstable fixed point. Otherwise, it is called a hidden attractor [26]. On the contrary, hidden solutions have attraction basin which does not overlap with the neighborhood of an equilibrium point, and thus may be difficult to find numerically [11, 27–34]. However, the localization of the latter was made possible using an algorithm proposed by Leonov et al. [35]. Such system types (with hidden attractors) can be potentially dangerous and very unpredictable (unrelated to butterfly effect). The multistability of the nonlinear system means that the system is able to exhibit different types of coexisting stable states and different forms of attraction basin for an identical set of system parameters but using different initial conditions [2–4, 8, 14, 36, 37]. Since the coexistence of attractors has been commonly used in image processing [16, 38], it becomes very urgent to control this phenomenon when, sometimes, periodic and chaotic orbits exist simultaneously. Up to date, the prominent methods reported in the relevant literature which enable to turn a multistable system to a monostable system are the noise selection [39], pseudo-forcing [12], short pulses [40], harmonic perturbation [41], intermittent feedback [42], temporal feedback [43], and linear augmentation [2, 3, 44–50]. Except for the temporal feedback and linear augmentation methods, in almost all other existing methods, the control is applied to one parameter of the system to remove on the attractors for all initial points. Thus, external control such as the temporal feedback or linear augmentation method would be preferred. Recall that, in many bistable dynamical systems, only one of the stable states is desired to track certain system performance. In this regard, Sharma et al. [47] presented control of some bistable systems with annihilation and selection of attractors using the linear augmentation scheme. This work has been carried out using two well-known paradigmatic systems that are the autonomous Chua oscillator and a neuronal system. Furthermore, the linear augmentation method has been successfully used in [46] to control the bistability property exhibited by the Lorenz–Rössler system. In 2015, the same research team [45] exploited the linear control scheme to stabilize a system to a fixed-point state even when the original system did not have any fixed point. Recently, in [43], the authors proposed the method of temporal feedback in autonomous as well as nonautonomous systems to target the coexisting attractor. The experimental realization of the introduced method was also addressed. However, all these results were based only on bistable systems.

Very recently, Fonzin Fozin et al. [2] investigated the annihilation of the coexistence of multiple stable states in a self-excited memristive hyperchaotic oscillator based on the linear augmentation method. Exploiting nonlinear analysis tools such as bifurcation diagrams, Lyapunov exponent spectrum, phase portraits, basins of attraction, and relative basin sizes, the authors show that when increasing the control parameter, the bifurcation routes followed by each of the three coexisting attractors were progressively merged in order to give a unique diagram. The results of the authors show that, for higher values of the control parameter, the multistable system with up to three coexisting attractors becomes a monostable one with only one surviving attractor. The same result was found when the same research team was addressing the control of multistability (involving three disconnected attractors) in simplified canonical Chua's oscillator with smooth hyperbolic sine nonlinearity using the linear augmentation scheme [3, 44]. Much recently, Tabekoueng Njitacke et al. [50] investigated the coexistence of firing patterns and their control in two neurons coupled through an asymmetric electrical synapse. Their numerical results show the effectiveness of the control strategy through annihilation of the periodic coexisting firing pattern. They found that, for higher values of the coupling strength, only a chaotic firing pattern survives. From these results, it can be seen that intensive works have been done on the multistability control of the nonlinear oscillators based on the linear augmentation method. Remark that all these successful results on the control of multistability were performed so far only on systems with unique equilibrium point [2, 3, 44, 50]. This unique equilibrium point excludes the possibility to target/select a desired attractor during the multistability control process. Henceforth, we propose in this work the following:

(a) To exploit the linear augmentation method to track and select one attractor among the four coexisting attractors using each of the three equilibrium points of the model

(b) To design an analog electronic circuit of controlled Chua's oscillator to further support the numerical investigation

The layout of the paper is as follows: in Section 2, we recall some basic properties of Chua's oscillator with a smooth nonlinearity. In Section 3, numerical tracking of the coexisting attractors using usual nonlinear dynamics tools is addressed. In Section 4, the linear augmentation scheme is exploited to track each of the three coexisting attractors which survive around each of the three equilibriums points. The circuit realization of the investigated model is provided in Section 5. In Section 6, some conclusions are summarized.

2. Description of Chua's Oscillator with Smooth Nonlinearity

Chua's oscillator with smooth cubic nonlinearity in which multistability is controlled in this work is given by dimensionless equation (1) as follows [5, 51]:

$$\begin{cases} \dfrac{dx}{dt} = k\alpha(y - x - f(x)), \\ \dfrac{dy}{dt} = k(x - y + z), \\ \dfrac{dz}{dt} = k(-\beta y - \gamma z), \end{cases} \tag{1}$$

where the nonlinear function $f(\cdot)$ is defined as

$$f(x) = ax^3 + bx. \tag{2}$$

The parameter values used in this work are the ones of the model studied in [5] and are set as $\gamma = -0.75087096$, $a = -0.0375582129$, $b = -0.8415410391$, and $k = -1$ with β and α being tunable. As it can be seen in equation (1), the model remains identical under the substitution $(x, y, z) \Leftrightarrow (-x, -y, -z)$. The stable state generated by the model will appear in symmetric pairs in (x, y, z) to re-establish the real symmetry of the model. If not, the stable states produced will remain symmetric if the real symmetry of the attractors has already been re-established. This approach has been widely exploited recently to find coexisting attractors in symmetrical systems such as jerk [6, 8, 52–56], hyperchaotic and chaotic Chua's oscillators [3, 44, 57–59], Hopfield neural networks [10, 36, 60, 61], and Duffing oscillator [9], just to name a few. In addition, it is easy to show that the model processes three equilibrium points given by the following expression: $S_0 = (0\ 0\ 0)$, and $S_{1,2} = (\pm \overline{x}_1, (\pm \overline{x}\gamma/\gamma + \beta), ((\mp \overline{x}\beta)/(\gamma + \beta)))$, in which $\overline{x}$ is given by $\overline{x} = \sqrt{(1/a)((\gamma/\beta + \gamma) - 1 - b)}$.

3. Selection of Coexisting Attractors: A Numerical Approach

3.1. Computational Method. In this section, we will use traditional nonlinear analysis tools such as bifurcation diagrams, graph of maximum Lyapunov exponent, phase portraits, two-parameter diagrams, standard Lyapunov stability diagrams, and attraction basins to hunt down windows in which controlled Chua's oscillator with a smooth nonlinearity exhibits either hysteretic dynamics of parallel bifurcation branches. These various tools are computed using the Runge–Kutta formula in Turbo Pascal software with variables and constants chosen in the extended precision mode. In this contribution, we use a constant time grid of $\Delta t = 0.002$, and investigations are carried out for a very long time. In this way, the transient behavior is suppressed. Some bifurcation diagrams in this work are computed either by increasing the control parameter stating from different initial conditions or using an upward and backward continuation technique. These methods are the best for finding windows in which the model displays the coexistence of bifurcations. Graph of Lyapunov exponent is calculated using the algorithm proposed by Wolf et al. [62]. Two-parameter diagrams and standard Lyapunov stability diagrams are computed by varying simultaneously two system parameters with making up of suitable colorful diagrams. These previous diagrams, as well as the basins of attraction, are obtained by numerically computing the maximum Lyapunov exponent on a grid of 350×350 values of the chosen space parameters.

3.2. Parallel Bifurcation Branches and Coexistence of Multiple Attractors. In the study of nonlinear dynamical systems, the coexistence of attractors for the same set of system parameters but using different initial conditions is known as multistability. Two curious and striking manifestations of such behavior are extreme or hidden extreme multistability [63, 64] and megastability phenomenon [17]. This phenomenon of multistability has already been found in several nonlinear systems including the memristor-based oscillator [8, 16, 57], jerk/hyperjerk systems [55, 56, 65], and hyperchaotic Chua's oscillator [3, 4], just to name a few.

Figure 1 represents a bifurcation obtained when varying the control parameter in the range $51 \leq \beta \leq 54.5$. Two sets of data with their corresponding graph of maximum Lyapunov exponent are superimposed. A large window of coexisting bifurcations which are related with parallel bifurcation branches is presented. As a result, this superposition of the bifurcations is the coexistence of multiple attractors for the same sets of system parameters. For example, when $\beta = 53.6$, Chua's circuit displays the coexistence of a symmetric pair of period-4 limit cycles (black and blue) and a symmetric pair of chaotic attractors (green and red), using different initial conditions, as depicted on the three-dimensional (3D) projection of the attractors in Figure 2(a). The set of initial conditions which enable to obtain each of the previous attractors is provided in Figure 2(b).

For this same value of the control parameter, the equilibrium points of the oscillator and their stability are checked as follows: $S_0 = (0\ 0\ 0)$ with eigenvalues given by $\lambda_1 = 31.0920$ and $\lambda_{2,3} = -0.1366 \pm 7.2349i$ and $S_{1,2} = (\pm 2.1441, \mp 0.0305, \mp 2.1746)$ with eigenvalues given by $\lambda_1 = 22.6638$ and $\lambda_{2,3} = -0.2219 + 7.1926i$. Since the eigenvalues of the investigated model around the fixed points are unstable for the set of the parameter used for the study and its basin of attraction intersects with any open neighborhood of an unstable fixed point, we conclude that the coexisting attractors found are self-excited [26]. When $\beta = 53.8$, Chua's circuit displays the coexistence of a symmetric pair of period-2 limit cycles (black and blue) and a symmetric pair of chaotic attractors (green and red), using different initial conditions, as depicted on the three-dimensional (3D) projection of the attractors in Figure 3(a). The basin of attraction associated to each coexisting attractor is provided in Figure 3(b). The equilibrium points of the model as well as the eigenvalues for that discrete value of the control parameter are given as $S_0 = (0\ 0\ 0)$ with eigenvalues given by $\lambda_1 = 31.0919$ and $\lambda_{2,3} = -0.1366 \pm 7.2485i$ and $S_{1,2} = (\pm 2.1438, \mp 0.0303, \mp 2.1741)$ with eigenvalues given by $\lambda_1 = 22.6662$ and $\lambda_{2,3} = -0.2218 + 7.2061i$, which further supported the unstable nature of the equilibria. From this attraction basin of Figures 2(b) and 3(b), it can be observed that each attractor has its set of initial conditions which intercepts with the one of its direct neighbor. For each

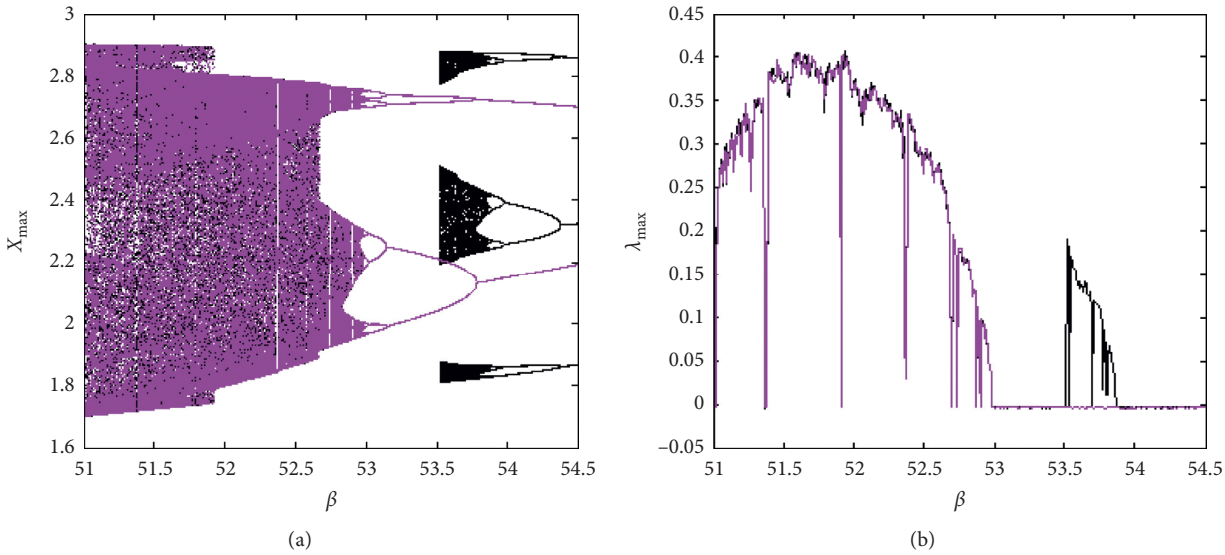

FIGURE 1: Bifurcation diagram (a) showing local maxima of coordinate x versus β and the corresponding graph (b) of the largest Lyapunov exponent (λ_{max}) plotted in the range $51 \leq \beta \leq 54.5$. Two sets of data are superimposed. The diagram in black is obtained when the control parameter is decreased from 54.5 to 51 starting with initial conditions $(1.2; 0; 0)$, while the one in magenta is obtained when decreasing the control parameter starting from the initial conditions $(1.52; 0; 0)$ with $\alpha = 16.6$.

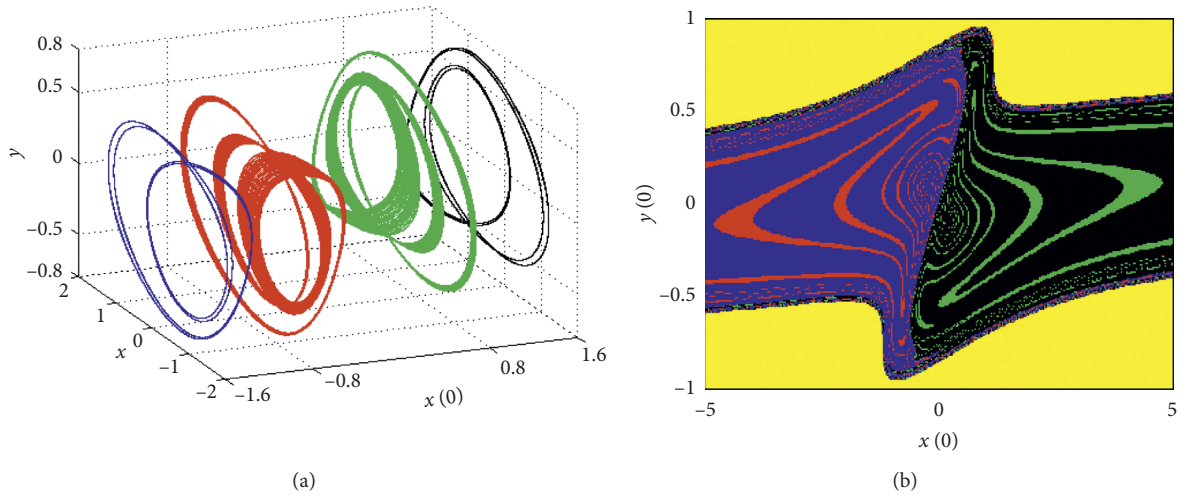

FIGURE 2: Three-dimensional projections of the coexisting attractors in the $(x(0), x, y)$ plane. (a) Coexistence of four different attractors (a pair of chaotic attractors and a pair of period-4 limit cycles) for $\beta = 53.6$. (b) Cross sections of the basin of attraction for $z(0) = 0$, corresponding to the asymmetric pair of period-4 cycles (black and blue) and the pair of chaotic attractors (red and green). Yellow regions correspond to unbounded motion.

basin of attraction, zones of unbounded motion are marked with yellow color, whereas the pair of coexisting attractors is painted in red and green, while the pair of periodic attractors is painted in blue and black.

4. Control of Coexisting Attractors Using the Linear Augmentation Method

4.1. Description of the Control Method. From the already published works [45–49], the theory of the linear augmentation control method consists of coupling the nonlinear system displaying multistable behavior with a linear system (V) as depicted by equation (3). Remark that the choice of scalar control was guided by recent results of control and synchronization on chaotic systems [66, 67]. Indeed, it has been demonstrated that control and synchronization of the chaotic system using scalars offer great flexibility than vectors. In fact, the drawback of using vector than scalar for control or synchronization is that the full states of the systems are involved in the process. When these full states of the systems are used, the energy and resource consumption are high.

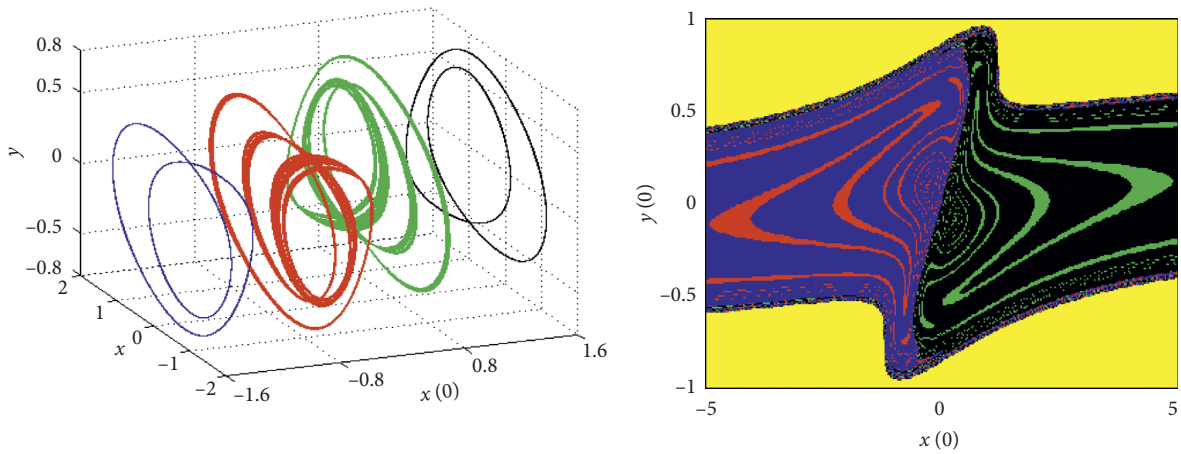

(a) (b)

FIGURE 3: Three-dimensional projections of the coexisting attractors in the $(x(0), x, y)$ plane. (a) Coexistence of four different attractors (a pair of chaotic attractors and a pair of period-2 limit cycles) for $\beta = 53.8$. (b) Cross sections of the basin of attraction for $z(0) = 0$, corresponding to the asymmetric pair of period-2 cycles (black and blue) and the pair of chaotic attractors (red and green). Yellow regions correspond to unbounded motion.

$$\begin{cases} \dot{X} = F(X) + \delta V, \\ \dot{V} = -\eta V - \delta(X - E). \end{cases} \tag{3}$$

In this equation, $\dot{X} = F(X)$ represents a standard form of a nonlinear dynamical system, X is an m-dimensional vector of the system variable, and $F(X)$ is the vector field on which it is associated. Parameter δ represents the connection weight which enables to link the nonlinear system and the linear one. Vector V stands for the dynamics of the linear system $\dot{V} = -\eta V$, where η represents its decay parameter. When the controller is off, i.e., $\delta = 0$, the linear system tends to zero with an exponential following a decay rate δ.

E represents another key parameter of controlled Chua's oscillator which will be used to track the wished stable state. It is generally selected at the neighborhood of the equilibria of the uncontrolled system [47]. These stable states, which can originate from unstable equilibria, are checked by certain sets of invariants, i.e., coexisting attractors and existing fixed points. The fixed points are found either in the center of the coexisting attractors or lying on the boundary separating the basins of attraction of the stable state. Then, by considering vector E identical with one of the unstable fixed points, one can obtain the death of some of the coexisting stable states through merging crises when increasing coupling/connection weight between the coupled oscillators. For superior values of the connection weight, only one surviving attractor is obtained which enables the system for chosen parameter sets to turn from multistable to a monostable one. The controlled scheme presented above is now used for Chua's oscillator. Coupling is applied along the x variable with the coupling strength δ as depicted in the following equation:

$$\begin{cases} \dfrac{dx}{dt} = k\alpha\left(y - x - ax^3 - bx\right) + \delta v, \\ \dfrac{dy}{dt} = k(x - y + z), \\ \dfrac{dz}{dt} = k(-\beta y - \gamma z), \\ \dfrac{dv}{dt} = -\eta v - \delta(x - \varepsilon). \end{cases} \tag{4}$$

The equilibrium points of controlled Chua's oscillator are obtained by solving the following equation:

$$\begin{cases} k\alpha\left(y - x - ax^3 - bx\right) + \delta v = 0, \\ k(x - y + z) = 0, \\ k(-\beta y - \gamma z) = 0, \\ -\eta v - \delta(x - \varepsilon) = 0. \end{cases} \tag{5}$$

After some algebraic manipulations, we obtain the expression of the equilibrium points as follows:

$$E_{1,2,3} = \left(\overline{x}, \frac{\overline{x}\gamma}{\gamma + \beta}, \frac{-\overline{x}\beta}{\gamma + \beta}, -\frac{\delta}{\eta}(\overline{x} - \varepsilon)\right), \tag{6}$$

where $\overline{x}$ is obtained by solving the following equation:

$$\overline{x}^3 + \frac{\overline{x}}{a}\left(1 + b + \frac{\delta^2}{k\alpha n} - \frac{\gamma}{\gamma + \beta}\right) - \frac{\delta^2 \varepsilon}{ak\alpha n} = 0. \tag{7}$$

Considering $p = (1/a)(1 + b + (\delta^2/k\alpha n) - (\gamma/\gamma + \beta))$ and $q = -(\delta^2 \varepsilon / ak\alpha n)$, equation (7) becomes

$$\overline{x}^3 + \overline{x}p + q = 0. \tag{8}$$

The roots of (8) can be derived using the Cardano–Tartaglia method. According to the Cardano discriminant [68, 69], if $\Delta > 0$, there is a real root and two complex roots. Since the fixed point cannot be a complex number, one equilibrium point exists.

$$\overline{x}_0 = \frac{-1 + i\sqrt{3}}{2} \times \sqrt[3]{-\frac{q}{2} + \sqrt{\Delta}} + \frac{-1 - i\sqrt{3}}{2} \times \sqrt[3]{-\frac{q}{2} - \sqrt{\Delta}}, \tag{9}$$

$$\overline{x}_1 = \sqrt[3]{-\frac{q}{2} + \sqrt{\Delta}} + \sqrt[3]{-\frac{q}{2} - \sqrt{\Delta}}, \tag{10}$$

$$\overline{x}_2 = \frac{-1 - i\sqrt{3}}{2} \times \sqrt[3]{-\frac{q}{2} + \sqrt{\Delta}} + \frac{-1 + i\sqrt{3}}{2} \times \sqrt[3]{-\frac{q}{2} - \sqrt{\Delta}}, \tag{11}$$

where $\Delta = (q/2)^2 + (p/3)^3$.

If $\Delta = 0$, equation (8) would have two real roots. Finally, if $\Delta < 0$, there are three real roots in equation (8), which manifests that controlled Chua's oscillator has three equilibrium points and can be obtained from equations (9)–(11). The rest of the circuit parameters are the same as those used in Figure 3. The stability of controlled Chua's oscillator is provided in Table 1. As it can be seen from Table 1, for some discrete values of the controller coefficient, controlled Chua's oscillator, under the consideration, conserves its stability, hence its ability to generate self-excited attractors because of the unstable nature of its equilibria. It is found that when the coupling strength is null, there are three values of $\overline{x}$, among which the origin S_0 and a symmetric pair $S_{1,2}$. When the coupling strength is increased, S_1 remains uniform, while S_0 and S_2 are attracted by decreasing (resp. increasing) the value of the equilibrium points S_0 and S_2.

4.2. Control of Multistability in Chua's Oscillator. An illustrative example of the linear control method is shown in Figure 4 using the two-parameter diagram and corresponding standard Lyapunov stability diagram in the parameter space (δ, β). The integration method adopted here is identical with the one used in the previous section. Cyan color is tied to periodic oscillations, while magenta color is tied with chaotic motions. Good accordance is observed between two-parameter diagrams (left) and corresponding standard Lyapunov stability diagrams (right). The diagrams are obtained by sweeping upward (Figure 4(a)) and downward (Figure 4(b)) both control parameters. From a general point of view, it can be seen that, on both diagrams, four regions, namely, (***R1***), (***R2***), (***R3***), and (***R4***), can be observed. Regions (***R1***), (***R2***), and (***R3***) correspond to the set of parameters for which the model displays hysteretic dynamics which gives birth to the phenomenon of coexistence of multiple stable states, whereas (***R4***) represents the set of parameters in which the model displays monostable dynamics, in other words, absence of multistability. These diagrams are very important since they enable the engineer to have a general overview on the dynamics of the multistable oscillator when the bifurcation parameter and the controller coupling strength are both varying.

Since coupling is introduced along the "x" variable, we fix $\varepsilon = 2.1438$ which is one among the two nontrivial equilibrium points. When increasing the control parameter δ in the range $[0 \longrightarrow 0.5]$ as it can be seen in Figure 5(a), four sets of data are superimposed in the bifurcation diagram. Each set of data (marked by red, black, blue, and green colors) corresponds to the route followed by each attractor during the control mechanism. As depicted in Figure 5(a), three crises enable all the plotted routes to merge along the one in black for higher values of the coupling strength. In region (***D1***) of Figure 6 and for very small values of δ (i.e., $\delta \approx 0.05$), four attractors coexist including two chaotic attractors (red color and green color) with two periodic attractors (black color and blue color).

At the upper boundary of (***D1***), the diagram in red (chaotic one) undergoes a merging crisis (first crisis) and blends with the diagram in blue. In region (***D2***), because of the previous merging crisis, there are only three distinct diagrams that follow their bifurcation sequences (see region (***D2***)). For a discrete value $\delta = 0.15$, we have the coexistence of three disconnected attractors, involving a period-2, period-3, and period-4 limit cycle as presented in Figure 6(a). The demarcation region of each coexisting attractor in region (***D2***) is provided in Figure 6(b). As it can be observed from Figure 6(b), the basin in blue has already absorbed the one in red, while the basin in black has started to absorb the one in green. At the upper boundary of (***D2***), a crisis (second crisis) enables the diagram in green displaying period-3 limit cycle to merge with the diagram in black. In region (***D3***), we observe the superposition of two diagrams including a periodic and chaotic one.

In this region for a discrete value $\delta = 0.3$, Chua's oscillator displays coexistence of a period-2 limit cycle with an asymmetric chaotic attractor (see Figure 7(a)). The basin of attraction associated with each coexisting attractor is computed and plotted in Figure 7(b). From this basin of attraction, it can be observed that the basin in black has already absorbed the one in green. At the upper boundary of (***D3***), a crisis (third crisis) enables the diagram in blue displaying chaotic behavior to merge with the diagram in black. In region (***D4***), when the critical value $\delta \approx 0.34$, all the diagrams have already merged with the black one, and the control goal is achieved as depicted in region (***D4***) when "ε" is fixed as $\varepsilon = 2.1438$. We can say that the route followed by the black diagram (see Figure 7(b)) is a magnetized route that attracts towards it all the other routes as the control parameter is increased.

As it can be observed in Figure 5(b), only two crises enable the control of the multistability around the origin ($\varepsilon = 0$). At the upper boundary of (***D1***), the first crisis enables the diagram in green to merge with the diagram in black. At the same time, the diagram in red merges with the one in blue. As presented in (***D2***), only a symmetrical pair of attractors coexists. At the upper boundary of (***D2***), the two coexisting diagrams undergo a symmetric restoring crisis

Table 1: Equilibrium points of controlled Chua's oscillator, the corresponding eigenvalues, and their stability for some discrete values of the control parameter.

Control parameter	Equilibria	Eigenvalues and stability
$\delta = 0$	$S_0 = (0, 0, 0, 0)$	31.0919, $-0.1366 \pm 7.2485i$, and -1.0 (unstable saddle focus (USF))
	$S_1 = (2.1438, -0.0303, -2.1741, 0)$	22.6662, $-0.2218 \pm 7.2061i$, and -1.0 (unstable saddle focus (USF))
	$S_2 = (-2.1438, +0.0303, +2.1741, 0)$	22.6662, $-0.2218 \pm 7.2061i$, and -1.0 (unstable saddle focus (USF))
$\delta = 0.2$	$S_1 = (2.1438, -0.0303, -2.1741, 0)$	22.6645, $-0.2218 \pm 7.2062i$, and -0.9983 (unstable saddle focus (USF))
	$S_0 = (-0.0304, 4.3e-04, 0.0308, 0.4348)$	31.089, $-0.1366 \pm 7.2485i$, and -0.9987 (unstable saddle focus (USF))
	$S_2 = (-2.1134, 0.0299, 2.1433, 0.8514)$	22.9005, $-0.2188 \pm 7.2081i$, and -0.9983 (unstable saddle focus (USF))
$\delta = 0.4$	$S_1 = (2.1438, -0.0303, -2.1741, 0)$	22.6596, $-0.2220 \pm 7.2064i$, and -0.9930 (unstable saddle focus (USF))
	$S_0 = (-0.1273, 0.0018, 0.1291, 0.9084)$	31.0571, $-0.1369 \pm 7.2485i$, and -0.9949 (unstable saddle focus (USF))
	$S_2 = (-2.0165, 0.0285, 2.0450, 1.6641)$	23.6260, $-0.2098 \pm 7.2136i$, and -0.9933(unstable saddle focus (USF))

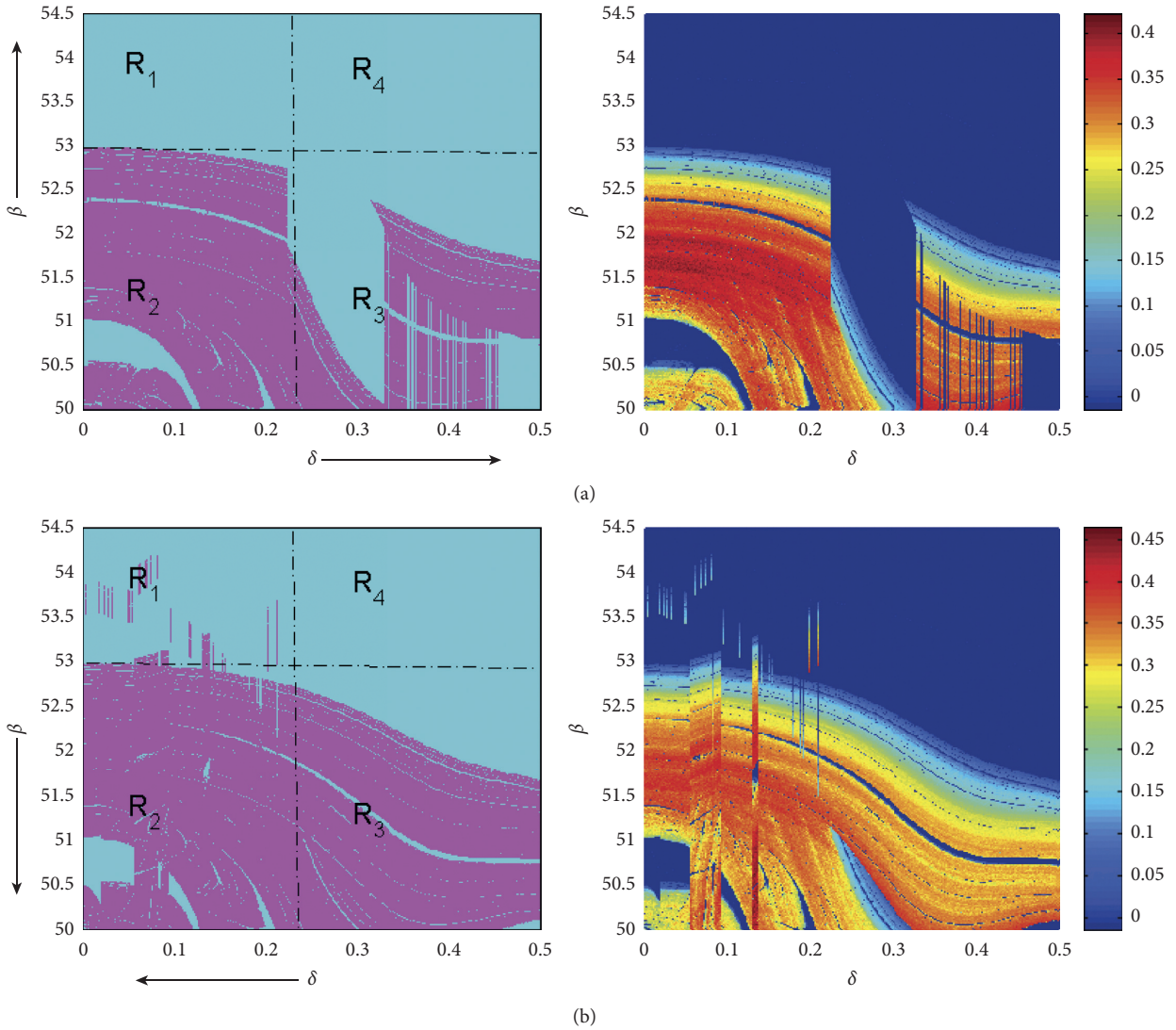

Figure 4: Two-parameter diagram (left) and the corresponding standard Lyapunov stability diagram (right) in the (δ, β) plane when increasing (a) and decreasing (b) both control parameters. Both diagrams show the effectiveness of the controller in the coexisting region for $\varepsilon = 2.1438$. Other parameters are those of Figure 1.

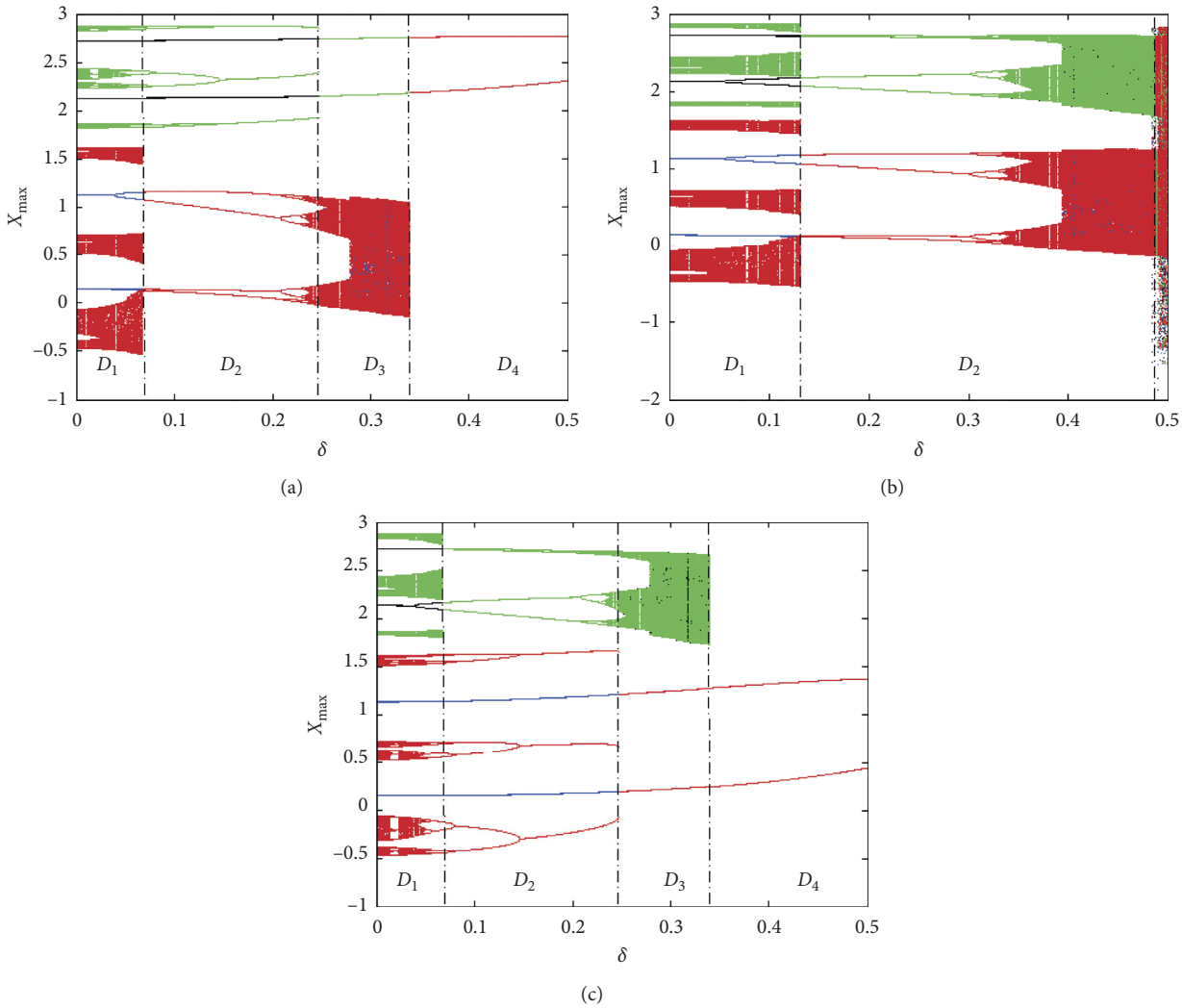

Figure 5: Bifurcation diagrams showing local maxima of the state variable x versus the control strength δ in the range $[0\ \ 0.5]$ of the controlled system (see equation (4)) showing multistability control with selection of attractors for different values of ε. Four separated diagrams are superimposed when increasing the coupling strength δ for four different initial conditions. Red is obtained with $(-0.56; 0; 0; 0)$, the one in black is obtained for $(1.6; 0; 0; 0)$, blue is obtained with $(-1.6; 0; 0; 0)$, and the one in green is obtained for $(0.56; 0; 0; 0)$. (a) For $\varepsilon = 2.1438$, (b) for $\varepsilon = 0$, and (c) for $\varepsilon = -2.1438$. For these diagrams, $\eta = 1$ and $\beta = 53.8$. Other parameters are those of Figure 1.

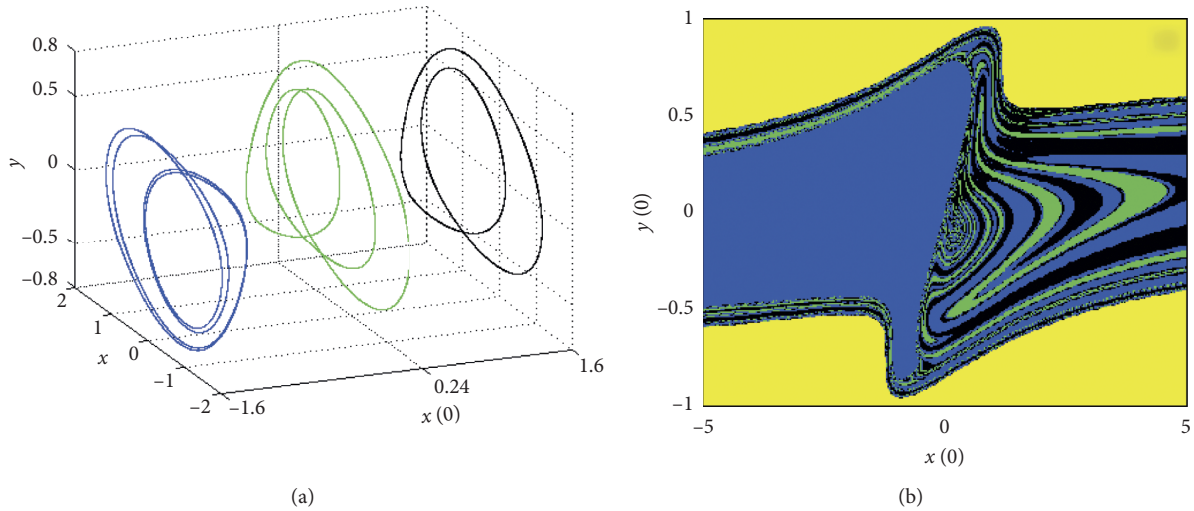

Figure 6: (a) Coexistence of three asymmetric periodic attractors showing multistability phenomenon with the basin of attraction (b) in the plane $(x(0), y(0))$ when $\delta = 0.15$.

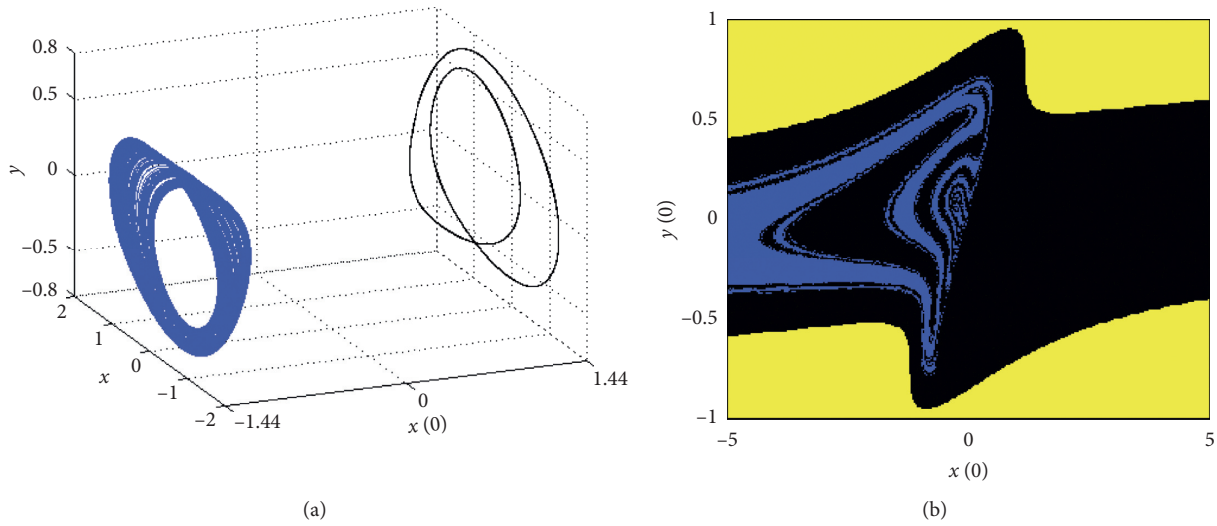

Figure 7: (a) Coexistence of an asymmetric chaotic attractor with a asymmetric periodic-2 limit cycle showing multistability phenomenon with the basin of attraction (b) in the plane $(x(0), y(0))$ when $\delta = 0.3$.

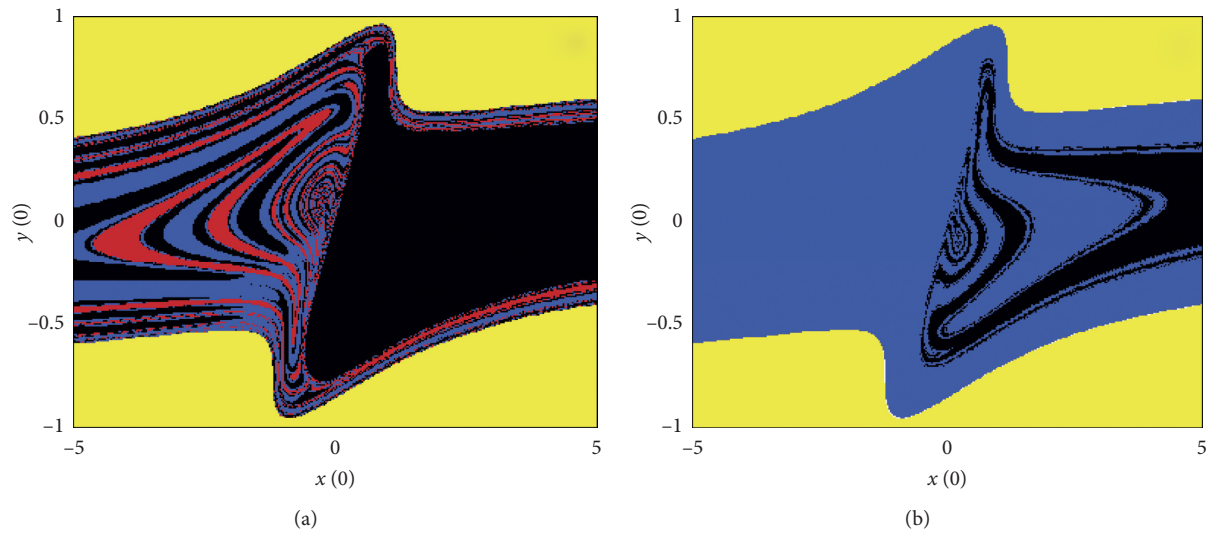

Figure 8: Basin of attractions in the plane $(x(0), y(0))$ for $\delta = 0.15$ (resp. $\delta = 0.3$) showing magnetization toward a unique stable state when the coupling strength is increased according to Figure 5(c).

and give birth to a unique diagram as depicted in region (***D3***).

Now, when tacking the other nontrivial equilibrium point ($\varepsilon = -2.1438$), the surviving attractor, when monitoring the control parameter, is obtained after three crises. These crises enable all the diagrams to finally merge with the diagram in blue. The details of this control process through merging of the diagrams are not provided for the sake of brevity. However, in Figure 8, we have provided some basins of attraction to illustrate merging of the basins of attraction. In Figure 8(a), the black diagram of Figure 5(c) has already merged with the green one. For that same value, the diagram in blue starts to absorb the one in red. In Figure 8(b), the diagram in blue has already completely merged with the red one, and only two coexisting attractors remain.

For $\delta = 0.5$, we have provided the unique attractors which have survived through the control scheme exhibited by Figures 5(a)–5(c) in Figure 9(a) and their corresponding basin of attraction in Figure 9(b). It is found that when the control, the techniques described in Figure 5(a), is exploited, the attractor in black is selected. When the control, the techniques described in Figure 5(c), is used, the attractor in blue is selected, and the control method displays by Figure 5(b) is used, the attractor in magenta is selected. These results clearly demonstrate that it is possible to target attractors based on steady points of the uncoupled system.

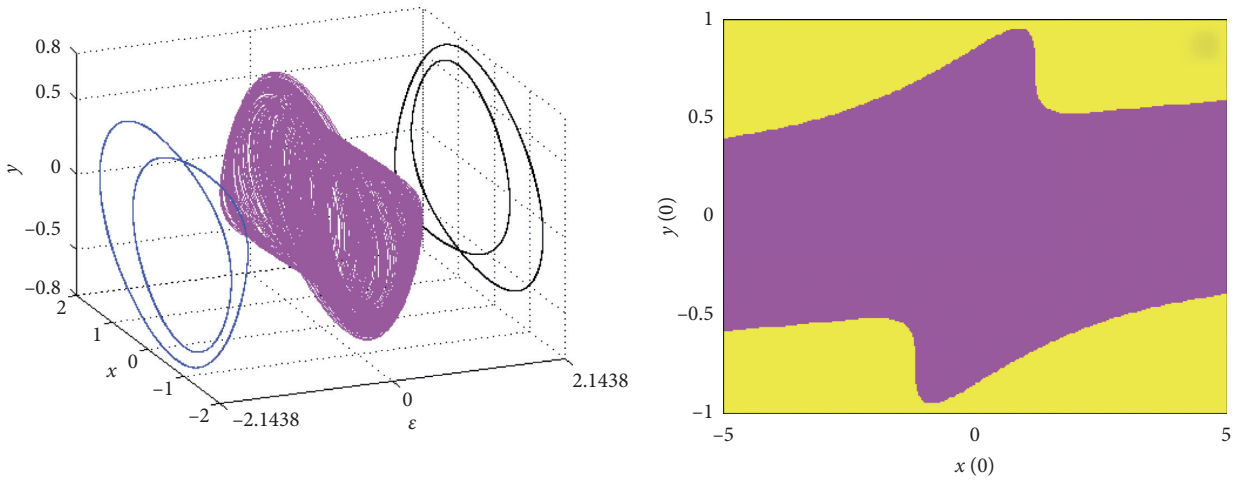

FIGURE 9: (a) Three-dimensional projections of the surviving stable states in the plane (ε, x, y) for the typical value of the coupling $\delta = 0.5$ for three distinct values of the equilibrium points, namely, S_0 and $S_{1,2}$. (b) Cross sections of the basin of attraction for $z(0) = 0$, corresponding to the domain of initial conditions which enable to obtain each attractor of Figure 9(a) in magenta color. Yellow regions correspond to unbounded motion.

Also, it is worth to emphasize here that the result of the multistability control of up to four coexisting attractors in Chua's system addressed in this work has never been presented before and thus merit to be shared.

5. The Circuit Implementation

In this part of our work, the aim is to be able to set up an analog circuit that will allow us to make a comparison between the theoretical/numerical results obtained previously and the experimental results [8, 10, 27, 61, 70, 71]. The circuit diagram that allows us to perform various simulations in PSpice software is presented in Figure 10. The circuit of controlled Chua's oscillator is designed using four capacitors C_1, C_2, C_3, and C_4, several resistors, eight op-amp TL082CD, a constant DC source, and two multipliers, which can be implemented practically using AD633JN versions of the AD633 four-quadrant voltage multiplier chips used to implement the nonlinear terms of our model. The signal (W) at the output is related to those at inputs $X_1(+)$, $X_2(-)$, $Y_1(+)$, $Y_2(-)$, and $Z(W = ((X_1 - X_2)(Y_1 - Y_2)/10) + Z)$. The circuit equation using Kirchhoff's electrical circuit laws can be obtained as

$$\begin{cases} C_1 \dfrac{dX}{dt} = \dfrac{1}{R_\alpha}\left(-Y + \dfrac{1}{R_a}X^3 + \dfrac{1}{R_{b+1}}X\right) + \dfrac{1}{R_\delta}V, \\ C_2 \dfrac{dY}{dt} = \dfrac{1}{R}(-X + Y - Z), \\ C_3 \dfrac{dZ}{dt} = \left(\dfrac{1}{R_\beta}Y + \dfrac{1}{R_\gamma}Z\right), \\ C_4 \dfrac{dV}{dt} = -\dfrac{1}{R_\eta}V - \dfrac{1}{R_\delta}(X - V_\varepsilon). \end{cases} \tag{12}$$

Setting $C_1 = C_2 = C_3 = C_4 = C = 5$ nF, $R = R_i = 100$ KΩ except R_α, R_{b+1}, R_γ, R_β, R_a, and R_δ and adopting the rescale of time $t = \tau RC$ and variables, $X = 1V \times x$, $Y = 1V \times y$, $Z = 1V \times z$, and $V = 1V \times v$, system (12) is the same with the one given in equation (4) with the following expression of parameters:

$$\begin{aligned} R_\alpha &= \frac{R}{\alpha} = 6.024\ \text{KΩ}, \\ R_\gamma &= \frac{R}{\gamma} = 133.178\ \text{KΩ}, \\ R_\beta &= \frac{R}{\beta} = 1.85\ \text{KΩ}, \\ R_a &= \frac{R}{a} = 2662.533\ \text{KΩ}, \\ R_{b+1} &= \frac{R}{-b+1} = 631.078\ \text{KΩ}, \\ R_\eta &= \frac{R}{\eta} = 100\ \text{KΩ}, \\ V_\varepsilon &= 1V \times \varepsilon, \\ R_\delta &= \frac{R}{\delta}. \end{aligned} \tag{13}$$

When the controller is OFF ($R_\delta \longrightarrow \infty$ or $\delta = 0$), the circuit implementation of controlled Chua's oscillator displays the phenomenon of the coexistence of up to four disconnected attractors as depicted in Figure 11. Thus, this result enables to support the fact that the previous obtained results on the coexistence of attractors in Chua's oscillator were not artifacts. When the controller is ON for $R_\delta = 180$ KΩ, selection of the attractor in controlled Chua's

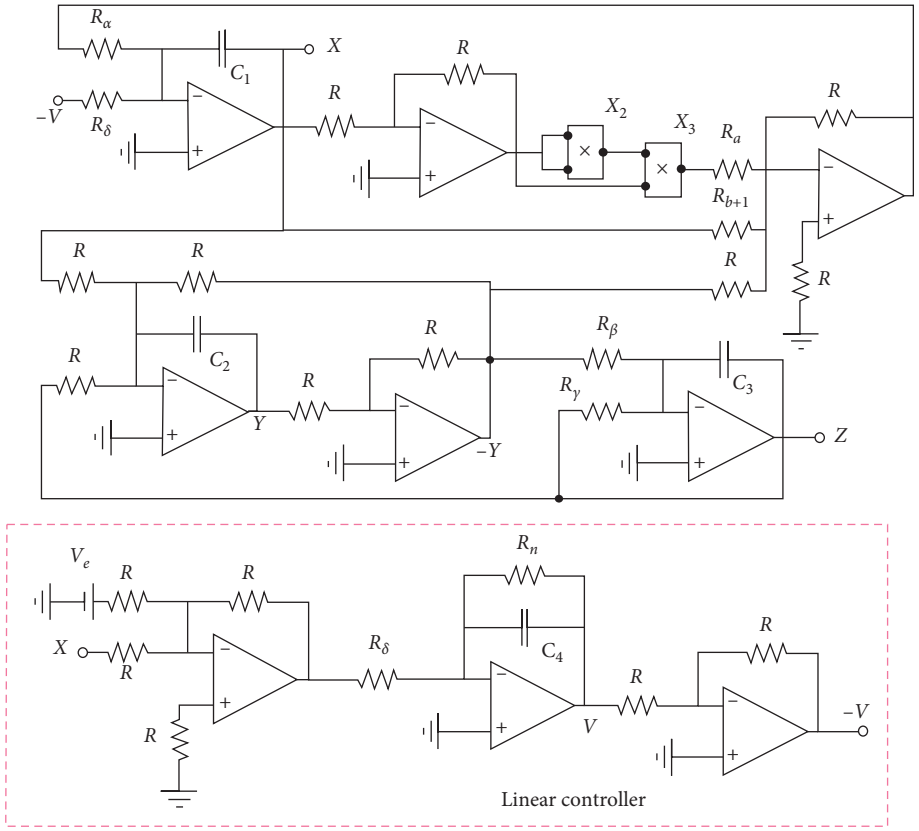

Figure 10: Schematic of Chua's oscillator coupled with the linear dynamical system.

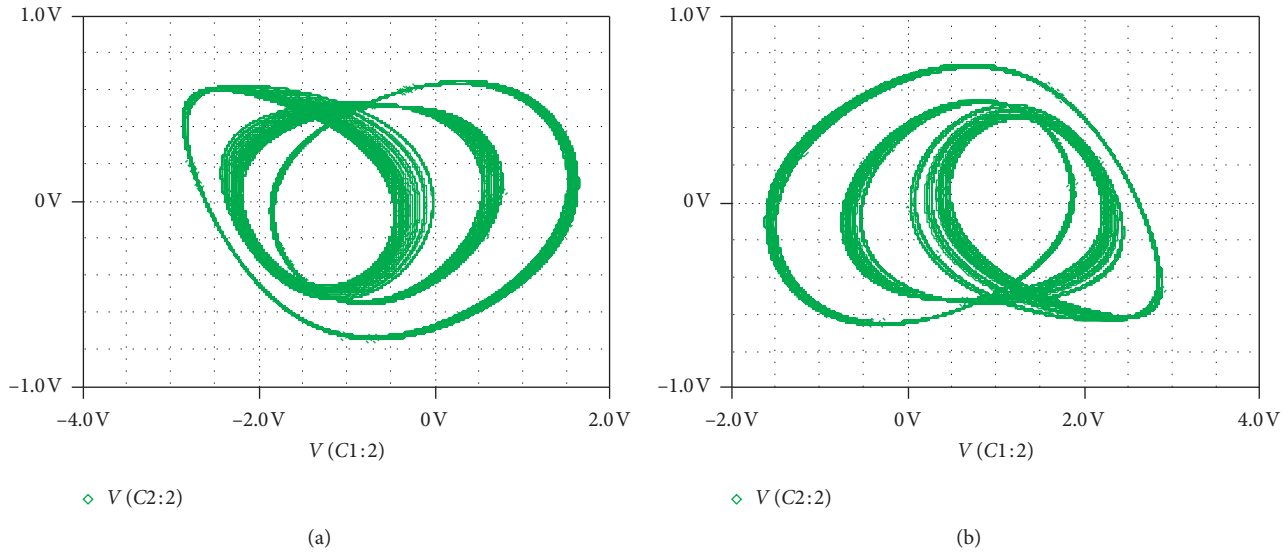

Figure 11: Continued.

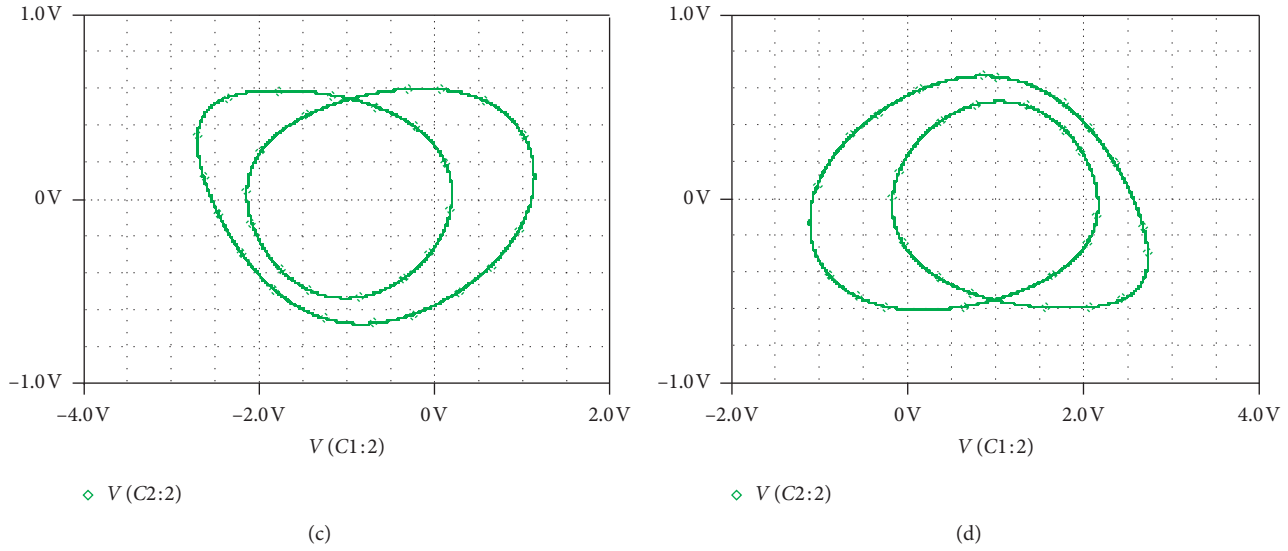

Figure 11: Phase portraits showing the coexistence of four different attractors using PSpice simulation (a pair of periodic and a pair of chaotic) for $R_\gamma = 133.178\,\text{K}\Omega$; initial conditions are $(\pm 4.3\,\text{V}, \pm 0.11\,\text{V}, 0\,\text{V})$ for the chaotic pair and $(\pm 4.3\,V, \pm 0\,\text{V}, \pm 0\,\text{V})$ for periodic attractors.

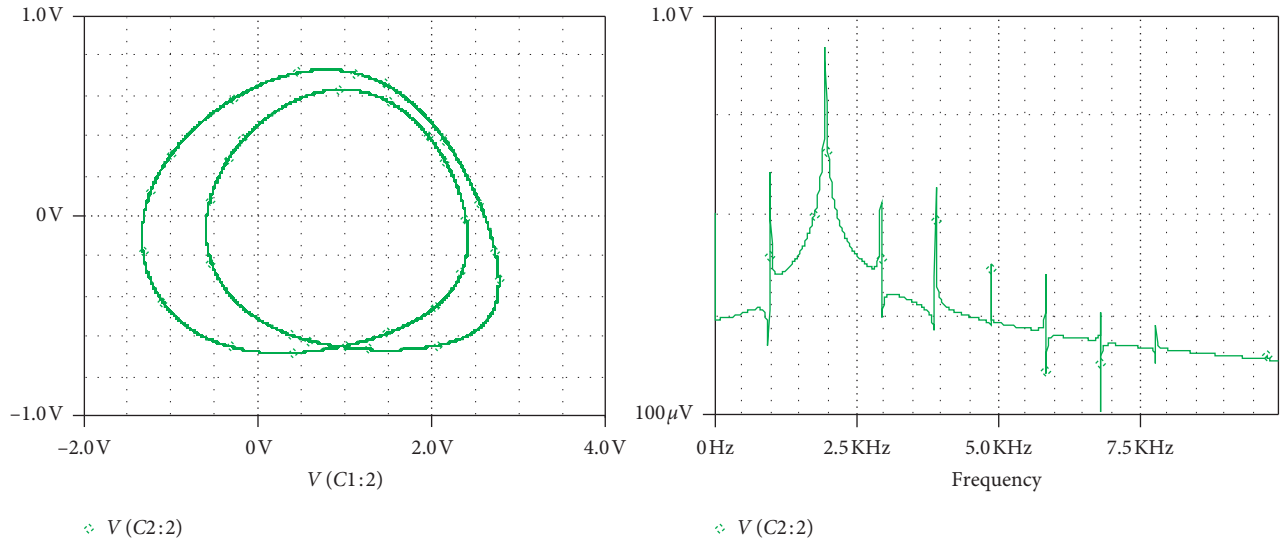

Figure 12: Continued.

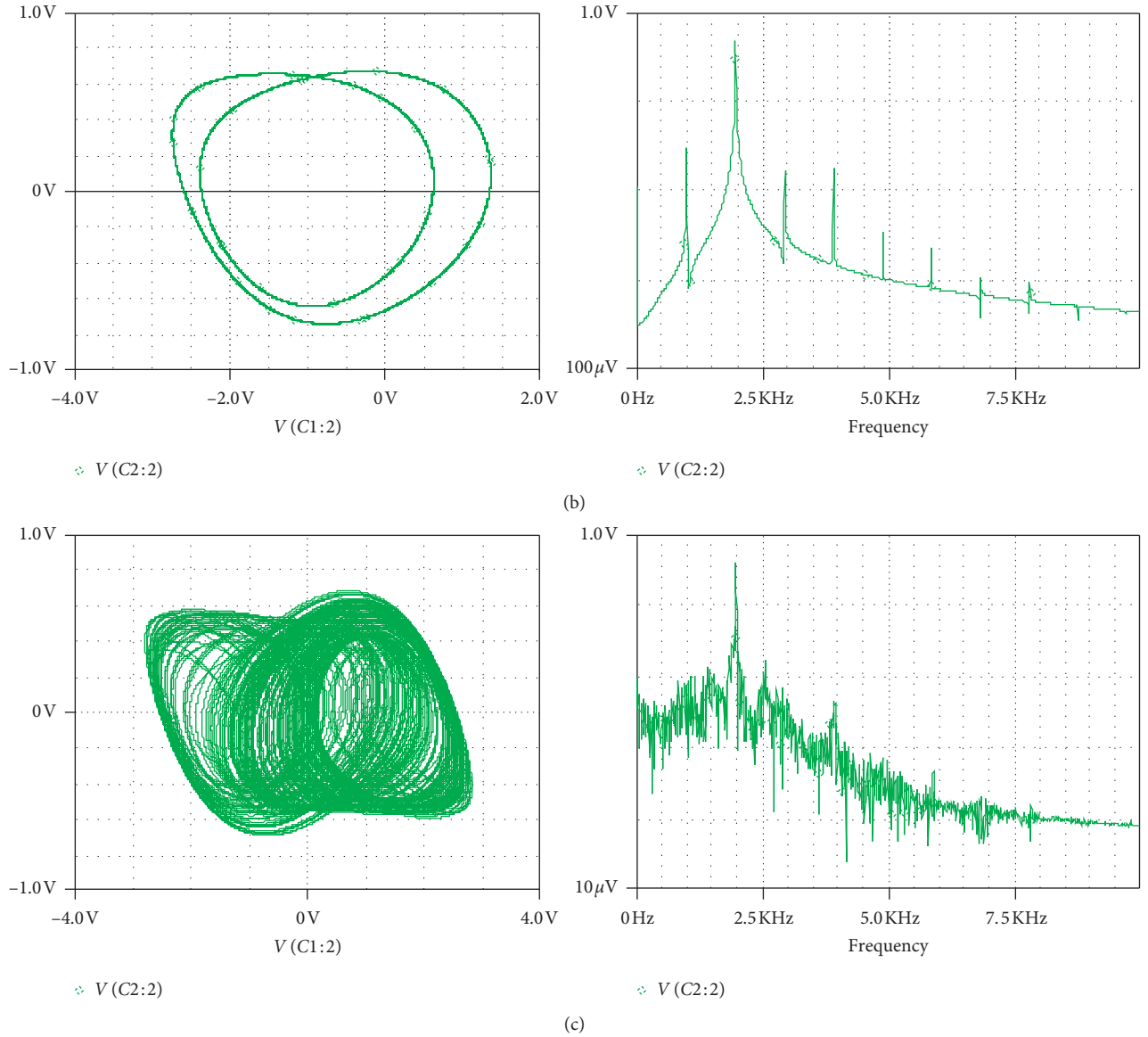

Figure 12: Phase portraits showing the unique surviving asymmetric and symmetric attractors for different values of the equilibrium points of the uncontrolled oscillator using PSpice simulation: (a) for $V_\varepsilon = 2.1438$ V, (b) for $V_\varepsilon = -2.1438$ V, and (c) for $V_\varepsilon = 0$ V. Parameter $R_\delta = 180$ KΩ, with initial conditions (4.3 V0 V, 0 V, 0 V).

oscillator occurs. For example, when $R_\delta = 180$ KΩ and $V_\varepsilon = 2.1438$ V, the attractor in Figure 12(a) is selected. When $R_\delta = 180$ KΩ and $V_\varepsilon = -2.1438$ V, the attractor in Figure 12(b) is selected. Finally, when $R_\delta = 180$ KΩ and $V_\varepsilon = 0$ V, the pair of the symmetric attractors of Figures 12(a) and 12(b) merges and gives the double-band chaotic attractor of Figure 12(c). Besides each selected attractor, its corresponding frequency spectrum is provided to further support the nature of the attractor.

6. Conclusion

This paper focused on selection of the coexisting attractor in multistable Chua's oscillator with a smooth nonlinearity. The choice of paradigmatic Chua's oscillator system within this work is based on the fact that it possesses three equilibrium points and thus opens the possibility to target or select a specific coexisting attractor located around unstable equilibria. Remark that the previous studies which focused on the multistability control were done on the system having three, four, and five coexisting attractors and only one equilibrium point [2, 3, 44, 50]. Based on linear augmentation, the unique equilibrium point excludes the possibility to target a coexisting attractor. This is why based on usual nonlinear techniques exploiting bifurcation diagrams, standard Lyapunov exponents, phase portraits, and cross-section basin of initial conditions, we show the possibility to control multistable Chua's oscillator (with three equilibria) towards three monostable states depending on the choice of the equilibrium point used during the linear augmentation.

These results clearly demonstrate that it is possible to select a coexisting attractor based on steady points of the uncoupled system such as predicted by Sharma et al. [47], where only bistable systems were investigated.

Data Availability

No data were used to support this study.

Conflicts of Interest

The authors declare that they have no conflicts of interest.

References

[1] W. Ai, K. Sun, and Y. Fu, "Design of multiwing-multiscroll grid compound chaotic system and its circuit implementation," *International Journal of Modern Physics C*, vol. 29, no. 6, Article ID 1850049, 2018.

[2] T. Fonzin Fozin, R. Kengne, J. Kengne, K. Srinivasan, M. Souffo Tagueu, and F. B. Pelap, "Control of multistability in a self-excited memristive hyperchaotic oscillator," *International Journal of Bifurcation and Chaos*, vol. 29, no. 9, Article ID 1950119, 2019.

[3] T. Fonzin Fozin, P. Megavarna Ezhilarasu, Z. Njitacke Tabekoueng et al., "On the dynamics of a simplified canonical Chua's oscillator with smooth hyperbolic sine nonlinearity: hyperchaos, multistability and multistability control," *Chaos: An Interdisciplinary Journal of Nonlinear Science*, vol. 29, no. 11, Article ID 113105, 2019.

[4] T. F. Fonzin, K. Srinivasan, J. Kengne, and F. Pelap, "Coexisting bifurcations in a memristive hyperchaotic oscillator," *AEU-international Journal of Electronics and Communications*, vol. 90, pp. 110–122, 2018.

[5] J. Kengne, "On the dynamics of Chua's oscillator with a smooth cubic nonlinearity: occurrence of multiple attractors," *Nonlinear Dynamics*, vol. 87, no. 1, pp. 363–375, 2017.

[6] J. Kengne, R. L. T. Mogue, T. F. Fozin, and A. N. K. Telem, "Effects of symmetric and asymmetric nonlinearity on the dynamics of a novel chaotic jerk circuit: coexisting multiple attractors, period doubling reversals, crisis, and offset boosting," *Chaos, Solitons & Fractals*, vol. 121, pp. 63–84, 2019.

[7] J. Kengne, Z. Njitacke Tabekoueng, V. Kamdoum Tamba, and A. Nguomkam Negou, "Periodicity, chaos, and multiple attractors in a memristor-based Shinriki's circuit," *Chaos: An Interdisciplinary Journal of Nonlinear Science*, vol. 25, no. 10, Article ID 103126, 2015.

[8] J. Kengne, Z. T. Njitacke, A. Nguomkam Negou, M. Fouodji Tsostop, and H. B. Fotsin, "Coexistence of multiple attractors and crisis route to chaos in a novel chaotic jerk circuit," *International Journal of Bifurcation and Chaos*, vol. 26, no. 5, Article ID 1650081, 2016.

[9] J. Kengne, Z. Njitacke Tabekoueng, and H. B. Fotsin, "Coexistence of multiple attractors and crisis route to chaos in autonomous third order Duffing-Holmes type chaotic oscillators," *Communications in Nonlinear Science and Numerical Simulation*, vol. 36, pp. 29–44, 2016.

[10] Z. T. Njitacke, J. Kengne, and H. B. Fotsin, "A plethora of behaviors in a memristor based Hopfield neural networks (HNNs)," *International Journal of Dynamics and Control*, vol. 7, no. 1, pp. 36–52, 2019.

[11] V.-T. Pham, C. Volos, S. Jafari, and T. Kapitaniak, "Coexistence of hidden chaotic attractors in a novel no-equilibrium system," *Nonlinear Dynamics*, vol. 87, no. 3, pp. 2001–2010, 2017.

[12] L. M. Pecora and T. L. Carroll, "Pseudoperiodic driving: eliminating multiple domains of attraction using chaos," *Physical Review Letters*, vol. 67, no. 8, pp. 945–948, 1991.

[13] Z. Huang, S. Mohamad, and H. Bin, "Multistability of HNNs with almost periodic stimuli and continuously distributed delays," *International Journal of Systems Science*, vol. 40, no. 6, pp. 615–625, 2009.

[14] Z. T. Njitacke, J. Kengne, R. W. Tapche, and F. B. Pelap, "Uncertain destination dynamics of a novel memristive 4D autonomous system," *Chaos, Solitons & Fractals*, vol. 107, pp. 177–185, 2018.

[15] V. F. Signing and J. Kengne, "Reversal of period-doubling and extreme multistability in a novel 4D chaotic system with hyperbolic cosine nonlinearity," *International Journal of Dynamics and Control*, vol. 7, pp. 439–451, 2019.

[16] C. Li, F. Min, Q. Jin, and H. Ma, "Extreme multistability analysis of memristor-based chaotic system and its application in image decryption," *AIP Advances*, vol. 7, no. 12, Article ID 125204, 2017.

[17] J. C. Sprott, S. Jafari, A. J. M. Khalaf, and T. Kapitaniak, "Megastability: coexistence of a countable infinity of nested attractors in a periodically-forced oscillator with spatially-periodic damping," *The European Physical Journal Special Topics*, vol. 226, no. 9, pp. 1979–1985, 2017.

[18] L. Fortuna, *Chua's Circuit Implementations: Yesterday, Today and Tomorrow*, World Scientific, Singapore, 2009.

[19] M. P. Kennedy, "Robust OP Amp realization of chua's circuit," *Frequenz*, vol. 46, pp. 66–80, 1992.

[20] T. Matsumoto, "A chaotic attractor from Chua's circuit," *IEEE Transactions on Circuits and Systems*, vol. 31, no. 12, pp. 1055–1058, 1984.

[21] T. Matsumoto, L. Chua, and K. Tokumasu, "Double scroll via a two-transistor circuit," *IEEE Transactions on Circuits and Systems*, vol. 33, no. 8, pp. 828–835, 1986.

[22] A. S. Elwakil and M. P. Kennedy, "Improved implementation of Chua's chaotic oscillator using current feedback op amp," *IEEE Transactions on Circuits and Systems I: Fundamental Theory and Applications*, vol. 47, no. 1, pp. 76–79, 2000.

[23] P. Arena, S. Baglio, L. Fortuna, and G. Manganaro, "Chua's circuit can be generated by CNN cells," *IEEE Transactions on Circuits and Systems I: Fundamental Theory and Applications*, vol. 42, no. 2, pp. 123–125, 1995.

[24] B. Bao, Q. Li, N. Wang, and Q. Xu, "Multistability in Chua's circuit with two stable node-foci," *Chaos: An Interdisciplinary Journal of Nonlinear Science*, vol. 26, Article ID 043111, 2016.

[25] N. Gunasekaran, R. Saravanakumar, M. Syed Ali, and Q. Zhu, "Exponential sampled-data control for T-S fuzzy systems: application to Chua's circuit," *International Journal of Systems Science*, vol. 50, no. 16, pp. 2979–2992, 2019.

[26] D. Dudkowski, S. Jafari, T. Kapitaniak, N. V. Kuznetsov, G. A. Leonov, and A. Prasad, "Hidden attractors in dynamical systems," *Physics Reports*, vol. 637, pp. 1–50, 2016.

[27] B. Bao, A. Hu, H. Bao, Q. Xu, M. Chen, and H. Wu, "Three-dimensional memristive Hindmarsh–Rose neuron model with hidden coexisting asymmetric behaviors," *Complexity*, vol. 2018, Article ID 3872573, 11 pages, 2018.

[28] S. Jafari, J. C. Sprott, and S. M. R. Hashemi Golpayegani, "Elementary quadratic chaotic flows with no equilibria," *Physics Letters A*, vol. 377, no. 9, pp. 699–702, 2013.

[29] H. Jiang, Y. Liu, Z. Wei, and L. Zhang, "A new class of three-dimensional maps with hidden chaotic dynamics,"

International Journal of Bifurcation and Chaos, vol. 26, no. 12, Article ID 1650206, 2016.

[30] V. T. Pham, S. Jafari, C. Volos, and L. Fortuna, "Simulation and experimental implementation of a line-equilibrium system without linear term," *Chaos, Solitons & Fractals*, vol. 120, pp. 213–221, 2019.

[31] V. T. Pham, C. Volos, T. Kapitaniak, S. Jafari, and X. Wang, "Dynamics and circuit of a chaotic system with a curve of equilibrium points," *International Journal of Electronics*, vol. 105, pp. 385–397, 2018.

[32] Z. Wei, P. Yu, W. Zhang, and M. Yao, "Study of hidden attractors, multiple limit cycles from Hopf bifurcation and boundedness of motion in the generalized hyperchaotic Rabinovich system," *Nonlinear Dynamics*, vol. 82, no. 1-2, pp. 131–141, 2015.

[33] Z. Wei, W. Zhang, Z. Wang, and M. Yao, "Hidden attractors and dynamical behaviors in an extended Rikitake system," *International Journal of Bifurcation and Chaos*, vol. 25, no. 2, Article ID 1550028, 2015.

[34] Z. Wei, W. Zhang, and M. Yao, "On the periodic orbit bifurcating from one single non-hyperbolic equilibrium in a chaotic jerk system," *Nonlinear Dynamics*, vol. 82, no. 3, pp. 1251–1258, 2015.

[35] G. A. Leonov, N. V. Kuznetsov, and V. I. Vagaitsev, "Localization of hidden Chua's attractors," *Physics Letters A*, vol. 375, no. 23, pp. 2230–2233, 2011.

[36] B. Bao, H. Qian, J. Wang et al., "Numerical analyses and experimental validations of coexisting multiple attractors in Hopfield neural network," *Nonlinear Dynamics*, vol. 90, no. 4, pp. 2359–2369, 2017.

[37] C. Li, J. C. Sprott, W. Hu, and Y. Xu, "Infinite multistability in a self-reproducing chaotic system," *International Journal of Bifurcation and Chaos*, vol. 27, no. 10, Article ID 1750160, 2017.

[38] G. Peng, F. Min, and E. Wang, "Circuit implementation, synchronization of multistability, and image encryption of a four-wing memristive chaotic system," *Journal of Electrical and Computer Engineering*, vol. 2018, Article ID 8649294, 13 pages, 2018.

[39] A. N. Pisarchik and U. Feudel, "Control of multistability," *Physics Reports*, vol. 540, no. 4, pp. 167–218, 2014.

[40] V. N. Chizhevsky and S. I. Turovets, "Small signal amplification and classical squeezing near period-doubling bifurcations in a modulated CO_2-laser," *Optics Communications*, vol. 102, no. 1-2, pp. 175–182, 1993.

[41] A. N. Pisarchik and B. K. Goswami, "Annihilation of one of the coexisting attractors in a bistable system," *Physical Review Letters*, vol. 84, no. 7, pp. 1423–1426, 2000.

[42] K. Yadav, N. K. Kamal, and M. D. Shrimali, "Intermittent feedback induces attractor selection," *Physical Review E*, vol. 95, Article ID 042215, 2017.

[43] K. Yadav, A. Prasad, and M. D. Shrimali, "Control of coexisting attractors via temporal feedback," *Physics Letters A*, vol. 382, no. 32, pp. 2127–2132, 2018.

[44] T. F. Fozin, G. D. Leutcho, A. T. Kouanou et al., "Multistability control of hysteresis and parallel bifurcation branches through a linear augmentation scheme," *Zeitschrift für Naturforschung A*, vol. 75, no. 1, pp. 11–21, 2019.

[45] P. R. Sharma, M. D. Shrimali, A. Prasad, N. V. Kuznetsov, and G. A. Leonov, "Control of multistability in hidden attractors," *The European Physical Journal Special Topics*, vol. 224, no. 8, pp. 1485–1491, 2015.

[46] P. R. Sharma, A. Sharma, M. D. Shrimali, and A. Prasad, "Targeting fixed-point solutions in nonlinear oscillators through linear augmentation," *Physical Review E*, vol. 83, Article ID 067201, 2011.

[47] P. R. Sharma, M. D. Shrimali, A. Prasad, and U. Feudel, "Controlling bistability by linear augmentation," *Physics Letters A*, vol. 377, no. 37, pp. 2329–2332, 2013.

[48] P. R. Sharma, M. D. Shrimali, A. Prasad, N. V. Kuznetsov, and G. A. Leonov, "Controlling dynamics of hidden attractors," *International Journal of Bifurcation and Chaos*, vol. 25, no. 4, Article ID 1550061, 2015.

[49] P. R. Sharma, A. Singh, A. Prasad, and M. D. Shrimali, "Controlling dynamical behavior of drive-response system through linear augmentation," *The European Physical Journal Special Topics*, vol. 223, no. 8, pp. 1531–1539, 2014.

[50] Z. Tabekoueng Njitacke, I. Sami Doubla, J. Kengne, and A. Cheukem, "Coexistence of firing patterns and its control in two neurons coupled through an asymmetric electrical synapse," *Chaos: An Interdisciplinary Journal of Nonlinear Science*, vol. 30, Article ID 023101, 2020.

[51] A. Tsuneda, "A gallery of attractors from smooth Chua's equation," *International Journal of Bifurcation and Chaos*, vol. 15, no. 1, pp. 1–49, 2005.

[52] J. Kengne, G. D. Leutcho, and A. N. K. Telem, "Reversals of period doubling, coexisting multiple attractors, and offset boosting in a novel memristive diode bridge-based hyperjerk circuit," *Analog Integrated Circuits and Signal Processing*, vol. 101, no. 3, pp. 379–399, 2019.

[53] J. Kengne and R. L. T. Mogue, "Dynamic analysis of a novel jerk system with composite tanh-cubic nonlinearity: chaos, multi-scroll, and multiple coexisting attractors," *International Journal of Dynamics and Control*, vol. 7, no. 1, pp. 112–133, 2019.

[54] L. K. Kengne, J. Kengne, and H. B. Fotsin, "The effects of symmetry breaking on the dynamics of a simple autonomous jerk circuit," *Analog Integrated Circuits and Signal Processing*, vol. 101, no. 3, pp. 489–512, 2019.

[55] G. D. Leutcho and J. Kengne, "A unique chaotic snap system with a smoothly adjustable symmetry and nonlinearity: chaos, offset-boosting, antimonotonicity, and coexisting multiple attractors," *Chaos, Solitons & Fractals*, vol. 113, pp. 275–293, 2018.

[56] G. D. Leutcho, J. Kengne, and R. Kengne, "Remerging Feigenbaum trees, and multiple coexisting bifurcations in a novel hybrid diode-based hyperjerk circuit with offset boosting," *International Journal of Dynamics and Control*, vol. 7, no. 1, pp. 61–82, 2019.

[57] M. Chen, M. Sun, H. Bao, Y. Hu, and B. Bao, "Flux–charge analysis of two-memristor-based chua's circuit: dimensionality decreasing model for detecting extreme multistability," *IEEE Transactions on Industrial Electronics*, vol. 67, no. 3, pp. 2197–2206, 2019.

[58] N. Tsafack and J. Kengne, "Complex dynamics of the chua's circuit system with adjustable symmetry and nonlinearity: multistability and simple circuit realization," *World Journal of Applied Physics*, vol. 4, no. 2, pp. 24–34, 2019.

[59] N. Tsafack and J. Kengne, "Multiple coexisting attractors in a generalized Chua's circuit with a smoothly adjustable symmetry and nonlinearity," *Journal of Physical Mathematics*, vol. 10, 2019.

[60] Z. T. Njitacke, J. Kengne, and H. B. Fotsin, "Coexistence of multiple stable states and bursting oscillations in a 4D Hopfield neural network," *Circuits, Systems, and Signal Processing*, vol. 39, no. 7, pp. 3424–3444, 2020.

[61] Z. T. Njitacke and J. Kengne, "Complex dynamics of a 4D Hopfield neural networks (HNNs) with a nonlinear synaptic

weight: coexistence of multiple attractors and remerging Feigenbaum trees," *AEU—International Journal of Electronics and Communications*, vol. 93, pp. 242–252, 2018.

[62] A. Wolf, J. B. Swift, H. L. Swinney, and J. A. Vastano, "Determining Lyapunov exponents from a time series," *Physica D: Nonlinear Phenomena*, vol. 16, no. 3, pp. 285–317, 1985.

[63] B. C. Bao, H. Bao, N. Wang, M. Chen, and Q. Xu, "Hidden extreme multistability in memristive hyperchaotic system," *Chaos, Solitons & Fractals*, vol. 94, pp. 102–111, 2017.

[64] S. Zhang, Y. Zeng, Z. Li, and C. Zhou, "Hidden extreme multistability, antimonotonicity and offset boosting control in a novel fractional-order hyperchaotic system without equilibrium," *International Journal of Bifurcation and Chaos*, vol. 28, no. 13, Article ID 1850167, 2018.

[65] A. N. Negou and J. Kengne, "A minimal three-term chaotic flow with coexisting routes to chaos, multiple solutions, and its analog circuit realization," *Analog Integrated Circuits and Signal Processing*, vol. 101, pp. 415–429, 2019.

[66] K.-Y. Lian, P. Liu, T.-S. Chiang, and C.-S. Chiu, "Adaptive synchronization design for chaotic systems via a scalar driving signal," *IEEE Transactions on Circuits and Systems I: Fundamental Theory and Applications*, vol. 49, pp. 17–27, 2002.

[67] J. H. Peng, E. J. Ding, M. Ding, and W. Yang, "Synchronizing hyperchaos with a scalar transmitted signal," *Physical Review Letters*, vol. 76, no. 6, pp. 904–907, 1996.

[68] C. Han, S. Yu, and G. Wang, "A sinusoidally driven Lorenz system and circuit implementation," *Mathematical Problems in Engineering*, vol. 2015, Article ID 706902, 11 pages, 2015.

[69] Q. Xu, Q. Zhang, B. Bao, and Y. Hu, "Non-autonomous second-order memristive chaotic circuit," *IEEE Access*, vol. 5, pp. 21039–21045, 2017.

[70] Z. T. Njitacke and J. Kengne, "Nonlinear dynamics of three-neurons-based Hopfield neural networks (HNNs): remerging Feigenbaum trees, coexisting bifurcations and multiple attractors," *Journal of Circuits, Systems and Computers*, vol. 28, no. 7, Article ID 1950121, 2019.

[71] Q. Xu, Q. Zhang, N. Wang, H. Wu, and B. Bao, "An improved memristive diode bridge-based band pass filter chaotic circuit," *Mathematical Problems in Engineering*, vol. 2017, Article ID 2461964, 11 pages, 2017.

Hindawi
Complexity
Volume 2020, Article ID 9410315, 26 pages
https://doi.org/10.1155/2020/9410315

Research Article

A Panoramic Sketch about the Robust Stability of Time-Delay Systems and Its Applications

Baltazar Aguirre-Hernández,[1] Raúl Villafuerte-Segura,[2] Alberto Luviano-Juárez,[3] Carlos Arturo Loredo-Villalobos,[1] and Edgar Cristian Díaz-González[1]

[1]*Departamento de Matemáticas, Universidad Autónoma Metropolitana Iztapalapa, 09340 Ciudad de Mexico, CDMX, Mexico*
[2]*Centro de Investigación en Tecnologías de Información y Sistemas, Universidad Autónoma del Estado de Hidalgo, Pachuca, HGO, Mexico*
[3]*Instituto Politécnico Nacional UPIITA, Ciudad de Mexico, CDMX, Mexico*

Correspondence should be addressed to Raúl Villafuerte-Segura; villafuerte@uaeh.edu.mx

Received 30 May 2020; Revised 20 August 2020; Accepted 5 September 2020; Published 27 September 2020

Academic Editor: Tila Bueno

Copyright © 2020 Baltazar Aguirre-Hernández et al. This is an open access article distributed under the Creative Commons Attribution License, which permits unrestricted use, distribution, and reproduction in any medium, provided the original work is properly cited.

This paper presents a brief review on the current applications and perspectives on the stability of complex dynamical systems, with an emphasis on three main classes of systems such as delay-free systems, time-delay systems, and systems with uncertainties in its parameters, which lead to some criteria with necessary and/or sufficient conditions to determine stability and/or stabilization in the domains of frequency and time. Besides, criteria on robust stability and stability of nonlinear time-delay systems are presented, including some numerical approaches.

1. Introduction

The importance of complex dynamical systems has been increasing dramatically since many real world applications have adopted this behavior. Some of them have become special areas of study such as smart grids [1–5], autonomous vehicles [6–10], biological systems [11–17], distribution networks [18–23], social interaction [24–27], communication systems [28–30], and animal monitoring [31–34], among others.

Among the structural properties in complex systems, controllability and observability are still discussion topics for a wide variety of dynamical systems, from classic linear time-invariant systems to other more complex families such as infinite-dimensional systems, stochastic systems, and hybrid systems, among others. This problem increases when they are subject to a large amount of connections, in which a classic handling is very difficult such as in complex networks [35], where the connection properties, such as symmetry [36, 37], and some computational tools have been developed to determine these properties [38].

In the case of stability of complex systems, two important aspects to consider are the time-delay between nodes (or the possible presence of time delay in the internal dynamics) and the robustness of the system (connection and internal) due to parametric variations. On the one hand, the time-delay induces infinite-dimensional dynamics whose equilibrium stability is still an active topic of research for, both, stability analysis itself and the use of the delay as a stabilizing element [39]. On the other hand, the parameter variations in a system demands a special stability treatment which has motivated some significant results such as Kharitonov's theorem [40] or H_∞ loop shaping in control design [41].

In this article, a stability review for a class of systems subject to parameter variations and time delays is addressed. The review includes a definition of the dynamics of a family of nonlinear time-delay systems, a brief historical outlook of the stability study development, and then it gives some approaches in time and frequency domain, as well as a numerical analysis to provide the stability operating regions. Then, the robustness aspect of stabilizing controls is discussed on the realm of Hurwitz polynomials families.

Finally, some perspectives of applications demanding these approaches are briefly provided.

2. Stability and Stabilization of Linear Systems

Characteristic root locations of linear systems or linear delay-free systems are completely related to system stability. The same criterion holds for linear time-delay system. Furthermore, many of the concepts and criteria for determining stability on time-delay system (TDS) are extensions or adaptations of the results initially proposed for linear delay-free systems. Accordingly, it is considered relevant to briefly address some classic stability criteria for this type of system.

In this section, some concepts and criteria regarding the stability of linear systems are analyzed. The section is divided as follows. In Section 2.1, the concept of stability in linear systems is addressed, Section 2.2 presents what can be the objectives in the stabilization of linear systems, and, finally, in Section 2.3, Kharitonov's theorem is analyzed and some families of polynomials to illustrate the importance of studying the stability in systems with uncertainties in the parameters are given.

2.1. Stability of Linear Systems. Lyapunov's doctoral thesis was perhaps the first systematic work on the subject of stability [42], although the study of stability theories was started by Maxwell, around 1868, in his work "on governors" [43]. Lyapunov presented a general definition of stability which referred to the stability of a solution of a differential equation, not necessarily at the equilibrium point.

Before Lyapunov, there were works that tried to explain the stability phenomenon in applications; it is worth mentioning the works of Lagrange and Dirichlet [44–48]. After Lyapunov's work, new concepts appeared such as uniform, global, exponential, and quasi asymptotic stability, among other types of them. In the following, some of the best known criteria for determining the stability of linear systems will be briefly mentioned.

A way to determine the asymptotic stability of continuous time-invariant systems is characterized by its eigenvalues. If all eigenvalues lie into open left half plane C^-, then the system is stable. A polynomial $p(s)$ that satisfies that all its roots are in C^- is called a Hurwitz polynomial or stable polynomial. Routh and Hurwitz showed, in independent works, that the stability of a matrix system could be determined by means of the coefficients of its characteristic polynomial. Their results are currently presented under the so-called Routh–Hurwitz criterion (see [49, 50]) and can be considered as a numerical criterion. In view of that, it is reduced to the calculation of determinants. Another useful approach used to test the stability is the Hermite–Biehler criterion [51, 52], which can be considered as an algebraic criterion, which expresses the stability in terms of even and odds parts of the characteristic polynomial. A pair of polynomials u and v are said to be a couple positive if the principal coefficients of u and v have the same sign and the roots μ_i of u and ν_i of v alternate orderly on the real axis, i.e., are real, distinct, and negative and satisfy the interlacing property. So, the Hermite–Biehler theorem states that a polynomial $p(x)$ that can be written in the form $p(x) = f(x^2) + xg(x^2)$ is stable if and only if f and g are a couple positive (see [49, 50], for details). There are others non-common stability criteria; it is worth mentioning some of them. The Lienard–Chipart conditions [53] reduce the positivity evaluation of the main minors of the Routh–Hurwitz criterion to half.

The Leohnard–Mihailov criterion [54], which expresses the stability in geometric terms, analyzes the argument of the complex polynomial $p(iw)$ associated with the characteristic polynomial p of the system. Routh's scheme gives rise to a recursive algorithm for testing the stability called Hurwitz stability test. Other approaches consider the Bezoutiant or the Cauchy indexes to verify stability of polynomials; for details, see [49, 50, 55].

Not less important are those systems, where uncertainty is considered and incorporated through parameters. The robust stability of parameter uncertainty systems and the families of polynomials are associated with them, and it is addressed in the subsequent sections.

2.2. Stabilizing Controls. In this section, the relation between stabilizing feedback and some families of Hurwitz polynomials is explained. Consider the controllable system:

$$\dot{x}(t) = Ax(t) + bu(t), \tag{1}$$

$x, b \in R^n$ and the controllable pair (A, b) is given in the canonical form:

$$A = \begin{pmatrix} 0 & 1 & 0 & \cdots & 0 \\ 0 & 0 & 1 & \cdots & 0 \\ \vdots & \vdots & \vdots & \cdots & \vdots \\ 0 & 0 & 0 & \cdots & 1 \\ -a_n & -a_{n-1} & -a_{n-2} & \cdots & -a_1 \end{pmatrix}, \quad b = \begin{pmatrix} 0 \\ 0 \\ \vdots \\ 0 \\ 1 \end{pmatrix}. \tag{2}$$

Note that the open-loop polynomial is given by $p_0(s) = s^n + a_1 s^{n-1} + \cdots + a_n$.

Now, let us define the feedback control u as follows:

$$u(t) = -kc^T x(t), \tag{3}$$

where $c \in R^n$ and $k > 0$. Then, the closed-loop polynomial is given by

$$p_c(s) = s^n + a_1 s^{n-1} + a_2 s^{n-2} + \cdots + a_n + k \cdot \left(c_1 s^{n-1} + c_2 s^{n-2} + \cdots + c_n\right). \tag{4}$$

Let us denote $p_c^*(s) = c_1 s^{n-1} + \cdots + c_2 s^{n-2} + \cdots + c_n$. Then, $p_c(s) = p_0(s) + k p_c^*(s)$. Now, let us suppose that the

$p_c^*(s)$ is a Hurwitz polynomial. When $k \longrightarrow \infty$ a closed-loop eigenvalue, say λ_1 satisfies $(\lambda_1/k) \longrightarrow -c_1$, the other eigenvalues converge to the zeroes of $p^*(s)$, that is, when $k \gg 1$, feedback (3) is a stabilizing control (see [56, 57]).

Also note that when $k \gg 1$, then high control gains kc^T are induced in the feedback (3); hence, feedback (3) is a high-gain feedback. There are several studies to analyze the properties of high-gain controls (see [56–64]).

Returning to the analysis of the closed-loop polynomial $p_c(s) = p_0(s) + kp_c^*(s)$, it can be seen that $p_c(s)$ is not necessarily Hurwitz for all $k > 0$, even when $p_0(s)$ is Hurwitz and $c \in R^n$ is chosen such that $p_c^*(s)$ is a Hurwitz polynomial (see [65–67]).

The last observation is illustrated with the following example, which was presented in [67].

Consider the system:

$$\dot{x}(t) = \begin{pmatrix} 0 & 1 & 0 \\ 0 & 0 & 1 \\ -5 & -11 & -7 \end{pmatrix} x(t) + \begin{pmatrix} 0 \\ 0 \\ 1 \end{pmatrix} + (-65k, -3k, -k)x(t). \tag{5}$$

Here, $p_0(s) = s^3 + 7s^2 + 11s + 5 = (s+1)^2(s+5)$ and $p_c^*(s) = s^2 + 3s + 65$, $p_0(s)$ and $p_c^*(s)$ are Hurwitz polynomials. However, $p_0(s) + kp_c^*(s)$ is not a Hurwitz polynomial for $k \in [3, 8]$; hence, the importance of have methods for choosing vectors c such that $u(t) = -kc^T x(t)$ is a stabilizing control. Consequently, it is necessary to study the Hurwitz stability of the ray of polynomials $p_0(s) + kp_c^*(s)$ with $k > 0$.

In the next section, a technique in terms of rays and segments of polynomials is presented.

2.2.1. Relation between Stabilizing Controls and Rays and Segments of Hurwitz Polynomials. As can be observed above, the control $u(t) = -kc^T x(t)$ is a stabilizing feedback if and only if the ray of polynomials $p_0(s) + kp_c^*(s)$ is a ray of Hurwitz polynomials. On the contrary, there is an obvious relation between Hurwitz rays and Hurwitz segments of polynomials: if $p_0(s) + kp_c^*(s)$ is a Hurwitz polynomial, then $(1/1+k)p_0(s) + (k/1+k)p_c^*(s)$ is a Hurwitz polynomial, which implies that the Hurwitz stability of the ray $p_0(s) + kp_c^*(s)$ is equivalent to the Hurwitz stability of the segment of polynomials $[p_0(s), p_c^*(s)]$.

The problem to establish conditions on the Hurwitz polynomials $f_0(s)$ and $f_1(s)$ such that the segment of polynomials determined by $f(s, \lambda) = \lambda f_0(s) + (1-\lambda) f_1(s)$ is Hurwitz stable for all $\lambda \in [0, 1]$ has been studied with different approaches (see [65–73]). The first reported work about this subject is Bialas's paper [68]. Bialas's theorem says that if $f_0(s)$ is a Hurwitz polynomial and $\deg(f_0) > \deg(f_1)$, then $f(s, \lambda)$ is Hurwitz for all $\lambda \in [0, 1]$ if and only if the matrix $H^{-1}(f_0)H(f_1)$ has no eigenvalues in $(-\infty, 0)$, where $H(p)$ is the Hurwitz matrix of the polynomial p (see [68, 74, 75]).

Other method which is known as the segment Lemma was obtained by Chapellat and Bhattacharyya (see [76, 77]). The segment lemma is an approach that presents conditions in the frequency domain. Based on the segment lemma, a computational algorithm was developed in [71] for testing the Hurwitz stability of segments of polynomials. On the contrary, Bose developed a technique to check the stability of segments of complex polynomials [78].

Based on Bose's test, in [69], a test for checking the stability of segment of complex polynomials was obtained. Another computational method is presented in [79]. Sufficient conditions to guarantee the Hurwitz stability of segments were obtained by Rantzer (see [72, 80]). On the contrary, an approach, where sufficient conditions in terms of matrix inequalities for checking the Hurwitz stability of segments of polynomials, has been presented in [65–67, 73]. The explanation of the aforementioned approach is the following: let $f_0(s) = s^n + a_1 s^{n-1} + \cdots + a_n$ be a Hurwitz polynomial.

Consider the matrix $E_{(n,n-1)} \in M_{n\times n}$ defined by

$$E_{(n,n-1)} = \begin{pmatrix} a_1 & -1 & 0 & 0 & \cdots & 0 & 0 \\ -a_3 & a_2 & -a_1 & 1 & \cdots & 0 & 0 \\ a_5 & -a_4 & a_3 & -a_2 & \cdots & 0 & 0 \\ \vdots & \vdots & \vdots & \vdots & \cdots & \vdots & \vdots \\ 0 & 0 & 0 & 0 & \cdots & a_{n-1} & -a_{n-2} \\ 0 & 0 & 0 & 0 & \cdots & 0 & a_n \end{pmatrix}, \tag{6}$$

and consider the matrix $D_{(n,n-1)} \in M_{n\times n}$ defined by

$$D_{(n,n-1)} = \begin{pmatrix} 1 & 0 & 0 & 0 & \cdots & 0 & 0 \\ -a_2 & a_1 & -1 & 0 & \cdots & 0 & 0 \\ a_4 & -a_3 & a_2 & -a_1 & \cdots & 0 & 0 \\ \vdots & \vdots & \vdots & \vdots & \cdots & \vdots & \vdots \\ 0 & 0 & 0 & 0 & \cdots & a_{n-2} & -a_{n-3} \\ 0 & 0 & 0 & 0 & \cdots & -a_n & a_{n-1} \end{pmatrix}. \tag{7}$$

Now, let $f_1(s) = c_1 s^{n-1} + c_2 s^{n-2} + \cdots + c_n$ be an arbitrary polynomial of degree $n-1$ with positive coefficients. If the vector $(c_1, c_2, \ldots, c_n)^T$ satisfies the system of linear inequalities $E_{(n,n-1)}c \gneqq 0$ or $D_{(n,n-1)}c \gneqq 0$, then $\lambda f_0(s) + (1-\lambda) f_1(s)$ is Hurwitz for every $\lambda \in [0, 1]$ (here the symbol $\succ 0$ ($\prec 0$) means that the components of a vector are nonnegative (nonpositive) and the symbol $\gneqq$ means that all of the components of a vector are nonnegative, but there is at least one positive component).

Other interesting references about segments of Hurwitz polynomials are the works [74, 76, 81–86]. Besides, in relation with Hurwitz polynomials, it is worth to consulting paper [87].

2.3. Robust Stability. The presence of several uncertain parameters in description of a LTI system manifests itself as variations in the coefficients of the characteristic polynomial. The determination of stability and stability margins under parametric uncertainty, structure uncertainty itself included, is the main purpose of the robust stability.

Perhaps, the most famous result about the Hurwitz polynomial families is the Kharitonov theorem, which is related to the interval-type polynomials. This section presents this theorem and addresses some related results.

2.3.1. The Kharitonov Theorem. The problem of stability under large parameter uncertainty was strongly promoted with the advent of a remarkable theorem due to the Russian control theorist V. L. Kharitonov.

Consider the interval family of polynomial defined by

$$P(s) = \alpha_0 + \alpha_1 s + \alpha_2 s^2 + \cdots + \alpha_n s^n, \tag{8}$$

where

$$\alpha_0 \in [a_0, b_0], \alpha_1 \in [a_1, b_1], \ldots, \alpha_n \in [a_n, b_n]. \tag{9}$$

Consider the following four elements of the family, named the Kharitonov polynomials:

$$\begin{aligned} k^1(s) &= \left(a_0 + a_1 s + b_2 s^2 + b_3 s^3 + a_4 s^4 + a_5 s^5 + \ldots\right), \\ k^2(s) &= \left(a_0 + b_1 s + b_2 s^2 + a_3 s^3 + a_4 s^4 + b_5 s^5 + \ldots\right), \\ k^3(s) &= \left(b_0 + a_1 s + a_2 s^2 + b_3 s^3 + b_4 s^4 + a_5 s^5 + \ldots\right), \\ k^4(s) &= \left(b_0 + b_1 s + a_2 s^2 + a_3 s^3 + b_4 s^4 + b_5 s^5 + \ldots\right). \end{aligned} \tag{10}$$

Kharitonov's theorem establishes that every polynomial in families (8) and (9) is Hurwitz if and only if the four Kharitonov polynomials 10(10) are Hurwitz. This result has been the motivation of different extensions, alternate proofs, and applications to some classes of families of polynomials, for instance,

(i) The problem to find conditions for family (8) to be Hurwitz was planted by Faedo [88]

(ii) The original proof was given by Kharitonov in [89], but different authors have presented other proofs (see [70, 77, 90–93])

(iii) Kharitonov extended his result to the complex case in 1979 [94]

(iv) Generalizations of Kharitonov's theorem are presented in [56, 95, 96]

(v) Applications of Kharitonov's theorem can be consulted in [97]

(vi) Recent information about Interval Families and Kharitonov's theorem was published in papers [65, 98, 99]

The appearance of Kharitonov's theorem led to a resurgence of interest in the study of robust stability under real parametric uncertainty. In Section 2.2, some results related to stability of certain families of polynomials such as the segments and the rays of polynomials were mentioned. Some other families worth mentioning are the ball of stable polynomials and polytope of polynomials. The ball of stable polynomials is a way of characterizing the largest region where the stability of a family of polynomials is preserved. Soh et al. [100] in 1985 adopted a point of view opposite to Kharitonov. Starting with an already stable polynomial $p(s)$, they gave a way to compute the radius of the largest stability ball in the space of polynomial coefficients around p. The estimation for the l_2-norm stability ball in the space of coefficients was calculated by Soh et al. For l_p-norm, the calculation was realized by Tsypkin and Polyak [101].

Otherwise, the main robust stability result related with polytope of polynomials is the celebrated Edge theorem of Bartlett et al. [102], which considers more general stability regions, and it is not restricted to Hurwitz stability. They considered a family of polynomials whose coefficients vary in an arbitrary polytope: $p(s) = a_1 Q_1(s) + a_2 Q_2(s) + \cdots + a_m Q_m(s)$ on R^{n+1}, with its edges not necessarily parallel to the coordinate axes as in Kharitonov's problem. They proved that the root space of the entire family is bounded by the root loci of the exposed edges. In particular, the entire family is stable in and only if all the edges are proved to be stable. The key idea behind this result is that we can reduce a multidimensional uncertainty problem into a finite number of one-parameter problems whose solution requires less effort.

One of the most used tools in the analysis of robust stability in families of polynomials, where the coefficients depend continuously on a set of parameters, is the *Boundary Crossing theorem* and its computational version the *Zero Exclusion principle*. Consider a family of polynomials $F(s, p)$ of degree n, where the real parameter p ranges over a connected set Ω. If it is known that one member of the family is stable, a useful technique of verifying robust stability of the family is to ascertain that $F(j\omega, p) \neq 0$ for all $p \in \Omega, \omega \in R$. This can also be written as the *zero exclusion condition* $0 \notin F(j\omega, \Omega)$, for all $\omega \in R$. This zero exclusion condition has been exploited to derive various types of robust stability and performance margins.

3. Stability and Stabilization of Time-Delay Systems

This section begins with a brief classification of nonlinear TDS, followed by a recurring classification in which the nonlinear TDS has a nominal part (linear part). The above allows to show basic and pillar results existing in the literature for the stability and stabilization analysis of linear TDS in two domains, frequency and temporal. Although it is typically believed that an analysis in the frequency domain is only limited to linear systems, recent results have shown that a study on polytope of quasi-polynomials (generalized characteristic quasi-polynomial) can determine stability conditions for a class of nonlinear TDS. Furthermore, in the time domain, the use of complete type Lyapunov–Krasovskii functionals can provide necessary and sufficient stability conditions for a class of linear TDS, while reduced type functionals only give sufficient conditions.

The understanding, analysis, and prediction of the dynamics of a system are topics that generate considerable interest in the scientific community. When this system presents nonlinearities and delays in its structure, the useful information is even richer, since it is more consistent to the dynamics observed in the systems/processes/prototypes of the physical world. These types of systems are known as nonlinear time-delay systems or nonlinear systems with

delays. Sometimes, nonlinear dynamics are phenomena that often introduce unpredictable chaotic behaviors into a system, whereas the delays are due to the fact that the rate of variation in the system dynamics depends on past states, which implies an analysis in an infinite-dimensional space, and this is in mathematical terms. Thus, the dynamics observed in communication networks [103–105], teleoperation [106, 107], chemical processes [108], population dynamics [109], biological phenomena [110], game theory and economic applications [111, 112], unmanned aerial vehicles [113], haptic interfaces [114], and robotic systems [115, 116], among others, can be mathematically modeled using nonlinear time-delay systems.

The nonlinear TDS are usually represented by functional differential equations (FDEs) also known as delay differential equations. Among functional differential equations, one may distinguish some particular classes as retarded functional differential equations (RFDEs) (or functional differential equations of retarded type), neutral functional differential equations (NFDEs) (or functional differential equations of neutral type), distributed functional differential equations (DFDEs) (or functional differential equations of distributed type), and differential-difference equations (DDEs). For illustrative purposes and to characterize the research space of the FDEs, the form of RFDE with one delay is presented below:

$$\begin{aligned} \dot{x}(t) &= f(t, x_t), \\ x(\theta) &= \phi(\theta), \quad \theta \in [-\tau, 0], \end{aligned} \tag{11}$$

where $f\colon R^+ \times \mathfrak{C} \longrightarrow R^n$ is continuous and satisfies a local Lipschitz condition regarding the second element of the argument. For $t \geq 0$, denote by $x(t, \phi) \in R^n$ the system solution with initial function (condition) $\phi \in \mathfrak{C}$, and by $\mathfrak{C} \coloneqq C([-\tau, 0], R^n)$ the Banach space with norm $\|\phi\|_\tau \coloneqq \max_{\theta \in [-\tau,0]} \|\phi(\theta)\|$. Here, $\|\cdot\|$ denotes the Euclidean norm. As a natural extension of the initial function, a solution segment of $x(t, \phi)$ in a time interval $[t - \tau, t]$ is denoted by

$$x_t = x(t + \theta) \in \mathfrak{C}, \quad \theta \in [-\tau, 0], \tag{12}$$

and called state of system (11). In turn, the above RFDE can be classified as follows:

(i) Time-invariant RFDE if the first term of the argument is omitted:

$$\begin{aligned} \dot{x}(t) &= f(x_t), \\ \text{or } \dot{x}(t) &= f(x(t), x(t - \tau)). \end{aligned} \tag{13}$$

(ii) RFDE with multiple delay if $0 = \tau_0 < \tau_1 < \cdots < \tau_m =$, that is,

$$\dot{x}(t) = f(t, x(t), x(t - \tau_1), x(t - \tau_2), \ldots, x(t - \tau_m)). \tag{14}$$

(iii) State-dependent delay RFDE if τ depends on state, x_τ:

$$\dot{x}(t) = f(t, x(t), x(t - \tau(x(t)))). \tag{15}$$

(iv) Time-varying delay RFDE if the delay τ depends on t:

$$\dot{x}(t) = f(t, x(t), x(t - \tau(t))). \tag{16}$$

(v) RFDE with distributive delay, also known as DFDE, if the delay is represented as a continuously distribution and it is not instantaneous:

$$\dot{x}(t) = f\left(t, x(t), \int_0^\infty x(t - \vartheta) d\vartheta\right). \tag{17}$$

(vi) RFDE with neutral delay or NFDE if the system also depends on the time derivative of the state:

$$\begin{aligned} \dot{x}(t) &= f(t, x_t, \dot{x}_t), \\ \text{or } \left(\frac{\mathrm{d}}{\mathrm{d}t}\right)[x(t) - g(t, x_t)] &= f(t, x_t). \end{aligned} \tag{18}$$

(vii) RFDE with discrete delay or DDE if τ is the interval between the successive sample instants t_{k-1} and t_k, $\tau = t_{k+1} - t_k \coloneqq \Delta t, k = 1, 2, \ldots, N$ and $t = (N - 1)$. Here, τ is called the sample period, and $x_k = x(t - (N - k)\tau) = x(t - (N - k)\Delta t)$ is an N-dimensional discrete mapping, and using any integral scheme we obtain

$$\begin{aligned} &x(t + \Delta t) = x(t) + f(x, x_\tau)\Delta t, \quad x_\tau = x(t - \tau) \text{ or,} \\ &x_1(k + 1) = x_N(k) + f(x_N(k), x_1(k))\Delta t, \\ &x_2(k + 1) = x_1(k + 1) + f(x_1(k + 1), x_2(k))\Delta t, \\ &\qquad \vdots \\ &x_N(k + 1) = x_{N-1}(k + 1) + f(x_{N-1}(k + 1), x_N(k))\Delta t. \end{aligned} \tag{19}$$

The above, as well as the possible combinations between these, are just some types of TDS. Currently, there is a broader classification of systems that are outside this basic classification. In addition, each type of TDS needs more appropriate concepts and descriptions for the research space and existence and uniqueness of the solution, among others. For further information, the reader is referred to the following authoritative references [52, 117–127]. Although these themes are very interesting, the focus of this review is on stability and stabilization. Therefore, it will be the next topic to discuss.

3.1. Stability of Time-Delay Systems. Undoubtedly, one of the most important research topics for the TDS research community is the analysis of stability. In this context, obtaining sufficient and/or necessary conditions to determine when the studied system remains stable or when it gains and/or loses stability is an important topic for the community. Furthermore, the knowledge of these conditions allows to solve other problems associated with this

topic such as analysis of robustness/adaptability/uncertainty/perturbation, design of observers, synthesis and tuning of controllers, determination of attraction regions estimates, and study of chaotic/hyperchaotic behaviors, to name just a few, [128–137].

Typically, the stability of the TDS is studied on two main frameworks: frequency domain and time domain. The fundamental results were proposed by Pontryagin [138, 139], Wright [140, 141], Bellman [142, 143], and Cooke [144] in the 1940s and 1950s. These results are in the frequency domain, which is based on a study of its corresponding characteristic equation (exponential polynomial, quasi-polynomial, and analytic function with transcendental terms) to determine the location of its roots in the complex plane or from the nontrivial solutions of a delayed Lyapunov matrix function. Later, Razumikhin [145] and Krasovskii [146] proposed to extend Lyapunov's results to analyze stability of TDS in the time domain.

The stability of nonlinear TDS has been studied for almost 80 years and most of the results proposed by the research community are about nonlinear systems with a specific structure. Among which, it is possible to apply techniques that benefit/facilitate the analysis of the stability of complex systems around an operating (equilibrium) point or even in a sector of it. Since, these allow to rewrite exactly or approximately a complex system in a more accessible system to study. Techniques such as sector nonlinearity [147], tangent linearization [148], feedback linearization approach (Lie derivative) [149, 150], passification [151–154], backstepping [155–158], immersion and invariance [159–162], and differential flatness [163–165], among others. On the contrary, in some cases, a linearization is proposed around an operating point. While in other cases, the nonlinear systems is represented with a dominant part (dominant linear part) plus nonlinear part is proposed. In this way, in the nonlinear part, disturbances, nonmodel dynamics, and parametric variations, among others, are usually introduced. Below, it is a classification of the aforementioned systems.

Let a nonlinear TDS be given in (11); in some cases, this system can be represented as

$$\dot{x}(t) = L(t, x_\tau) + g(t, x_t), \tag{20}$$

where L: $R^+ \times \mathfrak{C} \longrightarrow R^n$ is a linear operator and g: $R^+ \times \mathfrak{C} \longrightarrow R^n$ is a nonlinear operator, both properly defined. Typically, if g satisfies certain conditions (bounded, Lipschitz, and quasi-Lipschitz, among others), then g is considered as an uncertainty or/and perturbation of the nonlinear TDS, so the stability analysis of (20) focuses on the nominal system $\dot{x}(t) = L(t, x_\tau)$. A classification of the nominal part $L(t, x_\tau)$ proposed here is as follows:

(i) $L(t, x_\tau) = A_0(t)x(t) + A_1(t)x(t-\tau)$ is a linear time-variant (LTV) delay system of retarded type

(ii) $L(t, x_\tau) = A_0(\theta(t))x(t) + A_1(\theta(t))x(t-\tau)$ is a linear parameter varying (LPV) system with time delay, where θ are uncertain time-variant real parameters which satisfy $\underline{\theta} \le \theta(t) \le \overline{\theta}$

(iii) $L(t, x_\tau) = A_0x(t) + A_1x(t-\tau(t))$ is a linear system with time-varying delay, where $0 \le \tau(t) \le \overline{\tau}$ and $\dot{\tau}(t) \le \mu \le$, for all $t \ge 0$

(iv) $L(t, x_\tau) = A_0x(t) + A_1x(t-\tau)$ is a linear time-invariant (LTI) TDS of retarded type

(v) $L(t, x_\tau) = A_0x(t) + A_1x(t-\tau) + D_0\dot{x}(t) + D_1\dot{x}(t-\tau)$ is a linear NFDE (linear neutral time-delay systems or linear time-delay system of type neutral), where $|D_i| < 1$, for any matrix norm $|\cdot|$

(vi) $L(t, x_\tau) = A_0x(t) + A_1x(t-\tau) + \int_\tau^0 D(\vartheta)x(t+\vartheta)d$ is a linear DFDE or linear distributed time-delay system; here, $D(t)$ is a continuous matrix on $[-\tau, 0]$ of appropriate dimensions

(vii) $L(t, x_\tau) = \sum_{i=0}^m A_ix(t-\tau_i)$ is a LTI-TDS with multiple delays of retarded type, $0 = \tau_0 < \tau_1 < \cdots < \tau_m = \tau$

To learn more about the systems described above, the reader can consult the following references [52, 166–169]. Although the nonlinear part $g(t, x_\tau)$ is also important and its structure depends on the type of studied nonlinear system, it is more important to know the studies regarding the stability of the nominal part. Since the stability of the nominal part can contribute the obtaining of robust stability conditions in the presence of the nonlinear part. Therefore, some research studies on stability analysis of linear TDS in the frequency domain and time domain are presented below.

3.2. Stability in the Frequency Domain. It is well known that the analysis of stability and stabilization of a TDS in the frequency domain is based on a study of its corresponding characteristic equation to determine the location of its roots in the complex plane. This concept is inherited from the stability analysis of delay-free systems, mainly from Hurwitz's concept [170, 171]. However, when the delays are considered in a system, it involves the inclusion of transcendental terms in the characteristic equation, changing the analysis of a polynomial (free-delay systems) to a quasi-polynomial (TDS). This complicates the analysis of a finite number to an infinite number of roots [172], also this analysis is usually limited to LTI-TDS. However, in contrast with the time domain, this analysis allows obtaining necessary and sufficient stability conditions; recent results have shown that an analysis in the frequency domain can be applied to a class of nonlinear TDS, see [173, 174].

Given a LTI-TDS with multiple delays of retarded type,

$$\dot{x}(t) = \sum_{i=0}^m A_ix(t-\tau_i), \tag{21}$$

then its quasi-polynomial is of the form

$$\begin{aligned} Q(s) &= \det\left\{ sI_n - \sum_{k=0}^m A_k e^{-s\tau_k} \right\} \\ &= \sum_{k=0}^m p_k(s)e^{-s\tau_k} = 0, \end{aligned} \tag{22}$$

where I_n is the identity matrix of n-dimension, $0 = \tau_0 < \tau_1 < \cdots < \tau_m = \tau$, $p_k(s) = \sum_{j=0}^{r_k} a_{k_j} s^j$, $k = 0, 1, \ldots, m$, are polynomials with real coefficients and $\deg(p_0) \leq \deg(p_k)$, i.e., $r_0 \leq r_k$, $k = 1, \ldots, m$. Although $Q(s)$ given in 3.2 has an infinite number of roots, it is enough to know the location of the dominant roots as shown below.

Definition 1 (see [166]). The LTI-TDS with multiple delays of retarded type (21) is said to be σ-stable (exponentially stable) if the system response $x(t, \phi)$ satisfies the following inequality:

$$\|x(t, \phi)\| \leq Le^{-\sigma t}\|\phi\|_\tau, \quad t \geq 0, \tag{23}$$

where $L > 0$, $\sigma \geq 0$, and ϕ: $[-\tau, 0] \longrightarrow C([-\tau, 0], R^n)$ is the initial condition.

Under consideration, for LTI-TDS of retarded type, the exponential stability and asymptotic stability are equivalent.

Definition 2 (see [166]). Consider the quasi-polynomial 3.2, $\sigma \in R$ a positive constant and

$$s_0 = \max_{j=1,\ldots,\infty} \left\{ \mathrm{Re}\{s_j\} \,\middle|\, Q(s_j) = 0, s_j \in C \right\}, \tag{24}$$

where $\mathrm{Re}\{s_j\}$ denotes the real part of s_j. Then, the LTI-TDS with multiple delays of retarded type (22) is σ-stable if $s_0 \leq -\sigma$ (relative stability, [175]).

As can be seen in the above definitions, the stability of an LTI-TDS with multiple delays depends on the dominant roots of 3.2, which determine the abscissa $-\sigma$ (spectral abscissa) or vertical line on $-\sigma$ in the complex plane. Furthermore, the roots have continuous variations with respect to parametric variations of the system. This is known as continuity property.

Theorem 1 (see [176]). *If the matrices A_k or the delays τ_k, $k = 1, 2, \ldots, m$, are varied, then a loss or acquisition of exponential stability of the solution $x(t, \phi)$ of LTI-TDS with multiple delays (21) is associated with the dominant roots of the quasi-polynomial (22).*

This allows to obtain conditions of robustness when there are parametric variations and also the design and tuning of control laws for s-stabilize TDS are as shown in Section 3.4.

However, in the framework of TDS stability in the frequency domain, there are many results/criteria; among the first and most important are the following:

(i) The Pontryagin criterion [177] is considered as one of the most general analytical criteria, and it gives necessary and sufficient conditions for the stability of (22). However, it has strong limitations and may become very complicated for systems with more than one delay.

(ii) The Yesipovich–Svirskii criterion [178] is for systems with one discrete delay. The necessary and sufficient condition of the stability of (22) is given by means of the expression:

$$\sum_k \mathrm{sgn}\left(\left(\frac{1}{\mathrm{Re}\{F(u_k)\}}\right)\left(\frac{d\mathrm{Im}\{F(u_k)\}}{d(u_k)}\right)\right), \tag{25}$$

where

$$F(z) = \frac{1}{\tan(1/2z)} + \phi(z), \tag{26}$$

is a further transformation $s = iz$, $i^2 = -1, z \in C$, of $Q(s) = 0$, $\phi(z)$ is a function that does not contain transcendental terms, and u_k are the real roots of $\mathrm{Im}\phi(z) = 0$.

(iii) The τ-decomposition method [179] requires the transformation of the quasi-polynomial into the form

$$e^{\tau s} = D_0(\tau), \tag{27}$$

where $D_0(s)$ is a ration of two polynomials. This method is for systems with one discrete delay, and it is based on the analysis of the contour $D_0(iu)$, $u \in R^+$ around the unit circle in the complex plane.

(iv) The principle of argument [121] is used to determine the number N of roots of $Q(s)$ inside of an closed curve $C \subset C$, where

$$N = \left(\frac{1}{2\pi}\right)\Delta_{C\mathrm{arg}}\{Q(s)\}. \tag{28}$$

Here, $\Delta_C \mathrm{arg}\{Q(s)\}$ denotes the changes of the argument of Q along C.

(v) The Chebotarev criterion is the direct generalization of the Routh–Hurwitz. The analytical criterion needs to calculate an infinite number of Hurwitz determinants and the stability of the system with long delay is determined by determinants of high dimension, whereby it is not effective practically.

(vi) The D-partition (D-subdivision) method [180] is a geometric method to construct stability charts (regions) in the parameter space of the quasi-polynomial. It is very effective to determine stability based on system parameters. However, the number of parameters used is reduced.

(vii) The Nyquist [181] method is also a geometric method and the stability of the systems is determined by the relative position of the point $-1 + 0i$ and the contour $D(iu) \subset C$, $i^2 = -1$, $u \in R^+$, where $-1 = D(s)$ is a transformation of the quasi-polynomial.

(viii) The Bode and Nichols criteria and some others are transformations of the Nyquist criterion as Satche mentions in [182].

(ix) The Mikhailov criterion [183] is a consequence of the Cauchy Residue theorem in complex analysis. It can be applied to RFDE if there exists a scalar $\nu > 0$ such that the quasi-polynomial is bounded and analytical in any closed domain in $\{s: \mathrm{Re}\{s\} \succ \nu\}$; this is also known as Satche's diagram [184].

(x) The Hermite–Biehler criterion [51, 52] mentioned in the previous section can be applied for TDS using the imaginary and real parts of the quasi-polynomial, $Q(s = i\omega) = \mathrm{Re}\{Q(i\omega)\} + \mathrm{Im}\{Q(i\omega)\}$, $i = Q_r(\omega) + Q_i(\omega)i$; the stability of the system is determined by a continuous alternation between transformations of the real functions $Q_r(\omega)$ and $Q_i(\omega)$, when increasing phase condition $\omega > \omega^*$, for any $\omega^* \in (-\infty, \infty)$. See its extensions in [185, 186].

(xi) The Edge theorem [187], zero exclusion principle, and concept of convex direction [188] are graphical methods to determine stability of a set of quasi-polynomial family or convex polytope family.

The above criteria are the most recurrent on stability analysis of quasi-polynomials, see [176, 189–194], but there are quasi-polynomial classes of larger complexity that require special attention. Among this class, the quasi-polynomial of NFDE [195], polynomial family which is described by convex polytope in the coefficient space [196], and stability analysis of LPV-TDS through a generalized characteristic quasi-polynomial [173] can be found.

Consider a LTI-NFDE with multiple delays of the form:

$$\sum_{k=0}^{m} D_k \dot{x}(t - \tau_k) = \sum_{k=0}^{m} A_k x(t - \tau_k), \tag{29}$$

where $A_k, D_k \in R^{n\times n}$, $k = 0, 1, \ldots, m$ and $0 = \tau_0 < \tau_1 < \cdots < \tau_m = \tau$. The corresponding quasi-polynomial is given by

$$Q(s) = \det\left\{\left\{sI_n - \sum_{k=0}^{m} D_k\right\} - \sum_{k=0}^{m} A_k\right\} = 0. \tag{30}$$

A TDS has an infinite number of characteristic roots, but $Q(s)$ is an entire function, which implies that there can only be a finite number of characteristic roots within any bounded domain. These characteristic roots form root chains that are rather easy to describe. The quasi-polynomial has two types of root chains. The first type is retarded chains; here, the roots fall in the region $|\mathrm{Re}\{s + \mu \log s\}| < c$, for some $\mu > 0$ and $c > 0$. In other words, there may only be a finite number of roots on the right of the abscissa $\alpha = \mathrm{Re}\{s\}$ in the complex plane for any given α [195]. The second type is neutral chains; here, the roots are bounded by two abscissas $c_1 \le \mathrm{Re}\{s\} \le c_2$. The positions of such abscissas are determined by

$$\det\left\{\left(I_n - \sum_{k=0}^{m} D_k\right)\right\} = 0. \tag{31}$$

Additionally, if s^* is a solution of (31); then, there is a series of roots $s_l, l = 1, 2 \ldots$ of quasi-polynomial (30) such that $|s_l| \longrightarrow \infty$ and $\mathrm{Re}\{s_l\} \longrightarrow \mathrm{Re}\{s^*\}$. Due to all the above, the stability of (30) is associated with the stability of fd38(31). Furthermore, (31) can be sensitive to infinitesimal delay perturbations, which strongly affect the continuity property of the roots of (30). Moreover, in contrast with the retarded case, this property cannot be ensured with respect to parametric variations of the system. For more details on this type of systems, see [176, 195].

Another interesting study in the TDS research community is the stability analysis of convex sum of quasi-polynomials, known as polynomial family or convex polytope or polytope of quasi-polynomials. These are quasi-polynomials that are entire functions which include both degree of the independent variable and exponential functions and they appear when several subsystems with delays are interconnected. Consider a convex hull of quasi-polynomials of the form:

$$\mathbf{Q} = \left\{Q(s) = \sum_{r=1}^{M} \mu_r Q_r(s):\ \sum_{r=1}^{M} \mu_r = 1, \mu_r \ge 0, r = 1, 2, \ldots, M\right\}, \tag{32}$$

where the vertex quasi-polynomial $Q_r(s)$ is of form (22). The stability of this class of the quasi-polynomials of family $\mathbf{Q}$ is studied using the zero exclusion principle, the concepts of convex direction, and the Edge theorem [196–199]. Here, a coefficient vector $a = (a_{00}, \ldots, a_{0m}, a_{10}, \ldots, a_{1m}, \ldots, a_{r_k 0}, \ldots, a_{r_k m})$ is associated with every element $Q(s) \in Q$; then, family (32) can be described by the convex polytope:

$$M_{\mathbf{Q}} = \left\{a = \sum_{r=1}^{M} \mu_r a_r:\ \sum_{r=1}^{M} \mu_r = 1, \mu_r \ge 0, r = 1, 2, \ldots, M\right\}, \tag{33}$$

where the vector a_r corresponds to the vertex quasi-polynomial $Q_r(s)$. Thus, $E(M_{\mathbf{Q}})$ is the set of edges and $V(M_{\mathbf{Q}})$ is the set of vertexes of the polytope $M_{\mathbf{Q}}$. Every edge corresponds to the one-parameter family of quasi-polynomial of the form $\mu Q_p(s) + (1 - \mu)Q_q(s)$, $\mu \in [0, 1]$, i.e., the stability analysis for the families $\mathbf{Q}$ is reduced to a finite number of simpler problem stability to convex couples.

Theorem 2 (see [197]). *The family* $\mathbf{Q}$ *is stable if and only if all members of one-parameter family corresponding to the edges* $E(M_{\mathbf{Q}})$ *are stable.*

On stability analysis of LPV-TDS, it seems that this topic is one of the most relevant topics and the best opportunity field to direct the current research. An aircraft is one classic physical system where the mathematical model can be represented by a LPV system [200], while a system of distributed type can be seen in [201] and a LPV-TDS in [173].

Consider a LPV-TDS of the form:

$$\dot{x}(t) = \begin{pmatrix} 0 & 1 \\ \theta(t) - 2 & 0.1 \end{pmatrix} x(t) + \begin{pmatrix} 0 & 0 \\ -\theta(t) + 1 & 0 \end{pmatrix} x(t - \tau), \tag{34}$$

where $\theta(t) \in [-1, 1]$. Now, consider the LTV-TDS of the form:

$$\dot{x}(t) = \begin{pmatrix} 0 & 1 \\ \sin(t) - 2 & 0.1 \end{pmatrix} x(t) + \begin{pmatrix} 0 & 0 \\ -\cos(t) + 1 & 0 \end{pmatrix} x(t - \tau), \tag{35}$$

and the nonlinear TDS as follows:

$$\dot{x}(t) = \begin{pmatrix} 0 & 1 \\ \sin(x_1) - 2 & 0.1 \end{pmatrix} x(t) + \begin{pmatrix} 0 & 0 \\ -\cos(x_2) + 1 & 0 \end{pmatrix} x(t-\tau). \tag{36}$$

In terms of stability, the previous three systems (34)–(36) can have the same properties. In other words, the convex representation of the uncertainty of $\theta(t)$ and the nonlinear functions $(\sin(t), \cos(t))$ and $(\sin(x_1), \cos(x_2))$ are equivalent in a stability analysis if only the manipulation range of the previous variables is considered. This undoubtedly provides the opportunity to obtain stable conditions for a wide variety of types of systems. Furthermore, these conditions can be obtained using LMIs and by studying a generalized characteristic quasi-polynomial of the form

$$Q(s) = e^{s\tau_m} \det\{sI_n - A_1(\theta) - A_1(\theta)e^{-s\tau}\} = \sum_{k=0}^{n}\sum_{l=0}^{m} a_{kl}(\theta) s^k e^{s\tau_l}, \tag{37}$$

where $0 < \tau_0 < \tau_1 < \cdots < \tau_m$ and $a_{kl}(\theta)$ are the coefficients of a polynomial with a finite set of bounded uncertainties, which depend on the uncertainties θ. The quasi-polynomial (37) is exactly rewritten as a polytope whose interpolating functions exhibit mutual dependency. Therefore, the stability analysis of this type of polytopes implies the stability analysis of a class of nonlinear TDS, see [173, 174].

On the contrary and to finish this section, it is worth mentioning that some members of the scientific community have preferred to employ transformations, approximation methods or pseudo-delays to avoid the transcendental terms in the stability analysis of a TDS instead of using the direct methods presented above. Although, in many occasions, a direct approach to analyze the stability of a TDS is more efficient [202]. Among these, they can be found the Smith predictors [203], Rekasius transformation [204], and Padé approximation [205]. The Smith predictors allow to use a controller structure which takes the delay out of the control loop, which reduce the stability analysis to the one of a free-delay system. The employment of the Rekasius transformation implies an infinity-to-one holographic mapping (the mapping is asymmetric), and it is also impossible to track all of the infinitely many roots, especially, since the dominant root cannot be declared, as mentioned in [206]. The Padé approximation has been used to approximate the exponential function $e^{-s\tau}$, $s \in C$, through rational approximation of the form $(P_{mn}(s\tau)/P_{nm}(s\tau))$, where

$$P_{mn}(s\tau) = \sum_{j=0}^{m} \frac{(m+n-j)!m!}{j!(m-j)!}(-s\tau)^j,$$
$$P_{nm}(s\tau) = \sum_{j=0}^{n} \frac{(m+n-j)!n!}{j!(n-j)!}(s\tau)^j, \tag{38}$$

see [207].

3.3. Stability in the Time Domain. In this section, a brief description of the most well-known criteria for the stability analysis of TDS in the time domain will be given. Emphasize the results using two types of Lyapunov–Krasovskii functionals: reduced type and complete type. While the first type of functional is usually the favorite of the scientific community, perhaps due to the relative flexibility to propose the functional candidate and to accomplish the requirements of the system studied, it seems that this type of functional only can provide sufficient conditions of stability and stabilization. The second type of functional is used by a narrowed community, perhaps due to the relative complexity compared to the first, but this has been shown to be closer to obtaining the necessary and sufficient conditions of stability and stabilization, see [208].

This approach is based primarily on two methods: the use of Lyapunov–Krasovskii (L-K) functional [146] or Lyapunov–Razumikhin (L-R) functions [145]. Both methods are an extension of the Lyapunov direct method [42] for free-delay systems. These stability criteria usually provide sufficient stability conditions in terms of linear matrix inequalities (LMIs), [209], which can be effectively solved by means of convex optimization techniques [210]. Although these two methods have received a great deal of attention, the results only offer conservative and sufficient stability conditions. The Razumikhin results allow one to obtain stability results based on adapted Lyapunov functions to analyze the stability of the TDS, while the Krasovskii results employ Lyapunov functionals as a natural extension to TDS. Despite the two methods provide interesting results for stability studies, the last method is the predominant one in research.

The main idea of Krasovskii consists in proposing an appropriate functional which can satisfy extensions of concepts and criteria of Lyapunov for TDS. One of these stability concepts is the definition, while the most used criterion is given below.

Theorem 3 (see [122]). *Consider the TDS given in (11) and that there are u, v, w: $R^+ \longrightarrow R^+$ continuous nondecreasing functions, where $u(\alpha)$ and $v(\alpha)$ are positive for $\alpha > 0$ and $u(0) = v(0) = 0$.*

(i) If there exists a continuous differentiable functional V: $R^+ \times \mathfrak{C} \longrightarrow R^+$ such that

$$u(|\phi(0)|) \le V(t,\phi) \le v(|\phi|_\tau),$$
$$\dot{V}(t,\phi) \le -w(|\phi(0)|), \tag{39}$$

then the trivial solution of (11) is uniformly stable.

(ii) If the trivial solution of (11) is uniformly stable, and $w(\alpha) > 0$ for $\alpha > 0$, then the trivial solution of (11) is uniformly asymptotically stable.

(iii) If the trivial solution of (11) is uniformly asymptotically stable and if $\lim_{\alpha \longrightarrow \infty} u(\alpha) =$, then the trivial solution of (11) is globally uniformly asymptotically stable.

Consider the LTI-TDS of the form:

$$\dot{x}(t) = A_0 x(t) + A_1 x(t-\tau), \tag{40}$$

where A_0 and A_1 are matrices of appropriate dimensions. The functional ones proposed to satisfy the above conditions

are known as L-K functional candidates and their basic form is as follows:

$$V(x_t) = x^T(t)Px(t) + \int_{t-\tau}^{t} x^T(\alpha)Qx(\alpha)\mathrm{d}\alpha, \tag{41}$$

where $P = P^T > 0$ and $Q = Q^T > 0$ are positive definite matrices (symmetric matrices where every eigenvalue is positive). This functional satisfies the conditions of Theorem 3 if there are $P > 0$ and $Q > 0$ which satisfy $A_0^T P + PA_0 + PA_1 Q^{-1} A_1^T P + Q < 0$ or

$$\begin{pmatrix} A_0^T P + PA_0 + Q & PA_1 \\ * & -Q \end{pmatrix} < 0. \tag{42}$$

If this is true, then the functional is called L-K functional. However, this type of L-K functional only provides delay-independent sufficient stability conditions for LTI-TDS with one delay, namely, sufficient conditions that can only be applied to LTI-TDS that are stable for all $\tau > 0$. When the primary objective is to propose L-K functional candidates that provide delay-dependent stability conditions and that these conditions may be necessary and sufficient conditions to determine stability in a TDS, as well as for linear free-delay systems. Unfortunately, the above is still an open problem of the TDS. Therefore, most of the research studies carried out focus not only on the type of L-K functional, but also on mathematical properties that reduce the conservatism of the stability conditions (LMI-based stability conditions) and/or these can relax the conditions. Some of these properties follow immediately.

Lemma 1 (Schur complement). *Consider a given symmetric matrix* $S = \begin{pmatrix} S_{11} & S_{12} \\ * & S_{22} \end{pmatrix}$, *where* $S_{11} \in R^{r\times r}$; *then, the following conditions are equivalent:*

$$\begin{aligned} S &< 0, \\ S_{22} &< 0, \\ S_{11} - S_{12}^T S_{22}^{-1} S_{12} &< 0, \\ S_{11} &< 0, \\ S_{22} - S_{12}^T S_{11}^{-1} S_{12} &< 0. \end{aligned} \tag{43}$$

Lemma 2. *Let* $Q = Q^T$, H *and* E *given matrices with appropriate dimensions. Then,* $Q + HF(t)E + E^T F^T(t)H^T < 0$ *holds for all* $F(t)$ *such that* $F^T(t)F(t) \le I$ *if and only if there exists* $\epsilon > 0$ *such that* $Q + \epsilon^{-1} HH^T + \epsilon E^T E < 0$.

Lemma 3 (Jensen inequality, see [166]). *For any constant matrix* $M \in R^{m\times m}$, $M = M^T > 0$, *scalar* $\gamma > 0$, *vector function* ω: $[0, \gamma] \longrightarrow R^m$ *such that the integrations concerned are well defined, then*

$$\gamma \int_0^\gamma \omega^T(\beta)M\omega(\beta)\mathrm{d}\beta \ge \left(\int_0^\gamma \omega(\beta)\mathrm{d}\beta\right)^T M\left(\int_0^\gamma \omega(\beta)\mathrm{d}\beta\right). \tag{44}$$

Lemma 4 (see [122]). *Let* A, D, E, F, *and* P *be real matrices with appropriate dimensions, and let* $F^T F \le I$ *and* $P > 0$. *Then, the following propositions are true:*

(i) For any $x, y \in R^n$, $2x^T y \le x^T P^{-1} x + y^T P y$

(ii) For any $x, y \in R^n$ *and any* $\epsilon > 0$, $2x^T DFEy \le \varepsilon - 1x^T DD^T x + \varepsilon y^T E^T E y$

(iii) For any $\epsilon > 0$ *satisfying* $P - \epsilon DD^T > 0$, $(A + DFE)^T P^{-1}(A + DFE) \le \varepsilon^{-1} E^T E + A^T (P - \varepsilon DD^T)^{-1} A$

For decades the TDS research community has proposed different types of L-K functional candidates and/or also different mathematical properties in order to satisfy the postulated in (iii) of Theorem 3.3. One of the most observed trends is to add quadratic or cross terms to the functional candidate as follows.

Consider the following L-K functional candidate:

$$V(x_t) = x^T(t)\mathrm{P}\mathrm{x}(t) + \sum_{j=1}^{r} V_j(x_t), \tag{45}$$

where each term $V_j(x_t)$, $j = 1, 2, \ldots, r$ can be of the form: cross terms $x^T(t)\int_{-\tau}^{0} Qx(t+\alpha)\mathrm{d}\alpha$, quadratic terms $\int_{-\tau}^{0}\int_{t+\alpha}^{t} x^T(\alpha)Rx(\alpha)\mathrm{d}\alpha\mathrm{d}t$, quadratic terms for exponential terms $\int_{-\tau}^{0} x^T(t+\alpha)e^{2\sigma\alpha}Qx(t+\alpha)\mathrm{d}\alpha$, cross terms $x^T(t)\int_{-\tau}^{0} Q(\alpha)x(t+\alpha)\mathrm{d}\alpha$, and quadratic terms $\int_{-\tau}^{0}\int_{-\tau}^{0} x^T(t+\alpha)R(\alpha,\beta)x(\alpha+\beta)\mathrm{d}\alpha\mathrm{d}\beta$.

Typically, these terms (quadratic or crossed) are introduce depending on the type of system analyzed (RFDE, DFDE, and NFDE, among others) or the type of conditions required to obtain (robustness and exponential estimates, among others) as an effort to obtain the functional one that grants less restrictive conditions and more types of systems can be analyzed. Also, comparisons between various criteria of delay-dependent stability can be observed in the literature, to demonstrate the efficiency and loss of conservatism with the proposed conditions, see [211]. In this context, there are miles of contributions giving necessary conditions of stability, among which the following can be mentioned [39, 212–238]. In most of these contributions a type of functional known as reduced type functional is used. However, until now it is unknown what type of reduced-type functional is suitable for the type of TDS analyzed, [214, 239–241]. Therefore, some criteria for the construction of full size (complete) type L-K functionals have been developed with the intention of solving these problems.

The construction of the complete-type functional requires a prior proposal of the quadratic derivative of the functional and the construction of the so-called delay Lyapunov matrix. The first results were proposed in [242], followed by some interesting results such as those given in [243, 244] for RFDE with one delay, while in [245] some of the results have been extended to a general case of LTI-TDS. In the latter, it is also shown that the constructed functional requires additional information to admit a lower quadratic bound. In [213], an interesting numerical scheme for the construction of complete type L-K functionals has been

proposed using the LMI approach. In [246, 247], properties are clarified and completed for the construction of a functional with upper and lower quadratic bounds. This technique can be summarized in the following result.

Theorem 4 (see [123]). *Consider a prescribed quadratic functional of the form:*

$$\omega(x_t) = \omega_1(x(t), W_1) + \omega_2(x_t, W_2) + \omega_3(x(t-\tau), W_3), \tag{46}$$

where $\omega_1(x(t), W_1) = x^T(t)W_1x(t)$,

$$\begin{aligned} \omega_1(x_t, W_2) &= \int_{\tau}^{0} x^T(t+\alpha)W_2x(t+\alpha)\mathrm{d}\alpha, \\ \omega_2(x(t-\tau), W_3) &= x^T(t-\tau)W_3x(t-\tau), \end{aligned} \tag{47}$$

and W_1, W_2, *and* W_3 *are positive definite matrices of appropriate dimensions. If the LTI-TDS (40) is stable, then there is only one functional* $v(x_t)$ *such that*

$$\dot{v}(x_t) = -\omega(x_t). \tag{48}$$

This functional is known as complete type L-K functional and it is given by

$$\begin{aligned} v(x_t) = {} & x^T(t)U(0)x(t) + 2x^T(t)\int_{-\tau}^{0} U(-\tau-\alpha)A_1x(t+\alpha)d\alpha + \int_{-\tau}^{0}\int_{-\tau}^{0}\left[x^T(t+\alpha_1)A_1^TU(\alpha_1-\alpha_2)A_1x(t+\alpha_2)\right]d\alpha_1d\alpha_2 \\ & + \int_{-\tau}^{0} x^T(t+\alpha)\left[W_1 + (\tau+\alpha)W_2\right]x(t+\alpha)d\alpha, \end{aligned} \tag{49}$$

where

$$U(\varsigma) = \int_{0}^{\infty} K^T(t)WK(t+\varsigma)\mathrm{d}t, \quad \varsigma \in R, \tag{50}$$

is a counterpart of the classical Lyapunov matrix equation in the context of Lyapunov quadratic forms for the linear delay-free systems; therefore, it is called Lyapunov matrix for TDS (delay Lyapunov matrix). Here, $0 < W = W_0 + W_1 + \tau W_2 \in R^{n\times n}$ and $K(t)$: $R \longrightarrow R^{n\times n}$ is the fundamental matrix of LTI-TDS (40) and the solution of the matrix equation:

$$\dot{K}(t) = A_0K(t) + A_1K(t-\tau), \quad t \geq 0, \tag{51}$$

with initial condition $K(t) = 0$ for $t < 0$ y $K(0) = I_n$. In addition, the delay Lyapunov matrix satisfies the following conditions:

$$U'(\varsigma) = U(\varsigma)A_0 + U(\varsigma-\tau)A_1, \quad \varsigma \geq 0, \tag{52}$$

$$U(\varsigma) = U^T(-\varsigma), \quad \varsigma \geq 0, \tag{53}$$

$$-W = U(0)A_0 + A_0^TU(0) + U^T(\tau)A_1 + A_1^TU(\tau). \tag{54}$$

Equations (52)–(54) are known as dynamic property, symmetry property, and algebraic property, respectively.

One of the key points to use this type of functional are the existence, uniqueness, and numerical calculation of the delay Lyapunov matrix (50), for which several manuscripts have been dedicated to this sense, see [248–254]. Some of the functionals prescribed $w(x_t)$ to construct complete type L-K functionals $v(x_t)$ are as follows.

(i) For LTI-RFDE [255],

$$\omega(x_t) = x^T(t)W_1x(t) + 2x^T(t)ZA_1x(t-\tau) + x^T(t-\tau)W_2x(t-\tau) + \int_{\tau}^{0} x^T(t+\alpha)W_3x(t+\alpha)\mathrm{d}\alpha. \tag{55}$$

(ii) For LTI-DFDE [256],

$$\begin{aligned} \omega(x_t) = {} & x^T(t)W_1x(t) + x^T(t-\tau)W_2x(t-\tau) + \int_{\tau}^{0} x^T(t+\alpha)W_3x(t+\alpha)d\alpha + 2x^T(t)W_4x(t-\tau) \\ & + 2x^T(t)\int_{\tau}^{0} W_5x(t+\alpha)\mathrm{d}\alpha + 2x^T(t-\tau)\int_{\tau}^{0} W_6x(t+\alpha)\mathrm{d}\alpha. \end{aligned} \tag{56}$$

(iii) For RFDE with time-varying delay [257],

$$\omega(x_t) = x^T(t)W_1x(t) + \dot{x}^T(t)W_2\dot{x}(t). \tag{57}$$

(iv) For RFDE with uncertain coefficients $H\Delta A_0$ and $H\Delta A_1$ and an uncertain time-varying delay $\tau(t) = h_1 + \eta_1(t)$, with $h_1 \in R^+$ and $|\eta(t)| \leq \mu_1 \in R^+$ [258],

$$\omega(x_t) = x^T(t)W_1x(t) - 2\left[x^T(t)U^T(0) + \int_{-h_1}^{0} x^T(t+\alpha)A_1^TU(h_1+\alpha)\mathrm{d}\alpha\right] \times \left[H\Delta A_0x(t) + H\Delta A_1x(t-h_1) - H\Delta A_1 \cdot \int_{t-h_1-\eta_1}^{t-h_1} \dot{x}(\alpha)\mathrm{d}\alpha - A_1\int_{t-h_1-\eta_1}^{t-h_1} \dot{x}(\alpha)\mathrm{d}\alpha\right]. \tag{58}$$

This type of functional and the delay Lyapunov matrix are giving good results for the design of control laws such as linear quadratic suboptimal controllers [259]; recently, these have also been used to designing dynamic stabilizing controllers (predictor-based controls) for preserving the exponential stability of the closed-loop system after the replacement of the integrals by finite sums [260–263], robotic systems with constant input time delay through the active disturbance rejection paradigm and generalized proportional integral observers [264], design of delayed output-feedback controllers that optimize a quadratic cost function [265], necessary and sufficient exponential stability condition for systems with multiple delays [266], and partial differential equations [267]. Furthermore, these types of functionals can provide necessary and sufficient stability conditions for linear systems with pointwise and distributed delays [208]. Here, a stability criterion is presented for the exponential stability of systems with multiple point and distributed delays. These conditions are in terms of the delay Lyapunov matrix (50) using the evaluation of a complete type L-K functionals at a pertinent initial function that depends on the system fundamental matrix. Undoubtedly, this topic is solving important open problems in the area of TDS, whereby it is highly recommended to direct current and future research.

3.4. Numerical Methods (Applications). One of the most important aspects in the stability analysis of time-delay linear systems is the calculation of characteristic roots of the linear/linearized dynamics, being the root with the maximum real part a very important one [268]. The characteristic equation is a quasi-polynomial equation whose roots are computed through a numerical method for nonlinear equations.

In the contribution of Engelborghs [269], it is proposed a Matlab package for numerical bifurcation analysis of TDS, and the computation of the rightmost characteristic roots is carried out by using a linear multistep method (LMS method) [270].

The monograph of Breda et al. [271] presents a comprehensive set of pseudospectral techniques (Pseudospectral Differentiation Method and Piecewise Pseudospectral Differentiation Method) to analyze the stability of the solution of linear TDS with numerical implementations in Matlab.

In [272], Louisell establishes a method for determining the stability exponent and eigenvalue abscissas of a linear delay system based on examining the endpoint values of the solution to a functional equation occurring in the Lyapunov theory of delay equations. Other interesting related works are [273, 274]. In [275, 276], it is presented a methodology for calculating the Lyapunov matrix with a distributed delay, whose algorithm consist in solving a two points boundary value problem for a delay-free system.

Olgac and Sipahi provide an alternative procedure based on the cluster treatment of characteristic roots to analyze the stability of multiple time-delayed LTI dynamics. This methodology detects all the stable regions precisely, in the space of the time delays, by means of a set of curves (kernel and offspring) which count the possible imaginary root crossings for the system (see [206, 277–282] and references therein for a comprehensive treatment).

Concerning the eigenvalue problem, Michiels has come up with different procedures. In [283], it is provided a characterization of the solutions to an arbitrary nonlinear eigenvalue problem as the reciprocal eigenvalues of an infinite-dimensional operator, and the resulting algorithm is completely equivalent to the standard Arnoldi method, including many of its properties. An extension of last contribution [284] is used to compute the partial Schur factorization of a nonlinear eigenvalue problem. In [285], it is presented a procedure to compute solutions to a type of nonlinear eigenvalue problem with low-rank structure. The algorithm turns out to be equivalent to the Arnoldi method (even in the numerical behavior). In [286], first, the formula for the sensitivity of a simple eigenvalue with respect to a variation of a parameter is extended to the case of multiple non-semisimple eigenvalues. Also, it is provided a dual treatment of the delay eigenvalue problem, in one hand, at the level of the finite-dimensional nonlinear eigenvalue problem and, on the other hand, at the level of a standard operator eigenvalue problem. A numerical procedure to compute the pseudospectral abscissa is given in [287], whose main feature is that the approach is a pioneering applicable procedure for nonlinear problems.

The most complex systems have nonlinearities and delays, which can be easy to notice or sometimes not so much. A delay in a system is a phenomenon that can be seen as the dead time between transmitting and executing an action. In

this context, delays are due to the fact that system dynamics are associated with past events. In general, delays are undesirable phenomena in a system because they can instabilize or produce a poor performance in their response. However, in recent years, it has been shown that delays can also favor stabilizing and improving the performance of the system [288, 289].

The deliberate application of delays to stabilize systems is a latent topic in the literature, one of the most important contributions in this aspect is found in [290] that drove a whole stream of research in what is known as time-delayed feedback control (TDFC). The technique is to deliberately introduce delays into the control scheme to σ-stabilize a system with or without inherent delays [291–308]. This is due to the advantages that they have in applications on experimental platforms, such as noise attenuation, non-implementation of estimators, observers and speed sensors, avoiding filters, as well as its easy implementation. In addition, the σ-stability analysis or σ-stability regions allows a fragility analysis of the controllers gains, which can give a measure of the robustness of the closed-loop system under variations of the controller gains, see [303, 309–311].

4. Advances in Stability and Stabilization of Nonlinear Time-Delay Systems

In recent years, different concepts have emerged that are less restrictive to classical concepts to determine stability in nonlinear time-delay systems. Next, some of them are mentioned.

4.1. Complex Delay Complex Networks. One topic which has attracted attention from the scientific community is the analysis and control of complex networks [312, 313], which describe a wide variety of physical and social systems [314], from population interactions, brain activity, and language patterns to Internet traffic behavior among other interesting phenomena. One control problem derived from the complex systems control is the synchronization of delay coupled networks [315, 316]. In this sense, a formal stability analysis for the synchronization of complex networks, in particular for a set of oscillators, is usually given for linearized systems in a vicinity of the equilibrium point [317] by computing the stability regions in the delay parameters or using the circle criterion [318]. Some reported contributions can be found in [169, 238, 319–328].

4.2. Robotic Teleoperation and Predictor-Based Control. Robotic teleoperation and haptic teleoperation has been a highly active topic in last years, specially now with the active development of virtual reality and haptic interfaces [329–334]. The time delay in these applications arises mainly to the latency aspects of the virtual reality system [335–338], and the network traffic in a teleoperation system [339–342].

The stability analysis for teleoperation has the following general approaches:

(i) The use of predictors working on the stability of the system in the feedforward dynamics with nominal or robust criteria, see [203, 343–360]

(ii) Passivity-based approaches whose stability tests can be given in the Lyapunov–Krasovskii sense (see [106, 342, 361–374])

(iii) Robust and predictor-based schemes whose stability is given for time-delay dynamics tested by means of time- or frequency-based approaches [264, 375–378]

(iv) Other schemes which assume the delay as a disturbance to be compensated by robust or adaptive techniques [379–384]

4.3. Nonlinear and Fractional Order Systems. Lyapunov methods have shown very useful for the study of stability and the design of nonlinear control laws [130, 385, 386]. Here, discontinuous [387] and fractional order systems [388] represent an important challenge. Particularly, sliding mode control techniques is an active field of research where Lyapunov methods have been a key factor [389–393]. The main advantages of sliding mode control, including robustness and finite time convergence, are supported by no conventional Lyapunov methods.

On the contrary, fundamental research has shown that a large variety of physical signals can be described by means of functions with more varied topological properties [394–397], which can be continuous but not necessarily differentiable in any integer-order sense [398]. This has motivated the design of fractional order sliding mode-based controllers which have been proved to be robust against Hölder disturbances [399].

Fractional calculus has become an emerging approach for modeling complex systems, which has attracted the attention of several areas of study, including control systems. The use of fractional versions of PID controllers [400–406] has increased the interest and development of fractional control designs. As a natural consequence, this approach has been extended to a wider class of systems, especially time delay ones which has come up with stability studies and analyses.

Since classic methods for stability testing integer systems such as Routh–Hurwitz are not universally valid, the stability analysis for even linear fractional systems is more challenging. In particular, among the approaches of stability study for fractional time-delay systems, some pioneering contributions are given by Hwang and Cheng. In one hand, the Lambert W function is proposed for the stability analysis [407] and, on the other hand, in [408], the characteristic equation of the system is numerically analyzed for a BIBO stability test by means of Cauchy's integral theorem. In [409], a numerical procedure to obtain the delay values where there is a root crossing (from the left half plane to the right half and vice versa), for a further procedure of finding the stability zones in terms of the delay value. Other fundamental contributions are given in [410–415]. In [416], a Matlab toolbox for the H_∞-stability analysis of fractional

systems with commensurate delays is provided. L-K stability approaches for fractional systems are given in [417–419]. In [325, 420–424], some L-K stability approaches are given in the realm of neural network framework.

Concerning using Smith predictor-based stabilizing controllers, several applications are reported, see [425–432].

5. Conclusions

This paper has presented a set of criteria concerning robust stability of dynamical systems with or without delay, which is important for the analysis of complex systems which may not provide complete information, involving parameter uncertainties. On the one hand, the ideas of robust stability through families of polynomials were addressed and the main criteria discussed. On the other hand, an emerging topic in the area of complex systems such as time-delay systems stability was analyzed, including the motivation, basic results for its understanding, the difficulties involved with respect to systems without delay, the time and frequency approaches, applications involving complex oscillators, current trends in this field of research, and some interesting open problems. This review explored the stability as a fundamental structural property which is crucial in the analysis and development of studies and applications of complex dynamical systems, in which the couplings and dynamical behavior may come up with new developments in a wide variety of research areas.

Data Availability

No data were used to support this study.

Conflicts of Interest

The authors declare that there are no conflicts of interest regarding the publication of this paper.

Acknowledgments

In memory of Oscar Villafuerte-Segura, my brother, my partner, and unconditional friend. I will never forget you. This work was partially supported by Secretaría de Investigación y Posgrado-IPN under grant SIP20201675 (A. Luviano-Juárez).

References

[1] G. A. Pagani and M. Aiello, "Power grid complex network evolutions for the smart grid," *Physica A: Statistical Mechanics and its Applications*, vol. 396, pp. 248–266, 2014.

[2] C.-C. Chu and H. H.-C. Iu, "Complex networks theory for modern smart grid applications: a survey," *IEEE Journal on Emerging and Selected Topics in Circuits and Systems*, vol. 7, no. 2, pp. 177–191, 2017.

[3] W. Yu, G. Wen, X. Yu, Z. Wu, and J. Lü, "Bridging the gap between complex networks and smart grids," *Journal of Control and Decision*, vol. 1, no. 1, pp. 102–114, 2014.

[4] F. Dörfler, M. Chertkov, and F. Bullo, "Synchronization in complex oscillator networks and smart grids," *Proceedings of the National Academy of Sciences*, vol. 110, no. 6, pp. 2005–2010, 2013.

[5] S. Wollenberg and F Bruce, "Toward a smart grid: power delivery for the 21st century," *IEEE Power and Energy Magazine*, vol. 3, no. 5, pp. 34–41, 2005.

[6] M. Xue, W. Wang, and S. Roy, "Security concepts for the dynamics of autonomous vehicle networks," *Automatica*, vol. 50, no. 3, pp. 852–857, 2014.

[7] D. J. Stilwell, E. M. Bollt, and D. G. Roberson, "Sufficient conditions for fast switching synchronization in time-varying network topologies," *SIAM Journal on Applied Dynamical Systems*, vol. 5, no. 1, pp. 140–156, 2006.

[8] L. Iftekhar and R. Olfati-Saber, "Autonomous driving for vehicular networks with nonlinear dynamics," in *Proceedings of the 2012 IEEE Intelligent Vehicles Symposium*, pp. 723–729, Madrid, Spain, June 2012.

[9] C. J. E. Naranjo, R. Garcia, and T. de Pedro, "Lane-change fuzzy control in autonomous vehicles for the overtaking maneuver," *IEEE Transactions on Intelligent Transportation Systems*, vol. 9, no. 3, pp. 438–450, 2008.

[10] E. Frazzoli, M. A. Dahleh, and E. Feron, "Real-time motion planning for agile autonomous vehicles," *Journal of Guidance, Control, and Dynamics*, vol. 25, no. 1, pp. 116–129, 2002.

[11] B. H. Junker and F. Schreiber, *Analysis of Biological Networks*, John Wiley & Sons, Hoboken, New Jersey, USA, 2011.

[12] R.-S. Wang, S. Zhang, Y. Wang, X.-S. Zhang, and L. Chen, "Clustering complex networks and biological networks by nonnegative matrix factorization with various similarity measures," *Neurocomputing*, vol. 72, no. 1–3, pp. 134–141, 2008.

[13] E. Estrada, "Generalized walks-based centrality measures for complex biological networks," *Journal of Theoretical Biology*, vol. 263, no. 4, pp. 556–565, 2010.

[14] P. Wang, L. ü. Jinhu, and X. Yu, "Identification of important nodes in directed biological networks: a network motif approach," *PLoS One*, vol. 9, no. 8, 2014.

[15] M. Rosvall and C. T. Bergstrom, "Maps of random walks on complex networks reveal community structure," *Proceedings of the National Academy of Sciences*, vol. 105, no. 4, pp. 1118–1123, 2008.

[16] R. Pastor-Satorras, C. Castellano, P. Van Mieghem, and A. Vespignani, "Epidemic processes in complex networks," *Reviews of Modern Physics*, vol. 87, no. 3, pp. 925–979, 2015.

[17] D. Aguilar-Velázquez and L. Guzmán-Vargas, "Critical synchronization and 1/f noise in inhibitory/excitatory rich-club neural networks," *Scientific Reports*, vol. 9, no. 1, pp. 1–13, 2019.

[18] A. Yazdani and P. Jeffrey, "Robustness and vulnerability analysis of water distribution networks using graph theoretic and complex network principles," in *Proceedings of the 12th Annual Conference on Water Distribution Systems Analysis (WDSA)*, pp. 933–945, Tucson, AR, USA, September 2010.

[19] C. Ocampo-Martinez, V. Puig, G. Cembrano, and J. Quevedo, "Application of predictive control strategies to the management of complex networks in the urban water cycle applications of control," *IEEE Control Systems Magazine*, vol. 33, no. 1, pp. 15–41, 2013.

[20] R. Juárez, I. Y. Fernández, and L. Guzmán, "Characteristics of the oil transport network in the south of Mexico," *Journal of Physics: Conference Series*, vol. 792, Article ID 012096, 2017.

[21] Z. Ma, S. M. Jeter, and S. I. Abdel-Khalik, "Flow network analysis application in fuel cells," *Journal of Power Sources*, vol. 108, no. 1-2, pp. 106–112, 2002.

[22] Q. Ji, H.-Y. Zhang, and Y. Fan, "Identification of global oil trade patterns: an empirical research based on complex network theory," *Energy Conversion and Management*, vol. 85, pp. 856–865, 2014.

[23] M. Wang, Y. Chen, L. Tian, S. Jiang, Z. Tian, and R. Du, "Fluctuation behavior analysis of international crude oil and gasoline price based on complex network perspective," *Applied Energy*, vol. 175, pp. 109–127, 2016.

[24] K. Klemm, V. M. Eguíluz, R. Toral, and M. San Miguel, "Nonequilibrium transitions in complex networks: a model of social interaction," *Physical Review E*, vol. 67, no. 2, Article ID 026120, 2003.

[25] L. Guzmán-Vargas and R. Hernández-Pérez, "Small-world topology and memory effects on decision time in opinion dynamics," *Physica A: Statistical Mechanics and its Applications*, vol. 372, no. 2, pp. 326–332, 2006.

[26] M. Kitsak, L. K. Gallos, F. S. Havlin et al., "Identification of influential spreaders in complex networks," *Nature Physics*, vol. 6, no. 11, pp. 888–893, 2010.

[27] A.-L. Albert and R. Albert, "Emergence of scaling in random networks," *Science*, vol. 286, no. 5439, pp. 509–512, 1999.

[28] H. Zhang, N. Liu, X. Chu et al., "Network slicing based 5G and future mobile networks: mobility, resource management, and challenges," *IEEE Communications Magazine*, vol. 55, no. 8, pp. 138–145, 2017.

[29] A. E. Motter and Y.-C. Lai, "Cascade-based attacks on complex networks," *Physical Review E*, vol. 66, no. 6, Article ID 065102, 2002.

[30] R. Srikant, *The Mathematics of Internet Congestion Control*, Springer Science & Business Media, Berlin, Germany, 2004.

[31] R. Handcock, D. Swain, G. Bishop-Hurley et al., "Monitoring animal behaviour and environmental interactions using wireless sensor networks, GPS collars and satellite remote sensing," *Sensors*, vol. 9, no. 5, pp. 3586–3603, 2009.

[32] D. M. P. Jacoby, Y. P. Papastamatiou, and R. Freeman, "Inferring animal social networks and leadership: applications for passive monitoring arrays," *Journal of The Royal Society Interface*, vol. 13, no. 124, Article ID 20160676, 2016.

[33] A. G. Villa, A. Salazar, and F. Vargas, "Towards automatic wild animal monitoring: identification of animal species in camera-trap images using very deep convolutional neural networks," *Ecological informatics*, vol. 41, pp. 24–32, 2017.

[34] R. Vera-Amaro, M. E. Rivero-Ángeles, and A. Luviano-Juárez, "Data collection schemes for animal monitoring using WSNS-assisted by UAVS: Wsns-oriented or UAV-oriented," *Sensors*, vol. 20, no. 1, p. 262, 2020.

[35] Y.-Y. Liu, J.-J. Slotine, and A.-L. Barabási, "Controllability of complex networks," *Nature*, vol. 473, no. 7346, pp. 167–173, 2011.

[36] B. D. MacArthur, R. J. Sánchez-García, and J. W. Anderson, "Symmetry in complex networks," *Discrete Applied Mathematics*, vol. 156, no. 18, pp. 3525–3531, 2008.

[37] A. J. Whalen, S. N. Brennan, T. D. Sauer, and S. J. Schiff, "Observability and controllability of nonlinear networks: the role of symmetry," *Physical Review X*, vol. 5, no. 1, Article ID 011005, 2015.

[38] D. Leitold, Á. Vathy-Fogarassy, and J. Abonyi, "Controllability and observability in complex networks–the effect of connection types," *Scientific Reports*, vol. 7, no. 1, pp. 1–9, 2017.

[39] S.-I. Niculescu, "On delay-dependent stability under model transformations of some neutral linear systems," *International Journal of Control*, vol. 74, no. 6, pp. 609–617, 2001.

[40] V. L. Kharitonov, "Asymptotic stability of an equilibrium position of a family of systems of linear differential equations," *Differentsial'nye Uravneniya*, vol. 14, pp. 2086–2088, 1978.

[41] D. McFarlane and K. Glover, "A loop-shaping design procedure using H/sub infinity/synthesis," *IEEE Transactions on Automatic Control*, vol. 37, no. 6, pp. 759–769, 1992.

[42] A. Liapounoff, "Problème général de la stabilité du mouvement (in French)," *Annales de la Faculté des sciences de Toulouse: Mathématiques*, vol. 9, pp. 203–474, 1907.

[43] J. C. Maxwell, "I. On governors," *Proceedings of the Royal Society of London*, vol. 16, pp. 270–283, 1868.

[44] J. L. de La Grange, *Méchanique Analytique*, Veuve Desaint, 1788.

[45] J. L. Lagrange, "Sur l'altération des moyens mouvements des planetes mem," *Acad. Sci. Berlin*, vol. 199, 1776.

[46] G. L. Dirichlet, "Über die stabilität des gleichgewichts," *Journal für die reine und angewandte Mathematik*, vol. 32, pp. 85–88, 1846.

[47] B. Brogliato, "Absolute stability and the Lagrange-Dirichlet theorem with monotone multivalued mappings," *Systems & Control Letters*, vol. 51, no. 5, pp. 343–353, 2004.

[48] R. I. Leine, "The historical development of classical stability concepts: Lagrange, Poisson and Lyapunov stability," *Nonlinear Dynamics*, vol. 59, no. 1-2, p. 173, 2010.

[49] S. P. Bhattacharyya and L. H. Keel, "Robust control: the parametric approach," in *Advances in Control Education,* Elsevier, Amsterdam, Netherlands, 1995.

[50] D. Hinrichsen and A. J. Pritchard, *Mathematical Systems Theory I: Modelling, State Space Analysis, Stability and Robustness*, Springer, Berlin, Germany, 2005.

[51] C. Hermité, "Le nombre des racines d'une équation algebraique comprises entre des limites données," *Crelle's Journal*, vol. 52, pp. 1–6, 1895.

[52] R. E. Bellman and K. L Cooke, *Differential-difference Equations*, Rand Corporation, Santa Monica, CA, USA, 1963.

[53] P. A. Fuhrmann and B. N. Datta, "On bezoutians, van der monde matrices, and the lienard-chipart stability criterion," *Linear Algebra and its Applications*, vol. 120, pp. 23–37, 1989.

[54] M. Fu and Y. Z. Tsypkin, "Modified Mikhailov plots for robust absolute stability with non-parametric perturbations and uncertain nonlinearity," *International Journal of Control*, vol. 58, no. 4, pp. 925–932, 1993.

[55] B. Ross Barmish and E. I. Jury, "New tools for robustness of linear systems," *IEEE Transactions on Automatic Control*, vol. 39, no. 12, p. 2525, 1994.

[56] R. Tempo, "A dual result to Kharitonov's theorem," *IEEE Transactions on Automatic Control*, vol. 35, no. 2, pp. 195–198, 1990.

[57] K.-K. Young, P. Kokotovic, and V. Utkin, "A singular perturbation analysis of high-gain feedback systems," *IEEE Transactions on Automatic Control*, vol. 22, no. 6, pp. 931–938, 1977.

[58] A. Ilchmann and E. P. Ryan, "High-gain control without identification: a survey," *GAMM-Mitteilungen*, vol. 31, no. 1, pp. 115–125, 2008.

[59] L. Levaggi, "High-gain feedback and sliding modes in infinite dimensional systems," *Control and Cybernetics*, vol. 33, no. 1, pp. 33–50, 2004.

[60] H. Nogami, H. Maeda, S. Kodama, and M. Vidyasagar, "Robust stabilization of multivariable high gain feedback systems," *Transactions of the Society of Instrument and Control Engineers*, vol. 23, no. 4, pp. 364–370, 1987.

[61] J. Schumacher, "Almost stabilizability subspaces and high gain feedback," *IEEE Transactions on Automatic Control*, vol. 29, no. 7, pp. 620–628, 1984.

[62] Y. Z. Tsypkin and B. T. Polyak, "High-gain robust control," *European Journal of Control*, vol. 5, no. 1, pp. 3–9, 1999.

[63] J. L. Willems, "Disturbance isolation in linear feedback systems," *International Journal of Systems Science*, vol. 6, no. 3, pp. 233–238, 1975.

[64] J. Willems, "Almost invariant subspaces: an approach to high gain feedback design-part II: almost conditionally invariant subspaces," *IEEE Transactions on Automatic Control*, vol. 27, no. 5, pp. 1071–1085, 1982.

[65] B. Aguirre, C. Ibarra, and R. Suárez, "Sufficient algebraic conditions for stability of cones of polynomials," *Systems & Control Letters*, vol. 46, no. 4, pp. 255–263, 2002.

[66] B. Aguirre and R. Suárez, "Algebraic test for the Hurwitz stability of a given segment of polynomials," *Boletín de la Sociedad Matemática Mexicana*, vol. 12, no. 3, pp. 261–275, 2006.

[67] B. Aguirre Hernández, J. Solis-Daun, and R. Suárez, "Stabilization of linear systems: a polynomial approach," in *Advances in Dynamics, Instrumentation and Control,* World Scientific, Singapore, 2007.

[68] S. Bialas, "A necessary and sufficient condition for the stability of convex combinations of stable polynomials or matrices," *Bulletin of the Polish Academy of Sciences*, vol. 33, pp. 473–480, 1985.

[69] B. S. Bollepalli and L. R. Pujara, "On the stability of a segment of polynomials," *IEEE Transactions on Circuits and Systems I: Fundamental Theory and Applications*, vol. 41, no. 12, pp. 898–901, 1994.

[70] N. K. Bose, "A system-theoretic approach to stability of sets of polynomials," *Linear Algebra and its Role in Systems Theory*, vol. 47, pp. 25–34, 1985.

[71] H. Bouguerra, B. C. Chang, H. H. Yeh, and S. S. Banda, "Fast stability checking for the convex combination of stable polynomials," *IEEE Transactions on Automatic Control*, vol. 35, no. 5, pp. 586–588, 1990.

[72] D. Hinrichsen and V. L. Kharitonov, "Stability of polynomials with conic uncertainty," *Mathematics of Control, Signals, and Systems*, vol. 8, no. 2, pp. 97–117, 1995.

[73] J.-A. Lopez-Renteria, B. Aguirre-Hernandez, and F. Verduzco, "The boundary crossing theorem and the maximal stability interval," *Mathematical Problems in Engineering*, vol. 2011, Article ID 123403, 2011.

[74] B. Ross Barmish and E. I. Jury, "New tools for robustness of linear systems," *IEEE Transactions on Automatic Control*, vol. 39, no. 12, p. 2525, 1994.

[75] M. Fu and B. Ross Barmish, "Maximal unidirectional perturbation bounds for stability of polynomials and matrices," *Systems & Control Letters*, vol. 11, no. 3, pp. 173–179, 1988.

[76] S. P. Bhattacharyya and L. H. Keel, "Robust control: the parametric approach," in *Advances in Control Education,* Elsevier, Amsterdam, Netherlands, 1995.

[77] H. Chapellat and S. P. Bhattacharyya, "An alternative proof of Kharitonov's theorem," *IEEE Transactions on Automatic Control*, vol. 34, no. 4, pp. 448–450, 1989.

[78] N. K. Bose, "Tests for Hurwitz and Schur properties of convex combination of complex polynomials," *IEEE Transactions on Circuits and Systems*, vol. 36, no. 9, pp. 1245–1247, 1989.

[79] C. Hwang and S.-F. Yang, "The use of Routh array for testing the Hurwitz property of a segment of polynomials," *Automatica*, vol. 37, no. 2, pp. 291–296, 2001.

[80] A. Rantzer, "Stability conditions for polytopes of polynomials," in *Proceedings of the 29th IEEE Conference on Decision and Control*, pp. 27–31, Honolulu, HI, USA, 1990.

[81] J. Ackermann, *Robust Control: The Parameter Space Approach*, Springer Science & Business Media, Berlin, Germany, 2012.

[82] B. Aguirre-Hernández, F. R. García-Sosa, C. A. Loredo-Villalobos, R. Villafuerte-Segura, and E. Campos-Cantón, "Open problems related to the Hurwitz stability of polynomials segments," *Mathematical Problems in Engineering*, vol. 2018, Article ID 2075903, 2018.

[83] N. K. Bose, "Argument conditions for Hurwitz and Schur polynomials from network theory," *IEEE Transactions on Automatic Control*, vol. 39, no. 2, pp. 345-346, 1994.

[84] T. Büyükköroğlu and V. Dzhafarov, "On ray properties of Hurwitz polynomials," *IOSR Journal of Mathematics*, vol. 12, no. 6, pp. 87–90, 2016.

[85] M. Ń. Góra, "Stability of the convex combination of polynomials," *Control and Cybernetics*, vol. 36, no. 2, pp. 425–442, 2007.

[86] E. Zalot, "Criterions for the stability of the convex combination of polynomials," *Automatyka/Akademia Górniczo-Hutnicza im. StanisŃawa Staszica w Krakowie*, vol. 10, pp. 87–95, 2006.

[87] M.-T. Ming-Tzu Ho, A. Datta, and S. P. Bhattacharyya, "An elementary derivation of the Routh-Hurwitz criterion," *IEEE Transactions on Automatic Control*, vol. 43, no. 3, pp. 405–409, 1998.

[88] S. Faedo, "A new stability problem for polynomials with real coefficients,"Ann. Scuola Norm. Sup. Fis. Sci. Mat. Ser., vol. 3, pp. 53–63, 1953.

[89] V. L. Kharnitonov, "Asymtotic stability of an equilibrium position of a family of systems of linear di ential equations," *Differential Uravnen*, vol. 14, pp. 2086–2088, 1978.

[90] N. Bose and Y. Shi, "A simple general proof of Kharitonov's generalized stability criterion," *IEEE Transactions on Circuits and Systems*, vol. 34, no. 10, pp. 1233–1237, 1987.

[91] M. Mansour and B. D. O. Anderson, "Kharitonov's theorem and the second method of Lyapunov," *Systems & Control Letters*, vol. 20, no. 1, pp. 39–47, 1993.

[92] R. J. Minnichelli, J. J. Anagnost, and C. A. Desoer, "An elementary proof of Kharitonov's stability theorem with extensions," *IEEE Transactions on Automatic Control*, vol. 34, no. 9, pp. 995–998, 1989.

[93] K. Yeung and S. Wang, "A simple proof of Kharitonov's theorem," *IEEE Transactions on Automatic Control*, vol. 32, no. 9, pp. 822-823, 1987.

[94] V. L. Kharitonov, "Routh-Hurwitz problem for families of polynomials and quasi-polynomials," *Matematicheskaia Fizika*, vol. 1, no. 26, pp. 69–79, 1979.

[95] A. A. Kale and A. L. Tits, "On Kharitonov's theorem without invariant degree assumption," *Automatica*, vol. 36, no. 7, pp. 1075-1076, 2000.

[96] J. C. Willems and R. Tempo, "The Kharitonov theorem with degree drop," *IEEE Transactions on Automatic Control*, vol. 44, no. 11, pp. 2218–2220, 1999.

[97] T. Meressi, D. Chen, and B. Paden, "Application of Kharitonov's theorem to mechanical systems," *IEEE Transactions on Automatic Control*, vol. 38, no. 3, pp. 488–491, 1993.

[98] F. Asadi, S. Pongswatd, K. Eguchi, and N. L. Trung, "Modeling uncertainties in DC-DC converters," *Synthesis Lectures on Electrical Engineering*, vol. 3, no. 2, pp. 1–292, 2018.

[99] K. Panneerselvam and R. Ayyagari, "Computational complexity of Kharitonov's robust stability test," *International Journal of Control Science and Engineering*, vol. 3, no. 3, pp. 81–85, 2013.

[100] C. B. Soh, C. S. Berger, and K. P. Dabke, "On the stability properties of polynomials with perturbed coefficients," *IEEE Transactions on Automatic Control*, vol. 30, no. 10, pp. 1033–1036, 1985.

[101] Y. Z. Tsypkin and B. T. Polyak, "Frequency domain criteria for l_p-robust stability of continuos linear systems," *IEEE Transactions on Automatic Control*, vol. 36, no. 12, pp. 1464–1469, 1991.

[102] A. C. Bartlett, C. V. Hollot, and H. Lin, "Root locations of an entire polytope of polynomials: it suffices to check the edges," *Mathematics of Control, Signals, and Systems*, vol. 1, no. 1, pp. 61–71, 1988.

[103] F. Kelly, "Mathematical modelling of the Internet," in *Mathematics Unlimite–2001 and Beyond,* Springer, Berlin, Germany, 2001.

[104] R. M. Murray, *Control in an Information Rich World: Report of the Panel on Future Directions in Control, Dynamics, and Systems*, SIAM, Minneapolis, MN, USA, 2003.

[105] R. M. Murray, K. J. Astrom, S. P. Boyd, R. W. Brockett, and G. Stein, "Future directions in control in an information-rich world," *IEEE Control Systems Magazine*, vol. 23, no. 2, pp. 20–33, 2003.

[106] R. J. Anderson and M. W. Spong, "Bilateral control of teleoperators with time delay," *IEEE Transactions on Automatic Control*, vol. 34, no. 5, pp. 494–501, 1989.

[107] J. E. Speich and J. Rosen, "Medical robotics," *Encyclopedia of Biomaterials and Biomedical Engineering*, vol. 983, p. 993, 2004.

[108] J. F. M. Rubio, B. d. M. Cuéllar, and S. Olivier, "Control of delayed recycling systems with an unstable pole at forward path," in *Proceedings of the 2012 American Control Conference (ACC)*, pp. 5658–5663, Montreal, Canada, 2012.

[109] K. Gopalsamy, *Stability and Oscillations in Delay Differential Equations of Population Dynamics*, Springer Science & Business Media, Berlin, Germany, 2013.

[110] S.-I. Niculescu, C.-I. Morărescu, W. Michiels, and K. Gu, "Geometric ideas in the stability analysis of delay models in biosciences," in *Biology and Control Theory: Current Challenges,* Springer, Berlin, Germany, 2007.

[111] R. Villafuerte-Segura, E. Alvarado-Santos, and B. A. Itzá-Ortiz, "Conditions for stable equilibrium in Cournot duopoly models with tax evasion and time delay," *Chaos: An Interdisciplinary Journal of Nonlinear Science*, vol. 30, no. 1, Article ID 013142, 2020.

[112] B. A. Itzá-Ortiz, R. Villafuerte-Segura, and E. Alvarado-Santos, "Delay-dependent and delay-independent stability of Cournot duopoly model with tax evasion and time-delay," *Communications in Nonlinear Science and Numerical Simulation*, 2020.

[113] A. Ramirez, E. S. Espinoza, L. R. G. Carrillo, S. Mondié, A. García, and R. Lozano, "Stability analysis of a vision-based UAV controller," *Journal of Intelligent & Robotic Systems*, vol. 74, no. 1-2, pp. 69–84, 2014.

[114] J. Cheong, S.-I. Niculescu, A. Annaswamy, and M. A. Srinivasan, "Synchronization control for physics-based collaborative virtual environments with shared haptics," *Advanced Robotics*, vol. 21, no. 9, pp. 1001–1029, 2007.

[115] L. Vite-Hernández, R. Villafuerte-Segura, M. Ramírez-Neria, and G. Ochoa-Ortega, "σ-stabilization of a flexible joint robotic arm via delayed controllers," *Complexity*, vol. 2019, pp. 1–12, 2019.

[116] T. Ortega-Montiel, R. Villafuerte-Segura, C. Vázquez-Aguilera, and L. Freidovich, "Proportional retarded controller to stabilize underactuated systems with measurement delays: furuta pendulum case study," *Mathematical Problems in Engineering*, vol. 2017, Article ID 2505086, 2017.

[117] N. N. Krasovskii, *Stability of Motion*, Stanford University Press, Palo Alto, CA, USA, 1963.

[118] L. E. Elsgolts, *Introduction to the Theory of Differential Equations with Deviating Arguments*, Holden-Day, San Francisco, CA, USA, 1966.

[119] S. B. Norkin, *Introduction to the Theory and Application of Differential Equations with Deviating Arguments*, Academic Press, Cambridge, MA, USA, 1973.

[120] W. Hahn, *Stability of Motion*, Springer, Berlin, Germany, 1967.

[121] Vladimir Borisovich Kolmanovskii and Valerij Romanovič Nosov, *Stability of Functional Differential Equations*, Elsevier, Amsterdam, Netherlands, 1986.

[122] J. K. Hale and S. M. V. Lunel, *Introduction to Functional Differential Equations*, Springer Science & Business Media, Berlin, Germany, 1993.

[123] V. Kharitonov, *Time-delay Systems: Lyapunov Functionals and Matrices*, Springer Science & Business Media, Berlin, Germany, 2012.

[124] M. Wu, Y. He, and J.-H. She, *Stability Analysis and Robust Control of Time-Delay Systems*, Springer, Berlin, Germany, 2010.

[125] M. Lakshmanan and D. Vijayan Senthilkumar, *Dynamics of Nonlinear Time-Delay Systems*, Springer Science & Business Media, Berlin, Germany, 2011.

[126] C. Hua, L. Zhang, and X. Guan, *Robust Control for Nonlinear Time-Delay Systems*, Springer, Berlin, Germany, 2018.

[127] C. Sowmiya, R. Raja, J. Cao, and G. Rajchakit, "Impulsive discrete-time bam neural networks with random parameter uncertainties and time-varying leakage delays: an asymptotic stability analysis," *Nonlinear Dynamics*, vol. 91, no. 4, pp. 2571–2592, 2018.

[128] B. D. Hassard, B. D. Hassard, N. D. Kazarinoff, Y.-H. Wan, and Y. W. Wan, *Theory and Applications of Hopf Bifurcation*, CUP Archive, Cambridge, England, UK, 1981.

[129] M. Krstic, P. V. Kokotovic, and I. Kanellakopoulos, *Nonlinear and Adaptive Control Design*, John Wiley & Sons, Hoboken, NJ, USA, 1995.

[130] H. K. Khalil and J. W. Grizzle, *Nonlinear Systems*, Prentice-Hall, Upper Saddle River, NJ, USA, 2002.

[131] E. Fridman, A. Pila, and U. Shaked, "Regional stabilization and H_∞ control of time-delay systems with saturating actuators," *International Journal of Robust and Nonlinear Control*, vol. 13, no. 9, pp. 885–907, 2003.

[132] D. Melchor-Aguilar and S.-I. Niculescu, "On computing estimates of the attraction region for a class of nonlinear time-delay systems," *IFAC Proceedings Volumes*, vol. 39, no. 9, pp. 626–631, 2006.

[133] B. Ding and B. Huang, "Constrained robust model predictive control for time-delay systems with polytopic description," *International Journal of Control*, vol. 80, no. 4, pp. 509–522, 2007.

[134] R. Villafuerte, S. Mondié, and S.-I. Niculescu, "Stability analysis and estimate of the region of attraction of a human respiratory model," *IMA Journal of Mathematical Control and information*, vol. 27, no. 3, pp. 309–327, 2010.

[135] R. Sepulchre, M. Jankovic, and P. V. Kokotovic, *Constructive Nonlinear Control*, Springer Science & Business Media, Berlin, Germany, 2012.

[136] S. Sastry, *Nonlinear Systems: Analysis, Stability, and Control*, Springer Science & Business Media, Berlin, Germany, 2013.

[137] I. Alberto, *Nonlinear Control Systems Design 1989: Selected Papers from the IFAC Symposium, Capri, Italy, 14–16 June 1989*, Elsevier, Amsterdam, Netherlands, 2014.

[138] L. S. Pontryagin, "O nuliakh nekotorykh elementarnykh transtsendentnykh funktsii," Izvestiya Akademii Nauk SSSR, vol. 6, no. 1, pp. 115–134, 1942.

[139] L. S. Pontryagin, "On the zeros of some elementary transcendental functions," *American Mathematical Society Translations*, vol. 2, no. 1, pp. 95–110, 1955.

[140] E. M. Wright, "The non-linear difference-differential equation," *The Quarterly Journal of Mathematics*, vol. 17, no. 1, pp. 245–252, 1946.

[141] E. M. Wright, "The stability of solutions of non-linear difference-differential equations," *Proceedings of the Royal Society of Edinburgh. Section A. Mathematical and Physical Sciences*, vol. 63, no. 1, pp. 18–26, 1950.

[142] R. Bellman, "On the boundedness of solutions of nonlinear differential and difference equations," *Transactions of the American Mathematical Society*, vol. 62, no. 3, p. 357, 1947.

[143] R. E. Bellman and J. M. Danskin, "A survey of the mathematical theory of time-lag, retarded control, and hereditary processes," Technical report, Rand Corporation, Santa Monica, CA, USA, 1954.

[144] K. L. Cooke, "The asymptotic behavior of the solutions of linear and nonlinear differential-difference equations," *Transactions of the American Mathematical Society*, vol. 75, no. 1, p. 80, 1953.

[145] B. S. Razumikhin, "Stability of delay systems," *Prikl. Mat. Mekh*, vol. 20, no. 4, pp. 500–512, 1956.

[146] N. N. Krasovskii, "On the application of the second method of lyapunov for equations with time delays," *Prikl. Mat. Mekh*, vol. 20, no. 3, pp. 315–327, 1956.

[147] Z. Lendek, T. M. Guerra, R. Babuska, and B. De Schutter, *Stability Analysis and Nonlinear Observer Design Using Takagi-Sugeno Fuzzy Models*, Springer, Berlin, Germany, 2011.

[148] B. d'Andrea Novel, G. Bastin, and G. Campion, "Dynamic feedback linearization of nonholonomic wheeled mobile robots," in *Proceedings of the 1992 IEEE International Conference on Robotics and Automation*, pp. 2527–2532, Glasgow, Scotland, 1992.

[149] L. Hunt, R. Renjeng Su, and G. Meyer, "Global transformations of nonlinear systems," *IEEE Transactions on Automatic Control*, vol. 28, no. 1, pp. 24–31, 1983.

[150] H. Kokame and T. Mori, "Stability preserving transition from derivative feedback to its difference counterparts," in *Proceedings of the 15th Triennal IFAC World Congress*, Barcelona, Spain, 2002.

[151] M. S. Mahmoud and A. Ismail, "Passivity and passification of time-delay systems," *Journal of Mathematical Analysis and Applications*, vol. 292, no. 1, pp. 247–258, 2004.

[152] C. Li, H. Zhang, and X. Liao, "Passivity and passification of fuzzy systems with time delays," *Computers & Mathematics with Applications*, vol. 52, no. 6-7, pp. 1067–1078, 2006.

[153] R. Lozano, N. Chopra, and M. W. Spong, "Passivation of force reflecting bilateral teleoperators with time varying delay," in *Proceedings of the 8 Mechatronics Forum*, Enschede, Netherlands, June 2002.

[154] J. Lian, P. Shi, and Z. Feng, "Passivity and passification for a class of uncertain switched stochastic time-delay systems," *IEEE Transactions on Cybernetics*, vol. 43, no. 1, pp. 3–13, 2012.

[155] F. Mazenc and P.-A. Bliman, "Backstepping design for time-delay nonlinear systems," *IEEE Transactions on Automatic Control*, vol. 51, no. 1, pp. 149–154, 2006.

[156] C. Changchun Hua, X. Xinping Guan, and P. Peng Shi, "Robust backstepping control for a class of time delayed systems," *IEEE Transactions on Automatic Control*, vol. 50, no. 6, pp. 894–899, 2005.

[157] J. Zhou, C. Wen, and W. Wang, "Adaptive backstepping control of uncertain systems with unknown input time-delay," *Automatica*, vol. 45, no. 6, pp. 1415–1422, 2009.

[158] C. Changchun Hua, P. X. Liu, and X. Xinping Guan, "Backstepping control for nonlinear systems with time delays and applications to chemical reactor systems," *IEEE Transactions on Industrial Electronics*, vol. 56, no. 9, pp. 3723–3732, 2009.

[159] S. Monaco, D. Normand-Cyrot, and M. Mattioni, "Sampled-data stabilization of nonlinear dynamics with input delays through immersion and invariance," *IEEE Transactions on Automatic Control*, vol. 62, no. 5, pp. 2561–2567, 2016.

[160] C. Murguia, R. H. B. Fey, and H. Nijmeijer, "Immersion and invariance observers with time-delayed output measurements," *Communications in Nonlinear Science and Numerical Simulation*, vol. 30, no. 1–3, pp. 227–235, 2016.

[161] C. Murguia, R. H. B. Fey, and H. Nijmeijer, "Network synchronization using invariant-manifold-based diffusive dynamic couplings with time-delay," *Automatica*, vol. 57, pp. 34–44, 2015.

[162] E. Franco, "Immersion and invariance adaptive control for discrete-time systems in strict-feedback form with input delay and disturbances," *International Journal of Adaptive Control and Signal Processing*, vol. 32, no. 1, pp. 69–82, 2018.

[163] H. Mounier and J. Rudolph, "Flatness-based control of nonlinear delay systems: a chemical reactor example," *International Journal of Control*, vol. 71, no. 5, pp. 871–890, 1998.

[164] J. Rudolph and J. Winkler, "A generalized flatness concept for nonlinear delay systems: motivation by chemical reactor models with constant or input dependent delays," *International Journal of Systems Science*, vol. 34, no. 8-9, pp. 529–541, 2003.

[165] H. Mounier and J. Rudolph, "Flatness and quasi-static state feedback in non-linear delay systems," *International Journal of Control*, vol. 81, no. 3, pp. 445–456, 2008.

[166] K. Gu, J. Chen, and V. L. Kharitonov, *Stability of Time-Delay Systems*, Springer Science & Business Media, Berlin, Germany, 2003.

[167] F. Wu and K. M. Grigoriadis, "LPV systems with parameter-varying time delays: analysis and control," *Automatica*, vol. 37, no. 2, pp. 221–229, 2001.

[168] J.-H. Kim, "Note on stability of linear systems with time-varying delay," *Automatica*, vol. 47, no. 9, pp. 2118–2121, 2011.

[169] M. Iswarya, R. Raja, G. Rajchakit, J. Cao, J. Alzabut, and C. Huang, "A perspective on graph theory-based stability analysis of impulsive stochastic recurrent neural networks with time-varying delays," *Advances in Difference Equations*, vol. 2019, no. 1, pp. 1–21, 2019.

[170] A. Hurwitz, "Ueber die Bedingungen, unter welchen eine Gleichung nur Wurzeln mit negativen reellen Theilen besitzt," *Mathematische Annalen*, vol. 46, no. 2, pp. 273–284, 1895.

[171] A. Hurwitz, "Uber die bedingungen, unter welchen eine gleichung nur wurzeln mit negativen reellen theilen besitzt, stability theory (ascona, 1995)," *International Series of Numerical Mathematics*, vol. 121, pp. 239–249, 1995.

[172] E. A. Kalinina, "Stability and D-stability of the family of real polynomials," *Linear Algebra and its Applications*, vol. 438, no. 6, pp. 2635–2650, 2013.

[173] S. Angulo, R. Marquez, and M. Bernal, "Quasi-polynomial-based robust stability of time-delay systems can be less conservative than Lyapunov-Krasovskii approaches," *IEEE Transactions on Automatic Control*, vol. 65, no. 7, pp. 3164–3169, 2019.

[174] M. Bernal, V. Estrada, and R. Márquez, "Diseno e implementación de sistemas de control basados en estructuras convexas y desigualdades matriciales lineales," Pearson Mexico City, Mexico, 2019.

[175] K. Ogata and Y. Yang, *Modern Control Engineering*, Prentice-Hall, Upper Saddle River, NJ, USA, 2010.

[176] W. Michiels and S.-I. Niculescu, "Stability and stabilization of time-delay systems: an eigenvalue-based approach," *SIAM*, Minneapolis, MN, USA, 2007.

[177] L. S. Pontryagin, "On the zeros of some elementary transcendental functions," *American Mathematical Society Translations*, vol. 2, no. 1, pp. 95–110, 1955.

[178] Y. M. Yesipovich, "On the stability of the solution of a class of differential equations with delayed argument," *Prikl. Mat. Mech.,* vol. 1, no. 1, pp. 601–608, 1951.

[179] C. S. Hsu, "Application of the τ–decomposition method to dynamical systems subjected to retarded follower forces," *Journal of Applied Mechanics*, vol. 37, no. 1, pp. 258–266, 1970.

[180] J. I. Neimark, "D-decomposition of the space of quasi-polynomials (on the stability of linearized distributive systems)," *American Mathematical Society Translations*, vol. 102, pp. 95–131, 1973.

[181] H. Nyquist, "Regeneration theory," *Bell System Technical Journal*, vol. 11, no. 1, pp. 126–147, 1932.

[182] M. Satche, "Discussion on ANSOFF: stability of linear oscillating systems with constant time lag," *Journal of Applied Mechanics*, vol. 16, no. 1, pp. 419-420, 1949.

[183] A. W. Mikhailov, "Methods for harmonic analysis in the automatic control system theory (in Russian)," *Automatic Telemekh*, vol. 3, pp. 1–6, 1938.

[184] B. Porter, *Stability Criteria for Linear Dynamical Systems*, Oliver and Boyd, Edinburgh, London, UK, 1967.

[185] R. Farkh, K. Laabidi, and M. Ksouri, "Stabilizing sets of PI/PID controllers for unstable second order delay system," *International Journal of Automation and Computing*, vol. 11, no. 2, pp. 210–222, 2014.

[186] H. Wang, J. Liu, F. Yang, and Y. Zhang, "Proportional-integral controller for stabilization of second-order delay processes," *International Journal of Control, Automation and Systems*, vol. 12, no. 6, pp. 1197–1206, 2014.

[187] A. C. Bartlett, C. V. Hollot, and H. Lin, "Root locations of an entire polytope of polynomials: it suffices to check the edges," *Mathematics of Control, Signals, and Systems*, vol. 1, no. 1, pp. 61–71, 1988.

[188] E. Schwengeler, *Geometrisches über die Verteilung der Nullstellen spezieller ganzer Funktionen (Exponentialsummen)*, PhD thesis, ETH Zurich, Zürich, Switzerland, 1925.

[189] J. G. ZieglerB. Nathaniel et al., "Optimum settings for automatic controllers," *Transactions of ASME*, vol. 64, no. 11, 1942.

[190] M. Stojic and D. Siljak, "Generalization of Hurwitz, Nyquist, and Mikhailov stability criteria," *IEEE Transactions on Automatic Control*, vol. 10, no. 3, pp. 250–254, 1965.

[191] V. A. Oliveira, C. M. Marcelo, and L. Cossi, "Stabilizing a class of time delay systems using the hermite-biehler theorem," *Linear Algebra and its Applications*, vol. 369, pp. 203–216, 2003.

[192] G. Stépán, *Retarded Dynamical Systems: Stability and Characteristic Functions*, Longman Scientific & Technical, UK, 1989.

[193] M.-T. Ho, A. Datta, and S. P. Bhattacharyya, "Generalizations of the hermite–biehler theorem," *Linear Algebra and its Applications*, vol. 302, pp. 135–153, 1999.

[194] G. J. Silva, A. Datta, and S. P. Bhattacharyya, *PID Controllers for Time-Delay Systems*, Springer Science & Business Media, Berlin, Germany, 2007.

[195] K. Gu, "A review of some subtleties of practical relevance for time-delay systems of neutral type," *ISRN Applied Mathematics*, vol. 2012, Article ID 725783, 2012.

[196] V. L. Kharitonov and A. P. Zhabko, "Robust stability of time-delay systems," *IEEE Transactions on Automatic Control*, vol. 39, no. 12, pp. 2388–2397, 1994.

[197] M. Fu, A. W. Olbrot, and M. P. Polis, "Robust stability for time-delay systems: the edge theorem and graphical tests," *IEEE Transactions on Automatic Control*, vol. 34, no. 8, pp. 813–820, 1989.

[198] V. L. Kharitonov, J. A. Torres-Muñoz, and M. B. Ortiz-Moctezuma, "Polytopic families of quasi-polynomials: vertex-type stability conditions," *IEEE Transactions on Circuits and Systems I: Fundamental Theory and Applications*, vol. 50, no. 11, pp. 1413–1420, 2003.

[199] S. Mondie, J. Santos, and V. L. Kharitonov, "Robust stability of quasi-polynomials and the finite inclusions theorem," *IEEE Transactions on Automatic Control*, vol. 50, no. 11, pp. 1826–1831, 2005.

[200] G. Stein, G. Hartmann, and R. Hendrick, "Adaptive control laws for f-8 flight test," *IEEE Transactions on Automatic Control*, vol. 22, no. 5, pp. 758–767, 1977.

[201] J. S. Shamma and M. Athans, "Guaranteed properties of gain scheduled control for linear parameter-varying plants," *Automatica*, vol. 27, no. 3, pp. 559–564, 1991.

[202] K. Walton and J. E. Marshall, "Direct method for TDS stability analysis," *IEE Proceedings D Control Theory and Applications*, vol. 134, no. 2, pp. 101–107, 1987.

[203] J. M. Otto, "Closed control of loop with dead time," *Chemical Engineering Progress*, vol. 53, pp. 217–219, 1957.

[204] Z. Rekasius and J. Gibson, "Stability analysis of nonlinear control systems by the second method of Liapunov," *IRE Transactions on Automatic Control*, vol. 7, no. 1, pp. 3–15, 1962.

[205] O. Perron, *Die lehre von den kettenbriichen ii. Aufl., Teubner, Stuttgart (1954, 1957)*, 1957.

[206] R. Sipahi, H. Fazelinia, and N. Olgac, "Generalization of cluster treatment of characteristic roots for robust stability of multiple time-delayed systems," *International Journal of Robust and Nonlinear Control*, vol. 18, no. 14, pp. 1430–1449, 2008.

[207] J. Lam, "Model reduction of delay systems using Pade approximants," *International Journal of Control*, vol. 57, no. 2, pp. 377–391, 1993.

[208] A. V. Egorov, C. Cuvas, and S. Mondié, "Necessary and sufficient stability conditions for linear systems with pointwise and distributed delays," *Automatica*, vol. 80, pp. 218–224, 2017.

[209] I. V. Medvedeva and A. P. Zhabko, "Synthesis of Razumikhin and Lyapunov–Krasovskii approaches to stability analysis of time-delay systems," *Automatica*, vol. 51, pp. 372–377, 2015.

[210] M. J. Park, O. M. Kwon, J. H. Park, and S. M. Lee, "A new augmented Lyapunov-Krasovskii functional approach for stability of linear systems with time-varying delays," *Applied Mathematics and Computation*, vol. 217, no. 17, pp. 7197–7209, 2011.

[211] P.-L. Liu, "Exponential stability for linear time-delay systems with delay dependence," *Journal of the Franklin Institute*, vol. 340, no. 6-7, pp. 481–488, 2003.

[212] X. Li and C. E. De Souza, "Criteria for robust stability and stabilization of uncertain linear systems with state delay," *Automatica*, vol. 33, no. 9, pp. 1657–1662, 1997.

[213] K. Gu, "Discretized LMI set in the stability problem of linear uncertain time-delay systems," *International Journal of Control*, vol. 68, no. 4, pp. 923–934, 1997.

[214] L. Dugard and E. I. Verriest, *Stability and Control of Time-Delay Systems*, Springer, Berlin, Germany, 1998.

[215] P. G. Park, "A delay-dependent stability criterion for systems with uncertain time-invariant delays," *IEEE Transactions on Automatic Control*, vol. 44, no. 4, pp. 876-877, 1999.

[216] K. Gu, "An integral inequality in the stability problem of time-delay systems," in *Proceedings of the 39th IEEE Conference on Decision and Control*, pp. 2805–2810, Sydney, Australia, December 2000.

[217] E. Fridman, "New Lyapunov-Krasovskii functionals for stability of linear retarded and neutral type systems," *Systems & Control Letters*, vol. 43, no. 4, pp. 309–319, 2001.

[218] Y. S. Moon, P. Park, W. H. Kwon, and Y. S. Lee, "Delay-dependent robust stabilization of uncertain state-delayed systems," *International Journal of Control*, vol. 74, no. 14, pp. 1447–1455, 2010.

[219] E. Fridman and U. Shaked, "A descriptor system approach to H/sub ∞/control of linear time-delay systems," *IEEE Transactions on Automatic Control*, vol. 47, no. 2, pp. 253–270, 2002.

[220] Q.-L. Han, "Robust stability of uncertain delay-differential systems of neutral type," *Automatica*, vol. 38, no. 4, pp. 719–723, 2002.

[221] E. Fridman and U. Shaked, "An improved stabilization method for linear time-delay systems," *IEEE Transactions on Automatic Control*, vol. 47, no. 11, pp. 1931–1937, 2002.

[222] X. Zhang, P. Tsiotras, and C. Knospe, "Stability analysis of LPV time-delayed systems," *International Journal of Control*, vol. 75, no. 7, pp. 538–558, 2002.

[223] E. Fridman and U. Shaked, "Delay-dependent stability and H_∞ control: constant and time-varying delays," *International Journal of Control*, vol. 76, no. 1, pp. 48–60, 2003.

[224] V. L. Kharitonov and D. Hinrichsen, "Exponential estimates for time delay systems," *Systems & Control Letters*, vol. 53, no. 5, pp. 395–405, 2004.

[225] E. Fridman, A. Seuret, and J.-P. Richard, "Robust sampled-data stabilization of linear systems: an input delay approach," *Automatica*, vol. 40, no. 8, pp. 1441–1446, 2004.

[226] M. Wu, Y. He, and J.-H. She, "New delay-dependent stability criteria and stabilizing method for neutral systems," *IEEE Transactions on Automatic Control*, vol. 49, no. 12, pp. 2266–2271, 2004.

[227] Y. He, M. Wu, J.-H. She, and G.-P. Liu, "Parameter-dependent Lyapunov functional for stability of time-delay systems with polytopic-type uncertainties," *IEEE Transactions on Automatic Control*, vol. 49, no. 5, pp. 828–832, 2004.

[228] S. Mondie and V. L. Kharitonov, "Exponential estimates for retarded time-delay systems: an LMI approach," *IEEE Transactions on Automatic Control*, vol. 50, no. 2, pp. 268–273, 2005.

[229] S. Shengyuan, J. Xu, and J. Lam, "Improved delay-dependent stability criteria for time-delay systems," *IEEE Transactions on Automatic Control*, vol. 50, no. 3, pp. 384–387, 2005.

[230] S. Xu, J. Lam, and M. Zhong, "New exponential estimates for time-delay systems," *IEEE Transactions on Automatic Control*, vol. 51, no. 9, pp. 1501–1505, 2006.

[231] S. Xu and J. Lam, *Robust Control and Filtering of Singular Systems*, Springer, Berlin, Germany, 2006.

[232] X. Jiang and Q.-L. Han, "Delay-dependent robust stability for uncertain linear systems with interval time-varying delay," *Automatica*, vol. 42, no. 6, pp. 1059–1065, 2006.

[233] Y. He, Q.-G. Wang, C. Lin, and M. Wu, "Delay-range-dependent stability for systems with time-varying delay," *Automatica*, vol. 43, no. 2, pp. 371–376, 2007.

[234] H. Shao, "New delay-dependent stability criteria for systems with interval delay," *Automatica*, vol. 45, no. 3, pp. 744–749, 2009.

[235] J. Sun, G. P. Liu, J. Chen, and D. Rees, "Improved delay-range-dependent stability criteria for linear systems with time-varying delays," *Automatica*, vol. 46, no. 2, pp. 466–470, 2010.

[236] H.-B. Zeng, Y. He, M. Wu, and J. She, "Free-matrix-based integral inequality for stability analysis of systems with time-varying delay," *IEEE Transactions on Automatic Control*, vol. 60, no. 10, pp. 2768–2772, 2015.

[237] R. S. Kumar, G. Sugumaran, R. Raja, Q. Zhu, and U. K. Raja, "New stability criterion of neural networks with leakage delays and impulses: a piecewise delay method," *Cognitive Neurodynamics*, vol. 10, no. 1, pp. 85–98, 2016.

[238] S. Pandiselvi, R. Raja, J. Cao, X. Li, and G. Rajchakit, "Impulsive discrete-time GRNS with probabilistic time delays, distributed and leakage delays: an asymptotic stability issue," *IMA Journal of Mathematical Control and Information*, vol. 36, no. 1, pp. 79–100, 2019.

[239] V. Kharitonov, "Robust stability analysis of time delay systems: a survey," *Annual Reviews in Control*, vol. 23, no. 1, pp. 185–196, 1999.

[240] K. Gu and S.-I. Niculescu, "Survey on recent results in the stability and control of time-delay systems," *Journal of Dynamic Systems, Measurement, and Control*, vol. 125, no. 2, pp. 158–165, 2003.

[241] J.-P. Richard, "Time-delay systems: an overview of some recent advances and open problems," *Automatica*, vol. 39, no. 10, pp. 1667–1694, 2003.

[242] I. M. Repin, "Quadratic Liapunov functionals for systems with delay," *Journal of Applied Mathematics and Mechanics*, vol. 29, no. 3, pp. 669–672, 1965.

[243] R. Datko, "An algorithm for computing Liapunov functionals for some differential-difference equations," in *Ordinary Differential Equations,* Elsevier, Amsterdam, Netherlands, 1972.

[244] E. F. Infante and W. B. Castelan, *A Liapunov Functional for a Matrix Difference-Differential Equation*, Technical report, Brown University, Providence, RI, USA, 1977.

[245] H. Wenzhang, "Generalization of Liapunov's theorem in a linear delay system," *Journal of Mathematical Analysis and Applications*, vol. 142, no. 1, pp. 83–94, 1989.

[246] V. L. Kharitonov and A. P. Zhabko, "Lyapunov-Krasovskii approach to robust stability of time delay systems," *IFAC Proceedings Volumes*, vol. 34, no. 13, pp. 477–481, 2001.

[247] V. L. Kharitonov and A. P. Zhabko, "Lyapunov-Krasovskii approach to the robust stability analysis of time-delay systems," *Automatica*, vol. 39, no. 1, pp. 15–20, 2003.

[248] H. Garcia-Lozano and V. L. Kharitonov, "Lyapunov matrices for time delay system with commensurate delays," *IFAC Proceedings Volumes*, vol. 37, no. 21, pp. 91–95, 2004.

[249] H. Garcia-Lozano and V. L. Kharitonov, "Numerical computation of time delay Lyapunov matrices," *IFAC Proceedings Volumes*, vol. 39, no. 10, pp. 60–65, 2006.

[250] R. Villafuerte, S. Mondie, and O. Santos, "On the computation of estimates for time delay systems with Lyapunov-Krasovskii functionals of complete type," in *Proceedings of the 2006 3rd International Conference on Electrical and Electronics Engineering*, pp. 1–4, Veracruz, Mexico, September 2006.

[251] B. M. Ochoa and S. Mondie, "Approximations of Lyapunov-Krasovskii functionals of complete type with given cross terms in the derivative for the stability of time delay systems," in *Proceedings of the 2007 46th IEEE Conference on Decision and Control*, pp. 2071–2076, New Orleans, LO, USA, December 2007.

[252] V. L. Kharitonov, "Lyapunov matrices for a class of neutral type time delay systems," *International Journal of Control*, vol. 81, no. 6, pp. 883–893, 2008.

[253] J. E. Velázquez and V. L. Kharitonov, "Lyapunov–Krasovskii functionals for scalar neutral type time delay equations," *Systems & Control Letters*, vol. 58, no. 1, pp. 17–25, 2009.

[254] A. V. Egorov and V. L. Kharitonov, "Approximation of delay Lyapunov matrices," *International Journal of Control*, vol. 91, no. 11, pp. 2588–2596, 2018.

[255] S. Mondie, V. L. Kharitonov, and O. Santos, "Complete type Lyapunov-Krasovskii functionals with a given cross term in the time derivative," in *Proceedings of the 44th IEEE Conference on Decision and Control*, pp. 5060–5064, Seville, Spain, 2005.

[256] O. Santos, S. Mondie, and V. L. Kharitonov, "Robust stability conditions for systems with distributed delays," in *Proceedings of the 45th IEEE Conference on Decision and Control*, pp. 217–222, San Diego, CA, USA, December 2006.

[257] E. Fridman, "Stability of systems with uncertain delays: a new "complete" Lyapunov-Krasovskii functional," *IEEE Transactions on Automatic Control*, vol. 51, no. 5, pp. 885–890, 2006.

[258] E. Fridman and S.-I. Niculescu, "On complete Lyapunov-Krasovskii functional techniques for uncertain systems with fast-varying delays," *International Journal of Robust and Nonlinear Control*, vol. 18, no. 3, pp. 364–374, 2008.

[259] O. Santos, S. Mondié, and V. L. Kharitonov, "Linear quadratic suboptimal control for time delays systems," *IFAC Proceedings Volumes*, vol. 39, no. 10, pp. 96–101, 2006.

[260] V. L. Kharitonov, "Predictor based stabilization of neutral type systems with input delay," *Automatica*, vol. 52, pp. 125–134, 2015.

[261] V. L. Kharitonov, "Prediction-based control for systems with state and several input delays," *Automatica*, vol. 79, pp. 11–16, 2017.

[262] A. N. Aliseyko and V. L. Kharitonov, "Lyapunov-Krasovskii functionals for linear systems with input delay," *IFAC-PapersOnLine*, vol. 52, no. 18, pp. 19–24, 2019.

[263] L. Juárez, S. Mondié, and V. L. Kharitonov, "Dynamic predictor for systems with state and input delay: a time-domain robust stability analysis," *International Journal of Robust and Nonlinear Control*, vol. 30, no. 6, pp. 2204–2218, 2020.

[264] L. A. Castañeda, A. Luviano-Juárez, G. Ochoa-Ortega, and I. Chairez, "Tracking control of uncertain time delay systems: an ADRC approach," *Control Engineering Practice*, vol. 78, pp. 97–104, 2018.

[265] M. A. Gomez, W. Michiels, and S. Mondié, "Design of delay-based output-feedback controllers optimizing a quadratic cost function via the delay Lyapunov matrix," *Automatica*, vol. 107, pp. 146–153, 2019.

[266] M. A. Gomez, A. V. Egorov, and S. Mondié, "Lyapunov matrix based necessary and sufficient stability condition by finite number of mathematical operations for retarded type systems," *Automatica*, vol. 108, Article ID 108475, 2019.

[267] M. A. Gomez, A. V. Egorov, S. Mondié, and A. P. Zhabko, "Computation of the Lyapunov matrix for periodic time-delay systems and its application to robust stability analysis," *Systems & Control Letters*, vol. 132, Article ID 104501, 2019.

[268] A. Bellen and M. Zennaro, *Numerical Methods for Delay Differential Equations*, Oxford University Press, Oxford, UK, 2013.

[269] K. Engelborghs, T. Luzyanina, and D. Roose, "Numerical bifurcation analysis of delay differential equations using DDE-Biftool," *ACM Transactions on Mathematical Software*, vol. 28, no. 1, pp. 1–21, 2002.

[270] E. Hairer, S. P. Nørsett, and G. Wanner, "Solving ordinary differential equations *i* Nonstiff Problems," *Springer Series in Computational Mathematics*, vol. 8, Berlin, Germany, 1993.

[271] D. Breda, S. Maset, and R. Vermiglio, *Stability of Linear Delay Differential Equations: A Numerical Approach with MATLAB*, Springer, Berlin, Germany, 2014.

[272] J. Louisell, "Numerics of the stability exponent and eigenvalue abscissas of a matrix delay system," in *Stability and Control of Time-Delay Systems,* Springer, Berlin, Germany, 1998.

[273] J. Louisell, "Stability exponent and eigenvalue abscissas by way of the imaginary axis eigenvalues," in *Advances in Time-Delay Systems,* Springer, Berlin, Germany, 2004.

[274] J. Louisell, "A matrix method for determining the imaginary axis eigenvalues of a delay system," *IEEE Transactions on Automatic Control*, vol. 46, no. 12, pp. 2008–2012, 2001.

[275] G. Ochoa, S. Mondié, and V. L. Kharitonov, "Time delay systems with distributed delays: critical values," *IFAC Proceedings Volumes*, vol. 42, no. 14, pp. 272–277, 2009.

[276] G. Ochoa, V. L. Kharitonov, and S. Mondié, "Critical frequencies and parameters for linear delay systems: a Lyapunov matrix approach," *Systems & Control Letters*, vol. 62, no. 9, pp. 781–790, 2013.

[277] N. Olgac and R. Sipahi, "The cluster treatment of characteristic roots and the neutral type time-delayed systems," *Journal of Dynamic Systems, Measurement, and Control*, vol. 127, no. 1, pp. 88–97, 2004.

[278] R. Sipahi and N. Olgac, "A novel stability study on multiple time-delay systems (MTDS) using the root clustering paradigm," in *Proceedings of the 2004 American Control Conference*, pp. 5422–5427, Boston, MA, USA, June 2004.

[279] R. Sipahi and N. Olgac, "A unique methodology for the stability robustness of multiple time delay systems," *Systems & Control Letters*, vol. 55, no. 10, pp. 819–825, 2006.

[280] N. Olgac and R. Sipahi, "A practical method for analyzing the stability of neutral type LTI-time delayed systems," *Automatica*, vol. 40, no. 5, pp. 847–853, 2004.

[281] R. Sipahi and N. Olgac, "Complete stability robustness of third-order LTI multiple time-delay systems," *Automatica*, vol. 41, no. 8, pp. 1413–1422, 2005.

[282] R. Sipahi, *Cluster treatment of characteristic roots, CTCR, a unique methodology for the complete robustness analysis of linear time invariant multiple time delay systems against delay uncertainties*, PhD thesis, University of Connecticut, Mansfield, CT, USA, 2005.

[283] E. Jarlebring, W. Michiels, and K. Meerbergen, "A linear eigenvalue algorithm for the nonlinear eigenvalue problem," *Numerische Mathematik*, vol. 122, no. 1, pp. 169–195, 2012.

[284] E. Jarlebring, K. Meerbergen, and W. Michiels, "Computing a partial Schur factorization of nonlinear eigenvalue problems using the infinite arnoldi method," *SIAM Journal on Matrix Analysis and Applications*, vol. 35, no. 2, pp. 411–436, 2014.

[285] R. Van Beeumen, E. Jarlebring, and W. Michiels, "A rank-exploiting infinite arnoldi algorithm for nonlinear eigenvalue problems," *Numerical Linear Algebra with Applications*, vol. 23, no. 4, pp. 607–628, 2016.

[286] W. Michiels, I. Boussaada, and S.-I. Niculescu, "An explicit formula for the splitting of multiple eigenvalues for nonlinear eigenvalue problems and connections with the linearization for the delay eigenvalue problem," *SIAM Journal on Matrix Analysis and Applications*, vol. 38, no. 2, pp. 599–620, 2017.

[287] W. Michiels and N. Guglielmi, "An iterative method for computing the pseudospectral abscissa for a class of nonlinear eigenvalue problems," *SIAM Journal on Scientific Computing*, vol. 34, no. 4, pp. A2366–A2393, 2012.

[288] C. Abdallah, D. Peter, J. Benites-Read, and R. Byrne, "Delayed positive feedback can stabilize oscillatory systems," in *Proceedings of the 1993 American Control Conference*, pp. 3106-3107, San Francisco, CA, USA, June 1993.

[289] W. Michiels and S.-I. Niculescu, "Stability, control, and computation for time-delay systems: an eigenvalue-based approach," *SIAM*, vol. 27, 2014.

[290] K. Pyragas, "Continuous control of chaos by self-controlling feedback," *Physics Letters A*, vol. 170, no. 6, pp. 421–428, 1992.

[291] H. Chang, K. J. Åström, and K. Weng, "Refinements of the Ziegler–Nichols tuning formula," in *Proceedings of the IEEE D (Control Theory and Applications)*, pp. 111–118, 1991.

[292] M. E. Bleich and E. S. Joshua, "Stability of periodic orbits controlled by time-delay feedback," *Physics Letters A*, vol. 210, no. 1-2, pp. 87–94, 1996.

[293] M. de Sousa Vieira and A. J. Lichtenberg, "Controlling chaos using nonlinear feedback with delay," *Physical Review E*, vol. 54, no. 2, pp. 1200–1207, 1996.

[294] W. Just, T. Bernard, M. Ostheimer, E. Reibold, and H. Benner, "Mechanism of time-delayed feedback control," *Physical Review Letters*, vol. 78, no. 2, pp. 203–206, 1997.

[295] H. Suh and Z. Bien, "Use of time-delay actions in the controller design," *IEEE Transactions on Automatic Control*, vol. 25, no. 3, pp. 600–603, 1980.

[296] G. M. Swisher and S. Tenqchen, "Design of proportional-minus-delay action feedback controllers for second-and third-order systems," in *Proceedings of the 1988 American Control Conference*, pp. 254–260, Atlanta, GA, USA, 1988.

[297] Y. J. Huang, T. C. Kuo, and H. K. Lee, "Fuzzy-PD controller design with stability equations for electro-hydraulic servo systems," in *Proceedings of the 2007 International Conference on Control, Automation and Systems*, pp. 2407–2410, Seoul, Republic of Korea, 2007.

[298] C.-Y. LinY.-P. Chiu et al., "Catching algorithm for 2d robot manipulator using PD controller," in *Proceedings of the 2009 ICCAS-SICE*, pp. 46–50, Fukuoka, Japan, 2009.

[299] D. Simhachalam, C. Dey, and R. K. Mudi, "An auto-tuning PD controller for DC servo position control system," in *Proceedings of the 2012 2nd International Conference on Power, Control and Embedded Systems*, pp. 1–6, Allahabad, UP, India, December 2012.

[300] R. Kelly, R. Ortega, A. Ailon, and A. Loria, "Global regulation of flexible joint robots using approximate differentiation," *IEEE Transactions on Automatic Control*, vol. 39, no. 6, pp. 1222–1224, 1994.

[301] S. Mondié, R. Villafuerte, and R. Garrido, "Tuning and noise attenuation of a second order system using proportional retarded control," *IFAC Proceedings Volumes*, vol. 44, no. 1, pp. 10337–10342, 2011.

[302] R. Villafuerte, S. Mondié, and R. Garrido, "Tuning of proportional retarded controllers: theory and experiments," *IEEE Transactions on Control Systems Technology*, vol. 21, no. 3, pp. 983–990, 2012.

[303] J.-E. Hernández-Díez, C.-F. Méndez-Barrios, S. Mondié, S.-I. Niculescu, and E. J. González-Galván, "Proportional-delayed controllers design for LTI-systems: a geometric approach," *International Journal of Control*, vol. 91, no. 4, pp. 907–925, 2018.

[304] A. Ramírez, R. Garrido, and S. Mondié, "Integral retarded velocity control of DC servomotors," *IFAC Proceedings Volumes*, vol. 46, no. 3, pp. 558–563, 2013.

[305] A. Ramírez, R. Sipahi, S. Mondié, and R. Garrido, "Design of maximum decay rate for SISO systems with delayed output feedback using elimination theory," *IFAC-PapersOnLine*, vol. 48, no. 12, pp. 221–226, 2015.

[306] A. Ramirez, S. Mondié, R. Garrido, and R. Sipahi, "Design of proportional-integral-retarded (PIR) controllers for second-order LTI systems," *IEEE Transactions on Automatic Control*, vol. 61, no. 6, pp. 1688–1693, 2016.

[307] R. Villafuerte-Segura, F. Medina-Dorantes, L. Vite-Hernández, and B. Aguirre-Hernández, "Tuning of a time-delayed controller for a general class of second-order linear time invariant systems with dead-time," *IET Control Theory & Applications*, vol. 13, no. 3, pp. 451–457, 2018.

[308] G. Ochoa-Ortega, R. Villafuerte-Segura, M. Ramírez-Neria, and L. Vite-Hernández, σ-stabilization of a flexible joint robotic arm via delayed controllers," *Complexity*, vol. 2019, Article ID 7289689, 12 pages, 2019.

[309] D. Melchor-Aguilar and S.-I. Niculescu, "Computing non-fragile pi controllers for delay models of TCP/AQM networks," *International Journal of Control*, vol. 82, no. 12, pp. 2249–2259, 2009.

[310] Y. Yu, H. Dong, Z. Wang, W. Ren, and F. E. Alsaadi, "Design of non-fragile state estimators for discrete time-delayed neural networks with parameter uncertainties," *Neurocomputing*, vol. 182, pp. 18–24, 2016.

[311] J.-E. Hernandez-Diez, C.-F. Mendez-Barrios, S.-I. Niculescu, E.-J. Gonzalez-Galvan, G. Mejia-Rodriguez, and V. Ramirez-Rivera, "Closed-loop stability analysis of voltage mode buck using a proportional-delayed controller," in *Proceedings of the 2017 25th Mediterranean Conference on Control and Automation (MED)*, pp. 490–495, Valletta, Malta, July 2017.

[312] S. H. Strogatz, "Exploring complex networks," *Nature*, vol. 410, no. 6825, pp. 268–276, 2001.

[313] S. Boccaletti, V. Latora, Y. Moreno, M. Chavez, and D.-U. Hwang, "Complex networks: structure and dynamics," *Physics Reports*, vol. 424, no. 4-5, pp. 175–308, 2006.

[314] R. Barabási and A.-L. Barabási, "Statistical mechanics of complex networks," *Reviews of Modern Physics*, vol. 74, no. 1, pp. 47–97, 2002.

[315] C. P. Li, W. G. Sun, and J. Kurths, "Synchronization of complex dynamical networks with time delays," *Physica A: Statistical Mechanics and its Applications*, vol. 361, no. 1, pp. 24–34, 2006.

[316] L. Su, Y. Wei, W. Michiels, E. Steur, and H. Nijmeijer, "Robust partial synchronization of delay-coupled networks," *Chaos: An Interdisciplinary Journal of Nonlinear Science*, vol. 30, no. 1, Article ID 013126, 2020.

[317] W. Michiels and H. Nijmeijer, "Synchronization of delay-coupled nonlinear oscillators: an approach based on the stability analysis of synchronized equilibria," *Chaos: An interdisciplinary Journal of Nonlinear Science*, vol. 19, no. 3, Article ID 033110, 2009.

[318] M. G. Earl and S. H. Strogatz, "Synchronization in oscillator networks with delayed coupling: a stability criterion," *Physical Review E*, vol. 67, no. 3, Article ID 036204, 2003.

[319] U. Ernst, K. Pawelzik, and T. Geisel, "Delay-induced multistable synchronization of biological oscillators," *Physical Review E*, vol. 57, no. 2, pp. 2150–2162, 1998.

[320] E. M. Izhikevich, "Weakly pulse-coupled oscillators, fm interactions, synchronization, and oscillatory associative memory," *IEEE Transactions on Neural Networks*, vol. 10, no. 3, pp. 508–526, 1999.

[321] M. Y. Choi, H. J. Kim, D. Kim, and H. Hong, "Synchronization in a system of globally coupled oscillators with time delay," *Physical Review E*, vol. 61, no. 1, pp. 371–381, 2000.

[322] A. Papachristodoulou and J. Ali, "Synchronization in oscillator networks: switching topologies and non-homogeneous delays," in *Proceedings of the 44th IEEE Conference on Decision and Control*, pp. 5692–5697, Seville, Spain, 2005.

[323] H.-J. Wünsche, S. Bauer, J. Kreissl et al., "Synchronization of delay-coupled oscillators: a study of semiconductor lasers," *Physical Review Letters*, vol. 94, no. 16, Article ID 163901, 2005.

[324] A. A. Selivanov, Judith Lehnert, T. Dahms, P. Hövel, A. L. Fradkov, and E. Schöll, "Adaptive synchronization in delay-coupled networks of stuart-landau oscillators," *Physical Review E*, vol. 85, no. 1, Article ID 016201, 2012.

[325] C. Maharajan, R. Raja, J. Cao, G. Rajchakit, Z. Tu, and A. Alsaedi, "LMI-based results on exponential stability of bam-type neural networks with leakage and both time-varying delays: a non-fragile state estimation approach," *Applied Mathematics and Computation*, vol. 326, pp. 33–55, 2018.

[326] Q. Song, G. Lu, G. Wen, J. Cao, and F. Liu, "Bipartite synchronization and convergence analysis for network of harmonic oscillator systems with signed graph and time delay," *IEEE Transactions on Circuits and Systems I: Regular Papers*, vol. 66, no. 7, pp. 2723–2734, 2019.

[327] Y. Yang, W. He, Q.-L. Han, and C. Peng, "H_∞ synchronization of networked master-slave oscillators with delayed position data: the positive effects of network-induced delays," *IEEE Transactions on Cybernetics*, vol. 49, no. 12, pp. 4090–4102, 2019.

[328] R. Huan, D. Pu, X. Wang, and X. Wei, "Effects of phase delay on synchronization in a nonlinear micromechanical oscillator," *Applied Physics Letters*, vol. 114, no. 23, Article ID 233501, 2019.

[329] I. Choi, H. Culbertson, M. R. Miller, A. Olwal, and S. Follmer, "Grabity: a wearable haptic interface for simulating weight and grasping in virtual reality," in *Proceedings of the 30th Annual ACM Symposium on User Interface Software and Technology*, pp. 119–130, Québec, Canada, October 2017.

[330] Y. Song, S. Guo, X. Yin et al., "Design and performance evaluation of a haptic interface based on MR fluids for endovascular tele-surgery," *Microsystem Technologies*, vol. 24, no. 2, pp. 909–918, 2018.

[331] S. Yun, S. Park, B. Park, S. Ryu, S. M. Jeong, and K.-U. Kyung, "A soft and transparent Visuo-haptic interface pursuing wearable devices," *IEEE Transactions on Industrial Electronics*, vol. 67, no. 1, pp. 717–724, 2019.

[332] P. Polygerinos, F. Sebastian, Q. Fu, and M. Santello, "Soft robotic haptic interface with variable stiffness for rehabilitation of sensorimotor hand function," US Patent App. 16/212, 205, 2019.

[333] R. Brent Gillespie, "Haptic interface to virtual environments," in *Robotics and Automation Handbook,* CRC Press, Boca Raton, FL, USA, 2018.

[334] G. Hernández-Melgarejo, D. A. Flores-Hernández, A. Luviano-Juárez, L. A. Castañeda, I. Chairez, and S. Di Gennaro, "Mechatronic design and implementation of a bicycle virtual reality system," *ISA Transactions*, vol. 97, pp. 336–351, 2020.

[335] T. Waltemate, I. Senna, F. Hülsmann et al., "The impact of latency on perceptual judgments and motor performance in closed-loop interaction in virtual reality," in *Proceedings of the 22nd ACM Conference on Virtual Reality Software and Technology*, pp. 27–35, Munich, Germany, November 2016.

[336] M. S. Elbamby, C. Perfecto, M. Bennis, and K. Doppler, "Toward low-latency and ultra-reliable virtual reality," *IEEE Network*, vol. 32, no. 2, pp. 78–84, 2018.

[337] R. S. Allison, L. R. Harris, Michael Jenkin, U. Jasiobedzka, and J. E. Zacher, "Tolerance of temporal delay in virtual environments," in *Proceedings of the 2001 IEEE Virtual Reality*, pp. 247–254, Yokohama, Japan, March 2001.

[338] D. Delaney, T. Ward, and S. McLoone, "On consistency and network latency in distributed interactive applications: a survey-part I," *Presence: Teleoperators and Virtual Environments*, vol. 15, no. 2, pp. 218–234, 2006.

[339] N. Chopra, M. W. Spong, S. Hirche, and M. Buss, "Bilateral teleoperation over the Internet: the time varying delay," in *Proceedings of the American Control Conference (ACC)*, Denver, CO, USA, June 2003.

[340] N. Chopra, P. Berestesky, and M. W. Spong, "Bilateral teleoperation over unreliable communication networks," *IEEE Transactions on Control Systems Technology*, vol. 16, no. 2, pp. 304–313, 2008.

[341] P. F. Hokayem and M. W. Spong, "Bilateral teleoperation: an historical survey," *Automatica*, vol. 42, no. 12, pp. 2035–2057, 2006.

[342] D. A. Lawrence, "Stability and transparency in bilateral teleoperation," *IEEE Transactions on Robotics and Automation*, vol. 9, no. 5, pp. 624–637, 1993.

[343] K. J. Astrom, C. C. Hang, and B. C. Lim, "A new smith predictor for controlling a process with an integrator and long dead-time," *IEEE Transactions on Automatic Control*, vol. 39, no. 2, pp. 343–345, 1994.

[344] W. Zhang, Y. Sun, and X. Xu, "Two degree-of-freedom Smith predictor for processes with time delay," *Automatica*, vol. 34, no. 10, pp. 1279–1282, 1998.

[345] M. Velasco-Villa, B. del Muro-Cuellar, and A. Alvarez-Aguirre, "Smith-predictor compensator for a delayed omnidirectional mobile robot," in *Proceedings of the 2007 Mediterranean Conference on Control & Automation*, pp. 1–6, Athens, Greece, June 2007.

[346] M. Fliess, R. Marquez, and H. Mounier, "An extension of predictive control, PID regulators and Smith predictors to some linear delay systems," *International Journal of Control*, vol. 75, no. 10, pp. 728–743, 2002.

[347] M. Fliess, R. Marquez, and H. Mounier, "PID-like regulators for a class of linear delay systems," in *Proceedings of the 2001 European Control Conference (ECC)*, pp. 178–183, Porto, Portugal, 2001.

[348] R. Marquez, M. Fliess, and H. Mounier, "A non-conventional robust pi-controller for the smith predictor," in *Proceedings of the 40th IEEE Conference on Decision and Control*, pp. 2259-2260, Orlando, FL, USA, 2001.

[349] M. Fliess, R. Marquez, and H. Mounier, "On a generalization of PID regulators for delay systems," *IFAC Proceedings Volumes*, vol. 34, no. 23, pp. 13–18, 2001.

[350] R. Raja, R. Sakthivel, and S. M. Anthoni, "Stability analysis for discrete-time stochastic neural networks with mixed time delays and impulsive effects," *Canadian Journal of Physics*, vol. 88, no. 12, pp. 885–898, 2010.

[351] M. Ramirez-Neria, H. Sira-Ramírez, A. Luviano-Juarez, and A. Rodríguez-Angeles, "Smith predictor based generalized PI control for a class of input delayed nonlinear mechanical systems," in *Proceedings of the 2013 European Control Conference (ECC)*, pp. 1292–1297, Zurich, Switzerland, July 2013.

[352] H. Sira-Ramírez, A. Luviano-Juárez, M. Ramírez-Neria, and E. W. Zurita-Bustamante, *Active Disturbance Rejection Control of Dynamic Systems: A Flatness Based Approach*, Butterworth-Heinemann, Oxford, UK, 2017.

[353] P. Escudero-Gomez, H. Sira-Ramirez, and A. Rodriguez-Angeles, "Inventory trajectory tracking via an demand-atestimation using smithâ predictor," Congreso Nacional de Control Automáatico, Monterrey, Nuevo Leóon, Mexico, pp. 409–414, 2017.

[354] S. Chen, W. Xue, Yi Huang, and P. Liu, "On comparison between smith predictor and predictor observer based ADRCS for nonlinear uncertain systems with output delay," in *Proceedings of the 2017 American Control Conference (ACC)*, pp. 5083–5088, Seattle, WA, USA, May 2017.

[355] W. D. Zhang and Y. X. Sun, "Modified smith predictor for controlling integrator/time delay processes," *Industrial & Engineering Chemistry Research*, vol. 35, no. 8, pp. 2769–2772, 1996.

[356] T. Liu, W. D. Zhang, Y. Z. Cai, and D. Y. Gu, "New modified smith predictor scheme for integrating and unstable processes with time delay," *IEE Proceedings-Control Theory and Applications*, vol. 152, no. 2, pp. 238–246, 2005.

[357] H. U. Tianjian and X. Huang, "Active disturbance rejection control for space master-slave teleoperation," *Journal of Spacecraft TT & C Technology*, vol. 2011, no. 6, p. 8, 2011.

[358] T. J. Hu, X. X. Huang, and Q. Tan, "Active disturbance rejection controller for space teleoperation," in *Proceedings of the International Conference on Automatic Control and Artificial Intelligence*, pp. 334–337, Xiamen, China, March 2012.

[359] A. C. Smith and K. V. Hashtrudi-Zaad, "Neural network-based teleoperation using smith predictors," in *Proceedings of the IEEE International Conference Mechatronics and Automation*, vol. 3, pp. 1654–1659, Niagara Falls, Ontario, Canada, July 2005.

[360] A. C. Smith and K. Hashtrudi-Zaad, "Smith predictor type control architectures for time delayed teleoperation," *The International Journal of Robotics Research*, vol. 25, no. 8, pp. 797–818, 2006.

[361] G. Niemeyer and J.-J. E. Slotine, "Stable adaptive teleoperation," *IEEE Journal of Oceanic Engineering*, vol. 16, no. 1, pp. 152–162, 1991.

[362] G. Niemeyer and J.-J. E. Slotine, "Telemanipulation with time delays," *The International Journal of Robotics Research*, vol. 23, no. 9, pp. 873–890, 2004.

[363] D. Lee and M. W. Spong, "Passive bilateral teleoperation with constant time delay," *IEEE Transactions on Robotics*, vol. 22, no. 2, pp. 269–281, 2006.

[364] J.-H. Ryu, J. Artigas, and C. Preusche, "A passive bilateral control scheme for a teleoperator with time-varying communication delay," *Mechatronics*, vol. 20, no. 7, pp. 812–823, 2010.

[365] N. Chopra, M. W. Spong, and R. Lozano, "Synchronization of bilateral teleoperators with time delay," *Automatica*, vol. 44, no. 8, pp. 2142–2148, 2008.

[366] E. Nuño, L. Basañez, and R. Ortega, "Passivity-based control for bilateral teleoperation: a tutorial," *Automatica*, vol. 47, no. 3, pp. 485–495, 2011.

[367] E. Nuño, L. Basañez, R. Ortega, and M. W. Spong, "Position tracking for non-linear teleoperators with variable time delay," *The International Journal of Robotics Research*, vol. 28, no. 7, pp. 895–910, 2009.

[368] M. Franken, S. Stramigioli, S. Misra, C. Secchi, and A. Macchelli, "Bilateral telemanipulation with time delays: a two-layer approach combining passivity and transparency," *IEEE Transactions on Robotics*, vol. 27, no. 4, pp. 741–756, 2011.

[369] A. F. Villaverde, A. B. Blas, J. Carrasco, and A. B. Torrico, "Reset control for passive bilateral teleoperation," *IEEE Transactions on Industrial Electronics*, vol. 58, no. 7, pp. 3037–3045, 2010.

[370] J. Rebelo and A. Schiele, "Time domain passivity controller for 4-channel time-delay bilateral teleoperation," *IEEE Transactions on Haptics*, vol. 8, no. 1, pp. 79–89, 2014.

[371] D. Sun, F. Naghdy, and H. Du, "Neural network-based passivity control of teleoperation system under time-varying delays," *IEEE Transactions on Cybernetics*, vol. 47, no. 7, pp. 1666–1680, 2016.

[372] J. Artigas, J.-H. Ryu, and C. Preusche, "Time domain passivity control for position-position teleoperation architectures," *Presence: Teleoperators and Virtual Environments*, vol. 19, no. 5, pp. 482–497, 2010.

[373] V. Chawda and K. Marcia, "Position synchronization in bilateral teleoperation under time-varying communication delays," *IEEE/ASME Transactions on Mechatronics*, vol. 20, no. 1, pp. 245–253, 2014.

[374] Y. Ye, Y.-J. Pan, and T. Hilliard, "Bilateral teleoperation with time-varying delay: a communication channel Passification approach," *IEEE/ASME Transactions on Mechatronics*, vol. 18, no. 4, pp. 1431–1434, 2013.

[375] I. Estrada-Sánchez, M. Velasco-Villa, and H. Rodríguez-Cortés, "Prediction-based control for nonlinear systems with input delay," *Mathematical Problems in Engineering*, vol. 2017, Article ID 7415418, 2017.

[376] Z. Chen, F. Huang, C. Yang, and B. Yao, "Adaptive fuzzy backstepping control for stable nonlinear bilateral teleoperation manipulators with enhanced transparency

performance," *IEEE Transactions on industrial Electronics*, vol. 67, no. 1, pp. 746–756, 2019.

[377] D.-H. Zhai and Y. Xia, "Adaptive fuzzy control of multilateral asymmetric teleoperation for coordinated multiple mobile manipulators," *IEEE Transactions on Fuzzy Systems*, vol. 24, no. 1, pp. 57–70, 2015.

[378] C. Yang, X. Wang, Z. Li, Y. Li, and C.-Yi Su, "Teleoperation control based on combination of wave variable and neural networks," *IEEE Transactions on Systems, Man, and Cybernetics: Systems*, vol. 47, no. 8, pp. 2125–2136, 2016.

[379] L. Zhao, L. Liu, Y. Wang, and H. Yang, "Active disturbance rejection control for teleoperation systems with actuator saturation," *Asian Journal of Control*, vol. 21, no. 2, pp. 702–713, 2019.

[380] L. Á. Castañeda, L. Guzman-Vargas, I. Chairez, and A. Luviano-Juárez, "Output based bilateral adaptive control of partially known robotic systems," *Control Engineering Practice*, vol. 98, Article ID 104362, 2020.

[381] Y. Xia, G. P. Liu, P. Shi, J. Han, and D. Rees, "Active disturbance rejection control for uncertain multivariable systems with time-delay," *IET Control Theory & Applications*, vol. 1, no. 1, pp. 75–81, 2007.

[382] C. Join, M. Fliess, and F. Chaxel, "Model-free control as a service in the industrial internet of things: packet loss and latency issues via preliminary experiments," 2020, http://arxiv.org/abs//2004.12156.

[383] Y. Yang, C. Hua, and X. Guan, "Adaptive fuzzy finite-time coordination control for networked nonlinear bilateral teleoperation system," *IEEE Transactions on Fuzzy Systems*, vol. 22, no. 3, pp. 631–641, 2013.

[384] Z. Li, X. Cao, and N. Ding, "Adaptive fuzzy control for synchronization of nonlinear teleoperators with stochastic time-varying communication delays," *IEEE Transactions on Fuzzy Systems*, vol. 19, no. 4, pp. 745–757, 2011.

[385] V. Lakshmikantham, V. M. Matrosov, and S. Sivasundaram, *Vector Lyapunov Functions and Stability of Nonlinear Systems*, Kluwer Academic Publishers, Berlin, Germany, 1st edition, 1991.

[386] V. I. Vorotnikov, *Partial Stability and Control*, Birkhåuser, New York, NY, USA, 1998.

[387] A. F. Filippov, *Differential Equations with Discontinuities Right-Hand Sides*, Kluwer Academic Publisher, Dordrecht, Netherlands, 1988.

[388] I. Podlubny, *Fractional Differential Equations*, Academic Press, San Diego, CA, USA, 1999.

[389] V. Utkin, "On convergence time and disturbance rejection of super-twisting control," *IEEE Transactions on Automatic Control*, vol. 58, no. 8, pp. 2013–2017, 2013.

[390] J. A. Moreno and M. Osorio, "Strict Lyapunov functions for the super-twisting algorithm," *IEEE Transactions on Automatic Control*, vol. 57, no. 4, pp. 1035–1040, 2012.

[391] A. E. Polyakov and A. S. Poznyak, "Method of Lyapunov functions for systems with higher-order sliding modes," *Automation and Remote Control*, vol. 72, no. 5, pp. 944–963, 2011.

[392] V. I. Utkin and A. S. Poznyak, "Adaptive sliding mode control with application to super-twist algorithm: equivalent control method," *Automatica*, vol. 49, no. 1, pp. 39–47, 2013.

[393] Y. Shtessel, C. Edwards, L. Fridman, and A. Levant, *Sliding Mode Control and Observation*, Birkhåuser, New York, NY, USA, 2014.

[394] P. Flandrin, "Wavelet analysis and synthesis of fractional Brownian motion," *IEEE Transactions on Information Theory*, vol. 38, no. 2, pp. 910–917, 1992.

[395] B. B. Mandelbrot and J. W. Van Ness, "Fractional Brownian motions, fractional noises and applications," *SIAM Review*, vol. 10, no. 2, pp. 422–437, 1968.

[396] B. B. Mandelbrot, "Broken line process derived as an approximation to fractional noise," *Water Resources Research*, vol. 8, no. 5, pp. 1354–1356, 1972.

[397] J. Humphrey, C. A. Schuler, and B. Rubinsky, "On the use of the Weierstrass-Mandelbrot function to describe the fractal component of turbulent velocity," *Fluid Dynamics Research*, vol. 9, no. 1–3, pp. 81–95, 1992.

[398] B. Ross, S. Samko, and E. Love, "Functions that have no first order derivative might have fractional derivatives of all order less than one," *Real Analysis Exchange*, vol. 20, no. 2, pp. 140–157, 1994.

[399] A. J. Muñoz-Vázquez, V. Parra-Vega, and A. Sánchez-Orta, "Continuous fractional-order sliding PI control for nonlinear systems subject to non-differentiable disturbances," *Asian Journal of Control*, vol. 19, no. 1, pp. 279–288, 2017.

[400] C. A. Monje, Y. Q. Chen, B. M. Vinagre, D. Xue, and V. Feliu-Batlle, *Fractional-Order Systems and Controls: Fundamentals and Applications*, Springer Science & Business Media, Berlin, Germany, 2010.

[401] P. Shah and S. Agashe, "Review of fractional PID controller," *Mechatronics*, vol. 38, pp. 29–41, 2016.

[402] B. M. Vinagre, I. Podlubny, L. Dorcak, and V. Feliu, "On fractional PID controllers: a frequency domain approach," *IFAC Proceedings Volumes*, vol. 33, no. 4, pp. 51–56, 2000.

[403] D. Valério and J. S. da Costa, "Tuning of fractional PID controllers with Ziegler-Nichols-type rules," *Signal Processing*, vol. 86, no. 10, pp. 2771–2784, 2006.

[404] D. Valério and J. S. da Costa, "Tuning-rules for fractional PID controllers," in *Proceedings of the Second IFAC Symposium on Fractional Differentiation and its Applications (FDA06)*, Porto, Portugal, July 2006.

[405] B. M. Vinagre, C. A. Monje, A. J. Calderón, and J. I. Suárez, "Fractional PID controllers for industry application: a brief introduction," *Journal of Vibration and Control*, vol. 13, no. 9-10, pp. 1419–1429, 2007.

[406] L. Liu, F. Pan, and D. Xue, "Variable-order fuzzy fractional PID controller," *ISA Transactions*, vol. 55, pp. 227–233, 2015.

[407] C. Hwang and Y.-C. Cheng, "A note on the use of the lambert w function in the stability analysis of time-delay systems," *Automatica*, vol. 41, no. 11, pp. 1979–1985, 2005.

[408] C. Hwang and Y.-C. Cheng, "A numerical algorithm for stability testing of fractional delay systems," *Automatica*, vol. 42, no. 5, pp. 825–831, 2006.

[409] A. R. Fioravanti, C. Bonnet, H. Özbay, and S.-I. Niculescu, "A numerical method for stability windows and unstable root-locus calculation for linear fractional time-delay systems," *Automatica*, vol. 48, no. 11, pp. 2824–2830, 2012.

[410] C. Bonnet and J. R. Partington, "Coprime factorizations and stability of fractional differential systems," *Systems & Control Letters*, vol. 41, no. 3, pp. 167–174, 2000.

[411] C. Bonnet and J. R. Partington, "Analysis of fractional delay systems of retarded and neutral type," *Automatica*, vol. 38, no. 7, pp. 1133–1138, 2002.

[412] J. R. Partington and C. Bonnet, "H_∞ and BIBO stabilization of delay systems of neutral type," *Systems & Control Letters*, vol. 52, no. 3-4, pp. 283–288, 2004.

[413] C. Bonnet and J. R. Partington, "Stabilization of some fractional delay systems of neutral type," *Automatica*, vol. 43, no. 12, pp. 2047–2053, 2007.

[414] C. Bonnet, A. R. Fioravanti, and J. R. Partington, "Stability of neutral systems with commensurate delays and poles

asymptotic to the imaginary axis," *SIAM Journal on Control and Optimization*, vol. 49, no. 2, pp. 498–516, 2011.

[415] C. Bonnet, "Stabilization of MISO fractional systems with delays," *Automatica*, vol. 83, pp. 337–344, 2017.

[416] D. Avanessoff, A. R. Fioravanti, and C. Bonnet, "YALTA: a Matlab toolbox for the H_{∞}-stability analysis of classical and fractional systems with commensurate delays," *IFAC Proceedings Volumes*, vol. 46, no. 2, pp. 839–844, 2013.

[417] B. Dumitru, A. Ranjbar, S. J. Sadati, R. H. Delavari, and T. Abdeljawad, "Lyapunov-Krasovskii stability theorem for fractional systems with delay," *Romanian Journal of Physics*, vol. 56, no. 5-6, pp. 636–643, 2011.

[418] J.-B. Hu, G.-P. Lu, S.-B. Zhang, and L.-D. Zhao, "Lyapunov stability theorem about fractional system without and with delay," *Communications in Nonlinear Science and Numerical Simulation*, vol. 20, no. 3, pp. 905–913, 2015.

[419] W. Deng, C. Li, and J. Lü, "Stability analysis of linear fractional differential system with multiple time delays," *Nonlinear Dynamics*, vol. 48, no. 4, pp. 409–416, 2007.

[420] L. Chen, R. Wu, J. Cao, and J.-B. Liu, "Stability and synchronization of memristor-based fractional-order delayed neural networks," *Neural Networks*, vol. 71, pp. 37–44, 2015.

[421] H. Wang, Y. Yu, and G. Wen, "Stability analysis of fractional-order Hopfield neural networks with time delays," *Neural Networks*, vol. 55, pp. 98–109, 2014.

[422] H. Wang, Y. Yu, G. Wen, S. Zhang, and J. Yu, "Global stability analysis of fractional-order Hopfield neural networks with time delay," *Neurocomputing*, vol. 154, pp. 15–23, 2015.

[423] G. Velmurugan, R. Rakkiyappan, and J. Cao, "Finite-time synchronization of fractional-order memristor-based neural networks with time delays," *Neural Networks*, vol. 73, pp. 36–46, 2016.

[424] S. Tyagi, S. Abbas, and M. Hafayed, "Global mittag–leffler stability of complex valued fractional-order neural network with discrete and distributed delays," *Rendiconti del Circolo Matematico di Palermo Series 2*, vol. 65, no. 3, pp. 485–505, 2016.

[425] V. Feliu-Batlle, R. Rivas Pérez, F. J. Castillo García, and L. Sanchez Rodriguez, "Smith predictor based robust fractional order control: application to water distribution in a main irrigation canal pool," *Journal of Process Control*, vol. 19, no. 3, pp. 506–519, 2009.

[426] V. Feliu-Batlle, R. Rivas-Perez, and F. J. Castillo-Garcia, "Fractional order controller robust to time delay variations for water distribution in an irrigation main canal pool," *Computers and Electronics in Agriculture*, vol. 69, no. 2, pp. 185–197, 2009.

[427] V. Feliu-Batlle, R. Rivas-Perez, and F. J. Castillo-García, "Simple fractional order controller combined with a smith predictor for temperature control in a steel slab reheating furnace," *International Journal of Control, Automation and Systems*, vol. 11, no. 3, pp. 533–544, 2013.

[428] T. N. Luan Vu and M. Lee, "Smith predictor based fractional-order PI control for time-delay processes," *Korean Journal of Chemical Engineering*, vol. 31, no. 8, pp. 1321–1329, 2014.

[429] D. Boudjehem, M. Sedraoui, and B. Boudjehem, "A fractional model for robust fractional order Smith predictor," *Nonlinear Dynamics*, vol. 73, no. 3, pp. 1557–1563, 2013.

[430] C. I. Pop, C. Ionescu, R. De Keyser, and E. H. Dulf, "Robustness evaluation of fractional order control for varying time delay processes," *Signal, Image and Video Processing*, vol. 6, no. 3, pp. 453–461, 2012.

[431] P. Lanusse and A. Oustaloup, "Control of time-delay systems using robust fractional-order control and robust Smith predictor based control," in *Proceedings of the ASME 2005 International Design Engineering Technical Conferences and Computers and Information in Engineering Conference*, pp. 1475–1483, Long Beach, CA, USA, 2005.

[432] N. Maamri, M. Tenoutit, and J.-C. Trigeassou, "A comparison of fractional Smith predictors," in *Proceedings of the 2013 European Control Conference (ECC)*, pp. 3991–3996, Zurich, Switzerland, July 2013.

Hindawi
Complexity
Volume 2020, Article ID 9207650, 11 pages
https://doi.org/10.1155/2020/9207650

Research Article

Using Interval Operations in the Hungarian Method to Solve the Fuzzy Assignment Problem and Its Application in the Rehabilitation Problem of Valuable Buildings in Egypt

M. A. Elsisy, A. S. Elsaadany, and M. A. El Sayed

Benha Faculty of Engineering, Benha University, Benha, El Qalyoubia, Egypt

Correspondence should be addressed to M. A. Elsisy; mohamedelsisy2@gmail.com

Received 21 May 2020; Revised 23 August 2020; Accepted 29 August 2020; Published 14 September 2020

Academic Editor: Baltazar Aguirre Hernandez

Copyright © 2020 M. A. Elsisy et al. This is an open access article distributed under the Creative Commons Attribution License, which permits unrestricted use, distribution, and reproduction in any medium, provided the original work is properly cited.

Assignment problem (AP) is an entrenched tool for solving engineering and management problems. The Hungarian method is always used to fathom the AP in crisp cases. This paper presents an algorithm of finding the optimum solution of the fuzzy AP by using the modified Hungarian method. This method is utilized to get a minimum assignment cost in the fuzzy environment for a fuzzy AP. Firstly, we use the fuzzy numbers without any transformation. Secondly, the fuzzy AP is transformed into an interval AP based on the α-cut methodology. Then, the interval arithmetic operations and the order relations are applied to get the optimal solution by utilizing the modified Hungarian method. The proposed algorithm requires less efforts and time to reach optimality, compared to the existing methods. Numerical examples are given to ensure the efficiency and the validity of the proposed algorithm. A study on the reuse of many valuable buildings is presented after using different government and service buildings in a manner that does not fit with its original function and heritage value. We offer a solution based on the scientific and realistic basis for requalification according to the variables and requirements of the social, cultural, and economic environments in the environment surrounding the valuable buildings.

1. Introduction

The assignment problem (AP) is a very much evolved advancement issue in engineering and management sciences and has been broadly applied in both assembling and administration frameworks [1, 2]. In an AP, n jobs are to be performed by n people contingent upon their proficiency to carry out the job. The AP is used to determine the issue of appointing several origins to the equal number of destinations at the very least expense or most extreme benefit in the most ideal manner. It can appoint people to employments, classes to rooms, administrators to machines, drivers to trucks, trucks to conveyance courses, or issues to investigate groups, and so forth.

To deal with the AP, the decision parameters of the model must be fixed at deterministic values. In any case, to show real issues and to perform estimations, we ought to manage vulnerability and vagary. These vulnerability and vagary are a result of estimation botch, unraveling of physical models, assortments of the boundaries of the system, computational bungles, etc. Along these lines, we cannot viably use traditional old-style task issues, and from this time forward, the usage of fuzzy undertaking issues is progressively legitimate [3–8].

Several algorithms have been exhibited to solve APs, such as linear programming [1, 9, 10], Hungarian algorithm [11, 12], and particle swarm optimization [9]. Kar et al. resolved an AP with fuzzy cost by Yager's ranking index which transforms the fuzzy AP into a crisp one [7]. Different membership functions and the Yager ranking index for solving fuzzy APs and fuzzy travelling salesman problems were introduced by Kumar and Gupta [13]. Tapkan et al. considered a multiobjective generalized AP directly via bee's algorithm and fuzzy ranking [10]. Emrouznejad set up an algorithm using the data envelopment analysis method to solve the APs with fuzzy costs or fuzzy profits [3]. A new

method for solving fuzzy assignment problems was given by Pandian and Kavitha [14]. Thorani and Shankar explained in detail the application in the fuzzy AP [15]. Mary and Selvi proposed a model to solve the fuzzy AP using the centroid ranking method [16]. In [17], Traneva and Tranev presented the interval-valued intuitionistic fuzzy AP, in which the costs of assigning jobs to candidates are interval-valued intuitionistic fuzzy, depending on the experience, the education, and the professionalism of the applicants.

A basis in modeling uncertain systems is that an entangled model is not generally important to manage incomplete information and inaccurate data [18]. Interval numbers are a structure which helps to stay away from such an unnecessary complexity. Moore originally introduced interval numbers [19]. An interval number is a number whose exact value is unknown, but a range within which the value lies is known [20]. An interval number permits an expert to make his/her approximations about boundaries on a span as opposed to a crisp number. This adaptability caused interval numbers to have extraordinary applications in optimization issues. The literature studies on the applications of interval number in decision-making problems are so wide [21–23].

In most of the real-world problems, the parameters such as cost, time, and profit may not be precisely known in advance due to several uncontrollable factors such as human judgements and market fluctuations. In such situations, considering the values of uncertain parameters as fuzzy numbers or interval numbers is better than to approximate them as crisp values [21–25]. This led us to introduce the fuzzy AP that we transform into an interval AP.

The urban design and the architectural character represent an expressive characteristic of the prevailing culture in the society for the civilized value; the civilized value in architecture and urbanism reaches its highest levels when it is related to cultural connotations and concepts, so the negligence or neglect of civilizational heritage that enriches architecture and urbanism is only a lack of national awareness of civilized values wasting national wealth and retreating to the cultural dimension of the society [26–31]. As a result of accelerated urban development which is not indifferent to civilizational and heritage values during the second half of the twentieth century in Egypt, many distinguished buildings began to disappear to be replaced by other buildings that do not rise to the same architectural value, for example, the use of many valuable buildings as various government and service buildings in a manner that is not commensurate with their original function and heritage value, which led to deformation and visual pollution that has become a phenomenon in many Egyptian cities. We use some valuable buildings in the Arab Republic of Egypt as a comparative study. Their value is defined as being one of the philosophical concepts that can be described as "the criterion governing the degree to which a person accepts what is around him according to his desires and needs." This is because the value is a relative influence that depends on the nature of the recipient and the constituent conditions of his personality and on the temporal and spatial conditions. Also, most forms of the value are not acquired by the building during its design but rather over time [26–31]. The goal of reuse is to preserve historical buildings that are considered national wealth and part of the national economy, creating positive change in the population through contact with visitors, learning about new habits and lifestyles, and cultural exchange; however, the presence of some tourist establishments in areas of a somewhat conservative social nature does not contradict customs and traditions. It is preferable to reuse valuable buildings with an activity similar to the original activity for which the building was established as possible or by studying the needs of the surrounding environment and adapting the new activity according to the requirements of the surrounding environment.

In this article, the modified Hungarian method is introduced to solve the fuzzy AP. In our proposed model, due to several uncontrollable factors such as human judgements and market fluctuations, the cost is considered as a fuzzy number. The primary objective of this study is to propose a new method for solving the AP under an uncertain situation. Firstly, the fuzzy numbers are used without any transformation. Secondly, the fuzzy AP is transformed into an interval AP based on the α-cut methodology. Then, the interval arithmetic operations are applied to obtain the optimal solution by utilizing the modified Hungarian method. Also, the reuse and employment of the valuable buildings in Egypt are studied. It is used to clarify the impact on neighboring urban entities, which may help to find an economic basis on which to maintain those buildings to enter within the organic entity of the old city.

The composition of the article is organized as follows: preliminaries and notions of the fuzzy and interval numbers are reviewed in Section 2. Section 3 presents the mathematical formulation of the fuzzy AP. Section 4 provides the procedures for the modified Hungarian method. Also, numerical examples are presented in Section 4. In Section 5, we study the reuse and employment of the valuable buildings in Egypt. Finally, the conclusion is given in Section 6.

2. Preliminaries and Notions

In this section, some essential ideas and preparatory outcomes utilized as a part of this paper are quickly presented.

Definition 1 (fuzzy numbers). Let R^1 be the set of all real numbers. Then, a real fuzzy number $\tilde{a}$ is defined by its membership function $\mu_{\tilde{a}}(x)$ that satisfies [4, 32, 33]

(1) A continuous mapping from R^1 to the closed internal $[0, 1]$

(2) $\mu_{\tilde{a}}(x) = 0$ for all $x \in (-\infty, a]$

(3) Strictly increasing and continuous on $[a, b]$

(4) $\mu_{\tilde{a}}(x) = 1$ for all $x \in [b, c]$

(5) Strictly decreasing and continuous on $[c, d]$

(6) $\mu_{\tilde{a}}(x) = 0$ for all $x \in [d, +\infty)$ [8]

Definition 2 (triangular fuzzy number). $\tilde{a} = (a_0, b, c)$ is a triangular fuzzy number, where a_0 is the smallest value, b is the main value, and c is the highest value. The membership function $\mu_{\tilde{a}}(a; \vartheta), \vartheta \in [0,1]\,(0 \le \mu_{\tilde{a}}(a;\vartheta) \le \delta)$, where ϑ is the maximum value and $a = b$. Then [4, 32, 33],

$$\mu_{\tilde{a}}(a;\vartheta) = \begin{cases} 0, & \text{if } a < a_0, \text{ or } a > c, \\ \dfrac{(a-a_0)\vartheta}{b-a_0}, & \text{if } a_0 \le a \le b, \\ \dfrac{(c-a)\vartheta}{c-b}, & \text{if } b \le a \le c. \end{cases} \tag{1}$$

Definition 3 (the level set). The α-level set of the fuzzy number $\tilde{a}$ is defined as an ordinary set $L_\alpha(\tilde{a})$ for which the degree of its membership function exceeds the level set $\alpha \in [0,1]$, where [6, 32, 33]

$$L_\alpha(\tilde{a}) = \left\{a \in R^m \,\middle|\, \mu_{\tilde{a}}(x) \ge \alpha\right\} = \left\{a \in \left[\tilde{a}_\alpha^L, a_\alpha^U\right] \,\middle|\, \mu_{\tilde{a}}(x) \ge \alpha,\right\}, \tag{2}$$

where $\tilde{a}_\alpha^L = (1-\alpha)a_0 + \alpha b$, $\tilde{a}_\alpha^U = (1-\alpha)c + \alpha b$, and $\tilde{a}_\alpha^L$ and $\tilde{a}_\alpha^U$ represent the lower and upper cuts, respectively, as shown in Figure 1.

Definition 4 (interval numbers). An interval number is a number whose exact value is unknown, but a range within which the value lies is known [20]. Interval number is a number with both lower and upper bounds, $A = [a_L, a_R]$, where $a_L \le a_R$. The interval is also denoted by its center and width as

$$A = a_C, a_W = \{a:\ a_C - a_W \le a \le a_C + a_W, \quad a \in R\}, \tag{3}$$

where $a_C = (a_L + a_R)/2$ and $a_W = (a_R - a_L)/2$ are, respectively, the center and half width of A [20, 21, 23].

The main arithmetic operations can be defined on interval numbers. Let $A = [a_L, a_R] = \{a:\ a_L \le a \le a_R,\ a \in R\}$ and $B = [b_L, b_R] = \{b:\ b_L \le b \le b_R,\ b \in R\}$.

$$\begin{aligned} A + B &= [a_L, a_R] + [b_L, b_R] = [a_L + b_L, a_R + b_R], \\ A - B &= [a_L, a_R] - [b_L, b_R] = [a_L - b_R, a_R - b_L], \\ A \times B &= [\min(a_L b_L,\ a_L b_R,\ a_R b_L,\ a_R b_R), \\ &\qquad \max((a_L b_L,\ a_L b_R,\ a_R b_L,\ a_R b_R))], \\ A \div B &= [a_L, a_R] \times \left[\frac{1}{b_R}, \frac{1}{b_L}\right], \\ kA = k[a_L, a_R] &= \begin{cases} [ka_L, ka_R] & \text{if } k \ge 0, \\ [ka_R, ka_L] & \text{if } k < 0. \end{cases} \end{aligned} \tag{4}$$

Definition 5. The order relation $\le_{LR}$ between $A = [a_L, a_R]$ and $B = [b_L, b_R]$ is defined as [21, 23]

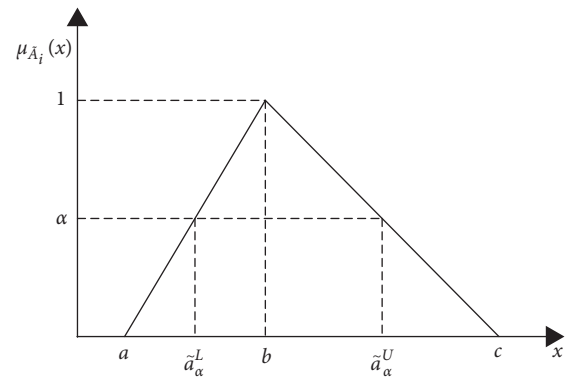

Figure 1: α-Cut of the triangular fuzzy number.

$$\begin{aligned} A \le_{LR} B &\quad \text{iff } a_L \le b_L \text{ and } a_R \le b_R, \\ A <_{LR} B &\quad \text{iff } A \le_{LR} B \text{ and } A \ne B. \end{aligned} \tag{5}$$

This order relation $\le_{LR}$ represents the decision maker's preference for the alternative with lower minimum cost and maximum cost, that is, if $A \le_{LR} B$, then A is preferred to B.

Definition 6. The order relation $\le_{CW}$ between $A = a_C, a_W$ and $B = b_C, b_W$ is defined as [20, 21]

$$\begin{aligned} A \le_{CW} B &\quad \text{iff } a_C \le b_C \text{ and } a_W \le b_W, \\ A <_{CW} B &\quad \text{iff } A \le_{CW} B \text{ and } A \ne B. \end{aligned} \tag{6}$$

This order relation $\le_{CW}$ represents the decision maker's preference for the alternative with lower minimum cost and maximum cost, that is, if $A \le_{CW} B$, then A is preferred to B.

We use the sum of all elements of the interval/fuzzy number as a scale to compare between intervals/fuzzy numbers. Zero interval/zero fuzzy number is the sum of all elements of the interval/fuzzy number which is equal to zero.

3. Fuzzy Assignment Problem

In a general AP, "n" works are to be performed by "n" people depending on their efficiency to do the job in one-one basis such that the assignment cost is minimum or maximum [24, 34]. If the objective of an AP is to minimize fuzzy cost $\tilde{c}_{ij}$, then we provide the AP of $n \times n$ matrix each cell having a fuzzy number in Table 1.

Firstly, we transform the fuzzy cost $\tilde{c}_{ij}$ into the interval cost $(\tilde{c}_{ij})_\alpha = [(\tilde{c}_{ij})_\alpha^L, (\tilde{c}_{ij})_\alpha^U]$ by utilizing the α-cut methodology. Thus, the fuzzy AP can be transformed into an interval AP with interval cost as shown in Table 2.

The above formulation of the problem is used in finding the optimal assignment when the values of parameters such as cost, time, and profit are precisely known in advance. However, in most of the realistic situations, the parameters such as cost, time, and profit may not be precisely known in advance due to several uncontrollable factors such as human judgements and market fluctuations. In such situations, considering the values of uncertain parameters as fuzzy numbers or interval numbers is better than to approximate

Table 1: Fuzzy assignment problem.

		Works						
				1	...	j	...	n
People	1	$\widetilde{c}_{11}$	...	...	...	$\widetilde{c}_{1n}$		
	...	...	...	...	...	...		
	i	...	...	$\widetilde{c}_{ij}$	...	...		
	...	...	...	...	...	...		
	n	$\widetilde{c}_{n1}$	...	...	...	$\widetilde{c}_{nn}$		

Table 2: Interval assignment problem.

		Works						
				1	...	j	...	n
People	1	$[(\widetilde{c}_{11})_\alpha^L, (\widetilde{c}_{11})_\alpha^U]$	...	...	...	$[(\widetilde{c}_{1n})_\alpha^L, (\widetilde{c}_{1n})_\alpha^U]$		
	...	...	...	...	...	...		
	i	...	...	$[(\widetilde{c}_{ij})_\alpha^L, (\widetilde{c}_{ij})_\alpha^U]$	...	...		
	...	...	...	...	...	...		
	n	$[(\widetilde{c}_{n1})_\alpha^L, (\widetilde{c}_{n1})_\alpha^U]$	...	...	...	$[(\widetilde{c}_{nn})_\alpha^L, (\widetilde{c}_{nn})_\alpha^U]$		

them as crisp values. Mathematically, the fuzzy AP can be stated as [5, 7, 35]

$$\begin{aligned} \min \quad & \widetilde{Z} = \sum_{i=1}^{n}\sum_{j=1}^{n} \widetilde{c}_{ij} x_{ij} \\ \text{subject to} \quad & \sum_{i=1}^{n} x_{ij} = 1, \quad j = 1, 2, \ldots, n \\ & \sum_{j=1}^{n} x_{ij} = 1, \quad i = 1, 2, \ldots, n, \\ x_{ij} = 0 \text{ or } 1, & \\ \text{for all } x_{ij} = & \begin{cases} 1, & \text{if } i^{\text{th}} \text{ person is assigned to } j^{\text{th}} \text{ work,} \\ 0, & \text{otherwise,} \end{cases} \end{aligned} \tag{7}$$

where $\widetilde{Z}$ denotes the fuzzy cost function, $\sum_{i=1}^{n} x_{ij} = 1$ (one work is done by the i^{th} person, $i = 1, 2 \ldots, n$), and $\sum_{j=1}^{n} x_{ij} = 1$ (only one person must be assigned to j^{th} work, $j = 1, 2 \ldots, n$), where x_{ij} denotes that j^{th} work is to be assigned to the i^{th} person. After applying the α-cut methodology to the fuzzy AP, the following interval AP is obtained:

$$\begin{aligned} \min \quad & Z = \sum_{i=1}^{n}\sum_{j=1}^{n} \left[\left(\widetilde{c}_{ij}\right)_\alpha^L, \left(\widetilde{c}_{ij}\right)_\alpha^U \right] x_{ij} \\ \text{subject to} \quad & \sum_{i=1}^{n} x_{ij} = 1, \quad j = 1, 2, \ldots, n \\ & \sum_{j=1}^{n} x_{ij} = 1, \quad i = 1, 2, \ldots, n, \\ x_{ij} = 0 \text{ or } 1, & \\ \text{for all } x_{ij} = & \begin{cases} 1, & \text{if } i^{\text{th}} \text{ person is assigned to } j^{\text{th}} \text{ work,} \\ 0, & \text{otherwise,} \end{cases} \end{aligned} \tag{8}$$

where $(\widetilde{c}_{ij})_\alpha^L$ and $(\widetilde{c}_{ij})_\alpha^U$ are the lower and upper cuts of the fuzzy cost. In this study, we solve both fuzzy APs by converting them into the interval AP by using the modified Hungarian method. Making best use of the interval arithmetic operations and order relations, the modified Hungarian method solves the interval AP.

4. The Proposed Algorithm

The Hungarian method solves the minimization APs with n workers and n jobs. It has been presented in [11, 12, 25]. So, in this section, we explain how the modified Hungarian method deals with the fuzzy AP by using the fuzzy number without transforming or converting it into interval APs. We apply the α-cut method to obtain the interval AP and use the interval arithmetic operations and the order relations to solve it. The modified Hungarian algorithm consists of the following four steps. The first two steps are executed once, while Steps 3 and 4 are repeated until an optimal assignment is found. The input of the algorithm is an $n \times n$ square matrix with only nonnegative elements. If the number of lines equals the number of rows (and columns), the test for the optimality is satisfied [17].

Step 1. Subtract row minima:

For each row, find the lowest interval and subtract it from each interval in that row based on interval arithmetic operations.

Step 2. Subtract column minima:

Similarly, for each column, find the lowest interval and subtract it from each interval in that column using interval arithmetic operations.

Step 3. Cover all zeros with a minimum number of lines:

Cover all zero or negative intervals in the resulting matrix using the minimum number of horizontal and vertical lines. If n lines are required, an optimal assignment exists among the zeros or negative interval. The algorithm

stops (an assignment can be made). If less than n lines are required, continue with Step 4.

Step 4. Create additional zeros:

Determine the minimum uncovered interval (call it H):

Subtract H from uncovered intervals.

(a) Add H to intervals covered by two lines

(b) Intervals covered by one line remain the same

(c) Then, go to Step 3

5. Numerical Examples

Example 1. Let us consider an AP with rows representing 4 people, A, B, C, and D, and columns representing 4 jobs, job I, job II, job III, and job IV. The cost matrix $[c_{ij}]$ is given whose elements are interval numbers. The problem is to find the optimal assignment so that the total cost of the job assignment becomes minimum, see Table 3.

The minimum interval is [1, 5] in column 1, [3, 7] in column 2, [1, 5] in column 3, and [0, 4] in column 4. By using interval arithmetic operations, we get Table 4.

The minimum interval is [−4, 4] in row 1, [−4, 4] in row 2, [−4, 4] in row 3, and [−2, 6] in row 4. By using interval arithmetic operations, we get Table 5.

The optimal assignment is $A \longrightarrow$ II, $B \longrightarrow$ IV, $C \longrightarrow$ III, and $D \longrightarrow$ I. Cost = $[3, 7] + [3, 7] + [1, 5] + [0, 5] = [7, 24]$.

Example 2 (see [25]). Let us consider a fuzzy AP with rows representing 4 people, A, B, C, and D, and columns representing 4 jobs, job I, job II, job III, and job IV. The fuzzy cost matrix $[\tilde{c}_{ij}]$ is given whose elements are triangular fuzzy numbers. The problem is to find the optimal assignment so that the total cost of the job assignment becomes minimum, shown in Table 6. This example is solved by the method found in [25], in which the fuzzy assignment problem has been transformed into a crisp assignment problem using Robust's ranking indices [5].

Firstly, we apply the modified Hungarian method to the fuzzy cost matrix utilizing the arithmetic operations of fuzzy numbers to get the optimal assignment, see Table 7.

The optimal assignment is $A \longrightarrow$ I, $B \longrightarrow$ III, $C \longrightarrow$ IV, and $D \longrightarrow$ II. The fuzzy optimal total cost = (5, 10, 15) + (5, 10, 15) + (5, 10, 15) + (5, 10, 15) = (20, 40, 60).

Secondly, we apply the α-cut methodology to obtain the interval cost matrix. Then, the modified Hungarian method is utilized with the help of the arithmetic operations of interval numbers to get the optimal assignment. We can transform the above problem elements into intervals at $\alpha = 0.5$, shown in Table 8.

We apply the proposed method on Table 8 to get Table 9 by using the arithmetic operations of the interval to get the optimal assignment.

The optimal assignment is $A \longrightarrow$ I, $B \longrightarrow$ III, $C \longrightarrow$ IV, and $D \longrightarrow$ II. We see the solution of the AP by our two methods is the same as the solution found in [25].

Table 3: Example 1.

	I	II	III	IV
A	[8, 12]	[3, 7]	[11, 15]	[13, 17]
B	[1, 5]	[7, 11]	[16, 20]	[0, 5]
C	[8, 12]	[5, 9]	[1, 5]	[0, 4]
D	[3, 7]	[9, 13]	[7, 11]	[5, 9]

Table 4: Subtraction of the minimum interval in each column.

	I	II	III	IV
A	[3, 11]	[−4, 4]	[6, 14]	[9, 17]
B	[−4, 4]	[0, 8]	[11, 19]	[−4, 4]
C	[3, 11]	[−2, 6]	[−4, 4]	[−4, 4]
D	[−2, 6]	[2, 10]	[2, 10]	[1, 5]

Table 5: Subtraction of the minimum interval in each row.

	I	II	III	IV
A	[−1, 15]	[−8, 8]	[2, 18]	[5, 21]
B	[−8, 8]	[−4, 12]	[7, 23]	[−8, 8]
C	[−1, 15]	[−6, 10]	[−8, 8]	[−8, 8]
D	[−8, 8]	[−4, 12]	[−4, 12]	[−5, 7]

Table 6: Example 2.

	I	II	III	IV
A	(5, 10, 15)	(5, 10, 20)	(5, 15, 20)	(5, 10, 15)
B	(5, 10, 20)	(5, 15, 20)	(5, 10, 15)	(10, 15, 20)
C	(5, 10, 20)	(10, 15, 20)	(10, 15, 20)	(5, 10, 15)
D	(10, 15, 25)	(5, 10, 15)	(10, 20, 30)	(10, 15, 25)

Table 7: Subtraction of the minimum interval in each column.

	I	II	III	IV
A	(−10, 0, 10)	(−10, 0, 15)	(−10, 5, 5)	(−10, 0, 10)
B	(−10, 0, 15)	(−10, 5, 15)	(−10, 0, 10)	(−5, 5, 15)
C	(−10, 0, 15)	(−5, 5, 15)	(−5, 5, 15)	(−10, 0, 10)
D	(−5, 5, 20)	(−10, 0, 10)	(−5, 10, 25)	(−5, 5, 20)

Table 8: Transformation of Table 6 at $\alpha = 0.5$.

	I	II	III	IV
A	[7.5, 12.5]	[7.5, 15]	[10, 17.5]	[7.5, 12.5]
B	[7.5, 15]	[10, 17.5]	[7.5, 12.5]	[12.5, 17.5]
C	[7.5, 15]	[12.5, 17.5]	[12.5, 17.5]	[7.5, 12.5]
D	[12.5, 20]	[7.5, 12.5]	[15, 20]	[12.5, 20]

Table 9: Subtraction of the minimum interval in each column.

	I	II	III	IV
A	[−5, 5]	[−5, 7.5]	[−2.5, 10]	[−5, 5]
B	[−5, 7.5]	[−2.5, 10]	[−5, 5]	[0, 10]
C	[−5, 7.5]	[0, 10]	[0, 10]	[−5, 5]
D	[0, 12.5]	[−5, 5]	[2.5, 17.5]	[0, 12.5]

Example 3 (see [4]). Let us consider a fuzzy AP with rows representing 4 people, A, B, C, and D, and columns representing 4 jobs, job I, job II, job III, and job IV. The fuzzy cost matrix $[\tilde{c}_{ij}]$ is given whose elements are trapezoidal fuzzy numbers. The problem is to find the optimal assignment so that the total fuzzy cost of the job assignment becomes minimum, shown in Table 10. This example is

Table 10: Example 3.

	I	II	III	IV
A	(3, 5, 6, 7)	(5, 8, 11, 12)	(9, 10, 11, 15)	(5, 8, 10, 11)
B	(7, 8, 10, 11)	(3, 5, 6, 7)	(6, 8, 10, 12)	(5, 8, 9, 10)
C	(2, 4, 5, 6)	(5, 7, 10, 11)	(8, 11, 13, 15)	(4, 6, 7, 10)
D	(6, 8, 10, 12)	(2, 5, 6, 7)	(5, 7, 10, 11)	(2, 4, 5, 7)

solved by the method found in [4]. In [4], the fuzzy AP was transformed into a crisp AP in the LPP form.

Firstly, we apply the modified Hungarian method to the fuzzy cost matrix utilizing the arithmetic operations of fuzzy numbers to get the optimal assignment, see Tables 11–13.

The optimal assignment is $A \longrightarrow$ III, $B \longrightarrow$ II, $C \longrightarrow$ I, and $D \longrightarrow$ IV. The fuzzy optimal total cost is calculated as $(2, 4, 5, 7) + (9, 10, 11, 15) + (2, 4, 5, 6) + (2, 4, 5, 7) = (16, 23, 27, 35)$.

Secondly, we apply the α-cut methodology to obtain the interval cost matrix. Then, the modified Hungarian method is utilized with the help of the arithmetic operations of interval numbers to get the optimal assignment. If the fuzzy number in the above problem transformed into interval at $\alpha = 0.5$, shown in Table 14.

We apply the proposed method on Table 14 to get Table 15 by using the arithmetic operations of the interval. Also, we get Tables 16 and 17.

The optimal assignment is $A \longrightarrow$ III, $B \longrightarrow$ II, $C \longrightarrow$ I, and $D \longrightarrow$ IV. We see the solution of the AP by our two methods is the same as the solution found in [25].

In the above examples, the fuzzy optimal total cost obtained by our two methods remains the same as that obtained by other methods.

6. Practical Application

In this section, we get acquainted with some basic definitions for the application study. First, a building of value (with a distinct architectural style) is defined as a building or facility that is distinguished by the historical, symbolic, architectural, artistic, urban, or social value. Also, it has been agreed that buildings and heritage installations of distinct architectural style should be characterized by accepting and positively interacting with the community, being expressive of material, moral, or intellectual phenomena in a specific period (social or cultural phenomenon). Its condition allows to be present and able to deal with it, and this is known as persistence and continuity. Heritage buildings are classified according to their condition into several levels, some of which are good, partially degraded, and totally degraded. The aim of this classification is to set priorities for dealing with heritage buildings as most important buildings are placed on top of the priorities of conservation plans [26–31]. A strategy for re-employment of valuable buildings is the creation of a job for the building other than the one for which it was established, and this employment may be accompanied by making some fundamental changes to the building to fit with the newly created job and an optional re-employment of buildings in the case of valuable buildings whose original function still exists until now. It is mandatory for buildings with the value of original extinct function such as ancient Egyptian temples and cemeteries. The methods of

Table 11: Subtraction of the minimum interval in each column.

	I	II	III	IV
A	(−4, −1, 1, 4)	(−2, 2, 6, 9)	(2, 4, 6, 12)	(−2, 2, 5, 8)
B	(0, 2, 5, 8)	(−4, −1, 1, 4)	(−1, 2, 5, 9)	(−2, 2, 4, 7)
C	(−4, −1, 1, 4)	(−1, 2, 6, 9)	(2, 6, 9, 13)	(−2, 1, 3, 8)
D	(−1, 3, 6, 10)	(−5, 0, 2, 5)	(−2, 2, 6, 9)	(−5, −1, 1, 5)

Table 12: Subtraction of the minimum interval in each row.

	I	II	III	IV
A	(−8, −2, 2, 8)	(−6, 1, 7, 13)	(−7, −2, 4, 14)	(−7, 1, 6, 13)
B	(−4, 1, 6, 12)	(−8, −2, 2, 8)	(−10, −4, 3, 11)	(−7, 1, 5, 12)
C	(−8, −2, 2, 8)	(−5, 1, 7, 13)	(−7, 0, 7, 15)	(−7, 0, 4, 13)
D	(−5, 2, 7, 14)	(−9, −1, 3, 9)	(−11, −4, 4, 11)	(−10, −2, 2, 10)

Table 13: Subtract (−7, −2, 4, 14) from uncovered intervals.

	I	II	III	IV
A	(−8, −2, 2, 8)	(−20, −3, 9, 20)	(−21, −6, 6, 21)	(−21, −3, 8, 20)
B	(−4, 1, 6, 12)	(−8, −2, 2, 8)	(−10, −4, 3, 11)	(−7, 1, 5, 12)
C	(−8, −2, 2, 8)	(−19, −3, 9, 20)	(−21, −4, 9, 22)	(−21, −4, 6, 20)
D	(−5, 2, 7, 14)	(−9, −1, 3, 9)	(−11, −4, 4, 11)	(−10, −2, 2, 10)

Table 14: Transformation of Table 10 at $\alpha = 0.5$.

	I	II	III	IV
A	[4, 6.5]	[6.5, 11.5]	[9.5, 13]	[6.5, 10.5]
B	[7.5, 10.5]	[4, 6.5]	[7, 11]	[6.5, 9.5]
C	[3, 5.5]	[6, 10.5]	[9.5, 14]	[5, 8.5]
D	[7, 11]	[3.5, 6.5]	[6, 10.5]	[3, 6]

Table 15: Subtraction of the minimum interval in each column.

	I	II	III	IV
A	[−2.5, 2.5]	[0, 7.5]	[3, 9]	[0, 6.5]
B	[1, 6.5]	[−2.5, 2.5]	[0.5, 7]	[0, 5.5]
C	[−2.5, 2.5]	[0.5, 7.5]	[4, 11]	[−0.5, 5.5]
D	[1, 8]	[−2.5, 3.5]	[0, 7.5]	[−3, 3]

Table 16: Subtraction of the minimum interval in each row.

	I	II	III	IV
A	[−5, 5]	[−2.5, 10]	[−4.5, 9]	[−3, 9.5]
B	[−1.5, 9]	[−5, 5]	[−7, 7]	[−3, 8.5]
C	[−5, 5]	[−2, 10]	[−3.5, 11]	[−3.5, 8.5]
D	[−1.5, 10.5]	[−5, 6]	[−7.5, 7.5]	[−6, 6]

Table 17: Subtract [−3.5, 8.5] from uncovered intervals.

	I	II	III	IV
A	[−5, 5]	[−11, 13.5]	[−13, 12.5]	[−11.5, 13]
B	[−5, 17.5]	[−5, 5]	[−7, 7]	[−3, 8.5]
C	[−5, 5]	[−10.5, 13.5]	[−12, 14.5]	[−12, 12]
D	[−5, 19]	[−5, 6]	[−7.5, 7.5]	[−6, 6]

rehabilitating the building are multiple such as modification in the formation of internal voids by deleting part of the building or by creating architectural elements and shapes to which each of these methods is added. The aim is to reach to provide the maximum possible space required for the new activity while giving freedom and flexibility to exploit existing surfaces, resizing the interior space of the building, taking into account the proportions between the elements, height, and scale, ensuring that the essence of the artistic content is not compromised.

The desired objectives of reuse and employment of valuable buildings are numerous, whether they relate to the archaeological building itself by preserving its heritage and architectural values or related to its surroundings and its urban environment or related to the social aspect. We will address in the research study the means of optimal reuse of the building in terms of social and the built environment. Therefore, there are several social and urban goals for reuse that are clear as follows.

Opening the building of value to the public makes it relevant to the surrounding environment and enables us to link the past to the present. The social goals are given as follows:

Developing the national awareness to preserve the monumental buildings as a cultural heritage that must be preserved

Achieving the national social affiliation through focusing on the symbolic value

Upgrading the general taste of individuals, especially children

Preserving the historical character of the city and reinforcing the sense of pride of the citizens

Finding interconnectedness and communication between the building and its users through the job the building performs for the surrounding community

Preserving historic buildings aims to protect them as artistic works and historical evidence. Therefore, it must be developed and transformed to perform new jobs that meet the renewable needs of the society and achieve urban and environmental goals through

Development of the community surrounding the archaeological building, which helps to preserve the distinctive urban character of the historic district

Reuse of historical buildings and areas within the framework of the reality of land use determined by the city's planning studies

Forming a merger and cohesion between the old and new urban fabric of the historical areas of the existing cities

Achieving the sustainability goals by providing the raw materials as one of the environmental goals for reuse, as the reuse of an existing building achieves

There is a problem in achieving a balance between preserving valuable buildings and society benefiting from them, especially according to previous experiences. So, we suggest that "in case the cultural job is preserved, it should be reformulated as part of a development plan that benefits the residents of the region." One of the global models for reemploying valuable buildings, including distinguished models such as converting the historic Presidio Hospital in San Francisco, USA, into a residential building that includes 154 apartments, is now a distinctive sign in the region; dining tables have been placed between pumps, and some equipment have been added without affecting the original design of the building.

6.1. Case Study. We present the practical application study of several valuable buildings of Egypt. We study many places from the community and the surrounding environment's viewpoint, and an economic view, such as the Khedive Abbas I Palace in the city of Benha, Arab Republic of Egypt. It was established in the nineteenth century AD and reused as a school; then, the activity was changed from an educational to an administrator and reused as an administrative building for Benha University, see Figure 2.

The Saffron Palace in Cairo was reused as an administrative building for Ain Shams University, see Figure 3.

Al-Jazzar Palace, Shibin El-Kom, was reused as an administrative building for Menoufia University, see Figure 4.

Al-Jazeera Palace was established by Khedive Ismail to receive guests at the opening of the Suez Canal in 1869 AD, and in 1879, the palace was sold to Egyptian Hotels Company to pay part of the debt of Khedive Ismail and was transferred to Al-Jazeera Palace Hotel. After the collapse of the tourist movement in Egypt during the First World War, the palace was sold in 1919 to one of the Lebanese princes, Prince Habib Lotfallah, who turned it into a private residence. In 1962, the palace was nationalized and converted again to a hotel in the name of Omar Khayyam Hotel. Then, in the early seventies, Marriott International took over the management of the hotel (Figure 5).

The questionnaire was distributed to the users of each building and the surrounding environment and a group of specialists to determine the extent of the reality of the new use of the building and its suitability for the surrounding community environment and its suitability for its artistic, symbolic, and architectural value. The questionnaire was carried out in two phases: the first stage at the level of specialists and the suitability of the building for the new activity in design, urban, and planning and the second phase of the questionnaire at the level of the surrounding environment and the users of the building after changing the activity. The questionnaire was divided into four phases of evaluation for each building activity (inappropriate, acceptable, appropriate, and very appropriate) which are shown in Table 18. The activity that received less than 50% of the votes is considered inappropriate, the activity that obtained between 50 and 60% of the votes is considered acceptable, the activity with a percentage ranging from 60 to 80% of the votes is considered appropriate, and the activity with more than 80% of the votes is a very appropriate activity, see Table 19. The graph indicates the extent of approval of the new activity of the building according to the view of the surrounding environment and users which is

Figure 2: Khedive Abbas I Palace.

Figure 3: Saffron Palace.

Figure 4: Al-Jazzar Palace.

Figure 5: Al-Jazeera Palace.

shown in Figure 6. The flowchart indicates the extent of approval of the new activity of the building according to the viewpoint of the specialists which is shown in Figure 7.

The proposed method was used to solve the application with the same steps explained before and applied in the illustrative examples. The results were continuously advising the

Table 18: Evaluation for each building activity.

	Administrative building		A hotel		A cultural building		In another activity	
	I	II	I	II	I	II	I	II
Khedive Abbas I Palace	Unsuitable	Acceptable	Suitable	Suitable	Acceptable	Unsuitable	Unsuitable	Suitable
Saffron Palace	Unsuitable	Unsuitable	Unsuitable	Unsuitable	Acceptable	Suitable	Acceptable	Suitable
Al-Jazzar Palace	Unsuitable	Unsuitable	Unsuitable	Acceptable	Suitable	Suitable	Acceptable	Acceptable
Al-Jazeera Palace	Unsuitable	Suitable	Very convenient	Very convenient	Unsuitable	Suitable	Acceptable	Suitable

Table 19: Comparison of the four palaces.

	Administrative	A hotel	A cultural	Another activity
Khedive Abbas I Palace	[3, 5.2]	6.5	[4, 5.5]	[2, 6.2]
Saffron Palace	[1, 2]	[1, 4]	[5.8, 6.2]	[5.4, 6.8]
Al-Jazzar Palace	[1, 2.5]	[1.8, 5.5]	6.3	5.3
Al-Jazeera Palace	[4, 6]	8.2	[4.3, 6.2]	[5, 6]

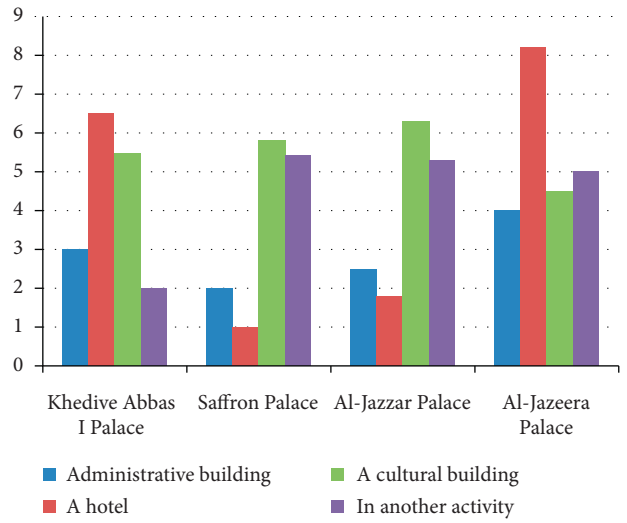

Figure 6: Graph indicating the extent of approval of the new activity of the building according to the view of the surrounding environment and users.

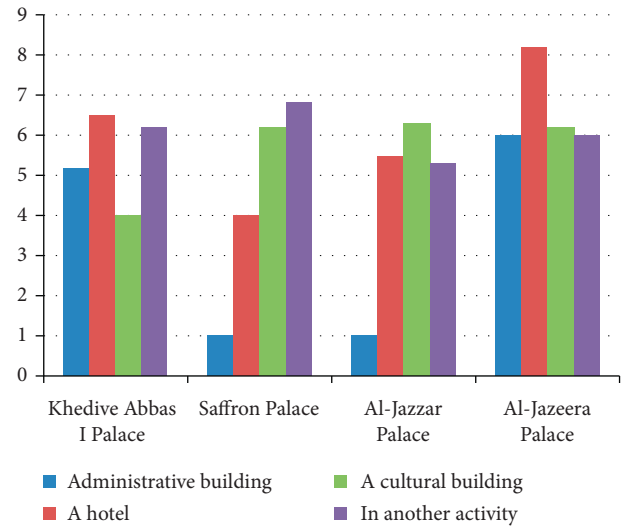

Figure 7: Flowchart indicating the extent of approval of the new activity of the building according to the viewpoint of the specialists.

use of the Khedive Abbas I Palace as an administrative building for Benha University and searching for a new use of the Saffron Palace and the use of Al-Jazzar Palace as a cultural building for Menoufia Governorate and the continuation of the Al-Jazeera Palace to be used as a hotel building. This is according to the view of the surrounding environment, dealers, and specialists.

The research study resulted in the success of some cases of reuse of valuable buildings through thinking out of the ordinary and finding unconventional solutions and the failure of some attempts through the deterioration of the construction status of the building and the general condition of the building. The principle of community participation must be adopted in developing plans for reuse operations so that local communities are involved in all stages of these operations and even make local communities' part of them. Also, valuable buildings should be reused with an activity similar to the original activity for which the building was established or by studying the needs of the surrounding environment and adapting the new activity according to the requirements of the surrounding environment.

7. Conclusions

In this paper, we introduce the modified Hungarian method for solving the interval and fuzzy AP. It is a novel and simple algorithm for solving the fuzzy and interval AP. We discussed finding a solution of an assignment problem in which cost coefficients are fuzzy numbers or intervals. The total optimal cost obtained by our method remains the same as that obtained by other researchers that convert the fuzzy cost into a crisp one by applying the ranking method. Also, we apply the modified Hungarian method in reuse of the valuable buildings in Egypt by making comparison between four valuable buildings that are reused in several activities for reaching the best benefit of building reuse, which should be matching with the basic purpose of the building and preserve on the value of the building. This method may be used in solving other types of optimization problems such as project schedules, transportation problems, and network flow problems.

Data Availability

All the data used to support the findings of this study are included within the article.

Conflicts of Interest

The authors declare that there are no conflicts of interest.

Authors' Contributions

M. A. Elsisy conceived the presented idea. M. A. Elsisy and M. A. El Sayed developed the theoretical framework and performed the numerical calculations. A.S. Elsaadany and M. A. Elsisy carried out the rehabilitation problem of valuable buildings in Egypt. M. A. Elsisy, A.S. Elsaadany, and M. A. El Sayed worked out almost all the technical details, performed the numerical calculations for the suggested application, and wrote the manuscript. All authors discussed the results, commented on the manuscript, and contributed to the final manuscript.

References

[1] C. Lin and U. Wen, "A labeling algorithm for the fuzzy assignment problem," *Fuzzy Sets and Systems*, vol. 142, no. 3, pp. 373–391, 2004.

[2] P. Malini and M. Ananthanarayanan, "Solving fuzzy assignment problem using ranking of generalized trapezoidal fuzzy numbers," *Indian Journal of Science and Technology*, vol. 9, no. 20, pp. 1–4, 2016.

[3] A. Emrouznejad, M. Zerafat Angiz L, and W. Ho, "An alternative formulation for the fuzzy assignment problem," *Journal of the Operational Research Society*, vol. 63, no. 1, pp. 59–63, 2012.

[4] A. N. Gani and V. N. Mohamed, "Solution of a fuzzy assignment problem by using a new ranking method," *International Journal of Fuzzy Mathematical Archive*, vol. 2, pp. 8–16, 2013.

[5] D. Gurukumaresan, C. Duraisamy, R. Srinivasan, and V. Vijayan, "Optimal solution of fuzzy assignment problem with centroid methods," *Materials Today: Proceedings*, 2020, in Press.

[6] S. Kar, K. Basu, and S. Mukherjee, "Solution of generalized fuzzy assignment problem with restriction on costs under fuzzy environment," *International Journal of Fuzzy Mathematics and Systems*, vol. 4, no. 2, pp. 169–180, 2014.

[7] S. Kar, K. Basu, and S. Mukherjee, "Generalized fuzzy assignment problem with restriction on the cost of job under hesitant fuzzy environment," *Opsearch*, vol. 52, no. 3, pp. 401–411, 2015.

[8] D. W. Pentico, "Assignment problems: a golden anniversary survey," *European Journal of Operational Research*, vol. 176, no. 2, pp. 774–793, 2007.

[9] H. Liu, A. Abraham, and M. Clerc, "A hybrid fuzzy variable neighborhood particle swarm optimization algorithm for solving quadratic assignment problems," *Journal of Universal Computer Science*, vol. 13, no. 9, pp. 1309–1331, 2007.

[10] P. Tapkan, L. Özbakır, and A. Baykasoğlu, "Solving fuzzy multiple objective generalized assignment problems directly via bees algorithm and fuzzy ranking," *Expert Systems with Applications*, vol. 40, no. 3, pp. 892–898, 2013.

[11] R. Jonker and T. Volgenant, "Improving the Hungarian assignment algorithm," *Operations Research Letters*, vol. 5, no. 4, pp. 171–185, 1986.

[12] H. W. Kuhn, "The Hungarian method for the assignment problem," *Naval Research Logistics Quarterly*, vol. 2, no. 1-2, pp. 83–97, 1955.

[13] A. Kumar and A. Gupta, "Methods for solving fuzzy assignment problems and fuzzy travelling salesman problems with different membership functions," *Fuzzy Information and Engineering*, vol. 3, no. 1, pp. 3–21, 2011, þ.

[14] P. Pandian and K. Kavitha, "A new method for solving fuzzy assignment problems," *Annals of Pure and Applied Mathematics*, vol. 1, no. 1, pp. 69–83, 2012.

[15] Y. L. P. Thorani and N. R. Shankar, "Application of fuzzy assignment problem," *Advances in Fuzzy Mathematics*, vol. 12, no. 4, pp. 911–939, 2017.

[16] R. Q. Mary and D. Selvi, *Solving Fuzzy Assignment Problem Using Centroid Ranking Method*, p. 55, IOP Publishing, Bristol, UK, 2018.

[17] V. Traneva and S. Tranev, "An interval-valued intuitionistic fuzzy approach to the assignment problem," in *International Conference on Intelligent and Fuzzy Systems*, pp. 1279–1287, Springer, Cham, Switzerland, 2019.

[18] S. Liu, K. Sheng, and J. Forrest, "On uncertain systems and uncertain models," *Kybernetes*, vol. 41, no. 5-6, pp. 548–558, 2012.

[19] R. E. Moore, *Interval Analysis*, Prentice-Hall, Englewood Cliffs, NJ, USA, 1996.

[20] R. E. Moore, R. B. Kearfott, and M. J. Cloud, *Introduction to Interval Analysis*, SIAM Press, Philadelphia, PA, USA, 2009.

[21] S. K. Das, A. Goswami, and S. S. Alam, "Multiobjective transportation problem with interval cost, source and destination parameters," *European Journal of Operational Research*, vol. 117, no. 1, pp. 100–112, 1999.

[22] S. H. R. Hajiagha, H. A. Mahdiraji, and S. S. Hashemi, "Multiobjective linear programming with interval coefficients," *Kybernetes*, vol. 42, no. 3, pp. 482–496, 2013.

[23] H. Lu, G. Huang, and L. He, "An inexact rough-interval fuzzy linear programming method for generating conjunctive water-allocation strategies to agricultural irrigation systems," *Applied Mathematical Modelling*, vol. 35, no. 9, pp. 4330–4340, 2011.

[24] N. Gupta, "Optimization of fuzzy bi-objective fractional assignment Problem," *Opsearch*, vol. 56, no. 3, pp. 1091–1102, 2019.

[25] R. Nagarajan and A. Solairaju, "Computing improved fuzzy optimal Hungarian assignment problems with fuzzy costs under robust ranking techniques," *International Journal of Computer Applications*, vol. 6, no. 4, p. 6, 2010.

[26] Al-Hathloul, *Tradition and Modernity in Architecture and Urbanism in the Islamic World, Symposium on Preserving Urban Heritage in the Emirates*, Dubai, UAE, 1995.

[27] A. D. Botton, *The Architecture of Happiness*, Vintage International, New York, NY, USA, 2008.

[28] D. Cruickshank, *Sir Banister Fletcher's A History of Architecture*, Princeton Architectural Press, New York, NY, USA, 20th edition, 1996.

[29] S. Elttony, *Urban Conservation of Older Housing Areas, Appropriating, the Process, IAHS, World Congress on Housing Trends Housing Projects*, Miami Florida, USA, 1986.

[30] P. Goldberger, *Why Architecture Matters*, Yale University Press, New Haven, CT, USA, 2009.

[31] T. C. James, "Life in the pharaohs, translated by ahmed zuhair amin," *Review: Mahmoud Maher Abdullah, General Book Authority*, 1997.

[32] S.-M. Chen, "Fuzzy system reliability analysis using fuzzy number arithmetic operations," *Fuzzy Sets and Systems*, vol. 64, no. 1, pp. 31–38, 1994.
[33] L. A. Zadeh, "Fuzzy sets," *Information and Control*, vol. 8, no. 3, pp. 338–353, 1965.
[34] P. S. Kumar and R. J. Hussain, "A method for finding an optimal solution of an assignment problem under mixed intuitionistic fuzzy environment," in *Proceedings in International Conference on Mathematical Sciences (ICMS-2014)*, Elsevier, Seoul, South Korea, pp. 417–421, August 2014.
[35] Y. L. P. Thorani and N. R. Shankar, "Fuzzy assignment problem with generalized fuzzy numbers," *Applied Mathematical Sciences*, vol. 7, pp. 3511–3537, 2013.

Hindawi
Complexity
Volume 2020, Article ID 2837916, 19 pages
https://doi.org/10.1155/2020/2837916

Research Article

Attitude Control with Auxiliary Structure Based on Adaptive Dynamic Programming for Reentry Vehicles

Xu Li, Zhongtao Cheng, Bo Wang, Yongji Wang, and Lei Liu

National Key Laboratory of Science and Technology on Multispectral Information Processing, School of Artificial Intelligence and Automation, Huazhong University of Science and Technology, Wuhan 430074, China

Correspondence should be addressed to Zhongtao Cheng; ztcheng@hust.edu.cn

Received 6 April 2020; Revised 8 August 2020; Accepted 19 August 2020; Published 2 September 2020

Academic Editor: Raúl Villafuerte-Segura

Copyright © 2020 Xu Li et al. This is an open access article distributed under the Creative Commons Attribution License, which permits unrestricted use, distribution, and reproduction in any medium, provided the original work is properly cited.

This paper presents an attitude control scheme combined with adaptive dynamic programming (ADP) for reentry vehicles with high nonlinearity and disturbances. Firstly, the nonlinear attitude dynamics is divided into inner and outer loops according to the time scale separation and the cascade control principle, and a general sliding mode control method is employed to construct the main controllers for the double loops. Considering the shortage of main controllers in handling nonlinearity and sudden disturbances, an ADP structure is introduced into the outer attitude loop as an auxiliary. And the ADP structure utilizes neural network estimators to minimize the cost function and generate optimal signals through online learning, so as to compensate defect of the main controllers' adaptability speed and accuracy. Then, the stability is analyzed by the Lyapunov method, and the parameter selection strategy of the ADP structure is derived to guide implementation. In addition, this paper puts forward skills to speed up ADP training. Finally, simulation results show that the control strategy with ADP possesses stronger adaptability and faster response than that without ADP for the nonlinear vehicle system.

1. Introduction

Attitude control for reentry vehicles has been a hotspot in the field of aerospace. The complex operating conditions and the high nonlinearity of vehicles themselves bring great challenges to attitude control. Fortunately, around these focuses, researchers continue to explore and ameliorate control schemes, developing a series of available control technologies.

For the control of space vehicles, some schemes have been investigated one after another. Some linear control methods, such as linear parameter varying (LPV) [1] and linear quadratic regulator (LQR), focus on linearizing the aircraft model. However, due to the highly nonlinear and coupling dynamic characteristics, to be honest, the capabilities of these linear control methods on actual nonlinear coupling vehicles are limited. Besides, some nonlinear control methods are widely employed, such as nonlinear dynamic inversion [2], sliding mode control, and backstepping method [3, 4]. Although these nonlinear control techniques can also effectively deal with the nonlinear nature of vehicles, they will still be slightly embarrassed and lack adaptability in the face of complex and changeable disturbances if without other auxiliary means. Therefore, in the recent development of vehicle control, more and more adaptive technologies have been favoured by researchers [5].

For the purpose of ameliorating the robustness of the controller by designing adaptive mechanism, observer-based adaptive control technology and other intelligent methods (as adaptive fuzzy control and iterative learning) have emerged one after another [6–8]. Especially, in recent years, thanks to the vigorous development of new artificial intelligence, reinforcement learning (RL) has attracted more and more attention, which has shown strong performance in solving adaptive and optimal control problems [9–11]. In the control domain, reinforcement learning is transformed into approximate or adaptive dynamic programming (ADP), which learns by interacting with the environment to determine what optimal actions to take to minimize a cost function over a period of time [12]. One of the core

approaches is the critic-action (CA) design, which approximates the cost function and obtains the optimal actions by solving the Hamilton–Jacobi–Bellman equation with function estimators [13]. ADP contains a variety of structural classifications, including heuristic [14], dual heuristic [15], and action-dependent dynamic programming (ADHDP), etc., which have been made preliminary explorations and achievements in the field of vehicle control [16]. Specifically, Luo et al. developed a direct heuristic dynamic programming (dHDP) for longitudinal control of hypersonic vehicles and introduced fuzzy neural networks to enhance the learning ability and robustness of dHDP [17]. There is also an application of ADDHP to study the optimal control of attitude maneuver for three-axis spacecraft [18]. Some creative researchers improve ADP by redefining the two optimization objectives and apply ADP to the in-orbit reconfiguration of the vehicle attitude system under multitask constraints through dual optimization indexes [19]. Moreover, ADP can be associated with traditional methods, such as nonlinear filter [20] and sliding mode control [21], to implement a data-driven ADHDP auxiliary control scheme for the speed and altitude system of an air-breathing hypersonic vehicle [21]. In [22], a switching adaptive active anti-interference control technique based on reduced-order observer technique and ADP is proposed, considering the parameter uncertainty and external disturbance of variable structure near-space vehicles. Furthermore, aiming at the guidance and control problem of the vertical take-off and landing (VTOL) system with multivariable disturbances, an online kernel DHP robust control strategy based on the sparse kernel theory is designed for VTOL vehicles [23]. Most of the above control strategies with ADP utilize neural network estimators to approximate the cost function and optimal control law online, while Zhou et al. creatively put forward an incremental ADP (iADP) combining the advantages of the incremental control method and ADP [24]. This iADP is based on Markov decision-making process and Bellman optimal principle to directly derive the explicit expression of optimal control law, greatly simplifying the design process of ADP, and successfully exploited to satellite [25] and aircraft [26]. Similarly, Sun and van Kampen also come up with an incremental model-based DHP technology for vehicle control, replacing the model network in traditional DHP with an incremental model [27, 28].

In a word, the development of ADP in the field of vehicle control is rapidly deepening and expanding [16], but as far as the current literature is concerned, ADP is still rarely applied to the control of all three channels' attitude angles of the vehicle. Moreover, most of the literature rarely mentions the internal weight convergence, parameter selection, training speed, and other issues of ADP based on critic-action networks, but these are problems to be concerned about. Therefore, this paper contributes to employ the ADP framework to the control of all three-channel attitude angles of a reentry vehicle. Inspired by the ADP as an auxiliary controller [21], this paper presents a framework combining conventional controller and ADP, and ADP is as the auxiliary means to enhance the rapidity and adaptivity of the whole attitude system. In addition, the internal convergence of the ADP structure and its parameter selection rules are discussed in depth. Aiming at the implementation problem, this paper considers the improvement measures to speed up ADP training, which will be provided to interested researchers for future discussion.

The rest of this paper is organized as follows. Firstly, the nonlinear dynamics of the three-channel attitude control system of the reentry vehicle is established in Section 2. Then, in Section 3, the control strategy based on the dual-loop main controller plus ADP is elaborated in detail. In Section 4, some issues about implementation are taken into consideration. Finally, the simulations and conclusions are presented in Sections 5 and 6, respectively.

2. Nonlinear Model

To describe the attitude change of the reentry phase, we give the rotation equations of the vehicle around the center of mass, including rotation dynamics and attitude kinematics. They determine the attitude angles of the vehicle around the center of mass and the angular rate of the three channels during the flight. Considering the influence of Earth rotation on attitude control, a three degree of freedom nonlinear attitude model in the body coordinate system can be obtained [29]:

$$\dot{\alpha} = -p\cos\alpha\tan\beta + q - r\sin\alpha\tan\beta + \left(\frac{\sin\mu}{\cos\beta}\right)\left(-\dot{\phi}\sin\chi\sin\vartheta + \dot{\chi}\cos\vartheta + \left(\dot{\theta} + \Omega_{\mathrm{E}}\right)(\cos\phi\cos\chi\sin\vartheta - \sin\phi\cos\vartheta)\right) - \left(\frac{\cos\mu}{\cos\beta}\right)\left(\dot{\vartheta} - \dot{\phi}\cos\chi - \left(\dot{\theta} + \Omega_{\mathrm{E}}\right)\cos\phi\sin\chi\right),$$

$$\dot{\beta} = p\sin\alpha - r\cos\alpha + \sin\mu\left(\dot{\vartheta} - \dot{\phi}\cos\chi + \left(\dot{\theta} + \Omega_{\mathrm{E}}\right)\cos\phi\sin\chi\right)$$

$$
\begin{aligned}
&+\cos\mu\left(\left(-\dot{\theta}+\Omega_{\mathrm{E}}\right)(\cos\phi\cos\chi\sin\vartheta-\sin\phi\cos\vartheta)+\dot{\chi}\cos\vartheta-\dot{\phi}\sin\chi\sin\vartheta\right),\\
\dot{\mu}&=-p\cos\alpha\cos\beta-q\sin\beta-r\sin\alpha\cos\beta+\dot{\alpha}\sin\beta\\
&\quad-\dot{\chi}\sin\vartheta-\dot{\phi}\sin\chi\cos\vartheta+\left(\dot{\theta}+\Omega_{\mathrm{E}}\right)(\sin\phi\sin\vartheta+\cos\phi\cos\chi\cos\vartheta),\\
\dot{p}&=\left(\frac{I_{=}M_x}{I_{xx}I_{zz}-I_{xz}^2}\right)+\left(\frac{I_{xz}M_z}{I_{xx}I_{zz}-I_{xz}^2}\right)+\left(\frac{\left(I_{xx}-I_{yy}+I_{zz}\right)I_{xz}}{I_{xx}I_z-I_{xz}^2}\right)pq+\left(\frac{\left(I_{yy}-I_{zz}\right)I_{zz}-I_{xz}^2}{I_{xx}I_{zz}-I_{xz}^2}\right)qr,\\
\dot{q}&=\left(\frac{M_y}{I_{yy}}\right)+\left(\frac{I_{xz}}{I_{yy}}\right)\left(r^2-p^2\right)+\left(\frac{I_{zz}-I_{xx}}{I_{yy}}\right)pr,\\
\dot{r}&=\left(\frac{I_{xz}M_x}{I_{xx}I_{zz}-I_{xz}^2}\right)+\left(\frac{I_{xx}M_z}{I_{xx}I_{zz}}\right)+\left(\frac{\left(I_{xx}-I_{yy}\right)I_{xx}-I_{xz}^2}{I_{xx}I_{zz}-I_{xz}^2}\right)pq+\left(\frac{\left(I_{yy}-I_{xx}-I_{zz}\right)I_{xz}}{I_{xx}I_{zz}-I_{xz}^2}\right)qr,
\end{aligned}
\tag{1}
$$

where α, β, and μ represent the angle of attack, sideslip, and bank angle, respectively; p, q, and r are the roll, pitch, and yaw rate, respectively. And M_x, M_y, and M_z denote the roll, pitch, and yaw control torques, respectively; $I_{ij}\,(i = x, y, z; j = x, y, z)$ is rotational inertia. ϕ, θ, χ, and ϑ are longitude, latitude, heading angle, and flight path angle, respectively; Ω_{E} is the Earth rotation angular velocity.

In actual control, vehicles can be regarded as an ideal rigid body. Considering that the rotation rate of the Earth is far less than that of vehicles, the rotation of the Earth is ignored. Besides, orbital motion is much slower than attitude motion, so the orbital motion terms of vehicles are described as $\dot{\phi} = \dot{\theta} = \dot{\vartheta} = \dot{\chi} = 0$. Finally, simplified dynamics can be obtained:

$$
\begin{aligned}
\dot{\alpha}&=-p\cos\alpha\tan\beta+q-r\sin\alpha\tan\beta,\\
\dot{\beta}&=p\sin\alpha-r\cos\alpha,\\
\dot{\mu}&=-p\cos\alpha\cos\beta-q\sin\beta-r\sin\alpha\cos\beta.
\end{aligned}
\tag{2}
$$

Above attitude kinematics equation (2) is abbreviated as

$$
\dot{\gamma}=\Gamma(\cdot)\omega, \tag{3}
$$

where $\gamma = [\alpha, \beta, \mu]^{\mathrm{T}} \in R^3$ and $\omega = [p, q, r]^{\mathrm{T}} \in R^3$. $\Gamma \in R^{3\times3}$ are defined as

$$
\Gamma=\begin{bmatrix}-\cos\alpha\tan\beta & 1 & -\sin\alpha\tan\beta\\ \sin\alpha & 0 & -\cos\alpha\\ -\cos\alpha\cos\beta & -\sin\beta & -\sin\alpha\cos\beta\end{bmatrix}. \tag{4}
$$

Similarly, rotational dynamics can be simplified as

$$
\dot{\omega}=-I^{-1}\Omega I\omega+I^{-1}M_c, \tag{5}
$$

where $I \in R^{3\times3}$ denotes inertial matrix; $M_c = [M_x, M_y, M_z]^{\mathrm{T}} \in R^3$ is a vector of control torques. $\Omega \in R^{3\times3}$ and $I \in R^{3\times3}$ are defined as

$$
\begin{aligned}
I&=\begin{bmatrix}I_{xx} & -I_{xy} & -I_{xz}\\ -I_{xy} & I_{yy} & -I_{yz}\\ -I_{xz} & -I_{yz} & I_{zz}\end{bmatrix},\\
\Omega&=\begin{bmatrix}0 & -r & q\\ r & 0 & -p\\ -q & p & 0\end{bmatrix}.
\end{aligned}
\tag{6}
$$

If there exist external disturbances, d_1 and d_2 are introduced into the vehicle system as follows:

$$
\begin{cases}\dot{\gamma}=\Gamma(\cdot)\omega+d_1,\\ \dot{\omega}=-I^{-1}\Omega I\omega+I^{-1}M_c+d_2,\end{cases} \tag{7}
$$

where $d_1 \in R^3$ and $d_2 \in R^3$ represent external disturbances.

Obviously, the attitude tracking control problem of the reentry vehicles can be described as

$$
\begin{aligned}
\lim_{t\longrightarrow\infty}\left\|\alpha-\alpha_d\right\|&=0,\\
\lim_{t\longrightarrow\infty}\left\|\beta-\beta_d\right\|&=0,\\
\lim_{t\longrightarrow\infty}\left\|\mu-\mu_d\right\|&=0.
\end{aligned}
\tag{8}
$$

3. Controller Design

In the previous section, the nominal attitude model of the reentry vehicle has been established by equations (3) and (5), which can be reorganized as equations (9a) and (9b). This section will devise a controller with an auxiliary according to this vehicle model:

$$
\dot{\gamma}=\Gamma(\cdot)\omega, \tag{9a}
$$

$$
\dot{\omega}=-I^{-1}\Omega I\omega+I^{-1}M_c. \tag{9b}
$$

It is well known that the attitude angles change more slowly than the angular rate. Therefore, according to the principle of time scale separation and cascade control,

equations (9a) and (9b) can be divided into attitude angle slow loop equation (9a) and angle rate fast loop equation (9b), also known as outer loop and inner loop, respectively. In this section, the ADP-based controller will be presented, and the overall control strategy is shown in Figure 1.

As shown in Figure 1, there are two control loops. The outer loop is an attitude control loop with two controllers. The controller 1 generates the main angular rate instruction ω_s according to the guidance instruction γ_d, and the ADP controller outputs the control instruction u_{ADP} according to the attitude angle error; both of which together yield the angular rate ω_c. Then, ω_c is a reference instruction for the inner angular rate loop so that the controller 2 of the inner loop generates the control torque M_c, which acts on the vehicle to output the actual attitude angles and complete the control task.

In this paper, the inner controller 1 and outer loop controller 2 are implemented based on conventional sliding mode control and serve as the main controllers. To increase the performance of the main controller of the outer loop, the ADP controller acts as an auxiliary and adopts an action-dependent structure such as ADHDP. Note that ADHDP belongs to the category of ADP, so it is called ADP in this paper. The output of the ADP serves as a supplementary reference signal for the inner loop. The focus of this paper is to discuss the auxiliary role of ADP structure. Of course, the main controllers can also choose other methods to design, but how to select the main controllers is not the focus of this paper. It should be pointed out that only the ADP auxiliary controller is introduced into the outer loop, mainly because the outer loop variable is the attitude angle and the inner loop variable is the angular rate, and the attitude angle changes slowly than the angular rate. Therefore, in each iteration, the iterative speed of the ADP is more easily matched with the update speed of the main controller 1. Perhaps we can similarly introduce the ADP auxiliary controller with the same structure into the inner loop, and its rationality and effectiveness will be researched and verified in future work.

In the following subsections: according to cascade control strategy, the outer loop controllers are first designed, including the main controller 1 and the ADP-based auxiliary controller. After the reference command signal ω_c is obtained by the outer loop controllers, the inner loop controller 2 is presented.

3.1. Outer Loop Controllers

3.1.1. Main Controller 1. The control objective of the outer loop is to operate the actual attitude angle γ to track γ_d within the desired accuracy. First, take the tracking error $e_\gamma = \gamma_d - \gamma \in R^3$. The sliding switching surface $S_\gamma \in R^3$ of the outer loop can be selected as

$$S_\gamma = \left[S_{\gamma 1}, S_{\gamma 2}, S_{\gamma 3}\right]^T = e_\gamma + \rho_\gamma \int_0^t e_\gamma \mathrm{d}\tau, \tag{10}$$

where $\rho_\gamma = \mathrm{diag}\left\{\rho_{\gamma 1}, \rho_{\gamma 2}, \rho_{\gamma 3}\right\} \in R^{3\times 3}$ and $\rho_{\gamma i} > 0$, $i = 1, 2, 3$ are the parameters to be designed [30]. Obviously, on the sliding surface $S_\gamma = 0$, the tracking error e_γ can be guaranteed to converge uniformly, that is,

$$S_\gamma = e_\gamma + \rho_\gamma \int_0^t e_\gamma \mathrm{d}\tau = 0. \tag{11}$$

In order to ensure the asymptotic convergence of the outer loop tracking error to the sliding surface, the virtual control law must be designed. First, take the derivative of S_γ as

$$\begin{aligned} \dot{S}_\gamma &= \dot{e}_\gamma + \rho_\gamma e_\gamma \\ &= \dot{\gamma}_d - \dot{\gamma} + \rho_\gamma e_\gamma \\ &= \dot{\gamma}_d - \Gamma\omega + \rho_\gamma e_\gamma. \end{aligned} \tag{12}$$

Take the following Lyapunov function:

$$L_1 = \left(\frac{1}{2}\right) S_\gamma^{\mathrm{T}} S_\gamma > 0, \tag{13}$$

and the derivative of L_1 is as

$$\dot{L}_1 = S_\gamma^{\mathrm{T}} \dot{S}_\gamma. \tag{14}$$

By Lyapunov stability, $\dot{L}_1 < 0$ has to be guaranteed. Therefore, the sliding mode approach law can be chosen as

$$\dot{S}_\gamma = -\tau_\gamma \mathrm{sign}\left(S_\gamma\right), \tag{15}$$

where designed parameter $\tau_\gamma > 0$ and $\mathrm{sign}(S_\gamma) = [\mathrm{sign}(S_{\gamma 1}), \mathrm{sign}(S_{\gamma 2}), \mathrm{sign}(S_{\gamma 3})]^{\mathrm{T}}$ denotes a sign function.

According to equations (12) and (15), there exists

$$\dot{\gamma}_d - \Gamma\omega + \rho_\gamma e_\gamma = -\tau_\gamma \mathrm{sign}\left(S_\gamma\right). \tag{16}$$

So, the virtual control law of the outer loop can be obtained as follows:

$$\omega_s = \Gamma^{-1}\left(\dot{\gamma}_d + \rho_\gamma e_\gamma + \tau_\gamma \mathrm{sign}\left(S_\gamma\right)\right). \tag{17}$$

In order to avoid or reduce the sliding mode chattering caused by the sign function in equation (17), a smooth continuous function can be adopted instead of the sign function. Because the saturation function is one of the most simple and effective ways, the virtual control law is redesigned as follows:

$$\omega_s = \Gamma^{-1}\left(\dot{\gamma}_d + \rho_\gamma e_\gamma + \tau_\gamma \mathrm{sat}\left(\frac{S_\gamma}{\xi_\gamma}\right)\right), \tag{18}$$

where $\mathrm{sat}(S_\gamma/\xi_\gamma) = [\mathrm{sat}(S_{\gamma 1}/\xi_\gamma), \mathrm{sat}(S_{\gamma 2}/\xi_\gamma), \mathrm{sat}(S_{\gamma 3}/\xi_\gamma)]^{\mathrm{T}}$ denotes a saturation function with width $\xi_\gamma > 0$ as follows:

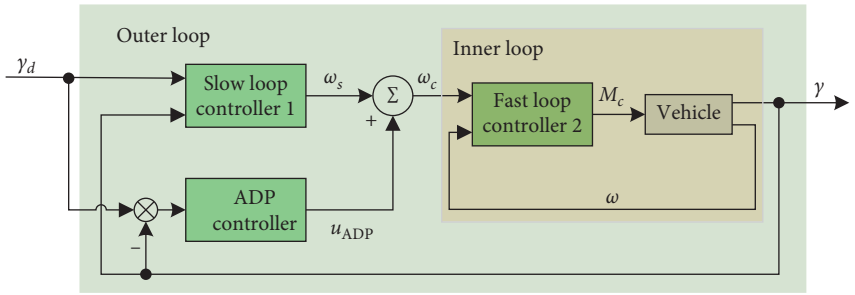

Figure 1: Dual-loop control structure based on ADP.

$$\operatorname*{sat}_{(i=1,2,3)}\left(\frac{S_{\gamma i}}{\xi_\gamma}\right)=\begin{cases}1, & \left(S_{\gamma i}>\xi_\gamma\right),\\ \left(\dfrac{S_{\gamma i}}{\xi_\gamma}\right), & \left(\left|S_{\gamma i}\right|\le\xi_\gamma\right),\\ -1, & \left(S_{\gamma i}<-\xi_\gamma\right).\end{cases}\tag{19}$$

Therefore, according to control law equation (18), the attitude angles can track the commands, and the error e_γ uniformly converges. Next, ω_s will be provided as the main reference signal to the inner loop.

3.1.2. ADP Auxiliary Controller. The idea of ADP is to take advantage of the function estimators to approximate the performance index functions and control strategies that meet the principle of optimality. By designing a critic-action structure, the critic network approximates the performance index J (the cost function) and J is defined as the forward accumulation of the utility function U with the discount factor λ [20, 21]:

$$J(k)=\sum_{i=k}^{\infty}\lambda^{i-k}U(i),\tag{20}$$

where U is usually defined as a quadratic. It can be seen that the cost function is also a quadratic convex function, with only a local minimum and at the same time a global minimum. The action network obtains the optimal control law u^* by minimizing J:

$$u^*(k)=\arg\min_{u(k)}\{U(k)+\lambda J(k+1)\}.\tag{21}$$

In this paper, only the auxiliary ADP controller is added to the outer loop to compensate for the attitude angle error generated by the main controller 1. ADP outputs u_{ADP} (u_{ADP} has the same dimension as ω_s), and the sum of u_{ADP} and ω_s inputs as a reference instruction to the inner loop. Obviously, the ADP controller is sensitive to the attitude angle error. It can be imagined that ADP will start to work when a certain error occurs; when the error meets the threshold requirements, the ADP does not need to work, which will balance the loss in accuracy and calculation speed. However, this does not seem to be the focus of this paper. It may be discussed in future research, such as the selection and optimization of the threshold.

In Figure 2, ADP adopts a network structure based on ADHDP, which includes an action network, a critic network, and attitude model (9a). The input of ADP is the attitude error, and the action network generates the control signal u_{ADP}. At the same time, the critic network approximates J. The specific design of each network is given below.

(1) Critic Network. In Figure 3, the critic network uses a single hidden-layer BP neural network with six input nodes, M hidden nodes, and one output node. The input contains the attitude angle error $\Delta\gamma$ and u_{ADP} generated by the action network. The output is the estimated $\widehat{J}$ of the cost function J. $\mathrm{Wc1}\in R^{M\times 6}$ is the weight matrix of the input layer to the hidden layer and $\mathrm{Wc1}_{ji}\,(i=1,\ldots,6;\ j=1,\ldots,M)$ represents the weight of the i-th input node to the j-th hidden node. $\mathrm{Wc2}\in R^{1\times M}$ is the weight matrix from the hidden-to-output layer, and $\mathrm{Wc2}_j$, $j=1,\ldots,M$ represents the connection weight of the j-th hidden node to the output. $\mathrm{Ch1}\in R^{M\times 1}$ and $\mathrm{Ch2}\in R^{M\times 1}$ are the input and output vectors of hidden nodes, respectively. The active functions of the hidden layer and the output layer are a bipolar sigmoid function and linear function, respectively. The attitude error is as follows:

$$\Delta\gamma=[\Delta\alpha,\Delta\beta,\Delta\mu]^{\mathrm{T}}=\left[\alpha_d-\alpha,\beta_d-\beta,\mu_d-\mu\right]^{\mathrm{T}}.\tag{22}$$

The input of the critic network is $\mathrm{INc}\in R^{6\times 1}$ as

$$\begin{aligned}\mathrm{INc}&=\left[\Delta\gamma;\Delta u_{\mathrm{ADP}}\right]\\&=\left[\Delta\alpha,\Delta\beta,\Delta\mu,u_{\mathrm{ADP}}(1),u_{\mathrm{ADP}}(2),u_{\mathrm{ADP}}(3)\right]^{\mathrm{T}}.\end{aligned}\tag{23}$$

The training of the critic network consists of two parts, one is the forward calculation, and the other is the error backpropagation of updating network weights. The forward process of step k is

$$\begin{aligned}\mathrm{Ch1}_j(k)&=\sum_{i=1}^{6}\mathrm{INc}_i(k)\cdot\mathrm{Wc1}_{ji}(k),\quad j=1,2,\ldots,M,\\ \mathrm{Ch2}_j(k)&=\frac{1-e^{-\mathrm{Ch1}_j(k)}}{1+e^{-\mathrm{Ch1}_j(k)}},\quad j=1,2,\ldots,M,\\ \widehat{J}(k)&=\sum_{j=1}^{M}\mathrm{Ch2}_j(k)\cdot\mathrm{Wc2}_j(k),\quad j=1,2,\ldots,M.\end{aligned}\tag{24}$$

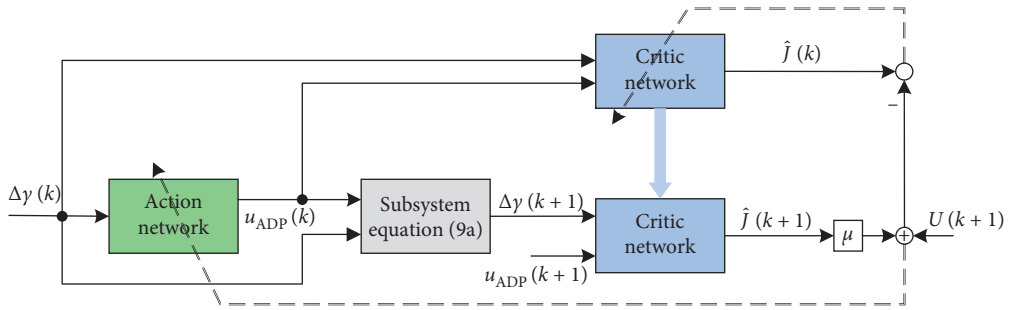

Figure 2: Structure of the ADP controller.

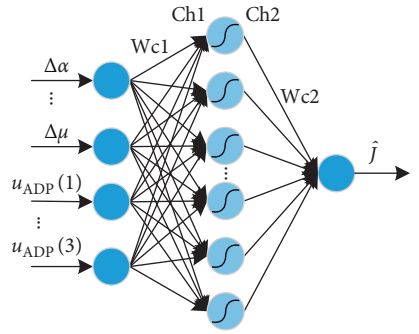

Figure 3: Structure of the critic network.

Equation (24) can be rewritten in matrix form as

$$\begin{aligned} \mathrm{Ch1}(k) &= \mathrm{Wc1} \cdot \mathrm{INc}, \\ \mathrm{Ch2}(k) &= \frac{(1-e)^{-\mathrm{Ch1}(k)}}{(1+e)^{-\mathrm{Ch1}(k)}}, \\ \hat{J}(k) &= \mathrm{Wc2}(k) \cdot \mathrm{Ch2}(k). \end{aligned} \tag{25}$$

Based on the Bellman optimality principle, the critic network approximates the cost function of the system. The actual $J(k)$ is defined as the cumulative return from the current state to the future:

$$J(k) = \sum_{i=k}^{\infty} \lambda^{i-k} U(i), \tag{26}$$

where $\lambda \in (0,1)$ is a discount factor or forgetting factor, indicating the influence of the future state on the current strategy. U is the utility function at each step, which is defined as a quadratic:

$$\begin{cases} U(k) = \Delta\gamma^T(k) \Lambda \Delta\gamma(k), \\ \Lambda = \mathrm{diag}\{\sigma, \sigma, \sigma\}, \quad \sigma > 0. \end{cases} \tag{27}$$

The following error E_c can be defined, and the critic network can approximate J by minimizing E_c:

$$\begin{cases} E_c = \left(\frac{1}{2}\right) e_c^2, \\ e_c = \hat{J}(k) - U(k+1) - \lambda \hat{J}(k+1). \end{cases} \tag{28}$$

Therefore, network weights can be updated through backpropagation of E_c.

(2) Updating the Weights Wc2. Using the gradient descent method, let $\Delta\mathrm{Wc2}$ be the gradient, so

$$\mathrm{Wc2}(k+1) = \mathrm{Wc2}(k) + \Delta\mathrm{Wc2}(k), \tag{29}$$

where each component of $\Delta\mathrm{Wc2}$ is represented as

$$\begin{aligned} \Delta\mathrm{Wc2}_j(k) &= \zeta_c(k) \cdot \left(-\frac{\partial E_c(k)}{\partial \mathrm{Wc2}_j(k)} \right), \quad j = 1, \ldots, M \\ &= -\zeta_c(k) \frac{\partial E_c(k)}{\partial \hat{J}(k)} \frac{\partial \hat{J}(k)}{\partial \mathrm{Wc2}_j(k)}, \quad j = 1, \ldots, M \\ &= -\zeta_c(k) \cdot e_c(k) \cdot \mathrm{Ch2}_j(k), \quad j = 1, \ldots, M, \end{aligned} \tag{30}$$

where $\zeta_c(k) \in (0,1)$ is the learning rate. Equation (30) is combined and rewritten into a matrix form as

$$\Delta\mathrm{Wc2}(k) = -\zeta_c(k) \cdot e_c(k) \cdot \mathrm{Ch2}^{\mathrm{T}}(k). \tag{31}$$

(3) Updating the Weights Wc1. Similarly, let $\Delta\mathrm{Wc1}$ be the gradient, so

$$\begin{aligned}
\mathrm{Wc1}(k+1) &= \mathrm{Wc1}(k) + \Delta\mathrm{Wc1}(k),\\
\Delta\mathrm{Wc1}_{ji}(k) &= \zeta_c(k)\cdot\left(-\frac{\partial E_c(k)}{\partial \mathrm{Wc1}_{ji}(k)}\right), \quad \begin{matrix} i=1,\ldots,6 \\ j=1,\ldots,M \end{matrix}\\
&= -\zeta_c(k)\frac{\partial E_c(k)}{\partial \widehat{J}(k)}\frac{\partial \widehat{J}(k)}{\partial \mathrm{Ch2}_j(k)}\frac{\partial \mathrm{Ch2}_j(k)}{\partial \mathrm{Ch1}_j(k)}\frac{\partial \mathrm{Ch1}_j(k)}{\partial \mathrm{Wc1}_{ji}(k)}\\
&= -\zeta_c(k)\cdot e_c(k)\cdot \mathrm{Wc2}_j(k)\cdot\left(\frac{1}{2}\right)\left[1-\mathrm{Ch2}_j^2(k)\right]\cdot \mathrm{INc}_i(k).
\end{aligned} \tag{32}$$

Combine the above formula into a simplified matrix form as follows:

$$\begin{aligned}
\Delta\mathrm{Wc1}(k) = &-\left(\frac{1}{2}\right)\cdot\zeta_c(k)\cdot e_c(k)\\
&\cdot\left\{\mathrm{Wc2}^{\mathrm{T}}(k)\times[1-\mathrm{Ch2}(k)\times\mathrm{Ch2}(k)]\right\}\cdot\mathrm{INc}^{\mathrm{T}}(k),
\end{aligned} \tag{33}$$

where the symbol "×" represents the Hadamard product of two matrices, that is, bitwise multiplication; "·" represents the ordinary multiplication of matrices. These symbols appearing in the later parts of this paper possess the same meaning.

(4) Action Network. As shown in Figure 4, the action network adopts a single hidden-layer BP neural network with three input nodes, N hidden nodes, and three output nodes. The network's input is $\mathrm{INa} = \Delta\gamma \in R^{3\times 1}$, and output is $u_{\mathrm{ADP}} \in R^{3\times 1}$. Other parameters are defined similarly to the critic network. The active functions of the hidden and output layer are a bipolar sigmoid function and linear function, respectively.

The training of the action network also includes forward calculation and error backpropagation. Firstly, the forward process is briefly presented as

$$\begin{aligned}
\mathrm{Ah1}(k) &= \mathrm{Wa1}\cdot\mathrm{INa},\\
\mathrm{Ah2}(k) &= \frac{(1-e)^{-\mathrm{Ah1}(k)}}{(1+e)^{-\mathrm{Ah1}(k)}},\\
u_{\mathrm{ADP}}(k) &= \mathrm{Wa2}(k)\cdot\mathrm{Ah2}(k).
\end{aligned} \tag{34}$$

The action network generates an optimal control strategy by minimizing the system cost function J. This goal can be achieved by minimizing the defined error E_a:

$$\begin{cases}
E_a(k) = \left(\frac{1}{2}\right)e_a^2(k),\\
e_a(k) = \widehat{J}(k).
\end{cases} \tag{35}$$

(5) Updating the Weights Wa2. With the gradient descent method, the update process of Wa2 is

$$\begin{aligned}
\mathrm{Wa2}(k+1) &= \mathrm{Wa2}(k) + \Delta\mathrm{Wa2}(k),\\
\Delta\mathrm{Wa2}(k) &= \zeta_a(k)\cdot\left(-\frac{\partial E_a(k)}{\partial \mathrm{Wa2}(k)}\right),
\end{aligned} \tag{36}$$

where $\zeta_a(k)$ represents the learning rate. The connection weight from the j-th hidden node to the ith output node is denoted as $\mathrm{Wa2}_{ij}\,(i=1,2,3;\ j=1,\ldots,N)$, so

$$\mathrm{Wa2}_{ij}(k+1) = \mathrm{Wa2}_{ij}(k) + \Delta\mathrm{Wa2}_{ij}(k), \quad \begin{matrix} i=1,2,3 \\ j=1,\ldots,N \end{matrix}, \tag{37}$$

$$\begin{aligned}
\Delta\mathrm{Wa2}_{ij}(k) &= \zeta_a(k)\cdot\left(-\frac{\partial E_a(k)}{\partial e_a(k)}\frac{\partial e_a(k)}{\partial \widehat{J}(k)}\frac{\partial \widehat{J}(k)}{\partial \mathrm{Wa2}_{ij}(k)}\right)\\
&= \zeta_a(k)\cdot\left(-e_a(k)\frac{\partial \widehat{J}(k)}{\partial u_{\mathrm{ADP}i}(k)}\frac{\partial u_{\mathrm{ADP}i}(k)}{\partial \mathrm{Wa2}_{ij}(k)}\right)\\
&= -\zeta_a(k)\cdot e_a(k)\cdot\frac{\partial \widehat{J}(k)}{\partial u_{\mathrm{ADP}i}(k)}\cdot\mathrm{Ah2}_j(k).
\end{aligned} \tag{38}$$

The middle term $(\partial\widehat{J}(k)/\partial u_{\mathrm{ADP}i}(k))$ in equation (38) indicates that the path of the backpropagated signal passes through the critic network when training the action network [31]. Furthermore, by the output and input of the critic network, $(\partial\widehat{J}(k)/\partial u_{\mathrm{ADP}i}(k))$ can be obtained:

$$\frac{\partial \widehat{J}(k)}{\partial u_{\mathrm{ADP}}(k)} = \frac{\partial \widehat{J}(k)}{\partial \mathrm{Ch2}(k)}\frac{\partial \mathrm{Ch2}(k)}{\partial \mathrm{Ch1}(k)}\frac{\partial \mathrm{Ch1}(k)}{\partial u_{\mathrm{ADP}}(k)}. \tag{39}$$

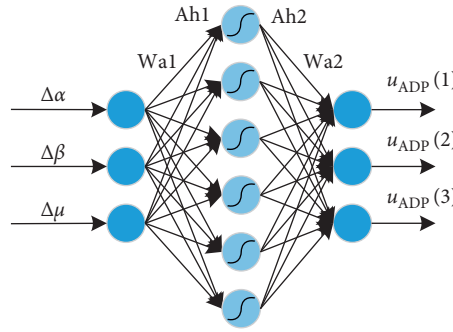

Figure 4: Structure of the action network.

So,

$$\frac{\partial \hat{J}(k)}{\partial u_{\mathrm{ADP}i}(k)} = \sum_{j=1}^{M}\left(\frac{\partial \hat{J}(k)}{\partial \mathrm{Ch2}_j(k)}\frac{\partial \mathrm{Ch2}_j(k)}{\partial \mathrm{Ch1}_j(k)}\frac{\partial \mathrm{Ch1}_j(k)}{\partial u_{\mathrm{ADP}i}(k)}\right), \quad i = 1, 2, 3$$

$$= \sum_{j=1}^{M}\left(\mathrm{Wc2}_j(k)\cdot\left(\frac{1}{2}\right)\left(1-\mathrm{Ch2}_j^2(k)\right)\cdot \mathrm{Wc1}_{(j,i+3)}(k)\right) \tag{40}$$

$$= \left(\frac{1}{2}\right)\cdot \mathrm{Wc1}_{(:,i+3)}{}^{\mathrm{T}}(k)\cdot\left(\mathrm{Wc2}^{\mathrm{T}}(k)\times(1-\mathrm{Ch2}(k)\times\mathrm{Ch2}(k))\right),$$

where $Wc1_{(:,i+3)}$ represents the $(i+3)$-th column of Wc1. Equation (40) can be rewritten in matrix form:

$$\frac{\partial \hat{J}(k)}{\partial u_{\mathrm{ADP}}(k)} = \left(\frac{1}{2}\right)\cdot \mathrm{Wc1}_{u_{\mathrm{ADP}}}{}^{\mathrm{T}}(k) \cdot\left(\mathrm{Wc2}^{\mathrm{T}}(k)\times(1-\mathrm{Ch2}(k)\times\mathrm{Ch2}(k))\right), \tag{41}$$

where $\mathrm{Wc1}_{u_{\mathrm{ADP}}} = \mathrm{Wc1}(:, 4{:}\ 6)$ represents columns 4 to 6 of Wc1, that is, the connection weights of the three input nodes corresponding to u_{ADP} and all hidden nodes in the critic network. From equations (37)–(41), ΔWa2 can be deduced as

$$\Delta\mathrm{Wa2}(k) = \zeta_a(k)\cdot\left(-\frac{\partial E_a(k)}{\partial e_a(k)}\frac{\partial e_a(k)}{\partial \hat{J}(k)}\frac{\partial \hat{J}(k)}{\partial \mathrm{Wa2}(k)}\right)$$

$$= -\zeta_a(k)\cdot e_a(k)\cdot\frac{\partial \hat{J}(k)}{\partial u_{\mathrm{ADP}}(k)}\cdot \mathrm{Ah2}^{\mathrm{T}}(k) \tag{42}$$

$$= -\left(\frac{1}{2}\right)\cdot\zeta_a(k)\cdot e_a(k)\cdot\left\{\mathrm{Wc1}_{u_{\mathrm{ADP}}}{}^{\mathrm{T}}(k)\cdot\left(\mathrm{Wc2}^{\mathrm{T}}(k)\times(1-\mathrm{Ch2}(k)\times\mathrm{Ch2}(k))\right)\right\}\cdot \mathrm{Ah2}^{\mathrm{T}}(k).$$

(6) Updating the Weights Wa1. Similar to the Wa2, the update of Wa1 is

$$\mathrm{Wa1}(k+1) = \mathrm{Wa1}(k) + \Delta\mathrm{Wa1}(k), \tag{43}$$

$$\begin{aligned}\Delta\mathrm{Wa1}(k) &= \zeta_a(k)\cdot\left(-\frac{\partial E_a(k)}{\partial \mathrm{Wa1}(k)}\right)\\ &= \zeta_a(k)\cdot\left(-\frac{\partial E_a(k)}{\partial e_a(k)}\frac{\partial e_a(k)}{\partial \widehat{J}(k)}\frac{\partial \widehat{J}(k)}{\partial u_{\mathrm{ADP}}(k)}\frac{\partial u_{\mathrm{ADP}}(k)}{\partial \mathrm{Ah2}(k)}\frac{\partial \mathrm{Ah2}(k)}{\partial \mathrm{Ah1}(k)}\frac{\partial \mathrm{Ah1}(k)}{\partial \mathrm{Wa1}(k)}\right)\\ &= -\zeta_a(k)\cdot e_a(k)\cdot\left\{\left(\mathrm{Wa2}^{\mathrm{T}}(k)\cdot\frac{\partial \widehat{J}(k)}{\partial u_{\mathrm{ADP}}(k)}\right)\times\left(\frac{1}{2}\cdot\left(1-\mathrm{Ah2}(k)\times\mathrm{Ah2}(k)\right)\right)\right\}\cdot\mathrm{INa}^{\mathrm{T}}(k).\end{aligned} \tag{44}$$

Substituting equation (41) into equation (44), ΔWa1 can be easily obtained.

So far, the training process is completed. And the optimal control signal u_{ADP} output by the action network will be combined with ω_s output by outer loop main controller 1, that is

$$\omega_c = \omega_s + u_{\mathrm{ADP}}, \tag{45}$$

where the angular rate signal $\omega_c \in R^{3\times1}$ will be input as the reference command of the inner loop controller 2, and the control torque M_c output by controller 2 will operate the vehicle to complete the attitude control task.

3.2. Inner Loop Controller. To ensure that the actual angular rate ω can stably track the expected reference angular rate ω_c, similar to controller 1, the sliding variable is selected for inner loop controller 2 as follows:

$$S_\omega = [S_{\omega1}, S_{\omega2}, S_{\omega3}]^T = e_\omega + \rho_\omega\int_0^t e_\omega \mathrm{d}\tau, \tag{46}$$

where $e_\omega = \omega_c - \omega \in R^{3\times1}$ and $\rho_\omega = \mathrm{diag}\{\rho_{\omega1}, \rho_{\omega2}, \rho_{\omega3}\} \in R^{3\times3}$ with $\rho_{\omega i} > 0$, $i = 1, 2, 3$. In order to ensure the inner loop tracking error e_ω asymptotically converges to the sliding surface $S_\omega = 0$, the actual control law M has to be designed.

The derivative of S_ω is

$$\begin{aligned}\dot{S}_\omega &= \dot{e}_\omega + \rho_\omega e_\omega\\ &= \dot{\omega}_c + I^{-1}\Omega I\omega - I^{-1}M_c + \rho_\omega e_\omega.\end{aligned} \tag{47}$$

Take the following Lyapunov function L_2:

$$\begin{aligned}L_2 &= \left(\frac{1}{2}\right)S_\omega^{\mathrm{T}}S_\omega > 0,\\ \dot{L}_2 &= S_\omega^{\mathrm{T}}\dot{S}_\omega.\end{aligned} \tag{48}$$

By Lyapunov stability, $\dot{L}_2 < 0$ has to be guaranteed. Therefore, the dynamics $\dot{S}_\omega$ can be chosen as

$$\dot{S}_\omega = -\tau_\omega \mathrm{sign}(S_\omega), \tag{49}$$

where designed parameter $\tau_\omega > 0$ and $\mathrm{sign}(S_\omega) = [\mathrm{sign}(S_{\omega1}), \mathrm{sign}(S_{\omega2}), \mathrm{sign}(S_{\omega3})]^{\mathrm{T}}$ denotes a sign function.

According to equations (47) and (49), there exists

$$\dot{\omega}_c + I^{-1}\Omega I\omega - I^{-1}M_c + \rho_\omega e_\omega = -\tau_\omega \mathrm{sign}(S_\omega). \tag{50}$$

So, the actual control law of the inner loop can be obtained as follows:

$$M_c = I\dot{\omega}_c + \Omega I\omega + I\rho_\omega e_\omega + \tau_\omega I\cdot\mathrm{sign}(S_\omega). \tag{51}$$

Similarly, a continuous saturation function is chosen to replace the sign function to reduce the chattering. Therefore, the actual control law is rewritten as follows:

$$M_c = I\dot{\omega}_c + \Omega I\omega + I\rho_\omega e_\omega + \tau_\omega I\cdot\mathrm{sat}\left(\frac{S_\omega}{\xi_\omega}\right). \tag{52}$$

where $\mathrm{sat}(S_\omega/\xi_\omega) = [\mathrm{sat}(S_{\omega1}/\xi_\omega), \mathrm{sat}(S_{\omega2}/\xi_\omega), \mathrm{sat}(S_{\omega3}/\xi_\omega)]^{\mathrm{T}}$ denotes a saturation function with width $\xi_\omega > 0$.

Therefore, for actual control law as equation (52), $\dot{L}_2 < 0$ holds. That is, the actual attitude angular rate ω converges asymptotically to the expected angular rate ω_c.

4. Implementation Issues

In Section 3, the design of ADP auxiliary controller is completed, but the parameter selection and training speed of ADP cannot be ignored in practical application. So, in this section, some issues are discussed about implementation of ADP structure, including parameter selection for networks and skills related to speed up training.

4.1. Network Parameters and Their Convergence. It is clear that the critic network with a single hidden layer and randomly initialized weights can approximate J with arbitrarily small errors, that is, $\lim_{k\longrightarrow\infty}\|\widehat{J}(k) - J(k)\| = 0$. Similarly, the action network with randomly initialized weights can minimize the cost function $\widehat{J}$ and its output can approximate to the optimal control law u_{ADP}^*, that is,

$$u_{\mathrm{ADP}}^* = \arg\min_{u_{\mathrm{ADP}}^*}\|\widehat{J}\|. \tag{53}$$

In other words, both the critic network and action network evolve towards the optimal direction to achieve their goals. Furthermore, considering equations (25) and (34), it is because of the adjustment of network weights Wc1, Wc2, Wa1, and Wa2 that the output of the networks reaches the desired optimal value. That is, when the optimal control strategy u_{ADP}^* is obtained, the network weights will also reach the optimal weights as follows [32]:

$$\begin{cases} \mathrm{Wc}^* = \arg\min_{\mathrm{Wc}} \|\widehat{J}(k) - U(k+1) - \lambda\widehat{J}(k+1)\|, \\ \mathrm{Wa}^* = \arg\min_{\mathrm{Wa}} \|\widehat{J}(k)\|, \end{cases} \tag{54}$$

where Wc^* and Wa^* represent the optimal weights of the critic and action network, respectively.

Lemma 1. *In critic and action network, the weights Wc and Wa are finally uniformly stable and approach the optimal weights Wc^* and Wa^*.*

Proof. It is well known that the weights of the input to hidden layer are similar to the weights of the hidden to output layer. In order to facilitate the elaboration, this paper only presents the uniform stability proof about Wc2 and Wa2, which are the weights of the hidden to output layer. Let the optimal weights corresponding to Wc2 and Wa2 be $\mathrm{Wc2}^*$ and $\mathrm{Wa2}^*$, respectively, and they are bounded. $\|\mathrm{Wc2}^*\| \le \kappa_c$, $\|\mathrm{Wa2}^*\| \le \kappa_a$, and κ_c, κ_a are positive constants.

Equation (28) can be rewritten as

$$\begin{aligned} E_c(k) &= \left(\frac{1}{2}\right)e_c^2(k), \\ e_c(k) &= \lambda\widehat{J}(k) - (\widehat{J}(k-1) - U(k)) \\ &= \lambda \cdot \mathrm{Wc2}(k) \cdot \mathrm{Ch2}(k) - (\lambda \cdot \mathrm{Wc2}(k-1) \\ &\quad \cdot \mathrm{Ch2}(k-1) - U(k)). \end{aligned} \tag{55}$$

From equations (29) to (31), the update of Wc2 can be rewritten as follows:

$$\begin{aligned} \mathrm{Wc2}(k+1) &= \mathrm{Wc2}(k) + \Delta\mathrm{Wc2}(k) \\ &= \mathrm{Wc2}(k) + \left(-\zeta_c(k) \cdot \frac{\partial E_c(k)}{\partial e_c(k)} \frac{\partial e_c(k)}{\partial \widehat{J}(k)} \frac{\partial \widehat{J}(k)}{\mathrm{Wc2}(k)}\right) \\ &= \mathrm{Wc2}(k) - \lambda \cdot \zeta_c(k) \cdot (\lambda \cdot \mathrm{Wc2}(k) \\ &\quad \cdot \mathrm{Ch2}(k) - ((\lambda \cdot \mathrm{Wc2}(k-1)) \cdot \mathrm{Ch2}(k-1) \\ &\quad - U(k))) \cdot \mathrm{Ch2}^{\mathrm{T}}(k). \end{aligned} \tag{56}$$

Similarly, the update of Wa2 is

$$\begin{aligned} \mathrm{Wa2}(k+1) &= \mathrm{Wa2}(k) + \Delta\mathrm{Wa2}(k), \\ &= \mathrm{Wa2}(k) + \zeta_a(k) \cdot \left(-\frac{\partial E_a(k)}{\partial \mathrm{Wa2}(k)}\right) \\ &= \mathrm{Wa2}(k) - \left(\frac{1}{2}\right) \cdot \zeta_a(k) \cdot e_a(k) \cdot \left\{\mathrm{Wc1}_{u_{\mathrm{ADP}}}{}^{\mathrm{T}}(k) \cdot \left(\mathrm{Wc2}^{\mathrm{T}}(k) \times (1 - \mathrm{Ch2}(k) \times \mathrm{Ch2}(k))\right)\right\} \cdot \mathrm{Ah2}^{\mathrm{T}}(k) \\ &= \mathrm{Wa2}(k) - \left(\frac{1}{2}\right) \cdot \zeta_a(k) \cdot \widehat{J}(k) \cdot \left(\Theta(k) \cdot \mathrm{Wc2}^{\mathrm{T}}(k) \cdot \mathrm{Ah2}^{\mathrm{T}}(k)\right) \\ &= \mathrm{Wa2}(k) - \left(\frac{1}{2}\right) \cdot \zeta_a(k) \cdot (\mathrm{Wc2}(k) \cdot \mathrm{Ch2}(k)) \cdot \left(\Theta(k) \cdot \mathrm{Wc2}^{\mathrm{T}}(k) \cdot \mathrm{Ah2}^{\mathrm{T}}(k)\right), \end{aligned} \tag{57}$$

where $\Theta(k) = \mathrm{Wc1}_{u_{\mathrm{ADP}}}{}^{\mathrm{T}}(k) \times [1 - \mathrm{Ch2}(k) \times \mathrm{Ch2}(k) \quad 1 - \mathrm{Ch2}(k) \times \mathrm{Ch2}(k) \quad 1 - \mathrm{Ch2}(k) \times \mathrm{Ch2}(k)]^{\mathrm{T}}$.

First, the Lyapunov method is adopted to analyse the convergence of Wc2:

$$V_c(k) = \frac{1}{\zeta_c(k)} \mathrm{tr}\left(\widetilde{\mathrm{W}}\mathrm{c2}(k)\widetilde{\mathrm{W}}\mathrm{c2}^{\mathrm{T}}(k)\right), \tag{58}$$

where $\widetilde{\mathrm{W}}\mathrm{c2}(k) = \mathrm{Wc2}(k) - \mathrm{Wc2}^*(k)$ is the error between actual and optimal weights. Then, the first-order difference of V_c is expressed as

$$\begin{aligned} \Delta V_c(k) = \frac{1}{\zeta_c(k)} \mathrm{tr}\Big(&\widetilde{\mathrm{W}}\mathrm{c2}(k+1)\widetilde{\mathrm{W}}\mathrm{c2}^{\mathrm{T}}(k+1) \\ &- \widetilde{\mathrm{W}}\mathrm{c2}(k)\widetilde{\mathrm{W}}\mathrm{c2}^{\mathrm{T}}(k)\Big). \end{aligned} \tag{59}$$

According to equation (56), (60) can be obtained:

$$\begin{aligned}\widetilde{\mathrm{Wc2}}(k+1) &= \mathrm{Wc2}(k+1) - \mathrm{Wc2}^{*} \\ &= \mathrm{Wc2}(k) - \lambda \cdot \zeta_c(k) \cdot [\lambda \cdot \mathrm{Wc2}(k) \cdot \mathrm{Ch2}(k) - (\lambda \cdot \mathrm{Wc2}(k-1) \cdot \mathrm{Ch2}(k-1) - U(k))] \cdot \mathrm{Ch2}^{\mathrm{T}}(k) - \mathrm{Wc2}^{*} \\ &= \widetilde{\mathrm{Wc2}}(k) - \lambda \cdot \zeta_c(k) \cdot [\lambda \cdot (\widetilde{\mathrm{Wc2}}(k) + \mathrm{Wc2}^{*}) \cdot \mathrm{Ch2}(k) - (\lambda \cdot \mathrm{Wc2}(k-1) \cdot \mathrm{Ch2}(k-1) - U(k))] \cdot \mathrm{Ch2}^{\mathrm{T}}(k) \\ &= \widetilde{\mathrm{Wc2}}(k) \cdot \left(I - \lambda^2 \cdot \zeta_c(k) \cdot \mathrm{Ch2}(k)\mathrm{Ch2}^{\mathrm{T}}(k)\right) - \lambda \cdot \zeta_c(k) \cdot [\lambda \cdot \mathrm{Wc2}^{*} \cdot \mathrm{Ch2}(k) - (\lambda \cdot \mathrm{Wc2}(k-1) \\ &\quad \cdot \mathrm{Ch2}(k-1) - U(k))] \cdot \mathrm{Ch2}^{\mathrm{T}}(k).\end{aligned} \tag{60}$$

In addition, denote the approximation error between actual and optimal output as

$$\delta_c(k) = (\mathrm{Wc2}(k) - \mathrm{Wc2}^{*}) \cdot \mathrm{Ch2}(k) = \widetilde{\mathrm{Wc2}}(k) \cdot \mathrm{Ch2}(k). \tag{61}$$

Substituting equations (60) and (61) into equation (59), $\Delta V_c(k)$ can be deduced:

$$\begin{aligned}\Delta V_c(k) = &-\lambda^2 \|\delta_c(k)\|^2 - \lambda^2 \left(1 - \lambda^2 \cdot \zeta_c(k) \|\mathrm{Ch2}(k)\|^2\right) \\ &\cdot \left\|\delta_c(k) + \mathrm{Wc2}^{*} \cdot \mathrm{Ch2}(k) + \left(\frac{1}{\lambda}\right) U(k) - \left(\frac{1}{\lambda}\right) \mathrm{Wc2}(k-1) \cdot \mathrm{Ch2}(k-1)\right\|^2 \\ &+ \|\lambda \cdot \mathrm{Wc2}^{*} \cdot \mathrm{Ch2}(k) + U(k) - \mathrm{Wc2}(k-1) \cdot \mathrm{Ch2}(k-1)\|^2.\end{aligned} \tag{62}$$

Furthermore, applying the Cauchy–Schwarz inequality [33], it can be deduced as

$$\begin{aligned}\Delta V_c(k) \le &-\lambda^2 \|\delta_c(k)\|^2 \\ &- \lambda^2 \left(1 - \lambda^2 \cdot \zeta_c(k) \|\mathrm{Ch2}(k)\|^2\right) \left\|\delta_c(k) + \mathrm{Wc2}^{*} \cdot \mathrm{Ch2}(k) + \frac{1}{\lambda} U(k) - \frac{1}{\lambda} \mathrm{Wc2}(k-1) \cdot \mathrm{Ch2}(k-1)\right\|^2 \\ &+ 2\left\|\lambda \cdot \mathrm{Wc2}^{*} \cdot \mathrm{Ch2}(k) + U(k) - \frac{1}{2} \mathrm{Wc2}(k-1) \cdot \mathrm{Ch2}(k-1) - \frac{1}{2} \mathrm{Wc2}^{*} \cdot \mathrm{Ch2}(k-1)\right\|^2 + \frac{1}{2} \|\delta_c(k-1)\|^2.\end{aligned} \tag{63}$$

Similarly, set $V_a(k) = (1/\psi\zeta_a(k))\mathrm{tr}(\widetilde{\mathrm{Wa2}}(k)\widetilde{\mathrm{Wa2}}^{\mathrm{T}}(k))$, $(\psi > 0)$.

Denote the approximation error of the action network between the actual and optimal output as $\delta_a(k) = (\mathrm{Wa2}(k) - \mathrm{Wa2}^{*}) \cdot \mathrm{Ah2}(k) = \widetilde{\mathrm{Wa2}}(k) \cdot \mathrm{Ah2}(k)$. Referring to ΔV_c, ΔV_a satisfies

$$\begin{aligned}\Delta V_a(k) \le \left(\frac{1}{\psi}\right) \Big\{ &-\left(\|\Theta(k) \cdot \mathrm{Wc2}^{\mathrm{T}}(k)\|^2 - \zeta_a(k) \cdot \|\Theta(k) \cdot \mathrm{Wc2}^{\mathrm{T}}(k)\|^2 \|\mathrm{Ah2}(k)\|^2\right) \cdot \|\mathrm{Wc2}(k) \cdot \mathrm{Ch2}(k)\|^2 \\ &+ \|\mathrm{Wc2}(k) \cdot \mathrm{Ch2}(k)\|^2 \|\delta_a(k)\|^2 + 4\|\mathrm{Wc2}^{*} \cdot \mathrm{Ch2}(k)\|^2 + 4\|\delta_c(k)\|^2 \Big\}.\end{aligned} \tag{64}$$

Furthermore, set $V_\delta(k) = (1/2)\|\delta_c(k-1)\|^2$, and then

$$\Delta V_\delta(k) = \left(\frac{1}{2}\right)\left(\|\delta_c(k)\|^2 - \|\delta_c(k-1)\|^2\right). \tag{65}$$

From the above derivation, we can finally take the total Lyapunov function $V(k)$ as

$$\begin{aligned} V(k) &= V_c(k) + V_a(k) + V_\delta(k) \\ &\le -\left(\lambda^2 - \frac{1}{2} - \frac{4}{\psi}\right)\left\|\delta_c(k)\right\|^2 \\ &\quad - \lambda^2\left(1 - \lambda^2 \cdot \zeta_c(k)\|\mathrm{Ch2}(k)\|^2\right) \cdot \left\|\delta_c(k) + \mathrm{Wc2}^* \cdot \mathrm{Ch2}(k) + \frac{1}{\lambda}U(k) - \frac{1}{\lambda}\mathrm{Wc2}(k-1) \cdot \mathrm{Ch2}(k-1)\right\|^2 \\ &\quad - \frac{1}{\psi}\left(\left\|\Theta(k) \cdot \mathrm{Wc2}^{\mathrm{T}}(k)\right\|^2 - \zeta_a(k) \cdot \left\|\Theta(k) \cdot \mathrm{Wc2}^{\mathrm{T}}(k)\right\|^2 \|\mathrm{Ah2}(k)\|^2\right) \cdot \|\mathrm{Wc2}(k) \cdot \mathrm{Ch2}(k)\|^2 \\ &\quad + 2\left\|\lambda \cdot \mathrm{Wc2}^*(k) \cdot \mathrm{Ch2}(k) + U(k) - \frac{1}{2}\mathrm{Wc2}(k-1) \cdot \mathrm{Ch2}(k-1) - \frac{1}{2}\mathrm{Wc2}^* \cdot \mathrm{Ch2}(k-1)\right\|^2 \\ &\quad + \frac{1}{\psi}\|\mathrm{Wc2}(k) \cdot \mathrm{Ch2}(k)\|^2\left\|\delta_a(k)\right\|^2 + \frac{4}{\psi}\left\|\mathrm{Wc2}^*(k) \cdot \mathrm{Ch2}(k)\right\|^2. \end{aligned} \tag{66}$$

Selecting some parameters as equation (67), then equation (68) holds:

$$\begin{aligned} \frac{1}{\sqrt{2}} &< \lambda < 1, \\ \zeta_c(k) &< \frac{1}{\lambda^2\|\mathrm{Ch2}(k)\|^2}, \\ \zeta_a(k) &< \frac{1}{\|\mathrm{Ah2}(k)\|^2}, \\ \psi &> \frac{4}{\lambda^2 - (1/2)}, \end{aligned} \tag{67}$$

$$\begin{aligned} \Delta V(k) \le & -\left(\lambda^2 - \frac{1}{2} - \frac{4}{\psi}\right)\left\|\delta_c(k)\right\|^2 - \lambda^2\left(1 - \lambda^2 \cdot \zeta_c(k)\|\mathrm{Ch2}(k)\|^2\right) \\ & \cdot \left\|\delta_c(k) + \mathrm{Wc2}^* \cdot \mathrm{Ch2}(k) + \frac{1}{\lambda}U(k) - \frac{1}{\lambda}\mathrm{Wc2}(k-1) \cdot \mathrm{Ch2}(k-1)\right\|^2 \\ & - \frac{1}{\psi}\left(\left\|\Theta(k) \cdot \mathrm{Wc2}^{\mathrm{T}}(k)\right\|^2 - \zeta_a(k) \cdot \left\|\Theta(k) \cdot \mathrm{Wc2}^{\mathrm{T}}(k)\right\|^2 \|\mathrm{Ah2}(k)\|^2\right) \cdot \|\mathrm{Wc2}(k) \cdot \mathrm{Ch2}(k)\|^2 + D^2, \end{aligned} \tag{68}$$

where D^2 represents

$$\begin{aligned} D^2 = & 2\left\|\lambda \cdot \mathrm{Wc2}^*(k) \cdot \mathrm{Ch2}(k) + U(k) - \frac{1}{2}\mathrm{Wc2}(k-1) \cdot \mathrm{Ch2}(k-1) - \frac{1}{2}\mathrm{Wc2}^* \cdot \mathrm{Ch2}(k-1)\right\|^2 \\ & + \frac{1}{\psi}\|\mathrm{Wc2}(k) \cdot \mathrm{Ch2}(k)\|^2\left\|\delta_a(k)\right\|^2 + \frac{4}{\psi}\left\|\mathrm{Wc2}^*(k) \cdot \mathrm{Ch2}(k)\right\|^2. \end{aligned} \tag{69}$$

Furthermore, applying the Cauchy–Schwarz inequality, we get

$$\begin{aligned} D^2 &\le 8\left(\lambda^2\left\|\mathrm{Wc2}^*(k)\cdot\mathrm{Ch2}(k)\right\|^2 + U^2(k) + \frac{1}{4}\|\mathrm{Wc2}(k-1)\cdot\mathrm{Ch2}(k-1)\|^2 + \frac{1}{4}\left\|\mathrm{Wc2}^*\cdot\mathrm{Ch2}(k-1)\right\|\right), \\ &+ \frac{2}{\psi}\left\|\Theta(k)\cdot\mathrm{Wc2}^T(k)\right\|^2\cdot\left(\|\mathrm{Wa2}(k)\cdot\mathrm{Ah2}(k)\|^2 + \left\|\mathrm{Wa2}^*\cdot\mathrm{Ah2}(k)\right\|^2\right) + \frac{4}{\psi}\left\|\mathrm{Wc2}^*(k)\cdot\mathrm{Ch2}(k)\right\|^2, \\ &\le \left(8\lambda^2 + 4 + \frac{4}{\psi}\right)\cdot\mathrm{Wc2}_{\max}^2\cdot\mathrm{Ch2}_{\max}^2 + \frac{4}{\psi}\cdot\mathrm{Wc2}_{\max}^2\cdot\Theta_{\max}^2\mathrm{Wa2}_{\max}^2\cdot\mathrm{Ah2}_{\max}^2 + 8U_{\max}^2 = D_{\max}^2, \end{aligned} \tag{70}$$

where the subscript "max" represents the upper bound of the corresponding parameters' 2-norm, such as $\|\mathrm{Wc2}\| \le \mathrm{Wc2}_{\max}$.

Therefore, for any

$$\left\|\zeta_c(k)\right\| > \left(\frac{D_{\max}}{\sqrt{\lambda - (1/2) - (4/\psi)}}\right), \tag{71}$$

$\Delta V(k) \le 0$ holds. This indicates that the actual weights will converge to the optimal weights. In other words, the weight error δ_c and δ_a are uniformly bounded. This also results in a stable ADP system and an optimal output.

Furthermore, note that the components of Ch2 and Ah2 are limited to [−1, 1] due to the activation functions of the hidden nodes, that are

$$\begin{aligned} -1 \le \mathrm{Ch2}_i \le 1, \quad i = 1, \ldots, M, \\ -1 \le \mathrm{Ah2}_j \le 1, \quad j = 1, \ldots, N. \end{aligned} \tag{72}$$

So, there exist

$$\begin{aligned} \|\mathrm{Ch2}(k)\|^2 &= \sum_{i=1}^{M}\left[\mathrm{Ch2}_i(k)\right]^2 \le M, \\ \|\mathrm{Ah2}(k)\|^2 &= \sum_{j=1}^{N}\left[\mathrm{Ah2}_j(k)\right]^2 \le N. \end{aligned} \tag{73}$$

According to equation (67), some networks' parameters should satisfy

$$\begin{aligned} \frac{1}{\sqrt{2}} < \lambda < 1, \\ \zeta_c(k) < \frac{1}{\lambda^2 M}, \\ \zeta_a(k) < \frac{1}{N}, \\ \psi > \frac{4}{\lambda^2 - (1/2)}. \end{aligned} \tag{74}$$

Equation (74) provides a simple and intuitive guidance to select networks' structure and learning rate, while maintaining the stability of weights and ADP structure.

4.2. Improvement in Implementation. In the previous literature, when it comes to the training of feedforward networks, all weights usually need to be adjusted, so there are serious dependencies between different layers. Moreover, the algorithm based on gradient descent is widely applied to the learning of various feedforward neural networks. However, it is obvious that the learning method based on gradient descent is usually very slow and time-consuming because of improper learning steps, or it is easy to be overtrained and falls into local minima.

In order to make the training process as time-saving as possible and better meet the time matching between online training and practical applications, we can consider two ideas: one is based on Igelnik and Pao's theory [34], that is, for a single hidden-layer forward neural network, if the weights of input to hidden layer are randomly initialized and kept constant, as long as the number of hidden nodes is sufficient, the approximation error of the network can be arbitrarily small. The second is based on the extreme learning machine (ELM) proposed by Huang et al. [35, 36]. For a single hidden layer forward neural network, the weights of the input to hidden layer are initialized randomly and kept constant, and then the hidden nodes are arbitrarily selected. The weights of hidden to output layer are directly determined analytically by the Moore–Penrose inverse, without necessary to derive and calculate partial derivatives layer by layer such as the gradient descent method. The speed of extreme learning methods has been proven to be tens or even thousands of times that of ordinary gradient descent methods, and it can effectively reduce complexity and avoid local minima [37].

To facilitate implementation, this paper will adopt the first idea to improve the performance; that is, the weights Wc1 and Wa1 are randomly initialized in a finite interval and kept constant, and only the weights Wc2 and Wa2 are adjusted by the gradient descent algorithm, resulting in effectively avoiding excessive time consumption. As for the thinking based on extreme learning machine, it is only given here without in-depth discussion due to the limited space of this paper and the lack of theoretical guidance in the application of vehicles. We may make further analysis and give more rigorous theories to support the application in practical vehicle control in future research.

5. Simulations

In this section, the control strategy with ADP derived above is implemented to vehicle attitude control, and the

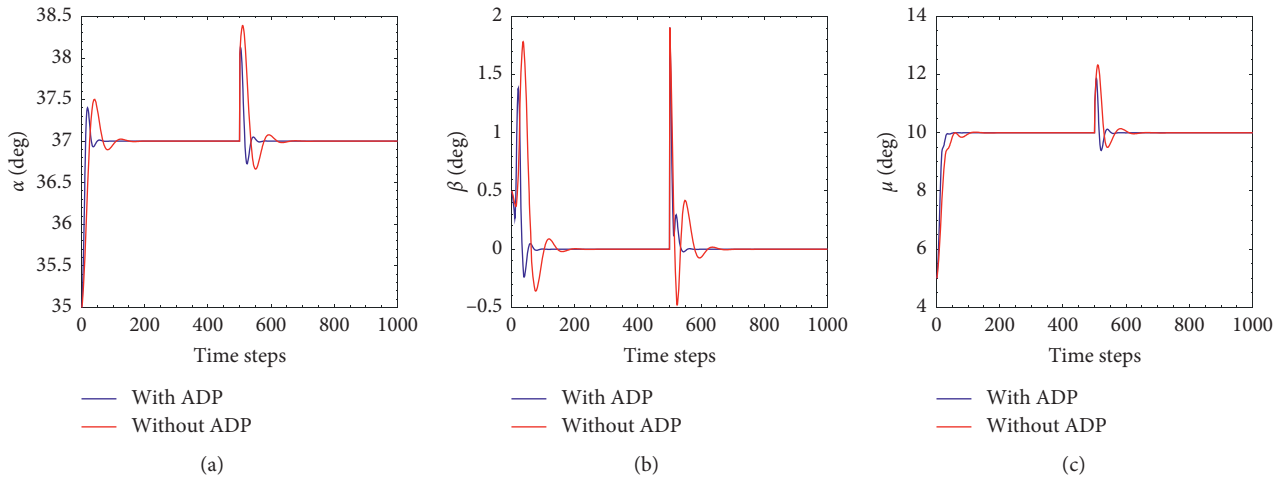

Figure 5: Tracking result of the three attitude angles. (a) The angle of attack α. (b) The sideslip angle β. (c) The bank angle μ.

effectiveness of the designed strategy is verified by comparing with the conventional controller without ADP.

According to a vehicle model in laboratory, the inertia matrix I is taken as

$$I = \begin{bmatrix} 135 & -20 & -1 \\ -20 & 1060 & -1 \\ -1 & -1 & 975 \end{bmatrix}. \quad (75)$$

The common parameters are taken as follows: $\rho_\gamma = \text{diag}\{1, 1, 1\}$, $\rho_w = \text{diag}\{0.5, 0.5, 0.5\}$; the width $\xi_\gamma = \xi_w = 2$ in the saturation function; $\tau_\gamma = \tau_w = 0.2$. The number of hidden nodes is $M = N = 8$. According to equation (74), the discount factor takes $\lambda = 0.9$ with learning rate $\zeta_c(k) < 0.155$, $\zeta_a(k) < 0.125$. Take $\Lambda = \text{diag}\{1, 1, 1\}$, and all weights are randomly initialized in $[-0.2, 0.2]$.

Set the initial flight state of the vehicle as $\gamma_0 = [35, 0.5, 5]^T$ deg and $w_0 = [0, 0, 0]^T$ (rad/s). The desired attitude instruction is $\gamma_d = [37, 0, 10]^T$ deg, and the simulation step size is 0.02 s. To verify the performance of the controller, pulsed disturbances $d_1 = d_2 = [10, 20, 10]$ will be added at 10 s.

Figure 5 presents the tracking results of the three attitude angles. As can be seen from these figures, the controller with ADP is more responsive than the controller without ADP. For example, the controller with ADP can accurately track instructions within 100 steps and cause less overshoot, while the controller without ADP requires about 200 steps. When external disturbances are added at 10 s, the controller with ADP also responds more quickly and with less overshoot. Through these, it can be seen that ADP improves the performance of the system.

The controller with ADP shows faster performance and less overshoot, which benefits from the ADP structure's auxiliary behaviour to the outer loop. Through the training process that meets the expected threshold, the ADP structure generates the auxiliary optimal control signal to compensate for the deficiency of the outer loop main controller 1 in eliminating attitude error. Figures 6–11 show the training process of the ADP network. Specifically,

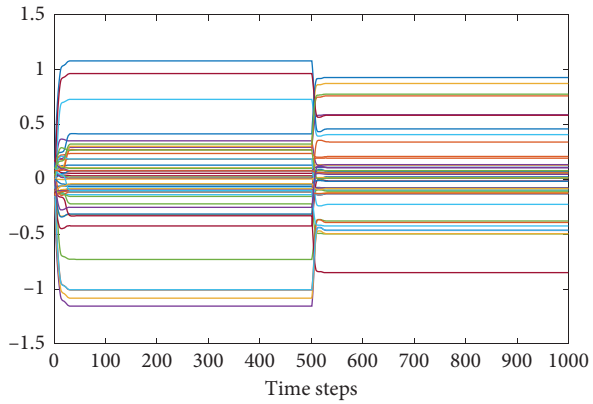

Figure 6: Wc1.

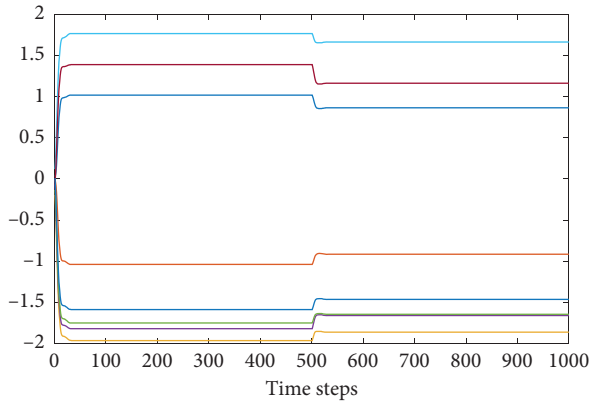

Figure 7: Wc2.

Figures 6–9 show the dynamic adjustment of network weights. Figures 10 and 11 are the estimated value of the cost function output by the critic network and the optimal control signal output by the action network. Compared to the previous Figures 5, 6–9 show the rapid adjustment of the network weights at the beginning stage to achieve the

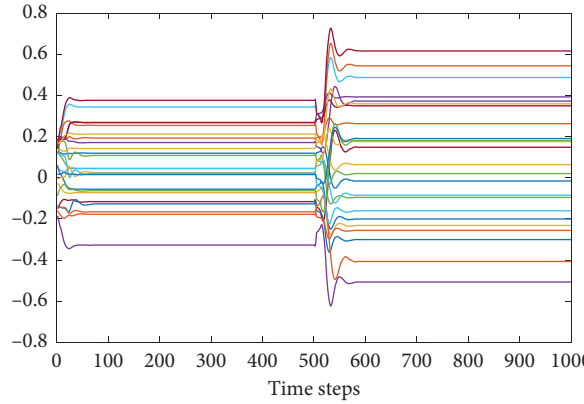

Figure 8: Wa1.

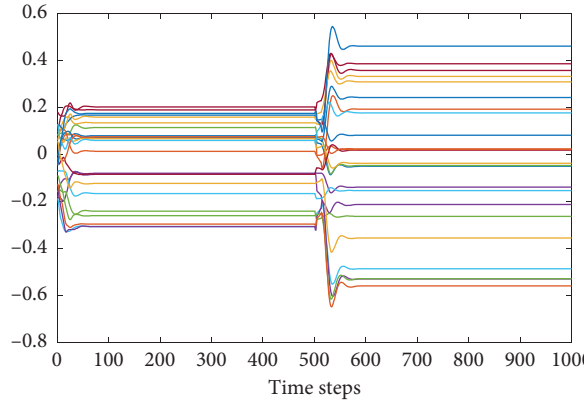

Figure 9: Wa2.

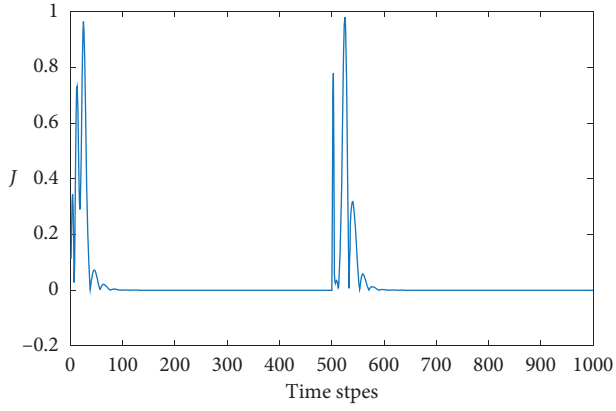

Figure 10: Estimated cost function J.

purpose of tracking instructions. As the system output gradually keeps up with the instructions, the weights also converge to the optimal weights (W^* as demonstrated in Section 4) and remain stable. When the external disturbances are added at 10 s, the network weights are adjusted again and tend to other optimal weights. It shows that ADP produces auxiliary output to play a certain role at the beginning and when disturbance appears.

According to the thinking and analysis in Section 4.2, when implementing this control strategy, it can be considered that randomly initializing the weights of the input to hidden layer (Wc1 and Wa1) and keeping them constant. During the training, only adjusting the weights Wc2 and Wa2 can not only achieve the same optimal control goal but also greatly reduce the time consumption. Figures 12 and 13 show the corresponding weight changes. Simultaneously, Figure 14 shows the comparison of time consumption in 12 group simulations. It can be further concluded that the average time consumption of maintaining the weights of the input-to-hidden layer (Wc1 and Wa1) and only adjusting the weights of the hidden-to-output layer (Wc2 and Wa2) is 31.9% lower than that of adjusting all weights. Although the sample in Figure 14 is limited, combined with the analysis in Section 4.2 and neural network theory, the effectiveness of this idea in reducing time consumption and improving efficiency is significant.

Furthermore, Figures 15–19 show the tracking control results of time-varying attitude commands, using the controller with ADP. The pulsed disturbances $d = [5, 1, 1]^{\mathrm{T}}$ and $d = [10, 2, 2]^{\mathrm{T}}$ are introduced at 10 s and 20 s, respectively, as shown by the yellow arrow in the figures. From Figures 15–17, it can be seen that the controller with ADP auxiliary structure can make the actual attitude angles accurately track the commands. Figures 18–19 show the weights of action network

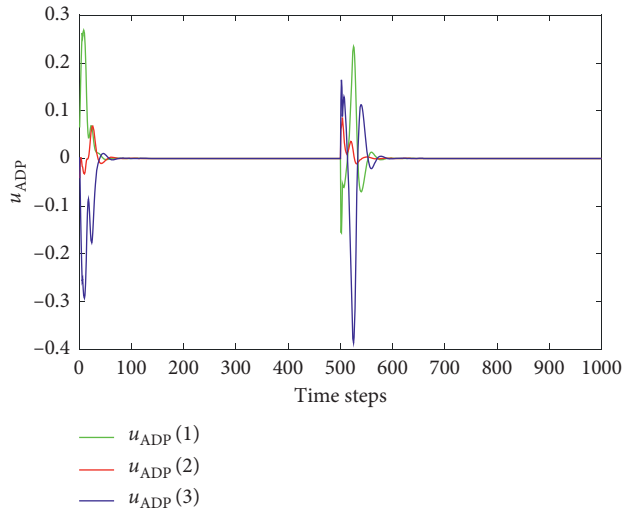

Figure 11: Optimal control signal u_{ADP}.

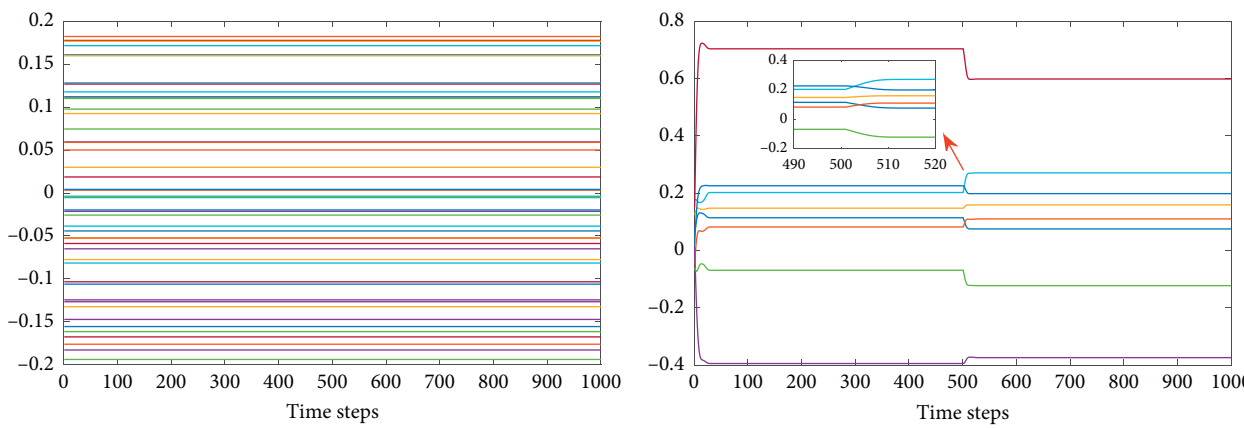

Figure 12: Keep (a) Wc1 and update (b) Wc2.

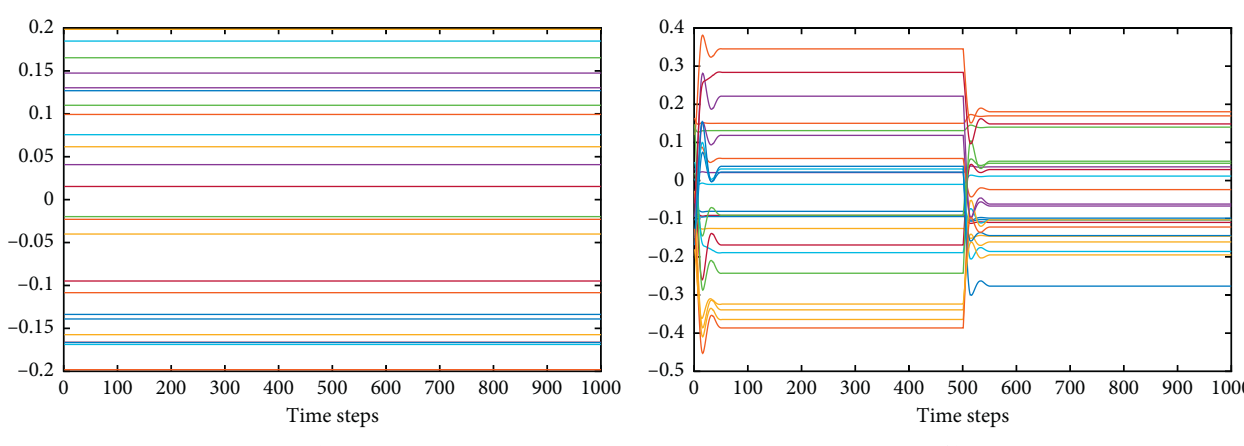

Figure 13: Keep (a) Wa1 and update (b) Wa2.

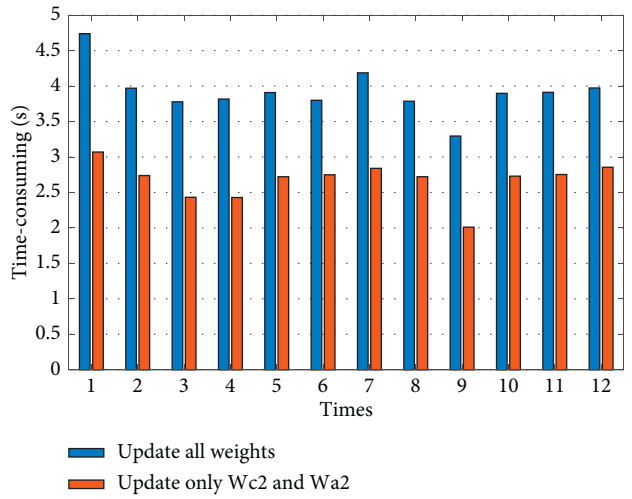

Figure 14: Comparison of time consumption in 12 group simulations.

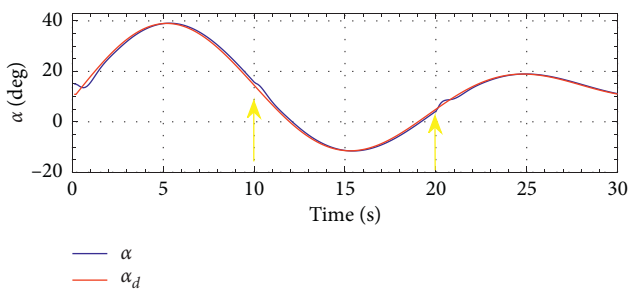

Figure 15: Tracking result of the angle of attack α.

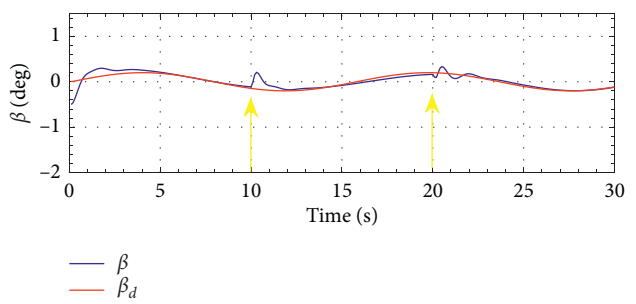

Figure 16: Tracking result of the sideslip angle β.

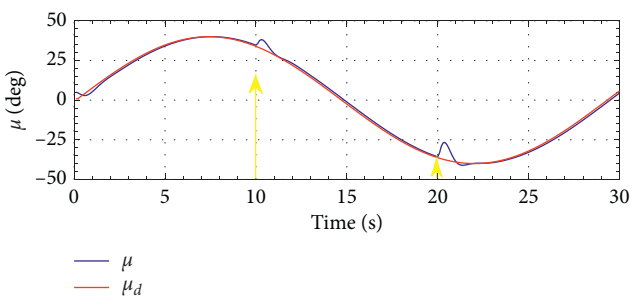

Figure 17: Tracking result of the bank angle μ.

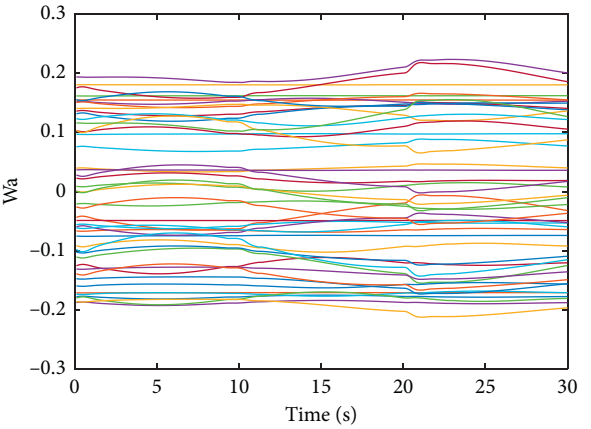

Figure 18: Wa1 of action network.

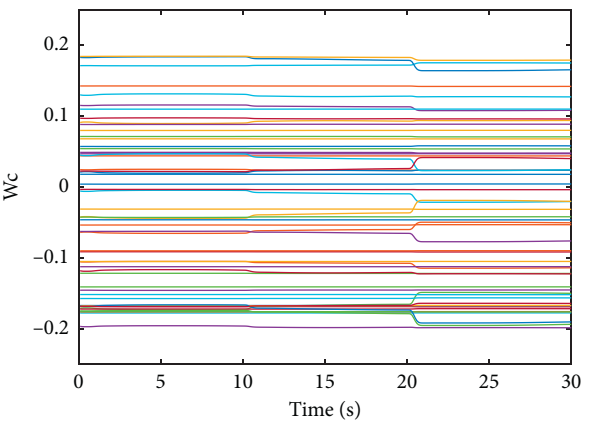

Figure 19: Wc1 of critic network.

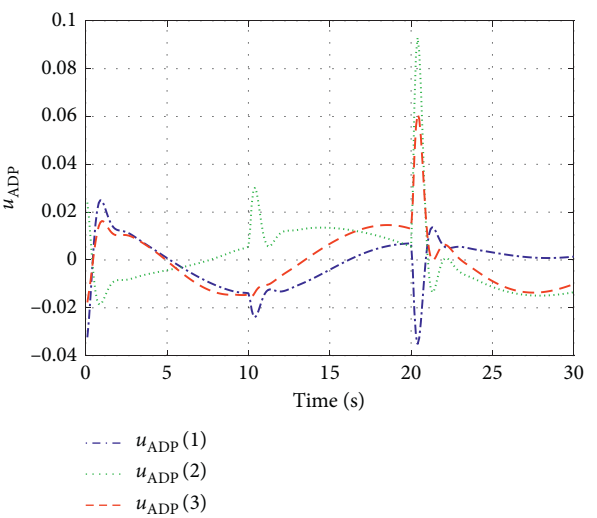

Figure 20: Optimal control signal u_{ADP}.

and critic network in ADP. The weights of the action network are dynamically adjusted to output the optimal auxiliary control signal u_{ADP} in real time, as shown in Figure 20. Figure 21 shows the control torque acting on the vehicle. From

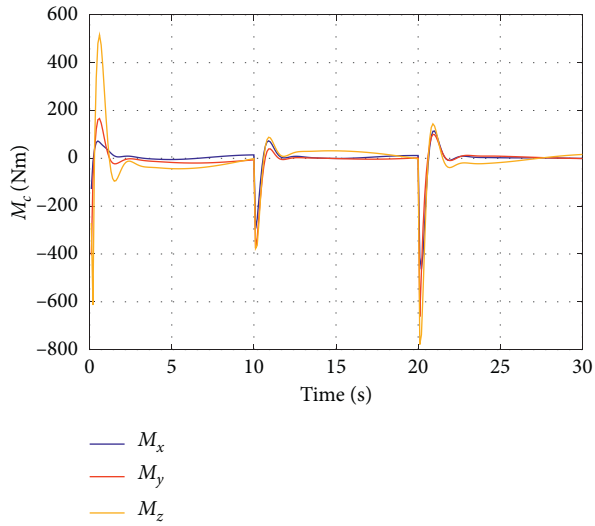

Figure 21: Control inputs M_c.

these, it can be seen that the controller with ADP auxiliary structure has good dynamic stability performance.

6. Conclusions

Combining the hottest reinforcement learning at present, this paper presents an ADP-based attitude control methodology for reentry vehicles, applying the ADP to the three-channel attitude control. First, a nonlinear model of the three-channel attitude system is established, and it is divided into inner and outer loops according to the principle of time scale separation. Both the inner and outer loops utilize a conventional sliding mode controller as the main controller, and an auxiliary ADP framework is introduced to the outer loop. When facing the vehicle's nonlinearity and sudden disturbances in particular, the main controller is easy to be weak due to its lack of sufficient adaptability. At this time, the auxiliary role of ADP will be fully exerted. Because ADP uses the critic network and action network, ADP structure has good learning ability. It generates the optimal auxiliary signal immediately after learning the tracking error to compensate for the deficiency of the main controller and improves the adaptability and response speed of the entire control system. For implementation, this paper discusses selection strategies of the ADP parameter and some tips for speeding up training. And the stability is proved by the Lyapunov method. Finally, simulation results of step and time-varying commands demonstrate the effectiveness of the designed scheme for the nonlinear attitude system.

In the future work, we will focus on some switching or event-triggered strategies for this structure with dual controllers. Imagining that if the ADP auxiliary structure is event-triggered rather than time-triggered, it will greatly reduce consumption of ADP's time and system resources, to improve efficiency.

Data Availability

Some data used in this article are confidential, but other public data can be obtained by contacting li_xu@hust.edu.cn.

Conflicts of Interest

The authors declare that there are no conflicts of interest regarding the publication of this paper.

Acknowledgments

This work was supported partially by the National Natural Science Foundation of China under grant nos. 61873319, 61903146, and 61803162.

References

[1] Z. Gao and J. Fu, "Robust LPV modeling and control of aircraft flying through wind disturbance," *Chinese Journal of Aeronautics*, vol. 32, no. 7, pp. 1588–1602, 2019.

[2] G. Wu, X. Meng, and F. Wang, "Improved nonlinear dynamic inversion control for a flexible air-breathing hypersonic vehicle," *Aerospace Science and Technology*, vol. 78, pp. 734–743, 2018.

[3] I. Ali, G. Radice, and J. Kim, "Backstepping control design with actuator torque bound for spacecraft attitude maneuver," *Journal of Guidance, Control, and Dynamics*, vol. 33, no. 1, pp. 254–259, 2010.

[4] Q. Hu, J. Cao, and Y. Zhang, "Robust backstepping sliding mode attitude tracking and vibration damping of flexible spacecraft with actuator dynamics," *Journal of Aerospace Engineering*, vol. 22, no. 2, pp. 139–152, 2009.

[5] Z. Zhen, P. Zhu, J. Jiang, and G. Tao, "Research progress of adaptive control for hypersonic vehicle in near space," *Journal of Astronautics*, vol. 39, no. 4, pp. 355–367, 2018.

[6] A. H. J. de Ruiter, "Observer-based adaptive spacecraft attitude control with guaranteed performance bounds," *IEEE Transactions on Automatic Control*, vol. 61, no. 10, pp. 3146–3151, 2016.

[7] Y. Liu, Z. Pu, and J. Yi, "Observer-based robust adaptive T2 fuzzy tracking control for flexible air-breathing hypersonic vehicles," *IET Control Theory & Applications*, vol. 12, no. 8, pp. 1036–1045, 2018.

[8] C. Wang, M. Liang, and Y. Chai, "Adaptive neural network control of a class of fractional order uncertain nonlinear MIMO systems with input constraints," *Complexity*, vol. 2019, Article ID 5643298, 17 pages, 2019.

[9] S. G. Khan, G. Herrmann, F. L. Lewis, T. Pipe, and C. Melhuish, "Reinforcement learning and optimal adaptive control: an overview and implementation examples," *Annual Reviews in Control*, vol. 36, no. 1, pp. 42–59, 2012.

[10] T. Mannucci, E.-J. van Kampen, C. de Visser, and Q. Chu, "Safe exploration algorithms for reinforcement learning controllers," *IEEE Transactions on Neural Networks and Learning Systems*, vol. 29, no. 4, pp. 1069–1081, 2018.

[11] J. Shin, T. A. Badgwell, K.-H. Liu, and J. H. Lee, "Reinforcement learning—overview of recent progress and implications for process control," *Computers & Chemical Engineering*, vol. 127, pp. 282–294, 2019.

[12] A. Heydari, "Theoretical and numerical analysis of approximate dynamic programming with approximation errors," *Journal of Guidance, Control, and Dynamics*, vol. 39, no. 2, pp. 301–311, 2016.

[13] C. Yang, Y. Xu, L. Zhou, and Y. Sun, "Model-free composite control of flexible manipulators based on adaptive dynamic programming," *Complexity*, vol. 2018, Article ID 9720309, 9 pages, 2018.

[14] Y. Sokolov, R. Kozma, L. D. Werbos, and P. J. Werbos, "Complete stability analysis of a heuristic approximate dynamic programming control design," *Automatica*, vol. 59, pp. 9–18, 2015.

[15] Z. Ni, H. He, X. Zhong, and D. V. Prokhorov, "Model-free dual heuristic dynamic programming," *IEEE Transactions on Neural Networks and Learning Systems*, vol. 26, no. 8, pp. 1834–1839, 2015.

[16] C. Mu, Y. Zhang, Y. Yu, and C. Sun, "An overview on robust control of aviation and aerospace aircraft based on adaptive dynamic programming," *Aerospace Control and Application*, vol. 45, no. 4, pp. 71–79, 2019.

[17] X. Luo, Y. Chen, J. Si, and F. Liu, "Longitudinal control of hypersonic vehicles based on direct heuristic dynamic programming using ANFIS," in *Proceedings of the 2014 International Joint Conference on Neural Networks (IJCNN)*, pp. 3685–3692, Beijing, China, July 2014.

[18] J. Zhu, X. Ge, and M. Wang, "Approximate dynamic programming for attitude control of three-axis satellite," *Journal of Beijing Information Science and Technology University*, vol. 33, no. 1, pp. 27–32, 2018.

[19] Y.-H. Cheng, B. Jiang, H. Li, and X.-d. Han, "On-orbit reconfiguration using adaptive dynamic programming for multi-mission-constrained spacecraft attitude control system," *International Journal of Control, Automation and Systems*, vol. 17, no. 4, pp. 822–835, 2019.

[20] C. Mu, Z. Ni, C. Sun, and H. He, "Data-driven tracking control with adaptive dynamic programming for a class of continuous-time nonlinear systems," *IEEE Transactions on Cybernetics*, vol. 47, no. 6, pp. 1460–1470, 2017.

[21] C. Mu, Z. Ni, C. Sun, and H. He, "Air-breathing hypersonic vehicle tracking control based on adaptive dynamic programming," *IEEE Transactions on Neural Networks and Learning Systems*, vol. 28, no. 3, pp. 584–598, 2017.

[22] C. Dong, C. Liu, Q. Wang, and L. Gong, "Switched adaptive active disturbance rejection control of variable structure near space vehicles based on adaptive dynamic programming," *Chinese Journal of Aeronautics*, vol. 32, no. 7, pp. 1684–1694, 2019.

[23] Q. Xie, F. Tan, B. Luo, and X. Guan, "Optimal control for vertical take-off and landing aircraft non-linear system by online kernel-based dual heuristic programming learning," *IET Control Theory & Applications*, vol. 9, no. 6, pp. 981–987, 2015.

[24] Y. Zhou, E.-J. van Kampen, and Q. P. Chu, "Incremental model based online dual heuristic programming for nonlinear adaptive control," *Control Engineering Practice*, vol. 73, pp. 13–25, 2018.

[25] Y. Zhou, E.-J. van Kampen, and Q. Chu, "Incremental approximate dynamic programming for nonlinear adaptive tracking control with partial observability," *Journal of Guidance, Control, and Dynamics*, vol. 41, no. 12, pp. 2554–2567, 2018.

[26] Y. Zhou, E.-J. van Kampen, and Q. Chu, "Nonlinear adaptive flight control using incremental approximate dynamic programming and output feedback," *Journal of Guidance, Control, and Dynamics*, vol. 40, no. 2, pp. 493–500, 2017.

[27] B. Sun and E.-J. van Kampen, "Incremental model-based global dual heuristic programming with explicit analytical calculations applied to flight control," *Engineering Applications of Artificial Intelligence*, vol. 89, Article ID 103425, 2020.

[28] B. Sun and E.-J. van Kampen, "Incremental model-based global dual heuristic programming for flight control," *IFAC-PapersOnLine*, vol. 52, no. 29, pp. 7–12, 2019.

[29] J. J. Recasens, Q. P. Chu, and J. A. Mulder, "Robust model predictive control of a feedback linearized system for a lifting-body re-entry vehicle," in *Proceedings of the AIAA Guidance, Navigation, and Control Conference and Exhibit (Guidance, Navigation, and Control and Co-Located Conferences*, pp. 1–33, American Institute of Aeronautics and Astronautics, San Francisco, CA, USA, August 2005.

[30] R. Zhai, R. Qi, and J. Zhang, "Compound fault-tolerant attitude control for hypersonic vehicle with reaction control systems in reentry phase," *ISA Transactions*, vol. 90, pp. 123–137, 2019.

[31] E.-J. van Kampen, Q. P. Chu, and J. A. Mulder, "Continuous adaptive critic flight control aided with approximated plant dynamics," in *Proceedings of the AIAA Guidance, Navigation, and Control Conference and Exhibit*, August 2006.

[32] J. Si and Y. T. Wang, "Online learning control by association and reinforcement," *IEEE Transactions on Neural Networks*, vol. 12, no. 2, pp. 264–276, 2001.

[33] S. Puntanen, G. P. H. Styan, and J. Isotalo, "The Cauchy–Schwarz inequality," in *Matrix Tricks for Linear Statistical Models*, pp. 415–426, Springer, Berlin, Germany, 2011.

[34] B. Igelnik and Y. H. Pao, "Stochastic choice of basis functions in adaptive function approximation and the functional-link net," *IEEE Transactions on Neural Networks*, vol. 6, no. 6, pp. 1320–1329, 1995.

[35] G. Huang, G.-B. Huang, S. Song, and K. You, "Trends in extreme learning machines: a review," *Neural Networks*, vol. 61, pp. 32–48, 2015.

[36] G. B. Huang, Q. Y. Zhu, and C. K. Siew, "Extreme learning machine: a new learning scheme of feedforward neural networks," in *Proceedings of the 2004 IEEE International Joint Conference on Neural Networks (IJCNN)*, vol. 1–4, pp. 985–990, Budapest, Hungary, July 2004.

[37] G. B. Huang, Q. Y. Zhu, and C. K. Siew, "Extreme learning machine: theory and applications," *Neurocomputing*, vol. 70, no. 1–3, pp. 489–501, 2006.

Hindawi
Complexity
Volume 2020, Article ID 3510396, 11 pages
https://doi.org/10.1155/2020/3510396

Research Article

A Robust Control Scheme for a PVTOL System Subject to Wind Disturbances

Carlos Alejandro Merlo-Zapata,[1] Carlos Aguilar-Ibanez,[2] Octavio Gutiérrez-Frías,[3] Mayra Antonio-Cruz,[4] Celso Márquez-Sánchez,[5] and Miguel S. Suarez-Castanon[6]

[1]*Tecnológico Nacional de México, Instituto Tecnológico de Iztapalapa, Departamento de Ciencias Básicas, Ciudad de México 09208, Mexico*
[2]*CIC, Instituto Politécnico Nacional, Unidad Profesional Adolfo López Mateos, Ciudad de México 07700, Mexico*
[3]*SEPI, UPIITA, Instituto Politécnico Nacional, La Laguna Ticoman, Ciudad de México 07340, Mexico*
[4]*Instituto Politécnico Nacional, UPIICSA, SEPI, Mexico City 08400, Mexico*
[5]*Tecnológico Nacional de México, Instituto Tecnológico de Iztapalapa, Departamento de Sistemas y Computación, Ciudad de México 09208, Mexico*
[6]*SEPI, ESCOM, Instituto Politécnico Nacional, Unidad Profesional Adolfo López Mateos, Ciudad de México 07700, Mexico*

Correspondence should be addressed to Octavio Gutiérrez-Frías; ogutierrezf@ipn.mx

Received 19 May 2020; Revised 21 July 2020; Accepted 31 July 2020; Published 1 September 2020

Guest Editor: Raúl Villafuerte-Segura

Copyright © 2020 Carlos Alejandro Merlo-Zapata et al. This is an open access article distributed under the Creative Commons Attribution License, which permits unrestricted use, distribution, and reproduction in any medium, provided the original work is properly cited.

In this study, a control scheme that allows performing height position regulation and stabilization for an unmanned planar vertical take-off and landing aerial vehicle, in the presence of disturbance due to wind, is presented. To this end, the backstepping procedure together with nested saturation function method is used. Firstly, a convenient change of coordinates in the aerial vehicle model is carried out to dissociate the rotational dynamics from the translational one. Secondly, the backstepping procedure is applied to obtain the height position controller, allowing the reduction of the system and expressing it as an integrator chain with nonlinear disturbance. Therefore, the nested saturation function method is used to obtain a stabilizing controller for the horizontal position and roll angle. The corresponding stability analysis is conducted via the Lyapunov second method. In addition, to estimate the disturbance due to wind, an extended state observer is used. The effectiveness of the proposed control scheme is assessed through numerical simulations, from which convincing results have been obtained.

1. Introduction

The Planar Vertical Take-Off and Landing (PVTOL) unmanned aerial vehicle is a representation of the Harrier Yab-8b aircraft when considering a minimum of inputs and outputs to obtain a vertical short take-off and landing behavior [1], which has been used as a test bed for automatic control applications. In fact, the PVTOL aerial vehicle is a simplified model that embodies the behavior of several actual vertical take-off and landing aircraft, which ultimately makes it a suitable benchmark to test new and existing controllers. Therefore, there is a vast literature on the subject. However, a current and open challenge is the design of robust controllers for the PVTOL system under wind disturbance in order to pursue outdoor applications. Thus, this paper presents a robust control scheme for a PVTOL system subjected to disturbance due to wind.

The works considered most relevant and closely related to the control problem treated in this study are mentioned as follows. In [1], an input-output linearization to achieve trajectory tracking control for the non-minimum phase nonlinear system is presented. In [2], the authors developed a nonlinear output-feedback controller for the trajectory tracking of a reference model by using a global exponential observer, coordinate transformations, the Lyapunov's method, and an extension of

backstepping. In [3], a global stabilization control derived from nonlinear combinations of linear saturation functions was presented, whereas in [4], a nonlinear controller for taking-off, hovering, tracking of a straight line, and landing of the PVTOL system was introduced. The corresponding experimental implementation of the controller was reported in [5], where a camera was used to estimate the position and orientation of the PVTOL vehicle. Also, in [6], a global configuration stabilization for the VTOL aircraft with a strong input coupling using a smooth static state feedback was reported. An alternative feedback-based stabilization law to the one introduced in [6] was presented in [7]. This law simplifies the term that connects the state vector with the dynamics error. In [8], the authors designed a stabilization control by transforming the system into an integrator chain plus a nonlinear disturbance, after which the saturation technique was used so that neither backstepping/forwarding approaches nor small gain analysis is required. Furthermore, a nonlinear controller for a PVTOL vehicle, based on prediction and partial feedback linearization, was designed in [9]. A robust and linear state-feedback gain-scheduled control to achieve hovering of a PVTOL system with uncertainties in the mass, the momentum of inertia, and the parasitic coupling parameter was introduced in [10], while a nested set stabilization approach to locally solve path following for the PVTOL system was introduced in [11]. The system center of mass was constrained to lie on the path, and the roll angle should be specified at any given point on the path. In [12], the authors developed a bounded backstepping method to achieve input-to-state stability, with respect to the actuator errors, and to force all trajectories of the system to track a reference trajectory for all initial configurations. Also, Zavala-Río et al. [13] introduced a finite-time observer-based output-feedback control for the global stabilization of both taking-off and landing of the PVTOL system. In [14–16], a solution for the regulation of a simplified version of the PVTOL system was reported, which consisted of two control actions that act simultaneously. Aguilar-Ibáñez et al. [14] used, as first action, a feedback linearization along with a saturation function to asymptotically stabilize the vertical position. For the second action, backstepping was exploited to stabilize both the horizontal and the angle positions. Similarly, Aguilar-Ibañez et al. [15] utilized as first action a feedback linearization in combination with a nonlinear controller to stabilize the vertical variable. The other action stabilizes the horizontal and angular variables to the desired rest position through an energy-control method, whereas Aguilar-Ibañez [16] employed again a feedback linearization with a saturation function to stabilize the vertical variable, while a PD-controller and a sliding-mode controller were used to stabilize both the horizontal and angular variables. Moreover, Yu-Chan et al. [17] dealt with the stabilization of the PVTOL system with unknown model parameters by applying a sliding-mode technique to design a state feedback control law. Recently, in [18], a controller for the stabilization of the PVTOL vehicle was designed on the basis of the immersion and invariance control technique. The controller gives priority to the control of the aircraft's altitude before controlling the lateral displacement. More recently, in [19], a cascade active disturbance rejection controller was introduced to counteract the adverse effects caused by an actuator failure in the PVTOL aircraft, while Escobar et al. [20] were focused on finding conditions to determine local asymptotic stability using a feedback linearization control for the PVTOL platform, so that reaching any singularity due to the transformation of the system is prevented. Aguilar-Ibanez et al. [21] introduced an output-feedback regulation control law for a PVTOL aircraft, based on a version of the matching control energy method. Such a control was improved to compensate bounded, smooth, and matching perturbations with a suitable finite time-varying identificator. Finally, Aguilar-Ibanez et al. [22] proposed a robust controller to solve the trajectory-tracking control problem of PVTOL aircraft under crosswind by applying an input-output feedback linearization to the PVTOL model under no crosswind conditions. Thus, the resulting linearized system under the crosswind effects is controlled using an active disturbance rejection control approach to counteract the effects of these perturbations.

Having reviewed the literature, it was found that almost all the works mentioned above were developed to test the PVTOL system indoor, mainly to avoid the undesirable effect produced by the wind (instability and, even, the collapse of the PVTOL system), which is not easy to counteract. Therefore, few controllers are robust under unknown model parameters, actuator failure, and crosswind. Thus, with the intention of contributing to overcome wind undesirable effects, a robust control scheme that combines a backstepping approach and a nested saturation function-based controller is proposed herein to perform taking-off maneuvers in the presence of disturbance due to wind. The backstepping is used to carry out the trajectory tracking task over the vertical position of the PVTOL system and, consequently, to control the height position. Then, from a set of convenient linear transformations, the system is represented as an integrator chain with a nonlinear perturbation, for which a nested saturation function-based controller is developed to stabilize the horizontal position and roll angle. This is carried out by satisfying stability conditions obtained from application of the second method of Lyapunov. Therefore, boundedness of each state and asymptotic convergence to the origin are ensured. Lastly, to estimate the disturbance due to the wind, an extended state observer is used.

The remaining of the paper is organized as follows. In Section 2, the PVTOL system and its dynamics are introduced. In Section 3 the design of the backstepping controller to perform trajectory tracking for the height position of the system is presented. In Section 4, the controller based on nested saturation functions for stabilization of the horizontal position and the roll angle is designed. The extended state observer is introduced in Section 5. In Section 6, the outcome of numerical simulations that show the behavior of the proposed control scheme is reported. Finally, Section 7 is devoted to the concluding remarks.

2. PVTOL System

Here, the PVTOL system and its dynamic model considering a disturbance due to wind are presented.

The PVTOL system emulates the vertical take-off and landing of an aerial vehicle, whereas it is automatically stabilized. Hence, in practice, this system has a rigid structure and two motors collocated at the ends of the structure, as can be seen in Figure 1, where θ_1 is the roll angle, x_1 is the horizontal position in the x axis, y_1 is the vertical position in the y axis, f_1 and f_2 are the forces produced by the motors, L is the distance between the center of the rigid structure to the center of the motors, m is the mass of the system, and g is the gravitational acceleration.

The representation in state variables of the PVTOL dynamic model, when L, m, and g are normalized, has been previously reported in [1] and used in [14, 23, 24], which is given by

$$\begin{aligned}
\dot{x}_1 &= \dot{x}_2,\\
\dot{x}_2 &= -u_1 \sin\theta_1 + \epsilon u_2 \cos\theta_1,\\
\dot{y}_1 &= y_2,\\
\dot{y}_2 &= u_1 \cos\theta_1 + \epsilon u_2 \sin\theta_1 - 1,\\
\dot{\theta}_1 &= \theta_2,\\
\dot{\theta}_2 &= u_2 + A_L,
\end{aligned} \tag{1}$$

where x_1, $x_2 = \dot{x}_1$, y_1, $y_2 = \dot{y}_1$, θ_1, and $\theta_2 = \dot{\theta}_1$ are the state variables, $u_1 = f_1 + f_2$ and $u_2 = f_1 - f_2$ are the control inputs, ϵ is the coefficient giving the coupling between the rolling moment and the lateral acceleration, and A_L is the rolling moment due to the air, defined by Gomes and Ramos [25] as

$$A_L = \left(\frac{1}{2}\right)\rho C_l U^2 V_a, \tag{2}$$

with ρ being the air density, C_l being the nondimensional coefficient of the rolling moment in the standard convention for airships, U being the air speed, and V_a being the airship model volume. That is, A_L is considered as a disturbance due to wind.

3. Height Position Control

To obtain the height position control, we apply the following global coordinate change [26] to model (1):

$$\begin{aligned}
\overline{x}_1 &= x_1 - \epsilon \sin\theta_1,\\
\overline{x}_2 &= x_2 - \epsilon\theta_2 \cos\theta_1,\\
\overline{y}_1 &= y_1 + \epsilon(\cos\theta_1 - 1),\\
\overline{y}_2 &= y_2 - \epsilon\theta_2 \sin\theta_1,\\
\overline{\theta}_1 &= \theta_1,\\
\overline{\theta}_2 &= \theta_2.
\end{aligned} \tag{3}$$

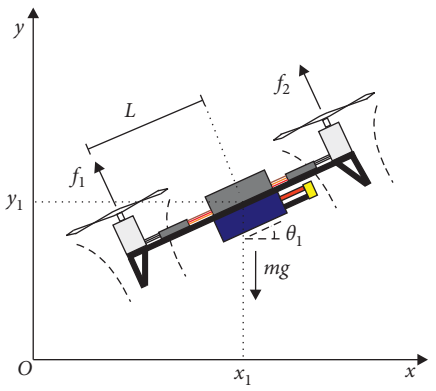

Figure 1: Diagram of the PVTOL system.

Also, we introduce $\overline{A}_L = A_L - \widehat{A}_L$, where $\widehat{A}_L$ is an estimation of the disturbance due to wind carried out by an extended state observer, which is described later in Section 5. Thus, model (1) is transformed into the following system:

$$\begin{aligned}
\dot{\overline{x}}_1 &= \overline{x}_2,\\
\dot{\overline{x}}_2 &= -\overline{u}_1 \sin\overline{\theta}_1 - \epsilon\overline{A}_L \cos\overline{\theta}_1,\\
\dot{\overline{y}}_1 &= \overline{y}_2,\\
\dot{\overline{y}}_2 &= \overline{u}_1 \cos\overline{\theta}_1 - \epsilon\overline{A}_L \sin\overline{\theta}_1 - 1,\\
\dot{\overline{\theta}}_1 &= \overline{\theta}_2,\\
\dot{\overline{\theta}}_2 &= u_2 + \overline{A}_L,
\end{aligned} \tag{4}$$

where $\overline{u}_1 = u_1 - \epsilon\overline{\theta}_2^2$ is a new control input.

From this point, the backstepping procedure can be applied to force the system to track a desired trajectory and, consequently, to reach a desired height position. To this end, an error is defined as follows:

$$e_y = \overline{y}_{1_d} - \overline{y}_1, \tag{5}$$

with $\overline{y}_{1_d}$ being the desired height position. Then, the method of Lyapunov is used, considering the following candidate function:

$$V(e_y) = \left(\frac{1}{2}\right)e_y^2, \tag{6}$$

which is positive definite and whose time derivative results in

$$\dot{V}(e_y) = e_y\left(\dot{\overline{y}}_{1_d} - \overline{y}_2\right). \tag{7}$$

To ensure the stabilization of e_y, the auxiliary control, $\overline{y}_2$, is proposed as

$$\overline{y}_2 = \dot{\overline{y}}_{1_d} + \alpha_1 e_y, \tag{8}$$

with $\alpha_1 > 0$, so that (7) results in the following negative semidefinite expression:

$$\dot{V}(e_y) = -\alpha_1 e_y^2. \tag{9}$$

Then, it is proceeded with the following change of variables:

$$e_{2y} = \overline{y}_2 - \dot{\overline{y}}_{1_d} - \alpha_1 e_y. \tag{10}$$

So, the augmented Lyapunov function is given by

$$V\left(e_y, e_{2y}\right) = \left(\frac{1}{2}\right)\left(e_y^2 + e_{2y}^2\right), \tag{11}$$

whose time derivative is determined by

$$\begin{aligned}\dot{V}\left(e_y, e_{2y}\right) = &-e_y e_{2y} - \alpha_1 e_y^2 + e_{2y} \\ &\cdot \left(\overline{u}_1 \cos\overline{\theta}_1 - 1 - \epsilon\overline{A}_L \sin\overline{\theta}_1\right) \\ &- e_{2y}\left[\ddot{\overline{y}}_{1_d} + \alpha_1\left(-e_{2y} - \alpha_1 e_y\right)\right].\end{aligned} \tag{12}$$

To facilitate the proposal of $\overline{u}_1$ that ensures stabilization of e_{2y}, let us make (12) equal to zero for a moment and solve for $\overline{u}_1$. Since $\ddot{\overline{y}}_{1_d} = 0$ is considered because it is the desired acceleration of the height position, $\overline{u}_1$ is found as follows:

$$\overline{u}_1 = \frac{1}{\cos\overline{\theta}_1}\left[e_y + \alpha_1\left(\frac{e_y^2}{e_{2y}}\right) + \alpha_1\left(-e_{2y} - \alpha_1 e_y\right) + 1 + \epsilon\overline{A}_L \sin\overline{\theta}_1\right]. \tag{13}$$

Note that in order to avoid indeterminate (13), $-(\pi/2) < \overline{\theta}_1 < +(\pi/2)$ is required.

Taking into account the previous result and proposing $\alpha_1(e_y^2/e_{2y}) = -(\alpha_2 e_{2y})$, it is clear that the stabilization of the control system is accomplished if $\overline{u}_1$ is selected as follows:

$$\overline{u}_1 = \frac{1}{\cos\overline{\theta}_1}\left[e_y - \alpha_2 e_{2y} + \alpha_1\left(-e_{2y} - \alpha_1 e_y\right) + 1 + \epsilon\overline{A}_L \sin\overline{\theta}_1\right], \tag{14}$$

because it achieves

$$\dot{V}\left(e_y, e_{2y}\right) = -\left(\alpha_1 e_y^2\right) - \left(\alpha_2 e_{2y}^2\right) < 0, \tag{15}$$

with $\alpha_1 > 0$, $\alpha_2 > 0$ and $-(\pi/2) < \overline{\theta}_1 < +(\pi/2)$. Hence, $\overline{y}_1 \longrightarrow \overline{y}_{1_d}$, that is, the PVTOL system reaches the desired height position.

4. Control of the Horizontal Position and Roll Angle

In this section, a nested saturation function-based controller for the stabilization of the horizontal position, $\overline{x}_1$, and roll angle, $\overline{\theta}_1$, is developed [27]. This technique has been used for the stabilization of nonlinear systems that can be approximately expressed as integrator chain [28–30]. To solve the PVTOL system stability problem, first a linear transformation to propose the stabilizing controller is used. Then, it is showed that the proposed controller guarantees the boundedness of all states and, after a finite time, the closed-loop system is asymptotically stable.

Before developing the control strategy, the definition of a saturation function is introduced.

Definition 1 (see [31]). A linear saturation function $\sigma_b(s)$: $\mathbb{R} \longrightarrow \mathbb{R}$ is defined as

$$\sigma_b(s) = \begin{cases} s, & \text{if } |s| \le b, \\ b \cdot \text{sign}(s), & \text{if } |s| > b, \end{cases} \tag{16}$$

with $b > 0$ being the upper bound of the function.

4.1. System as an Integrator Chain. After applying the controller $\overline{u}_1$, the transformed system (4) can be reduced to the subsystem $(\overline{x}_1, \overline{\theta}_1)$, that is:

$$\begin{aligned}\dot{\overline{x}}_1 &= \overline{x}_2, \\ \dot{\overline{x}}_2 &= -\tan\overline{\theta}_1 - \epsilon\overline{A}_L \sec\overline{\theta}_1, \\ \dot{\overline{\theta}}_1 &= \overline{\theta}_2, \\ \dot{\overline{\theta}}_2 &= u_2 + \overline{A}_L.\end{aligned} \tag{17}$$

To express system (17) as an integrator chain, with a nonlinear perturbation, and to propose a controller for the stabilization of the subsystem $(\overline{x}_1, \overline{\theta}_1)$, it is proceeded similarly as in [32], so that the following global nonlinear transformation is defined:

$$\begin{aligned}w_1 &= -\tan\overline{\theta}_1, \\ w_2 &= -\overline{\theta}_2 \sec^2\overline{\theta}_1, \\ \nu &= -u_2 \sec^2\overline{\theta}_1 + 2\overline{\theta}_2^2 \tan\overline{\theta}_1 \sec^2\overline{\theta}_1.\end{aligned} \tag{18}$$

Hence, the transformed system as an integrator chain is given by

$$\begin{aligned}\dot{\overline{x}}_1 &= \overline{x}_2, \\ \dot{\overline{x}}_2 &= w_1 - \epsilon\overline{A}_L \sec\overline{\theta}_1, \\ \dot{w}_1 &= w_2, \\ \dot{w}_2 &= \nu + \overline{A}_L \sec^2\overline{\theta}_1,\end{aligned} \tag{19}$$

whose matrix representation can be expressed as

$$\dot{\xi} = (A\xi + B\nu + \omega), \tag{20}$$

where $\xi = (\overline{x}_1, \overline{x}_2, w_1, w_2)$ is the new state vector,

$$A = \begin{bmatrix} 0 & 1 & 0 & 0 \\ 0 & 0 & 1 & 0 \\ 0 & 0 & 0 & 1 \\ 0 & 0 & 0 & 0 \end{bmatrix},$$
$$B = \begin{bmatrix} 0 \\ 0 \\ 0 \\ 1 \end{bmatrix}, \tag{21}$$
$$\omega = \begin{bmatrix} 0 \\ -\epsilon \overline{A}_L \sec\overline{\theta}_1 \\ 0 \\ \overline{A}_L \sec^2\overline{\theta}_1 \end{bmatrix}.$$

4.2. Nested Saturation Function-Based Controller. In order to obtain the stabilizing controller for system (20) and inspired by [27], the linear transformation $q = S\xi$ is used, in which S must satisfy

$$SAS^{-1} = \begin{bmatrix} 0 & 1 & 1 & 1 \\ 0 & 0 & 1 & 1 \\ 0 & 0 & 0 & 1 \\ 0 & 0 & 0 & 1 \end{bmatrix},$$
$$SB = \begin{bmatrix} 1 \\ 1 \\ 1 \\ 1 \end{bmatrix}. \tag{22}$$

The matrix S that achieves the aforementioned equalities is given by [31]

$$S = \begin{bmatrix} 1 & 3 & 3 & 1 \\ 0 & 1 & 2 & 1 \\ 0 & 0 & 1 & 1 \\ 0 & 0 & 0 & 1 \end{bmatrix}. \tag{23}$$

Thus, q results in

$$q = \begin{bmatrix} q_1 \\ q_2 \\ q_3 \\ q_4 \end{bmatrix} = \begin{bmatrix} 1 & 3 & 3 & 1 \\ 0 & 1 & 2 & 1 \\ 0 & 0 & 1 & 1 \\ 0 & 0 & 0 & 1 \end{bmatrix}, \tag{24}$$

which transforms system (20) into

$$\begin{aligned} \dot{q}_1 &= q_2 + q_3 + q_4 + \nu + \overline{A}_L \sec^2\overline{\theta}_1 - 3\epsilon \overline{A}_L \sec\overline{\theta}_1, \\ \dot{q}_2 &= q_3 + q_4 + \nu + \overline{A}_L \sec^2\overline{\theta}_1 - \epsilon \overline{A}_L \sec\overline{\theta}_1, \\ \dot{q}_3 &= q_4 + \nu + \overline{A}_L \sec^2\overline{\theta}_1, \\ \dot{q}_4 &= \nu + \overline{A}_L \sec^2\overline{\theta}_1, \end{aligned} \tag{25}$$

for which, the following nested saturation function-based stabilizing controller is proposed:

$$\nu = -q_4 - \sigma_\alpha\left(q_3 + \sigma_\beta\left(q_2 + \sigma_\gamma(q_1)\right)\right), \tag{26}$$

where $\sigma_\alpha(\cdot)$, $\sigma_\beta(\cdot)$, and $\sigma_\gamma(\cdot)$ are linear saturation functions as defined in (16) and α, β, and γ are the upper bounds of each nested saturation function.

Finally, departing from (18) and using (26), u_2 can be constructed as follows:

$$u_2 = -\left(\frac{1}{\sec^2\overline{\theta}_1}\right)\nu + \left(2\overline{\theta}_2^2 \tan\overline{\theta}_1\right). \tag{27}$$

4.3. Boundedness of All States. Now, it is proved that the proposed closed-loop system, (25) with (26), ensures that all the states are bounded and that the bound of each of them directly depends on the design parameters of the controller.

Step 1: to show that the state q_4 is bounded, the following positive definite function is defined:

$$V_4 = \left(\frac{1}{2}\right)q_4^2, \tag{28}$$

whose time derivative is expressed as

$$\dot{V}_4 = -q_4^2 - q_4\left[\sigma_\alpha\left(q_3 + \sigma_\beta\left(q_2 + \sigma_\gamma(q_1)\right)\right) - \overline{A}_L \sec^2\overline{\theta}_1\right]. \tag{29}$$

It is clear that $\dot{V}_4 < 0$ is accomplished when $|q_4| \geq \alpha + (\overline{A}_L \sec^2\overline{\theta})$. Therefore, there exists a finite time $T_1 > 0$, such that

$$\left|q_4(t)\right| < \alpha + \overline{A}_L \sec^2\overline{\theta}_1, \quad \forall t > T_1. \tag{30}$$

Step 2: now, the behavior of q_3 is analyzed. For this, a positive definite function is introduced as follows:

$$V_3 = \left(\frac{1}{2}\right)q_3^2. \tag{31}$$

Differentiating it with respect to time and after substituting (26) into $\dot{q}_3$, the following is obtained:

$$\dot{V}_3 = -q_3\left[\sigma_\alpha\left(q_3 + \sigma_\beta\left(q_2 + \sigma_\gamma(q_1)\right)\right) - \overline{A}_L \sec^2\overline{\theta}_1\right]. \tag{32}$$

To ensure $\dot{V}_3 < 0$ is achieved, the following conditions must be satisfied:

$$\alpha > 2\beta + \overline{A}_L \sec^2\overline{\theta}_1, \quad |q_3| > \beta + \overline{A}_L \sec^2\overline{\theta}_1. \tag{33}$$

Then, there exists a finite time $T_2 > T_1$ after which

$$\left|q_3(t)\right| < \beta + \overline{A}_L \sec^2\overline{\theta}_1, \quad \forall t > T_2. \tag{34}$$

Thus, when conditions in (33) are satisfied, q_3 is bounded and the stabilization controller (26) takes the following structure:

$$\nu = -q_4 - q_3 - \sigma_\beta\left(q_2 + \sigma_\gamma(q_1)\right), \quad \forall t > T_2. \tag{35}$$

Step 3: substituting (35) into the second differential equation of (25), the following is obtained:

$$\dot{q}_2 = -\sigma_\beta\left(q_2 + \sigma_\gamma(q_1)\right) - \epsilon\overline{A}_L \sec\overline{\theta}_1 + \overline{A}_L \sec^2\overline{\theta}_1. \tag{36}$$

Then, the following definite positive function is defined:

$$V_2 = \left(\frac{1}{2}\right)q_2^2, \tag{37}$$

whose first time derivative is obtained using (36), as follows:

$$\dot{V}_2 = -q_2\left[\sigma_\beta\left(q_2 + \sigma_\gamma(q_1)\right) + \epsilon\overline{A}_L \sec\overline{\theta}_1 - \overline{A}_L \sec^2\overline{\theta}_1\right]. \tag{38}$$

With the purpose of performing $\dot{V}_2 < 0$, it is required that β and γ satisfy the below conditions:

$$\begin{aligned} \beta &> 2\gamma - \epsilon\overline{A}_L \sec\overline{\theta}_1 + \overline{A}_L \sec^2\overline{\theta}, \\ \left|q_2\right| &> \gamma - \epsilon\overline{A}_L \sec\overline{\theta}_1 + \overline{A}_L \sec^2\overline{\theta}_1. \end{aligned} \tag{39}$$

Hence, there exists a finite time $T_3 > T_2$, after which

$$\left|q_2(t)\right| < \gamma - \epsilon\overline{A}_L \sec\overline{\theta}_1 + \overline{A}_L \sec^2\overline{\theta}_1. \tag{40}$$

Consequently, q_2 is bounded and the control ν turns out to be

$$\nu = -q_4 - q_3 - q_2 - \sigma_\gamma(q_1), \quad \forall t > T_3. \tag{41}$$

Step 4: substituting (41) into the first equation of (25), the following is obtained:

$$\dot{q}_1 = -\sigma_\gamma(q_1) - 3\epsilon\overline{A}_L \sec\overline{\theta}_1 + \overline{A}_L \sec^2\overline{\theta}_1. \tag{42}$$

To demonstrate that q_1 is bounded, a definite positive function is defined as follows:

$$V_1 = \left(\frac{1}{2}\right)q_1^2. \tag{43}$$

Differentiating V_1 along the trajectories of (42), the following is obtained:

$$\dot{V}_1 = -q_1\left[\sigma_\gamma(q_1) + 3\epsilon\overline{A}_L \sec\overline{\theta}_1 - \overline{A}_L \sec^2\overline{\theta}_1\right], \tag{44}$$

where γ must be selected so that $\gamma > -3\epsilon\overline{A}_L \sec\overline{\theta}_1 + \overline{A}_L \sec^2\overline{\theta}_1$ and $|q_1| > -3\epsilon\overline{A}_L \sec\overline{\theta}_1 + \overline{A}_L \sec^2\overline{\theta}_1$ to achieve $\dot{V}_1 < 0$. Therefore, there exists a finite time $T_4 > T_3$, such that

$$\left|q_1(t)\right| < -3\epsilon\overline{A}_L \sec\overline{\theta}_1 + \overline{A}_L \sec^2\overline{\theta}_1, \quad \forall t > T_4. \tag{45}$$

Consequently, q_1 is also bounded. Finally, the values of the parameters α, β, and γ can be determined as follows:

$$\begin{aligned} \alpha &> 2\beta + \overline{A}_L \sec\overline{\theta}_1\left(\sec\overline{\theta}_1\right), \\ \beta &> 2\gamma + \overline{A}_L \sec\overline{\theta}_1\left(\sec\overline{\theta}_1 - \epsilon\right), \\ \gamma &> \overline{A}_L \sec\overline{\theta}_1\left(\sec\overline{\theta}_1 - 3\epsilon\right). \end{aligned} \tag{46}$$

Since $\sec\overline{\theta}_1 > \sec\overline{\theta}_1 - \epsilon > \sec\overline{\theta}_1 - 3\epsilon$, $r > |\overline{A}_L \sec^2\overline{\theta}_1| > 0$ can be introduced, which is directly related to the magnitude of the system disturbance, to select the upper bounds of the saturation functions as

$$\alpha = 7r, \quad \beta = 3r, \quad \gamma = r. \tag{47}$$

4.4. Convergence of All States to Zero. Here, we prove that the closed-loop system, provided by (25) and (26) satisfying (47), is asymptotically stable.

Note that after $t > T_4$, controller (26) is no longer saturated. That is,

$$\nu = -q_1 - q_2 - q_3 - q_4, \tag{48}$$

and the closed-loop system turns out to be

$$\begin{aligned} \dot{q}_1 &= -q_1 + \overline{A}_L \sec^2\overline{\theta}_1 - 3\epsilon\overline{A}_L \sec\overline{\theta}_1, \\ \dot{q}_2 &= -q_1 - q_2 + \overline{A}_L \sec^2\overline{\theta}_1 - \epsilon\overline{A}_L \sec\overline{\theta}_1, \\ \dot{q}_3 &= -q_1 - q_2 - q_3 + \overline{A}_L \sec^2\overline{\theta}_1, \\ \dot{q}_4 &= -q_1 - q_2 - q_3 - q_4 + \overline{A}_L \sec^2\overline{\theta}_1. \end{aligned} \tag{49}$$

To demonstrate convergence to zero of all the states, the following Lyapunov function is used:

$$V = \left(\frac{1}{2}\right)q^T q, \tag{50}$$

and differentiating it along the trajectories of (49), the following is obtained:

$$\begin{aligned} \dot{V} = &-q^T M q + (q_1 + q_2 + q_3 + q_4)\overline{A}_L \sec^2\overline{\theta}_1 \\ &- (3q_1 + q_2)\epsilon\overline{A}_L \sec\overline{\theta}_1, \end{aligned} \tag{51}$$

where

$$M = \begin{bmatrix} 1 & 1/2 & 1/2 & 1/2 \\ 1/2 & 1 & 1/2 & 1/2 \\ 1/2 & 1/2 & 1 & 1/2 \\ 1/2 & 1/2 & 1/2 & 1 \end{bmatrix}, \tag{52}$$

is positive definite with $\lambda_{\min} = (1/2)$. Therefore, (51) is strictly negative, when $\overline{A}_L \longrightarrow 0$. Then, the vector of states q exponentially converges to zero after some time $t > T_4$.

5. Extended State Observer

In this section, the extended state observer needed to estimate the disturbance due to wind, A_L, is introduced [33].

Consider only the disturbed coordinate:

$$\dot{\theta}_2 = u_2 + A_L. \tag{53}$$

The following extended state observer is designed:

$$\begin{aligned} \dot{\widehat{\theta}}_2 &= u_2 + \widehat{A}_L - \lambda_1\left(\widehat{\theta}_2 - \theta_2\right), \\ \dot{\widehat{A}}_L &= -\lambda_2\left(\widehat{\theta}_2 - \theta_2\right), \end{aligned} \tag{54}$$

where $\widehat{\theta}_2$ is the estimate of the roll velocity, $\widehat{A}_L$ is the estimate of the disturbance due to wind, λ_1 and λ_2 are the gains of the observer, which must satisfy the following condition: $\lambda_1 \ll \lambda_2$, and lastly u_2 is redefined and proposed as

$$u_2 = \overline{u}_2 - \widehat{A}_L, \tag{55}$$

where $\overline{u}_2 = -(1/\sec^2\overline{\theta}_1)\nu + 2\overline{\theta}_2^2\tan\overline{\theta}_1$ represents a fictitious controller, acting on the coordinate θ_2.

6. Simulation Results

In this section, the outcomes of some numerical tests are presented in order to validate that the proposed control scheme successfully achieves that $(x_1, x_2, y_1, y_2, \theta_1, \theta_2) \longrightarrow (0, 0, y_{1_d}, 0, 0, 0)$. That is, the control scheme carries out height position regulation, through performing trajectory tracking task, and stabilization of the horizontal position and roll angle for the PVTOL system in the presence of random disturbance due to wind.

The simulations were performed with the normalized model (1) in MATLAB-Simulink, using Euler's numerical method with fixed step and a sample time of 1 ms. In that direction, the coefficient giving the coupling between the rolling moment and the lateral acceleration was chosen as in [1], i.e., $\epsilon = 0.001$. Also, the desired trajectory, y_{1_d}, was proposed as the following Bézier polynomial:

$$y_{1_d} = \nu_1 + (\nu_2 - \nu_1)P_d(t), \tag{56}$$

where $\nu_1 = 0$ m and $\nu_2 = 2$ m are the constant values, $P_d(t)$ is defined by

$$P_d(t) = \begin{cases} 0, & \text{if} \quad t \le t_i, \\ \left(\dfrac{t - t_i}{t_f - t_i}\right)^5 \left[r_1 + r_2\left(\dfrac{t - t_i}{t_f - t_i}\right) + r_3\left(\dfrac{t - t_i}{t_f - t_i}\right)^2 + r_4\left(\dfrac{t - t_i}{t_f - t_i}\right)^3 + r_5\left(\dfrac{t - t_i}{t_f - t_i}\right)^4 + r_6\left(\dfrac{t - t_i}{t_f - t_i}\right)^5\right], & \text{if} \quad t_i < t < t_f, \\ 1, & \text{if} \quad t \ge t_f, \end{cases} \tag{57}$$

which smoothly interpolates between ν_1 and ν_2 in the interval $[t_i, t_f]$, with t_i being the initial time, t_f being the final one, and r_1, r_2, r_3, r_4, r_5, and r_6 selected as

$$\begin{aligned} r_1 &= 252, \\ r_2 &= -1050, \\ r_3 &= 1800, \\ r_4 &= -1575, \\ r_5 &= 700, \\ r_6 &= -126. \end{aligned} \tag{58}$$

Regarding the disturbance due to wind given in (2), the air density of the Mexico City was used for ρ and the aerodynamic coefficient C_l was characterized as the following linear approximation:

$$C_l = m_1\theta_1, \tag{59}$$

with m_1 being the slope and θ_1 being the roll angle of the PVTOL system in degrees. It is important to mention that this linear approximation was determined from the results of C_l, obtained with respect to the variation of the roll angle of an aircraft similar to the PVTOL system, by using a wind

chamber [34]. Furthermore, the air speed U was generated as follows:

$$U = A_U \cos\left(\frac{\mathrm{t}}{\mathrm{P}}\right) + \phi + a, \tag{60}$$

where A_U is a random amplitude, t is time, P is a random period, ϕ is a random phase, and a is a random offset. Therefore, (2) is random and can be rewritten as

$$A_L = \left(\frac{1}{2}\right)\rho\left(m_1\theta_1\right)\left[A_U \cos\left(\frac{t}{P}\right) + \phi + a\right]^2 V_a. \tag{61}$$

The whole parameters to construct A_L are shown in Table 1.

On the other hand, the tuning parameters of u_1 were set at

$$\begin{aligned} \alpha_1 &= 8, \\ \alpha_2 &= 8. \end{aligned} \tag{62}$$

The parameter $r = 1$ was chosen for u_2 so that

$$\begin{aligned} \alpha &= 7, \\ \beta &= 3, \\ \gamma &= 1. \end{aligned} \tag{63}$$

The gains implemented for the extended state observer were selected as

$$\begin{aligned} \lambda_1 &= 5, \\ \lambda_2 &= 20. \end{aligned} \tag{64}$$

The initial conditions of the PVTOL system were set as indicated in Table 2.

The corresponding simulation results are shown in Figure 2. With the intention of comparing the performance of the proposed control scheme with a classical controller, Figure 2 also presents simulation results when using a PID structure for u_1 and u_2 to carry out regulation of the system. For the simulation of the normalized system in closed loop with the PID controllers, (61) with parameters in Table 1 was preserved, the initial conditions in Table 2 were set, the gains of the observer were maintained, and the gains of the controllers were tuned as

$$\begin{aligned} k_{p1} &= 1.5, \\ k_{i1} &= 1.5, \\ k_{d1} &= 3, \end{aligned} \tag{65}$$

Table 1: Parameters of A_L.

Parameter	Value
ρ	0.908906 kg/m^2
m_1	−0.0013
A_U	[4, 12]
P	[1.6, 4.8] s
ϕ	[12°, 21°]
a	[−2, 2]
V_a	0.1 m^3

Table 2: Initial conditions.

State	Value
x_1	0.1 m
x_2	0 m/s
y_1	0 m
y_2	0 m/s
θ_1	0.15 rad
θ_2	0 rad/s

for u_1 and

$$\begin{aligned} k_{p2} &= 0.1, \\ k_{i2} &= 0, \\ k_{d2} &= 0.5, \end{aligned} \tag{66}$$

for u_2. To distinguish the results, the ones associated with the PID controllers are denoted with the subscript PID.

In Figure 2, it can be observed that the proposed control scheme allows achieving successfully the height position regulation, through the trajectory tracking task, and stabilization of the horizontal position and roll angle when the system is subjected to random disturbance due to wind. That is, $(x_1, x_2, y_1, y_2, \theta_1, \theta_2) \longrightarrow (0, 0, y_{1_d}, 0, 0, 0)$ is accomplished. Note that the execution of the trajectory tracking task in the vertical position provides maneuverability when taking-off the PVTOL system. However, with the PID controllers, the regulation of state x_1 cannot be achieved, but only for the positions y_1 and θ_1. That is, stabilization of the whole system is not achieved. Although PID structure can achieve the height position regulation when the system is far from the desired height, it requires excessive values for u_1 and u_2 and does not allow the taking-off of the system in a controlled way. Thus, advantages of the proposal presented herein are maneuverability and whole stabilization, when the system is under the undesired effect caused by wind.

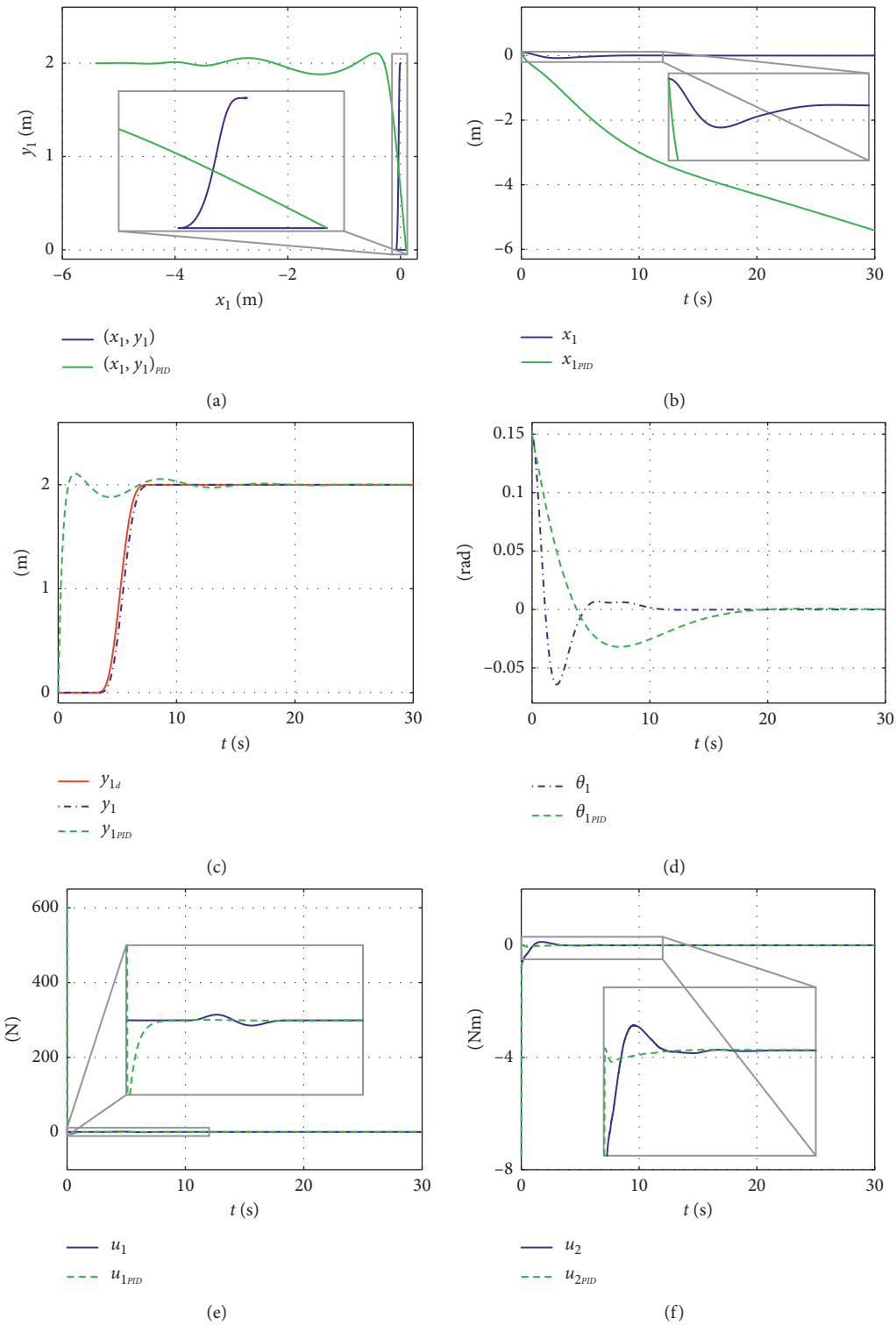

Figure 2: Continued.

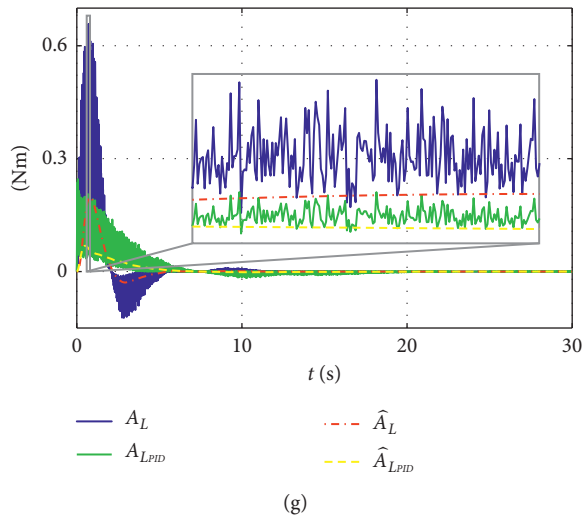

(g)

Figure 2: Simulation results.

7. Conclusions

In this study, a nested saturation function-based controller, in combination with a backstepping controller, for stabilizing the PVTOL system under a disturbance due to wind was used. With this approach, the control design complexity of a higher-order system is reduced to design a control for a lower-order nonlinear subsystem of the original system. Thus, the proposed control approach allows designing a controller based on nested saturation functions, which contemplates perturbations, guaranteeing the convergence of the roll angle to zero within a finite time and, consequently, the convergence to zero of the horizontal state. The stability analysis of the closed-loop system was based on the second method of Lyapunov, using a simple candidate function. It is important to remark that the controller, based on backstepping and nested saturation functions, allows performing take-off maneuvers in the presence of exogenous disturbances, which are found when aircraft carries out actual maneuvers. Furthermore, an extended state observer is used to estimate the disturbance due to wind. Numerical simulations were carried out to test the effectiveness of the proposed controller, having obtained convincing results. Finally, the proposed scheme was compared with a classical controller, finding that the controller based on backstepping and nested saturation functions presented herein has better performance.

It is worth mentioning that an experimental platform that allows configuring the PVTOL system has been designed, whose construction is in process. Thus, experimental implementation of the control scheme proposed herein is considered as a future work.

Data Availability

The data used to support the conclusion of this study are available from the corresponding author upon request.

Conflicts of Interest

The authors declare that there are no conflicts of interest regarding the publication of this article.

Acknowledgments

This study was supported by the Secretaría de Investigación y Posgrado of the Instituto Politécnico Nacional under the research grants 20201829, 20200162, 20201623, and 20200671. C. A. Merlo-Zapata acknowledges financial support from Instituto Tecnológico de Iztapalapa. M. Antonio-Cruz and C. Márquez-Sánchez thank the support from the Sistema Nacional de Investigadores-CONACYT.

References

[1] J. Hauser, S. Sastry, and G. Meyer, "Nonlinear control design for slightly non-minimum phase systems: application to v/stol aircraft," *Automatica*, vol. 28, no. 4, pp. 665–679, 1992.

[2] K. D. Do, Z. P. Jiang, and J. Pan, "On global tracking control of a vtol aircraft without velocity measurements," *IEEE Transactions on Automatic Control*, vol. 48, no. 12, pp. 2212–2217, 2003.

[3] A. Zavala-Río, I. Fantoni, and R. Lozano, "Global stabilization of a pvtol aircraft model with bounded inputs," *International Journal of Control*, vol. 767, no. 8, pp. 1833–1844, 2003.

[4] R. Lozano, P. Castillo, and A. Dzul, "Global stabilization of the pvtol: real-time application to a mini-aircraft," *International Journal of Control Proceedings Volumes*, vol. 77, no. 8, pp. 735–740, 2004.

[5] A. Palomino, P. Castillo, I. Fantoni, R. Lozano, and C. Pégard, "Control strategy using vision for the stabilization of an experimental pvtol aircraft setup," *IEEE Transactions on Control Systems Technology*, vol. 13, no. 5, pp. 847–850, 2005.

[6] R. Olfati-Saber, "Global configuration stabilization for the vtol aircraft with strong input coupling," *IEEE Transactions on Automatic Control*, vol. 47, no. 11, pp. 1949–1952, 2002.

[7] R. Wood and B. Cazzolato, "An alternative nonlinear control law for the global stabilization of the pvtol vehicle," *IEEE Transactions on Automatic Control*, vol. 52, no. 7, pp. 1282–1287, 2007.

[8] H. Ye, H. Wang, and H. Wang, "Stabilization of a pvtol aircraft and an inertia wheel pendulum using saturation technique," *IEEE Transactions on Control Systems Technology*, vol. 15, no. 6, pp. 1143–1150, 2007.

[9] A. Chemori and N. Marchand, "A prediction-based nonlinear controller for stabilization of a non-minimum phase pvtol aircraft," *International Journal of Robust and Nonlinear Control*, vol. 18, no. 8, pp. 876–889, 2008.

[10] S.-L. Wu, P.-C. Chen, K.-Y. Chang, and C.-C. Huang, "Robust gain-scheduled control for vertical/short take-off and landing aircraft in hovering with time-varying mass and moment of inertia," *Proceedings of the Institution of Mechanical Engineers, Part G: Journal of Aerospace Engineering*, vol. 222, no. 4, pp. 473–482, 2008.

[11] L. Consolini, M. Maggiore, C. Nielsen, and M. Tosques, "Path following for the pvtol aircraft," *Automatica*, vol. 46, no. 8, pp. 1284–1296, 2010.

[12] A. Gruszka, M. Malisoff, and F. Mazenc, "Tracking control and robustness analysis for planar vertical takeoff and landing aircraft under bounded feedbacks," *International Journal of Robust and Nonlinear Control*, vol. 22, no. 17, pp. 1899–1920, 2012.

[13] A. Zavala-Río, I. Fantoni, and G. Sanahuja, "Finite-time observer-based output-feedback control for the global stabilisation of the pvtol aircraft with bounded inputs," *International Journal of Systems Science*, vol. 47, no. 7, pp. 1543–1562, 2014.

[14] C. Aguilar-Ibáñez, J. H. Sossa-Azuela, and M. S. Suarez-Castanon, "A backstepping-based procedure with saturation functions to control the pvtol system," *Nonlinear Dynamics*, vol. 83, no. 3, pp. 1247–1257, 2016.

[15] C. Aguilar-Ibañez, M. S. Suarez-Castanon, J. Mendoza-Mendoza, J. D. J. Rubio, and J. C. Martínez-García, "Output-feedback stabilization of the pvtol aircraft system based on an exact differentiator," *Journal of Intelligent & Robotic Systems*, vol. 90, no. 3-4, pp. 443–454, 2018.

[16] C. Aguilar-Ibañez, "Stabilization of the pvtol aircraft based on a sliding mode and a saturation function," *International Journal of Robust and Nonlinear Control*, vol. 27, no. 5, pp. 843–859, 2017.

[17] C. Yu-Chan, M. Bao-Li, and X. Wen-Jing, "Robust stabilization of nonlinear pvtol aircraft with parameter uncertainties," *Asian Journal of Control*, vol. 19, no. 3, pp. 1239–1249, 2017.

[18] F. Hernández-Castañeda, V. Santibáñez, and F. Jurado, "Priority altitude pvtol aircraft control via immersion and invariance," *International Journal of Control*, vol. 2018, pp. 1–12, 2018.

[19] X. Xu and C. Zhang, "Cascade ADRCbased fault-olerant control for a hovering PVTOL aircraft," in *Robotics and Mechatronics, Mechanisms and MachineScience*, R. Yang, Y. Takeda, C. Zhang, and G. Fang, Ed., vol. 72, pp. 239–249, Springer, Cham, Switzerland, 2019.

[20] J. C. Escobar, R. Lozano, and M. Bonilla Estrada, "PVTOL control using feedback linearisation with dynamic extension," *International Journal of Control*, vol. 2019, pp. 1–10, 2019.

[21] C. Aguilar-Ibanez, M. S. Suarez-Castanon, J. Meda-Campaña, O. Gutierrez-Frias, C. Merlo-Zapata, and J. A. Martinez-Castro, "A simple approach to regulate a pvtol system using matching conditions," *Journal of Intelligent & Robotic Systems*, vol. 98, no. 2, pp. 511–524, 2019.

[22] C. Aguilar-Ibanez, H. Sira-Ramirez, M. S. Suarez-Castanon, and R. Garrido, "Robust trajectory-tracking control of a pvtol under crosswind," *Asian Journal of Control*, vol. 21, no. 3, pp. 1293–1306, 2019.

[23] P. C. Garcia, R. Lozano, and A. Dzul, *Modelling and Control of Mini-Flying Machines*, Springer-Verlag, London, UK, 2006.

[24] L. E. Munoz, O. Santos, and P. Castillo, "Robust nonlinear real-time control strategy to stabilize a pvtol aircraft in crosswind," in *Proceedings of the 2010 IEEE/RSJ International Conference on Intelligent Robots and Systems*, pp. 1606–1611, Taipei, TW, 2010.

[25] S. B. V. Gomes and J. G. Ramos, "Airship dynamic modeling for autonomous operation," *IEEE International Conference on Robotics and Automation (Cat. No. 98CH36146)*, vol. 4, pp. 3462–3467, 1998.

[26] R. Olfati-Saber, *Nonlinear Control of Underactuated Mechanical Systems with Application to Robotics and Aerospace Vehicles*, Ph.D. dissertation, Massachusetts Institute of Technology, Massachusetts, MA, USA, 2001.

[27] A. R. Teel, "Global stabilization and restricted tracking for multiple integrators with bounded controls," *Systems & Control Letters*, vol. 18, no. 3, pp. 165–171, 1992.

[28] P. Castillo, R. Lozano, and A. Dzul, "Stabilization of a mini rotorcraft with four rotors," *IEEE Control Systems Magazine*, vol. 25, no. 6, pp. 45–55, 2005.

[29] C. A. Ibánez, O. G. Frías, and M. S. Castañón, "Controlling the strongly damping inertia wheel pendulum via nested saturation functions," *Computación y Sistemas*, vol. 12, no. 4, pp. 436–449, 2009.

[30] C. Aguilar-Ibañez, J. C. Martínez-García, A. Soria-López, and J. D. J. Rubio, "On the stabilization of the inverted-cart pendulum using the saturation function approach," *Mathematical Problems in Engineering*, vol. 2011, pp. 1–14, 2011.

[31] C. A. Ibañez and O. G. Frias, "Controlling the inverted pendulum by means of a nested saturation function," *Nonlinear Dynamics*, vol. 53, no. 4, pp. 273–280, 2008.

[32] Y. Lozano Hernández, O. Gutiérrez Frías, N. Lozada-Castillo, and A. Luviano Juárez, "Control algorithm for taking off and landing manoeuvres of quadrotors in open navigation environments," *International Journal of Control, Automation and Systems*, vol. 17, no. 9, pp. 2331–2342, 2019.

[33] H. Sira-Ramírez, A. Luviano-Juárez, M. Ramírez-Neria, and E. W. Zurita-Bustamante, *Active Disturbance Rejection Control of Dynamic Systems: A Flatness Based Approach*, Butterworth-Heinemann, London, UK, 2018.

[34] F. Mohamad, W. Wisnoe, R. E. M. Nasir, K. I. Sainan, and N. Jenal, "Yaw stability analysis for UiTM's BWB baseline-II UAV E-4," *Applied Mechanics and Materials*, vol. 393, pp. 323–328, 2013.

Hindawi
Complexity
Volume 2020, Article ID 2160743, 18 pages
https://doi.org/10.1155/2020/2160743

Research Article

Cascade Delayed Controller Design for a Class of Underactuated Systems

G. Ochoa-Ortega,[1] **R. Villafuerte-Segura**,[2] **A. Luviano-Juárez**,[3] **M. Ramírez-Neria**,[4] **and N. Lozada-Castillo**[3]

[1]*Universidad Politécnica del Valle de México, Av. Mexiquense s/n Colonia Villa Esmeralda, Tultitlán 54910, Mexico*
[2]*Universidad Autónoma del Estado de Hidalgo, CITIS, Carretera Pachuca-Tulancingo km. 4.5, Col. Carboneras, Mineral de la Reforma 42184, Mexico*
[3]*Instituto Politécnico Nacional-UPIITA, Av. IPN 2580 Colonia Barrio la Laguna Ticomán, Ciudad de México 07340, Mexico*
[4]*InIAT Universidad Iberoamericana Ciudad de México, Prolongación Paseo de la Reforma 880, Colonia Lomas de Santa Fé, Ciudad de México CP 01219, Mexico*

Correspondence should be addressed to R. Villafuerte-Segura; villafuerte@uaeh.edu.mx

Received 16 April 2020; Revised 11 July 2020; Accepted 22 July 2020; Published 25 August 2020

Academic Editor: Alejandro F. Villaverde

Copyright © 2020 G. Ochoa-Ortega et al. This is an open access article distributed under the Creative Commons Attribution License, which permits unrestricted use, distribution, and reproduction in any medium, provided the original work is properly cited.

In this paper, a delayed control strategy for a class of nonlinear underactuated fourth-order systems is developed. The proposal is based on the implementation of the tangent linearization technique, differential flatness, and a study of the σ-stabilization of the characteristic equation of the closed-loop system. The tangent linearization technique allows obtaining a local controllability property for the analyzed class of systems. Also, it can reduce the complexity of the global control design, through the use of a cascade connection of two second-order controllers instead of designing a global controller of the fourth-order system. The stabilizing behavior of the delayed controller design is supported by the σ-stability criterion, which provides the controller parameter selection to reach the maximum exponential decay rate on the system response. To illustrate the efficiency of the theoretical results, the proposal is experimentally assessed in two cases of study: a flexible joint system and a pendubot.

1. Introduction

The control of underactuated systems has attracted some attention from the academic community, as noticed in the growing list of articles and new approaches to solve the problems of estimation, regulation, and trajectory tracking involving both linear and nonlinear underactuated systems. In the literature, there are a variety of control strategies, including controlled Lyapunov functions [1, 2], energy-based control [3–5], passivity approaches [6, 7], active disturbance rejection [8–10], planning algorithms, and feedback stabilization schemes [11].

One of the most important problems of nonlinear underactuated systems is the fact that the controllability property may be subject to singularities (ill-conditioned relative degree [12]), which conditions the controllable (normal) forms of the models to a certain class of systems [13]. An alternative to locally overcome the aforementioned problem is the use of the tangent linearization technique, since the tangent linearized models of an important class of underactuated systems are differentially flat [9]. The last fact means that the linearized systems are controllable and there exists a set of variables, named flat outputs, which can characterize them [14]. Besides the flatness of the linearized system, another important advantage for this class of systems is the called cascade form [15], which allows finding a relation between $2n-$ th-order time derivatives (fourth-order, sixth-order, and so on) of the flat output and a measurable variable of the system. This form can reduce the complexity of the global control design in which, instead of designing a global controller of a $2n-$ th-order system, the task can be the cascade connection of second-order

controllers, which is especially important for sensitive systems or noise amplification effects due to high-order observer designs, among others. In particular, for the case of fourth-order systems, this scheme allows, instead of stabilizing a fourth-order integrator, implementing a cascade control arrangement of two second-order systems, for instance, classic controllers with derivative action. The implementation of the derivative action has at least three natural disadvantages. Firstly, the estimation algorithms typically increase the controller design. Secondly, the application of filters or compensators often increases the order of the closed-loop system. Thirdly, the use of measurement tools (encoders) is usually very noisy. An alternative is the use of delayed controllers, which means to deliberately include retarded actions (time delays) in the controller. Delayed controllers have better performance in practical applications compared to controllers with derivative actions [16]. Since these controllers type noise attenuation, they do not require estimators or filters to approximate the time derivative, providing soft control signals which do not damage actuators, and their numerical implementation is computationally more efficient than other low-order controllers. Moreover, a delayed controller has a simple structure which is easy to implement, like classic controllers.

The deliberate use of retarded actions to stabilize a system is a topic that has been investigated in recent decades, among which are the pioneering contributions of [17–28]. Concerning derivative-free control based schemes, such as the proportional retarded (PR) scheme [19, 25, 29–31], which consists in using the relation between the time derivative approximations in terms of a differential difference equation, involving a time delay. This approximation is taken as a baseline to avoid using a derivative compensation, but a proportional retarded one.

The use of delayed controllers has been previously studied for the stabilization of chains of integrators. It has been proven [32–34] that a chain of n integrators cannot be stabilized with less than n delay blocks, which increases significantly the complexity of the closed-loop system. The migration of a double imaginary characteristic root to the left half-plane or the right half-plane under the variation of two parameters of a quasi-polynomial is given in [35]. However, in none of the above proposals, there are criteria or methodologies to explicitly tune the controller gains.

For the class of underactuated systems satisfying the cascade property, the use of a cascade control structure of PR controllers (delayed controller) can be a derivative-free alternative of stabilizing control, including the complete dynamics (some reported schemes based on the linearization deal with a part of the dynamics such as the switched control [36]). However, the existing analyses are restricted to a class of second-order LTI systems, and the system to analyze becomes a cascade of two-order systems, whose analysis cannot be considering the isolated dynamics but the cascade structure.

The stability analysis of delayed controllers can be commonly addressed on the study of the relative stability of degree σ of the characteristic function, also known as σ-stability. This approach in conjunction with the $\mathcal{D}$-decomposition methodology (see [37–40]) can lead us to obtain conditions, under which the system response can reach the maximal exponential decay rate.

Thus, the contributions of this manuscript are listed as follows:

(1) It analyzed a class of underactuated systems, especially those whose tangent linearization is controllable (flat). Moreover, it developed a controller through the use of the cascade property in the flat linearized system, which allows reducing the complexity of the control loops.

(2) The control approach consists in using a cascade structure of proportional retarded controllers in each of the second-order structures derived from the cascade system. In this proposal, the fourth-order system is controlled by a tandem array of PR controllers in which two delays are used for the main structure.

(3) The stability analysis considers the complete fourth-order structure and provides the tuning conditions for the controller design and, moreover, provides competitive experimental results, which denote the importance of using a more complex controller with the aim of obtaining appropriate results for noisy measurements, in which additional filtering schemes are demanded. In addition, the tuning procedure is reported and the involved numerical algorithms are provided for practitioners.

(4) The combination of the aforementioned concepts provides an alternative control approach for a class of fourth-order underactuated systems subject to noisy measurements, with a possible extension to the highest-order systems.

(5) The analysis and synthesis of a cascade proportional retarded controllers for a class of underactuated systems in cascade structure are proposed (Figure 1). Also, analytic conditions, on the parameters of the controller, to reach the maximal exponential decay rate of the system response are proposed.

(6) Experimental implementations of the proposal, which validate its practical effectiveness, are also proposed. Two classic challenging systems were used for the assessment: a rotatory flexible link and a pendubot.

The remaining of the contribution is organized as follows. In Section 2, the basic concepts related to time-delay systems and differentially flatness are presented. In Section 3, a methodology based on the differential flatness to represent a class of fourth-order underactuated systems as a cascade arrangement of two-order systems is presented. The main contributions of the present manuscript are introduced in Section 4, where the σ-stability of the system is analyzed and analytic conditions to reach the maximal exponential decay rate of the system response are provided. Section 5 is devoted to the implementation results in trajectory tracking tasks. The article ends with some concluding remarks.

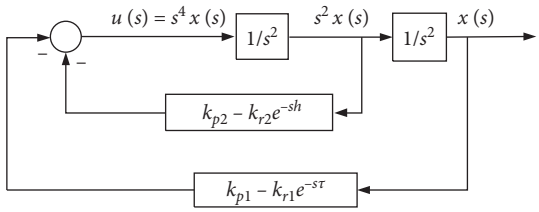

Figure 1: Schematic of the PR controller for a cascade structure.

Notation. Given a vector $x(t) \in \mathbb{R}^n$, $x^\intercal(t)$ denotes its transpose and $\|x(t)\|$ stands for the Euclidean norm. Let $s \in \mathbb{C}$; then, $\mathrm{Re}(s)$ and $\mathrm{Im}(s)$ denote its real and imaginary parts, respectively. For a function $x(t)$, $x^{(i)}(t)$, $i \in \mathbb{Z}^+$ denotes the i-th time derivative of the function.

2. Mathematical Preliminaries

In this section, we introduce some basic concepts, concerning both time-delay systems and differentially flat systems, necessary for the development of this contribution.

2.1. Differentially Flat Systems. In this subsection, the flatness concept for single-input single-output (SISO) systems of nonlinear and linear types is taken. Further comprehensive information can be taken from [14, 41, 42] and references therein.

Definition 1. Let us consider a nonlinear system of the following form:

$$\dot{x}(t) = f(x(t), u(t)), \tag{1}$$

where $x(t) \in \mathbb{R}^n$, $u(t) \in \mathbb{R}$, and $f(\cdot) = [\, f_1(\cdot)\ f_2(\cdot) \cdots f_n(\cdot)]^\intercal$ is a smooth function of $x(t), u(t)$, and the rank of the Jacobian matrix, and $(\partial f(\cdot))/(\partial u(t))$ is equal to 1. System (1) is said to be differentially flat if there exists a differential function, denoted as $y(t) \in \mathbb{R}$, given by

$$y(t) = r\left(x(t), u(t), \dot{u}(t), \ddot{u}(t), \ldots, u^{(\alpha)}(t)\right), \quad \alpha \in \mathbb{Z}^+, \tag{2}$$

which completely differentially parametrizes all the variables of the system. This means that states, inputs, and original output variables in the system can be written as differential functions of the flat output $y(t)$, that is,

$$\begin{aligned} x(t) &= \phi\left(y(t), \dot{y}(t), \ldots, y^{(\gamma)}(t)\right), \\ u(t) &= \psi\left(y(t), \dot{y}(t), \ldots, y^{(\gamma+1)}(t)\right), \quad \gamma \in \mathbb{Z}^+. \end{aligned} \tag{3}$$

Flatness is a structural property of the system that trivializes the exact linearization procedure of a nonlinear system even when it is not expressed in an affine form. It also allows an easier manner of designing control laws in trajectory tracking tasks, by taking advantage of the differential parametrization. For the case of linear SISO systems, the flatness property can be directly related to the controllability of the system.

Definition 2. Consider the linear time-invariant SISO system:

$$\dot{x}(t) = Ax(t) + bu(t), \tag{4}$$

with $A \in \mathbb{R}^{n\times n}$, $b \in \mathbb{R}^n$, $x(t) \in \mathbb{R}^n$, and $u(t) \in \mathbb{R}$. Let the pair (A, b) be controllable, that is, the controllability matrix:

$$K_c = \left[\, b \ \ Ab \ \ A^2b \ \cdots \ A^{n-1}b \,\right], \tag{5}$$

which has full rank n. Then, it is said that system (4) is controllable; hence, it is differentially flat with the flat output given by

$$y(t) = \left[\, 0 \ \ 0 \ \cdots \ 1 \,\right] K_c^{-1} x(t). \tag{6}$$

2.2. Time-Delay Systems. In the present section, some definitions and general results concerning linear time-delay systems are introduced; for these purposes, it is considered a basic system of the following form:

$$\dot{x}(t) = A_0 x(t) + A_1 x(t-\tau) + A_2 x(t-h), \quad t \geq 0. \tag{7}$$

Here, $A_0, A_1 \in \mathbb{R}^{n\times n}$, and $\tau, h \in \mathbb{R}^+$ are time delays. Now, some stability concepts related to system (7) are presented.

Definition 3 (see [43]). The solution $x(t, \varphi)$ of a system of the form (7) is said to be exponentially stable, if there exist $L, \sigma \in \mathbb{R}^+$ such that the following inequality holds:

$$\|x(t, \varphi)\| \leq Le^{-\sigma t}\|\varphi\|_H, \quad t \geq 0. \tag{8}$$

Here, $H = \max\{\tau, h\}$, $\varphi\colon [-H, 0] \longrightarrow \mathfrak{C}$ denotes the initial function and $\mathfrak{C} \coloneqq C([-H, 0], \mathbb{R}^n)$ is a Banach space of continuous functions in $[-H, 0]$ with the norm $\|\varphi\|_H = \max_{\theta\in[-H,0]}\|\varphi(\theta)\|$.

Definition 4 (see [43]). A $s_0 \in \mathbb{C}$ is said to be an eigenvalue of system (7) if it is a root of the characteristic function; that is,

$$Q(s_0, \tau, h) = \det\left(s_0 I - A_0 - A_1 e^{-s_0\tau} - A_2 e^{-s_0 h}\right) = 0. \tag{9}$$

The set of all the distinct eigenvalues of the system is called the spectrum of system (7) and this is denoted as $\Lambda(Q)$.

An equivalent definition of exponential stability is given hereinafter.

Definition 5 (see [43]). System (7) is exponentially stable if and only if the spectrum of the system lies in the open left half-plane of the complex plane; that is, $\mathrm{Re}(s_j) < 0$, $\forall s_j \in \Lambda(Q)$.

Definition 6. A linear time-delay system of the form (7) is said to be σ-stable, if

$$s^* = -\sigma, \tag{10}$$

for $\sigma \in \mathbb{R}^+$ and $s^* = \max_{j=1,\ldots,\infty}\{\mathrm{Re}(s_j)\colon s_j \in \Lambda(Q)\}$.

From these definitions, note that σ-stability ensures exponential stability with the decay rate σ in the system response (7).

In the following section, a class of fourth-order underactuated systems is described.

3. Preliminary Results

Euler-Lagrange underactuated systems of the fourth order can generally be described by

$$P(q(t))u(t) = M(q(t))\ddot{q}(t) + C(q(t), \dot{q}(t))\dot{q}(t) + g(q(t)), \tag{11}$$

where $q(t) \coloneqq [\, q_1(t) \;\; q_2(t) \,]^{\intercal}$ represents the generalized coordinates, $M(q(t)) \in \mathbb{R}^{2\times 2}$ is the inertia matrix, and $C(q(t), \dot{q}(t)) \in \mathbb{R}^{2\times 2}$ describes the Coriolis matrix and centrifugal forces. Let $g(q(t)) \in \mathbb{R}^2$ be the vector of gravitational forces and $P(q(t)) \in \mathbb{R}^2$ is the vector mapping the external forces. Finally, $u(t) \in \mathbb{R}$ denotes the control input.

Systems of the form (11) can be rewritten in a state-space representation as follows:

$$\begin{aligned} \dot{x}_a(t) &= x_b(t), \\ \dot{x}_b(t) &= f\left(x_a(t), t x_b n(t)\right) + \zeta\left(x_a(t)\right)u(t), \end{aligned} \tag{12}$$

where $x_a(t)$ stands for the vector of joint positions $[\, q_1(t) \;\; q_2(t) \,]^{\intercal}$, $x_b(t)$ denotes the articular velocities vector $[\, \dot{q}_1(t) \;\; \dot{q}_2(t) \,]^{\intercal}$, and

$$\begin{aligned} f\left(x_a(t), x_b(t)\right) &= -M(q(t))^{-1}[C(q(t), \dot{q}(t))\dot{q}(t) + g(q(t))], \\ \zeta\left(x_a(t)\right) &= M(q(t))^{-1}P(q(t)). \end{aligned} \tag{13}$$

After a slight rearrangement of the state vector as $x(t) = [\, q_1(t) \;\; \dot{q}_1(t) \;\; q_2(t) \;\; \dot{q}_2(t) \,]^{\intercal}$ and by denoting $\overline{x}(t)$ as an equilibrium point of the nonlinear representation (12), a tangent linearization around the equilibrium point $\overline{x}(t)$ is given by

$$\dot{x}_\delta(t) = Ax_\delta(t) + Bu_\delta(t). \tag{14}$$

Here, $x_\delta(t) = x(t) - \overline{x}(t)$ and $u_\delta(t) = u(t) - \overline{u}(t)$. The controllability matrix of system (14) is given by

$$K_c = \left[\, bA \;\; bA^2 \;\; bA^3 \;\; b \,\right]. \tag{15}$$

Under the assumption that $\det(K_c) \neq 0$, the system is controllable and hence, according to [14, 42], differentially flat. The flat output can be obtained as follows:

$$y_f(t) = C_f x_\delta(t), \tag{16}$$

where $C_f \in \mathbb{R}^n$ and defined as

$$C_f \epsilon \coloneqq \epsilon [\, 0 \;\; 0 \;\; 0 \;\; 1 \,] K_c^{-1}. \tag{17}$$

Here, $\epsilon \in \mathbb{R}/\{0\}$ is an arbitrary constant. In order to determine the relative degree of system (14), we first need to compute the high-order time derivatives. To this end, notice that the following relations hold:

$$C_f b = C_f Ab = C_f A^2 b = 0, \quad C_f A^3 b \neq 0, \tag{18}$$

and the time derivatives of the flat output are given by

$$\begin{aligned} y_f(t) &= C_f x_\delta(t), \\ \dot{y}_f(t) &= C_f A x_\delta(t), \\ \ddot{y}_f(t) &= C_f A^2 x_\delta(t), \\ y_f^{(3)}(t) &= C_f A^3 x_\delta(t), \\ y_f^{(4)}(t) &= C_f A^4 x_\delta(t) + C_f A^3 b u_\delta(t). \end{aligned} \tag{19}$$

Since $C_f A^3 b \neq 0$, then, the relative degree of the system is four. It is worth noting that the even time derivatives of $y_f(t)$ can be expressed as a linear combination of the flat output, which correspond to those variables that can be measured and coincide with the vector of generalized positions $q(t)$.

Now, let us define the output estimation error as

$$e_i(t) \coloneqq y_f^{(i-1)}(t) - y_f^{*(i-1)}(t), \quad i = 1, \ldots, 4. \tag{20}$$

Here, $y_f^*(t)$ denotes the desired output. Then, the error dynamics is governed by

$$\begin{aligned} \dot{e}_1(t) &= e_2(t), \\ \dot{e}_2(t) &= e_3(t), \\ \dot{e}_3(t) &= e_4(t), \\ \dot{e}_4(t) &= y_f^{(4)}(t) - y_f^{*(4)}(t), \end{aligned} \tag{21}$$

by proposing the auxiliary control

$$u_\delta(t) = \left(C_f A^3 b\right)^{-1}\left[u(t) - C_f A^4 x_\delta(t) + y_f^{*(4)}(t)\right], \tag{22}$$

and then (21) can be expressed as a fourth-order integration chain; that is,

$$\begin{aligned} \dot{e}_1(t) &= e_2(t), \\ \dot{e}_2(t) &= e_3(t), \\ \dot{e}_3(t) &= e_4(t), \\ \dot{e}_4(t) &= u(t). \end{aligned} \tag{23}$$

Now, a delayed controller $u(t)$ that fulfills the cascade control structure proposed in Figure 1 is given as follows:

$$u(t) = -k_{p_1} e_1(t) + k_{r_1} e_1(t - \tau) - k_{p_2} e_3(t) + k_{r_2} e_3(t - h), \tag{24}$$

where $\tau, h \in \mathbb{R}^+$ are the delays and $k_{p_{1,2}}, k_{r_{1,2}} \in \mathbb{R}^+$ are the control gains. Thus, the closed-loop representation of system (23) is now

$$\dot{e}(t) = A_0 e(t) + A_1 e(t - \tau) + A_2 e(t - h). \tag{25}$$

Here,

$$A_0 = \begin{bmatrix} 0 & 1 & 0 & 0 \\ 0 & 0 & 1 & 0 \\ 0 & 0 & 0 & 1 \\ -k_{p_1} & 0 & -k_{p_2} & 0 \end{bmatrix},$$

$$A_1 = \begin{bmatrix} 0 & 0 & 0 & 0 \\ 0 & 0 & 0 & 0 \\ 0 & 0 & 0 & 0 \\ k_{r_1} & 0 & 0 & 0 \end{bmatrix}, \tag{26}$$

$$A_2 = \begin{bmatrix} 0 & 0 & 0 & 0 \\ 0 & 0 & 0 & 0 \\ 0 & 0 & 0 & 0 \\ 0 & 0 & k_{r_2} & 0 \end{bmatrix},$$

and $e(t) = [\, e_1(t) \;\; e_2(t) \;\; e_3(t) \;\; e_4(t) \,]^{\intercal}$. Thus, the characteristic function or characteristic quasi-polynomial of system (25) is given by

$$Q\left(s, k_{p_{1,2}}, k_{r_{1,2}}, \tau, h\right) = s^4 + k_{p_2} s^2 + k_{p_1} - k_{r_1} e^{-s\tau} - s^2 k_{r_2} e^{-sh}. \tag{27}$$

4. Main Results

In the present section, analytic conditions on the parameters of the delayed controller (24) are presented. Here, a general form of quasi-polynomial (27) is considered:

$$Q\left(s, k_{p_{1,2}}, k_{r_{1,2}}, \tau, h\right) = P_1\left(s, k_{p_{1,2}}\right) + P_2\left(s, k_{r_1}\right) e^{-s\tau} + P_3(s) k_{r_2} e^{-\mathrm{sh}}, \tag{28}$$

where $P_i(\cdot)$, $i = 1, 2, 3$, are polynomials with real coefficients which satisfy the following degree condition: $\deg(P_1(\cdot)) > \deg(P_{2,3}(\cdot))$. In order to analyze the σ-stability of the quasi-polynomial (28), the change of variable $s \longrightarrow (s - \sigma)$ is considered; thus, (28) is now in the following form:

$$\begin{aligned} Q\left(s - \sigma, k_{p_{1,2}}, k_{r_{1,2}}, \tau, h\right) &\coloneqq Q_\sigma\left(s, k_{p_{1,2}}, k_{r_{1,2}}, \tau, h\right) \\ &= P_{\sigma_1}\left(s, k_{p_{1,2}}\right) + P_{\sigma_2}\left(s, k_{r_1}\right) e^{-\tau(s-\sigma)} \\ &\quad + P_{\sigma_3}(s) e^{\sigma h} k_{r_2} e^{-\mathrm{sh}}. \end{aligned} \tag{29}$$

Based on the $\mathscr{D}$-decomposition methodology [44], the σ-stability regions of the modified characteristic function (29) can be now obtained. This procedure will play a key role in determining the analytic conditions to obtain the maximal decay rate σ^*.

Proposition 1. *Let us consider a quasi-polynomial of the form (28), with given control parameters $k_{p_1}, k_{p_2}, k_{r_1}$, and τ. Let $\sigma \in \mathbb{R}^+$ be fixed; then, by defining*

$$\Gamma(s, \sigma) = P_{\sigma_1}\left(s, k_{p_{1,2}}\right) + P_{\sigma_2}\left(s, k_{r_1}\right) e^{-(s-\sigma)\tau}, \tag{30}$$

the σ-stability regions on the (h, k_r) parametric space are bounded by the following conditions.

When $s = 0$,

$$k_{r_2}(h) = -\frac{\Gamma(0, \sigma)}{P_{\sigma_3}(0) e^{\sigma h}}, \quad h \in \mathbb{R}^+. \tag{31}$$

When $s = i\omega$, $\omega \in \mathbb{R}^+$,

$$h(\omega) = \frac{1}{\omega} \cot^{-1}\left(-\frac{\mathrm{Re}\left(\left(\Gamma(i\omega, \sigma)\right)/\left(P_{\sigma_3}(i\omega)\right)\right)}{\mathrm{Im}\left(\left(\Gamma(i\omega, \sigma)\right)/\left(P_{\sigma_3}(i\omega)\right)\right)} \right) + \frac{\pi n}{\omega}, \quad n = 0, \pm 1, \pm 2, \ldots, \tag{32}$$

$$k_{r_2}(h, \omega) = \frac{1}{e^{\sigma h} \sin(\omega h)} \mathrm{Im}\left(\frac{\Gamma(i\omega, \sigma)}{P_{\sigma_3}(i\omega)} \right). \tag{33}$$

Proof. It should be noted that the σ crossing boundaries of the quasi-polynomial (28), in the parametric space (h, k_r), are given by the critical crossings roots of quasi-polynomial (29), which occur when $s = 0$ and $s = \pm i\omega$. In this regard, on the one hand, the solutions of quasi-polynomial (29) when $s = 0$ are given by

$$\begin{aligned} 0 = Q_\sigma\left(s, k_{p_{1,2}}, k_{r_{1,2}}, \tau, h\right)\Big|_{s=0} &= P_{\sigma_1}\left(0, k_{p_{1,2}}\right) + P_{\sigma_2}\left(0, k_{r_1}\right) e^{\tau\sigma} \\ &\quad + P_{\sigma_3}(0) e^{\sigma h} k_{r_2}, \end{aligned} \tag{34}$$

or equivalently

$$k_{r_2} = -\frac{P_{\sigma_1}\left(0, k_{p_{1,2}}\right) + P_{\sigma_2}\left(0, k_{r_1}\right) \mathrm{e}^{\tau\sigma}}{P_{\sigma_3}(0) \mathrm{e}^{\sigma h}}. \tag{35}$$

On the other hand, the solutions of the quasi-polynomial (29) when $s = i\omega$ are given by

$$\begin{aligned} 0 = Q_\sigma\left(s, k_{p_{1,2}}, k_{r_{1,2}}, \tau, h\right)\Big|_{s=i\omega} &= P_{\sigma_1}\left(i\omega, k_{p_{1,2}}\right) + P_{\sigma_2}\left(i\omega, k_{r_1}\right) e^{-(i\omega-\sigma)\tau} \\ &\quad + P_{\sigma_3}(s) e^{\sigma h} k_{r_2} e^{-i\omega h}. \end{aligned} \tag{36}$$

Thereby,

$$-\frac{1}{k_{r_2} e^{\sigma h}} \left(\frac{\Gamma(i\omega, \sigma)}{P_{\sigma_3}(i\omega)} \right) = e^{-i\omega h} = \cos(\omega h) - i \sin(\omega h), \tag{37}$$

from which

$$\begin{aligned} \cos(\omega h) &= -\frac{1}{k_{r_2} e^{\sigma h}} \mathrm{Re}\left(\frac{\Gamma(i\omega, \sigma)}{P_{\sigma_3}(i\omega)} \right), \\ \sin(\omega h) &= \frac{1}{k_{r_2} e^{\sigma h}} \mathrm{Im}\left(\frac{\Gamma(i\omega, \sigma)}{P_{\sigma_3}(i\omega)} \right). \end{aligned} \tag{38}$$

From the above equation, it follows that

$$\frac{\cos(\omega h)}{\sin(\omega h)}\mathrm{Im}\left(\frac{\Gamma(i\omega,\sigma)}{P_{\sigma_3}(i\omega)}\right) = -\mathrm{Re}\left(\frac{\Gamma(i\omega,\sigma)}{P_{\sigma_3}(i\omega)}\right). \tag{39}$$

Then, the solutions of (39) (with respect to h) are of the following form:

$$h = \frac{1}{\omega}\cot^{-1}\left(-\frac{\mathrm{Re}\left(\left(\Gamma(i\omega,\sigma)\right)/\left(P_{\sigma_3}(i\omega)\right)\right)}{\mathrm{Im}\left(\left(\Gamma(i\omega,\sigma)\right)/\left(P_{\sigma_3}(i\omega)\right)\right)}\right) + \frac{\pi n}{\omega}, \tag{40}$$

$$n = 0, \pm 1, \pm 2, \ldots, \text{and } \omega \in \mathbb{R}^+.$$

Finally, solving k_{r_2} from (38), equation (33) follows.

In the following corollary, the σ-stability boundaries in the (h, k_{r_2}) parametric space are written particularly for the quasi-polynomial (23), where $P_1(s, k_{p_{1,2}}) = s^4 + k_{p_2}s^2 + k_{p_1}$, $P_2(s, k_{r_1}) = -k_{r_1}$, and $P_3(s) = -s^2$. □

Corollary 1. *Consider the quasipolynomial of the form (23). Then, the σ-stability boundaries (31)–(33) look as follows.*

For $s = 0$,

$$k_{r_2}(h) = \frac{k_{p_2}\sigma^4 + k_{p_2}\sigma^2 + k_{p_1} - k_{r_1}e^{\sigma\tau}}{\sigma^2 e^{\sigma h}}. \tag{41}$$

For $s = i\omega$, $\omega \in \mathbb{R}^+$,

$$\begin{aligned} h(\omega) &= \frac{1}{\omega}\cot^{-1}\left(-\frac{\Phi}{\Psi}\right) + \frac{\pi n}{\omega}, \\ k_{r_2}(h,\omega) &= \frac{\Psi}{e^{\sigma h}\sin(\omega h)\left(\sigma^2+\omega^2\right)^2}. \end{aligned} \tag{42}$$

Here, $n = 0, \pm 1, \pm 2, \ldots$, and Ψ and Φ are defined as

$$\begin{aligned} \Psi &= 2\omega\sigma\left(k_{p_1} - \left(\sigma^2+\omega^2\right)^2\right) \\ &\quad - k_{r_1}e^{\tau\sigma}\left(2\sigma\omega\cos(\omega\tau) - \left(\sigma^2-\omega^2\right)\sin(\omega\tau)\right), \\ \Phi &= \left(\sigma^2-\omega^2\right)\left(\sigma^2\omega^2 + k_{p_1} - k_{r_1}e^{\tau\sigma}\cos(\omega\tau)\right) \\ &\quad + k_{p_2}\left(\sigma^2+\omega^2\right)^2 - 2k_{r_1}\sigma\omega e^{\tau\sigma}\sin(\omega\tau) + \left(\sigma^6-\omega^6\right). \end{aligned} \tag{43}$$

The methodology to graphically determine the σ-stability boundaries (31)–(33) is as follows:

(1) Propose an initial value of $\sigma \in \mathbb{R}^+$ close to zero, denoted by σ_0

(2) For the critical frequencies $s = 0$: from (31), graph the parametric boundaries for $k_{r_2}(h)$ on the parametric space (h, k_{r_2}) considering $h \in (0, \overline{h}]$, $\overline{h} \in \mathbb{R}^+$, and σ_0

(3) For the critical frequencies $s = i\omega$:

(a) From (32), calculate h considering $\omega \in (0, \overline{\omega}]$, $\overline{\omega} \in \mathbb{R}^+$, and σ_0

(b) From (33), compute k_{r_2} considering $\omega \in (0, \overline{\omega}]$, σ_0, and h (from (a))

(c) Plot the values of h and k_{r_2}, obtained in the previous steps, on the parametric space (h, k_{r_2})

(4) Detect the closed regions/curves in the parametric plane (h, k_{r_2}) and discard the unstable ones; the remaining regions are considered as the σ-stability regions of (28)

(5) Select $\sigma_1 > \sigma_0$

(6) Repeat steps 2–5, considering σ_1, until the σ-stability regions collapse in a single point

Proposition 1 and Corollary 1 provide conditions to determine the σ-stability boundaries in the parametric plane (h, k_{r_2}) of quasi-polynomial (28). Next, the main result of the contribution is presented, where analytic expressions relative to the tuning of the controller gains h^* and $k_{r_2}^*$ to reach the maximal decay rate σ^* are obtained. The result is based on the fact that when the maximal decay rate σ^* is reached, there exist three dominant roots of the quasi-polynomial (28) in $s = -\sigma$; this phenomenon occurs when the concentric σ-stability regions collapse in a single point, denoted by $(h^*, k_{r_2}^*)$, as σ increases. The value of σ, when the collapse occurs, determines the maximal decay rate σ^*; see [25, 30]. Then, the analytical equations are determined to obtain the parameters h^* and $k_{r_2}^*$, considering that there are three dominant roots on σ^*.

Proposition 2. *Let us consider the closed-loop system (25). Then, the quasi-polynomial (28) has a root of multiplicity at least three on* $s = -\sigma^*$ *if* $k_{r_2}^*$ *and* h^* *satisfy the following equations:*

$$h^* = h(\sigma^*) = \left[\frac{(\partial/\partial s)P_{\sigma_3}(s)}{P_{\sigma_3}(0)} - \frac{(\partial/\partial s)\left(\Gamma(s,\sigma^*)\right)}{\Gamma(0,\sigma^*)}\right]\Bigg|_{s=0}, \tag{44}$$

$$k_{r_2}^* = k_{r_2}(\sigma^*, h^*) = \frac{-(\partial/\partial s)\left(\Gamma(s,\sigma^*)\right)\big|_{s=0}}{e^{\sigma^* h^*}\left((\partial/\partial s)P_{\sigma_3}(s)\big|_{s=0} - h^* P_{\sigma_3}(0)\right)}, \tag{45}$$

and σ^* *is the smallest positive real root of*

$$\begin{aligned} &f\left(\sigma, k_{p_1}, k_{p_2}, k_{r_1}, \tau\right) \\ &= P_{\sigma_3}(0)^2\left[\Gamma(0,\sigma)\frac{\partial^2}{\partial s^2}\left(\Gamma(s,\sigma) - \frac{\partial}{\partial s}\Gamma(s,\sigma)^2\right)\right]\Bigg|_{s=0} \\ &\quad + \Gamma(0,\sigma)^2\left[\left(\frac{\partial}{\partial s}P_{\sigma_3}(s)\right)^2 - P_{\sigma_3}(0)\frac{\partial^2}{\partial s^2}P_{\sigma_3}(s)\right]\Bigg|_{s=0}. \end{aligned} \tag{46}$$

Proof. Clearly, quasi-polynomial (28) presents three dominant roots at the point $s = -\sigma$ if the quasi-polynomial (29) has three dominant roots at $s = 0$. Thus, the conditions

$$\begin{aligned} Q_\sigma(\cdot)\big|_{s=0} &= 0, \\ \frac{\mathrm{d}}{\mathrm{d}s}Q_\sigma(\cdot)\Big|_{s=0} &= 0, \\ \frac{\mathrm{d}^2}{\mathrm{d}s^2}Q_\sigma(\cdot)\Big|_{s=0} &= 0, \end{aligned} \tag{47}$$

must be satisfied; consequently,

$$0 = \Gamma(0,\sigma) + P_{\sigma_3}(0)k_{r_2}e^{\sigma h}, \tag{48}$$

$$0 = \left(\frac{\partial}{\partial s}\Gamma(s,\sigma)\right)\Big|_{s=0} + k_{r_2}\mathrm{e}^{\sigma h}\left(\frac{\partial}{\partial s}P_{\sigma_3}(s)\mathrm{e}^{-sh}\right)\Big|_{s=0}, \tag{49}$$

$$0 = \left(\frac{\partial^2}{\partial s^2}\Gamma(s,\sigma)\right)\Big|_{s=0} + k_{r_2}\mathrm{e}^{\sigma h}\left(\frac{\partial^2}{\partial s^2}P_{\sigma_3}(s)\mathrm{e}^{-sh}\right)\Big|_{s=0}. \tag{50}$$

The first two (44) and (45) can be easily verified. First, expression (45) follows directly from (49). Now, to obtain (44), from (48) and (49), it follows that

$$0 = \left(\frac{\partial}{\partial s}\Gamma(s,\sigma)\right)\Big|_{s=0} - \frac{\Gamma(0,\sigma)}{P_{\sigma_3}(0)}\frac{\partial}{\partial s}P_{\sigma_3}(s)\Big|_{s=0} + h\Gamma(0,\sigma), \tag{51}$$

and we get (44):

$$h = \left[\frac{(\partial/\partial s)P_{\sigma_3}(s)}{P_{\sigma_3}(0)} - \frac{(\partial/\partial s)(\Gamma(s,\sigma))}{\Gamma(0,\sigma)}\right]\Big|_{s=0}. \tag{52}$$

To address (46), from (48) and (50), it follows that

$$\begin{aligned} 0 &= \left(\frac{\partial^2}{\partial s^2}\Gamma(s,\sigma)\right)\Big|_{s=0} + k_{r_2}\mathrm{e}^{\sigma h}\frac{\partial^2}{\partial s^2}P_{\sigma_3}(s)\mathrm{e}^{-\mathrm{sh}}\Big|_{s=0} \\ &= \left(\frac{\partial^2}{\partial s^2}\Gamma(s,\sigma)\right)\Big|_{s=0} - \frac{\Gamma(0,\sigma)}{P_{\sigma_3}(0)}\frac{\partial^2}{\partial s^2}P_{\sigma_3}(s)\Big|_{s=0} \\ &\quad + 2h\frac{\Gamma(0,\sigma)}{P_{\sigma_3}(0)}\frac{\partial}{\partial s}P_{\sigma_3}(s)\Big|_{s=0} - h^2\Gamma(0,\sigma). \end{aligned} \tag{53}$$

Substituting (52) in the above equation yields

$$\begin{aligned} 0 = {} & P_{\sigma_3}(0)^2\left[\Gamma(0,\sigma)\frac{\partial^2}{\partial s^2}\Gamma(s,\sigma) - \left(\frac{\partial}{\partial s}\Gamma(s,\sigma)\right)^2\right]\Big|_{s=0} \\ & + \Gamma(0,\sigma)^2\left[\left(\frac{\partial}{\partial s}P_{\sigma_3}(s)\right)^2 - P_{\sigma_3}(0)\frac{\partial^2}{\partial s^2}P_{\sigma_3}(s)\right]\Big|_{s=0}, \end{aligned} \tag{54}$$

which ends proof.

In the following corollary, conditions (44)–(46) are written particularly for the quasi-polynomial (27), where $P_1(s,k_{p_{1,2}}) = s^4 + k_{p_2}s^2 + k_{p_1}$, $P_2(s,k_{r_1}) = -k_{r_1}$, and $P_3(s) = -s^2$. □

Corollary 2. *Consider the quasi-polynomial of the form (27); then, the controller gains h^*, $k_{r_2}^*$ and the function $f(\sigma,\cdot)$ given by equations (44)–(46) look as*

$$\begin{aligned} f\left(\sigma,k_{p_{1,2}},k_{r_1},\tau\right) = {} & \sigma^4\left(2\sigma\left(k_{p_2}-2\sigma^2\right) - k_{r_1}\tau e^{\sigma\tau}\right)^2 \\ & + \sigma^2\kappa\left[\sigma^2\left(2k_{p_2}+12\sigma^2-k_{r_1}\tau^2e^{\sigma\tau}\right)\right]2\sigma^2\kappa^2, \end{aligned} \tag{55}$$

where $\kappa = k_{p_1} - k_{r_1}e^{\sigma\tau} + \sigma^2(\sigma^2 + k_{p_2})$ and

$$\begin{aligned} h^*\left(\sigma,k_{p_{1,2}},k_{r_1},\tau\right) &= \frac{2\sigma\mu_1 - k_{r_1}\tau e^{\sigma\tau}}{k_{p_1} - k_{r_1}e^{\sigma\tau} + \sigma^2\mu_2} - \frac{2}{\sigma}, \\ k_{r_2}^*\left(\sigma,k_{p_{1,2}},k_{r_1},h,\tau\right) &= e^{\sigma h}\frac{2\sigma\mu_1 - k_{r_1}\tau e^{\sigma\tau}}{\sigma(2+h\sigma)}, \end{aligned} \tag{56}$$

with $\mu_1 = k_{p_2} + 2\sigma^2$ and $\mu_2 = \mu_1 - \sigma^2$.

The conditions introduced in this section are only focused on the appropriate selection of the control parameters σ^*, $k_{r_2}^*$, and h^* that guarantee reaching the maximal exponential decay rate, but there are no conditions involving the remaining control parameters. In the following, a simple approach for the approximate selection of the control parameters is presented. On the one hand, let us consider quasi-polynomial (27), where the exponential terms are estimated by its first-order Taylor series truncated expansion; that is,

$$\begin{aligned} Q\left(s,k_{p_{1,2}},k_{r_{1,2}},\tau,h\right) &= \left(s^4 + k_{p_2}s^2 + k_{p_1}\right) - k_{r_1}(1-s\tau) \\ &\quad - k_{r_2}s^2(1-sh) \\ &= s^4 + hk_{r_2}s^3 + \left(k_{p_2} - k_{r_2}\right)s^2 + \tau k_{r_1}s \\ &\quad + \left(k_{p_1} - k_{r_1}\right). \end{aligned} \tag{57}$$

Now, let us propose a Hurwitz stable polynomial of the following form:

$$p(s) = \left(s^2 + 2\xi_c\omega_c s + \omega_c^2\right)^2, \tag{58}$$

where $\xi_c, \omega_c \in \mathbb{R}^+$. Thus, the dynamics of the previous polynomial is matched with (57). Then, simple calculations show that the controller gain parameters $k_{p_1}, k_{p_2}, k_{r_1}$, and τ can be chosen according to the following conditions (for $\alpha_1 > 1$ and $\alpha_2 > 2$):

$$\begin{aligned} k_{p_1} &> \alpha_1\omega_c^4, \\ k_{p_2} &> \alpha_2\omega_c^2\left(1+2\xi_c^2\right), \end{aligned} \tag{59}$$

$$\begin{aligned} k_{r_1} &= k_{p_1} - \omega_c^4, \\ \tau &= \frac{4\xi_c\omega_c^3}{k_{r_1}}. \end{aligned} \tag{60}$$

Remark 1. Due to the simple nature of conditions (54) and (60), they must be considered only as a starting point in the process of tuning the delayed control law (24) and subsequently adjusted according to the performance of the system.

5. Cases of Study

5.1. Rotatory Flexible Link. The rotatory flexible link platform consists of a rotating base driven by a belt-pulley mechanism actuated by a DC motor, a link is attached to the rotating base by two springs of identical nature, which results in a flexible joint. The schematic of such a manipulator is presented in Figure 2. The variables $\theta_1(t)$ and $\theta_2(t)$ denote

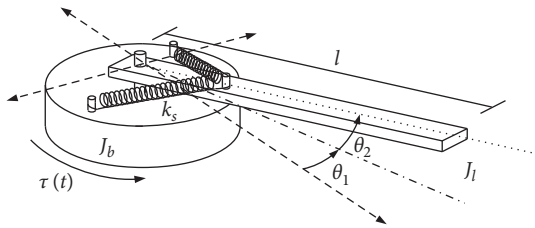

Figure 2: Schematics of the rotatory flexible link.

the angular positions of the rotating base and the link, respectively, l represents the length of the link, J_b stands for the inertia of the rotating base, and J_l is the moment of inertia of the link. Finally, k_s denotes the stiffness of the spring and $u(t)$ is the torque input applied to the system.

The problem formulation is stated as follows. For the rotatory flexible link, a smooth rest to rest angular position reference trajectory for the rotating base is demanded while the nonactuated link is desired to remain in a vicinity zero position, avoiding oscillations during the tracking maneuver.

5.1.1. The Dynamic Model. Following the methodology presented in Section 3 the Euler-Lagrange formalism (11) is used to represent the mathematical model of the rotatory flexible link system, where the viscous friction is neglected and the unmodeled nonlinear terms are ignored:

$$M(q(t))\ddot{q}(t) + C(q(t), \dot{q}(t))\dot{q}(t) + g(q(t)) = P\tau(t), \tag{61}$$

with

$$\begin{aligned} M(q) &= \begin{bmatrix} J_b + J_l & J_l \\ J_l & J_l \end{bmatrix}, \\ C(q, \dot{q}) &= \begin{bmatrix} 0 & 0 \\ 0 & 0 \end{bmatrix}, \\ g(q) &= \begin{bmatrix} 0 \\ k_s\theta_2(t) \end{bmatrix}, \\ q(t) &= \begin{bmatrix} \theta_1(t) & \theta_2(t) \end{bmatrix}^\intercal, \\ P &= \begin{bmatrix} 1 & 0 \end{bmatrix}^\intercal, \end{aligned} \tag{62}$$

or in an equivalent form:

$$\begin{aligned} \ddot{\theta}_1(t) &= \frac{k_s}{J_b}\theta_2(t) + \frac{\tau(t)}{J_b}, \\ \ddot{\theta}_2(t) &= -k_s\left(\frac{J_b + J_l}{J_b J_l}\right)\theta_2(t) - \frac{\tau(t)}{J_b}. \end{aligned} \tag{63}$$

5.1.2. Cascade Structure Representation. Let us introduce the state vector:

$$\begin{aligned} x(t) &= \begin{bmatrix} x_1(t) & x_2(t) & x_3(t) & x_4(t) \end{bmatrix}^\intercal \\ &= \begin{bmatrix} \theta_1(t) & \dot{\theta}_1(t) & \theta_2(t) & \dot{\theta}_2(t) \end{bmatrix}^\intercal. \end{aligned} \tag{64}$$

Then, the applied torque can be expressed as $\tau(t) = N\tau_m$, where $\tau_m = (k_\tau/R_m)V(t)$ is the torque in terms of the input voltage, N represents the gear ratio, k_τ is the torque constant, and R_m denotes the motor armature resistance. Since (63) is linear, it can be rewritten in space state representation (24) as follows:

$$\dot{x}(t) = Ax(t) + bV(t), \tag{65}$$

$$\begin{aligned} A &= \begin{bmatrix} 0 & 1 & 0 & 0 \\ 0 & 0 & \dfrac{k_s}{J_b} & 0 \\ 0 & 0 & 0 & 1 \\ 0 & 0 & -\left(\dfrac{J_l + J_b}{J_l J_b}\right)k_s & 0 \end{bmatrix}, \\ b &= \begin{bmatrix} 0 \\ \dfrac{Nk_\tau}{R_m J_b} \\ 0 \\ -\dfrac{Nk_\tau}{R_m J_b} \end{bmatrix}. \end{aligned} \tag{66}$$

Let us define the Kalman controllability matrix as in (5). Direct calculations show that the pair (A, b) is controllable and consequently, by Definition 2, it is flat. The flat output can be computed according to (16), where by defining $\varepsilon = (R_m J_b J_l)/(k_\tau k_s N)$, the flat output $y_f(t)$ is expressed as

$$y_f(t) = x_1(t) + x_3(t). \tag{67}$$

The flat output time derivatives are

$$\begin{aligned} y_f(t) &= x_1(t) + x_2(t), \\ \dot{y}_f(t) &= x_2(t) + x_4(t), \\ \ddot{y}_f(t) &= -\frac{k_s}{J_l}x_3(t), \\ y_f^{(3)}(t) &= -\frac{k_s}{J_l}x_4(t), \\ y_f^{(4)}(t) &= \frac{k_s^2(J_l + J_b)}{J_l^2 J_b}x_3(t) + \frac{k_\tau k_s N}{R_m J_b J_l}V(t). \end{aligned} \tag{68}$$

Let us define the output error as in (20); then, its dynamics are

$$\begin{aligned} \dot{e}_1(t) &= e_2(t), \\ \dot{e}_2(t) &= e_3(t), \\ \dot{e}_3(t) &= e_4(t), \\ \dot{e}_4(t) &= \frac{k_s^2(J_l + J_b)}{J_l^2 J_b}x_3(t) + \frac{k_\tau k_s N}{R_m J_b J_l}V(t) - y_f^{*(4)}(t), \end{aligned} \tag{69}$$

where the auxiliary control $V(t)$ is proposed as

$$V(t) = a_1\left[u(t) - \frac{k_s^2(J_l + J_b)}{J_l^2 J_b}x_3(t) + y_f^{*(4)}(t)\right],$$
$$a_1 = \frac{R_m J_b J_l}{k_\tau k_s N}. \tag{70}$$

5.1.3. Delayed Control Law. If the following delayed controller, $u(t) = {}_u(t)$ is considered:

$$u_D(t) = -k_{p_1}e_1(t) + k_{r_1}e_1(t-\tau) - k_{p_2}e_3(t) + k_{r_2}e_3(t-h). \tag{71}$$

The chain of integrators representation (25) is obtained.

Remark 2. It is worth noting that both the auxiliary control $V(t)$ and the delayed controller $u_D(t)$ depend completely on the measurable variables that correspond to angular positions $x_1(t) = \theta_1(t)$ and $x_3(t) = \theta_2(t)$.

5.1.4. Feedback State Control Law. In order to compare the proposed delayed controller with a classical scheme, a feedback state control is designed as follows:

$$u_{\mathrm{FS}}(t) = -\kappa_1 e_1(t) - \kappa_2 e_2 - \kappa_3 e_3(t) - \kappa_4 e_4(t), \tag{72}$$

where the set of gains $[\kappa_1, \kappa_2, \kappa_3, \kappa_4]$ is chosen as $\kappa_1 = \varpi^4$, $\kappa_2 = 4\bar{\varsigma}\varpi^3$, $\kappa_3 = 4\bar{\varsigma}^2\varpi^2 + 2\varpi^2$, and $\kappa_4 = 4\bar{\varsigma}\varpi$.

Remark 3. Now, the auxiliary control $V(t)$ and the feedback state control law $u_{\mathrm{FS}}(t)$ depend on the complete vector state $x(t)$, due to the fact that the velocity states $x_2(t) = \dot{\theta}_1(t)$ and $x_4(t) = \dot{\theta}_2(t)$ are not available; then, a low pass filter with transfer function $G(s) = (200s)/(s + 200)$ is used to estimate the velocity using the measurable variables $x_1(t) = \theta_1(t)$ and $x_3(t) = \theta_2(t)$; this methodology allows us to reduce the noise generated by the estimation of the so-called "dirty derivative" [45].

5.1.5. Experimental Results. In Figure 3, the rotatory flexible link experimental platform is presented. The prototype consists of a DC motor NISCA model NC5475 attached to the rotating base by means of a belt-pulley system with a 16 : 1 ratio. The angular position of both the rotating base and the link is measured by means of incremental encoders with a resolution of 1000 counts per revolution. The data acquisition is carried out with a data card Sensoray, model 626. The data card acquires the signals from the optical incremental encoders and supplies the control voltages to the power amplifiers (Quanser amplifier model VoltPAQ-X2). The control scheme is implemented in the Matlab-Simulink platform with a sampling time of 0.001[s].

The rotatory flexible link parameters are

Inertias: $J_b = 0.0481$ [Kg − m^2] and $J_l = 0.0036$ [Kg − m^2].

Length of the link: $l = 0.55$ [m].

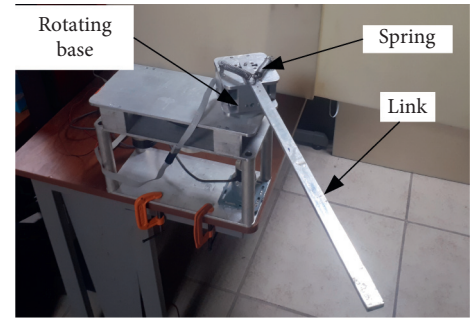

Figure 3: Rotatory flexible link prototype.

Stiffness of the spring: $k_s = 4$ [N − m/rad].

Armature resistance: $k_\tau = 0.0724$ [Ω].

Torque constant: $\tau_m = 2.983$ [Ω].

Mechanical advantage: $N = 16$.

In this experiment, the tracking trajectory problem is addressed. The initial conditions are $x(0) = 0$. The desired trajectory $y_f^*(t)$ consists of a path initialized at $y_f^*(0) = 0$[rad]. After two seconds in this position, the mechanism moves, in an interval of 0.7[s], to $y_f^*(2) = \pi/2$[rad] where it stands still for 7.3[s]. Finally, the reference path returns to its initial condition in an interval of 0.7[s].

The parameters of the controller were selected as follows. According to (38) and (39), the following values were proposed $\omega_c = 52$ and $\xi_c = 1.2$; thus, $k_{p_1} = 29246464$, $k_{p_2} = 33572.864$, $k_{r_1} = 21934848$, and $\tau = 0.02$. Now, the conditions presented in Corollary 4 lead to $\sigma^* = 66.65$ and consequently $k_{r_2}^* = 18839.729$ and $h^* = 0.00476$.

The σ-stability boundaries were calculated following Corollary 1, which is illustrated in Figure 4. The red mark symbolizes the maximal achievable decay rate σ^* and, as it can be seen, represents the point where all the σ-stable regions collapse.

Figure 5 depicts the rightmost root locus of the closed-loop system, where it can be appreciated that a triple real dominant root is located at the point $\sigma^* = 66.65$ as stated in Proposition 3.

The set of gains for the feedback state controller were chosen as $\varpi = 52$ and $\bar{\varsigma} = 1.2$. The main challenge when controlling the rotatory flexible link platform is to avoid the oscillations that appear intrinsically due to the flexible nature of the system. In Figure 6, the rotatory flexible link tracking trajectory task under the control actions of the proposed cascade PR scheme and feedback state is presented. The desired trajectory $y_f^*(t)$ is represented by a black line, while the flat output $y_{\mathrm{fD}}(t)$ with the delayed controller is depicted in blue and the $y_{\mathrm{fFS}}(t)$ with the feedback is represented by a red line. It can be seen that the tracking task is carried out satisfactorily by both controllers, avoiding oscillations and reaching the reference without overshooting. The tracking errors are detailed in Figure 7, noticing that both errors e_D and e_{FS} are restricted to the interval $[-0.075, 0.075]$[rad] with similar performance. Figures 8 and 9 represent the evolution of the angular positions θ_1 and θ_2

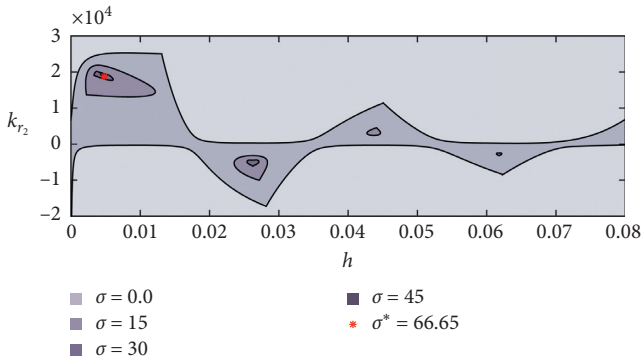

Figure 4: σ-stability boundaries.

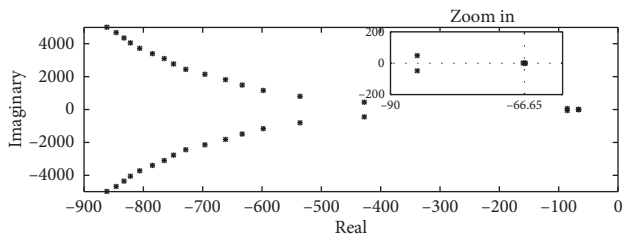

Figure 5: Root locus.

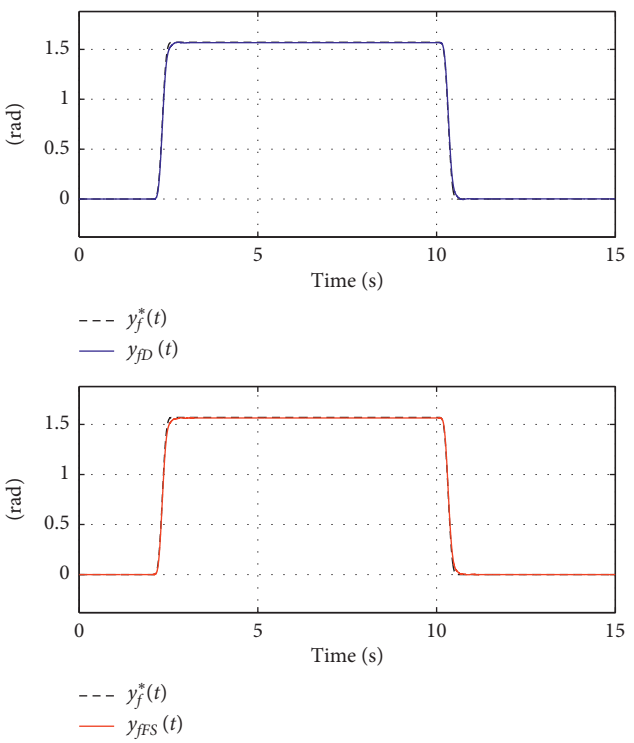

Figure 6: Trajectory tracking results.

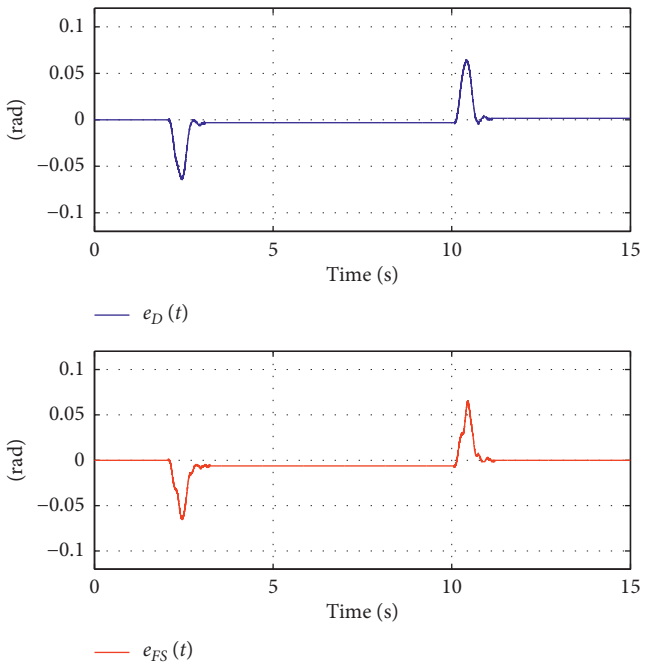

Figure 7: Tracking error.

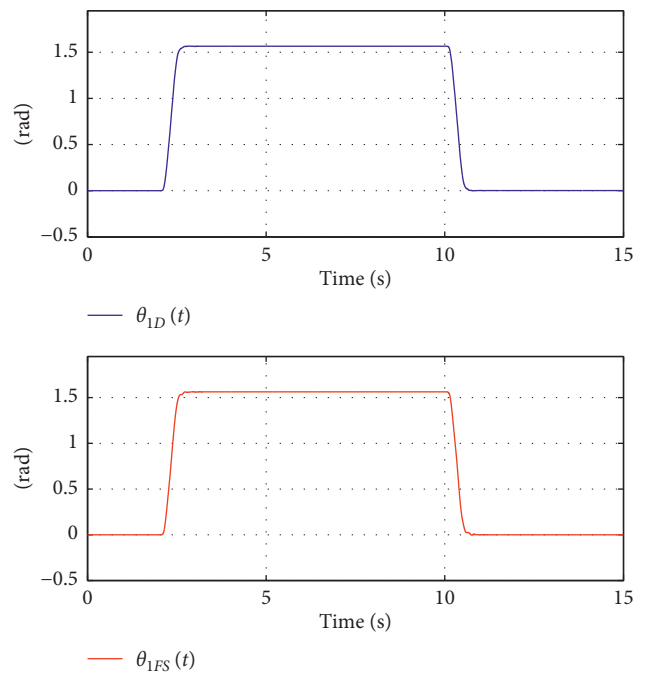

Figure 8: θ_1 evolution.

when the system follows the reference trajectory. Figure 10 shows the control voltages of both schemes. Notice that the peak voltage V_D does not exceed ±10[Volts] but V_{FS} presents a larger amplitude. As a consequence of avoiding the use of the time derivatives in the proposed control scheme, the voltage V_D signal appears relatively free of noise, as expected but V_{FS} presents high-frequency components; it can be corroborated in Figure 11 where a Power Spectrum Density of control signals V_D and V_{FS} is presented. Here, it can be observed that FS_{PSD} presents more frequency components in comparison with D_{PSD}. Finally, the performance of the system is evaluated by means of a quadratic index of the applied voltage (see Figure 12) where it can be noticed that V_{FS} consumes more energy.

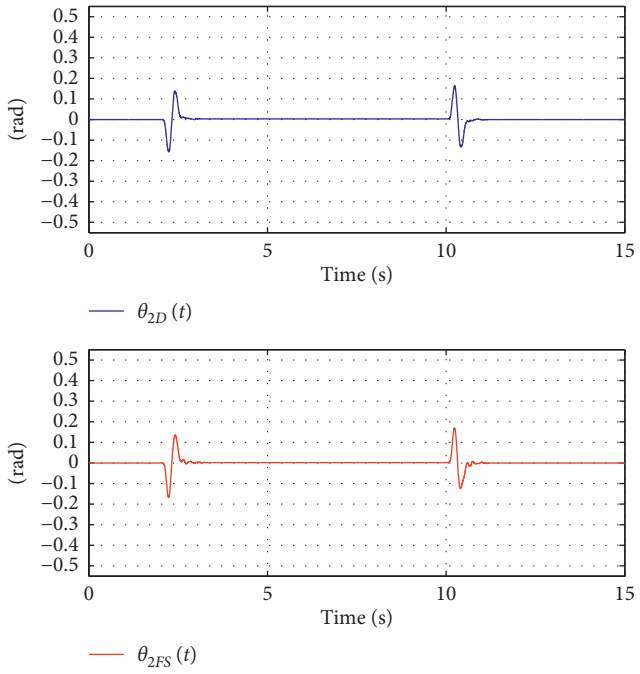

Figure 9: θ_2 evolution.

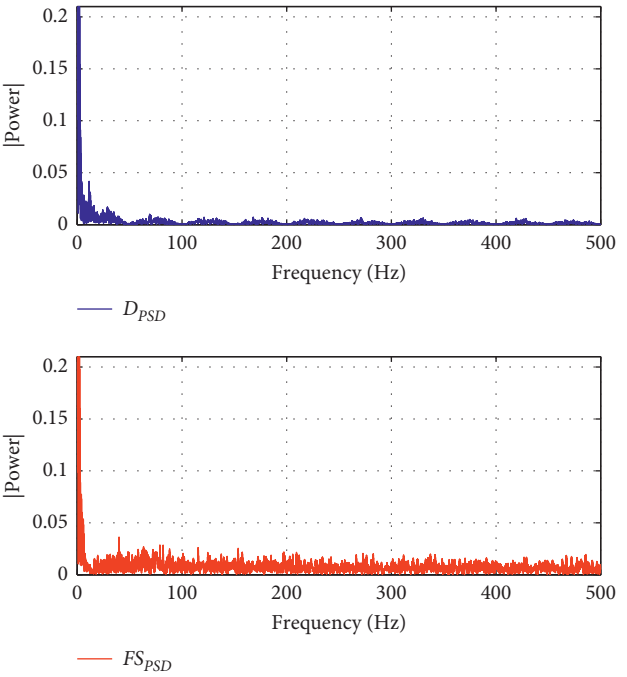

Figure 11: Power spectrum density.

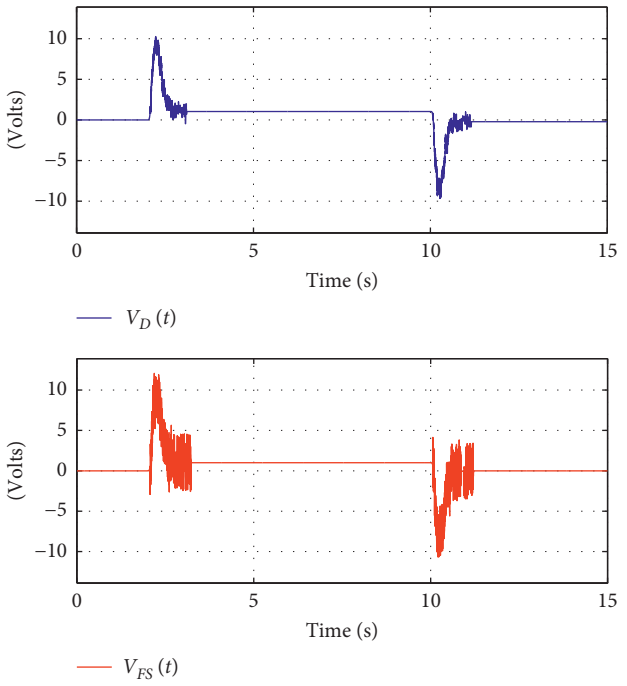

Figure 10: Control input voltage.

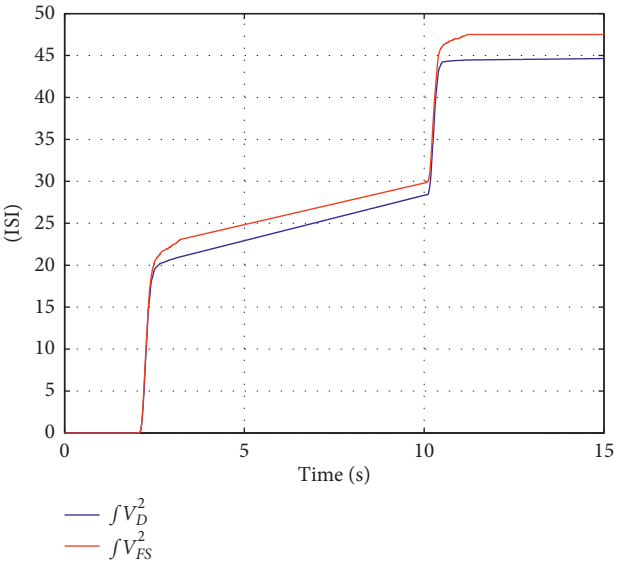

Figure 12: Performance index of the controller.

5.2. Pendubot System. The pendubot consists of a planar double inverted pendulum, whose schematic is presented in Figure 13. The first link is driven by a DC motor while the second link is an underactuated simple pendulum. The variables θ_1 and θ_2 denote the angular positions of the links, u represents the control torque input, and the parameters m_1 and m_2 denote the masses of the links. The lengths of the links are represented as l_1 and l_2, while l_{c_1} and l_{c_2} are the distances to the center of the masses. Finally, I_1 and I_2 denote the inertias of the links.

The problem formulation is given as follows: a smooth rest to rest angular position reference trajectory for the first link is demanded, while the nonactuated second link is desired to remain around its unstable vertical position, without falling during the entire tracking maneuver or moving away from the equilibrium point.

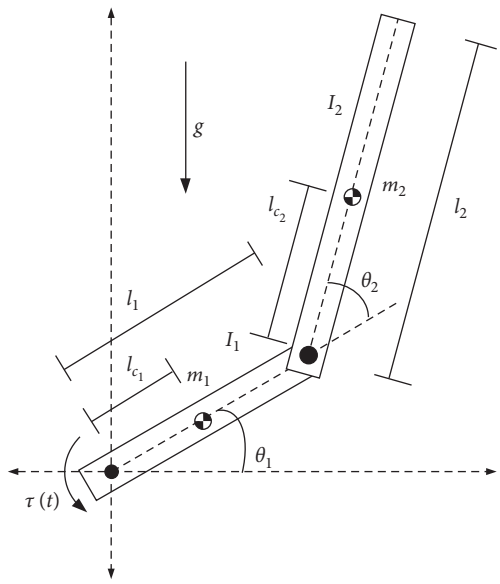

Figure 13: Schematics of the pendubot system.

5.2.1. The Nonlinear Dynamic Model. As carried out for the flexible link system, the Euler-Lagrange formalism is used to represent the dynamic model of the considered system:

$$M(q(t))\ddot{q}(t) + C(q(t), \dot{q}(t))q(t) + g(q(t)) = P\tau(t), \tag{73}$$

with $q(t) = [\,\theta_1(t)\ \ \theta_2(t)\,]^\intercal$ and $P = [\,1\ \ 0\,]^\intercal$. Here,

$$M(q) = \begin{bmatrix} \beta_1 + \beta_2 + 2\beta_3\cos(\theta_2(t)) & M_{1,2}(\theta) \\ \beta_2 + \beta_3\cos(\theta_2(t)) & \beta_2 \end{bmatrix},$$

$$C(q, \dot{q}) = \begin{bmatrix} -\beta_3\dot{\theta}_1(t)\sin(\theta_2(t)) & \beta_3 C_{1,2}(\theta) \\ \beta_3\dot{\theta}_1(t)\sin(\theta_2(t)) & 0 \end{bmatrix},$$

$$g(q) = \begin{bmatrix} \beta_4 g\cos(\theta_1(t)) + \beta_5 g\cos(\theta_1(t) + \theta_2(t)) \\ \beta_5 g\cos(\theta_1(t) + \theta_2(t)) \end{bmatrix}, \tag{74}$$

where

$$\begin{aligned} \beta_1 &= m_1 l_{c_1}^2 + m_2 l_{c_2}^2 + I_1, \\ \beta_2 &= m_2 l_{c_2}^2 + I_2, \\ \beta_3 &= m_2 l_1 l_{c_2}, \\ \beta_4 &= m_1 l_{c_1} + m_1 l_1, \beta_5 = m_2 l_{c_2}, \\ M_{1,2}(\theta) &= \beta_2 + \beta_3\cos(\theta_2(t)), \\ C_{1,2}(\theta) &= \left(\dot{\theta}_1(t) + \dot{\theta}_2(t)\right)\sin(\theta_2(t)). \end{aligned} \tag{75}$$

5.2.2. Cascade Structure Representation. In this section, the procedure presented in Section 3 is applied. The state vector is defined as

$$\begin{aligned} x(t) &= [\,x_1(t)\ \ x_2(t)\ \ x_3(t)\ \ x_4(t)\,]^\intercal \\ &= [\,\theta_1(t)\ \ \dot{\theta}_1(t)\ \ \theta_2(t)\ \ \dot{\theta}_2(t)\,]^\intercal. \end{aligned} \tag{76}$$

The applied torque can be expressed as $\tau(t) = (k_\tau/R_m)V(t)$ in terms of the input voltage, where k_τ is the torque constant and R_m represents the motor armature resistance. For $V = 0$, the considered equilibrium point $\overline{x}(t)$ is

$$\overline{x}(t) = \left[\,\frac{\pi}{2}\ \ 0\ \ 0\ \ 0\,\right]^\intercal. \tag{77}$$

Then, the tangent linearization looks as

$$\dot{x}_\delta(t) = Ax_\delta(t) + bV(t), \tag{78}$$

where $x_\delta(t) = [\,x_1(t) - \pi 2\ \ x_2(t)\ \ x_3(t)\ \ x_4(t)\,]^\intercal$,

$$A = \begin{bmatrix} 0 & 1 & 0 & 0 \\ \dfrac{(\beta_3\beta_5 - \beta_2\beta_4)g}{\beta_3^2 - \beta_1\beta_2} & 0 & \dfrac{\beta_3\beta_5 g}{\beta_3^2 - \beta_1\beta_2} & 0 \\ 0 & 0 & 0 & 1 \\ \dfrac{((\beta_2 + \beta_3)\beta_4 - (\beta_1 + \beta_3)\beta_5)g}{\beta_3^2 - \beta_1\beta_2} & 0 & \dfrac{(\beta_1 + \beta_3)\beta_5 g}{\beta_3^2 - \beta_1\beta_2} & 0 \end{bmatrix},$$

$$b = \begin{bmatrix} 0 & -\dfrac{k_\tau\beta_2}{R_m\left(\beta_3^2 - \beta_1\beta_2\right)} & 0 & \dfrac{k_\tau(\beta_2 + \beta_3)}{R_m\left(\beta_3^2 - \beta_1\beta_2\right)} \end{bmatrix}^T. \tag{79}$$

By defining the Kalman controllability matrix as $K_c = [\,b\ \ Ab\ \ A^2b\ \ A^3b\,]$, the pair (A, b) is controllable since K_c has full rank. Then, according to Definition 2, it implies that system (42) is flat, and the corresponding flat output is computed as

$$y_f(t) = \varepsilon[\,0\ \ 0\ \ 0\ \ 1\,]K_c^{-1}x_\delta(t) = \frac{\beta_2 + \beta_3}{\beta_2}x_{\delta 1}(t) + x_{\delta 3}(t). \tag{80}$$

Here, ε is selected as $\varepsilon = (R_m\beta_2(\beta_3^2 - \beta_1\beta_2))/(k_\tau\beta_3\beta_5 g)$. Now, by straightforward calculations, the flat output time derivatives (10) are given by

$$\begin{aligned} y_f(t) &= \frac{\beta_2 + \beta_3}{\beta_2}x_{\delta 1}(t) + x_{\delta 3}(t), \\ \dot{y}_f(t) &= \frac{\beta_2 + \beta_3}{\beta_2}x_{\delta 2}(t) + x_{\delta 4}(t), \\ \ddot{y}_f(t) &= \frac{g\beta_5}{\beta_2}\left(x_{\delta 1}(t) + x_{\delta 3}(t)\right), \\ y_f^{(3)}(t) &= \frac{g\beta_5}{\beta_2}\left(x_{\delta 2}(t) + x_{\delta 4}(t)\right), \\ y_f^{(4)}(t) &= \rho_1 x_{\delta 1}(t) - \rho_2\left(x_{\delta 1}(t) + x_{\delta 3}(t)\right) + \rho_3 V(t), \end{aligned} \tag{81}$$

with

$$\rho_1 = \frac{(\beta_3\beta_4\beta_5)g^2}{\beta_2\left(\beta_3^2 - \beta_1\beta_2\right)},$$

$$\rho_2 = \frac{\beta_1\beta_5^2 g^2}{\beta_2\left(\beta_3^2 - \beta_1\beta_2\right)}, \tag{82}$$

$$\rho_3 = \frac{k_\tau\beta_3\beta_5 g}{R_m\beta_2\left(\beta_3^2 - \beta_1\beta_2\right)}.$$

By defining the output error as in (20), then, the set of error dynamics (21) are given as follows:

$$\begin{aligned}
\dot{e}_1(t) &= e_2(t),\\
\dot{e}_2(t) &= e_3(t),\\
\dot{e}_3(t) &= e_4(t),\\
\dot{e}_4(t) &= \rho_1 x_{\delta 1}(t) - \rho_2\left(x_{\delta 1}(t) + x_{\delta 3}(t)\right)\\
&\quad + \rho_3 u_{\delta 1}(t) - y_f^{*(4)}(t).
\end{aligned} \tag{83}$$

Now, by proposing the auxiliary control

$$\begin{aligned}
V(t) &= \rho_3^{-1}\left[u(t) - \rho_1 x_{\delta 1}(t) + \rho_2\left(x_{\delta 1}(t) + x_{\delta 3}(t)\right)\right]\\
&\quad + \rho_3^{-1} y_f^{*(4)}(t),
\end{aligned} \tag{84}$$

and by considering the delayed control law

$$\begin{aligned}
u(t) = u_D(t) &= -k_{p_1} e_1(t) + k_{r_1} e_1(t-\tau) - k_{p_2} e_3(t)\\
&\quad + k_{r_2} e_3(t-h),
\end{aligned} \tag{85}$$

the desired chain of integrators representation (25) is obtained.

Remark 4. As in the previous experiment, the auxiliary control $V(t)$ and the delayed control law $u_D(t)$ depend completely on the measurable variables that correspond to the angular positions.

5.2.3. Feedback State Control Law. As in the previous test, feedback state control is designed in order to compare its performance with the proposed delayed controller:

$$u_{\mathrm{FS}}(t) = -\kappa_1 e_1(t) - \kappa_2 e_2 - \kappa_3 e_3(t) - \kappa_4 e_4(t), \tag{86}$$

where the following set of gains $[\kappa_1, \kappa_2, \kappa_3, \kappa_4]$ is chosen as $\kappa_1 = \bar{\omega}^4$, $\kappa_2 = 4\bar{\varsigma}\bar{\omega}^3$, $\kappa_3 = 4\bar{\varsigma}^2\bar{\omega}^2 + 2\bar{\omega}^2$, and $\kappa_4 = 4\bar{\varsigma}\bar{\omega}$.

Remark 5. The velocity states $x_2(t)$ and $x_4(t)$ are estimated using a low pass filter with transfer function $G(s) = (200s/s + 200)$.

5.2.4. Experimental Results. Figure 14 shows the experimental pendubot prototype. It consists of a DC motor NISCA model NC5475, which drives the first link. The angular position of both links is measured by means of incremental encoders with a resolution of 10000 counts per revolution. The same data acquisition model of the former example was used. The power amplifier consists of a Quanser amplifier model VoltPAQ-X2. The control strategy was implemented in the Matlab-Simulink platform, and the sampling time was set to be 0.001[s]. The pendubot parameters are as follows.

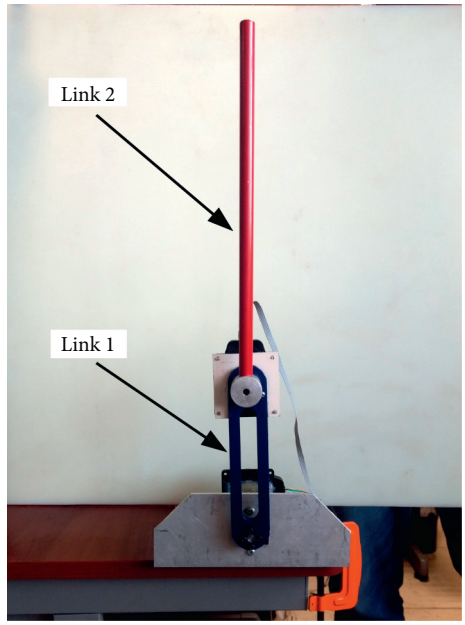

Figure 14: Pendubot prototype.

The test on the pendubot was carried out as follows:

Links Inertias: $I_1 = 0.00053$ [Kg − m^2] and $I_2 = 0.00077$ [Kg − m^2].

Mass of the links: $m_1 = 0.210$ [Kg] and $m_2 = 0.1$ [Kg].

Length of the links: $l_1 = 0.15$ [m] and $l_2 = 0.3$ [m].

Distance to the center of mass: $l_{c_1} = 0.12$ [m] and $l_{c_2} = 0.15$ [m].

Armature resistance: $k_\tau = 0.0724$ [Ω].

Torque constant: $\tau_m = 2.983$ [Ω].

The initial conditions are set as $x_1(0) = \pi/2$[rad] and $x_3(0) = 0$[rad]. The desired trajectory consists of a rest to rest smooth trajectory, described as follows:

$$\begin{aligned}
y_f^*(t) &= \frac{\beta_2 + \beta_3}{\beta_2} x_{\delta 1}^*(t) + x_{\delta 3}^*(t),\\
y_f^*(t) &= \frac{\beta_2 + \beta_3}{\beta_2}\left(\theta_1^*(t) - \frac{\pi}{2}\right) + \theta_2^*(t).
\end{aligned} \tag{87}$$

At $t = 0$, the trajectory is set at $y_f^*(0) = 0$; it implies that $\theta_1^*(t) = \pi/2$ and $\theta_2^*(t) = 0$; when the time reaches $t = 4.5$, the desired trajectory moves to $y_f^*(6) = ((\beta_2 + \beta_3)/\beta_2)(\pi/6) - (\pi/6)$ with $\theta_1^*(t) = (2/3)\pi$ and $\theta_2^*(t) = -(\pi/6)$ on a lapse of 2.5 seconds. Then, when time is $t = 9.5$[s], it moves to $y_f^*(13.5) = -((\beta_2 + \beta_3)/\beta_2)(\pi/6) + (\pi/6)$ with $\theta_1^*(t) = (\pi/3)$ and $\theta_2^*(t) = -(\pi/6)$ in 4 seconds, and finally, when $t = 17.5$[s], it returns to the initial position and remains in this position until the test is finished. Figure 15 shows the desired rest to rest positions of the pendubot system.

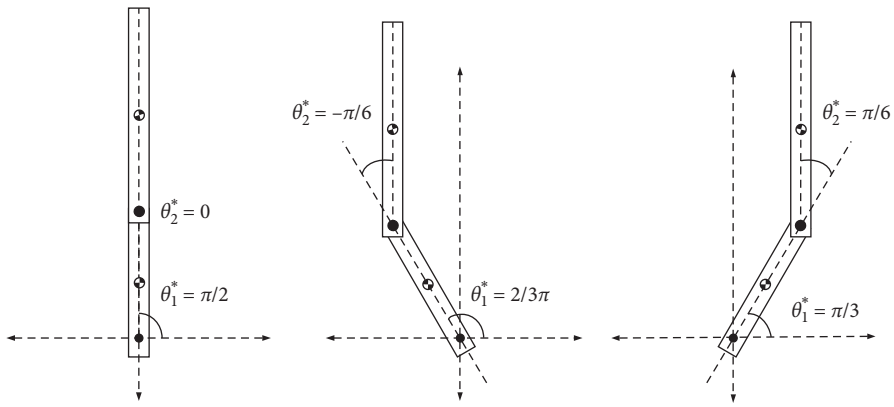

Figure 15: Pendubot desired rest to rest positions.

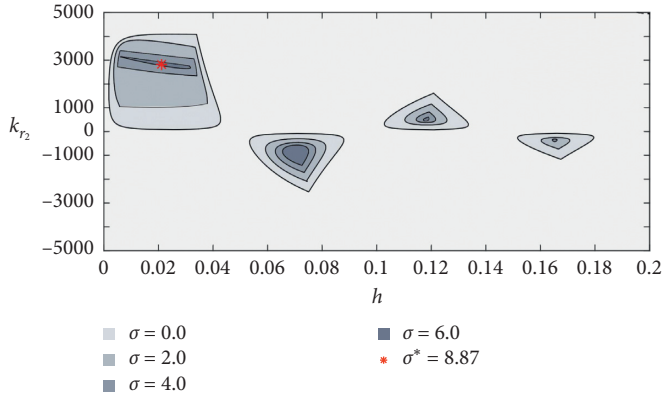

Figure 16: σ-stability boundaries.

The parameters of the controller were chosen according to (59 and 60), selecting $\omega_c = 14$ and $\xi_c = 1.2$ and then $k_{p_1} = 460992$, $k_{p_2} = 4562.88$, $k_{r_1} = 422576$, and $\tau = 0.0311$. The remainder of the parameters are calculated following Corollary 2, leading to $\sigma^* = 8.8477$, $k_{r_2} = 2832.39$, and $h^* = 0.021$. The σ-stability boundaries are computed by means of Corollary 1, see Figure 16, where the maximal achievable decay rate σ^* is marked as a red spot. Here, the zone outside the concentric regions corresponds to the unstable region. The set of gains for the feedback state controller were chosen as $\bar{\omega} = 14$ and $\bar{\varsigma} = 1.2$. Notice that the gain value coincides with the gain value used to select the proposed delayed control.

Figure 17 shows the flat output trajectory tracking performance of both controllers, the reference trajectory $y_f^*(t)$ is depicted in black line, the delayed controller response $y_D(t)$ is shown in the blue line, and the feedback controller response is shown in the red line $y_{\mathrm{FS}}(t)$, where it can be seen that the pendubot tracks the desired trajectory with adequate results, even when it is far from the equilibrium point. Figure 18 shows that the tracking errors $e_D(t)$ and $e_{\mathrm{FS}}(t)$ are bounded in an interval of approximately $[-0.025, 0.025]$[rad]. Figures 19 and 20 show the variation of the positions of the links during the tracking trajectory task. Figure 21 exhibits the control input voltage V_D calculated without using any time derivatives, which shows less noise

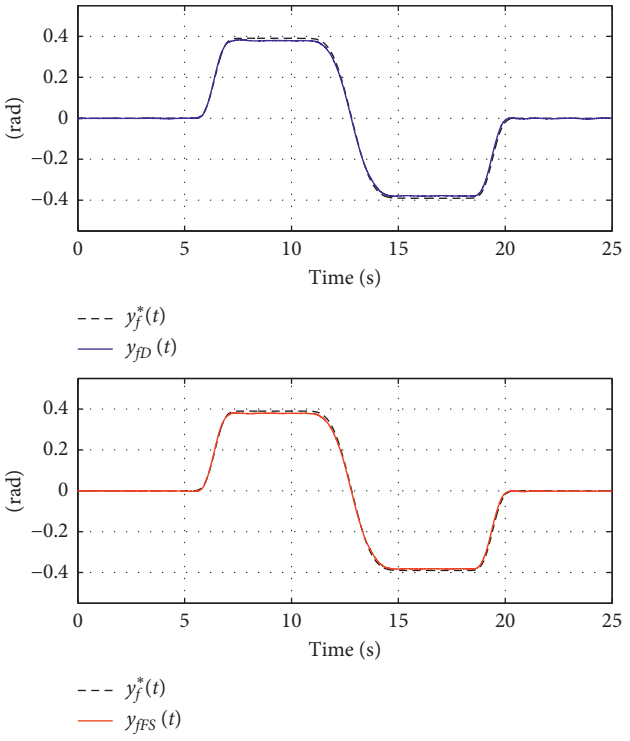

Figure 17: Flat output trajectory tracking.

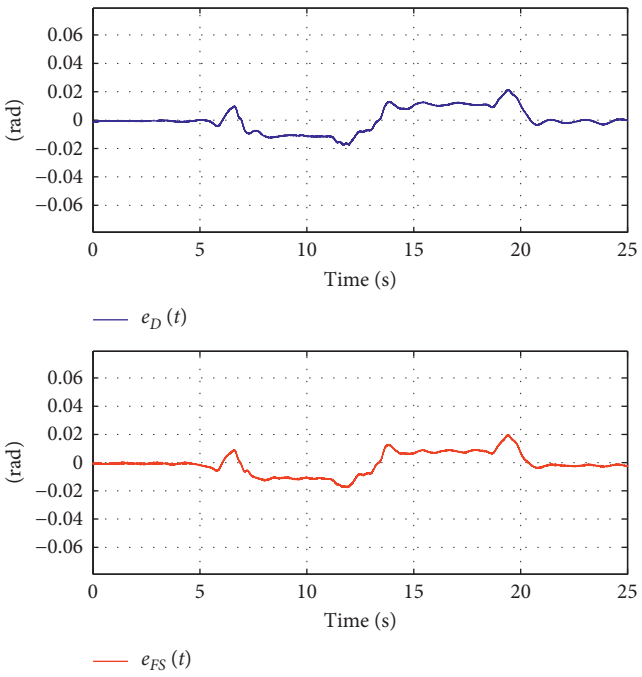

Figure 18: Tracking error.

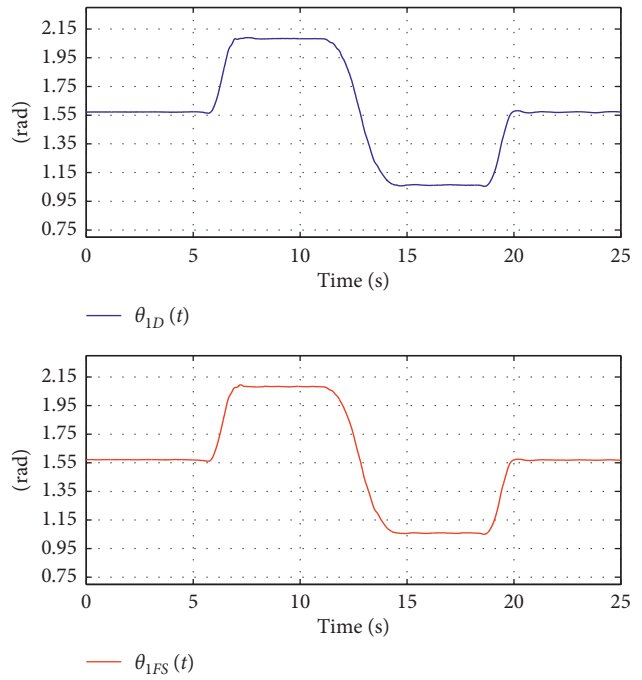

Figure 19: θ_1 performance.

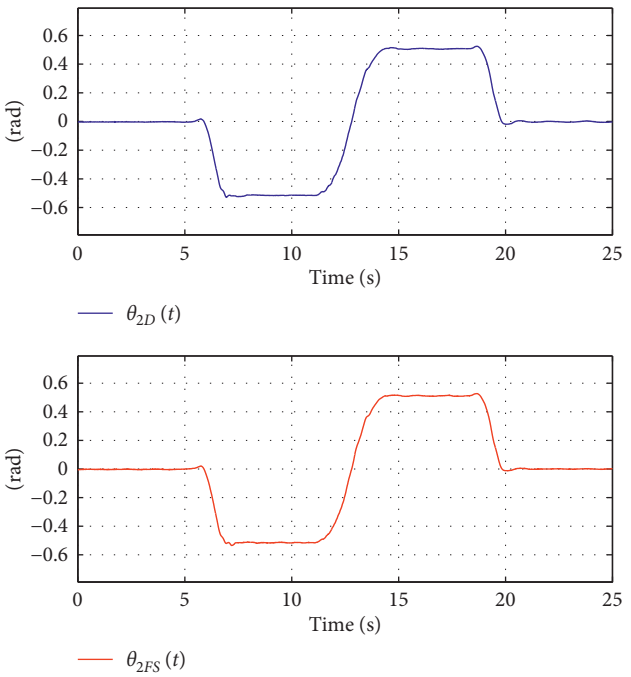

Figure 20: θ_2 performance.

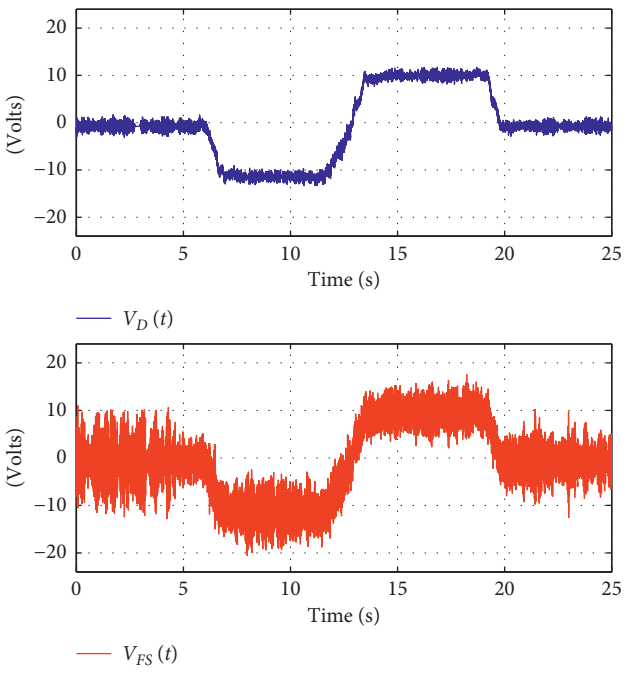

Figure 21: Control input voltage.

and less amplitude in contrast with V_{FS}. The performance of both controllers is similar to good results; the main difference is on the voltage control. The Power Spectrum Density of V_D and V_{FS} is depicted in Figure 22. Notice that FS_{PSD} shows high-frequency components with a peak on 50 [Hz]. Figure 23 shows an analysis using a quadratic index of the voltage, where V_{FS} consumes more energy. Thus, the proposed delay controller represents an attractive alternative to control a set of underactuated mechanical systems. A sensitivity analysis with a quadratic error index of the

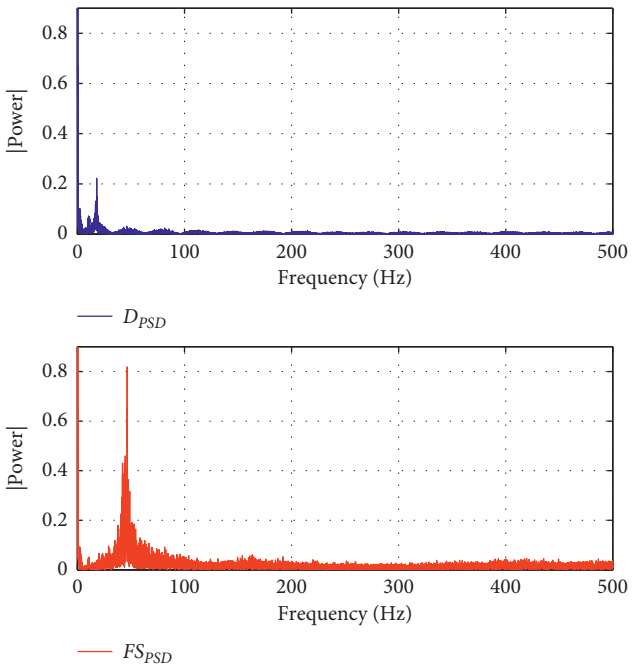

Figure 22: Power spectrum density.

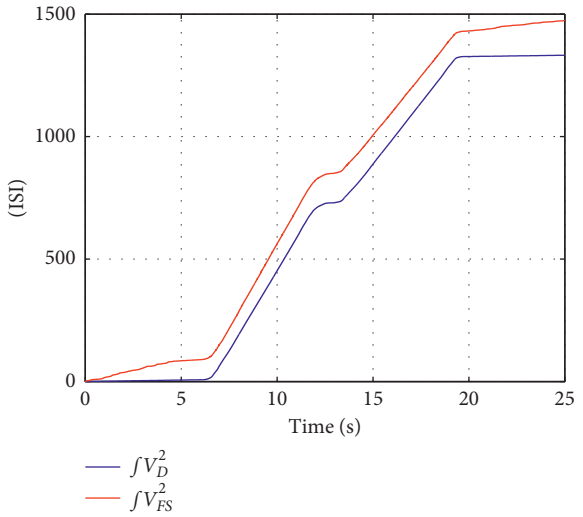

Figure 23: Performance index of the controller.

trajectory tasks was performed in simulation using a set of initial conditions for the angular positions $\theta_1(0)$ and $\theta_2(0)$. Figure 24 shows the first link performance; notice that the PR controller rank of initial conditions $\theta_{1D}(0)$ remains on $[-8, 8]$ degrees, in comparison with the FS controller rank of initial conditions $\theta_{1FS}(0)$ that remains on the interval $[-7, 7]$ degrees. Similarly, Figure 25 shows the second link performance, the rank of the initial conditions for $\theta_{2D}(0)$ is $[-12, 12]$ degrees, while $\theta_{2FS}(0)$ is $[-11, 11]$. Notice that the PR controller can control the pendubot system with further

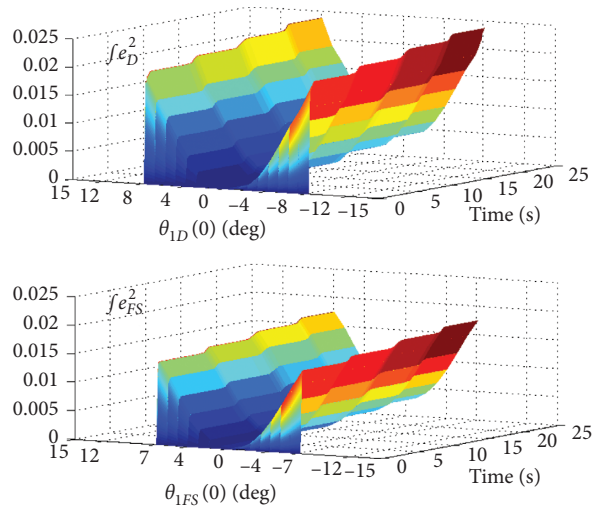

Figure 24: Assessment of the quadratic error index for the first link.

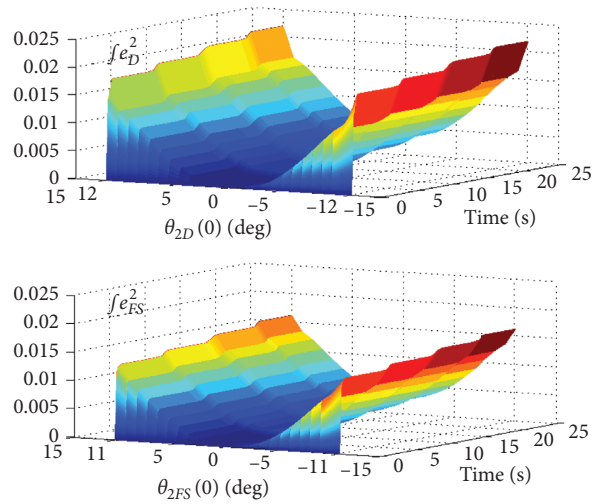

Figure 25: Assessment of the quadratic error index for the second link.

initial conditions from the equilibrium point than the PD controller.

6. Conclusion

In this paper, an alternative approach to control a class of underactuated systems of the fourth order through proportional retarded based controllers was proven and experimentally tested, leading to smooth tracking results thanks to the derivative-free control philosophy. The tuning procedure allows the practitioner to find appropriate control gains (the proposal is constructive). The cascade form of the tangent linearization of the underactuated system is an important design tool for the model simplification and the

local controllability property for the design of a wide variety of controllers. Future research concerning the topic deals with the extension of the procedure to larger order systems as well as a more comprehensive development of the conditions involving all the control parameters. The case of study can be also extended for disturbed dynamics, in which integral actions can be proposed and tested.

Data Availability

All the data generated or analyzed during this study are included in this paper.

Conflicts of Interest

The authors declare that there are no conflicts of interest regarding the publication of this paper.

Acknowledgments

This paper is in memory of Oscar Villafuerte-Segura. This work was partially supported by "Secretaría de Investigación y Posgrado-IPN" under Grants SIP20201675 and SIP20201830, and CONACYT-México and InIAT Universidad Iberoamericana Ciudad de México.

References

[1] C. A. Ibañez and O. G. Frias, "Controlling the inverted pendulum by means of a nested saturation function," *Nonlinear Dynamics*, vol. 53, no. 4, pp. 273–280, 2008.

[2] C. A. Ibañez, O. G. Frias, and M. S. Castañón, "Lyapunov-based controller for the inverted pendulum cart system," *Nonlinear Dynamics*, vol. 40, no. 4, pp. 367–374, 2005.

[3] I. Fantoni, R. Lozano, and M. W. Spong, "Energy based control of the pendubot," *IEEE Transactions on Automatic Control*, vol. 45, no. 4, pp. 725–729, 2000.

[4] B. Lu, Y. Fang, and N. Sun, "Continuous sliding mode control strategy for a class of nonlinear underactuated systems," *IEEE Transactions on Automatic Control*, vol. 50, 2018.

[5] R. Xu and Ü. Özgüner, "Sliding mode control of a class of underactuated systems," *Automatica*, vol. 44, no. 1, pp. 233–241, 2008.

[6] R. Ortega, A. Loría, P. Nicklasson, and H. Sira-Ramirez, *Passivity-based Control of Euler-Lagrange Systems: Mechanical, Electrical and Electromechanical Applications*, Springer Science & Business Media, Berlin, Germany, 1998.

[7] M. Spong, *Underactuated Mechanical Systems*, Springer, Berlin, Germany, 1998.

[8] J. Li, X. Qi, Y. Xia, and Z. Gao, "On asymptotic stability for nonlinear ADRC based control system with application to the ball-beam problem," 2016.

[9] M. Ramírez-Neria, H. Sira-Ramírez, R. Garrido-Moctezuma, and A. Luviano-Juárez, "Linear active disturbance rejection control of underactuated systems: the case of the furuta pendulum," *ISA Transactions*, vol. 53, no. 4, pp. 920–928, 2014.

[10] W. Tan and C. Fu, "Linear active disturbance-rejection control: analysis and tuning via imc," *IEEE Transactions on Industrial Electronics*, vol. 63, pp. 2350–2359, 2016.

[11] M. Reyhanoglu, A. van der Schaft, N. H. McClamroch, and I. Kolmanovsky, "Dynamics and control of a class of underactuated mechanical systems," *IEEE Transactions on Automatic Control*, vol. 44, no. 9, pp. 1663–1671, 1999.

[12] J. Hauser, S. Sastry, and P. Kokotovic, "Nonlinear control via approximate input-output linearization: the ball and beam example," *IEEE Transactions on Automatic Control*, vol. 37, no. 3, pp. 392–398, 1992.

[13] R. Olfati-Saber, "Normal forms for underactuated mechanical systems with symmetry," *IEEE Transactions on Automatic Control*, vol. 47, no. 2, pp. 305–308, 2002.

[14] M. Fliess, J. Lévine, P. Martin, and P. Rouchon, "Flatness and defect of non-linear systems: introductory theory and examples," *International Journal of Control*, vol. 61, no. 6, pp. 1327–1361, 1995.

[15] H. Sira-Ramírez, A. Luviano-Juárez, M. Ramírez-Neria, and E. W. Zurita-Bustamante, *Active Disturbance Rejection Control of Dynamic Systems: A Flatness Based Approach*, Butterworth-Heinemann, New York, NY, USA, 2017.

[16] N. S. Özbek and İ. Eker, "Investigation of time-delayed controller design strategies for an electromechanical system," *IEEE*, vol. 170, pp. 181–186, 2017.

[17] C. Abdallah, P. Dorato, J. Benites-Read, and R. Byrne, "Delayed positive feedback can stabilize oscillatory systems," *1993 American Control Conference*, vol. 53, pp. 3106-3107, 1993.

[18] K. Gu, S.-I. Niculescu, and J. Chen, "On stability crossing curves for general systems with two delays," *Journal of Mathematical Analysis and Applications*, vol. 311, no. 1, pp. 231–253, 2005.

[19] J.-E. Hernández-Díez, C.-F. Méndez-Barrios, S. Mondié, S.-I. Niculescu, and E. J. González-Galván, "Proportional-delayed controllers design for LTI-systems: a geometric approach," *International Journal of Control*, vol. 91, no. 4, pp. 907–925, 2018.

[20] C. Hwang and J. H. Hwang, "Stabilisation of first-order plus dead-time unstable processes using PID controllers," *IEE Proceedings-Control Theory and Applications*, vol. 151, no. 1, pp. 89–94, 2004.

[21] W. Just, T. Bernard, M. Ostheimer, E. Reibold, and H. Benner, "Mechanism of time-delayed feedback control," *Physical Review Letters*, vol. 78, no. 2, pp. 203–206, 1997.

[22] S.-I. Niculescu, K. Gu, and C. T. Abdallah, "Some remarks on the delay stabilizing effect in SISO systems," *IEEE*, vol. 3, 2003.

[23] N. Olgac, A. F. Ergenc, and R. Sipahi, ""Delay scheduling": a new concept for stabilization in multiple delay systems," *Journal of Vibration and Control*, vol. 11, no. 9, pp. 1159–1172, 2005.

[24] K. Pyragas, "Continuous control of chaos by self-controlling feedback," *Physics Letters A*, vol. 170, no. 6, pp. 421–428, 1992.

[25] A. Ramírez, S. Mondié, R. Garrido, and R. Sipahi, "Design of proportional-integral-retarded (PIR) controllers for second-order LTI systems," *IEEE Transactions on Automatic Control*, vol. 61, no. 6, pp. 1688–1693, 2016.

[26] M. de Sousa Vieira and A. J. Lichtenberg, "Controlling chaos using nonlinear feedback with delay," *Physical Review E*, vol. 54, no. 2, pp. 1200–1207, 1996.

[27] G. M. Swisher and S. Tenqchen, "Design of proportional-minus-delay action feedback controllers for second-and third-order systems," *IEEE*, vol. 63, 1988.

[28] Q.-C. Zhong and H.-X. Li, "A delay-type PID controller," *IFAC Proceedings Volumes*, vol. 35, no. 1, pp. 265–270, 2002.

[29] S. Mondié, R. Villafuerte, and R. Garrido-Moctezuma, "Tuning and noise attenuation of a second order system using proportional retarded control," 2011.

[30] R. Villafuerte, S. Mondié, and R. Garrido, "Tuning of proportional retarded controllers: theory and experiments," *IEEE*

Transactions on Control Systems Technology, vol. 21, no. 3, pp. 983–990, 2013.

[31] R. Villafuerte, S. Mondié, C. Vazquez, and J. Collado, "Proportional retarded control of a second order system," in *Proceedings of the International Conference on Electrical Engineering, Computing Science and Automatic Control, CCE*, New York, NY, USA, 2009.

[32] V. L. Kharitonov, S.-I. Niculescu, J. Moreno, and W. Michiels, "Static output feedback stabilization: necessary conditions for multiple delay controllers," *IEEE Transactions on Automatic Control*, vol. 50, pp. 82–86, 2005.

[33] F. Mazenc, S. Mondié, and S.-I. Niculescu, "Global stabilization of oscillators with bounded delayed input," *Systems & Control Letters*, vol. 53, no. 5, pp. 415–422, 2004.

[34] S.-I. Niculescu and W. Michiels, "Stabilizing a chain of integrators using multiple delays," *IEEE Transactions on Automatic Control*, vol. 49, no. 5, pp. 802–807, 2004.

[35] D. A. Irofti, K. Gu, I. Boussaada, and S.-I. Niculescu, "Some insights into the migration of double imaginary roots under small deviation of two parameters," *Automatica*, vol. 88, pp. 91–97, 2018.

[36] M. W. Spong, P. Corke, and R. Lozano, "Nonlinear control of the reaction wheel pendulum," *Automatica*, vol. 37, no. 11, pp. 1845–1851, 2001.

[37] E. N. Gryazina, "The D-decomposition theory," *Automation and Remote Control*, vol. 65, no. 12, pp. 1872–1884, 2004.

[38] E. N. Gryazina and B. T. Polyak, "Stability regions in the parameter space: D-decomposition revisited," *Automatica*, vol. 42, no. 1, pp. 13–26, 2006.

[39] E. N. Gryazina, B. T. Polyak, and A. A. Tremba, "D-decomposition technique state-of-the-art," *Automation and Remote Control*, vol. 69, no. 12, pp. 1991–2026, 2008.

[40] Y. I. Neimark, "D-partition and robust stability," *Computational Mathematics and Modeling*, vol. 9, no. 2, pp. 160–166, 1998.

[41] J. Levine, *Analysis and Control of Nonlinear Systems: A Flatness-Based Approach*, Springer Science & Business Media, Berlin, Germany, 2009.

[42] H. Sira-Ramirez and S. Agrawal, *Differentially Flat Systems*, CRC Press, New York, NY, USA, 2004.

[43] V. Kharitonov, *Time-delay Systems: Lyapunov Functionals and Matrices*, Springer Science & Business Media, Berlin, Germany, 2012.

[44] J. I. Neimark, "D-decomposition of the space of quasi-polynomials (on the stability of linearized distributive systems)," *American Mathematical Society Translations*, vol. 102, pp. 95–131, 1973.

[45] G. Escobar, R. Ortega, and H. Sira-Ramírez, "Output-feedback global stabilization of a nonlinear benchmark system using a saturated passivity-based controller," *IEEE Transactions on Control Systems Technology*, vol. 7, no. 2, pp. 289–293, 1999.

Hindawi
Complexity
Volume 2020, Article ID 3951381, 19 pages
https://doi.org/10.1155/2020/3951381

Research Article

Input-to-State Stabilization of a Class of Uncertain Nonlinear Systems via Observer-Based Event-Triggered Impulsive Control

Xiangru Xing and Jin-E Zhang

College of Mathematics and Statistics, Hubei Normal University, Huangshi 435002, China

Correspondence should be addressed to Jin-E Zhang; zhang86021205@163.com

Received 4 May 2020; Revised 22 June 2020; Accepted 21 July 2020; Published 17 August 2020

Guest Editor: Edgar Cristian Díaz González

Copyright © 2020 Xiangru Xing and Jin-E Zhang. This is an open access article distributed under the Creative Commons Attribution License, which permits unrestricted use, distribution, and reproduction in any medium, provided the original work is properly cited.

This article concerns the problem of input-to-state stabilization for a group of uncertain nonlinear systems equipped with nonabsolutely available states and exogenous disturbances. To appropriately cope with these partially measurable state variables as well as dramatically minimize controller updating burden and communication costs, an event-triggered mechanism is skillfully devised and an observer-based impulsive controller with the combination of sample control is correspondingly presented. By resorting to the iterative method and Lyapunov technology, some sufficient criteria are established to guarantee the input-to-state stability of the newly uncertain controlled system under the employed controller, in which an innovative approximation condition as to the uncertain term is proposed and the linear matrix inequality technique is utilized for restraining sophisticated parameter uncertainties. Furthermore, the Zeno behavior in the proposed event-triggered strategy is excluded. The control gains and event-triggered mechanism parameters are conjointly designed by resolving some inequalities of linear matrix. Eventually, the availability and feasibility of the achieved theoretical works are elucidated by two simulation examples.

1. Introduction

Since it is originally put forward by [1, 2], input-to-state stabilization has caught widespread attention [3–5], attributing to its performance in characterizing dynamical systems reaction to exogenous disturbances with bounded magnitude. The property of input-to-state stabilization, crudely speaking, symbolizes that the system state will ultimately approach the origin neighborhood whose dimension is in direct proportion to the size of the system input regardless of the magnitude of the initial state. With this characteristic, a system is asymptotically stabilizable under disturbance-free condition and has the evolution of bounded state in the bounded perturbation circumstance. Indeed, input-to-state stability behavior can characterize robustness and stability on dynamic systems possessed disturbances, in which the corresponding stabilization problem has a great signality for the control issue of [5–7]. Input-to-state stability is incipiently introduced for continuous systems to evaluate dynamical behaviors, which is especially a fundamental conception for investigating robust dynamics on nonlinear systems influenced by noise, inputs, or interferences [8]. Afterwards, it is diffusely capitalized for stabilizing controller synthesis and stabilization analysis of diverse discontinuous systems, to name a few, switched systems [9, 10], stochastic systems [5, 11], and fuzzy systems [12, 13].

Accompanied by the prompt development of some technologies such as digital control for resource-limited models and sensors incorporated embedded microprocessors, event-triggered impulsive control strategy, more recently, has been highly valued. On the one hand, the impulsive system, composed of discrete dynamics and continuous dynamics, is an important hybrid system in which the uncontinuous behavior is a momentary state jump occurring at given moments, while the consecutive behavior is usually expressed as differential equation. Correspondingly, impulsive control is a control approach that the control signals are transmitted to a system only at certain moments. In comparison with continuous control [14, 15], it

has the advantages of only discrete control which is required for deriving the desired performance, discontinuity, and stronger robustness. Consequently, the control approach is extensively applied in practice, such as ecosystem management [16, 17], satellite orbit transfer [18], secure communication [19], pharmacokinetics [20], and complex switched network [21]. Furthermore, controlling the operation of systems all the while is unnecessary or even impossible in practice. In population model [16], for example, it is merited to release predators at appropriate discrete circumstances, rather than the continuous instances for controlling the amount of a category insect. Moreover, as [22] amply demonstrated, impulsive control allows utilizing small control impulses as much as possible to stabilize a type of chaotic system. Not merely does it reduce redundant information transmission, but it increases the robustness of disturbances rejection. On the other hand, event-based control, as the name implies, is the strategy that event is triggered by some elaborate state-based or output-based event conditions to update the control input, which compared to the conventional time-triggered control is capable of avoiding unnecessary communication since a system adjusts the sampling rate adaptively according to the current situation [23, 24]. Specifically, the issue of self-learning optimal supervision on discrete systems via event-driven formulation is investigated in [24]. And the critics learning standard is improved for the design of nonlinear H_∞ state-feedback control based on events [25]. Distinct from the extant achievements involving sectionally continuous or consecutive control inputs, event-triggered impulsive control is able to dramatically minimize communication load and communication cost as well as enhance robustness, which, for these reasons, is deserving increasing attention. Simultaneously, the integration of two control strategies also creates tremendous challenges in designing appropriate controller.

As yet, some (but few) significant accomplishments about the event-triggered impulsive control such as [26–29] have been reported. Taking [26] as an instance, the synchronization issue on multiple neural networks with disconnected switching topology and delay under this control strategy is studied. Nevertheless, systems are generally affected by some uncertain factors such as human error, random disturbance, information loss, inherent deviation, or environmental noise. The uncertainty caused by these factors is referred to as the parametric uncertainty that is perhaps foremost provenance of model uncertainty [30]. Without taking model uncertainty into account, it seems to be far-fetched and preposterous in reality for analyzing performances of various systems like estimating the property indexes on steady state. In this condition, none of the beforementioned results are valid. Besides, in the control engineering application, when it comes to the fact that the system states may not be fully available because of implementation costs or physical restrictions, it becomes crucial and inevitable to formulate the event-triggered impulsive control strategy according to practical observer measurements. At this juncture, once the incomplete testability of states and the uncertainty of parameters are incorporated into the characterization of nonlinear systems, then these uncertainties may give rise to a totally new rule with more uncertain antecedents and results. What is exhilarating is that there is no work on the observer-based event-triggered impulsive control strategy to achieve the input-to-state property of uncertain nonlinear systems. After all, it is of more difficulty to find a feasible analytical framework compared with the nominal nonlinear systems. Moreover, in comparison with the previous methods, the robust handling for uncertain parameters during the course of system performance implementation becomes increasingly tricky as the number of uncertain parameters surges. Therefore, the theoretical challenges and technical deficiencies urge us to explore the actual performance evaluation for nonlinear systems with parametric uncertainties under observer-based control.

The abovementioned analysis motivates us to focus on issues of both input-to-state stability and event-triggered impulsive control scheme design on a type of uncertain nonlinear systems with incomplete measurable state variables and exogenous disturbances in this paper. Firstly, we establish a category of newly uncertain nonlinear systems, where the uncertainty terms are legitimately estimated by capitalizing on a creationary approximation condition of uncertainties, matrix synthesis method, and some inequalities of linear matrix. Secondly, a novel observer is constructed on the uncertain nonlinear system, in which the information between plant and observer is transmitted as impulses. In particular, the impulsive controllers are dependent upon the partial measurement output of observer and plant, which can eliminate the adverse effects of output data loss attributed to the external environment. Thirdly, an applicable observer-based event-triggered mechanism is designed and an event-triggered impulsive control strategy is correspondingly constructed, which could lessen burden of sampling and information transmission. At last, several sufficient criteria on excluding the Zeno behavior and analyzing the input-to-state stability property are developed, meanwhile, which suggest that a more extensible framework in complex dynamics can be explored through taking full advantage of a range of the employed ideas and methods.

The content of the remaining sections is summarized as follows. Section 2 puts forward the model and preparatory works for a kind of uncertain nonlinear systems. Section 3 furnishes primary research results. In addition, Section 4 corroborates the validity of the derived results by two numerical simulations. Finally, conclusion is exhibited in Section 5.

2. Preliminaries and Model Description

2.1. Notations. Throughout this article, $\mathbb{R}^{q\times p}$, $\mathbb{R}^q$, and $\mathbb{N}^+$ are separately the set of all $q\times p$ real matrices and q−dimensional Euclidean space and the set of positive integers. I stands for an identity matrix with matched dimensionality in matrices or matrix inequalities. 0 in matrices is a zero matrix of appropriate dimensions. Let $\|\mathscr{D}\|$ and $\|\mathscr{D}\|_{\mathcal{S}}$ denote the 2-norm of matrix $\mathscr{D}$ and the supremum of $\|\mathscr{D}\|$ on the interval $\mathcal{S}$, respectively. For a matrix $\mathscr{D}$, $\mathscr{D}^{-1}$,

$\mathscr{D}^T$, $\lambda_{\max}(\mathscr{D})$, and $\lambda_{\min}(\mathscr{D})$ represent severally its inverse, transposition, maximum eigenvalue, and minimum eigenvalue. The symbol $*$ is defined as the symmetric term in a matrix. $s\vee d$ and $s\wedge d$ represent the maximum and minimum of s and d, respectively. $\mathscr{D} > 0$ and $\mathscr{D} < 0$ mean that $\mathscr{D}$ are symmetric positive definite and symmetric negative definite separately. Let $He(\mathscr{D}) = \mathscr{D} + \mathscr{D}^T$, $\mathscr{K}_\infty = \{\phi \in \mathscr{C}(\mathbb{R}^+, \mathbb{R}^+) \mid \phi(0) = 0, \lim \phi(s) = \infty$, and $\phi(s)$ is strictly increasing in $s\}$, and $\mathscr{KL}^\infty = \{\psi \in \mathscr{C}(\mathbb{R}^+ \times \mathbb{R}^+, \mathbb{R}^+) \mid \psi(s, j)$, for each fixed $j \geq 0$, belongs to the function of class $\mathscr{K}$ as regards s, but $\psi(s, j)$, for each fixed $s \geq 0$, is strictly decreasing to 0 as $j \longrightarrow \infty\}$.

2.2. Some Preliminaries and Problem Formulation. A class of uncertain nonlinear systems incorporated exogenous disturbances is of the following form:

$$\begin{aligned} \dot{x}(t) &= (B + \Delta B)x(t) + \left(B_d + \Delta B_d\right) f(x(t)) \\ &\quad + (A + \Delta A)u(t) + (C + \Delta C)v(t), \\ y(t) &= (D + \Delta D)x(t), \end{aligned} \tag{1}$$

in which $t \geq t_0$, $x(t) \in \mathbb{R}^n$, $y(t) \in \mathbb{R}^p$, and $v(t) \in \mathbb{R}^n$ are the system state, the measurement output, and measurable locally bounded exogenous disturbances, respectively; $u(t) = u_1(t) + u_2(t)$ means the control input in which $u_1(t)$ is the sample control input and $u_2(t)$ is the Dirac delta control input; a nonlinear vector-valued function $f: \mathbb{R}^n \longrightarrow \mathbb{R}^n$ satisfies some conditions that will be provided in the sequel, and $\dot{x}(t)$ represents the right-hand derivative of $x(t)$. B, B_d, A, C, and D are constant matrices, and ΔB, ΔB_d, ΔA, ΔC, and ΔD are the norm-bounded uncertain parameters.

Given that the incompletely procurable system states can generate the ineffectiveness of state-feedback controllers, an observer-based controller is considered in this paper, and the state observer for uncertain system (1) is constructed by

$$\begin{aligned} \dot{\overline{x}}(t) &= B\overline{x}(t) + B_d f(\overline{x}(t)) + Au_3(t) + Cv(t), \\ \overline{y}(t) &= D\overline{x}(t), \end{aligned} \tag{2}$$

where $t \geq t_0$; $\overline{x}(t) \in \mathbb{R}^n$; and $\overline{y}(t) \in \mathbb{R}^p$ are separately the estimated state and the estimated output. The control input $u_3(t)$ of observer is described as

$$u_3(t) = \sum_{a=1}^{\infty} \left(\overline{K}y(t) + K\overline{y}(t) - \overline{K}\overline{y}(t)\right)\delta\left(t - t_a\right), \tag{3}$$

where $t \in [t_a, t_{a+1})$; K and $\overline{K}$ are control gains; δ is the Dirac delta function, which is also called the impulsive control function. And the impulsive time sequence $\{t_a\}_{a=1}^{\infty}$ satisfies $t_1 < t_2 < \cdots < t_a < \cdots$ and $\lim_{a\longrightarrow\infty} t_a = +\infty$. It is well-known that the Dirac delta function has two properties: for any constants c and $\Delta_1 > 0$ and function $g(t)$, (1) $\delta(t - c) = 0$ only when $t \neq c$; (2) $\int_{c-\Delta_1}^{c+\Delta_1} g(t)\delta(t - c)\mathrm{d}t = g(c)$. Then, by virtue of (2) and (3) and the properties of function δ, what we can see is that $u_3(t) = 0$ at $t \neq t_a$ and $a \in \mathbb{N}^+$, and for any constant $\Delta(>0)$ that is small enough,

$$\begin{aligned} &\overline{x}(t_a + \Delta) - \overline{x}(t_a - \Delta) \\ &= \int_{t_a-\Delta}^{t_a+\Delta} \left[B\overline{x}(s) + B_d f(\overline{x}(s)) + Cv(s)\right]\mathrm{d}s \\ &\quad + \int_{t_a-\Delta}^{t_a+\Delta} \sum_{a=1}^{\infty} A\left(\overline{K}yt(s)n + qKh\overline{y}(s)x - 7\overline{K}C\overline{y};(s)\right)\delta\left(s - t_a\right)\mathrm{d}s \\ &= \int_{t_a-\Delta}^{t_a+\Delta} \left[B\overline{x}(s) + B_d f(\overline{x}(s)) + Cv(s)\right]\mathrm{d}s \\ &\quad + A\left(\overline{K}y(t_a) + K\overline{y}(t_a) - \overline{K}\overline{y}(t_a)\right), \end{aligned} \tag{4}$$

where $\int_{t_a-\Delta}^{t_a+\Delta} \sum_{a=1}^{\infty} A\left(\overline{K}y(s) + K\overline{y}(s) - \overline{K}\overline{y}(s)\right)\delta(s - t_a)\mathrm{d}s$, which can be regarded as the convolution in the interval $[t_a - \Delta, t_a + \Delta]$ based on the properties of function δ, represents the sum of the effects of all unit impulses on the observer state over $[t_a - \Delta, t_a + \Delta]$.

Let $\Delta \longrightarrow 0$ and $\Delta\overline{x}(t) = \overline{x}(t_a^+) - \overline{x}(t_a^-)$; then we can infer that

$$\Delta\overline{x}(t) = A\left(\overline{K}y\left(t_a\right) + K\overline{y}\left(t_a\right) - \overline{K}\overline{y}\left(t_a\right)\right), \quad t = t_a. \tag{5}$$

By means of the above calculation, the controller $u_3(t)$ with function δ can make the observer state change instantaneously in the discrete time sequence $\{t_a\}_{a=1}^{\infty}$ so as to achieve the impulsive effect. Thus, observer (2) is converted into an impulsive control system as follows:

$$\begin{aligned} \dot{\overline{x}}(t) &= B\overline{x}(t) + B_d f(\overline{x} \\ \Delta\overline{x}(t) &= A\left(\overline{K}y(t^-) + K\overline{y}(t^-) - \overline{K}\overline{y}(t^-)\right), \quad t = t_a, \\ \overline{y}(t) &= D\overline{x}(t), \end{aligned} \tag{6}$$

where the left-continuous case of the estimate of $x(t)$ is always considered; that is, $\overline{x}(t) = \overline{x}(t^-) \triangleq \lim_{\Delta\longrightarrow 0}\overline{x}(t - \Delta)$.

According to the aforementioned observer, the control inputs $u_1(t)$ and $u_2(t)$ are devised as

$$\begin{aligned} u_1(t) &= L\overline{x}\left(t_a\right), \quad t \in \left[t_a, t_{a+1}\right), \\ u_2(t) &= \sum_{a=1}^{\infty} K\overline{y}(t)\delta\left(t - t_a\right), \quad t \in \left[t_a, t_{a+1}\right), \end{aligned} \tag{7}$$

where L is the gain of $u_1(t)$. In a similar way, uncertain system (1) can be transformed into

$$\begin{aligned} \dot{x}(t) &= (B + \Delta B)x(t) + \left(B_d + \Delta B_d\right) f(x(t)) \\ &\quad + (A + \Delta A)L\overline{x}\left(t_a\right) + (C + \Delta C)v(t), \quad t \neq t_a, \\ \Delta x(t) &= (A + \Delta A)K\overline{y}(t^-), \quad t = t_a, \\ y(t) &= (D + \Delta D)x(t). \end{aligned} \tag{8}$$

Without loss of generality, we always assume that the state of system (8) is left-continuous. For forward complete impulsive systems, there is no fundamental difference between utilizing left-continuous model and employing right-continuous model. Then by defining the tracking error $e(t) = x(t) - \overline{x}(t)$, the error system can be expressed as

$$\begin{aligned}\dot{e}(t) &= Be(t) + B_d(f(x(t)) - f(\overline{x}(t))) + (A+\Delta A)L\overline{x}(t_a)\\ &\quad + (C+\Delta C)\nu(t) + \Delta Bx(t) + \Delta B_d f(x(t)), \quad t \neq t_a,\\ \Delta e(t) &= (-\Delta AKD - A\overline{K}D)e(t^-)\\ &\quad + (\Delta AKD - A\overline{K}\Delta D)x(t^-), \quad t = t_a.\end{aligned} \tag{9}$$

Remark 1. Since uncertain system (1) is a category of impulsive systems, coupled with the incomplete measurability of the system state, we need to construct an appropriate observer and subsequently establish an applicable error system related to plant and observer. Based on the prerequisite of ensuring real-time monitoring, fault-tolerant control, easy realization, and so on, as a result, it is necessary and natural to construct observer (2) which is only influenced by impulsive. One more point needs noting that the controllers $u_2(t)$ and $u_3(t)$ designed by us can exert positive effects on the unstable systems and meanwhile control them only at the impulsive instant. In this way, $u_2(t)$ and $u_3(t)$ can stabilize systems (1) and (2), respectively, for ages, while reducing unnecessary computing costs.

Let

$$\begin{aligned}\wp(t) &= \left(x^T(t), e^T(t)\right)^T,\\ \zeta(t) &= \left(\nu^T(t), \nu^T(t)\right)^T,\\ \mathscr{F}(t) &= \left(f^T(x(t)), f^T(x(t)) - f^T(\overline{x}(t))\right)^T,\end{aligned} \tag{10}$$

and then the argument system can be deduced as

$$\begin{aligned}\dot{\wp}(t) &= \widetilde{B}\wp(t) + \widetilde{B}_d\mathscr{F}(t) + \widetilde{A}\widetilde{L}\wp(t_a) + \widetilde{C}\zeta(t), \quad t \neq t_a,\\ \wp(t) &= \widetilde{K}\wp(t^-), \quad t = t_a,\end{aligned} \tag{11}$$

where

$$\begin{aligned}B &= \begin{bmatrix} B+\Delta B & 0\\ \Delta B & B\end{bmatrix},\\ \widetilde{B}_d &= \begin{bmatrix} B_d+\Delta B_d & 0\\ \Delta B_d & B_d\end{bmatrix},\\ \widetilde{A} &= \begin{bmatrix} A+\Delta A & 0\\ 0 & A+\Delta A\end{bmatrix},\\ \widetilde{L} &= \begin{bmatrix} L & -L\\ L & -L\end{bmatrix},\\ \widetilde{C} &= \begin{bmatrix} C+\Delta C & 0\\ 0 & C+\Delta C\end{bmatrix},\\ \widetilde{K} &= \begin{bmatrix} I+(A+\Delta A)KD & -(A+\Delta A)KD\\ \Delta AKD - A\overline{K}\Delta D & I-\Delta AKD - A\overline{K}D\end{bmatrix}.\end{aligned} \tag{12}$$

Furthermore, $\forall t \in [t_a, t_{a+1}], a \in \mathbb{N}^+$, argument system (11) is rewritten as

$$\begin{aligned}\dot{\wp}(t) &= A_1\wp(t) + A_2\mathscr{F}(t) + A_3\varrho(t) + A_4\zeta(t), \quad t \neq t_a,\\ \wp(t) &= \widetilde{K}\wp(t^-), \quad t = t_a,\end{aligned} \tag{13}$$

where $\varrho(t) = \wp(t_a) - \wp(t)$;

$$\begin{aligned}A_1 &= \begin{bmatrix} B+\Delta B+(A+\Delta A)L & -(A+\Delta A)L\\ \Delta B+(A+\Delta A)L & B-(A+\Delta A)L\end{bmatrix},\\ A_2 &= \widetilde{B}_d = \begin{bmatrix} B_d+\Delta B_d & 0\\ \Delta B_d & B_d\end{bmatrix},\\ A_3 &= \widetilde{A}\widetilde{L} = \begin{bmatrix} (A+\Delta A)L & -(A+\Delta A)L\\ (A+\Delta A)L & -(A+\Delta A)L\end{bmatrix},\\ A_4 &= \widetilde{C} = \begin{bmatrix} C+\Delta C & 0\\ 0 & C+\Delta C\end{bmatrix}.\end{aligned} \tag{14}$$

An adaptive event-triggered mechanism, determining the continuously updated controller works at the instants $\{t_a \mid a \in \mathbb{N}^+\}$ known as the triggered time sequence, is introduced to decrease the burden of updating and communication in control. It is notable that the system states are imperfectly accessible, so the event-triggered mechanism included exogenous disturbances as well as the system and observer output is designed. By defining

$$\begin{aligned}\mathfrak{F}(t) &= \left(y^T(t), (y(t)-\overline{y}(t))^T\right)^T,\\ \widetilde{D} &= \begin{bmatrix} D+\Delta D & 0\\ \Delta D & D\end{bmatrix},\\ \overline{\varrho}(t) &= \widetilde{D}\varrho(t),\end{aligned} \tag{15}$$

the event-triggered mechanism is formulated as

$$\begin{aligned}t_{a+1} &= t^\star_{a+1} \wedge (t_a + \ell),\\ t^\star_{a+1} &= \inf\left\{t \geq t_a \,\middle|\, \mathscr{H}(t) \geq 0\right\},\end{aligned} \tag{16}$$

where the event generator function $\mathscr{H}(t) = \|\overline{\varrho}(t)\|^2 - \eta\|\mathfrak{F}(t_a)\|^2 - \rho\|\zeta(t)\|^2_{[t_0,t]}$, $t \in [t_a, t_{a+1})$; parameters $\eta > 0$, $\rho > 0$, and $\ell > 0$ in which ℓ is a forced triggered constant. Denote by $\{t^\star_a\}_{a=1}^\infty$ the event-triggered time sequence that it is determined by function $\mathscr{H}(t)$. For $t \geq t_a (a \in \mathbb{N}^+)$, the next event $t^\star_{a+1}$ will be triggered only when the correlative measurement reaches or surpasses the stated threshold, and then, the next triggered instant (impulsive instant) will be generated by comparing the obtained event-triggered time with the forced triggered time. In addition, it is worth mentioning that the aforesaid two sequences may differ depending on the selected parameters ℓ, η, and ρ.

In what follows, two assumptions are proposed around the uncertain terms and the nonlinear function.

Assumption 1

$$\begin{bmatrix}\Delta B & \Delta B_d & \Delta A & \Delta C & \Delta D\end{bmatrix} = ME(t)\begin{bmatrix}F_1 & F_2 & F_3 & F_4 & F_5\end{bmatrix}, \tag{17}$$

in which $E(t)$ is the unknown time-varying matrix with $\alpha I \le E^T(t)E(t) \le I$, the adjustment coefficient of the uncertain term $\alpha \in (0,1]$, and F_1, F_2, F_3, F_4, and F_5 are constant matrices with compatible dimensionality.

Remark 2. Different from existing achievements, such as [21, 30, 31], this paper has more uncertain parameters. Note that, in the practical application, each program will inevitably be subjected to the actual limitation of imprecise modeling for controlled plant and affected by external factors like environmental noise. Therefore, it is favorable and urgent for increasing the number of uncertainties to describe a larger range nonlinear system.

Remark 3. Only the norm-bounded uncertainties are taken into account in this article to efficaciously avoid needlessly intricate notations and restrain parameter uncertainty. In accordance with Assumption 1 and several linear matrix inequalities, the uncertainties ΔB, ΔB_d, ΔA, ΔC, and ΔD can be reasonably eliminated. Moreover, compared with the conventional constraint conditions of uncertain terms, the adjustment coefficient α is added in this paper, which not merely does not change the norm value range of the uncertain terms but also can ingeniously resolve the input-to-state stability problem of fairly sophisticated system. Even though the uncertainty parameters are also present at other singular structures, the subsequent results could be popularized to this circumstance in parallel.

Assumption 2. Suppose that there exists a scalar $\beta > 0$ such that the nonlinearity f satisfies $|f(y_1) - f(y_2)| \le \beta |y_1 - y_2|$, $\forall y_1, y_2 \in \mathbb{R}^n$. Particularly, $f(0) = 0$.

Hereafter, a definition and several lemmas are introduced for latter use.

Definition 1. For every initial condition $(t_0, \wp_0)$ and each measurable locally bounded exogenous disturbance $\zeta(t)$ (see [1]), system (13) is said to be input-to-state stabilizable under the given event-triggered mechanism (16) if there exist functions $\mathscr{Y} \in \mathscr{KL}$ and $\mathscr{Z} \in \mathscr{K}_\infty$ such that the solution $\wp(t)$ satisfies

$$\|\wp(t)\| \le \mathscr{Y}\left(\|\wp_0\|, t - t_0\right) + \mathscr{Z}\left(\|\zeta(t)\|_{[t_0,t]}\right), \quad t \ge t_0. \tag{18}$$

Lemma 1. *Given constant matrices $\mathscr{U}$, $\mathscr{P}$, and $\mathscr{V}$ with suitable dimensionality and a matrix function $\mathscr{M}(t)$ (see [23, 32]),*

(1) $\forall \varepsilon_1 > 0$ and $\mathscr{M}^T(t)\mathscr{M}(t) \le I$, then

$$\mathscr{P}\mathscr{M}(t)\mathscr{V} + \mathscr{V}^T\mathscr{M}^T(t)\mathscr{P}^T \le \frac{1}{\varepsilon_1}\mathscr{P}\mathscr{P}^T + \varepsilon_1\mathscr{V}^T\mathscr{V}. \tag{19}$$

(2) $\forall \varepsilon_2 > 0$ such that $\varepsilon_2\mathscr{V}^T\mathscr{V} < I$ and $\mathscr{M}^T(t)\mathscr{M}(t) \le I$, then

$$\begin{aligned}&(\mathscr{U} + \mathscr{P}\mathscr{M}(t)\mathscr{V})(\mathscr{U} + \mathscr{P}\mathscr{M}(t)\mathscr{V})^T \\ &\le \mathscr{U}\left(I - \varepsilon_2\mathscr{V}^T\mathscr{V}\right)^{-1}\mathscr{U}^T + \frac{1}{\varepsilon_2}\mathscr{P}\mathscr{P}^T.\end{aligned} \tag{20}$$

Particularly, when $\mathscr{U} \equiv 0$, we obtain

$$\mathscr{P}\mathscr{M}(t)\mathscr{V}(\mathscr{P}\mathscr{M}(t)\mathscr{V})^T \le \frac{1}{\varepsilon_2}\mathscr{P}\mathscr{P}^T. \tag{21}$$

Lemma 2. *$\forall s_1, s_2 \in \mathbb{R}^q$ (see [33]), the inequality*

$$s_1^T s_2 + s_2^T s_1 \le s_1{}^T R s_1 + s_2^T R^{-1} s_2, \tag{22}$$

holds, where $R \in \mathbb{R}^{q\times q}$ is a positive definite matrix.

Lemma 3. *Given constant matrices $\mathscr{B}_1, \mathscr{B}_2$, and $\mathscr{B}_3$ (see [34]), where $\mathscr{B}_1 = \mathscr{B}_1^T$ and $\mathscr{B}_2 > 0$, then*

$$\mathscr{B}_1 + \mathscr{B}_3^T\mathscr{B}_2^{-1}\mathscr{B}_3 < 0, \tag{23}$$

if and only if

$$\begin{bmatrix} \mathscr{B}_1 & \mathscr{B}_3^T \\ \mathscr{B}_3 & -\mathscr{B}_2 \end{bmatrix} < 0, \quad \text{or} \quad \begin{bmatrix} -\mathscr{B}_2 & \mathscr{B}_3 \\ \mathscr{B}_3^T & \mathscr{B}_1 \end{bmatrix} < 0. \tag{24}$$

3. Main Results

This section is devoted to the following tripartite through theoretical analysis and demonstrates the following:

(T1) The presence of the lower bound of adjacent impulse instants is testified, whereafter, the Zeno behavior can be excluded.

(T2) The resultant augmented system which is equipped with parameter uncertainties and exogenous disturbances is input-to-state stabilizable where the uncertainties are tactfully subdued.

(T3) The control gains and event-triggered scheme parameters are devised without strong constrained condition under system (13) corresponding stability.

Before verifying the above statements, it is necessary to introduce some symbols:

$$\mathscr{B}=\begin{bmatrix}B & 0\\ 0 & B\end{bmatrix},$$

$$\Delta\mathscr{B}=\begin{bmatrix}\Delta B & 0\\ \Delta B & 0\end{bmatrix},$$

$$\mathscr{B}_d=\begin{bmatrix}B_d & 0\\ 0 & B_d\end{bmatrix},$$

$$\Delta\mathscr{B}_d=\begin{bmatrix}\Delta B_d & 0\\ \Delta B_d & 0\end{bmatrix},$$

$$\mathscr{A}=\begin{bmatrix}A & 0\\ 0 & A\end{bmatrix},$$

$$\Delta\mathscr{A}=\begin{bmatrix}\Delta A & 0\\ 0 & \Delta A\end{bmatrix},$$

$$\mathscr{C}=\begin{bmatrix}C & 0\\ 0 & C\end{bmatrix},$$

$$\Delta\mathscr{C}=\begin{bmatrix}\Delta C & 0\\ 0 & \Delta C\end{bmatrix},\tag{25}$$

$$\mathscr{D}=\begin{bmatrix}D & 0\\ 0 & D\end{bmatrix},$$

$$\Delta\mathscr{D}=\begin{bmatrix}\Delta D & 0\\ \Delta D & 0\end{bmatrix},$$

$$\mathscr{M}=\begin{bmatrix}M & 0\\ 0 & M\end{bmatrix},$$

$$\mathscr{E}(t)=\begin{bmatrix}E(t) & 0\\ 0 & E(t)\end{bmatrix},$$

$$\mathscr{K}_1=\begin{bmatrix}I+AKD & -AKD\\ 0 & I-A\overline{K}D\end{bmatrix},$$

$$\mathscr{K}_2=\begin{bmatrix}KD & -KD\\ KD & -KD\end{bmatrix},$$

$$\mathscr{K}_3=\begin{bmatrix}0 & 0\\ 0 & -A\overline{K}\end{bmatrix}.$$

According to Assumption 1, we have

$$\begin{aligned}&\left[\Delta\mathscr{B}\ \ \Delta\mathscr{B}_d\ \ \Delta\mathscr{A}\ \ \Delta\mathscr{C}\ \ \Delta\mathscr{D}\right]\\&\quad=\mathscr{M}\mathscr{E}(t)\left[\mathscr{F}_1\ \ \mathscr{F}_2\ \ \mathscr{F}_3\ \ \mathscr{F}_4\ \ \mathscr{F}_5\right],\end{aligned}\tag{26}$$

where

$$\begin{aligned}\mathscr{F}_1&=\begin{bmatrix}F_1 & 0\\ F_1 & 0\end{bmatrix},\\ \mathscr{F}_2&=\begin{bmatrix}F_2 & 0\\ F_2 & 0\end{bmatrix},\\ \mathscr{F}_3&=\begin{bmatrix}F_3 & 0\\ 0 & F_3\end{bmatrix},\\ \mathscr{F}_4&=\begin{bmatrix}F_4 & 0\\ 0 & F_4\end{bmatrix},\\ \mathscr{F}_5&=\begin{bmatrix}F_5 & 0\\ F_5 & 0\end{bmatrix}.\end{aligned}\tag{27}$$

Theorem 1. *Under event-triggered scheme (16), then (T1) holds, where the positive lower bound $\mathscr{J}$ of adjoining impulsive moments conforms to $\mathscr{J}=(ln((\varphi_1(\eta\wedge\rho)/\varphi_2\vee\varphi_3)+1)/\varphi_1)\wedge\ell$, constants η, ρ, and ℓ are specified in (16), and*

$$\begin{aligned}\varphi_1&=2\|\mathscr{B}+\mathscr{A}\tilde{L}\|+2\|\mathscr{M}\|\cdot\left\|\mathscr{F}_1\right\|+2\|\mathscr{M}\|\cdot\left\|\mathscr{F}_3\tilde{L}\right\|\\&\quad+2\beta\left\|\mathscr{B}_d\right\|+2\beta\|\mathscr{M}\|\cdot\left\|\mathscr{F}_2\right\|+2\|\mathscr{A}\tilde{L}\|\\&\quad+2\|\mathscr{M}\|\cdot\left\|\mathscr{F}_3\tilde{L}\right\|\varphi_3,\\ \varphi_2&=\|\mathscr{B}+\mathscr{A}\tilde{L}\|+\|\mathscr{M}\|\cdot\left\|\mathscr{F}_1\right\|+\|\mathscr{M}\|\cdot\left\|\mathscr{F}_3\tilde{L}\right\|+\beta\left\|\mathscr{B}_d\right\|\\&\quad+\beta\|\mathscr{M}\|\cdot\left\|\mathscr{F}_2\right\|,\\ \varphi_3&=\|\mathscr{C}\|\cdot\|\mathscr{D}\|+\|C\|\cdot\|\mathscr{M}\|\cdot\|\mathscr{F}_5\|+\|D\|\cdot\|\mathscr{M}\|\cdot\|\mathscr{F}_4\|\\&\quad+\|\mathscr{M}\|^2\cdot\|\mathscr{F}_4\|\cdot\|\mathscr{F}_5\|.\end{aligned}\tag{28}$$

Proof. For the sake of checking on (T1), we consider the following three cases:

Case (i). The generation of the triggered time sequence $\{t_a\}_{a=1}^{\infty}$ depends entirely on the event-triggered time sequence $\{t_a^*\}_{a=1}^{\infty}$. Based on $\overline{\varrho}(t)=\widetilde{D}\varrho(t)=\mathfrak{T}(t_a)-\mathfrak{T}(t)$, in this case, the upper right Dini derivative of $\overline{\varrho}(t)$ in the interval $[t_a,t_{a+1})$ is calculated as

$$
\begin{aligned}
&D^+\|\overline{\varrho}(t)\|^2\\
&\quad=2\|\overline{\varrho}(t)\|D^+\|\overline{\varrho}(t)\|\\
&\quad=2\|\overline{\varrho}(t)\|\cdot\|\tilde{D}\dot{\wp}(t)\|\\
&\quad\le 2\|\overline{\varrho}(t)\|\cdot\left\|\tilde{D}A_1t\wp n(t)q+h\tilde{D}A_2x\mathscr{F}7(t)C+;\right.\\
&\qquad\left.\cdot\tilde{D}A_3\varrho(t)+\tilde{D}A_4\zeta(t)\right\|\\
&\quad\le 2\|\overline{\varrho}(t)\|\cdot\|A_1\|\cdot\|\mathfrak{F}(t)\|+2\beta\|\overline{\varrho}\\
&\qquad+2\|A_3\|\cdot\|\overline{\varrho}(t)\|^2+2\|\overline{\varrho}\\
&\quad\le\|A_1\|\left(\|\overline{\varrho}(t)\|^2+\|\mathfrak{F}(t)\|^2\right)+\beta\|A_2\|\left(\|\overline{\varrho}(t)\|^2+\|\mathfrak{F}(t)\|^2\right)\\
&\qquad+2\|A_3\|\cdot\|\overline{\varrho}(t)\|^2+\|\tilde{D}\|\cdot\|A_4\|\left(\|\overline{\varrho}(t)\|^2+\|\mathfrak{F}(t)\|^2\right)\\
&\quad\le\|A_1\|\left(\|\overline{\varrho}(t)\|^2+\left\|\mathfrak{F}(t_a)-\overline{\varrho}(t)\right\|^2\right)\\
&\qquad+\beta\|A_2\|\left(\|\overline{\varrho}(t)\|^2+\left\|\mathfrak{F}(t_a)-\overline{\varrho}(t)\right\|^2\right)\\
&\qquad+2\|A_3\|\cdot\|\overline{\varrho}(t)\|^2+\|\tilde{D}\|\cdot\|A_4\|\left(\|\overline{\varrho}(t)\|^2+\|\zeta(t)\|^2\right)\\
&\quad\le\left(2\|A_1\|+2\beta\|A_2\|+2\|A_3\|+\|\tilde{D}\|\cdot\|A_4\|\right)\|\overline{\varrho}(t)\|^2\\
&\qquad+\left(\|A_1\|+\beta\|A_2\|\right)\|\mathfrak{F}(t_a)\|^2+\|\tilde{D}\|\cdot\|A_4\|\cdot\|\zeta(t)\|^2\\
&\quad\le\left(2\|\mathscr{B}+\mathscr{A}\tilde{L}\|+2\|\mathscr{M}\|\cdot\|\mathscr{F}_1\|+2\|\mathscr{M}\|\cdot\|\mathscr{F}_3\tilde{L}\|\right.\\
&\qquad+2\beta\|\mathscr{B}_d\|+2\beta\|\mathscr{M}\|\cdot\|\mathscr{F}_2\|+2\|\mathscr{A}\tilde{L}\|+2\|\mathscr{M}\|\cdot\|\mathscr{F}_3\tilde{L}\|\\
&\qquad\left.+\left(\|\mathscr{D}\|+\|\mathscr{M}\|\cdot\|\mathscr{F}_5\|\right)\cdot\left(\|\mathscr{C}\|+\|\mathscr{M}\|\cdot\|\mathscr{F}_4\|\right)\right)\|\overline{\varrho}(t)\|^2\\
&\qquad+\left(\|\mathscr{B}+\mathscr{A}\tilde{L}\|+\|\mathscr{M}\|\cdot\|\mathscr{F}_1\|+\|\mathscr{M}\|\cdot\|\mathscr{F}_3\tilde{L}\|+\beta\|\mathscr{B}_d\|\right.\\
&\qquad\left.+\beta\|\mathscr{M}\|\cdot\|\mathscr{F}_2\|\right)\|\mathfrak{F}(t_a)\|^2\\
&\qquad+\left(\|\mathscr{D}\|+\|\mathscr{M}\|\cdot\|\mathscr{F}_5\|\right)\cdot\left(\|\mathscr{C}\|+\|\mathscr{M}\|\cdot\|\mathscr{F}_4\|\right)\cdot\|\zeta(t)\|^2\\
&\quad\le\varphi_1\|\overline{\varrho}(t)\|^2+\varphi_2\|\mathfrak{F}(t_a)\|^2+\varphi_3\|\zeta(t)\|^2_{[t_0,t_{a+1})}.
\end{aligned}
\tag{29}
$$

Let $\varphi_a=\varphi_2\|\mathfrak{F}(t_a)\|^2+\varphi_3\|\zeta(t)\|^2_{[t_0,t_{a+1})}$; then,

$$
D^+\|\overline{\varrho}(t)\|^2\le\varphi_1\|\overline{\varrho}(t)\|^2+\varphi_a,\quad\forall t\in[t_a,t_{a+1}).
\tag{30}
$$

Using $e^{-\varphi_1(t-t_a)}$ to premultiplication and post-multiplication in (30) results in

$$
D^+\left(e^{-\varphi_1(t-t_a)}\|\overline{\varrho}(t)\|^2\right)\le\varphi_a e^{-\varphi_1(t-t_a)}.
\tag{31}
$$

By considering $\overline{\varrho}(t_0)=0$ and integrating both sides of (31) from t_a to t, we have

$$
\|\overline{\varrho}(t)\|^2\le\frac{\varphi_a}{\varphi_1}\left(e^{\varphi_1(t-t_a)}-1\right),\quad\forall t\in[t_a,t_{a+1}).
\tag{32}
$$

When mechanism (16) is triggered, we can derive $\eta\|\mathfrak{F}(t_a)\|^2+\rho\|\zeta(t)\|^2_{[t_0,t_{a+1})}=\|\overline{\varrho}(t_{a+1})\|^2$. Together with $\varphi_a=\varphi_2\|\mathfrak{F}(t_a)\|^2+\varphi_3\|\zeta(t)\|^2_{[t_0,t_{a+1})}$, it follows that

$$
\begin{aligned}
&(\eta\wedge\rho)\left(\left\|\mathfrak{F}(t_a)\right\|^2+\|\zeta(t)\|^2_{[t_0,t_{a+1})}\right)\\
&\quad\le\frac{e^{\varphi_1(t_{a+1}-t_a)}-1}{\varphi_1}\times(\varphi_2\vee\varphi_3)\times\left(\left\|\mathfrak{F}(t_a)\right\|^2\right.\\
&\qquad\left.+\|\zeta(t)\|^2_{[t_0,t_{a+1})}\right),
\end{aligned}
\tag{33}
$$

which indicates that

$$
t_{a+1}-t_a\ge\frac{\ln\left((\varphi_1(\eta\wedge\rho)/\varphi_2\vee\varphi_3)+1\right)}{\varphi_1}>0,\quad a\in\mathbb{N}^+.
\tag{34}
$$

Case (ii). Only the forced triggered time sequence $\{t_0+n\ell\}_{a=1}^{\infty}$ exists in the sequence $\{t_a\}_{a=1}^{\infty}$. Obviously, in this case, $t_{a+1}-t_a=\ell>0, a\in\mathbb{N}^+$.

Case (iii). The sequence $\{t_a\}_{a=1}^{\infty}$ is composed of the event-triggered instants t_s^* ($s\in\mathbb{N}^+$) and the forced triggered instants t_j ($j\in\mathbb{N}^+$). If the Zeno behavior lives in argument system (13), it must be that a finite time interval owns infinite impulse jumps in this case. To exhibit this phenomenon, suppose that T presents the accumulation time (or Zeno time) on the finite time interval $[t_0,T]$. By defining $\varsigma=(T-([\ell/2]))\vee t_0$, it is apparent that countless of impulsive instants appears in the interval $[\varsigma,T]$. Denote by $\{t_{N_0+s}\}_{s=1}^{\infty}\in[\varsigma,T]$ the subsequence of $\{t_a\}_{a=1}^{\infty}$ satisfying $t_{N_0+s}\longrightarrow T$ as $s\longrightarrow\infty$, where integer $N_0\ge 0$. If there is no forced triggered moment in $[\varsigma,T]$, similar to the discussion of Case (i), we conclude that $t_{N_0+s}\longrightarrow\infty$ as $s\longrightarrow\infty$, which contradicts the definition of the accumulation time T. If there exists $t_j\in\{t_{N_0+s}\}_{s=1}^{\infty}$ for some $j\in\mathbb{Z}^+$ over the interval $[\varsigma,T]$, recalling the definition of ς, it can be deduced that only one $t_j\in\{t_{N_0+s}\}_{s=1}^{\infty}$, which implies that the triggered moments totally consist of the event-triggered moments in $(t_j,T]$. Then it follows from Case (i) that $t_{N_0+s}\longrightarrow\infty$ as $s\longrightarrow\infty$. Hence, the Zeno behavior is precluded in Case (iii).

From the foregoing discussion, the lower bound of neighboring impulsive instants is ultimately acquired, which symbolizes that the Zeno behavior can be eliminated.

Remark 4. When designing event-triggered mechanism (16), $\|\zeta(t)\|^2_{[t_0,t]}$ cannot be superseded by $\|\zeta(t)\|^2$. It is on account of a discovery that the correlation $\|\zeta(t)\|^2$ over $[t_a,t_{a+1})$ and $\|\zeta(t_{a+1})\|^2$ is not easily obtained in the abovementioned reasoning process of excluding the Zeno phenomenon. Therefore, it is essential for the device of (16)

to take the supremum of $\|\zeta(t)\|^2$ in $[t_0, t]$. In addition, the study in [29] assists us in detecting the indispensability of the forced trigger condition in (16).

Remark 5. As described earlier, mechanism (16) is presented to select the optimal triggered moment according to the steady state of resulting system (13). Based on the results of Theorem 1, it can be proved that the designed event-triggered mechanism is effective. By comparison with the existing results of the uncertain models, such as [21, 35, 36], although they reduce the transmission of information, impulsive controller with fixed impulsive moments, in design, is still conservative. Now, in this paper, the controller based on event-triggered mechanism only is updated at the triggered moment. By this means, the burden of controller update can be decreased without affecting accurate control. Moreover, the sampling control adopted in this paper is only dependent on the state information of observer at the triggered moment, which can reduce the communication between the equipment under test and the observer.

Assumption 3. $\widetilde{K}$ is a nonsingular matrix, and there exists a constant $\gamma > 0$ such that $\lambda_{\max}(\widetilde{K}) \le e^{-(1/2)\gamma}$.

Theorem 2. *Uncertain system (13) is input-to-state stable via the event-triggered scheme (16); suppose that for given parameters $\eta \in (0, (1/2))$, $\rho > 0$, and $\ell > 0$ and the control gains K, $\overline{K} \in \mathbb{R}^{q\times p}$, and $L \in \mathbb{R}^{q\times n}$, there exist matrices $P > 0$ and $H_\iota > 0\,(\iota = 1, 2, 3)$ and constants $\widetilde{\vartheta} > 0$, $\vartheta > 0$, $\gamma > 0$, and $\varepsilon_b > 0\,(b = 1, 2, 3, \ldots, 58)$, such that*

$$\begin{bmatrix} \Psi_1 & 0 & 0 \\ * & \Psi_2 & 0 \\ * & * & \Psi_3 \end{bmatrix} > 0, \tag{35}$$

$$\begin{bmatrix} \Omega_1 & \mathscr{D}^T P \mathscr{D} \mathscr{B}_d & \mathscr{D}^T P \mathscr{D} \mathscr{A} \widetilde{L} & \mathscr{D}^T P \mathscr{D} \mathscr{C} \\ * & -H_1 & 0 & 0 \\ * & * & -H_2 & 0 \\ * & * & * & -H_3 \end{bmatrix} < 0, \tag{36}$$

$$\begin{bmatrix} \Omega_2 & \mathscr{M} & \mathscr{K}_2^T \mathscr{F}_3^T & \mathscr{K}_3 \mathscr{M} & \mathscr{F}_5^T \\ * & -\varepsilon_{57} I & 0 & 0 & 0 \\ * & * & -\dfrac{1}{\varepsilon_{57}} I & 0 & 0 \\ * & * & * & -\varepsilon_{58} I & 0 \\ * & * & * & * & -\dfrac{1}{\varepsilon_{58}} I \end{bmatrix} \le 0, \tag{37}$$

$$\gamma - \widetilde{\vartheta}\ell > 0, \tag{38}$$

where

$$\Psi_1 = \begin{bmatrix} I & \mathscr{F}_5 \mathscr{M} \\ * & \dfrac{1}{\omega_1} I \end{bmatrix},$$

$$\Psi_2 = \begin{bmatrix} I & \Lambda_2 \mathscr{M} \\ * & \dfrac{1}{\omega_2} I \end{bmatrix},$$

$$\Psi_3 = \begin{bmatrix} I & \mathscr{M}^T P \mathscr{M} \\ * & \dfrac{1}{\omega_3} I \end{bmatrix},$$

$$\Omega_1 = -\vartheta I + \mathscr{R}_1, \Omega_2 = He(\mathscr{K}_1) - 2e^{-(1/2)\gamma} I,$$

$$\widetilde{\vartheta} = \widehat{\vartheta} + \frac{(1-2\eta)\left(\|\mathscr{D}\| + \alpha\|\mathscr{M}\| \cdot \|\mathscr{F}_5\|\right)^2 \vartheta + 2\eta\lambda_{\max}(\mathscr{R}_2)}{(1-2\eta)\left(\|\mathscr{D}\| + \alpha\|\mathscr{M}\| \cdot \|\mathscr{F}_5\|\right)^2 \lambda_{\min}(P)},$$

$$\begin{aligned} \mathscr{R}_1 = {} & He\left(\mathscr{D}^T P \mathscr{D} \Lambda_1\right) + \mu_1 \Lambda_3^T \Lambda_3 + \mu_2 \Lambda_2^T \Lambda_2 + \mu_3 \mathscr{F}_5^T \mathscr{F}_5 \\ & + \mu_4 \mathscr{F}_1^T \mathscr{F}_1 + \mu_5 \widetilde{L}^T \mathscr{F}_3^T \mathscr{F}_3 \widetilde{L} + \mu_6 \Lambda_1^T \mathscr{F}_5^T \mathscr{F}_5 \Lambda_1 \\ & + \frac{1}{\varepsilon_8} \Lambda_1^T \Lambda_2^T \Lambda_2 \Lambda_1 + \mu_7 \beta \mathscr{F}_2^T \mathscr{F}_2 \beta \\ & + \mu_8 \beta \mathscr{B}_d^T \mathscr{F}_5^T \mathscr{F}_5 \mathscr{B}_d \beta + \frac{1}{\varepsilon_{25}} \beta \mathscr{B}_d^T \Lambda_2^T \Lambda_2 \mathscr{B}_d \beta + \beta H_1 \beta, \end{aligned}$$

$$\begin{aligned} \mathscr{R}_2 = {} & \mu_9 \widetilde{L}^T \mathscr{F}_3^T \mathscr{F}_3 \widetilde{L} + \mu_{10} \widetilde{L}^T \mathscr{A}^T \mathscr{F}_5^T \mathscr{F}_5 \mathscr{A} \widetilde{L} \\ & + \frac{1}{\varepsilon_{37}} \widetilde{L}^T \mathscr{A}^T \Lambda_2^T \Lambda_2 \mathscr{A} \widetilde{L} + H_2, \end{aligned}$$

$$\Lambda_1 = \mathscr{B} + \mathscr{A}\widetilde{L},$$

$$\Lambda_2 = \mathscr{M}^T P \mathscr{D},$$

$$\Lambda_3 = \mathscr{M}^T \mathscr{D}^T P \mathscr{D},$$

$$\omega_1 = \max\{\varepsilon_5, \varepsilon_7, \varepsilon_{17}, \varepsilon_{20}, \varepsilon_{24}, \varepsilon_{32}, \varepsilon_{36}, \varepsilon_{44}, \varepsilon_{48}, \varepsilon_{56}\},$$

$$\omega_2 = \max\{\varepsilon_{10}, \varepsilon_{12}, \varepsilon_{27}, \varepsilon_{39}, \varepsilon_{51}\},$$

$$\omega_3 = \max\{\varepsilon_{14}, \varepsilon_{16}, \varepsilon_{19}, \varepsilon_{29}, \varepsilon_{31}, \varepsilon_{41}, \varepsilon_{43}, \varepsilon_{53}, \varepsilon_{55}\},$$

$$\mu_1 = \varepsilon_1 + \varepsilon_2 + \varepsilon_{21} + \varepsilon_{33} + \varepsilon_{45},$$

$$\mu_2 = \varepsilon_3 + \varepsilon_4 + \varepsilon_6 + \varepsilon_{22} + \varepsilon_{23} + \varepsilon_{34} + \varepsilon_{35} + \varepsilon_{46} + \varepsilon_{47},$$

$$\begin{aligned} \mu_3 = {} & \varepsilon_8 + \varepsilon_9 + \varepsilon_{11} + \varepsilon_{13} + \varepsilon_{15} + \varepsilon_{18} + \varepsilon_{25} + \varepsilon_{26} \\ & + \varepsilon_{28} + \varepsilon_{30} + \varepsilon_{37} + \varepsilon_{38} + \varepsilon_{40} + \varepsilon_{42} + \varepsilon_{49} \\ & + \varepsilon_{50} + \varepsilon_{52} + \varepsilon_{54}, \end{aligned}$$

$$\mu_4 = \frac{1}{\varepsilon_1} + \frac{1}{\varepsilon_4 \varepsilon_5} + \frac{1}{\varepsilon_9 \varepsilon_{10}} + \frac{1}{\varepsilon_{15} \varepsilon_{16} \varepsilon_{17}},$$

$$\mu_5 = \frac{1}{\varepsilon_2} + \frac{1}{\varepsilon_6 \varepsilon_7} + \frac{1}{\varepsilon_{11} \varepsilon_{12}} + \frac{1}{\varepsilon_{18} \varepsilon_{19} \varepsilon_{20}},$$

$$\mu_6 = \frac{1}{\varepsilon_3} + \frac{1}{\varepsilon_{13} \varepsilon_{14}},$$

$$\mu_7 = \frac{1}{\varepsilon_{21}} + \frac{1}{\varepsilon_{23} \varepsilon_{24}} + \frac{1}{\varepsilon_{26} \varepsilon_{27}} + \frac{1}{\varepsilon_{30} \varepsilon_{31} \varepsilon_{32}},$$

$$\mu_8 = \frac{1}{\varepsilon_{22}} + \frac{1}{\varepsilon_{28} \varepsilon_{29}},$$

$$\mu_9 = \frac{1}{\varepsilon_{33}} + \frac{1}{\varepsilon_{35} \varepsilon_{36}} + \frac{1}{\varepsilon_{38} \varepsilon_{39}} + \frac{1}{\varepsilon_{42} \varepsilon_{43} \varepsilon_{44}},$$

$$\mu_{10} = \frac{1}{\varepsilon_{34}} + \frac{1}{\varepsilon_{40} \varepsilon_{41}}. \tag{39}$$

Proof. Suppose that $\wp(t) = \wp(t, t_0, \wp(0))$ is the solution of system (13) with the initial value $(t_0, \wp(0))$. Due to the imperfect measurability of the system states, the Lyapunov functional related to the relevant outcomings is considered as $V(t) = \mathfrak{F}^T(t)P\mathfrak{F}(t)$. $\forall t \in [t_a, t_{a+1})$, $a \in \mathbb{Z}^+$, the derivative of $V(t)$ can be calculated that

$$\begin{aligned}\dot{V} &= 2\mathfrak{F}^T(t)P\dot{\mathfrak{F}}(t)\\ &= 2\wp^T(t)\tilde{D}^T P\tilde{D}\dot{\wp}(t)\\ &\le 2\wp^T(t)\tilde{D}^T P\tilde{D}A_1\wp(t) + \hat{\vartheta}\wp^T(t)\tilde{D}^T P\tilde{D}\wp(t)\\ &\quad + 2\wp^T(t)\tilde{D}^T P\tilde{D}A_2\mathcal{F}(t) + 2\wp^T(t)\tilde{D}^T P\tilde{D}A_3\varrho(t)\\ &\quad + 2\wp^T(t)\tilde{D}^T P\tilde{D}A_4\zeta(t).\end{aligned} \tag{40}$$

It follows from Lemma 1 and conditions (26) and (35) that

$$He\left(\mathscr{D}^T P\mathscr{D}\left[\begin{array}{cc}\Delta\mathscr{B} & \Delta\mathscr{A}\tilde{L}\end{array}\right]\right)$$

$$\le \left[\begin{array}{cc}\frac{1}{\varepsilon_1}\mathscr{F}_1^T\mathscr{F}_1 & \frac{1}{\varepsilon_2}\tilde{L}^T\mathscr{F}_3^T\mathscr{F}_3\tilde{L}\end{array}\right] + \Lambda_3^T\Lambda_3\left[\begin{array}{cc}\varepsilon_1 I & \varepsilon_2 I\end{array}\right],$$

$$He\left(\mathscr{D}^T P\Delta\mathscr{D}\left[\begin{array}{ccc}\Lambda_1 & \Delta\mathscr{B} & \Delta\mathscr{A}\tilde{L}\end{array}\right]\right)$$

$$\le \left[\begin{array}{ccc}\frac{1}{\varepsilon_3}\Lambda_1^T\mathscr{F}_5^T\mathscr{F}_5\Lambda_1 & \frac{1}{\varepsilon_4\varepsilon_5}\mathscr{F}_1^T\mathscr{F}_1 & \frac{1}{\varepsilon_6\varepsilon_7}\tilde{L}^T\mathscr{F}_3^T\mathscr{F}_3\tilde{L}\end{array}\right] + \Lambda_2^T\Lambda_2\left[\begin{array}{ccc}\varepsilon_3 I & \varepsilon_4 I & \varepsilon_6 I\end{array}\right],$$

$$He\left(\Delta\mathscr{D}^T P\mathscr{D}\Lambda_1\right) \le \varepsilon_8\mathscr{F}_5^T\mathscr{F}_5 + \frac{1}{\varepsilon_8}\Lambda_1^T\Lambda_2^T\Lambda_2\Lambda_1,$$

$$He\left(\Delta\mathscr{D}^T P\mathscr{D}\left[\begin{array}{cc}\Delta\mathscr{B} & \Delta\mathscr{A}\tilde{L}\end{array}\right]\right)$$

$$\le \left[\begin{array}{cc}\frac{1}{\varepsilon_9\varepsilon_{10}}\mathscr{F}_1^T\mathscr{F}_1 & \frac{1}{\varepsilon_{11}\varepsilon_{12}}\tilde{L}^T\mathscr{F}_3^T\mathscr{F}_3\tilde{L}\end{array}\right] + \mathscr{F}_5^T\mathscr{F}_5\left[\begin{array}{cc}\varepsilon_9 I & \varepsilon_{11} I\end{array}\right],$$

$$He\left(\Delta\mathscr{D}^T P\Delta\mathscr{D}\left[\begin{array}{ccc}\Lambda_1 & \Delta\mathscr{B} & \Delta\mathscr{A}\tilde{L}\end{array}\right]\right)$$

$$\le \left[\begin{array}{ccc}\frac{1}{\varepsilon_{13}\varepsilon_{14}}\Lambda_1^T\mathscr{F}_5^T\mathscr{F}_5\Lambda_1 & \frac{1}{\varepsilon_{15}\varepsilon_{16}\varepsilon_{17}}\mathscr{F}_1^T\mathscr{F}_1 & \frac{1}{\varepsilon_{18}\varepsilon_{19}\varepsilon_{20}}\tilde{L}^T\mathscr{F}_3^T\mathscr{F}_3\tilde{L}\end{array}\right] + \mathscr{F}_5^T\mathscr{F}_5\left[\begin{array}{ccc}\varepsilon_{13} I & \varepsilon_{15} I & \varepsilon_{18} I\end{array}\right],$$

$$2\wp^T(t)\mathscr{D}^T P\mathscr{D}\Delta\mathscr{B}_d\mathcal{F}(t)$$

$$\le \frac{1}{\varepsilon_{21}}\mathcal{F}^T(t)\mathcal{F}_2^T\mathcal{F}_2\mathcal{F}(t) + \varepsilon_{21}\wp^T(t)\Lambda_3^T\Lambda_3\wp(t),$$

$$2\wp^T(t)\mathscr{D}^T P\Delta\mathscr{D}\left[\begin{array}{cc}\mathscr{B}_d\mathcal{F}(t) & \Delta\mathscr{B}_d\mathcal{F}(t)\end{array}\right]$$

$$\le \left[\begin{array}{cc}\frac{1}{\varepsilon_{22}}\mathcal{F}^T(t)\mathscr{B}_d^T\mathscr{F}_5^T\mathscr{F}_5\mathscr{B}_d\mathcal{F}(t) & \frac{1}{\varepsilon_{23}\varepsilon_{24}}\mathcal{F}^T(t)\mathcal{F}_2^T\mathcal{F}_2\mathcal{F}(t)\end{array}\right] + \wp^T(t)\Lambda_2^T\Lambda_2\wp(t)\left[\begin{array}{cc}\varepsilon_{22} I & \varepsilon_{23} I\end{array}\right],$$

$$2\wp^T(t)\Delta\mathscr{D}^T P\mathscr{D}\left[\begin{array}{cc}\mathscr{B}_d\mathcal{F}(t) & \Delta\mathscr{B}_d\mathcal{F}(t)\end{array}\right]$$

$$\le \left[\begin{array}{cc}\frac{1}{\varepsilon_{25}}\mathcal{F}^T(t)\mathscr{B}_d^T\Lambda_2^T\Lambda_2\mathscr{B}_d\mathcal{F}(t) & \frac{1}{\varepsilon_{26}\varepsilon_{27}}\mathcal{F}^T(t)\mathcal{F}_2^T\mathcal{F}_2\mathcal{F}(t)\end{array}\right]$$

$$
\begin{aligned}
&+\wp^{T}(t)\mathscr{F}_{5}^{T}\mathscr{F}_{5}\wp(t)\left[\begin{array}{cc}\varepsilon_{25}I & \varepsilon_{26}I\end{array}\right],\\
&2\wp^{T}(t)\Delta\mathscr{D}^{T}P\Delta\mathscr{D}\left[\begin{array}{cc}\mathscr{B}_{d}\mathscr{F}(t) & \Delta\mathscr{B}_{d}\mathscr{F}(t)\end{array}\right]\\
&\quad\leq\left[\begin{array}{cc}\dfrac{1}{\varepsilon_{28}\varepsilon_{29}}\mathscr{F}^{T}(t)\mathscr{B}_{d}^{T}\mathscr{F}_{5}^{T}\mathscr{F}_{5}\mathscr{B}_{d}\mathscr{F}(t) & \dfrac{1}{\varepsilon_{30}\varepsilon_{31}\varepsilon_{32}}\mathscr{F}^{T}(t)\mathscr{F}_{2}^{T}\mathscr{F}_{2}\mathscr{F}(t)\end{array}\right]\\
&\qquad+\wp^{T}(t)\mathscr{F}_{5}^{T}\mathscr{F}_{5}\wp(t)\left[\begin{array}{cc}\varepsilon_{28}I & \varepsilon_{30}I\end{array}\right],\\
&2\wp^{T}(t)\mathscr{D}^{T}P\mathscr{D}\Delta\mathscr{A}\tilde{L}\varrho(t)\\
&\quad\leq\frac{1}{\varepsilon_{33}}\varrho^{T}(t)\tilde{L}^{T}\mathscr{F}_{3}^{T}\mathscr{F}_{3}\tilde{L}\varrho(t)+\varepsilon_{33}\wp^{T}(t)\Lambda_{3}^{T}\Lambda_{3}\wp(t),\\
&2\wp^{T}(t)\mathscr{D}^{T}P\Delta\mathscr{D}\left[\begin{array}{cc}\mathscr{A}\tilde{L}\varrho(t) & \Delta\mathscr{A}\tilde{L}\varrho(t)\end{array}\right]\\
&\quad\leq\left[\begin{array}{cc}\dfrac{1}{\varepsilon_{34}}\varrho^{T}(t)\tilde{L}^{T}\mathscr{A}^{T}\mathscr{F}_{5}^{T}\mathscr{F}_{5}\mathscr{A}\tilde{L}\varrho(t) & \dfrac{1}{\varepsilon_{35}\varepsilon_{36}}\varrho^{T}(t)\tilde{L}^{T}\mathscr{F}_{3}^{T}\mathscr{F}_{3}\tilde{L}\varrho(t)\end{array}\right]\\
&\qquad+\wp^{T}(t)\Lambda_{2}^{T}\Lambda_{2}\wp(t)\left[\begin{array}{cc}\varepsilon_{34}I & \varepsilon_{35}I\end{array}\right],\\
&2\wp^{T}(t)\Delta\mathscr{D}^{T}P\mathscr{D}\left[\begin{array}{cc}\mathscr{A}\tilde{L}\varrho(t) & \Delta\mathscr{A}\tilde{L}\varrho(t)\end{array}\right]\\
&\quad\leq\left[\begin{array}{cc}\dfrac{1}{\varepsilon_{37}}\varrho^{T}(t)\tilde{L}^{T}\mathscr{A}^{T}\Lambda_{2}^{T}\Lambda_{2}\mathscr{A}\tilde{L}\varrho(t) & \dfrac{1}{\varepsilon_{38}\varepsilon_{39}}\varrho^{T}(t)\tilde{L}^{T}\mathscr{F}_{3}^{T}\mathscr{F}_{3}\tilde{L}\varrho(t)\end{array}\right]\\
&\qquad+\wp^{T}(t)\mathscr{F}_{5}^{T}\mathscr{F}_{5}\wp(t)\left[\begin{array}{cc}\varepsilon_{37}I & \varepsilon_{38}I\end{array}\right],\\
&2\wp^{T}(t)\Delta\mathscr{D}^{T}P\Delta\mathscr{D}\left[\begin{array}{cc}\mathscr{A}\tilde{L}\varrho(t) & \Delta\mathscr{A}\tilde{L}\varrho(t)\end{array}\right]\\
&\quad\leq\left[\begin{array}{cc}\dfrac{1}{\varepsilon_{40}\varepsilon_{41}}\varrho^{T}(t)\tilde{L}^{T}\mathscr{A}^{T}\mathscr{F}_{5}^{T}\mathscr{F}_{5}\mathscr{A}\tilde{L}\varrho(t) & \dfrac{1}{\varepsilon_{42}\varepsilon_{43}\varepsilon_{44}}\varrho^{T}(t)\tilde{L}^{T}\mathscr{F}_{3}^{T}\mathscr{F}_{3}\tilde{L}\varrho(t)\end{array}\right]\\
&\qquad+\wp^{T}(t)\mathscr{F}_{5}^{T}\mathscr{F}_{5}\wp(t)\left[\begin{array}{cc}\varepsilon_{40}I & \varepsilon_{42}I\end{array}\right],\\
&2\wp^{T}(t)\mathscr{D}^{T}P\mathscr{D}\Delta\mathscr{C}\zeta(t)\\
&\quad\leq\varepsilon_{45}\wp^{T}(t)\Lambda_{3}^{T}\Lambda_{3}\wp(t)+\frac{1}{\varepsilon_{45}}\zeta^{T}(t)\mathscr{F}_{4}^{T}\mathscr{F}_{4}\zeta(t),\\
&2\wp^{T}(t)\mathscr{D}^{T}P\Delta\mathscr{D}\left[\begin{array}{cc}\mathscr{C}\zeta(t) & \Delta\mathscr{C}\zeta(t)\end{array}\right]\\
&\quad\leq\left[\begin{array}{cc}\dfrac{1}{\varepsilon_{46}}\zeta^{T}(t)\mathscr{C}^{T}\mathscr{F}_{5}^{T}\mathscr{F}_{5}\mathscr{C}\zeta(t) & \dfrac{1}{\varepsilon_{47}\varepsilon_{48}}\zeta^{T}(t)\mathscr{F}_{4}^{T}\mathscr{F}_{4}\zeta(t)\end{array}\right]\\
&\qquad+\wp^{T}(t)\Lambda_{2}^{T}\Lambda_{2}\wp(t)\left[\begin{array}{cc}\varepsilon_{46}I & \varepsilon_{47}I\end{array}\right],\\
&2\wp^{T}(t)\Delta\mathscr{D}^{T}P\mathscr{D}\left[\begin{array}{cc}\mathscr{C}\zeta(t) & \Delta\mathscr{C}\zeta(t)\end{array}\right]\\
&\quad\leq\left[\begin{array}{cc}\dfrac{1}{\varepsilon_{49}}\zeta^{T}(t)\mathscr{C}^{T}\Lambda_{2}^{T}\Lambda_{2}\mathscr{C}\zeta(t) & \dfrac{1}{\varepsilon_{50}\varepsilon_{51}}\zeta^{T}(t)\mathscr{F}_{4}^{T}\mathscr{F}_{4}\zeta(t)\end{array}\right]\\
&\qquad+\wp^{T}(t)\mathscr{F}_{5}^{T}\mathscr{F}_{5}\wp(t)\left[\begin{array}{cc}\varepsilon_{49}I & \varepsilon_{50}I\end{array}\right],\\
&2\wp^{T}(t)\Delta\mathscr{D}^{T}P\Delta\mathscr{D}\left[\begin{array}{cc}\mathscr{C}\zeta(t) & \Delta\mathscr{C}\zeta(t)\end{array}\right]\\
&\quad\leq\left[\begin{array}{cc}\dfrac{1}{\varepsilon_{52}\varepsilon_{53}}\zeta^{T}(t)\mathscr{C}^{T}\mathscr{F}_{5}^{T}\mathscr{F}_{5}\mathscr{C}\zeta(t) & \dfrac{1}{\varepsilon_{54}\varepsilon_{55}\varepsilon_{56}}\zeta^{T}(t)\mathscr{F}_{4}^{T}\mathscr{F}_{4}\zeta(t)\end{array}\right]\\
&\qquad+\wp^{T}(t)\mathscr{F}_{5}^{T}\mathscr{F}_{5}\wp(t)\left[\begin{array}{cc}\varepsilon_{52}I & \varepsilon_{54}I\end{array}\right],
\end{aligned}
\tag{41}
$$

and from Assumption 2 and Lemma 2, we derive

$$\begin{aligned}
&\mathscr{F}(t) \le \beta\wp(t)\\
&2\wp^T(t)\mathscr{D}^T P\mathscr{D}\mathscr{B}_d\mathscr{F}(t) \le \wp^T(t)\mathscr{D}^T P\mathscr{D}\mathscr{B}_d H_1^{-1}\mathscr{B}_d^T\mathscr{D}^T P\mathscr{D}\wp(t)\\
&\quad + \wp^T(t)\beta H_1\beta\wp(t),\\
&2\wp^T(t)\mathscr{D}^T P\mathscr{D}\mathscr{A}\tilde{L}\varrho(t) \le \wp^T(t)\mathscr{D}^T P\mathscr{D}\mathscr{A}\tilde{L}H_2^{-1}\tilde{L}^T\mathscr{A}^T\mathscr{D}^T P\mathscr{D}\wp(t)\\
&\quad + \varrho^T(t)H_2\varrho(t),\\
&2\wp^T(t)\mathscr{D}^T P\mathscr{D}\mathscr{C}\zeta(t) \le \wp^T(t)\mathscr{D}^T P\mathscr{D}\mathscr{C}H_3^{-1}\mathscr{C}^T\mathscr{D}^T P\mathscr{D}\wp(t)\\
&\quad + \zeta^T(t)H_3\zeta(t).
\end{aligned} \tag{42}$$

And then we infer that

$$\begin{aligned}
&2\wp^T(t)\tilde{D}^T P\tilde{D}A_1\wp(t) + 2\wp^T(t)\tilde{D}^T P\tilde{D}A_2\mathscr{F}(t)\\
&\quad = 2\wp^T(t)(\mathscr{D}+\Delta\mathscr{D})^T P(\mathscr{D}+\Delta\mathscr{D})(\Lambda_1+\Delta\mathscr{B}+\Delta\mathscr{A}\tilde{L})\wp(t)\\
&\qquad + 2\wp^T(t)(\mathscr{D}+\Delta\mathscr{D})^T P(\mathscr{D}+\Delta\mathscr{D})(\mathscr{B}_d+\Delta\mathscr{B}_d)\mathscr{F}(t)\\
&\quad \le \wp^T(t)\mathscr{R}_1\wp(t) + \wp^T(t)\mathscr{D}^T P\mathscr{D}\mathscr{B}_d H_1^{-1}\mathscr{B}_d^T\mathscr{D}^T P\mathscr{D}\wp(t),
\end{aligned} \tag{43}$$

$$\begin{aligned}
&2\wp^T(t)\tilde{D}^T P\tilde{D}A_3\varrho(t)\\
&\quad = 2\wp^T(t)(\mathscr{D}+\Delta\mathscr{D})^T P(\mathscr{D}+\Delta\mathscr{D})(\mathscr{A}\tilde{L}+\Delta\mathscr{A}\tilde{L})\varrho(t)\\
&\quad \le \varrho^T(t)\mathscr{R}_2\varrho(t) + \wp^T(t)\mathscr{D}^T P\mathscr{D}\mathscr{A}\tilde{L}H_2^{-1}\tilde{L}^T\mathscr{A}^T\mathscr{D}^T P\mathscr{D}\wp(t),
\end{aligned} \tag{44}$$

$$\begin{aligned}
&2\wp^T(t)\tilde{D}^T P\tilde{D}A_4\zeta(t)\\
&\quad = 2\wp^T(t)(\mathscr{D}+\Delta\mathscr{D})^T P(\mathscr{D}+\Delta\mathscr{D})(\mathscr{C}+\Delta\mathscr{C})\zeta(t)\\
&\quad \le \zeta^T(t)\mathscr{R}_3\zeta(t) + \wp^T(t)\mathscr{D}^T P\mathscr{D}\mathscr{C}H_3^{-1}\mathscr{C}^T\mathscr{D}^T P\mathscr{D}\wp(t),
\end{aligned} \tag{45}$$

where

$$\begin{aligned}
\mathscr{R}_3 &= \left(\frac{1}{\varepsilon_{45}} + \frac{1}{\varepsilon_{47}\varepsilon_{48}} + \frac{1}{\varepsilon_{50}\varepsilon_{51}} + \frac{1}{\varepsilon_{54}\varepsilon_{55}\varepsilon_{56}}\right)\mathscr{F}_4^T\mathscr{F}_4\\
&\quad + \left(\frac{1}{\varepsilon_{46}} + \frac{1}{\varepsilon_{52}\varepsilon_{53}}\right)\mathscr{C}^T\mathscr{F}_5^T\mathscr{F}_5\mathscr{C} + \frac{1}{\varepsilon_{49}}\mathscr{C}^T\Lambda_2^T\Lambda_2\mathscr{C} + H_3.
\end{aligned} \tag{46}$$

Consequently, under Lemma 3 and (35), substituting (43)–(45) into (40) gives that, $\forall t \in [t_a, t_{a+1}), a \in \mathbb{N}^+$,

$$\begin{aligned}
\dot{V} &\le \vartheta\wp^T(t)\wp(t) + \widehat{\vartheta}\wp^T(t)\tilde{D}^T P\tilde{D}\wp(t)\\
&\quad + \varrho^T(t)\mathscr{R}_2\varrho(t) + \zeta^T(t)\mathscr{R}_3\zeta(t)\\
&\le \widehat{\vartheta}V(t) + \vartheta\|\wp(t)\|^2 + \lambda_{\max}(\mathscr{R}_2)\|\varrho(t)\|^2\\
&\quad + \lambda_{\max}(\mathscr{R}_3)\|\zeta(t)\|^2.
\end{aligned} \tag{47}$$

$\forall t \in [t_a, t_{a+1})$, it holds from Assumption 1, (26), and the fact $\|\overline{\varrho}(t)\|^2 \le \eta\|\mathfrak{T}(t_a)\|^2 + \rho\|\zeta(t)\|^2_{[t_0,t]}$ that

$$\begin{aligned}
\|\varrho(t)\|^2 &\le \frac{2\eta}{(1-2\eta)\left(\|\mathscr{D}\| + \alpha\|\mathscr{M}\|\cdot\|\mathscr{F}_5\|\right)^2}\|\mathfrak{T}(t)\|^2\\
&\quad + \frac{\rho}{(1-2\eta)\left(\|\mathscr{D}\| + \alpha\|\mathscr{M}\|\cdot\|\mathscr{F}_5\|\right)^2}\|\zeta(t)\|^2_{[t_0,t]},
\end{aligned} \tag{48}$$

which supplied into (47) yields that

$$\dot{V}(t) \le \widetilde{\vartheta}V(t) + \psi\left(\|\zeta(t)\|_{[t_0,t]}\right), \quad \forall t \in [t_a, t_{a+1}), \tag{49}$$

where

$$\psi(c) = \left(\lambda_{\max}(\mathscr{R}_3) + \frac{\rho\lambda_{\max}(\mathscr{R}_2)}{(1-2\eta)\left(\|\mathscr{D}\| + \alpha\|\mathscr{M}\|\cdot\|\mathscr{F}_5\|\right)^2}\right)c^2. \tag{50}$$

By virtue of condition (38), a positive constant $\overline{\vartheta} > \widetilde{\vartheta}$ could be spotted with ease such that $\gamma - \overline{\vartheta}\ell > 0$, and it could be derived that

$$\dot{V}(t) \le \overline{\vartheta}V(t), \tag{51}$$

whenever $V(t) \ge \sigma\psi(\|\zeta(t)\|_{[t_0,t]})$, $\sigma = 1/(\overline{\vartheta} - t\widetilde{\vartheta})$.

When $t = t_{a+1}$, it is deduced from (13) that

$$\begin{aligned}
V(t) &= \mathfrak{T}^T(t)P\mathfrak{T}(t) = \wp^T(t)\tilde{D}^T P\tilde{D}\wp(t)\\
&= \wp^T(t^-)\tilde{K}^T\tilde{D}^T P\tilde{D}\tilde{K}\wp(t^-).
\end{aligned} \tag{52}$$

By Assumption 3, there exists an invertible matrix $\mathfrak{R}$ such that

$$\mathfrak{R}^{-1}\tilde{K}\mathfrak{R} \le e^{-(1/2)\gamma}I. \tag{53}$$

In accordance with Lemma 1, we discover that

$$\begin{aligned}
He(\Delta\mathscr{A}\mathscr{K}_2) &\le \frac{1}{\varepsilon_{57}}\mathscr{M}\mathscr{M}^T + \varepsilon_{57}\mathscr{K}_2^T\mathscr{F}_3^T\mathscr{F}_3\mathscr{K}_2,\\
He(\mathscr{K}_3\Delta\mathscr{D}) &\le \frac{1}{\varepsilon_{58}}\mathscr{K}_3\mathscr{M}\mathscr{M}^T\mathscr{K}_3^T + \varepsilon_{58}\mathscr{F}_5^T\mathscr{F}_5.
\end{aligned} \tag{54}$$

Afterwards, combined with Lemma 3, (37), (52), and (53), we obtain

$$V(t) \le e^{-\gamma}V(t^-). \tag{55}$$

Pay attention that $V(t_0) > \sigma\psi(\|\zeta(t_0)\|)$. Accordingly, we can define $\widehat{t}_1 = \inf\left\{t \ge t_0 \mid V(t) \le \sigma\psi(\|\zeta(t)\|_{[t_0,t]})\right\}$, which symbolizes that $V(t) \ge \sigma\psi(\|\zeta(t)\|_{[t_0,t]}), \forall t \in [t_0, \widehat{t}_1)$. Consider this case that $\widehat{t}_1 < \infty$ initially. If there is no impulse over $[t_0, \widehat{t}_1)$, it gives from (51) that

$$V(t) \le e^{\overline{\vartheta}(t-t_0)}V(t_0), \quad \forall t \in [t_0, \widehat{t}_1). \tag{56}$$

If there exist a few impulsive moments $t_{11} < t_{12} < \cdots < t_{1m} < \cdots$ on $[t_0, \widehat{t}_1)$, we can deduce that

$$V(t) \le e^{\overline{\vartheta}(t-t_0)}V(t_0), \quad t \in [t_0, \widehat{t}_1). \tag{57}$$

Based on (55), we get

$$V(t_{11}) \le e^{-\gamma} V(t_{11}^{-}) \le e^{-\gamma+\overline{\vartheta}(t_{11}-t_0)} V(t_0), \tag{58}$$

which illustrates that

$$V(t) \le e^{\overline{\vartheta}(t-t_{11})} V(t_{11}) \le e^{-\gamma+\overline{\vartheta}(t_{11}-t_0)} V(t_0), \quad t \in [t_{11}, t_{12}). \tag{59}$$

Equally, the inequality $V(t_{12}) \le e^{-2\gamma+\overline{\vartheta}(t_{12}-t_0)} V(t_0)$ holds. Paralleling to the above deduction, we could get an inference that, $\forall t \in [t_0, \widehat{t}_1)$,

$$V(t) \le e^{-\varkappa(t,t_0)\gamma+\overline{\vartheta}(t-t_0)} V(t_0) \le e^{-\varkappa(t,t_0)\overline{\gamma}+\overline{\vartheta}\ell} V(t_0), \tag{60}$$

where $\varkappa(t, t_0)$ denote the number of impulsive moments in the corresponding interval and $\overline{\gamma} = \gamma - \overline{\vartheta}\ell > 0$.

As a result, when $\widehat{t}_1 < \infty$, whether impulse exists in $[t_0, \widehat{t}_1)$ or not, the following inequality is always attainable:

$$V(t) \le e^{-\varkappa(t,t_0)\overline{\gamma}+\overline{\vartheta}\ell} V(t_0), \quad \forall t \in [t_0, \widehat{t}_1). \tag{61}$$

When $\widehat{t}_1 = \infty$, executing the similar argument as the case of $\widehat{t}_1 < \infty$, we could reason out

$$V(t) \le e^{-\varkappa(t,t_0)\overline{\gamma}+\overline{\vartheta}\ell} V(t_0), \quad \forall t \in [t_0, \infty). \tag{62}$$

Associating with the situation of $\widehat{t}_1 < \infty$, let $\check{t}_1 = \inf\{t \ge \widehat{t}_1 \mid V(t) \ge \sigma\psi(\|\zeta(t)\|_{[t_0,t]})\}$; the priority concern is the case of $\check{t}_1 < \infty$. Evidently, whether impulse appears on $[\widehat{t}_1, \check{t}_1)$ or not, it can be invariably obtained that

$$V(t) \le \sigma\psi\left(\|\zeta(t)\|_{[t_0,t]}\right), \quad \forall t \in [\widehat{t}_1, \check{t}_1). \tag{63}$$

Similarly, when $\check{t}_1 = \infty$; $V(t) \le \sigma\psi(\|\zeta(t)\|_{[t_0,t]})$, $\forall t \in [\widehat{t}_1, \infty)$.

Combined with the circumstance that $\check{t}_1 < \infty$, it follows that

$$V(t) \le e^{-\varkappa(t,t_0)\overline{\gamma}+\overline{\vartheta}\ell} V(t_0) + \sigma\psi\left(\|\zeta(t)\|_{[t_0,t]}\right), \quad \forall t \in [t_0, \check{t}_1), \tag{64}$$

and then let $\widehat{t}_2 = \inf\{t \ge \check{t}_1 \mid V(t) \le \sigma\psi(\|\zeta(t)\|_{[t_0,\check{t}]})\}$. When $\widehat{t}_2 < \infty$, we give priority to the case of no impulse over $[\check{t}_1, \widehat{t}_2)$; we could derive from $V(\check{t}_1) = \sigma\psi(\|\zeta(t)\|_{[t_0,\check{t}_1)})$ that

$$V(t) \le e^{\overline{\vartheta}(t-\check{t}_1)} V(\check{t}_1) \le e^{-\overline{\vartheta}\ell} \sigma\psi\left(\|\zeta(t)\|_{[t_0,t]}\right), \quad t \in [\check{t}_1, \widehat{t}_2). \tag{65}$$

If there exist impulsive moments $t_{21} < t_{22} < \cdots < t_{2m} < \cdots$, it holds that

$$V(t) \le e^{\overline{\vartheta}(t-\check{t}_1)} \sigma\psi\left(\|\zeta(t)\|_{[t_0,t]}\right), \quad \forall t \in [\check{t}_1, t_{21}). \tag{66}$$

According to (55), we have

$$V(t_{21}) \le e^{-\gamma} V(t_{21}^{-}) \le e^{-\gamma+\overline{\vartheta}(t_{21}-\check{t}_1)} \sigma\psi\left(\|\zeta(t)\|_{[t_0,t]}\right), \tag{67}$$

which suggests that

$$V(t) \le e^{-\gamma+\overline{\vartheta}(t-\check{t}_1)} \sigma\psi\left(\|\zeta(t)\|_{[t_0,t]}\right), \quad \forall t \in [t_{21}, t_{22}). \tag{68}$$

On account of $\gamma - \overline{\vartheta}\ell > 0$, performing semblable operation, we get

$$V(t) \le e^{\overline{\vartheta}\ell} \sigma\psi\left(\|\zeta(t)\|_{[t_0,t]}\right), \quad \forall t \in [\check{t}_1, \widehat{t}_2). \tag{69}$$

When $\widehat{t}_2 = \infty$, it can be inferred in repeating similar iterations that

$$V(t) \le e^{\overline{\vartheta}\ell} \sigma\psi\left(\|\zeta(t)\|_{[t_0,t]}\right), \quad \forall t \in [\check{t}_1, \infty). \tag{70}$$

Together with $\widehat{t}_2 < \infty$, we derive

$$V(t) \le e^{-\varkappa(t,t_0)\overline{\gamma}+\overline{\vartheta}\ell} V(t_0) + e^{\overline{\vartheta}\ell} \sigma\psi\left(\|\zeta(t)\|_{[t_0,t]}\right), \quad \forall t \in [t_0, \widehat{t}_2). \tag{71}$$

Arguing in the identical manner, we conclude that

$$V(t) \le e^{-\varkappa(t,t_0)\overline{\gamma}+\overline{\vartheta}\ell} V(t_0) + e^{\overline{\vartheta}\ell} \sigma\psi\left(\|\zeta(t)\|_{[t_0,t]}\right), \quad \forall t \in [t_0, \infty), \tag{72}$$

which fulfills the proof of (T2) based on Definition 1.

Remark 6. Obviously, Assumption 3 and condition (37) play a complementary role in the proof, which simultaneously explains the rationality and significance of Assumption 3.

Next, for the purpose of achieving (T3), the following hypothesis needs to be proposed.

Assumption 4. Matrices D and A with appropriate dimensionality are of full-row rank and full-column rank separately.

Theorem 3. *Assume that, for given constants ε_ι ($\iota = 1, 2, 3$), there exist matrices $P > 0$, $S_i > 0$, Ξ_i, and Θ_i, $i = 1, 2$, and constants $\widehat{\vartheta} > 0$, $\vartheta > 0$, $\gamma > 0$, and $\varepsilon_b > 0$ ($b = 1, 2, 3, \ldots, 58$) such that (35) and*

$$\begin{bmatrix} He(\Sigma_1) & \mathscr{M} & \Sigma_2^T \mathscr{F}_3^T & \Sigma_3 \mathscr{M} & \mathscr{F}_5^T \\ * & -\varepsilon_{57} I & 0 & 0 & 0 \\ * & * & -\dfrac{1}{\varepsilon_{57}} I & 0 & 0 \\ * & * & * & -\varepsilon_{58} I & 0 \\ * & * & * & * & -\dfrac{1}{\varepsilon_{58}} I \end{bmatrix} < 0, \tag{73}$$

$$\begin{bmatrix} \Omega & S\mathscr{D}^T P \mathscr{D} \mathscr{B}_d S & S\mathscr{D}^T P \mathscr{D} \mathscr{A} \Theta & S\mathscr{D}^T P \mathscr{D} \mathscr{C} S \\ * & -\varepsilon_1 S & 0 & 0 \\ * & * & -\varepsilon_2 S & 0 \\ * & * & * & -\varepsilon_3 S \end{bmatrix} < 0, \tag{74}$$

where

$$\Sigma_1 = \begin{bmatrix} \left(1 - e^{-\frac{1}{2}\gamma}\right)I + A\Xi_1 & -A\Xi_1 \\ 0 & \left(1 - e^{-\frac{1}{2}\gamma}\right)I - \Xi_2 D \end{bmatrix},$$

$$\Sigma_2 = \begin{bmatrix} \Xi_1 & -\Xi_1 \\ \Xi_1 & -\Xi_1 \end{bmatrix},$$

$$\Sigma_3 = \begin{bmatrix} 0 & 0 \\ 0 & -\Xi_2 \end{bmatrix},$$

$$S = \begin{bmatrix} S_1 & 0 \\ 0 & S_2 \end{bmatrix},$$

$$\Theta = \begin{bmatrix} \Theta_1 & -\Theta_2 \\ \Theta_1 & -\Theta_2 \end{bmatrix},$$

$$\Omega = -\vartheta S^2 + \overline{\mathscr{R}}_1,$$

$$\begin{aligned} \overline{\mathscr{R}}_1 = {} & \mu_1 S\mathscr{D}^T P\mathscr{D}\mathscr{M}\mathscr{M}^T\mathscr{D}^T P\mathscr{D}S + \mu_2 S\mathscr{D}^T P\mathscr{M}\mathscr{M}^T P\mathscr{D}S \\ & + \mu_3 S\mathscr{F}_5^T\mathscr{F}_5 S + \mu_4 S\mathscr{F}_1^T\mathscr{F}_1 S + \mu_5\Theta^T\mathscr{F}_3^T\mathscr{F}_3\Theta \\ & + \mu_6 S\mathscr{B}^T\mathscr{F}_5^T\mathscr{F}_5\mathscr{B}S + \mu_6\Theta^T\mathscr{A}^T\mathscr{F}_5^T\mathscr{F}_5\mathscr{A}\Theta \\ & + \frac{1}{\varepsilon_8} S\mathscr{B}^T\mathscr{D}^T P\mathscr{M}\mathscr{M}^T P\mathscr{D}\mathscr{B}S \\ & + \frac{1}{\varepsilon_8}\Theta^T\mathscr{A}^T\mathscr{D}^T P\mathscr{M}\mathscr{M}^T P\mathscr{D}\mathscr{A}\Theta + \mu_7\beta S\mathscr{F}_2^T\mathscr{F}_2 S\beta \\ & + \mu_8\beta S\mathscr{B}_d^T\mathscr{F}_5^T\mathscr{F}_5\mathscr{B}_d S\beta + He\left(S\mathscr{D}^T P\mathscr{D}\mathscr{B}S\right) \\ & + \frac{1}{\varepsilon_{25}}\beta S\mathscr{B}_d^T\mathscr{D}^T P\mathscr{M}\mathscr{M}^T P\mathscr{D}\mathscr{B}_d S\beta + He\left(S\mathscr{D}^T P\mathscr{D}\mathscr{A}\Theta\right) + \varepsilon_1\beta S\beta, \end{aligned}$$

$$\mu_1 = \varepsilon_1 + \varepsilon_2 + \varepsilon_{21} + \varepsilon_{33} + \varepsilon_{45},$$

$$\mu_2 = \varepsilon_3 + \varepsilon_4 + \varepsilon_6 + \varepsilon_{22} + \varepsilon_{23} + \varepsilon_{34} + \varepsilon_{35} + \varepsilon_{46} + \varepsilon_{47},$$

$$\begin{aligned} \mu_3 = {} & \varepsilon_8 + \varepsilon_9 + \varepsilon_{11} + \varepsilon_{13} + \varepsilon_{15} + \varepsilon_{18} + \varepsilon_{25} + \varepsilon_{26} \\ & + \varepsilon_{28} + \varepsilon_{30} + \varepsilon_{37} + \varepsilon_{38} + \varepsilon_{40} + \varepsilon_{42} + \varepsilon_{49} \\ & + \varepsilon_{50} + \varepsilon_{52} + \varepsilon_{54}, \end{aligned}$$

$$\mu_4 = \frac{1}{\varepsilon_1} + \frac{1}{\varepsilon_4\varepsilon_5} + \frac{1}{\varepsilon_9\varepsilon_{10}} + \frac{1}{\varepsilon_{15}\varepsilon_{16}\varepsilon_{17}},$$

$$\mu_5 = \frac{1}{\varepsilon_2} + \frac{1}{\varepsilon_6\varepsilon_7} + \frac{1}{\varepsilon_{11}\varepsilon_{12}} + \frac{1}{\varepsilon_{18}\varepsilon_{19}\varepsilon_{20}},$$

$$\mu_6 = \frac{1}{\varepsilon_3} + \frac{1}{\varepsilon_{13}\varepsilon_{14}},$$

$$\mu_7 = \frac{1}{\varepsilon_{21}} + \frac{1}{\varepsilon_{23}\varepsilon_{24}} + \frac{1}{\varepsilon_{26}\varepsilon_{27}} + \frac{1}{\varepsilon_{30}\varepsilon_{31}\varepsilon_{32}},$$

$$\mu_8 = \frac{1}{\varepsilon_{22}} + \frac{1}{\varepsilon_{28}\varepsilon_{29}}, \tag{75}$$

and then system (13) is input-to-state stabilizable under event-triggered strategy (16). In addition, the control gains K, $\overline{K}$, and L and parameters η, ρ, and ℓ are jointly devised by

$$\begin{aligned} & K = \Xi_1 D^T\left(DD^T\right)^{-1}, \\ & \overline{K} = \left(A^T A\right)^{-1} A^T \Xi_2, \\ & L = \Theta_1 S_1^{-1} \\ & 0 < \eta < \frac{\kappa}{2 + 2\kappa}, \\ & 0 < \ell < \frac{\lambda_{\min}(P)\gamma}{\lambda_{\min}(P)\widehat{\vartheta} + \vartheta}, \\ & \rho > 0, \end{aligned} \tag{76}$$

where

$$\kappa = \frac{\lambda_{\min}(P)\lambda_{\min^2}(S)\left((\gamma/\ell) - \widehat{\vartheta} - (\vartheta/\lambda_{\min}(P))\right)\left(\|\mathscr{D}\| + \alpha\|\mathscr{M}\| \cdot \|\mathscr{F}_5\|\right)^2}{\lambda_{\max}\left(\overline{\mathscr{R}}_2\right)},$$

$$\begin{aligned} \overline{\mathscr{R}}_2 = {} & \mu_9\Theta^T\mathscr{F}_3^T\mathscr{F}_3\Theta + \mu_{10}\Theta^T\mathscr{A}^T\mathscr{F}_5^T\mathscr{F}_5\mathscr{A}\Theta \\ & + \frac{1}{\varepsilon_{37}}\Theta^T\mathscr{A}^T\mathscr{D}^T P\mathscr{M}\mathscr{M}^T P\mathscr{D}\mathscr{A}\Theta + \epsilon_2\lambda_{\min^2}(S)S^{-1}, \end{aligned}$$

$$\mu_9 = \frac{1}{\varepsilon_{33}} + \frac{1}{\varepsilon_{35}\varepsilon_{36}} + \frac{1}{\varepsilon_{38}\varepsilon_{39}} + \frac{1}{\varepsilon_{42}\varepsilon_{43}\varepsilon_{44}},$$

$$\mu_{10} = \frac{1}{\varepsilon_{34}} + \frac{1}{\varepsilon_{40}\varepsilon_{41}}. \tag{77}$$

Proof. The controller gains K and $\overline{K}$, under Theorem 2, could be determined by (73), which leads to (37). Meanwhile, let $H_\iota = \varepsilon_\iota S^{-1}$ $(\iota = 1, 2, 3)$; then we use $\mathrm{diag}\{S^{-1}, S^{-1}, S^{-1}, S^{-1}\}$ to postmultiplication and premultiplication in inequality (74); condition (36) can be derived. Furthermore, condition (38) is linearized to (76). This accomplishes the proof.

Remark 7. More recently, the design problems of adaptive controller are studied for uncertain nonlinear systems with diverse structures, such as lower triangular structure [37], nonlower-triangular structure [38, 39], and nonstrict-feedback structure [40, 41]. Inspired by these interesting and pioneering works, the event-triggered impulsive control scheme designed and the approach adopted in this paper may be extended in these areas. In addition, through the enlightenment of some excellent works like [42–44], whether our model can be extended to various memristive neural network models would be a probable and rewarding research topic.

4. Illustrative Examples

For the purpose of corroborating the merit and effectiveness of the developed results, two numerical examples are considered in this section.

Example 1. Consider a dynamic model of a vehicle radar servo system. Following [45, 46], the nonlinear dynamic model with parametrized uncertainties can be modeled as

$$\begin{aligned}\dot{x}_1 &= x_2,\\ \dot{x}_2 &= -(b+\Delta b)x_2 + (c+\Delta c)u - (d+\Delta d)\left(F_c + fV_f\right),\\ y &= x_1,\end{aligned} \tag{78}$$

where x_1 and x_2 are the angular and the angular speed of the motor, respectively; $b = (B_r/J + m(r^2/G^2))$, $\Delta b = (\Delta B_r/\Delta J + m(r^2/G^2))$, $c = (K_f/J + m(r^2/G^2))$, $\Delta c = (\Delta K_f/\Delta J + m(r^2/G^2))$, $d = (r/GJ + m(r^2/G^2))$, and $\Delta d = (r/G\Delta J + m(r^2/G^2))$; J, m, r, G, B_r, K_f, i_q, F_c, and f are the rotor inertia, the mass of radar antenna, the radius of the gearing wheel, the gearing ratio, the rotor shaft friction, the torque constant, the current in q axis, the dry friction force, and the wind resistance coefficient, respectively; V_f is a nonlinear function in regard to radar antenna velocity. Besides, the parameters ΔB_r, ΔJ, and ΔK_f are not precisely known, which are dependent on several factors in the nonlinear dynamics; for instance, the direction of the radar antenna changes with vehicle vibration and gusty winds. Suppose that F_c is an interfering variable that varies over time. To stabilize this system in the input-to-state sense, now, some parameters are selected as

$$\begin{aligned}B_r &= 1.7\times 10^{-4}\mathrm{N}\cdot\mathrm{m}\cdot s,\\ J &= 48\times 10^{-3}\mathrm{kg}\cdot\mathrm{m}^2,\\ m &= 1000\mathrm{kg},\\ r &= 50\mathrm{mm},\\ G &= 1,\\ K_f &= 1.2\frac{\mathrm{N}\cdot\mathrm{m}}{\mathrm{A}},\\ f &= 1.4,\\ F_c &= \tanh t,\\ V_f &= 0.2\tanh(x_2),\\ \Delta B_r &= 0.2\times 10^{-4}\sin t\mathrm{N}\cdot\mathrm{m}\cdot\mathrm{s},\\ \Delta J &= 3\times 10^{-3}\cos t\mathrm{kg}\cdot\mathrm{m}^2,\\ \Delta K_f &= 0.2\sin t\frac{\mathrm{N}\cdot\mathrm{m}}{\mathrm{A}}.\end{aligned} \tag{79}$$

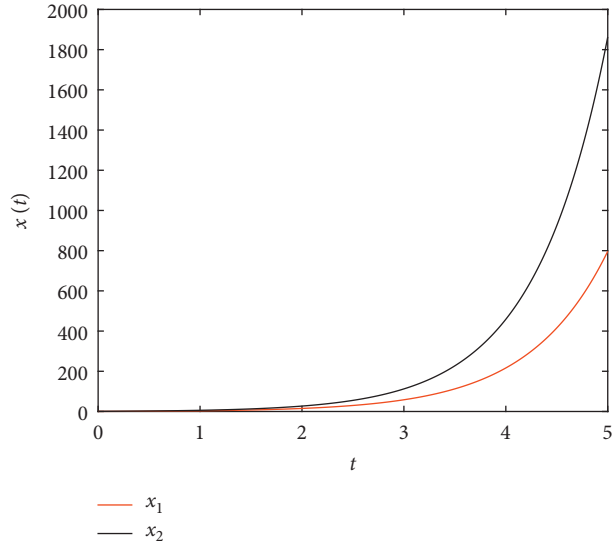

Figure 1: Responses of $x_1(t)$ and $x_2(t)$.

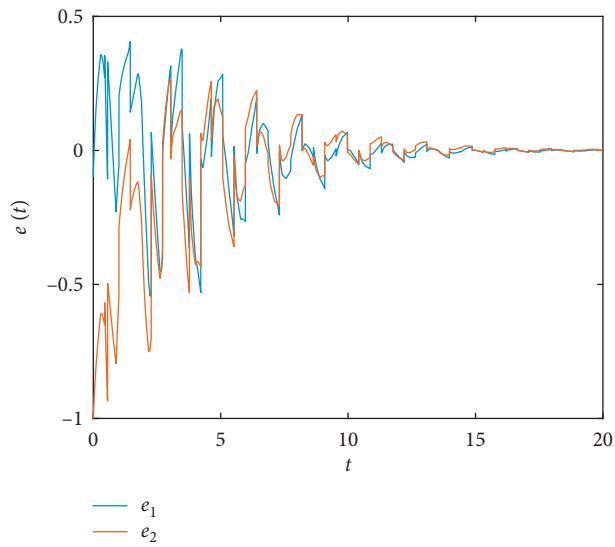

Figure 2: Responses of $e_1(t)$ and $e_2(t)$.

Based on Theorem 2 proposed in this paper, let $\varepsilon_i = 20, i = 1, 2, \ldots, 29$, $\varepsilon_j = 25, j = 30, 31, \ldots, 49$, $\varepsilon_l = 30$, and $l = 50, 51, \ldots, 58$, and choose $\widehat{\vartheta} = 0.45$, $\vartheta = 3\times 10^{-6}$, and $\gamma = 0.03$. Then, the control gains and the event-triggered mechanism parameters can be designed by utilizing MATLAB toolbox as follows:

$$\begin{aligned}K &= [\,-0.2164 \quad -0.1922\,],\\ \overline{K} &= [\,0.2149 \quad 0.1974\,],\\ L &= [\,-1.6450 \quad -1.1250\,],\\ 0 &< \eta < 0.2253\times 10^{-3}, 0 < \ell < 0.56.\end{aligned} \tag{80}$$

In order to achieve simulation, we choose $\eta = 0.18\times 10^{-3}$, $\rho = 0.1$, and $\ell = 0.4$. When the designed

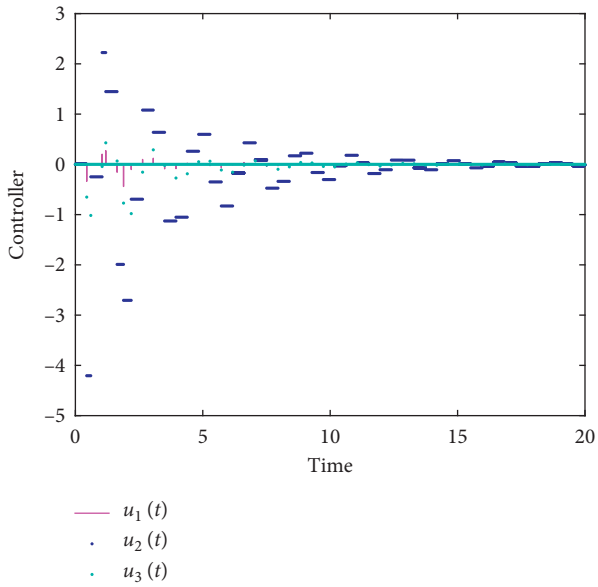

Figure 3: The dynamics of control inputs.

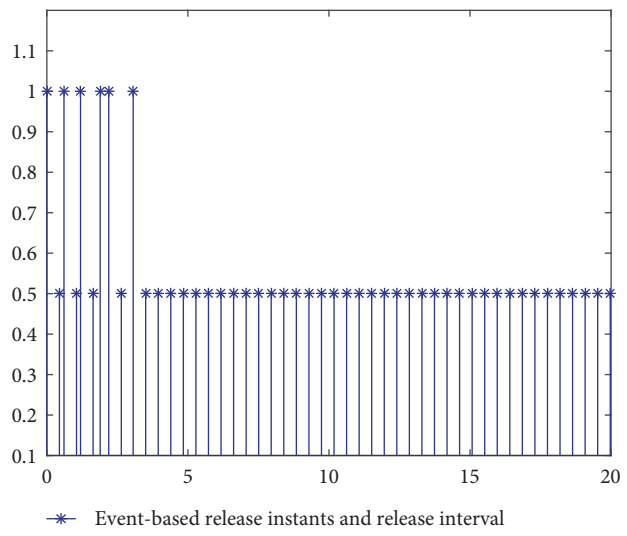

Figure 4: The dynamics of event-triggered mechanism.

controller does not act on system (78), as shown in Figure 1, then the system is unstable. However, under control, the change trend of error between the observer state and the system state, the dynamics of the controller updates (the points on the t-axis mean that the controller does not update), and the sampling dynamics of the event triggering mechanism are illustrated in Figures 2–4, respectively. Thereinto, in Figure 4, the point with a value of 1 corresponds to the event trigger sampling time, and the point with a value of 0.5 corresponds to the forced trigger sampling time. Assume that the total elapsed time of system is 20 s, if the output signal is transmitted by a fixed impulsive time sequence or time-triggered scheme, and the sampling period is 0.05 s; then the number of data traffic will be 400, whereas, as shown in Table 1, the amount of data communication can be dramatically decreased by adopting the designed event-triggered scheme. In conclusion, the aforementioned simulation outcomes reflect that when the system state is not completely measurable and uncertainties and external interferences exist in the system, the vehicle radar servo system can accurately estimate the corresponding input in real time and save unnecessary communication resources.

Table 1: Amount of date communication under varying ℓ, η, and ρ.

(ℓ, η)	$(0.1, 0.00043)$	$(0.2, 0.00024)$	$(0.4, 0.00018)$
$\rho = 0.01$	85	68	55
$\rho = 0.05$	74	61	51
$\rho = 0.1$	71	59	48

Example 2. To ensure the participation of more uncertainties and the establishment of Assumption 4, uncertain nonlinear system (1) incorporating two subsystems is taken into consideration, whose parameters are set as follows:

$$
\begin{aligned}
B &= \begin{bmatrix} 1 & 0 \\ 0 & 1 \end{bmatrix}, \\
B_d &= \begin{bmatrix} -1.7 & 0 \\ 0 & -1.7 \end{bmatrix}, \\
A &= \begin{bmatrix} 0.2 \\ 0.2 \end{bmatrix}, \\
C &= \begin{bmatrix} 420.3819 & 0 \\ 0 & 420.3819 \end{bmatrix}, \\
D &= \begin{bmatrix} -3526.2 & 0 \\ 0 & -3526.2 \end{bmatrix}, \\
f(x) &= \begin{bmatrix} 0.3\tanh(x_1) \\ 0.2\tanh(x_2) \end{bmatrix}, \\
\nu(t) &= \begin{bmatrix} \sin(t) \\ \tanh(t) \end{bmatrix}, \\
M &= \begin{bmatrix} -149.5759 & 0 \\ 0 & -149.5759 \end{bmatrix}, \\
F_1 &= \begin{bmatrix} 0.11 & 0 \\ 0 & 0.11 \end{bmatrix}, \\
F_2 &= \begin{bmatrix} 1 & 0 \\ 0 & 1 \end{bmatrix}, \\
F_3 &= \begin{bmatrix} -0.000545 \\ -0.000545 \end{bmatrix}, \\
F_4 &= F_5
\end{aligned}
\tag{81}
$$

If system (1) has no the control input, as portrayed in Figure 5, its dynamic behavior is unstable under exogenous disturbance and uncertainties. Next, without capturing the information of system states, an observer-based event-triggered impulsive controller will be designed to implement the input-to-state stabilization attribute on system (1). In accordance with Theorem 3, let $\varepsilon_i = 15, i = 1, 2, \ldots, 29$;

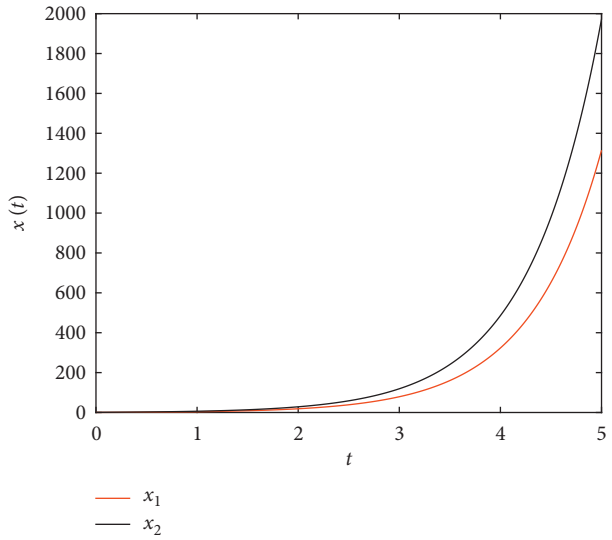

Figure 5: Responses of $x_1(t)$ and $x_2(t)$.

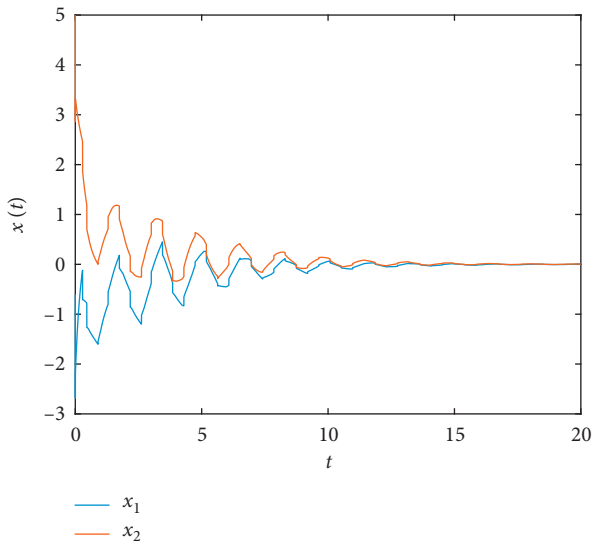

Figure 6: Responses of $x_1(t)$ and $x_2(t)$.

$\varepsilon_j = 18$, $\underline{j} = 30, 31, \ldots, 49$; $\varepsilon_l = 20$, $l = 50, 51, \ldots, 58$ and choose $\vartheta = 0.1$, $\vartheta = 10^{-10}$, $\gamma = 0.001$, $\varepsilon_1 = 160$, $\varepsilon_2 = 36520$, $\varepsilon_3 = 36971$, and $\beta = 18.9505$; then we devise the control gains as

$$\begin{aligned} K &= [\,2.6446 \;\; 2.6446\,], \\ \overline{K} &= [\,-3.8464 \;\; -3.8464\,], \\ L &= [\,0.01 \;\; 0\,], \end{aligned} \tag{82}$$

and the parameter of event-triggered mechanism as $0 < \eta < 0.0267$, $\rho > 0$, and $0 < \ell < 0.643$, so as to achieve the control performance of the input-to-state stabilization. To facilitate the simulation, we select $\eta = 0.02$, $\rho = 0.4$, and $\ell = 0.4$; then event-triggered mechanism (16) can be given by

$$\begin{aligned} t_{a+1} &= t_{a+1}^{\star} \wedge (t_a + 0.4), \\ t_{a+1}^{\star} &= \inf\{t \geq t_a \,|\, \mathscr{H}(t) \geq 0\}, \end{aligned} \tag{83}$$

where

$$\mathscr{H}(t) = \|\overline{\varrho}(t)\|^2 - 0.2\|\mathfrak{I}(t_a)\|^2 - 0.4\|\zeta(t)\|^2_{[t_0,t]}. \tag{84}$$

By exploiting such mechanism and controller gains, the trajectories of states and errors are separately illustrated in Figures 6 and 7, where the evolution of control inputs is exhibited in Figure 8. Moreover, viewed from the triggered dynamics of Figure 9, the event-triggered scheme lessens unnecessary sampling and avoids repeated sampling.

The advantage of the presented strategy in reducing data traffic, in the following, will be further verified. Assume that

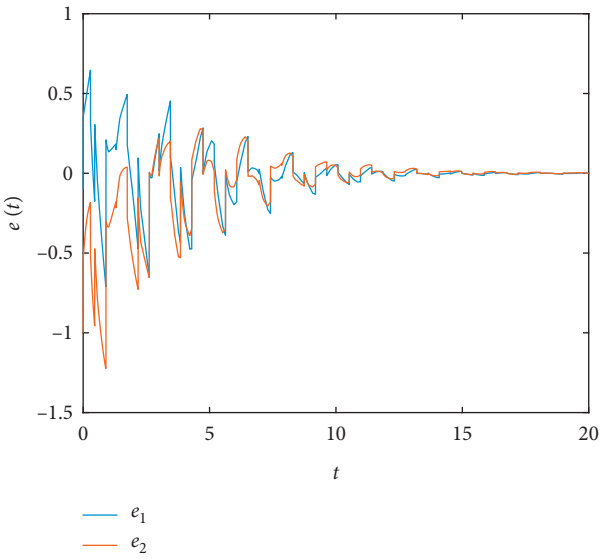

Figure 7: Responses of $e_1(t)$ and $e_2(t)$.

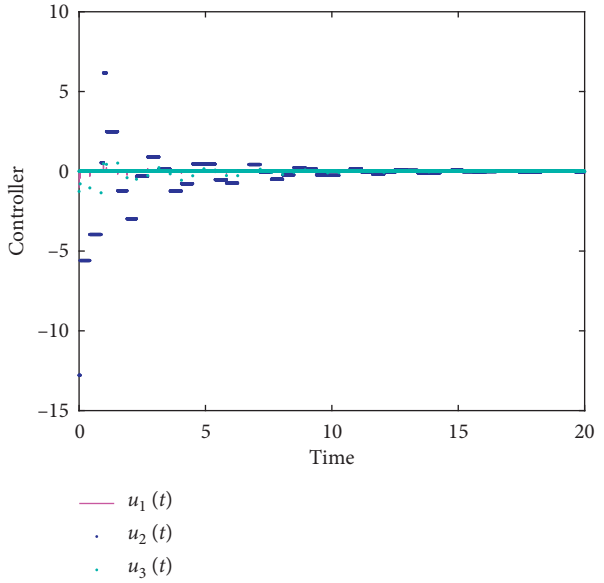

Figure 8: The dynamics of control inputs.

the total elapsed time of the closed-loop system (13) is 20s, analyzing in the same way as Example 1, then we can clearly observe from Table 2 that the event-triggered scheme proposed in this paper is superior to the periodic sampling scheme put forward in [21, 35, 36]. This table also exhibits that the sampling amount varies with the parameters ℓ, η, and ρ. It can be seen that the greater the value of ℓ or ρ is, the less the data communication would be generated and thus the more resources would be saved.

5. Concluding Remarks

This article investigates innovatively the input-to-state stabilization and controller design for a type of uncertain nonlinear systems included partially measurable states and exogenous disturbances. A suitable event-triggered mechanism is constructed which decides when the controllers are updated. With the combination of sample control, subsequently, an observer-based impulsive controller has been devised to warrant the performance of input-to-state stabilization on the uncertain controlled system. Particularly, the Zeno behavior in presented control scheme has been eliminated. With the aid of several analysis strategies and the linear matrix inequality technology, some sufficient criteria are deduced to guarantee the input-to-state stabilization. In addition, substantial uncertain parameters are reasonably estimated by exploiting some constant matrix inequalities and an innovative hypothesis. Although the reasoning process is slightly more complicated, fortunately, the result of theoretical analysis and simulations can demonstrate that the observer-based event-triggered impulsive scheme can work well. In some circumstances, the controller perhaps oversteps its physical restrictions that possibly lead to the controlled system subjected to rigorous performance degradation. Consequently, it is a probable research work for observer-based event-triggered saturated impulsive control on a category of nonlinear controlled systems in the future.

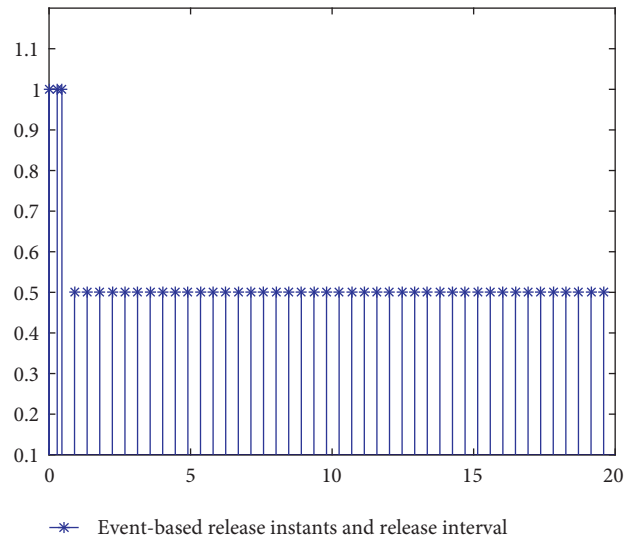

Figure 9: The dynamics of event-triggered mechanism.

Table 2: Amount of date communication under varying ℓ, η, and ρ

(ℓ, η)	$(0.1, 0.39)$	$(0.2, 0.13)$	$(0.4, 0.02)$
$\rho = 0.2$	82	66	52
$\rho = 0.3$	72	59	49
$\rho = 0.4$	69	56	46

Data Availability

No data were used to support this study.

Conflicts of Interest

The authors declare that there are no conflicts of interest regarding the publication of this paper.

Authors' Contributions

This study was carried out by the Master's student Xiangru Xing under the direction of Assistant Professor Jin-E Zhang.

Acknowledgments

This work was supported by the Natural Science Foundation of China under Grants 61976084 and 61773152.

References

[1] E. D. Sontag, "Smooth stabilization implies coprime factorization," *IEEE Transactions on Automatic Control*, vol. 34, no. 4, pp. 435–443, 1989.

[2] E. D. Sontag, "Further facts about input to state stabilization," *IEEE Transactions on Automatic Control*, vol. 35, no. 4, pp. 473–476, 1990.

[3] D. Angeli, "Intrinsic robustness of global asymptotic stability," *Systems & Control Letters*, vol. 38, no. 4-5, pp. 297–307, 1999.

[4] T. Kameneva and D. Nešić, "Robustness of nonlinear control systems with quantized feedback," *Nonlinear Analysis: Hybrid Systems*, vol. 4, no. 2, pp. 306–318, 2010.

[5] B. Li, Z. D. Wang, Q.-L. Han, and H. J. Liu, "Input-to-state stabilization in probability for nonlinear stochastic systems under quantization effects and communication protocols," *IEEE Transactions on Cybernetics*, vol. 49, no. 9, pp. 3242–3254, 2019.

[6] B. Li, Z. Wang, L. Ma, and H. Liu, "Observer-based event-triggered control for nonlinear systems with mixed delays and disturbances: the input-to-state stability," *IEEE Transactions on Cybernetics*, vol. 49, no. 7, pp. 2806–2819, 2019.

[7] D. Liberzon and D. Nesic, "Input-to-state stabilization of linear systems with quantized feedback," in *Proceedings of the 44th IEEE Conference on Decision and Control, and the European Control Conference*, pp. 8197–8202, Seville, Spain, December 2005.

[8] A. Isidori, *Nonlinear Control Systems II*, Springer, Berlin, Germany, 1999.

[9] J. Liu, X. Liu, and W.-C. Xie, "Input-to-state stability of impulsive and switching hybrid systems with time-delay," *Automatica*, vol. 47, no. 5, pp. 899–908, 2011.

[10] F.-L. Sun, Z.-H. Guan, X.-H. Zhang, and J.-C. Chen, "Exponential-weighted input-to-state stability of hybrid impulsive switched systems," *IET Control Theory & Applications*, vol. 6, no. 3, pp. 430–436, 2012.

[11] F. Zhao, Q. L. Zhang, X.-G. Yan, M. Cai, and J. C. Ren, "Stochastic input-to-state stability and H_∞ filtering for a class of stochastic nonlinear systems," *Applied Mathematics & Computation*, vol. 227, no. 15, pp. 672–686, 2014.

[12] T. Zhang, G. Feng, and X.-J. Zeng, "Output tracking of constrained nonlinear processes with offset-free input-to-state stable fuzzy predictive control," *Automatica*, vol. 45, no. 4, pp. 900–909, 2009.

[13] Y. Wen and A. Ferreyra, "System identification with state-space recurrent fuzzy neural networks," in *Proceedings of the 43rd IEEE Conference on Decision and Control*, vol. 5, pp. 5106–5111, Nassau, Bahamas, December 2005.

[14] R. C. Ma, Q. Chen, S. Z. Zhao, and J. Fu, "Dwell-time-based exponential stabilization of switched positive systems with actuator saturation," *IEEE Transactions on Systems, Man, and Cybernetics: Systems*, In press.

[15] H. Li, Y. Liu, and Y. Huang, "Event-triggered controller via adaptive output-feedback for a class of uncertain nonlinear systems," *International Journal of Control*, pp. 1–9, 2020.

[16] W. M. Haddad, V. Chellaboina, and S. G. Nersesov, *Impulsive and Hybrid Dynamical Systems: Stability, Dissipativity, and Control*, Princeton University Press, Princeton, NJ, USA, 2006.

[17] C. E. Neuman and V. Costanza, "Deterministic impulse control in native forest ecosystems management," *Journal of Optimization Theory and Applications*, vol. 66, no. 2, pp. 173–196, 1990.

[18] Y. Masutani, M. Matsushita, and F. Miyazaki, "Flyaround maneuvers on a satellite orbit by impulsive thrust control," in *Proceedings of the IEEE International Conference on Robotics and Automation*, vol. 1, pp. 421–426, Seoul, South Korea, May 2001.

[19] T. Yang and L. O. Chua, "Impulsive stabilization for control and synchronization of chaotic systems: theory and application to secure communication," *IEEE Transactions on Circuits and Systems I: Fundamental Theory and Applications*, vol. 44, no. 10, pp. 976–988, 1997, In press.

[20] R. Bellman, "Topics in pharmacokinetics, III: repeated dosage and impulse control," *Mathematical Biosciences*, vol. 12, no. 1-2, pp. 1–5, 1971.

[21] J.-E. Zhang, "Stabilization of uncertain fractional-order complex switched networks via impulsive control and its application to blind source separation," *IEEE Access*, vol. 6, pp. 32780–32789, 2018.

[22] X. Yang, X. D. Li, X. Li, Q. Xi, and P. Duan, "Review of stability and stabilization for impulsive delayed systems," *Mathematical Biosciences & Engineering*, vol. 15, no. 6, pp. 1495–1515, 2018.

[23] J.-E. Zhang and H. Liu, "Global robust exponential synchronization of multiple uncertain neural networks subject to event-triggered strategy," *Complexity*, vol. 2019, Article ID 7672068, 16 pages, 2019.

[24] D. Wang, M. Ha, and J. Qiao, "Self-learning optimal regulation for discrete-time nonlinear systems under event-driven formulation," *IEEE Transactions on Automatic Control*, vol. 65, no. 3, pp. 1272–1279, 2020.

[25] D. Wang, H. He, and D. Liu, "Improving the critic learning for event-based nonlinear H_∞ control design," *IEEE Transactions on Cybernetics*, vol. 47, no. 10, pp. 3417–3428, 2017.

[26] J. Chen, B. Chen, and Z. Zeng, "Synchronization in multiple neural networks with delay via impulsive control with event-triggered strategy and disconnected switching topology," *IEEE Transactions on Industrial Electronics*, p. 1, 2020, In press.

[27] W. Du, S. Y. S. Leung, Y. Tang, and A. V. Vasilakos, "Differential evolution with event-triggered impulsive control," *IEEE Transactions on Cybernetics*, vol. 47, no. 1, pp. 244–257, 2017.

[28] X. G. Tan, J. D. Cao, and X. D. Li, "Consensus of leader-following multiagent systems: a distributed event-triggered impulsive control strategy," *IEEE Transactions on Cybernetics*, vol. 49, no. 3, pp. 792–801, 2019.

[29] X. Li, H. Zhu, and S. Song, "Input-to-state stability of nonlinear systems using observer-based event-triggered impulsive control," *IEEE Transactions on Systems, Man, and Cybernetics: Systems*, pp. 1–9, 2020, In press.

[30] A. L. Wu, H. Liu, and Z. G. Zeng, "Observer design and H_∞ performance for discrete-time uncertain fuzzy-logic systems," *IEEE Transactions on Cybernetics*, 2020.

[31] T. Zhan, S. Ma, X. Liu, and H. Chen, "Exponential stability and H_∞ control of uncertain singular nonlinear switched

systems with impulsive perturbations," *International Journal of Systems Science*, vol. 50, no. 13, pp. 2424–2436, 2019, In press.

[32] Y. Wang, L. Xie, and C. E. De Souza, "Robust control of a class of uncertain nonlinear systems," *Systems & Control Letters*, vol. 19, no. 2, pp. 139–149, 1992.

[33] S. Boyd, L. EI Ghaoui, E. Feron, and V. Balakrishnan, *Linear Matrix Inequalities in System and Control Theory*, SIAM, Philadelphia, PA, USA, 1994.

[34] J. Yu, K. Zhang, and S. Fei, "Further results on mean square exponential stability of uncertain stochastic delayed neural networks," *Communications in Nonlinear Science and Numerical Simulation*, vol. 14, no. 4, pp. 1582–1589, 2009.

[35] G. Wen, X. Zhai, Z. Peng, and A. Rahmani, "Fault-tolerant secure consensus tracking of delayed nonlinear multi-agent systems with deception attacks and uncertain parameters via impulsive control," *Communications in Nonlinear Science and Numerical Simulation*, vol. 82, Article ID 105043, 2020.

[36] Suriguga, Y. Kao, C. Wang, and H. Xia, "Robust mean square stability of delayed stochastic generalized uncertain impulsive reaction-diffusion neural networks," *Journal of the Franklin Institute*, 2020, In press.

[37] B. Niu, P. Zhao, J.-D. Liu, H.-J. Ma, and Y.-J. Liu, "Global adaptive control of switched uncertain nonlinear systems: an improved MDADT method," *Automatica*, vol. 115, Article ID 108872, 2020.

[38] B. Niu, Y. J. Liu, W. L. Zhou, H. T. Li, P. Y. Duan, and J. Q. Li, "Multiple lyapunov functions for adaptive neural tracking control of switched nonlinear nonlower-triangular systems," *IEEE Transactions on Cybernetics*, vol. 50, no. 5, pp. 1877–1886, 2020.

[39] B. Niu, D. Wang, M. Liu, X. M. Song, H. Q. Wang, and P. Y. Duan, "Adaptive neural output-feedback controller design of switched nonlower triangular nonlinear systems with time delays," *IEEE Transactions on Neural Networks and Learning Systems*, 2020, In press.

[40] L. Ma, X. Huo, X. Zhao, B. Niu, and G. Zong, "Adaptive neural control for switched nonlinear systems with unknown backlash-like hysteresis and output dead-zone," *Neurocomputing*, vol. 357, pp. 203–214, 2019.

[41] B. Niu, D. Wang, N. D. Alotaibi, and F. E. Alsaadi, "Adaptive neural state-feedback tracking control of stochastic nonlinear switched systems: an average dwell-time method," *IEEE Transactions on Neural Networks and Learning Systems*, vol. 30, no. 4, pp. 1076–1087, 2019.

[42] H. Liu, Z. Wang, B. Shen, and H. Dong, "Delay-distribution-dependent H_∞ state estimation for discrete-time memristive neural networks with mixed time-delays and fading measurements," *IEEE Transactions on Cybernetics*, vol. 50, no. 2, pp. 440–451, 2020.

[43] H. J. Liu, Z. D. Wang, B. Shen, and X. H. Liu, "Event-triggered H_∞ state estimation for delayed stochastic memristive neural networks with missing measurements: the discrete time case," *IEEE Transactions on Neural Networks and Learning Systems*, vol. 29, no. 8, pp. 3726–3737, 2018.

[44] H. Liu, Z. Wang, B. Shen, T. Huang, and F. E. Alsaadi, "Stability analysis for discrete-time stochastic memristive neural networks with both leakage and probabilistic delays," *Neural Networks*, vol. 102, pp. 1–9, 2018.

[45] D. Deb, "Nonlinear adaptive control of vehicular radar servo systems with system and sensor uncertainties," in *Proceedings of the IEEE Applied Electromagnetics Conference*, pp. 1–4, Kolkata, India, December 2011.

[46] X. Liu, Q. Huang, and Y. Chen, "Robust adaptive controller with disturbance observer for vehicular radar servo system," *International Journal of Control, Automation and Systems*, vol. 9, no. 1, pp. 169–175, 2011.

Hindawi
Complexity
Volume 2020, Article ID 1468109, 11 pages
https://doi.org/10.1155/2020/1468109

Research Article

Constrained Uncertain System Stabilization with Enlargement of Invariant Sets

Walid Hamdi,[1,2] **Wissal Bey**,[1] **and Naceur Benhadj Braiek**[1,2]

[1]*Laboratory of Advanced Systems (LAS), Polytechnic School of Tunisia, Carthage University, BP 743, 2078 La Marsa, Tunisia*
[2]*National Higher Engineering School of Tunis (ENSIT), University of Tunis, 5 Avenue Taha Hussein, BP 56, 1008 Tunis, Tunisia*

Correspondence should be addressed to Walid Hamdi; hamdi.walid987@gmail.com

Received 31 March 2020; Revised 21 June 2020; Accepted 15 July 2020; Published 10 August 2020

Guest Editor: Baltazar Aguirre-Hernández

Copyright © 2020 Walid Hamdi et al. This is an open access article distributed under the Creative Commons Attribution License, which permits unrestricted use, distribution, and reproduction in any medium, provided the original work is properly cited.

An enhanced method able to perform accurate stability of constrained uncertain systems is presented. The main objective of this method is to compute a sequence of feedback control laws which stabilizes the closed-loop system. The proposed approach is based on robust model predictive control (RMPC) and enhanced maximized sets algorithm (EMSA), which are applied to improve the performance of the closed-loop system and achieve less conservative results. In fact, the proposed approach is split into two parts. The first is a method of enhanced maximized ellipsoidal invariant sets (EMES) based on a semidefinite programming problem. The second is an enhanced maximized polyhedral set (EMPS) which consists of appending new vertices to their convex hull to minimize the distance between each new vertex and the polyhedral set vertices to ensure state constraints. Simulation results on two examples, an uncertain nonisothermal CSTR and an angular positioning system, demonstrate the effectiveness of the proposed methodology when compared to other works related to a similar subject. According to the performance evaluation, we recorded higher feedback gain provided by smallest maximized invariant sets compared to recently studied methods, which shows the best region of stability. Therefore, the proposed algorithm can achieve less conservative results.

1. Introduction

Model predictive control (MPC) is a main concern for control design applied in different systems such as linear or nonlinear [1–3], continuous or discrete [4], and monovariable or multivariable [5]. Actually, MPC is a common technique for the dynamical systems' stabilization. This method is applicable already in numerous domains in industry [6] as regulation and control. Generally, real processes are nonlinear, complex, and uncertain [7–10]. Therefore, a robust model predictive control (RMPC) has been introduced to guarantee robustness as well as constraint satisfaction against uncertainty. Moreover, model predictive control is an interesting approach to represent systems using fuzzy logic for designing controllers. Several works have focused on the use of fuzzy-model-based sliding mode control of nonlinear systems in combination with MPC algorithms [11–14]. In fact, the fuzzy logic technique is quite attractive in terms of time, simplicity of implementation, relatively low cost, and ability to rapidly model complex systems.

For constrained control problems processing, robust MPC is an effectual stabilization algorithm. This technique employs a specific model procedure based on input and output constraints, for each sampling time, in order to optimize system behavior through the prediction horizon. The controller implements merely the initial calculated input and reproduces these computations at the next sampling time, despite the fact that more than one input shift is calculated [15]. The major aim is to determine the state feedback control law to facilitate the minimization of the worst-case performance cost.

At each time phase, the convex problem is considered as an optimization problem including linear matrix inequalities (LMI). The main common current algorithm for RMPC is demonstrated to guarantee robust stability. But, due to the fact that the optimization problem is truly settled at each sampling time, it needs high computational time in online

implementation. On the other hand, such problems rise appreciably with the size of the polytopic uncertainty set [16].

Many efforts have been made to design the state feedback control law which minimizes the worst-case performance cost. However, in future RMPC research [17], some constructive simulation experiences still remain. Several techniques have been performed in this field where practical treatments of RMPC are still a challenging task for model predictive control. Wan and Kothare [15] proposed an algorithm based on an offline robust constrained MPC by the use of ellipsoidal invariant sets subject to linear matrix inequality (LMI). This algorithm provides a detailed explicit control laws sequence corresponding to stable invariant ellipsoidal sequence asymptotically constructed offline in the state space. In the work of Bumroongsri and Kheawhom [18], the algorithm of Wan and Kothare [15] is developed in order to ensure the performance of the closed-loop system focused on polyhedral invariant sets. An offline approach for the stabilization of constrained uncertain system is presented in this study. Various approaches have been proposed to investigate, estimate, or enlarge the maximum region of the state space where the system can operate without violating state and stabilization constraints. In fact, the obtainable difficulty is associated with the determination of controlled invariant sets [19, 20]. The computation of the maximal controlled invariant set process introduced in [21] and the corresponding state feedback control laws for linear systems subject to polyhedral input and state constraints have been studied in [22, 23]. Kouvaritakis et al. [24] developed an advanced method to enlarge the terminal invariant set using a linear programming approach. In the study by Henrion et al. [25], convex optimization problems are formulated for the region enlargement and hence tuning parameters for the positively invariant set improvement.

Many researchers [26–28] were interested in an automatic enlargement of invariant sets. In the work by Li and Lin [26], the characterization of the maximal contractively invariant ellipsoid associated with a given positive definite matrix is proposed for discrete-time linear systems. This description can be used to establish an algebraic computational approach and thus determine such maximal contractively invariant ellipsoids based on inputs from saturated linear feedback. In this field, the authors first divide the state space into several regions according to the saturation status of each input. Second, the possible maximal contractively invariant ellipsoids are computed in each region. Note that if none of the inputs saturate on their intersections, no region has been calculated. The minimal one among these possible maximal contractively invariant ellipsoids is the maximal contractively invariant ellipsoids of the system.

In this work, a new approach for maximizing ellipsoidal and polyhedral invariant sets associated with the determination of the corresponding state feedback control laws is developed. The contributions of this paper are twofold: firstly, to highlight the robust control of states, an RMPC algorithm [15, 18] was applied. This approach is based on a computation method of maximal controlled invariant sets [21]. Secondly, the combination of MPC method and maximized invariant sets procedure is proposed in order to precisely advance the performance of the employed system. The considered techniques are realized to enlarge ellipsoidal and polyhedral invariant sets. For invariant ellipsoidal sets maximization, a semidefinite problem is used based on quadratic Lyapunov function. Besides, the proposed method for polyhedral sets enlargement consists of the iterative expansion of an initial invariant set precomputed by the LMI method, adding new vertices to its convex hull. This is achieved by minimizing the distance between each new vertex from the vertices of the polyhedral set. Finally, an online implementation strategy has been applied.

So, in summary, using this proposed approach, we recorded these two contributions:

Maximization of the invariant ellipsoidal and polyhedral sets in order to increase the region of stability

Providing less conservative results and efficient system performance in terms of computational time

This paper is organized as follows. Section 2 describes the proposed methodology based on robust model predictive control. In Section 3, simulation results and discussions of the whole proposed approach are reported using two examples: an uncertain nonisothermal CSTR and an angular positioning system. The conclusion is provided in Section 4. All preliminaries and notations used in this paper are revealed in Table 1.

Schur's Lemma 1 (see [16]). Let R, S, T be given matrices with appropriate sizes and assume that $Q > 0$; then the LMI $\begin{bmatrix} R & S \\ S^T & Q \end{bmatrix} > 0$ (respectively, ≥ 0) is feasible if and only if the nonlinear constraint $R - SQ^{-1}ST > 0$ (respectively, ≥ 0) is feasible.

2. Methods

2.1. Description of Robust Model Predictive Control. In this work, robust model predictive control (RMPC) analysis is the employed procedure to emphasize stability and effectively improve the performance of the uncertain discrete-time linear systems. RMPC method is a typical scheme for minimizing the worst-case performance cost in order to determine the state feedback control law. This technique consists of two tasks: (i) offline part is introduced to search the feedback gain K_i based on the resolution of Bumroongsri and Kheawhom problem [18]; (ii) online part, at each sampling time, determines the smallest invariant set containing the measured state and implements the corresponding state feedback control law to the process. In general, RMPC preprocessing strategy is suitable for stabilization process, decreasing computational time. Here, the regulated output is demonstrated to considerably evolve the system state faster to the origin. The step-by-step method of RMPC is described as follows.

Step 1. The linear discrete-time system described by Wan and Kothare [15] is considered with the following polytopic uncertainty:

Table 1: Preliminaries and notation.

Notation	Signification
Capital letters	Real matrices
A^T	Transpose of matrix A
$\det(A)$	Determinant of matrix A
$A \geq 0$	Symmetric matrix A is positive and semidefinite
$A > 0$	Symmetric matrix A is positive and definite
x_i	The i th element of x
$S = \text{conv}\{v_1, \ldots, v_q\}$	The convex hull of $\{v_1, \ldots, v_q\}$

$$\begin{cases} x(k+1) = A(k)x(k) + B(k)u(k), \\ y(k) = C(k)x(k), \end{cases} \tag{1}$$

where $x(k) \in \mathbb{R}^{n_x}$, $u(k) \in \mathbb{R}^{n_u}$, and $y(k) \in \mathbb{R}^{n_y}$ are state, control, and output variables of the system, respectively. Then,

$$\begin{aligned} &[A(k), B(k)] \in \Omega, \\ &\Omega = \text{conv}\{[A_1, B_1], [A_2, B_2], \ldots, [A_L, B_L]\}, \end{aligned} \tag{2}$$

where conv is the convex hull, Ω is a polytope, and $[A_j, B_j]$ are vertices of the polytope, where $j = 1, 2, \ldots, L$.

Step 2. Research to the feedback control law is as follows:

$$u\left(\frac{k+i}{k}\right) = Kx(k+i). \tag{3}$$

Equation (3) stabilizes system (1) with the following cost:

$$\min_{u(k+i/k)} \max_{[A(k+i),B(k+i)]\in\Omega, i\geq 0} J_\infty(k),$$

$$J_\infty(k) = \sum_{i=0}^{\infty} \begin{bmatrix} x\left(\frac{k+i}{k}\right) \\ u\left(\frac{k+i}{k}\right) \end{bmatrix}^T \begin{bmatrix} \Theta & 0 \\ 0 & R \end{bmatrix} \begin{bmatrix} x\left(\frac{k+i}{k}\right) \\ u\left(\frac{k+i}{k}\right) \end{bmatrix}, \tag{4}$$

subject to

$$\begin{aligned} &\left| u_h \frac{k+1}{k} \right| \leq u_{h,\max}, \quad h = 1, 2, \ldots, n_u, \\ &\left| y_r \frac{k+1}{k} \right| \leq y_{r,\max}, \quad r = 1, 2, \ldots, n_y, \end{aligned} \tag{5}$$

where $\Theta > 0$ and $R > 0$ are symmetric weighting matrices.

Step 3. Choose a state sequence x_i, $i = 1, 2, \ldots, N$, and solve problem (6)–(10) to get the state feedback gains $K_i = Y_i Q_i^{-1}$, where Y_i and Q_i, $i = 1, 2, \ldots, N$, are solutions of the following problem:

$$\min_{\gamma_i, Q_i, Y_i} \gamma_i, \tag{6}$$

subject to

$$\begin{bmatrix} Q_i & Q_i A_j^T + Y_i^T B_j^T & Q_i \Theta^{1/2} & Y_i^T R^{1/2} \\ A_j Q_i + B_j Y_i & Q_i & 0 & 0 \\ \Theta^{1/2} Q_i & 0 & \gamma_i I & 0 \\ R^{1/2} Y_i & 0 & 0 & \gamma_i I \end{bmatrix} \geq 0, \tag{7}$$

$$\forall j = 1, 2, \ldots, L,$$

$$\begin{bmatrix} 1 & x_i^T \\ x_i & Q_i \end{bmatrix} \geq 0, \tag{8}$$

$$\begin{bmatrix} X & Y_i \\ Y_i^T & Q_i \end{bmatrix} \geq 0, \tag{9}$$

$$X_{hh} \leq u_{h,\max}^2, \quad h = 1, 2, \ldots, n_u,$$

$$\begin{bmatrix} S & C\left(A_j Q_i + B_j Y_i\right) \\ \left(A_j Q_i + B_j Y_i\right)^T C^T & Q_i \end{bmatrix} \geq 0, \tag{10}$$

$$S_{rr} \leq y_{r,\max}^2, \quad r = 1, 2, \ldots, n_y, \ \forall j = 1, 2, \ldots, L,$$

where Q is a symmetric matrix.

Step 4. For each K_i, the corresponding polyhedral invariant set $S_i = \{x_i / M_i x_i \leq d_i\}$ is constructed in [18].

2.2. The Proposed Methodology. As illustrated in Figure 1, the proposed methodology is composed of three steps:

Step 1. Enhanced maximized sets algorithm: by the combination of an RMPC technique proposed by Bumroongrsi and Kheawhom [18] and the enhanced maximized invariant sets approach, a successful progress of the closed-loop system performance was obtained. Two methods are developed to maximize the ellipsoidal and polyhedral invariant sets constructed by the RMPC algorithm. The ellipsoidal invariant sets approach referred to in Section 2.2.1 is a semidefinite programming method. Based on the work of Athanasopoulos and Bitsoris [21], a second linear programming approach is used to enlarge polyhedral sets.

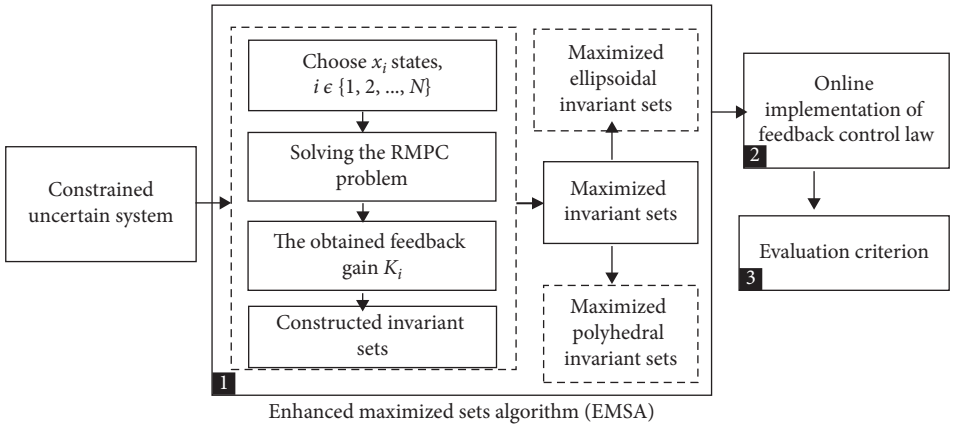

Figure 1: Flowchart of the proposed methodology.

It consists of adding new vertices to their convex hull by minimizing the distance between each new vertex and the polyhedral set vertices for securing the state constraints. The polyhedral invariant sets process is presented in Section 2.2.2.

Step 2. Online implementation of the feedback control law: at each sampling time, determine the smallest invariant set containing the measured state and implement the corresponding state feedback control law to the process.

Step 3. Evaluation criterion: the computational time (CT) required for the proposed approach has been reduced.

2.2.1. Enhanced Maximized Ellipsoidal Invariant Sets (EMES). Subsequent to the RMPC problem resolution and the feedback gains determination, an invariant ellipsoidal sets sequence is built.

Let the following inequalities be

$$x\left(\frac{k}{k}\right)^{\mathrm{T}} Px\left(\frac{k}{k}\right) \leq 1, \tag{11}$$

which is equivalent to

$$x\left(\frac{k}{k}\right)^{\mathrm{T}} Q^{-1} x\left(\frac{k}{k}\right) \leq 1, \tag{12}$$

where $P = Q^{-1}$.

To maximize the ellipsoidal region

$$\xi = \left\{x \mid x^{\mathrm{T}} Px \leq 1\right\} = \left\{x \mid x^{\mathrm{T}} Q^{-1} x \leq 1\right\}, \tag{13}$$

by guaranteeing a wider stability domain, a semidefinite programming problem will be used.

Let us consider the quadratic Lyapunov function $V(x(k)) = x(k)^{\mathrm{T}} Px(k)$. Then, we have

$$\begin{aligned} \Delta V(x(k)) &= V(x(k+1)) - V(x(k)) \leq 0 \\ &= x(k)^{\mathrm{T}} \left[(A+BK)^{\mathrm{T}} P(A+BK) - P\right] x(k) \leq 0. \end{aligned} \tag{14}$$

Condition (14) is true if and only if

$$(A+BK)^{\mathrm{T}} P(A+BK) - P \leq 0. \tag{15}$$

Using Schur's lemma, the following condition with $Q = P^{-1}$ and $K = YQ^{-1}$ is obtained:

$$\begin{bmatrix} Q & \left(A_j Q_i + B_j Y_i\right)^{\mathrm{T}} \\ A_j Q_i + B_j Y_i & Q \end{bmatrix} \geq 0. \tag{16}$$

A natural objective enables increasing the ellipsoid volume which is proportional to $\det(Q)$. Hence, if the maximal invariant ellipsoid volume corresponds to state feedback law, solving the following semidefinite programming is required:

$$\max_{Q,Y} \log(\det(Q)), \tag{17}$$

subject to

$$\begin{bmatrix} Q & \left(A_j Q_i + B_j Y_i\right)^{\mathrm{T}} \\ A_j Q_i + B_j Y_i & Q \end{bmatrix} \geq 0, \quad \begin{bmatrix} u_{\max} & Y \\ Y^{\mathrm{T}} & Q \end{bmatrix} \geq 0, \quad u_{\max} \geq |u|. \tag{18}$$

2.2.2. Enhanced Maximized Polyhedral Invariant Sets (EMPS). Given the state feedback gains $K_i = Y_i Q_i^{-1}$, $i = 1, \ldots, N$, calculated from RMPC algorithm, for each K_i, the corresponding polyhedral invariant set $S_i = \{x_i / M_i x_i \leq d_i\}$ is constructed. The enhanced maximized polyhedral invariant sets (EMPS) algorithm is given as follows.

Step 1. Let the polyhedral invariant sets S_i be the convex hull of its vertices:

$$S_i = \operatorname{conv}\left\{v_i^1, \ldots, v_i^q\right\}, \quad i = 1, 2, \ldots, N. \tag{19}$$

Step 2. Consider new sets $S_i' = \operatorname{conv}\left\{v_i^1, \ldots, v_i^q, v_{\sup}\right\}$, $i = 1, 2, \ldots, N$, $q = 1, 2, \ldots, n$, and choose a point $v^{\mathrm{ch}} \notin S_i$.

Step 3. Solve the following EMPS problem:

$$\min_{v_{\sup},p,u_{\sup},\varepsilon}\left\{\left\|v_{\sup}-v^{\mathrm{ch}}\right\|_{\infty}\right\}, \tag{20}$$

subject to

$$Av_{\sup}+Bu_{\sup}=\sum_{i=1}^{j}p_iv_i^j+p_{j+1}v_{\sup}, \tag{21}$$

$$p_i\geq 0,\quad i=1,\ldots,j+1, \tag{22}$$

$$\sum_{i=1}^{j+1}p_i\leq\varepsilon, \tag{23}$$

$$0<\varepsilon<1, \tag{24}$$

$$M_iv_{\sup}\leq d_i, \tag{25}$$

where $p_{j+1}\in[0,1]$.

Once the problem is solved, an optimal vertex $v_{\sup}$ is obtained, and thus, the following maximized polyhedral set is constructed:

$$S_i'=\mathrm{conv}\left\{v_i^1,\ldots,v_i^q,v_{\sup}\right\}. \tag{26}$$

Relations (21)–(23) imply the positive invariance and attractivity of S_i', while (24) and (25) guarantee constraint satisfaction.

Step 4. At each sampling time, determine the smallest maximized polyhedral invariant set containing the measured state and implement the corresponding state feedback control law $u(k/k)=K_ix(k/k)$ to the process.

3. Results

3.1. Example 1. An uncertain nonisothermal CSTR [15] is considered where the exothermic reaction $A\longrightarrow B$ takes place. The reaction is irreversible and the rate of reaction is primary order with respect to component A. A cooling coil is employed to eliminate heat which is released in the exothermic reaction. The uncertain parameters are the reaction rate constant k_0 and the heat of reaction H_{rxn}. The linearized model focused on the component balance and the energy balance is given by the following state equations:

$$\begin{cases}\dot{x}(t)=Ax(t)+Bu(t),\\ y(t)=Cx(t),\end{cases} \tag{27}$$

where $\begin{bmatrix}C_A\\T\end{bmatrix}$ is the state vector $x(t)$ and $\begin{bmatrix}C_{A,F}\\F_C\end{bmatrix}$ is the input control vector $u(t)$. Matrices are defined by

$$\begin{aligned}A&=\begin{bmatrix}0.85-0.0986\alpha(k) & -0.0014\alpha(k)\\ 0.9864\alpha(k)\beta(k) & 0.0487+0.01403\alpha(k)\beta(k)\end{bmatrix},\\ B&=\begin{bmatrix}0.15 & 0\\ 0 & -0.912\end{bmatrix},\\ C&=\begin{bmatrix}1 & 0\\ 0 & 1\end{bmatrix},\end{aligned} \tag{28}$$

where C_A is the concentration of A in the reactor, $C_{A,F}$ presents the feed concentration of A, T denotes the reactor temperature, and F_C is the coolant flow. The operating parameters are as follows:

$$\begin{aligned}F&=1\,\mathrm{m}^3/\mathrm{min}, V=1\,\mathrm{m}^3\\ k_0&=10^9-10^{10}\,\mathrm{min}^{-1}\\ E/R&=8330.1\,\mathrm{K}\\ -\Delta H_{rxn}&=10^7-10^8\,\mathrm{cal/kmol}\\ \rho&=10^6\,\mathrm{g/m}^3\\ U_A&=5.3410^6\,\mathrm{cal/(K\,min)}\\ C_p&=1\,\mathrm{cal/(g\,K)}\end{aligned}$$

Let $\overline{C}_A=C_A-C_{A,\mathrm{eq}}$, $\overline{C}_{A,F}=C_{A,F}-C_{A,F,\mathrm{eq}}$, and $\overline{F}_C=F_C-F_{C,\mathrm{eq}}$, where the subscript eq is used to denote the corresponding variable at equilibrium condition. By discretization, using a sampling time (ST = 0.15 min), the discrete-time model with $\begin{bmatrix}\overline{C}_A(k)\\ \overline{T}(k)\end{bmatrix}$ and $\begin{bmatrix}\overline{C}_{A,F}\\ \overline{F}_C(k)\end{bmatrix}$, as state and control vectors, respectively, is given as follows:

$$\begin{cases}x(k+1)=Ax(k)+Bu(k),\\ y(k)=Cx(k),\end{cases} \tag{29}$$

$$\begin{cases}x(k+1)=\begin{bmatrix}\overline{C}_A(k+1)\\ \overline{T}(k+1)\end{bmatrix}\\ =\begin{bmatrix}0.85-0.0986\alpha(k) & -0.0014\alpha(k)\\ 0.9864\alpha(k)\beta(k) & 0.0487+0.01403\alpha(k)\beta(k)\end{bmatrix}\begin{bmatrix}\overline{C}_A(k)\\ \overline{T}(k)\end{bmatrix}\\ +\begin{bmatrix}0.15 & 0\\ 0 & -0.912\end{bmatrix}\begin{bmatrix}\overline{C}_{A,F}\\ \overline{F}_C(k)\end{bmatrix},\\ y(k)=\begin{bmatrix}1 & 0\\ 0 & 1\end{bmatrix}\begin{bmatrix}\overline{C}_A(k)\\ \overline{T}(k)\end{bmatrix},\end{cases} \tag{30}$$

where $1\leq\alpha(k)=k_0/10^9\leq 10$ and $1\leq\beta(k)=-\Delta H_{rxn}/10^7\leq 10$.

The two parameters $\alpha(k)$ and $\beta(k)$ are independent of each other. Then, we consider the following polytopic uncertain model with four vertices:

$$\Omega=\mathrm{conv}\left\{\begin{bmatrix}0.751 & -0.0014\\ 0.986 & 0.063\end{bmatrix},\begin{bmatrix}0.751 & -0.0014\\ 9.864 & 0.189\end{bmatrix},\begin{bmatrix}-0.136 & -0.014\\ 9.864 & 0.189\end{bmatrix},\begin{bmatrix}-0.136 & -0.014\\ 98.644 & 1.451\end{bmatrix}\right\}. \tag{31}$$

By manipulating $\overline{C}_{A,F}$ and $\overline{F}_C$, the control of concentration $\overline{C}_A$ and the reactor temperature $\overline{T}$ return to the origin. These variables are constrained having $|\overline{C}_{A,F}| \leq 0.5\,\text{kmol/m}^3$ and $|\overline{F}_C| \leq 1.5\,\text{m}^3/\text{min}$.

The cost function is given by (4) with $\Theta = I$ and $R = 0.1I$.

The sequence of the chosen states is

$$x_i = \left\{ \begin{array}{ll} (0.0525, 0.0525), & (0.0475, 0.0475) \\ (0.0425, 0.0425), & (0.0375, 0.0375) \\ (0.0325, 0.0325), & (0.0275, 0.0275) \end{array} \right\}. \quad (32)$$

These sequences are used to compute six offline feedback gains K_i, $i = 1, 2, \ldots, 6$. This allows building an ellipsoidal and polyhedral invariant sets sequences.

Focused on the EMSA method, the maximized ellipsoidal and polyhedral invariant sets are larger compared to invariant sets [15, 18]. The difference between these sets is, respectively, shown in Figures 2 and 3.

For both techniques, the invariant sets, ellipsoidal (Figure 2) and polyhedral ones (Figure 3), are constructed based on the choice of the same states sequence x_i, $i = 1, \ldots, 6$.

The maximized polyhedral invariant sets enable us to obtain an appreciably larger domain of stability compared to the polyhedral invariant ones in [18], for each chosen state x_i. This is due to the additional vertex of the obtained sets that have been added by the EMPS approach. Figure 3 reveals the comparison between the stabilizable sets of two feedback gains in terms of A and B points. As shown in Figure 3, it is clear that the maximized polyhedral invariant sets stabilize the states at point A by the use of feedback gain K_1 since the states are contained in the maximized sets S_1. Contrariwise, the polyhedral sets [18] are not able to stabilize the states at point A because they are not contained in the initial invariant set. As illustrated in Figures 2 and 3, beginning at the point B, the polyhedral set can stabilize the states to the origin taking on the lowest feedback gain K_1. In brief, the proposed approach EMPS algorithm can regulate the states at point B to the origin using a higher feedback gain K_6 in the fact that the points are contained in S_6. In this case, EMPS method achieves the higher feedback gain, when compared to previous studies. Consequently, the proposed maximized approach attains less conservative results. To significantly clarify our results, Figures 4 and 5 demonstrate the regulated outputs. Here, we report that the considered EMSA method provides less conservative results and efficient system performance, when the state evolves faster to the origin. Compared to the previous work [15, 18], the proposed strategy seems to be helpful for uncertain system control. As demonstrated in Table 2, we can deduce from the stabilization validation results that the EMSA technique is more efficient compared to the other model predictive control methods [15, 18] in terms of stabilizable region and computational time (CT). EMSA strategy provides rigorous results in terms of CT (4.951 s) and larger stabilization region in different points. Although the construction of maximized polyhedral invariants sets requests more computational time than the standard ellipsoidal and polyhedral invariants sets, it is still more precise in enlargement of stability domain. Table 3 summarizes the cumulative cost obtained in Example 1.

3.2. Example 2. We consider the angular positioning system described by the following discrete-time equation [29]:

$$\left\{ \begin{array}{l} \begin{bmatrix} \theta(k+1) \\ \dot{\theta}(k+1) \end{bmatrix} = \begin{bmatrix} 1 & 0.1 \\ 0 & 1 - 0.1\alpha(k) \end{bmatrix} \begin{bmatrix} \theta(k) \\ \dot{\theta}(k) \end{bmatrix} \\ + \begin{bmatrix} 0 \\ 0.0787 \end{bmatrix} u(k), \\ y(k) = \begin{bmatrix} 1 & 0 \end{bmatrix} \begin{bmatrix} \theta(k) \\ \dot{\theta}(k) \end{bmatrix}, \end{array} \right. \quad (33)$$

where $\theta(k)$ is the angular position of the antenna, $\dot{\theta}(k)$ is the angular velocity, and $u(k)$ is the input voltage of the motor. It is assumed that the uncertain parameter is arbitrarily time varying: $0.1 \leq \alpha(k) \equiv k_0/10^9 \leq 10$.

Let $\overline{\theta} = \theta - \theta_{\text{eq}}$, $\dot{\overline{\theta}} = \dot{\theta} - \dot{\theta}_{\text{eq}}$, and $\overline{u} = u - u_{\text{eq}}$, where the subscript eq denotes the corresponding variable at equilibrium condition Figure 6. The obtained system can be written as follows:

$$\left\{ \begin{array}{l} \begin{bmatrix} \overline{\theta}(k+1) \\ \dot{\overline{\theta}}(k+1) \end{bmatrix} = \begin{bmatrix} 1 & 0.1 \\ 0 & 1 - 0.1\alpha(k) \end{bmatrix} \begin{bmatrix} \overline{\theta}(k) \\ \dot{\overline{\theta}}(k) \end{bmatrix} \\ + \begin{bmatrix} 0 \\ 0.0787 \end{bmatrix} u(k), \\ y(k) = \begin{bmatrix} 0 & 1 \end{bmatrix} \begin{bmatrix} \overline{\theta}(k) \\ \dot{\overline{\theta}}(k) \end{bmatrix}. \end{array} \right. \quad (34)$$

System (34) has the following polytopic structure:

$$A(k) \in \text{conv}\left\{ \begin{bmatrix} 1 & 0.1 \\ 0 & 0.9 \end{bmatrix}, \begin{bmatrix} 1 & 0.1 \\ 0 & 0 \end{bmatrix} \right\}. \quad (35)$$

The input constraint is

$$|\overline{u}(k)| \leq 2\,\text{volts}. \quad (36)$$

The weighting matrices Θ and R are given by

$$\Theta = \begin{bmatrix} 1 & 0 \\ 0 & 0 \end{bmatrix}, \quad R = 0.00002I. \quad (37)$$

Let us choose the following seven states sequence:

$$x_i = \left\{ \begin{array}{lll} (0.35, 0.35), & & (0.3, 0.3) \\ (0.25, 0.25), & & (0.02, 0.02) \\ (0.15, 0.15), & (0.1, 0.1), & (0.05, 0.05) \end{array} \right\}. \quad (38)$$

In this example, the sequence of seven states x_i, $i = 1, \ldots, 7$, is used to compute seven state feedback gains K_i corresponding to seven ellipsoidal and polyhedral invariant sets. Using the EMSA algorithm, the maximized ellipsoidal and polyhedral invariant sets are drawn compared to invariant sets [15, 18]. Figure 7 exemplifies the comparison between the maximized ellipsoidal and polyhedral invariant sets.

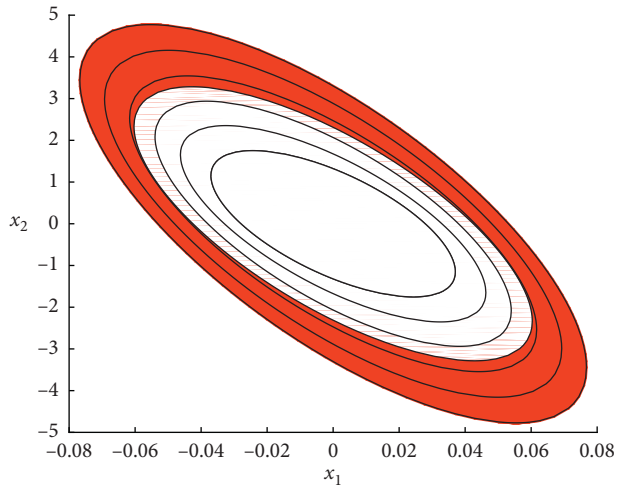

Figure 2: Resulting maximized ellipsoidal invariant sets (in red).

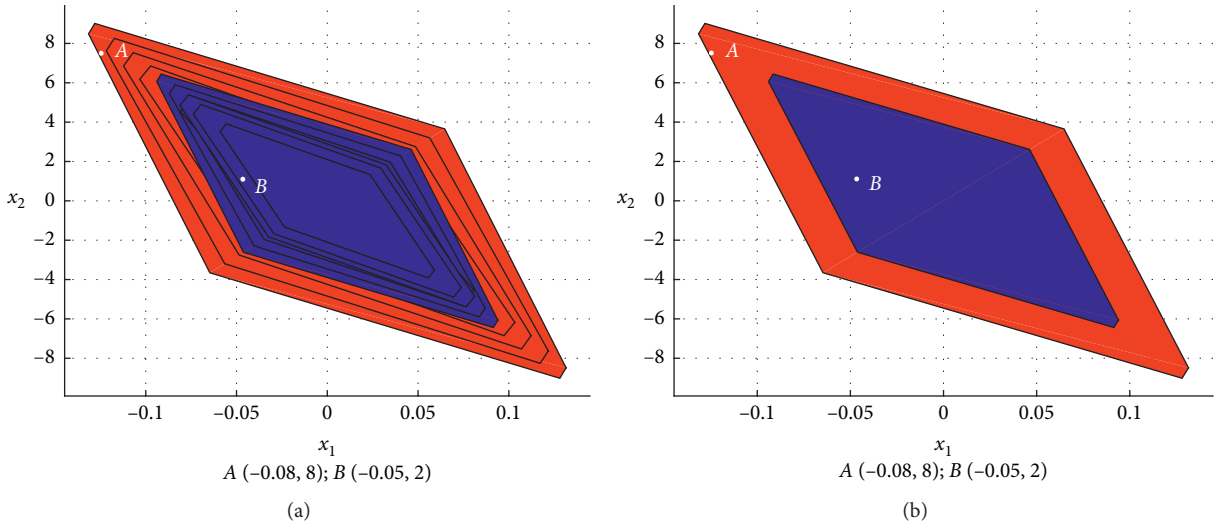

Figure 3: Examples of maximized polyhedral invariant sets from (a) six imprecated sets and (b) first set compared to [18].

Compared to the invariant set [18], the maximized invariant set has a significantly larger domain of stability, for each chosen state x_i, $i = 1, \ldots, 7$. Figure 7 reveals the comparison between the stabilizable sets of three feedback gains in terms of A, B, and C points. Simulation results illustrated in Figure 7 highlight the robustness of the proposed method using maximized polyhedral invariant sets which stabilize the states at point A employing the feedback gain K_1 (the states are contained in the maximized set S_1). On the other hand, the polyhedral [18] and the maximized ellipsoidal sets are not able to stabilize the states at point A (the states are not contained in the original polyhedral and maximized ellipsoidal sets). Concerning the point B, the polyhedral set [18] can stabilize the states to the origin corresponding to the lowest feedback gain K_1. In addition, the proposed EMPS approach can regulate the states at point B to the origin utilizing a higher feedback gain K_5 (points contained in S_5). On the contrary, the maximized ellipsoidal set and the ellipsoidal set [15] cannot control the states at point B because they are not situated in these invariant sets. Also, starting by the point C, it is obvious that the maximized invariant set obtained from EMES approach can stabilize the states to the origin containing the lowest feedback gain K_1. The proposed EMSA model can control the states at this point to the origin exploiting higher feedback gain K_7 (points contained in S_7). Note that previous studies [18] are capable of stabilizing these states at points C from the feedback gain K_6. Figures 8 and 9 display the regulated outputs. In this case, it is evident that the projected EMSA method supplies less conservative results. If the state evolves faster to the origin, the

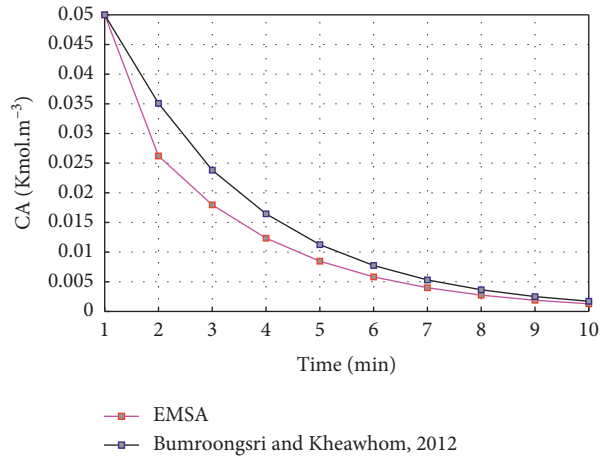

Figure 4: The concentration of A in the reactor of the regulated output obtained with EMPS algorithm.

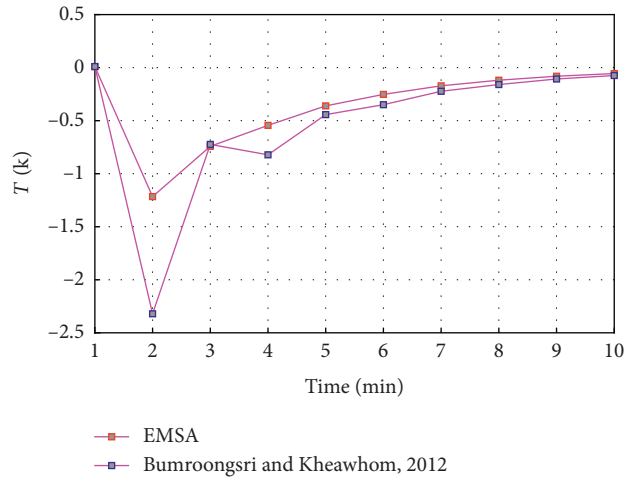

Figure 5: The reactor temperature of the regulated output obtained with EMPS algorithm.

Table 2: Performance comparison with previous works.

Methods	Years	Stabilizable region *Different points* A (−0.05, 3)	B (−0.08, 4)	C (−0.1, 8)	Stabilization domain	Invariant sets number	Maximization methods	Computational time (s)
Wan and Kothare [15]	2003	×	×	✓	Ellipsoidal invariant sets	6	×	3.672
Bumroongsri and Kheawhom [18]	2012	×	✓	✓	Polyhedral invariant sets	6	×	4.372
The proposed method		✓	✓	✓	Maximized invariant sets	6	Semidefine and linear programming	4.951

Table 3: Cumulative cost in Example 1.

Methods	Cumulative cost	Cumulative equation
Wan and Kothare [15]	20.48	$\sum_{i=0}^{\infty} x_i^T \Theta x_i + u_i^T R u_i$
Bumroongsri and Kheawhom [18]	19, 02	
Proposed approach	17, 9	

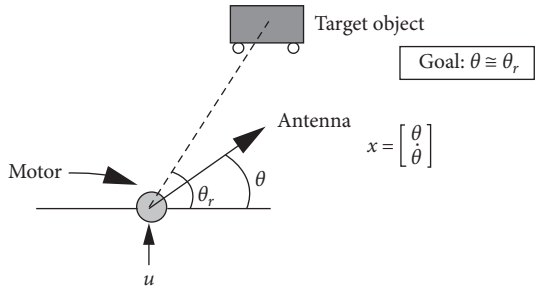

Figure 6: Angular positioning system.

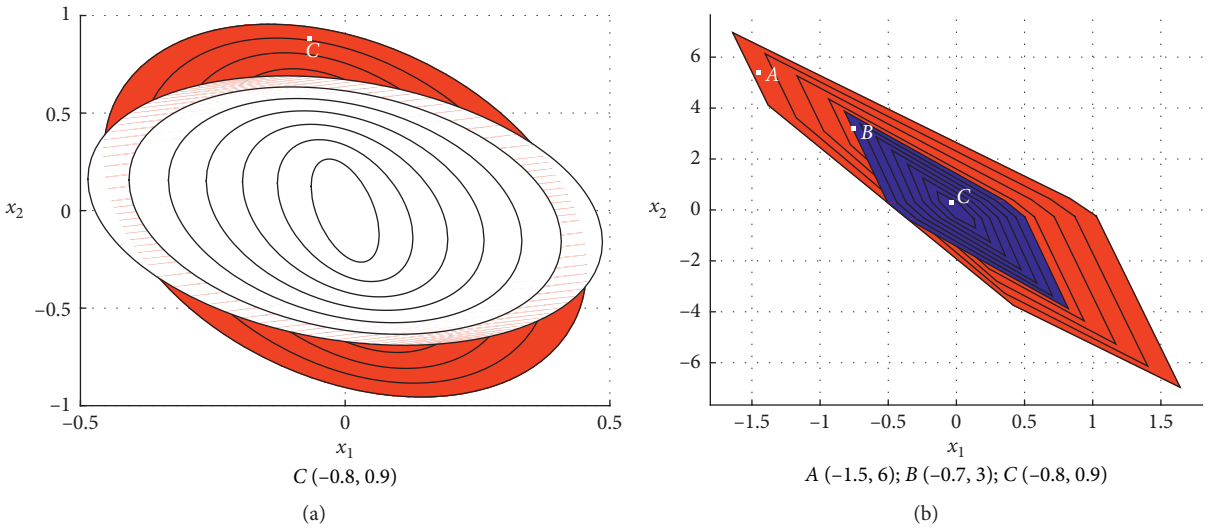

Figure 7: (a) Maximized ellipsoidal invariant sets compared to [15] and (b) maximized polyhedral invariant sets compared to [18].

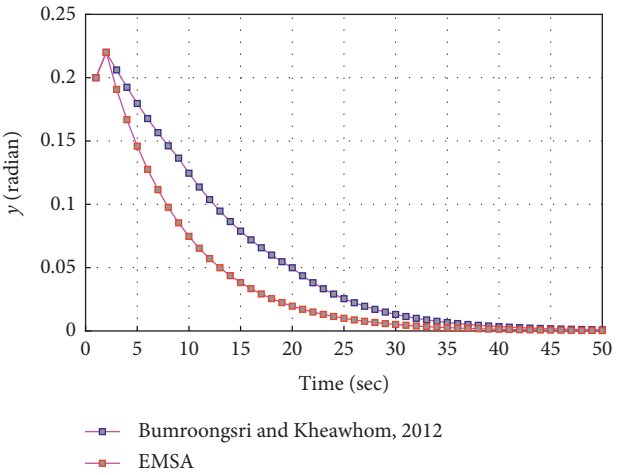

Figure 8: The regulated output obtained with EMPS approach.

applied approach reaches better performance system. The resolution of the predictive control problem based on the proposed EMSA algorithm aims to improve the uncertain system performances under consideration. Depending on the result of Table 4, we can assume that the proposed scheme is more successfully having a larger stabilizable region. Table 5 resumes the cumulative cost in the second example.

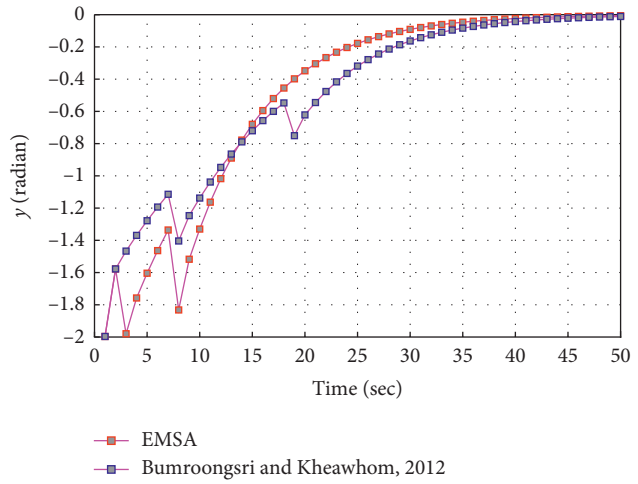

Figure 9: The control input obtained with EMPS approach.

Table 4: Performance comparison with previous works.

Methods	Years	Stabilizable region: Different points			Stabilization domain	Invariant sets number	Maximization methods	Computational time (s)
		A (−0.2, 0.4)	B (0, 2)	C (1.5, −3)				
Wan and Kothare [15]	2003	×	×	✓	Ellipsoidal invariant sets	7	×	2.831
Bumroongsri and Kheawhom [18]	2012	×	✓	✓	Polyhedral invariant sets	7	×	3.541
The proposed method		✓	✓	✓	Maximized invariant sets	7	Semidefine and linear programming	4.183

Table 5: Cumulative cost in Example 2.

Methods	Cumulative cost	Cumulative equation
Wan and Kothare [15]	0.19	$\sum_{i=0}^{\infty} x_i^T \Theta x_i + u_i^T R u_i$
Bumroongsri and Kheawhom [18]	0.12	
Proposed approach	0.9	

4. Conclusion

In this paper, we described an enhanced method which can be used for constrained uncertain discrete-time linear systems stabilization. A useful RMPC technique was applied to emphasize the robust control and improve the state stabilization. The proposed procedure gives appropriate optimization and notable precision when compared to existing model predictive control results. Then, we have suggested the combined RMPC method and maximized invariant sets process that can accurately progress the performance of the closed-loop system. The included methods are used to enlarge ellipsoidal and polyhedral invariant sets constructed by the RMPC algorithm. An online implementation for the obtained feedback control laws has been made. The proposed method has been compared with some existing algorithms in order to enlarge stability domain. Experiment results demonstrate that the proposed method can permanently control system states having a larger stabilizable region. Therefore, the performance of the proposed strategy furnishes a rigid basis in support of solving the control problem. As future works, we propose to use deep learning to obtain flexible models for nonlinear model predictive control (MPC).

Data Availability

No data were used to support this study.

Conflicts of Interest

The authors declare that they have no conflicts of interest.

References

[1] L. Cavanini, G. Cimini, and G. Ippoliti, "Computationally efficient model predictive control for a class of linear parameter-varying systems," *IET Control Theory and Applications*, vol. 12, no. 10, pp. 1384–1392, 2018.

[2] M. V. Kothare, V. Balakrishnan, and M. Morari, "Robust constrained model predictive control using linear matrix inequalities," *Automatica*, vol. 32, no. 10, pp. 1361–1379, 1996.

[3] N. Saraf and A. Bemporad, *An Efficient Non-condensed Approach for Linear and Nonlinear Model Predictive Control with Bounded Variables*, ArXiv, 1908.07247, 2019.

[4] D. Angeli, A. Casavola, and E. Mosca, "Constrained predictive control of nonlinear plants via polytopic linear system embedding," *International Journal of Robust and Nonlinear Control*, vol. 10, no. 13, pp. 1091–1103, 2000.

[5] M. J. Grimble, P. Majecki, and M. R. Katebi, "Extended NGMV predictive control of quasi-LPV systems," *IFAC-PapersOnLine*, vol. 50, no. 1, pp. 4101–4107, 2017.

[6] J. H. Lee, "Model predictive control: review of the three decades of development," *International Journal of Control, Automation and Systems*, vol. 9, no. 3, pp. 415–424, 2011.

[7] C. M. Massera, M. H. Terra, and D. F. Wolf, "Guaranteed cost approach for robust model predictive control of uncertain linear systems," in *Proceedings of the 2017 American Control Conference (ACC)*, pp. 4135–4140, Seattle, WA, USA, May 2017.

[8] M. Mirzaei, N. K. Poulsen, and H. H. Niemann, "Robust model predictive control of a nonlinear system with known scheduling variable and uncertain gain," *IFAC Proceedings Volumes*, vol. 45, no. 13, pp. 616–621, 2012.

[9] D. Saoudi and C. Mechmeche, "TS fuzzy bilinear observer for a class of nonlinear system," in *Proceedings of the 18th IEEE Mediterranean Conference on Control and Automation*, pp. 1395–1400, Marrakech, Morocco, June 2010.

[10] A. S. Tlili and N. Benhadj Braiek, "H_∞ optimization-based decentralized control of linear interconnected systems with nonlinear interconnections," *Journal of the Franklin Institute*, vol. 351, no. 6, pp. 3286–3304, 2014.

[11] C. Ghorbel, A. Tiga, and N. Benhadj Braiek, "Proportional PDC design-based robust stabilization and tracking control strategies for uncertain and disturbed TS model," *Complexity*, vol. 2020, Article ID 8910132, 9 pages, 2020.

[12] J. Luo and H. Liu, "Adaptive fractional fuzzy sliding mode control for multivariable nonlinear systems," *Discrete Dynamics in Nature and Society*, vol. 2014, no. 6, Article ID 541918, 10 pages, 2014.

[13] A. O. Sahed, K. Kara, and M. L. Hadjili, "Constrained fuzzy predictive control using particle swarm optimization," *Applied Computational Intelligence and Soft Computing*, vol. 2015, Article ID 437943, 15 pages, 2015.

[14] N. M. N. Lima, L. Z. Liñan, R. M. Filho, M. R. W. Maciel, M. Embiruçu, and F. Grácio, "Modeling and predictive control using fuzzy logic: application for a polymerization system," *AIChE Journal*, vol. 56, no. 4, pp. 965–978, 2010.

[15] Z. Wan and M. V. Kothare, "An efficient off-line formulation of robust model predictive control using linear matrix inequalities," *Automatica*, vol. 39, no. 5, pp. 837–846, 2003.

[16] W. Hamdi, W. Bey, and N. B. Braiek, "Stabilization of constrained uncertain systems by an off-line approach using zonotopes," *Advances in Science, Technology and Engineering Systems Journal*, vol. 3, no. 1, pp. 281–287, 2018.

[17] X. Liu, S. Feng, and M. Ma, "Robust MPC for the constrained system with polytopic uncertainty," *International Journal of Systems Science*, vol. 43, no. 2, pp. 248–258, 2012.

[18] P. Bumroongsri and S. Kheawhom, "An off-line robust MPC algorithm for uncertain polytopic discrete-time systems using polyhedral invariant sets," *Journal of Process Control*, vol. 22, no. 6, pp. 975–983, 2012.

[19] F. Blanchini and S. Miani, *Set-Theoretic Methods in Control*, Birkhuser, Boston, MA, USA, 2008.

[20] W. Zheng, Y. Li, D. Zhang, C. Zhou, and P. Wu, "Envelope protection for aircraft encountering upset condition based on dynamic envelope enlargement," *Chinese Journal of Aeronautics*, vol. 31, no. 7, pp. 1461–1469, 2018.

[21] N. Athanasopoulos and G. Bitsoris, "A novel approach to the computation of the maximal controlled invariant set for constrained linear systems," in *Proceedings of the 2009 European Control Conference (ECC)*, pp. 3124–3129, Budapest, Hungary, August 2009.

[22] X.-B. Hu and W.-H. Chen, "Model predictive control: terminal region and terminal weighting matrix," *Proceedings of the Institution of Mechanical Engineers, Part I: Journal of Systems and Control Engineering*, vol. 222, no. 2, pp. 69–79, 2008.

[23] V. Rakovic and M. E. Villanueva, "The maximal positively invariant set: polynomial setting," 2017, https://arxiv.org/abs/1712.01150.

[24] B. Kouvaritakis, M. Cannon, A. Karas, B. Rohal-Ilkiv, and C. Belavy, "Asymmetric constraints with polytopic sets in mpc with application to coupled tanks system," *International Journal of Robust and Nonlinear Control*, vol. 14, no. 4, pp. 341–353, 2004.

[25] D. Henrion, S. Tarbouriech, and V. Kučera, "Control of linear systems subject to input constraints: a polynomial approach," *Automatica*, vol. 37, no. 4, pp. 597–604, 2001.

[26] Y. Li and Z. Lin, "The maximal contractively invariant ellipsoids for discrete-time linear systems under saturated linear feedback," *Automatica*, vol. 76, pp. 336–344, 2017.

[27] N. Michel, S. Olaru, S. Bertrand, G. Valmorbida, and D. Dumur, "Invariant set design for constrained discrete-time linear systems with bounded matched disturbance," *IFAC-PapersOnLine*, vol. 51, no. 25, pp. 55–60, 2018.

[28] M. Nilsson, E. Klintberg, P. Rumschinski, and L. J. Mrdh, "Admissible sets for slowly-varying discrete-time systems," *Automatica*, vol. 112, no. 1, pp. 108–676, 2020.

[29] X. Cheng, "A generalization of almost-Schur lemma for closed Riemannian manifolds," *Annals of Global Analysis and Geometry*, vol. 43, no. 2, pp. 153–160, 2013.

Hindawi
Complexity
Volume 2020, Article ID 1614894, 12 pages
https://doi.org/10.1155/2020/1614894

Research Article

Dynamic Complexity in a Prey-Predator Model with State-Dependent Impulsive Control Strategy

Chuanjun Dai [1,2]

[1]*Zhejiang Provincial Key Laboratory for Water Environment and Marine Biological Resources Protection, Wenzhou University, Wenzhou, Zhejiang 325035, China*
[2]*School of Life and Environmental Science, Wenzhou University, Wenzhou, Zhejiang 325035, China*

Correspondence should be addressed to Chuanjun Dai; chuanjdai@wzu.edu.cn

Received 3 March 2020; Revised 25 May 2020; Accepted 16 June 2020; Published 6 July 2020

Guest Editor: Raúl Villafuerte-Segura

Copyright © 2020 Chuanjun Dai. This is an open access article distributed under the Creative Commons Attribution License, which permits unrestricted use, distribution, and reproduction in any medium, provided the original work is properly cited.

In this paper, an ecological model described by a couple of state-dependent impulsive equations is studied analytically and numerically. The theoretical analysis suggests that there exists a semitrivial periodic solution under some conditions and it is globally orbitally asymptotically stable. Furthermore, using the successor function, we study the existence, uniqueness, and stability of order-1 periodic solution, and the boundedness of solution is also presented. The relationship between order-k successor function and order-k periodic solution is discussed as well, thereby giving the existence condition of an order-3 periodic solution. In addition, a series of numerical simulations are carried out, which not only support the theoretical results but also show the complex dynamics in the model further, for example, the coexistence of multiple periodic solutions, chaos, and period-doubling bifurcation.

1. Introduction

Since mathematical models represented by differential equations were introduced into biological and ecological systems, it has been proved that they are very useful tools to deal with practical problems such as emerging disease [1] and population dynamics between plankton and nutrient [2–4], which also promote the development of the theory of differential equation further. Especially, in the process, there is a significant development in impulsive differential equations [5–9] because many reality systems exhibit the abrupt jumps phenomena in population sizes during the evolution processes. Additionally, a theoretical method is urgently needed to provide a guide for the management of some practical problems such as pest outbreaks, phytoplankton blooms, vaccination, and so on. Accordingly, impulsive differential equation theory may prove to be one of the most potential theories to strategize about the approach of management for these problems, as impulsive differential equation can model abrupt jump behaviors induced by management, for example, some management occurs at fixed time, which can be modeled using the models with impulses at fixed times [10–13].

State-dependent impulsive differential equation, as a branch of impulsive differential equation, has the advantage to model the control behaviors depending on the population state. In recent years, the studies on state-dependent impulsive differential equation have been paid increasing attention [13–16]. Many studies devote to the properties of periodic solutions [17–20], including the existence, stability and periodicity, etc. It has been confirmed that the Poincaré map is a very useful tool to prove the existence of periodic solution in state-dependent impulsive differential equations [21–23]. In addition, Simeonov and Bainov [24] gave analogue of Poincaré criterion in ref. [25], which contributes to the stability of the periodic solution. Based on the Poincaré map, it can be proved theoretically that the positive periodic solution can bifurcate from the trivial periodic solution through a transcritical bifurcation [25]. Particularly, Chen [26] introduced the successor function a in semicontinuous dynamical system described by state-dependent impulsive differential equation to prove the existence of periodic

solution. Using the successor function, Dai et al. [27] studied homoclinic bifurcation in a semicontinuous dynamical system [28]. The successor function has been extensively employed to investigate the existence of periodic solution and even stability and bifurcation in state-dependent impulsive differential equation [28–38]. These studies enrich the theory of state-dependent impulsive differential equation further.

In this paper, we will present a prey-predator two-species model with state-dependent impulsive control strategy to study the dynamics induced by impulsive control. Firstly, a model describing population dynamics of prey and predator is given below.

$$\begin{cases} \dfrac{\mathrm{d}x}{\mathrm{d}t} = rx\left(1 - \dfrac{x}{K}\right) - \dfrac{bxy}{a+x}, \\ \dfrac{\mathrm{d}y}{\mathrm{d}t} = \dfrac{\alpha bxy}{a+x} - my, \end{cases} \tag{1}$$

where x and y denote the densities of prey and predator, respectively; r is the intrinsic growth rate of the prey; K is the carrying capacity of the prey; b is the maximum growth rate; a represents the half-saturation concentration; α is the assimilation efficiency of predator; and m is the specific mortality rate of predator. Here, we employ a Holling II functional response to present the interaction between prey and predator because some results suggest that the population dynamic following Holling II may exist in reality [2, 3, 39, 40].

For some species, when their densities are beyond a certain value, some seriously negative effects will emerge, for instance, algal bloom. For this reason, their densities should be kept below the critical value by harvest or/and released natural enemy. Obviously, the occurrence of control will rely on the density of the species. Here, under the assumption that the interaction between prey x and predator y follows model (1), we investigate the dynamics of impulsive control and control strategies for prey x using state-dependent impulsive differential equation, and the model can be described as

$$\begin{cases} \left.\begin{aligned} \dfrac{\mathrm{d}x}{\mathrm{d}t} &= rx\left(1 - \dfrac{x}{K}\right) - \dfrac{bxy}{a+x} \\ \dfrac{\mathrm{d}y}{\mathrm{d}t} &= \dfrac{\alpha bxy}{a+x} - my \end{aligned}\right\} & x < h, \\ \left.\begin{aligned} \Delta x &= -px \\ \Delta y &= -qy + \tau \end{aligned}\right\} & x = h, \end{cases} \tag{2}$$

where $h > 0$ denotes the critical value below which the density of prey x should be kept. $0 < p < 1$ is the harvest rate of prey x; $\tau \geq 0$ is the releasing amounts of predator y; and $0 < q < 1$ represents the harvest rate of predator y or the level of negative effect caused by the harvest of prey x on predator y.

The rest of the paper is organized as follows. In Section 2, some notations, basic definitions, and lemmas are given. In Section 3, a semitrivial solution and its stability are studied; we also study the existence, uniqueness, and stability of an order-1 periodic solution; moreover, the boundedness of solution and some propositions of periodic solution are discussed as well. Whereafter, a series of numerical results are carried out to study the dynamics of model (2) further in Section 4. Finally, the paper ends with the conclusion in Section 5.

2. Preliminaries

In model (1), there exist three equilibria, $E_0 = (0, 0)$, $E_1 = (K, 0)$, and $E_* = (x_*, y^*)$, where $x_* = ma/(\alpha b - m)$ and $y^* = r(K - x_*)(a + x_*)/(bK)$. When the condition $\max(0, \alpha b(K - a)/(K + a)) < m < K\alpha b/(a + K)$ holds, E_* is a stable positive focus or node. We assume that the following condition holds throughout the paper: (H) $0 < m < K\alpha b/(a + K)$.

The vertical isocline and the horizontal isocline can be defined as follows:

$$\begin{aligned} L_1 &: y = \frac{r(K - x)(a + x)}{bK} = f(x), \\ L_2 &: x = \frac{ma}{\alpha b - m}. \end{aligned} \tag{3}$$

Furthermore, let $N = \{(x, y) \mid x = (1 - p)h,\ y \geq 0\}$ be the phase set, and $M = \{(x, y) | x = h,\ y \geq 0\}$ denotes the impulsive set. Under condition (H), we assume that L_1 intersects with the phase set N at point $O(x_O, y_O)$ and the impulsive set M at point $H(x_H, y_H)$ in the first quadrant when $h < x_*$. We define $\Pi = \{(x, y) | (1 - p)h \leq x \leq h,\ 0 \leq y \leq f(x)\}$ and $\Omega = \{(x, y) | 0 \leq x \leq h,\ y \geq 0\}$.

Let $z(t) = (x(t), y(t))$ be any solution of model (2); then, we define the positive trajectory initializing at point $z_0 = z(t_0) \in R_+^2 = \{(x, y) | x \geq 0,\ y \geq 0\}$ for $t \geq t_0$ as $\pi(t; z_0, t_0) = \{z(t) \mid z(t) \in R_+^2,\ t \geq t_0 \geq 0,\ z(t_0) = z_0\}$.

In this paper, some notions are always mentioned, including phased point, impulsive point, and successor point. From works in [20, 23, 26], we state the following definition.

Definition 1. Take the point $A_0 \in N$; set $\pi(t; A_0, t_0)$ as the trajectory initializing at point A_0 in model (2). If there exists $t_k > t_0$ such that the trajectory $\pi(t; A_0, t_0)$ intersects the impulsive set M at $A_k = (h, y_k)$ when $t = t_k$ $(k = 1, 2, 3, \ldots)$, then a point A_k^+ exists in the phase set N, where point $A_k^+ = ((1 - p)h, y_k^+ = (1 - q)y_k + \tau)$. The point A_k^+ is called the phased point of point A_k, and the point A_k is called the impulsive point of point A_k^+. The point A_k^+ is called the order-k successor point of point A_0, and the vector $\overrightarrow{A_k A_k^+}$ is called an impulsive line.

Definition 2. Set point $E = N \cap \{(x, y) | x \geq 0, y = 0\}$; then, we define a number axis L in the phase N, and set point E as the origin of the number axis L. $\forall A_0 \in N$, set the direction of

vector $\overrightarrow{EA_0}$ as the positive direction of number axis L, and set $a_0 = |\overrightarrow{EA_0}|$ as the coordinate of point A_0 in the number axis L. Then, a map F_k: $R_+ \longrightarrow R (k = 1, 2, 3, \ldots)$ can be defined as $F_k(a_0) = a_k - a_0$, where $a_k = |\overrightarrow{EA_k^+}|$ and A_k^+ is the order-k successor point of point A_0. The map F_k is called the order-k successor function, that is, $F_k(A_0) = y_{A_k^+} - y_{A_0}$.

Definition 3. Take a point S in the phase set N; then, $\pi(t; S, t_0)$ is a solution of model (2). If there exists a positive integer $k \geq 1$ such that k is the smallest integer for $F_k(S) = 0$, then the solution $\pi(t; S, t_0)$ is called order-k periodic solution.

Lemma 1 (see [26]). *The successor function $F_k(S)$ is continuous, where the point $S \in N$.*

Obviously, we can obtain the following lemma by Lemma 1.

Lemma 2. *If there exist two points $S_1 = ((1-p)h, y_{S_1})$ and $S_2 = ((1-p)h, y_{S_2})$ in model (2) and $(y_{S_1} - y_O)(y_{S_2} - y_O) \geq 0$ such that $F_1(S_1)F_1(S_2) < 0$, then model (2) has an order-1 periodic solution.*

For the point O, we always assume the point $O_k^+ = ((1-p)h, y_{O_k^+})$ is the order-k successor point of the point O, and the point $O_k = (h, y_{O_k})$ is the impulsive point of point O_k^+, where $k = 1, 2, 3, \ldots$.

3. Main Results

When the values of parameters in model (1) are given, the dynamics of model (2) only depend on the parameters h, p, q, and τ. In this paper, we are interested in the effect of impulsive control on dynamics of model (2). Hence, we will investigate the dynamical behaviors of model (2) under the condition that the parameters of model (1) are fixed.

For points O and H, it is obvious that

(1) $y_O > y_H$ if $(1 - p/2)h > K - a/2$.

(2) $y_O < y_H$ if $(1 - p/2)h < K - a/2$ and $K > a$.

In this section, we just show the proof with respect to case $(K - a)/2 < (1 - p)h < (1 - p/2)h$ in the figure of illustration. The proof corresponding to other cases is similar, which has been omitted.

By model (1), it is obvious that $h < x_*$ implies $\mathrm{d}y/\mathrm{d}t < 0$. Additionally, $y(t^+) < y(t)$ always holds when $q \in (0, 1)$.

In model (2) with $\tau = 0$, it is obvious that the following semitrivial periodic solution exists for $t \in ((n-1)T, nT]$ $(n = 1, 2, 3, \ldots)$ when the predator $y = 0$,

$$\begin{cases} \xi(t) = \dfrac{(1-p)he^{r(t-(n-1)T)}K}{(1-p)he^{r(t-(n-1)T)} + (K - (1-p)h)}, \\ \eta(t) = 0, \end{cases} \tag{4}$$

where the period $T = (1/r)\ln(K - (1-p)h/(1-p)(K-h))$. Set $\Gamma = (\xi(t), \eta(t))$. Then, we can get the following theorem.

Theorem 1. *Under condition (H), if $h < x_*$ and $\tau = 0$, then semitrivial periodic solution Γ is globally orbitally asymptotically stable in model (2) for any $q \in (0, 1)$ and $p \in (0, 1)$.*

Proof. For $\tau = 0$, solutions of model (2) will enter the space Π eventually. Hence, we study the stability of the semitrivial periodic solution in this space.

For any $\varepsilon > 0$, set $N_\varepsilon = ((1-p)h, \varepsilon)$ and $M_\varepsilon = (h, \varepsilon)$. Then, we assume that the trajectory $\pi(t; N_\varepsilon, t_0)$ intersects with impulsive set M at point $P = (h, y_P)$, and $y_P < y_{N_\varepsilon} = \varepsilon$ under condition (H). Set $\delta = \varepsilon$; then, for any point $G = ((1-p)h, y_G)$ where $0 < y_G < \delta = y_{N_\varepsilon}$, we have $y_{G_1^+} < y_P$ under condition (H) because $h < x_*$ and $q \in (0, 1)$ (see Figure 1(a)), which suggests that the distance

$$d = d(\pi(t; G, t_0), \Gamma) = \inf_{P_0 \in \Gamma} |\pi(t; G, t_0) - P_0| < \varepsilon, \tag{5}$$

holds for all $t > t_0$, where $\Gamma = (\xi(t), \eta(t))$. Hence, according to the definition of orbital stability in ref. [40], the semitrivial periodic solution Γ is orbitally stable.

For any $G_0 \in N$, take a sequence of number $\{t_k\}$ $(k = 1, 2, 3, \ldots)$, where $0 < t_k < t_{k+1}$ and $\lim_{k \longrightarrow +\infty} t_k = +\infty$, such that $\pi(t_k; G_0, t_0) = ((1-p)h, y_k) \in N$. Then, the sequence of number $\{y_k\}$ is a strictly decreasing positive sequence because $h < x_*$ and $q \in (0, 1)$. Hence, there exists a $y_* \geq 0$, such that $\lim_{k \longrightarrow +\infty} y_k = y_* \geq 0$, but $y_k \geq y_*$. Set $Q_* = ((1-p)h, y_*)$, and let point Q_* be the order-1 successor point of point $Q_\# = ((1-p)h, y_\#)$ if $y_* > 0$, where $y_\# > y_*$. Then, for any point $Q \in \overline{Q_* Q_\#}$ (i.e., $y_{Q_*} < y_Q < y_{Q_\#}$), its order-1 successor point is below the point Q_* (see Figure 1(b)), that is, $y_{Q^+} \leq y_*$.

Because $\lim_{k \longrightarrow +\infty} y_k = y_*$, there exists a positive integer Θ_1 such that $y_{Q_*} < y_k < y_{Q_\#}$ for $k > \Theta_1$. According to above analysis, there exists a positive integer $\Theta_2 > \Theta_1$ such that $y_k < y_*$ when $k > \Theta_2$, which contradicts with $y_k \geq y_*$. Hence, $\lim_{k \longrightarrow +\infty} y_k = y_* = 0$, which means that the semitrivial periodic solution Γ is orbitally attractive. So, the semitrivial periodic solution Γ is orbitally asymptotically stable. Since the attraction domain is Ω, the semitrivial periodic solution Γ is globally orbitally asymptotically stable.

This completes the proof.

Suppose that M is a positive constant, and then we have the following theorem for any $M \in (0, +\infty)$. □

Theorem 2. *Under condition (H), if $h < x_*$ and $\tau \in (0, M]$, then there exists a unique order-1 periodic solution in model (2) for any $q \in (0, 1)$ and $p \in (0, 1)$.*

Proof. For any $\tau > 0$, Figure 2(a) displays the relation between point O and its order-1 successor point O_1^+ under condition (H), where $h < x_*$. Obviously, $\overline{OO_1O}$ is an order-1 periodic solution if $y_O = y_{O_1^+}$. If $y_O < y_{O_1^+}$, we have $F_1(O) = y_{O_1^+} - y_O > 0$ and $F_1(O_1^+) = y_{O_2^+} - y_{O_1^+} < 0$, where O_2^+ is the successor point of point O_1^+. According to Lemmas 1 and 2, there exists an order-1 periodic solution in model (2).

If $y_O > y_{O_1^+}$, we take a point $R = ((1-p)h, \tau)$ in phase set N. Then, let the point R_1^+ be the order-1 successor point of point R and point R_1 be the impulsive point of point R_1^+, and $y_{R_1^+} = (1-q)y_{R_1} + \tau > \tau = y_R$ (see Figure 2(a)), so $F_1(R) > 0$.

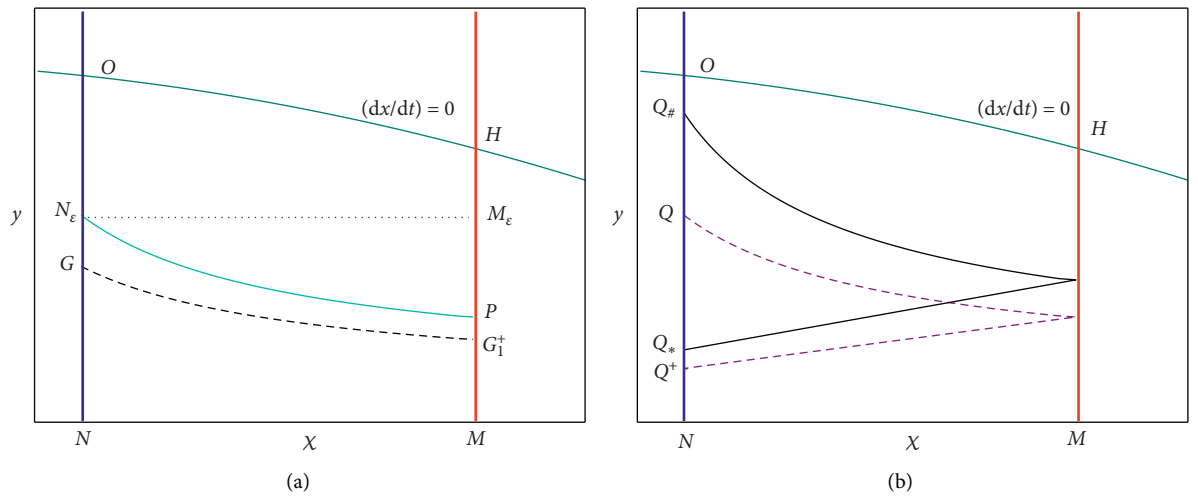

Figure 1: Illustration corresponding to the orbital (a) stability and (b) attractability of semitrivial periodic solution in model (2).

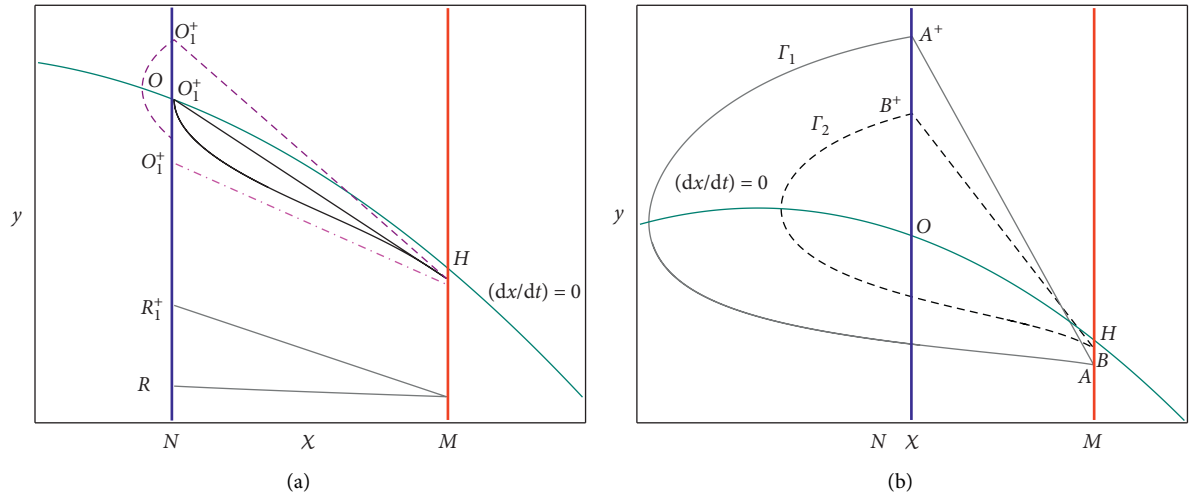

Figure 2: Illustration with respect to (a) existence and (b) uniqueness of the order-1 periodic solution in model (2).

By $F_1(O) = y_{O_1^+} - y_O < 0$, there exists an order-1 periodic solution in model (2) using Lemmas 1 and 2.

Hence, there exists an order-1 periodic solution for any $q \in (0, 1)$ and $p \in (0, 1)$ when $h < x_*$ and $\tau > 0$.

Suppose there are two order-1 periodic solutions in model (2), which are Γ_1 and Γ_2, respectively. Let point $A^+ = ((1-p)h, y_{A^+})$ and $A = (h, y_A)$ be the phase point and impulsive point of Γ_1, respectively, and point $B^+ = ((1-p)h, y_{B^+})$ and $B = (h, y_B)$ be the phase point and impulsive point of Γ_2, respectively. Without loss of generality, set $y_{A^+} > y_{B^+}$. Then, the relation among A^+, B^+, and O is (i) $B^+ \in \overline{OA^+}$ $(y_O < y_{B^+} < y_{A^+})$; (ii) $A^+ \in \overline{B^+O}$ $(y_{B^+} < y_{A^+} < y_O)$; and (iii) $O \in \overline{B^+A^+}$ $(y_{B^+} < y_O < y_{A^+})$.

Figure 2(b) shows case (i); it is obvious that Γ_1 and Γ_2 cannot coexist by disjoint property of trajectory of model (1). Hence, the order-1 periodic solution is unique for this case.

For case (ii), because $A^+ \in \overline{B^+O}$, we only need to focus on the region Π. We rewrite the model (1) in the region Π as the following initial-value problem:

$$\begin{cases} \dfrac{dy}{dx} = \dfrac{g(x,y)}{f(x,y)} \triangleq \Psi(x,y), \\ \\ y(x_0) = y_0, \quad (x,y) \in \Pi, \end{cases} \tag{6}$$

where $f(x,y) = rx(1 - x/K) - bxy/a + x$, $g(x,y) = \alpha bxy/a + x - my$.

Obviously, the function $\Psi(x,y)$ is continuously differentiable and monotone decreasing in y on the space Π. Then, the solution of model (6) is equivalent to the following integral equation:

$$y(x, y_0) = y_0 + \int_{x_0}^{x} \Psi(s, y(s, y_0))ds. \tag{7}$$

By equation (7), set

$$y_i(x) = y(x, y_{i^+}) = y_{i^+} + \int_{(1-p)h}^{x} \Psi(s, y_i(s))ds, \tag{8}$$

where $i = A, B$; then, $y_A = y_A(h)$ and $y_B = y_B(h)$. Because $y_{A^+} > y_{B^+}$, we have $y_A(x) > y_B(x)$ on the space Π by the disjoint property of trajectory of model (1). Hence,

$$\begin{aligned} y_A - y_B &= y_A(h) - y_B(h) \\ &= y_{A^+} + \int_{(1-p)h}^{h} \Psi(x, y_A(x))\mathrm{d}x - y_{B^+} \\ &\quad - \int_{(1-p)h}^{h} \Psi(x, y_B(x))\mathrm{d}x \\ &< y_{A^+} - y_{B^+}. \end{aligned} \tag{9}$$

On the other hand, because both Γ_1 and Γ_2 are order-1 periodic solutions, we have $y_{A^+} - y_{B^+} = (1-q)(y_A - y_B) < (y_A - y_B)$ by model (2), which is a contradiction with inequality (9). Hence, the order-1 periodic solution is unique for this case.

For case (iii), the proof is similar with case (ii), so it is omitted.

Hence, there exists a unique order-1 periodic solution in model (2) for any $q \in (0, 1)$ and $p \in (0, 1)$ when $h < x_*$ and $\tau > 0$.

This completes the proof.

From Theorem 2, we can find that the existence and stability of order-1 periodic solution depend on parameter τ. Suppose point $((1-p)h, y(\tau))$ is the phase point of the order-1 periodic solution, then we can get the following proposition. □

Proposition 1. *Under condition (H), when $h < x_*$ and $\tau > 0$, $y = y(\tau)$ is a monotonously increasing function with respect to τ.*

Proof. Let θ be the angle between the impulsive line and the x-axis. Then, $\tan\theta = -qy + \tau/-ph$, so $\mathrm{d}\theta/\mathrm{d}\tau = (\mathrm{d}/\mathrm{d}\tau)\tan^{-1}(-qy + \tau/-ph) < 0$. Hence, $\theta(\tau)$ is a monotonously decreasing function in τ. Given an order-1 periodic solution Γ_*, let points $U = (x_U, y_U)$ and $W = (x_W, y_W)$ be the phased point and impulsive point of Γ_*, respectively; then, $\tau_1 = y_U - (1-q)y_W$ guarantees the existence of the order-1 periodic solution Γ_*.

For any $\varepsilon > 0$, when $\tau = \tau_1 + \varepsilon$, the order-1 periodic solution Γ_* will disappear. Let point $U^+ = (x_{U^+}, y_{U^+})$ be the order-1 successor point of point U; then, $y_{U^+} > y_U$ because $\theta(\tau)$ is a monotonously decreasing function. In addition, $F_1(U) > 0$ and $F_1(U^+) < 0$. Therefore, there exists an order-1 periodic solution whose phase point belongs to $\overline{UU^+}$. By the uniqueness of order-1 periodic solution, $y = y(\tau)$ is a monotonously increasing function in τ.

This completes the proof.

By Theorem 2, we know that the trajectory $\overline{OO_1O}$ is an order-1 periodic solution of model (2) when $\tau = y_O - (1-q)y_{O_1} \triangleq \tau_c$. Then, we can get the following theorem. □

Theorem 3. *Under condition (H), if $h < x_*$, then the order-1 periodic solution is globally orbitally asymptotically stable in model (2) for any $q \in (0, 1)$ and $p \in (0, 1)$ when $\tau \in (0, \tau_c)$.*

Proof. When $\tau \in (0, \tau_c)$, the order-1 periodic solution of model (2) must belong to space Π under condition (*H*). Γ^+ denotes an order-1 periodic solution of model (2), whose phased point and impulsive point are point $C = (x_C, y_C)$ and point $D = (x_D, y_D)$, respectively. In addition, the solutions of model (2) will enter the space Π eventually when $\tau \in (0, \tau_c)$. Hence, we only need to study the stability of order-1 periodic solution on the space Π.

For any $\varepsilon > 0$, we assume that the trajectory $\pi(t; N_{\varepsilon 1}, t_0)$ meets impulsive set M at point $P_1 = (x_{P_1}, y_{P_1})$, where $N_{\varepsilon 1} = ((1-p)h, \varepsilon + y_C)$ (see Figure 3(a)); then, $y_{P_1} < y_{N_{\varepsilon 1}} = y_C + \varepsilon$. Take $\delta = \varepsilon$; for any point $G_1 = (x_{G_1}, y_{G_1})$, where $x_{G_1} = (1-p)h$ and $y_C < y_{G_1} < y_C + \delta = y_{N_{\varepsilon 1}}$, we assume that the trajectory $\pi(t; G_1, t_0)$ intersects with impulsive set at point $G_2 = (h, y_{G_2})$; then, $y_{G_1} > (1-q)y_{G_2} + \tau$; otherwise, another order-1 periodic solution exists above Γ^+, which contradicts with the uniqueness of order-1 periodic solution. Hence, the distance

$$d = d(\pi(t; G_1, t_0), \Gamma^+) = \inf_{P_0 \in \Gamma^+} |\pi(t; G_1, t_0) - P_0| < \varepsilon \tag{10}$$

holds for all $t > t_0$ according to equation (9).

On the other hand, for any $0 < \varepsilon < y_C$, given $\delta = \varepsilon$, when $y_C - \delta < y_{G_1} < y_C$, we still have

$$d = d(\pi(t; G_1, t_0), \Gamma^+) = \inf_{P_0 \in \Gamma^+} |\pi(t; G_1, t_0) - P_0| < \varepsilon, \tag{11}$$

using the same method. Hence, according to definition of orbital stability in ref. [41], the order-1 periodic solution Γ^+ is orbitally stable.

For any $G_0 \in N$, take a numerical sequence $\{t_k\}$ $(k = 1, 2, 3, \ldots)$, where $0 < t_k < t_{k+1}$ and $\lim_{k \longrightarrow +\infty} t_k = +\infty$, such that $\pi(t_k; G_0, t_0) = ((1-p)h, y_k) \in N$. Due to disjoint of impulsive line, there are two cases on the numerical sequence $\{y_k\}$ when $\tau \in (0, \tau_c)$ and $h < x_*$: (1) $\{y_k\}$ is a strictly decreasing positive sequence; (2) $\{y_k\}$ is a strictly increasing positive sequence.

For case (1) (see Figure 3(b)), we have $\lim_{k \longrightarrow +\infty} y_k = y_* \geq y_C$ and $y_k \geq y_*$. Let $Q_* = ((1-p)h, y_*)$; there exists a point $Q_\# = ((1-p)h, y_\#)$ when $y_* > y_C$, where $y_\# > y_*$, such that point Q_* is the order-1 successor point of point $Q_\#$. For any point $Q \in \overline{Q_* Q_\#}$ (i.e., $y_{Q_*} < y_Q < y_{Q_\#}$), its order-1 successor point is below the point Q_*. Let point Q^+ be the order-1 successor point of Q, then $y_{Q^+} < y_*$.

Because $\lim_{k \longrightarrow +\infty} y_k = y_*$ and $y_k \geq y_*$, there exists a positive integer Θ_1 such that $y_{Q_*} < y_k < y_{Q_\#}$ for $k > \Theta_1$. According to above analysis, there exists a positive integer $\Theta_2 > \Theta_1$ such that $y_k < y_*$ when $k > \Theta_2$, which contradicts with $y_k \geq y_*$. So, $\lim_{k \longrightarrow +\infty} y_k = y_C$. Likewise, $\lim_{k \longrightarrow +\infty} y_k = y_C$ also holds for case (2), which says the order-1 periodic solution Γ^+ is orbitally attractive.

Hence, the order-1 periodic solution Γ^+ is orbitally asymptotically stable. Since the attraction domain is Ω, the order-1 periodic solution Γ^+ is globally orbitally asymptotically stable.

This completes the proof. □

Proposition 2. *Under condition (H), when $h < x_*$ and $\tau > 0$, if there exists an order-k $(k \geq 3)$ periodic solution in model*

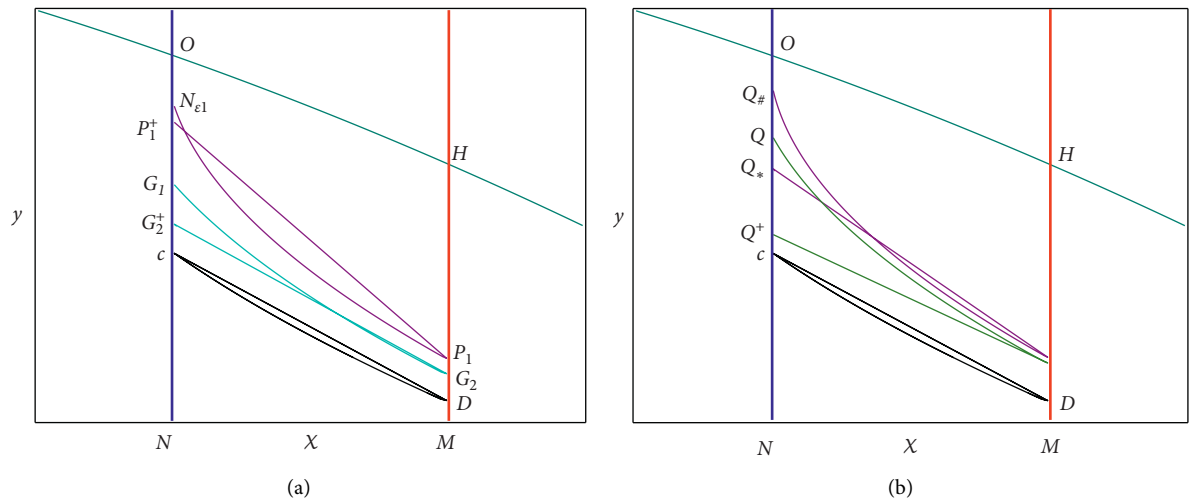

Figure 3: Illustration corresponding to the orbital (a) stability and (b) attractability of order-1 periodic solution in model (2).

(2), setting points $((1-p)h, y_i)(i = 1, \ldots, k)$ *as the phase points of the order-k periodic solution, then* $y_O \in (\min_{i=1,\ldots,k}(y_i), \max_{i=1,\ldots,k}(y_i))$.

Proof. If $y_O \geq \max_{i=1,\ldots,k}(y_i)$, it is obvious that there is no order-k $(k \geq 2)$ according to the proofs in the previous theorems. Hence, we only need to consider $y_O \leq \min_{i=1,\ldots,k}(y_i)$. Let points $(h, y_i^+)(i = 1, 2, \ldots, k)$ be the impulsive point of the order-k periodic solution and $y_{i+1} = (1-q)y_i^+ + \tau$; then, $y_1 = (1-q)y_k^+ + \tau$. Because $y_O \leq \min_{i=1,\ldots,k}(y_i)$, for any $l, j \in \{1, 2, \ldots, k\}$, if $y_l > y_j$, then $y_l^+ > y_j^+$ by the disjoint of trajectory of model (1).

For $y_O \leq \min_{i=1,\ldots,k}(y_i)$, the relationship among y_1, y_2, and y_3 is one of the following cases because of the disjoint of the trajectory of model (1) and the disjoint of the impulsive line of model (2):

① $y_1 > y_3 > y_2$
② $y_3 > y_1 > y_2$
③ $y_2 > y_1 > y_3$
④ $y_2 > y_3 > y_1$

For $y_1 > y_3 > y_2$, we get $y_1^+ < y_3^+ < y_2^+$, so $y_2 < y_4 < y_3 < y_1$ using $y_{i+1} = (1-q)y_i^+ + \tau$. Hence, we claim

$$y_2 < \cdots < y_{2n} < y_{2n-1} < \cdots < y_1. \tag{12}$$

When $n = 1, 2$, it is obvious that inequality (12) holds. Now, suppose inequality (12) holds when $n = \sigma$. In the following, we will prove that inequality (12) also holds when $n = \sigma + 1$. Because $y_2 < \cdots < y_{2\sigma} < y_{2\sigma-1} < \cdots < y_1$, we have $y_2^+ > \cdots > y_{2\sigma}^+ > y_{2\sigma-1}^+ > \cdots > y_1^+$. Consequently, $y_1 > y_3 > \cdots > y_{2\sigma+1} > y_{2\sigma} > \cdots > y_2$, that is, inequality (12) holds when $n = \sigma + 1$. Hence, inequality (12) holds when $y_1 > y_3 > y_2$.

In this case, obviously, for an order-k periodic solution, we have $(1-q)y_k^+ + \tau < y_1$ when $y_1 > y_3 > y_2$, which contradicts to $y_1 = (1-q)y_k^+ + \tau$. Hence, the order-k periodic solution does not exist. Using similar procedure, it is proved that the order-k $(k \geq 3)$ periodic solution does not exist for cases ②, ③, and ④. So, there is no order-k $(k \geq 3)$ periodic solution in model (2) when $y_O \leq \min_{i=1,\ldots,k}(y_i)$. Therefore, $y_O \in (\min_{i=1,\ldots,k}(y_i), \max_{i=1,\ldots,k}(y_i))$ when an order-k $(k \geq 3)$ periodic solution exists in model (2).

This completes the proof.

By Proposition 2, the following theorem will exist. □

Theorem 4. *Under condition (H), if* $h < x_*$ *and* $\tau \geq y_O$, *then there exists a globally orbitally asymptotically stable and unique order-1 periodic solution or a unique order-1 periodic solution and an order-2 solution coexists in model (2) for any* $q \in (0, 1)$, *and there is no order-k* $(k \geq 3)$ *periodic solution.*

Proof. By Proposition 2, it is obvious that there is no order-k $(k \geq 3)$ periodic solution in model (2) because $(1-q)y + \tau > \tau \geq y_O$ for any $y > 0$. If order-2 periodic solution does not exist, then a globally orbitally asymptotically stable and unique order-1 periodic solution exists using Theorems 2 and 3. If an order-2 periodic solution exists, then the order-2 periodic solution coexists with a unique order-1 periodic solution by Theorem 2.

This completes the proof. □

Theorem 5. *Under condition (H), if* $h < x_*$, *for given* $\tau > 0$, *then all the non-negative solutions of model (2) which start in* Ω *are ultimately bounded, and the bound depends on parameter* τ, q, p, *and* h.

Proof. By model (2) and the space Ω, obviously, $0 < \lim_{t \longrightarrow +\infty} \sup x(t) \leq h$ and $0 \leq \lim_{t \longrightarrow +\infty} \sup y(t)$ hold. In addition, set $\Lambda_N = \{y \mid y \text{ is the ordinate of phase point}\}$ and $\Lambda_M = \{y \mid y \text{ is the ordinate of impulsive point}\}$. Then, $y_{O_1} = \max(\Lambda_M)$, so we can obtain $y_{O_1^+} = \max(\Lambda_N)$ by $y_{O_1^+} = (1-q)y_{O_1} + \tau$. Hence, $\lim_{t \longrightarrow +\infty} \sup y(t) \leq y_{O_1^+}$, which obviously depends on τ, q, p, and h.

This completes the proof.

From Theorem 5, it is not difficult to find that there is a rough estimate of the bound, and we have the following remark. □

Remark 1. Under condition (*H*), if $h < x_*$, then $0 < \lim_{t\longrightarrow+\infty} \sup x(t) \le h$ and $0 \le \lim_{t\longrightarrow+\infty} \sup y(t) < (1-q)y_H + \tau$.

Proposition 3. *Under condition (H), if there exists a point S such that $F_k(S) = 0$ in model (2) when $h < x_*$, then there exists an order-k_f periodic solution, where the positive integer k_f is a factor of the positive integer k, including 1 and k.*

Proof. Suppose positive integer k_f is not a factor of the positive integer k, then let k_r be the remainder of k/k_f and k_q be the quotient of k/k_f. Because there exists an order-k_f periodic solution in model (2), without loss of generality, assume $F_{k_f}(S) = 0$. Obviously, we have $F_{k_q k_f}(S) = 0$, but $F_{k_r}(S) \neq 0$. Hence, the equation $F_{k_q k_f + k_r}(S) \neq 0$, which is a contradiction with $F_k(S) = 0$ because $k = k_q k_f + k_r$. So, the positive integer k_f is a factor of the positive integer k. When the positive integer k_f is a factor of the positive integer k, $F_k(S) = 0$ is obvious if there exists an order-k_f periodic solution in model (2).

This completes the proof. □

Proposition 4. *Under condition (H), if there exists a point O_0 below point O such that $F_3(O_0) < 0$ holds when $h < x_*$, $0 < \tau < y_O$, $p \in (0,1)$, and $q \in (0,1)$, then model (2) has an order-3 periodic solution when $F_1(O) > 0$, and the order-3 periodic solution coexists with an order-1 periodic solution.*

Proof. Setting $E = N \cap \{(x,y) | 0 < x \le h,\ y = 0\}$, we have $F_1(E) > 0$, $F_2(E) > 0$ and $F_3(E) > 0$. Hence, there exists a point $O_* \in \overline{EO_0}$ such that $F_3(O_*) = 0$ because $F_3(O_0) < 0$, so an order-k (k = 1or3) periodic solution exists by Proposition 3. However, owing to $F_1(O) > 0$, it is obvious that there is no order-1 periodic solution in space Π by the proof of Theorem 2. Thus, the periodic solution is the order-3 one. Furthermore, because $F_1(O) > 0$, there exists an order-1 periodic solution according to the proof of Theorem 2, and its phased point is above point O. Therefore, the order-3 periodic solution coexists with an order-1 periodic solution.

This completes the proof.

Although it is not proved that point O_0 must exist in Proposition 4, it provides a method to search an order-3 periodic solution for numerical analysis. Furthermore, the existence of order-3 periodic solution means that order-k ($k > 3$) periodic solution and chaos exist in model (2) by Sarkovskii's theorem [42] and Li and Yorke's theorem [43]. □

4. Numerical Results

In the previous section, we have analyzed the properties of periodic solution in model (2), including the existence, uniqueness, stability, and boundedness. In this section, we will further show the complex dynamics induced by impulsive control using the numerical simulations. Since the focus of this paper is the role of impulsive control in the population dynamics, the parameters of model (1) are fixed: $r = 0.9, K = 100, b = 1.2, a = 7, \alpha = 0.7$, and $m = 0.7$, and we can obtain the equilibrium $E_* = (35, 20.475)$ with index +1. Obviously, condition (*H*) always holds under this parameter set.

By Theorem 1, there only exists a semitrivial periodic solution in model (2) when $\tau = 0$ and $h < x_*$. Given $h = 3, p = 0.6, q = 0.5$, and $\tau = 0$, we get a semitrivial periodic solution as shown in Figure 4(a), and its period is about 1.309. In addition, we also obtain the theoretical value of the period by $T = (1/r)\ln(K-(1-p)h/(1-p)(K-h))$, which is the same as the numerical one. When $h = 3$ and $p = 0.6$, the point O is fixed at (1.2, 6.0762). The numerical simulation shows that all the successor points of any trajectory except the semitrivial solution are below initial point in model (2) and these trajectories converge towards the semitrivial periodic solution (see Figure 4(b)).

When $\tau > 0$, however, the semitrivial periodic solution disappears. Then, an order-1 periodic solution emerges and it should be unique by Theorem 2. In phase set N, because the order-1 successor point of any point above point O is below point O_1^+, we compute the order-1 successor function $F_1(y)$ where $y \in (0, y_{O_1^+}]$ for different values of τ (see Figure 5(a)), where $h = 32, p = 0.1$, and $q = 0.1$. In the rest of this section, we will employ this control parameter set unless otherwise specified.

From Figure 5(a), it is not difficult to find that the equation $F_1(y) = 0$ has a unique root, which means that there exists a unique order-1 periodic solution. Hence, we carry out some numerical simulations with respect to these roots of $F_1(y) = 0$, and the results verify that these solutions are order-1 periodic solutions as shown in Figure 5(b). But we find that some of these order-1 periodic solutions are unstable, which indicates that there may exist order-k periodic solution for some values of τ.

In order to illustrate the existence of order-k periodic solution, we further compute order-1 successor function, order-2 successor function, and order-3 successor function, and the results are very interesting and are shown in Figure 6(a). From Figure 6(a), it is easy to find that the equation $F_1(y) = 0$ has a unique root, the equation $F_2(y) = 0$ has three roots, and the equation $F_3(y) = 0$ has seven roots. Furthermore, we can find that the root of $F_1(y) = 0$ is the common root of three equations: $F_1(y) = 0$, $F_2(y) = 0$, and $F_3(y) = 0$, which means that there exists an order-1 periodic solution corresponding to this root. Except this root, the equation $F_2(y) = 0$ still has two roots which indicate an order-2 periodic solution exists in virtue of the uniqueness of order-1 periodic solution. For order-3 successor function $F_3(y)$, the equation $F_3(y) = 0$ has six roots except for the root of $F_1(y) = 0$.

Except for the root of $F_1(y) = 0$, it is not difficult to find that $F_1(y)$ and $F_2(y)$ are positive or negative definite in a small neighborhood of each root of $F_3(y) = 0$, which means that there may exist two order-3 periodic solutions in model (2). Thus, we perform some numerical simulations to show the solutions corresponding to these roots. The results show that a stable order-3 periodic solution coexists with an unstable order-3 periodic solution, an unstable order-2 periodic solution, and an unstable order-1 periodic solution (see Figure 6(b)). Additionally, the numerical solutions for

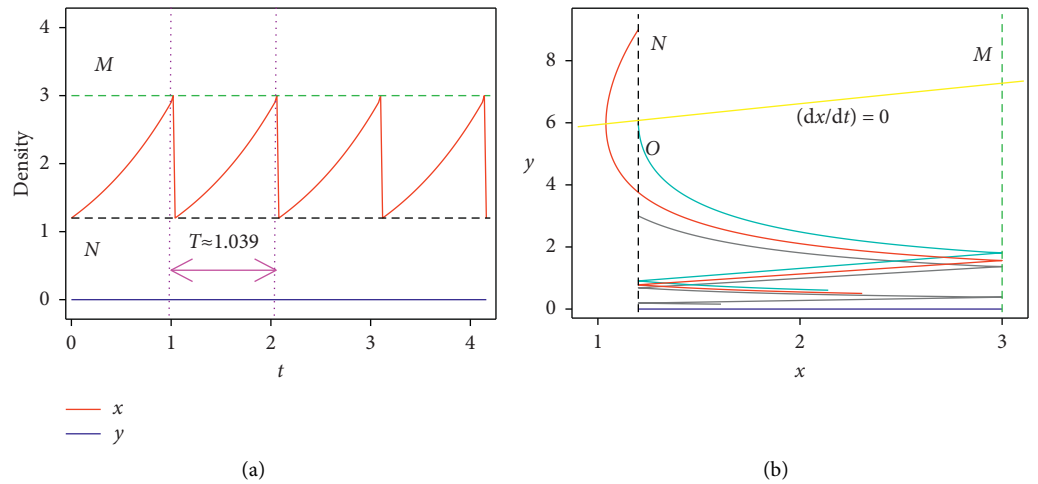

FIGURE 4: (a) The semitrivial periodic solution of model (2) (the red curve denotes the density of population x and the blue line denotes the density of population y). (b) The proof of trajectory whose successor points are below initial points.

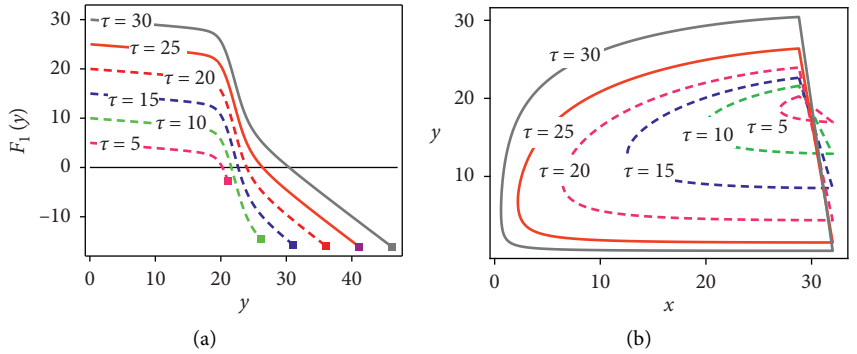

FIGURE 5: (a) The order-1 successor function $F_1(y)$ for $y \in (0, y_S)$, where the solid square denotes the value of y_S. (b) Order-1 periodic solutions corresponding to roots of $F_1(y) = 0$, where the dashed curves denote the unstable order-1 periodic solutions and the solid curves denote the stable ones.

prey y are given to further exhibit these periodic solutions, as shown in Figure 6(c).

The above results indicate that the order-1 periodic solutions are not always stable. Using order-1 and order-2 successor functions, we compute y – value with respect to the phased point of order-1 periodic solution to simulate its variation as parameter τ increases (see Figure 7(a)). From Figure 7(a), the order-1 periodic solution is stable before parameter τ reaches line l_1, and the order-1 periodic solution is still stable near l_1 when parameter τ is beyond l_1. This result is in accord with Theorem 3. Keeping parameter τ increasing, the order-1 periodic solution loses its stability until it is beyond l_3. It is well worth noting that model (2) only has order-1 and order-2 periodic solution when parameter τ is between l_2 and l_3, which agrees with Theorem 4. Furthermore, Figure 7(a) demonstrates that the order-1 periodic solution is unique, which supports the result in Theorem 2. Additionally, Figure 7(a) also shows that $y = y(\tau)$ is a monotonously increasing function with respect to τ, which is consistent with Proposition 1.

In addition, our numerical results also indicate that the phased point of order-1 periodic solution rises along phase set as parameter τ increases. In order to present the stability of order-1 periodic solution, we compute two groups of order-k successor points whose initial point is on the sides of the phased point of order-1 periodic solution, respectively. It is revealed that these points monotonously converge towards the phased point of order-1 periodic solution (see Figure 7(b)). Hence, this order-1 periodic solution is stable due to the nonexistence of other periodic solutions.

In order to display complex dynamics, we chose parameter τ as the controlled parameter and ran numerous simulations using a wide range of parameter τ to show the bifurcation diagram (see Figure 8(a)). Since the stability of order-1 periodic solution has been discussed above (Figure 7(a)), we will present the dynamics when the order-1 periodic solution is unstable. From Figure 8(a), increased parameter τ can generate chaos by a cascade of period-doubling bifurcation. Keeping parameter τ increasing, an order-3 periodic solution bifurcates from chaos. Subsequently, chaos occurs again with the increase of parameter τ. Finally, chaos disappears again via a cascade of inverse period-doubling bifurcation at higher values in the

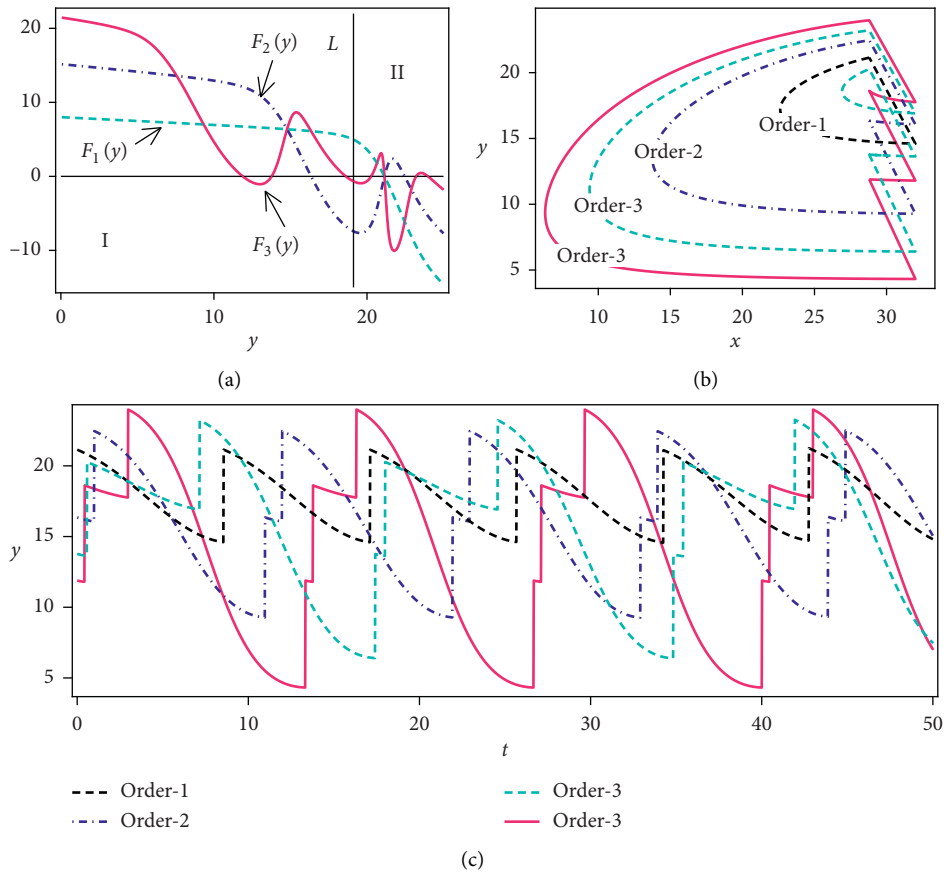

FIGURE 6: (a) The order-1 successor function $F_1(y)$, the order-2 successor function $F_2(y)$, and the order-3 successor function $F_3(y)$, where the line L denotes line $y = y_O$. (b) An order-1 periodic solution corresponding to the root of $F_1(y) = 0$, an order-2 periodic solution corresponding to roots of $F_2(y) = 0$, and two order-3 periodic solutions corresponding to roots of $F_3(y) = 0$, where the dashed curves denote the unstable periodic solutions and the solid curves denote the stable ones. (c) Time-series of population y corresponding to the periodic solutions in (b), where $\tau = 8$.

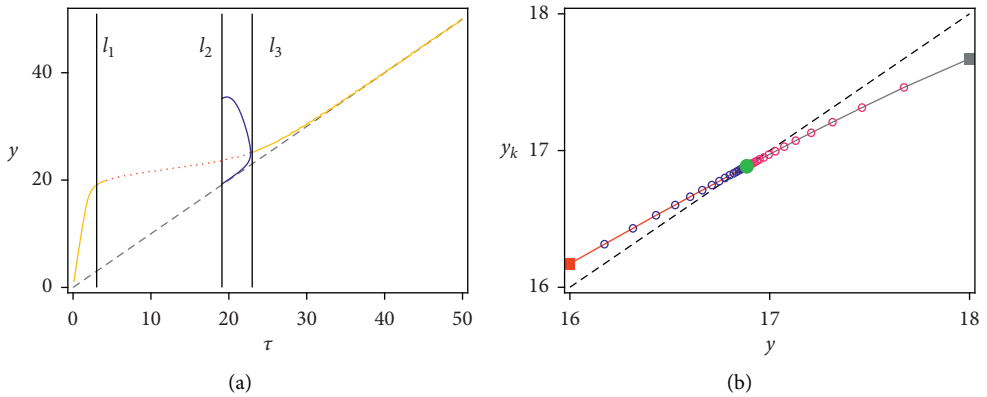

FIGURE 7: (a) The existence and stability of the order-1 periodic solution (the solid yellow curve represents stability of the order-1 periodic solution, the dashed red curve represents instability of the order-1 periodic solution, and the solid blue curve represents the stable order-2 periodic solution; the line l_1 denotes $\tau = y_S - (1-q)\pi(t_1; O, t_0)$, where t_1 is the moment when the trajectory $\pi(t_1; O, t_0)$ first met line $x = h$, the line l_2 denotes $\tau = y_O$, and the line l_3 denotes the critical value of parameter τ where the order-1 periodic solution obtain its stability again). (b) The proof of stability of the order-1 periodic solution (the solid squares represent initial points, the lines with circles denote the successor points, and the solid green circle denotes the phase point of order-1 periodic solution).

simulated range of parameter τ. To confirm the occurrence of chaos further, we calculate the largest Lyapunov exponents in the same range of parameter τ as Figure 8(a), which agrees with the bifurcation diagram (see Figure 8(b)). In addition, dozens of time-series of population y for differently initial values are given in Figure 8(c) to further show

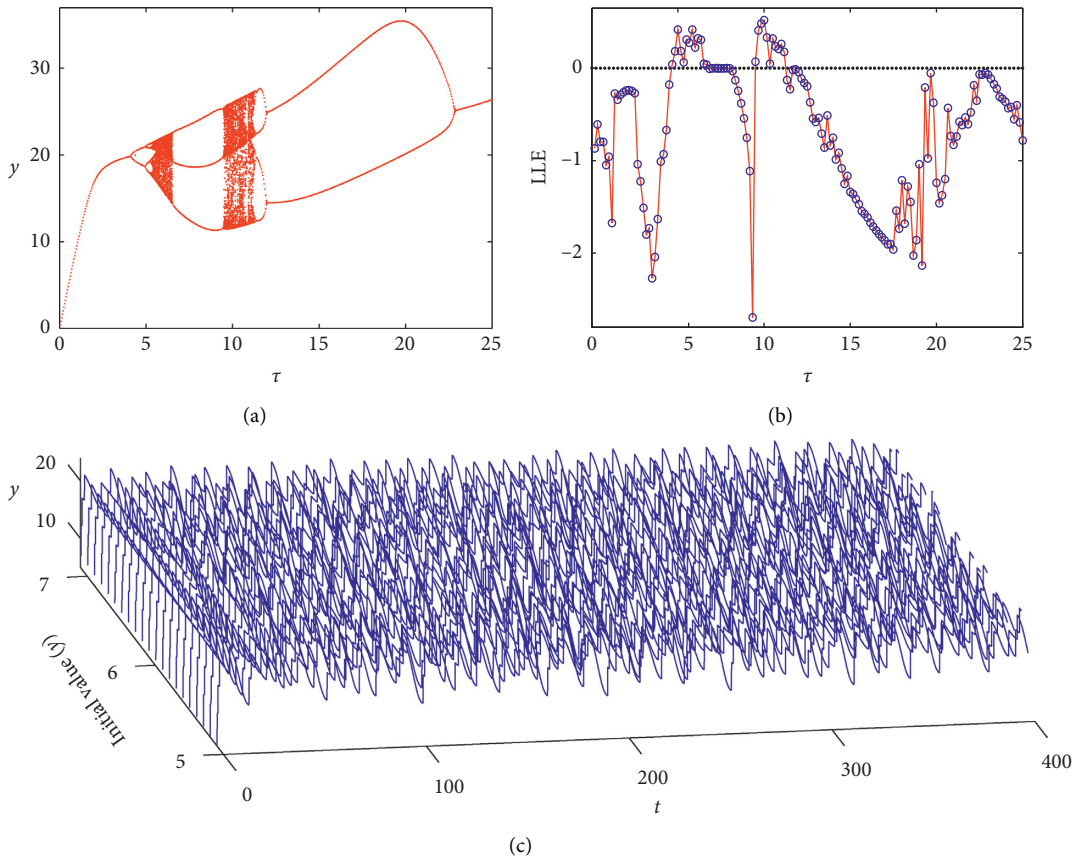

FIGURE 8: (a) The bifurcation diagram with respect to parameter τ for model (2). (b) The variation of the Lyapunov exponents with respect to the parameter τ, where the symbol "LLE" denotes the largest Lyapunov exponent. (c) Time-series of population y with different initial values for $\tau = 6$.

chaos, which suggests that all states described by these time-series are in disorder.

5. Conclusion

In this paper, we proposed an ecological model with state-dependent impulsive control strategy to investigate the effect of impulsive control on prey-predator dynamics. Theoretical results suggest that model (2) has a globally orbitally asymptotically stable semitrivial periodic solution when parameter $\tau = 0$ and $h < x_*$, where condition (H) holds to guarantee existence of positive equilibrium E_*. When $\tau > 0$, the semitrivial periodic solution disappears, but the theoretical analysis shows that a unique order-1 periodic solution emerges for any $q \in (0, 1)$ and $p \in (0, 1)$.

Furthermore, we find that the order-1 periodic solution is globally orbitally asymptotically stable when the value of τ is below τ_c. Additionally, when the value of τ is beyond y_o, theoretical analysis reveals that a globally orbitally asymptotically stable order-1 periodic solution exists or coexistence of a unique order-1 periodic solution and order-2 periodic solution occurs.

Additionally, the existence of order-k is theoretically analyzed based on equation $F_k(y) = 0$, which demonstrates that an order-k_f periodic solution exists when $F_k(y) = 0$, and k_f is a factor of the positive integer k, including 1 and k. According to this result, we discuss the existence of order-3 periodic solution. Although we cannot get the exact range of parameter τ with respect to the existence of order-3 periodic solution, our results imply that the order-3 periodic solution may exist for $\tau \in (\tau_c, y_O)$, which even means that chaos may occur.

In order to study dynamics induced by impulsive control further, a series of numerical simulations are carried out, which agreed with the theoretical results well. Numerical simulations show that order-1, order-2, and order-3 periodic solutions can coexist. Specially, we find the coexistence of double order-3 periodic solutions. Moreover, numerical bifurcation analysis shows that an unstable order-1 periodic solution and a stable order-2 periodic solution can coexist for $\tau > y_o$, but there exists only a stable order-1 periodic solution when τ is beyond some critical value. In addition, numerical simulations show that chaos occurs. Obviously, dynamics induced by impulsive control is much richer.

The theoretical and numerical results predict that the population x can be controlled using the state-dependent impulsive control strategies. Because $h < x_*$, the method by impulsive harvesting population x was a unique choice which can keep the density of population x below the critical value. Our results shows that the control period is much lower when the released amount τ is much smaller, which means that the control frequency is much higher. But from

the viewpoint of management for some ecological problems (e.g., pest outbreak, phytoplankton blooms, etc.), it is always hoped that the control period is much longer. Thus, much more predators are needed to be released. However, our results also indicate that chaos may occur for some values of τ, which is unfavourable for prediction of control period. Hence, the released amount of predator should be chosen carefully. Obviously, our results are much more interesting, and we expect that these results are helpful to the management of ecological problems.

Data Availability

The data used to support the findings of this study are included within the article.

Conflicts of Interest

The author declares that there are no conflicts of interest.

Acknowledgments

This study was supported by the Zhejiang Provincial Natural Science Foundation of China (grant no. LQ18C030002) and the National Natural Science Foundation of China (grant no. 61901303).

References

[1] A. Dobson, "Mathematical models for emerging disease," *Science*, vol. 346, pp. 1294-1295, 2014.

[2] G. A. Jackson, "Phytoplankton growth and zooplankton grazing in oligotrophic oceans," *Nature*, vol. 284, pp. 439–441, 1980.

[3] J. Huisman, T. Pham, N. Nga, D. M. Karl, and B. Sommeijer, "Reduced mixing generates oscillations and chaos in the oceanic deep chlorophyll maximum," *Nature*, vol. 439, pp. 322–325, 2006.

[4] C. J. Dai, H. G. Yu, Q. Guo et al., "Dynamics induced by delay in a nutrient-phytoplankton model with multiple delays," *Complexity*, vol. 2019, Article ID 3879626, 16 pages, 2019.

[5] V. Lakshmikantham, D. D. Bainov, and P. S. Simeonov, *Theory of Impulsive Differential Equations*, World Scientific, Singapore, 1989.

[6] D. D. Bainov and P. S. Simeonov, *Systems with Impulsive Effect: Stability, Theory and Applications*, Wiley, New York, NY, USA, 1989.

[7] E. M. Bonotto and M. Federson, "Limit sets and the Poincaré Bendixson theorem in impulsive semidynamical systems," *Journal of Differential Equations*, vol. 224, no. 9, pp. 2334–2349, 2008.

[8] J. J. Nieto and D. O'Regan, "Variational approach to impulsive differential equations," *Nonlinear Analysis: Real World Applications*, vol. 10, no. 2, pp. 680–690, 2009.

[9] R. P. Agarwal, A. S. Awan, D. O'Regan, and A. Younus, "Linear impulsive Volterra integro-dynamic system on time scales," *Advances in Difference Equations*, vol. 2014, Article ID 6, 2014.

[10] A. J. Terry, "Biocontrol in an impulsive predator-prey model," *Mathematical Biosciences*, vol. 256, pp. 102–115, 2014.

[11] X. D. Li, M. Bohner, and C. K. Wang, "Impulsive differential equations: periodic solutions and applications," *Automatica*, vol. 52, pp. 173–178, 2015.

[12] J. Yang, Y. S. Tan, and R. A. Cheke, "Modelling effects of a chemotherapeutic dose response on a stochastic tumour-immune model," *Chaos, Solitons & Fractals*, vol. 123, pp. 1–13, 2019.

[13] S. Y. Tang and R. A. Cheke, "State-dependent impulsive models of integrated pest management (IPM) strategies and their dynamic consequences," *Journal of Mathematical Biology*, vol. 50, no. 3, pp. 257–292, 2005.

[14] J. Yang and Y. S. Tan, "Effects of pesticide dose on Holling II predator-prey model with feedback control," *Journal of Biological Dynamics*, vol. 12, no. 1, pp. 527–550, 2018.

[15] G. R. Jiang, Q. S. Lu, and L. N. Qian, "Complex dynamics of a Holling type II prey- predator system with state feedback control," *Chaos, Solitons & Fractals*, vol. 31, pp. 448–461, 2007.

[16] C. J. Dai and M. Zhao, "Mathematical and dynamic analysis of a prey-predator model in the presence of alternative prey with impulsive state feedback control," *Discrete Dynamics in Nature and Society*, vol. 2012, Article ID 724014, 19 pages, 2012.

[17] C. J. Dai, M. Zhao, and L. S. Chen, "Dynamic complexity of an Ivlev-type prey-predator system with impulsive state feedback control," *Journal of Applied Mathematics*, vol. 2012, Article ID 534276, 17 pages, 2012.

[18] L. F. Nie, J. G. Peng, Z. D. Teng, and L. Hu, "Existence and stability of periodic solution of a Lotka-Volterra predator-prey model with state dependent impulsive effects," *Journal of Computational and Applied Mathematics*, vol. 224, no. 2, pp. 544–555, 2009.

[19] K. B. Sun, T. H. Zhang, and Y. Tian, "Dynamics analysis and control optimization of a pest management predator-prey model with an integrated control strategy," *Applied Mathematics and Computation*, vol. 292, pp. 253–271, 2017.

[20] G. P. Pang and L. S. Chen, "Periodic solution of the system with impulsive state feedback control," *Nonlinear Dynamics*, vol. 78, no. 1, pp. 743–753, 2014.

[21] S. Y. Tang, B. Tang, A. L. Wang, and Y. N. Xiao, "Holling II predator-prey impulsive semi-dynamic model with complex Poincaré map," *Nonlinear Dynamics*, vol. 81, no. 3, pp. 1575–1596, 2015.

[22] J. Yang, Y. S. Tan, and R. A. Cheke, "Complex dynamics of an impulsive Chemostat model," *International Journal of Bifurcation and Chaos*, vol. 29, no. 8, Article ID 1950101, 2019.

[23] D. Z. Li, H. D. Cheng, and Y. Liu, "Dynamic analysis of Beddington-DeAngelis predator-prey system with nonlinear impulse feedback control," *Complexity*, vol. 2019, Article ID 5308014, 13 pages, 2019.

[24] P. S. Simeonov and D. D. Bainov, "Orbital stability of periodic solutions of autonomous systems with impulse effect," *International Journal of Systems Science*, vol. 19, no. 12, pp. 2561–2585, 1988.

[25] L. N. Qian, Q. S. Lu, Q. G. Meng, and Z. S. Feng, "Dynamical behaviors of a prey-predator system with impulsive control," *Journal of Mathematical Analysis and Applications*, vol. 363, no. 1, pp. 345–356, 2010.

[26] L. S. Chen, "Pest control and geometric theory of semi-dynamical systems," *Journal of Beihua University*, vol. 12, pp. 1–9, 2011.

[27] C. J. Dai, M. Zhao, and L. S. Chen, "Homoclinic bifurcation in semi-continuous dynamic systems," *International Journal of Biomathematics*, vol. 5, no. 6, Article ID 1250059, 2012.

[28] H. J. Guo, X. Y. Song, and L. S. Chen, "Qualitative analysis of a Korean pine forest model with impulsive thinning measure," *Applied Mathematics and Computation*, vol. 234, pp. 203–213, 2014.

[29] X. H. Ji, S. L. Yuan, and L. S. Chen, "A pest control model with state-dependent impulses," *International Journal of Biomathematics*, vol. 8, no. 1, Article ID 1550009, 2015.
[30] Y. Tian, K. B. Sun, and L. S. Chen, "Geometric approach to the stability analysis of the periodic solution in a semi-continuous dynamic system," *International Journal of Biomathematics*, vol. 7, no. 2, Article ID 1450018, 2014.
[31] T. Zhang, X. Meng, R. Liu, and T. Zhang, "Periodic solution of a pest management Gompertz model with impulsive state feedback control," *Nonlinear Dynamics*, vol. 78, no. 2, pp. 921–938, 2014.
[32] M. Z. Huang and X. Y. Song, "Periodic solutions and homoclinic bifurcations of two predator-prey systems with nonmonotonic functional response and impulsive harvesting," *Journal of Applied Mathematics*, vol. 2014, Article ID 803764, 11 pages, 2014.
[33] Q. Z. Xiao, B. X. Dai, B. X. Xu, and L. S. Bao, "Homoclinic bifurcation for a general state-dependent Kolmogorov type predator-prey model with harvesting," *Nonlinear Analysis: Real World Applications*, vol. 26, pp. 263–273, 2015.
[34] C. J. Wei and L. S. Chen, "Periodic solution and heteroclinic bifurcation in a predator- prey system with Allee effect and impulsive harvesting," *Nonlinear Dynamics*, vol. 76, no. 2, pp. 1109–1117, 2014.
[35] M. Z. Huang, S. Z. Liu, X. Y. Song, and L. S. Chen, "Dynamics of unilateral and Bilateral control systems with state feedback for renewable resource management," *Complexity*, vol. 2020, Article ID 9453941, 16 pages, 2020.
[36] Z. Z. Shi, J. M. Wang, Q. J. Li, and H. D. Cheng, "Control optimization and homoclinic bifurcation of a prey-predator model with ratio-dependent," *Advances in Difference Equations*, vol. 2019, no. 1, 2019.
[37] B. Liu and Y. Tian, "Dynamics on a Holling II predator-prey model with state-dependent impulsive control," *International Journal of Biomathematics*, vol. 5, no. 3, Article ID 1260006, 2012.
[38] G. P. Pang, Z. Q. Liang, W. J. Xu, L. J. Li, and G. Fu, "A pest management model with stage structure and impulsive state feedback control," *Discrete Dynamics in Nature and Society*, vol. 2015, Article ID 617379, , 2015.
[39] T. Yoshida, L. E. Jones, S. P. Ellner, G. F. Fussmann, and N. G. Hairston Jr., "Rapid evolution drives ecological dynamics in a predator-prey system," *Nature*, vol. 424, no. 6946, pp. 303–306, 2003.
[40] G. F. Fussmann, S. P. Ellner, K. W. Shertzer, and N. G. Hairston Jr., "Crossing the Hopf bifurcation in a live predator-prey system," *Science*, vol. 290, pp. 1358–1360, 2000.
[41] D. W. Jordan and P. Smith, *Nonlinear Ordinary Differential Equations: An Introduction for Scientists and Enginerrs*, Oxford University, New York, NY, USA, 4th edition, 2007.
[42] R. L. Devaney, *An Introduction to Chaotic Dynamical Systems*, Westview Press, Bounlder, CO, USA, 2003.
[43] T. Y. Li and J. A. Yorke, "Period three implies chaos," *The American Mathematical Monthly*, vol. 82, pp. 985–992, 1975.

Hindawi
Complexity
Volume 2020, Article ID 9614670, 12 pages
https://doi.org/10.1155/2020/9614670

Research Article

Stability of a Nonlinear Stochastic Epidemic Model with Transfer from Infectious to Susceptible

Yanmei Wang [1,2] **and Guirong Liu** [1]

[1]*School of Mathematical Sciences, Shanxi University, Taiyuan, Shanxi 030006, China*
[2]*School of Applied Mathematics, Shanxi University of Finance and Economics, Taiyuan, Shanxi 030006, China*

Correspondence should be addressed to Guirong Liu; lgr5791@sxu.edu.cn

Received 3 April 2020; Revised 16 May 2020; Accepted 19 May 2020; Published 31 May 2020

Guest Editor: Carlos Arturo Loredo Villalobos

Copyright © 2020 Yanmei Wang and Guirong Liu. This is an open access article distributed under the Creative Commons Attribution License, which permits unrestricted use, distribution, and reproduction in any medium, provided the original work is properly cited.

We investigate a stochastic SIRS model with transfer from infectious to susceptible and nonlinear incidence rate. First, using stochastic stability theory, we discuss stochastic asymptotic stability of disease-free equilibrium of this model. Moreover, if the transfer rate from infectious to susceptible is sufficiently large, disease goes extinct. Then, we obtain almost surely exponential stability of disease-free equilibrium, which implies that noises can lead to extinction of disease. By the Lyapunov method, we give conditions to ensure that the solution of this model fluctuates around endemic equilibrium of the corresponding deterministic model in average time. Furthermore, numerical simulations show that the fluctuation increases with increase in noise intensity. Finally, these theoretical results are verified by numerical simulations. Hence, noises play a vital role in epidemic transmission. Our results improve and extend previous related results.

1. Introduction

Mathematical models have become a crucial tool in understanding dynamics of population growth [1–3]. In recent decades, some realistic mathematical models have been established to investigate dynamics of epidemic [4–10]. In order to simulate epidemic transmission process, many dynamic models have been established, such as SIS, SEIR, and SIRS models [11–13]. In these models, the incidence rate is crucial. Classical disease transmission models adopt the standard or bilinear incidence rate. However, in the course of epidemic propagation, nonlinear incidence may be more realistic than other incidence rates [14]. In addition, infected individuals may recover after a period of treatment or become susceptible individuals directly due to transient antibody. In [15], a deterministic SIRS model with transfer from infectious to susceptible and nonlinear incidence can be modeled as follows:

$$\begin{cases} \dot{S} = \Lambda + \gamma_1 I + \delta R - \beta S f(I) - \mu S, \\ \dot{I} = \beta S f(I) - (\alpha + \gamma_1 + \gamma_2 + \mu) I, \\ \dot{R} = \gamma_2 I - (\delta + \mu) R. \end{cases} \tag{1}$$

Here, S, I, and R denote numbers of susceptible, infectious, and recovered individuals, respectively. Λ is the recruitment rate of susceptible; β denotes the disease propagation coefficient; μ and α denote, respectively, the natural death rate and mortality caused by the disease; δ denotes the immunity loss rate; γ_1 represents the transfer rate from infectious to susceptible; γ_2 denotes the recovery rate of infectious individuals. In addition, $\Lambda > 0$, $\mu > 0$, $\gamma_1 \geq 0$, $\gamma_2 \geq 0$, $\delta \geq 0$, and $\alpha \geq 0$.

From [15], (1) has disease-free equilibrium $E_0(\Lambda/\mu, 0, 0)$ which is globally asymptotic stable in $\{(S, I, R) \in \mathbb{R}^3_+ : S + I + R \leq \Lambda/\mu\}$ if $\mathscr{R}_0 = (\beta\Lambda)/[\mu(\gamma_1 + \gamma_2 + \mu + \alpha)] < 1$. If $\mathscr{R}_0 > 1$, there exists a globally asymptotic stable endemic equilibrium $E^*(S^*, I^*, R^*)$.

However, dynamics of epidemic is often disturbed by some random factors. Hence, stochastic epidemic models are more realistic and have attracted much attention [16–19]. In [20], the authors discussed threshold behavior for a stochastic SIS model. In [21], asymptotic properties of a stochastic SIR model were considered. In [22, 23], the authors investigated persistence and extinction for a stochastic SIRS model. In [24], the authors studied stability of a stochastic SIRS model. Fatini et al. [25] considered stochastic

stability and instability for a stochastic SIR model. Recently, Wang et al. [26] established a stochastic SIRS epidemic model:

$$\begin{cases} \mathrm{d}S = \left[\Lambda + \gamma_1 I + \delta R - \beta S f(I) - \mu S\right]\mathrm{d}t - \sigma S f(I)\mathrm{d}B(t), \\ \mathrm{d}I = \left[\beta S f(I) - (\alpha + \gamma_1 + \gamma_2 + \mu) I\right]\mathrm{d}t + \sigma S f(I)\mathrm{d}B(t), \\ \mathrm{d}R = \left[\gamma_2 I - (\mu + \delta) R\right]\mathrm{d}t, \end{cases} \tag{2}$$

with initial values $S_0 > 0, I_0 > 0,$ and $R_0 > 0$. Here, $B(t)$ represents Brownian motion on $(\Omega, \mathscr{F}, \mathbb{P})$ which is a complete probability space. σ^2 denotes the intensity of $B(t)$. Other parameters are defined as (1). Model (2) covers many stochastic models as particular cases (see, for example, [15, 22, 27]). In [26], extinction and persistence are obtained.

As is well known, stability of the dynamic system means that solutions are insensitive to small changes of initial value. Hence, stability is one of the important topics encountered in applications. However, because of the complexity of stochastic dynamics, there are not many results on stability of stochastic differential equations.

Motivated by the above work, we consider (2) and obtain stochastic stability of disease-free equilibrium and asymptotic behavior around endemic equilibrium of corresponding deterministic model (1).

Throughout this paper, we give the following hypotheses:

($\mathbf{H}_1$) f is locally Lipschitz on $[0, \infty)$; $f(I) > 0$ for $I > 0$; $f(0) = 0$

($\mathbf{H}_2$) $\lim_{I \longrightarrow 0^+} f(I)/I = 1$ and $f(I)/I$ is nonincreasing on $(0, \infty)$

From ($\mathbf{H}_1$), (2) has disease-free equilibrium $E_0(\Lambda/\mu, 0, 0)$. By ($\mathbf{H}_2$), if $I \in (0, \infty)$, then

$$I \geq f(I). \tag{3}$$

2. Preliminaries

We will give some definitions and lemmas. Consider

$$\mathrm{d}x = F(x,t)\mathrm{d}t + G(x,t)\mathrm{d}W(t), t \geq t_0. \tag{4}$$

Here, F and G are, respectively, $\mathbb{R}^d$–valued and $\mathbb{R}^{d \times n}$–valued functions defined on $\mathbb{R}^d \times [t_0, \infty)$ and $\mathbb{R}^d \times [t_0, \infty)$. $\{W(t)\}$ denotes n-dimensional Brownian motion on $(\Omega, \mathscr{F}, \{\mathscr{F}_t\}_{t \geq 0}, \mathbb{P})$. Assume that existence-and-uniqueness theorem is fulfilled. For $t \geq t_0$, $G(0,t) = 0$ and $F(0,t) = 0$. Denote $\overline{\mathbb{R}}_+ = \mathbb{R}_+ \cup \{0\}$ and $\mathrm{K} = \{\mu \in C(\overline{\mathbb{R}}_+, \overline{\mathbb{R}}_+) : \mu$ is nondecreasing; $\mu(0) = 0; \mu(r) > 0$ if $r > 0\}$. Set $S_h = \{x \in \mathbb{R}^d : |x| < h\}$.

Definition 1 ([[28], p.108])

(i) Assume that V is continuous on $S_h \times [t_0, \infty)$ and $V(0,t) \equiv 0$. If there is $\mu \in \mathrm{K}$ such that, for $(x,t) \in S_h \times [t_0, \infty)$,

$$V(x,t) \geq \mu(|x|), \tag{5}$$

then V is positive-definite. In addition, V is negative-definite if $-V$ is positive-definite.

(ii) Assume that V is nonnegative and continuous on $S_h \times [t_0, \infty)$. If there is $\mu \in \mathrm{K}$, satisfying for $(x,t) \in S_h \times [t_0, \infty)$,

$$V(x,t) \leq \mu(|x|), \tag{6}$$

then V is decrescent.

Definition 2 ([[28], p.110])

(i) If for any $r > 0$ and $\varepsilon \in (0,1)$, there is $\delta = \delta(\varepsilon, r, t_0) > 0$, satisfying for any $x_0 \in \mathbb{R}^d$ with $|x_0| < \delta$,

$$\mathbb{P}\left\{|x(t; t_0, x_0)| < r \text{ for } t \geq t_0\right\} \geq 1 - \varepsilon, \tag{7}$$

then trivial solution to (4) is stochastically stable.

(ii) The trivial solution to (4) is stochastically asymptotically stable if it is stochastically stable, and for any $\varepsilon \in (0,1)$, there is $\delta_0 = \delta_0(\varepsilon, t_0) > 0$ satisfying

$$\mathbb{P}\left\{\lim_{t \longrightarrow \infty} x(t; t_0, x_0) = 0\right\} \geq 1 - \varepsilon, \tag{8}$$

whenever $|x_0| < \delta_0$.

(iii) If for any $x_0 \in G \subset \mathbb{R}^d$, $\limsup_{t \longrightarrow \infty} (\ln|x(t; t_0, x_0)|)/t < 0$ a.s., then trivial solution to (4) is almost surely exponentially stable in G.

Lemma 1 ([[28], p.112]). *If $V \in C^{2,1}(S_h \times [t_0, \infty); \overline{\mathbb{R}}_+)$ is positive-definite and decrescent, and $LV(x,t)$ is negative-definite, then trivial solution to (4) is stochastically asymptotically stable.*

By Theorem 1 and Remark 1 in [26], the following result holds.

Lemma 2 (see [26]). *For $(S_0, I_0, R_0) \in \mathbb{R}^3_+$, there is a unique global positive solution to (2). Moreover,*

$$D = \left\{(S, I, R) \in \mathbb{R}^3_+ : S + I + R \leq \frac{\Lambda}{\mu}\right\} \tag{9}$$

is positively invariant.

3. Stability of Disease-Free Equilibrium

In epidemiology, stability has important practical significance.

Theorem 1. *If $\mathscr{R}_0 < 1$, $(\sigma^2 \Lambda^2)/(2\mu^2) < (\mu + \gamma_1 + \gamma_2 + \alpha)(1 - \mathscr{R}_0)$, then disease-free equilibrium E_0 to (2) is stochastically asymptotically stable in D.*

Proof. Denote $x = (x_1, x_2, x_3) = (-S + \Lambda/\mu, I, R)$. Define Lyapunov function

$$V_2(x) = x_1^2 + bx_2^2 + x_3^2 \tag{10}$$

for $(S, I, R) \in D$, where $b > 0$ is to be chosen later. Clearly, V_2 is positive-definite. Note that $V_2(x) \le (1 \vee b)|x|^2 =: \mu(|x|)$. From Definition 1 (ii), it follows that V_2 is decrescent. Now, we show that LV_2 is negative-definite.

From Itô formula, for any $(S, I, R) \in D$,

$$\begin{aligned}
\mathrm{LV}_2(x) &= -2\left(\frac{\Lambda}{\mu} - S\right)(\Lambda - \mu S - \beta S f(I) + \delta R + \gamma_1 I) \\
&\quad + 2bI[\beta S f(I) - (\mu + \alpha + \gamma_1 + \gamma_2)I] \\
&\quad + 2R[\gamma_2 I - (\delta + \mu)R] + (1 + b)(\sigma S f(I))^2 \\
&\le -2\mu\left(\frac{\Lambda}{\mu} - S\right)^2 + 2\left(\frac{\Lambda}{\mu} - S\right)(\beta S - \gamma_1)I \\
&\quad + \left[2b\beta S - 2b(\mu + \gamma_1 + \gamma_2 + \alpha) + (1 + b)\sigma^2 S^2\right]I^2 \\
&\quad + 2\gamma_2 IR - 2\delta\left(\frac{\Lambda}{\mu} - S\right)R - 2(\delta + \mu)R^2 \\
&\le -2\mu\left(\frac{\Lambda}{\mu} - S\right)^2 + 2\left(\frac{\Lambda}{\mu} - S\right)\left(\frac{\beta\Lambda}{\mu} - \gamma_1\right)I \\
&\quad + \left[\frac{2b\beta\Lambda}{\mu} - 2b(\mu + \gamma_1 + \gamma_2 + \alpha) + \frac{(1 + b)\sigma^2\Lambda^2}{\mu^2}\right]I^2 \\
&\quad + 2\gamma_2 IR - 2\delta(I + R)R - 2(\delta + \mu)R^2.
\end{aligned} \tag{11}$$

Obviously, we have

$$\begin{aligned}
&-\mu\left(\frac{\Lambda}{\mu} - S\right)^2 + \left(\frac{\Lambda}{\mu} - S\right)\left(\frac{\beta\Lambda}{\mu} - \gamma_1\right)I \\
&\quad = -\mu\left[\left(\frac{\Lambda}{\mu} - S\right) - \frac{1}{2\mu^2}(\beta\Lambda - \gamma_1\mu)I\right]^2 + \frac{1}{4\mu^3}(\beta\Lambda - \gamma_1\mu)^2 I^2,
\end{aligned} \tag{12}$$

$$\begin{aligned}
-(\mu + 2\delta)R^2 + (\gamma_2 - \delta)IR &= -(\mu + 2\delta)\left[R - \frac{\gamma_2 - \delta}{2(\mu + 2\delta)}I\right]^2 \\
&\quad + \frac{(\gamma_2 - \delta)^2}{4(\mu + 2\delta)}I^2.
\end{aligned} \tag{13}$$

Substituting (12) and (13) into (11) yields

$$\begin{aligned}
LV_2(x) \le &-2\mu\left[\left(\frac{\Lambda}{\mu} - S\right) - \frac{1}{2\mu^2}(\beta\Lambda - \gamma_1\mu)I\right]^2 \\
&+ \frac{1}{2\mu^3}(\beta\Lambda - \gamma_1\mu)^2 I^2 + \frac{(\gamma_2 - \delta)^2}{2(\mu + 2\delta)}I^2 + \frac{\sigma^2\Lambda^2}{\mu^2}I^2 \\
&- 2b\left[\mu + \gamma_1 + \gamma_2 + \alpha - \frac{\beta\Lambda}{\mu} - \frac{\sigma^2\Lambda^2}{2\mu^2}\right]I^2 \\
&- 2(\mu + 2\delta)\left[R - \frac{\gamma_2 - \delta}{2(\mu + 2\delta)}I\right]^2 \le \\
&- 2\mu\left[\left(\frac{\Lambda}{\mu} - S\right) - \frac{1}{2\mu^2}(\beta\Lambda - \gamma_1\mu)I\right]^2 \\
&- 2(\mu + 2\delta)\left[R - \frac{\gamma_2 - \delta}{2(\mu + 2\delta)}I\right]^2 \\
&- \left[2b\left(\mu + \gamma_1 + \gamma_2 + \alpha - \frac{\beta\Lambda}{\mu} - \frac{\sigma^2\Lambda^2}{2\mu^2}\right)\right. \\
&\left. - \frac{1}{2\mu^3}(\beta\Lambda - \gamma_1\mu)^2 - \frac{\sigma^2\Lambda^2}{\mu^2} - \frac{(\gamma_2 - \delta)^2}{2(\mu + 2\delta)}\right]I^2.
\end{aligned} \tag{14}$$

Note $(\sigma^2\Lambda^2)/(2\mu^2) < (\alpha + \gamma_1 + \gamma_2 + \mu)(1 - \mathscr{R}_0)$. Then, $\alpha + \gamma_1 + \gamma_2 + \mu - (\beta\Lambda)/\mu - (\sigma^2\Lambda^2)/(2\mu^2) > 0$. Take

$$b > \frac{(1/2\mu^3)(\beta\Lambda - \gamma_1\mu)^2 + \sigma^2\Lambda^2/\mu^2 + (\gamma_2 - \delta)^2/2(\mu + 2\delta)}{2(\mu + \gamma_1 + \gamma_2 + \alpha - (\beta\Lambda/\mu) - (\sigma^2\Lambda^2/2\mu^2))}. \tag{15}$$

This yields that LV_2 is negative-definite. From Lemma 1, E_0 is stochastically asymptotically stable in D. □

Lemma 3. *For any $(S_0, I_0, R_0) \in D$, solution (S, I, R) of (2) satisfies the following:*

(i) If $\sigma^2 > (\beta\mu)/\Lambda$, then

$$\limsup_{t\longrightarrow\infty} \frac{1}{t}\ln\left[I + R + \left(\frac{\Lambda}{\mu} - S\right)\right] \leq \frac{\beta^2 - 2\mu\sigma^2}{2\sigma^2}. \tag{16}$$

(ii) If $\sigma^2 \leq (\beta\mu)/\Lambda$, then

$$\limsup_{t\longrightarrow\infty} \frac{1}{t}\ln\left[I + R + \left(\frac{\Lambda}{\mu} - S\right)\right] \leq \frac{\beta\Lambda}{\mu} - \mu - \frac{\Lambda^2\sigma^2}{2\mu^2}. \tag{17}$$

Proof. Obviously, $(S, I, R) \in D$ for $t \geq 0$. Define

$$V_3(S, I, R) = \ln\left[I + R + \left(\frac{\Lambda}{\mu} - S\right)\right]. \tag{18}$$

Then,

$$\begin{aligned} \mathrm{LV}_3 &= \frac{-\Lambda + 2\beta S f(I) + \mu S - \gamma_1 I - \delta R - (\mu + \alpha + \gamma_1 + \gamma_2) I - (\delta + \mu) R + \gamma_2 I}{I + R + ((\Lambda/\mu) - S)} - 2\left[\frac{\sigma S f(I)}{I + R + ((\Lambda/\mu) - S)}\right]^2 \\ &= \frac{2\beta S f(I)}{I + R + ((\Lambda/\mu) - S)} + \frac{-\gamma_1 I - \delta R - (\gamma_1 + \alpha) I - \delta R}{I + R + ((\Lambda/\mu) - S)} - \mu - 2\sigma^2\left[\frac{S f(I)}{R + I + ((\Lambda/\mu) - S)}\right]^2 \\ &\leq -\mu - 2\sigma^2\left[\frac{S f(I)}{R + I + ((\Lambda/\mu) - S)}\right]^2 + \frac{2\beta S f(I)}{I + R + ((\Lambda/\mu) - S)}. \end{aligned} \tag{19}$$

Let $Z = (S f(I))/(I + R + (\Lambda/(\mu - S)))$ and $\Psi(Z) = -2\sigma^2 Z^2 + 2\beta Z - \mu$. From $S + I + R \leq \Lambda/\mu$ and (3),

$$Z \leq \frac{SI}{I + R + ((\Lambda/\mu) - S)} \leq \frac{SI}{2(I + R)} \leq \frac{S}{2} \leq \frac{\Lambda}{2\mu}. \tag{20}$$

Let $r_0 = \sup_{Z\in(0,\Lambda/(2\mu))}\Psi(Z)$. Then,

$$\begin{aligned} \mathrm{d}V_3 &= \mathrm{LV}_3\mathrm{d}t + \frac{2\sigma S f(I)}{I + R + ((\Lambda/\mu) - S)}\mathrm{d}B(t) \leq \Psi(Z)\mathrm{d}t \\ &\quad + 2\sigma Z\mathrm{d}B(t) \leq r_0\mathrm{d}t + 2\sigma Z\mathrm{d}B(t), \end{aligned} \tag{21}$$

which yields

$$\begin{aligned} \ln\left[I(t) + R(t) + \left(\frac{\Lambda}{\mu} - S(t)\right)\right] &\leq \ln\left[I_0 + R_0 + \left(\frac{\Lambda}{\mu} - S_0\right)\right] \\ &\quad + r_0 t + \int_0^t 2\sigma Z(s)\mathrm{d}B(s). \end{aligned} \tag{22}$$

From the strong law of large numbers,

$$\lim_{t\longrightarrow\infty} \frac{1}{t}\int_0^t 2\sigma Z(s)\mathrm{d}B(s) = 0 \; a.s. \tag{23}$$

Then,

$$\limsup_{t\longrightarrow\infty} \frac{1}{t}\ln\left[R(t) + I(t) + \left(\frac{\Lambda}{\mu} - S(t)\right)\right] \leq r_0. \tag{24}$$

Obviously, if $\sigma^2 > (\beta\mu)/\Lambda$, then $r_0 = \Psi(\beta/(2\sigma^2)) = (\beta^2 - 2\mu\sigma^2)/(2\sigma^2)$; if $\sigma^2 \leq (\beta\mu)/\Lambda$, then $r_0 = \Psi(\Lambda/(2\mu)) = (\beta\Lambda)/\mu - \mu - (\Lambda^2\sigma^2)/(2\mu^2)$. Lemma 3 holds.

By Lemma 3, the following result holds. □

Theorem 2. *Assume that*

(i) $\sigma^2 > \max\{(\beta\mu)/\Lambda, \beta^2/(2\mu)\}$
or
(ii) $2\beta(\mu/\Lambda)(1 - \mu^2/(\beta\Lambda)) < \sigma^2 \leq (\beta\mu)/\Lambda$.

Then, disease-free equilibrium E_0 of (2) is almost surely exponentially stable in D.

Remark 1

(i) If $\mathscr{R}_0 < 1$ and $\sigma^2 = 0$, then $(\sigma^2\Lambda^2)/(2\mu^2) < (\mu + \gamma_1 + \gamma_2 + \alpha)(1 - \mathscr{R}_0)$ holds. From Theorem 1, if $\mathscr{R}_0 < 1$, then disease-free equilibrium E_0 of (1) is asymptotically stable in D. Hence, Theorem 1 extends Theorem 2.1 in [15].

(ii) From Theorem 2, if $\mathscr{R}_0 < 1, \beta\Lambda < \mu^2$, then disease-free equilibrium E_0 of (1) is exponentially stable in D. Hence, Theorem 2 partially improves Theorem 2.1 in [15].

(iii) From Theorem 1, if $\gamma_1 > (\sigma^2\Lambda^2)/(2\mu^2) + \beta(\Lambda/\mu) - \mu - \gamma_2 - \alpha$, then disease-free equilibrium E_0 of (2) is stochastically asymptotically stable in D.

Remark 2

(i) Assume that $((2\beta\mu)/\Lambda)[1 - \mu(\mu + \gamma_1 + \gamma_2 + \alpha)/(\Lambda\beta)] > \beta^2/(2\mu)$ and $\mathscr{R}_0 > 2$. From condition *(i)* in Theorem 2, if $\sigma^2 > \max\{(\beta\mu)/\Lambda, \beta^2/(2\mu)\} = \beta^2/(2\mu)$, then disease-free equilibrium E_0 of (2) is almost surely exponentially stable in D. However, Theorem 2 in [26] implies that disease of (2) will become extinct if (C_3) of Theorem 2 in [26] holds, i.e., $\sigma^2 > \max\{((\beta\mu)/\Lambda)\cdot(\mathscr{R}_0/2), ((2\beta\mu)/\Lambda)(1 - \mu(\mu + \gamma_1 + \gamma_2 + \alpha)/(\Lambda\beta))\}$.

(ii) Assume that $\beta^2/(2\mu) < (\beta\mu)/\Lambda < ((2\beta\mu)/\Lambda)(1-\mu(\gamma_1+\gamma_2+\alpha+\mu)/(\Lambda\beta))$ and $\mathscr{R}_0 < 2$. From Theorem 2 (i), E_0 is almost surely exponentially stable in D if $\sigma^2 > \max\{(\beta\mu)/\Lambda, \beta^2/(2\mu)\} = (\beta\mu)/\Lambda$, whereas disease will become extinct with probability one if $\sigma^2 > \max\{(\beta\mu)/\Lambda, ((2\beta\mu)/\Lambda)(1-\mu(\mu+\gamma_1+\gamma_2+\alpha)/(\Lambda\beta))\}$ in [26].

Obviously, condition (i) of Theorem 2 is weaker than condition (C_3) of Theorem 2 in [26].

Remark 3. Let $\beta^2/(2(\gamma_1+\gamma_2+\mu+\alpha)) > ((2\beta\mu)/\Lambda)(1-\mu^2/(\beta\Lambda))$. By Theorem 2, E_0 is almost surely exponentially stable in D if condition (ii) holds. However, disease will become extinct if $\max\{\beta^2/(2(\gamma_1+\gamma_2+\mu+\alpha)), ((2\beta\mu)/\Lambda)(1-\mu(\gamma_1+\gamma_2+\mu+\alpha)/(\Lambda\beta))\} < \sigma^2 < (\beta\mu)/\Lambda$ in [26]. Thus, condition (ii) of Theorem 2 is weaker than condition (C_2) of Theorem 2 in [26].

Remark 4. From Remarks 2 and 3, Theorem 2 partially improves Theorem 2 in [26].

4. Asymptotic Properties around Endemic Equilibrium

In studying epidemic dynamics, we have interest in persistence of epidemic. We consider the behavior of solutions to (2) around endemic equilibrium $E^*(S^*, I^*, R^*)$ of corresponding deterministic model (1). Denote

$$a_1 = \frac{\alpha}{\gamma_2},$$
$$a_2 = \frac{[2\mu(2\mu+\gamma_2+\alpha)+2\mu\delta+\alpha\delta]I^*}{\beta\delta f(I^*)}, \tag{25}$$
$$a_3 = \frac{2\mu}{\delta}.$$

Theorem 3. *If $\mathscr{R}_0 > 1$ and $\sigma^2 < \mu(a_3+1)/(a_2 I^*)$, then*

$$\limsup_{t\longrightarrow\infty} \frac{1}{t}\mathbb{E}\int_0^t \left[\eta_1(S-S^*)^2 + \eta_2(I-I^*)^2 + \eta_3(R-R^*)^2\right]ds \leq a_2 I^*(S^*)^2\sigma^2, \tag{26}$$

where (S, I, R) be the solution of (2) with $(S_0, I_0, R_0) \in \mathbb{R}^3_+$ and

$$\eta_1 = (a_3+1)\mu - a_2 I^*\sigma^2,$$
$$\eta_2 = a_3(\mu+\gamma_2+\alpha) + \mu + \alpha, \tag{27}$$
$$\eta_3 = a_1(\mu+\delta) + \mu.$$

Proof. Define $V_4 : \mathbb{R}^3_+ \longrightarrow \mathbb{R}_+$ by

$$V_4(S, I, R) = a_1 W_1(R) + a_2 W_2(I) + a_3 W_3(S, I) + W_4(S, I, R), \tag{28}$$

where

$$W_1(R) = \frac{1}{2}(R-R^*)^2,$$
$$W_2(I) = I - I^* - I^*\ln\left(\frac{I}{I^*}\right),$$
$$W_3(S, I) = \frac{1}{2}(S-S^*+I-I^*)^2, \tag{29}$$
$$W_4(S, I, R) = \frac{1}{2}(S-S^*+R-R^*+I-I^*)^2.$$

From It $\hat{o}$ formula, (3), and (H_2),

$$\begin{aligned} LW_1 &= (R-R^*)[\gamma_2 I - (\mu+\delta)R] \\ &= -(\delta+\mu)(R-R^*)^2 + \gamma_2(I-I^*)(R-R^*), \end{aligned} \tag{30}$$

$$\begin{aligned} LW_2 &= (I-I^*)\left[-(\gamma_1+\gamma_2\mu+\alpha) + \beta S f(I)\frac{1}{I}\right] + \frac{1}{2}I^*\left(\sigma S f(I)\frac{1}{I}\right)^2 \\ &= (I-I^*)\left[\beta(S-S^*)f(I^*)\frac{1}{I^*} + \beta S\left(f(I)\frac{1}{I} - f(I^*)\frac{1}{I^*}\right)\right] + \frac{1}{2}I^*\sigma^2 S^2\left(f(I)\frac{1}{I}\right)^2 \\ &\leq \beta(I-I^*)(S-S^*)f(I^*)\frac{1}{I^*} + \beta S(I-I^*)\left(f(I)\frac{1}{I} - f(I^*)\frac{1}{I^*}\right) + \sigma^2 I^*(S-S^*)^2 \\ &\quad + \sigma^2 I^*(S^*)^2 \leq \beta(I-I^*)(S-S^*)f(I^*)\frac{1}{I^*} \\ &\quad + \sigma^2 I^*(S-S^*)^2 + \sigma^2 I^*(S^*)^2, \end{aligned} \tag{31}$$

$$\begin{aligned} LW_3 &= (S-S^*+I-I^*)[\Lambda + \delta R - \mu S - (\gamma_2+\mu+\alpha)I] \\ &= (S-S^*+I-I^*)[-\mu(S-S^*) \\ &\quad + \delta(R-R^*) - (\gamma_2+\mu+\alpha)(I-I^*)] \\ &= -\mu(S-S^*)^2 - (\gamma_2+\alpha+2\mu)(S-S^*)(I-I^*) \\ &\quad - (\gamma_2+\alpha+\mu)(I-I^*)^2 + \delta(R-R^*)[(S-S^*)+(I-I^*)], \end{aligned} \tag{32}$$

$$\begin{aligned} LW_4 &= [R+I+S-(R^*+I^*+S^*)][\Lambda - \mu S - (\mu+\alpha)I - \mu R] \\ &= (R-R^*+S-S^*+I-I^*)[-\mu(S-S^*) - \mu(R-R^*) \\ &\quad - (\alpha+\mu)(I-I^*)] \\ &= -\mu(R-R^*)^2 - \mu(S-S^*)^2 - (\alpha+\mu)(I-I^*)^2 \\ &\quad - (\alpha+2\mu)(I-I^*)(S-S^*) \quad - 2\mu(R-R^*)(S-S^*) \\ &\quad - (\alpha+2\mu)(R-R^*)(I-I^*). \end{aligned} \tag{33}$$

From (25)–(33),

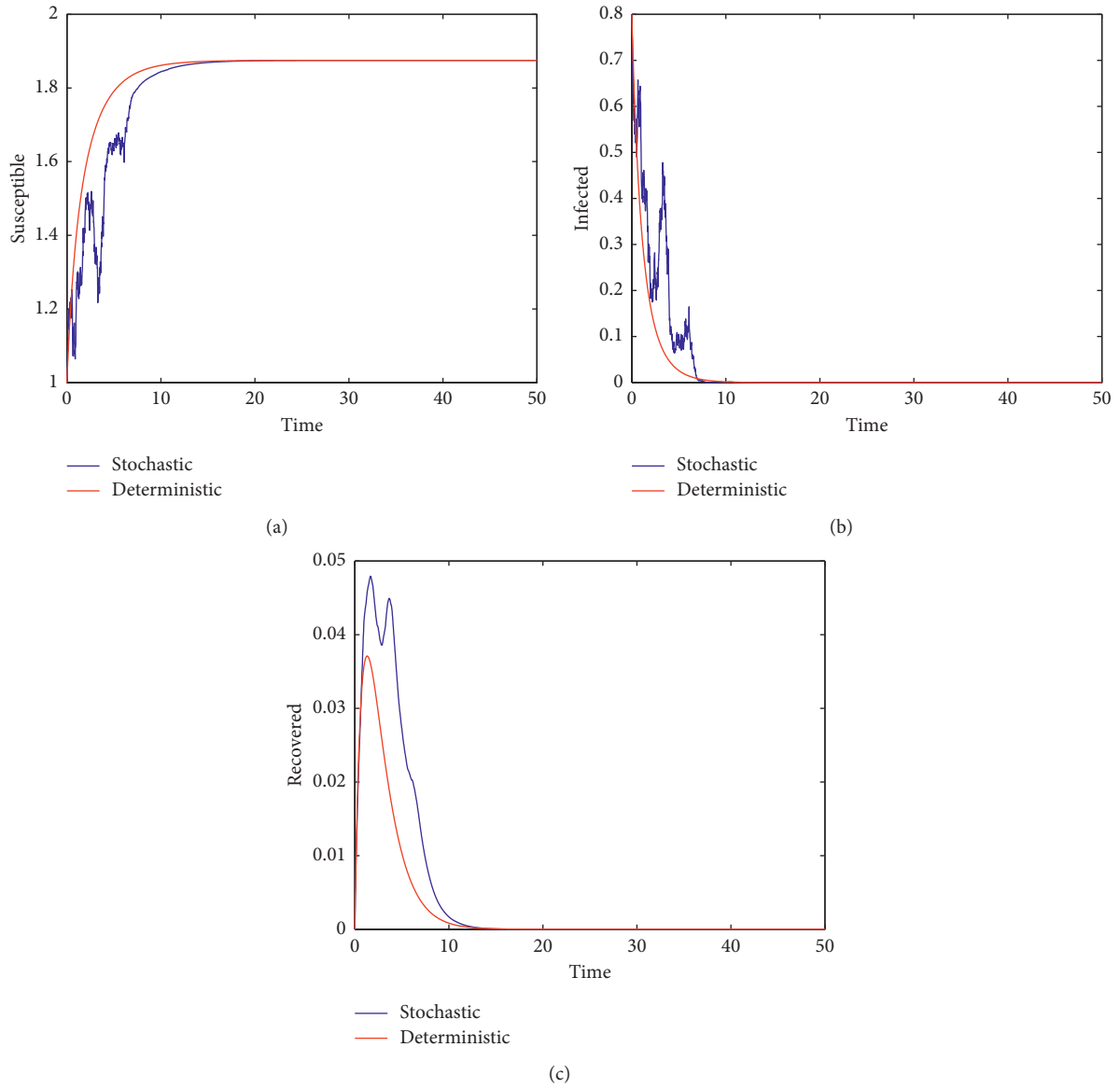

Figure 1: Trajectories of deterministic model (1) and stochastic model (2) with (a) $\beta = 0.3$, (b) $\gamma_1 = 0.57$, and (c) $\sigma^2 = 0.2$.

$$
\begin{aligned}
\mathrm{LV}_4 \le\ & a_1\gamma_2\left(R-R^*\right)\left(I-I^*\right) - a_1\left(\delta+\mu\right)\left(R-R^*\right)^2 + \frac{a_2\beta f\left(I^*\right)}{I^*}\left(S-S^*\right)\left(I-I^*\right) + a_2 I^*\sigma^2\left(S-S^*\right)^2 \\
& + a_2 I^*\sigma^2\left(S^*\right)^2 - a_3\mu\left(S-S^*\right)^2 - a_3\left(2\mu+\alpha+\gamma_2\right)\left(I-I^*\right)\left(S-S^*\right) - a_3\left(\mu+\alpha+\gamma_2\right)\left(I-I^*\right)^2 \\
& + a_3\delta\left(S-S^*\right)\left(R-R^*\right) + a_3\delta\left(R-R^*\right)\left(I-I^*\right) - \mu\left(S-S^*\right)^2 - \mu\left(R-R^*\right)^2 \\
& - \left(\alpha+\mu\right)\left(I-I^*\right)^2 - \left(\alpha+2\mu\right)\left(I-I^*\right)\left(S-S^*\right) \\
& - 2\mu\left(R-R^*\right)\left(S-S^*\right) - \left(\alpha+2\mu\right)\left(R-R^*\right)\left(I-I^*\right) \\
=\ & -\left(a_3\mu+\mu-a_2 I^*\sigma^2\right)\left(S-S^*\right)^2 - \left[\mu+\alpha+a_3\left(\gamma_2+\alpha+\mu\right)\right]\left(I-I^*\right)^2 \\
& - \left[\mu+a_1\left(\delta+\mu\right)\right]\left(R-R^*\right)^2 + a_2 I^*\left(S^*\right)^2\sigma^2 \\
=\ & -\eta_1\left(S-S^*\right)^2 - \eta_2\left(I-I^*\right)^2 - \eta_3\left(R-R^*\right)^2 + a_2 I^*\left(S^*\right)^2\sigma^2.
\end{aligned}
\tag{34}
$$

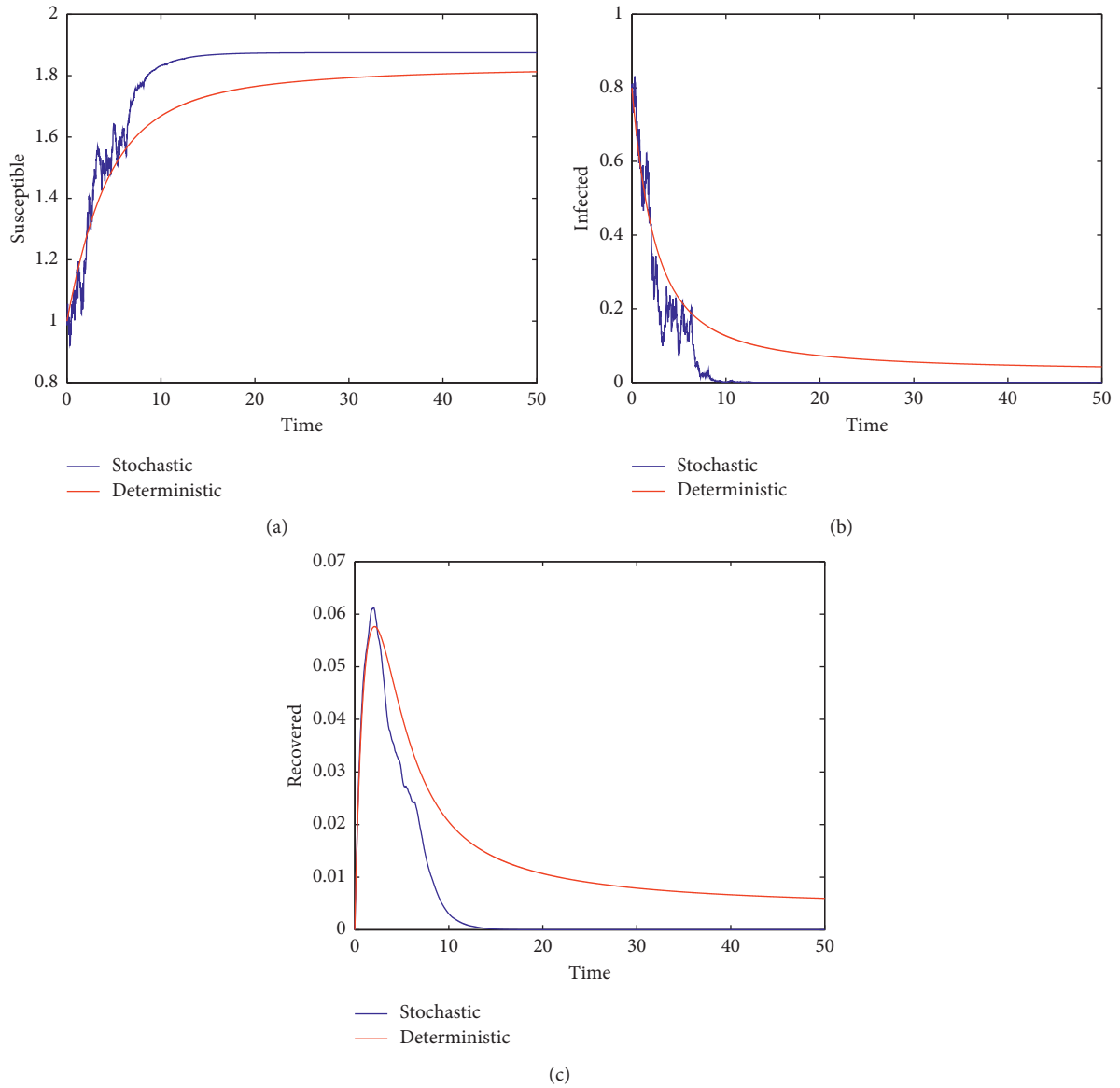

Figure 2: Trajectories of deterministic SIRS model (1) and stochastic SIRS model (2) with (a) $\beta = 0.3$, (b) $\gamma_1 = 0.01$, and (c) $\sigma^2 = 0.3$.

Hence, we have

$$\begin{aligned} dV(S,I,R) \le & \left[a_2 I^* (S^*)^2 \sigma^2 - \eta_1 (S - S^*)^2 - \eta_2 (I - I^*)^2 \right. \\ & \left. - \eta_3 (R - R^*)^2\right] dt + \sigma S (I - I^*) f(I) \frac{1}{I} dB(t). \end{aligned} \tag{35}$$

It follows from (35) that

$$\begin{aligned} & V(S(t), I(t), R(t)) - V(S_0, I_0, R_0) \\ & \le \int_0^t \left[-\eta_2 (I(s) - I^*)^2 - \eta_1 (S(s) - S^*)^2 \right. \\ & \quad \left. - \eta_3 (R(s) - R^*)^2\right] ds \\ & \quad + a_2 I^* (S^*)^2 \sigma^2 t + \int_0^t \sigma \frac{f(I(s))}{I(s)} S(s) (I(s) - I^*) dB(s). \end{aligned} \tag{36}$$

From (36),

$$\begin{aligned} & \mathbb{E} V(S(t), I(t), R(t)) - \mathbb{E} V(S_0, I_0, R_0) \\ & \le \mathbb{E} \int_0^t \left[-\eta_2 (I(s) - I^*)^2 - \eta_1 (S(s) - S^*)^2 \right. \\ & \quad \left. - \eta_3 (R(s) - R^*)^2\right] ds + a_2 I^* (S^*)^2 \sigma^2 t. \end{aligned} \tag{37}$$

Consequently,

$$\begin{aligned} & \limsup_{t \longrightarrow \infty} \frac{1}{t} \mathbb{E} \int_0^t \left[\eta_1 (S(s) - S^*)^2 + \eta_2 (I(s) - I^*)^2 \right. \\ & \quad \left. + \eta_3 (R(s) - R^*)^2\right] ds \le a_2 I^* (S^*)^2 \sigma^2. \end{aligned} \tag{38}$$

□

Remark 5. Theorem 3 shows that if $\mathcal{R}_0 > 1$, σ is small enough and then solution to (2) fluctuates around E^*; that is, disease will persist. Furthermore, if $\sigma = 0$, then (34) becomes

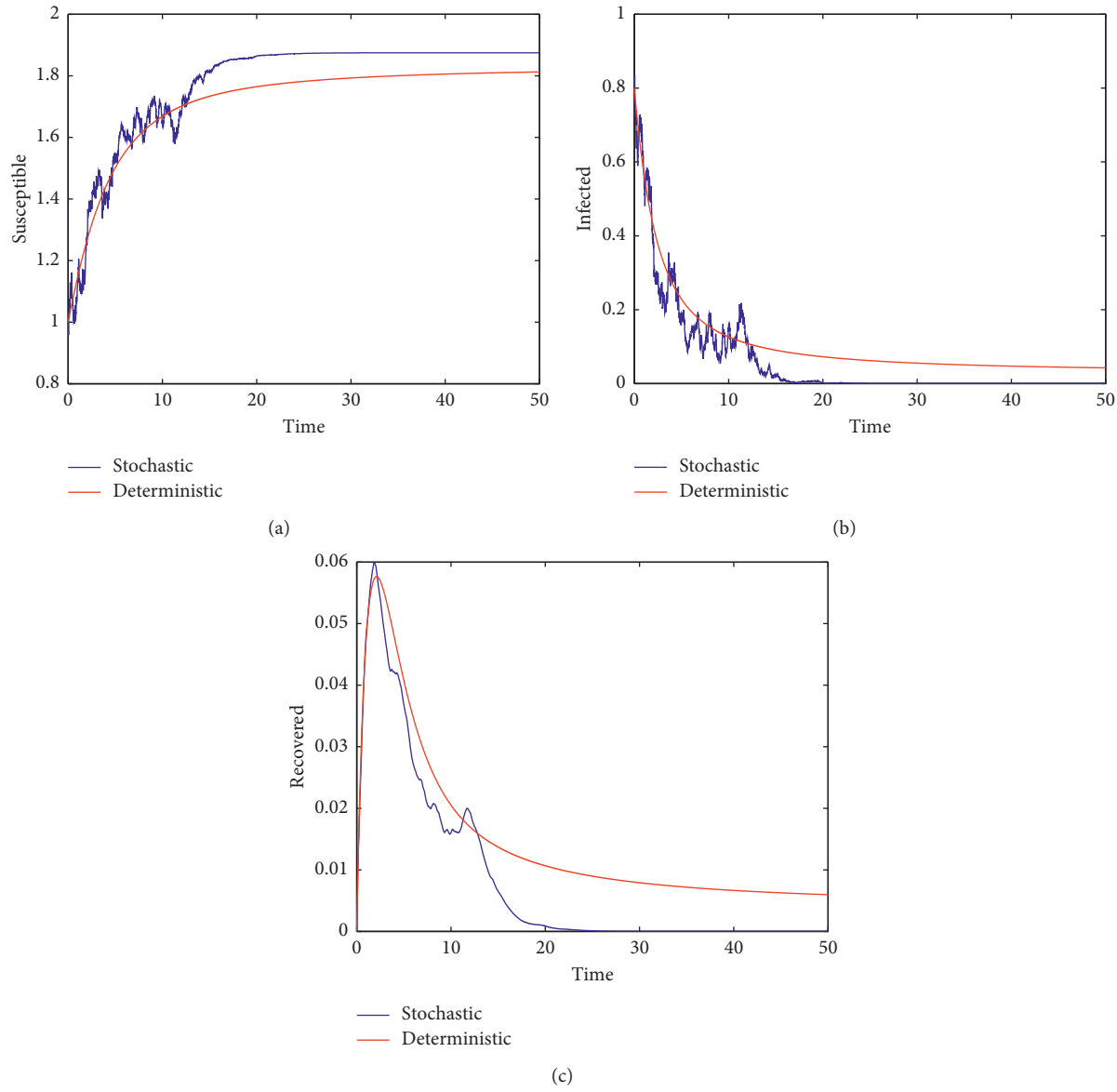

FIGURE 3: Trajectories of deterministic SIRS model (1) and stochastic SIRS model (2) with (a) $\beta = 0.3$, (b) $\gamma_1 = 0.01$, and (c) $\sigma^2 = 0.15$.

$$\mathrm{LV}_4 \leq -\eta_1 (S - S^*)^2 - \eta_2 (I - I^*)^2 - \eta_3 (R - R^*)^2, \quad (39)$$

which yields that for (1), E^* is globally asymptotically stable in $\mathbb{R}^3_+$. This is consistent with Corollary 2.3 in [15]. Hence, Theorem 3 generalizes Corollary 2.3 in [15].

5. Numerical Simulations

By numerical simulation, we analyze the asymptotic behavior of model (2) so that readers can better understand our results. Let $f(I) = I/(1 + I)$. Then, $I \geq f(I)$ for $I \geq 0$. Let

$$\Lambda = 0.6,\ \mu = 0.32,\ \gamma_2 = 0.1,\ \alpha = 0.1,\ \delta = 0.4,$$
$$(S_0, I_0, R_0) = (1, 0.8, 0). \quad (40)$$

Example 1. Take $\beta = 0.3, \gamma_1 = 0.57$, and $\sigma^2 = 0.2$. By a simple computation, we obtain $\mathscr{R}_0 \approx 0.516 < 1$, $0.352 \approx (\sigma^2\Lambda^2)/(2\mu^2) < (\mu + \gamma_1 + \gamma_2 + \alpha)(1 - \mathscr{R}_0) \approx 0.5276$, $\beta\Lambda - \gamma_1\mu = -0.0024 < 0$, and $\gamma_2 - \delta = -0.3 < 0$. Hence, the conditions of Theorem 1 hold. Furthermore, for (2), $E_0(1.875, 0, 0)$ is stochastically asymptotically stable. Figure 1 supports the result.

Example 2. Take $\beta = 0.3, \gamma_1 = 0.01$, and $\sigma^2 = 0.3$. Hence, $\mathscr{R}_0 \approx 1.0613 > 1$ and $\max\{(\beta\mu)/\Lambda, \beta^2/(2\mu)\} = 0.16 < \sigma^2$. Then, according to conclusion (i) in Theorem 2, solutions of (2) will tend almost surely exponentially to $E_0(1.875, 0, 0)$. However, from Corollary 2.3 in [15], the solution of deterministic model (1) will converge to $E^*(1.8261, 0.0337, 0.0047)$. This demonstrates that noises

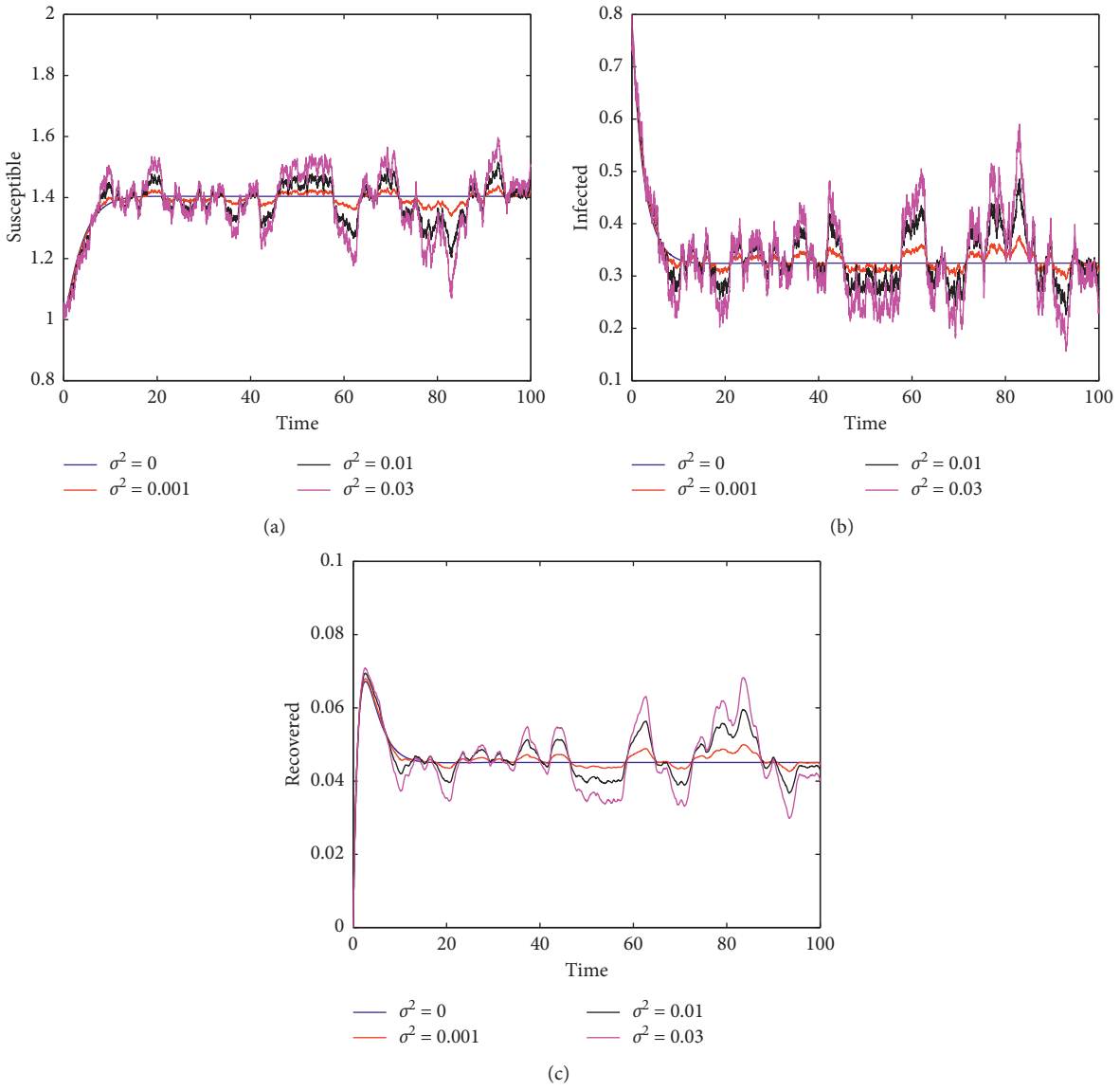

FIGURE 4: Trajectories of deterministic SIRS model (1) and stochastic SIRS model (2) for different σ^2 with $\beta = 0.5$ and $\gamma_1 = 0.01$.

can result in extinction of disease. Figure 2 clearly supports these results.

Example 3. Let $\beta = 0.3, \gamma_1 = 0.01$, and $\sigma^2 = 0.15$ such that $\mathcal{R}_0 \approx 1.0613 > 1$ and $(2\beta\mu/\Lambda)(1 - \mu^2/(\beta\Lambda)) \approx 0.1380 < \sigma^2 < (\beta\mu)/\Lambda = 0.16$. Then, according to conclusion (ii) in Theorem 2, solutions of (2) will tend almost surely exponentially to $E_0(1.875, 0, 0)$. However, from Corollary 2.3 in [15], endemic equilibrium $E^*(1.8261, 0.0337, 0.0047)$ of (1) is globally asymptotically stable in $\mathbb{R}^3_+$. This represents the extinction of disease due to noise. Figure 3 clearly supports these results.

Example 4. Take $\beta = 0.5, \gamma_1 = 0.01$. Then, $\mathcal{R}_0 \approx 1.7689 > 1$ and $\sigma^2 < \mu(a_3 + 1)/(a_2 I^*) \approx 0.4644$. By Theorem 3, solutions of (2) fluctuate around endemic equilibrium $E^*(1.404, 0.3245, 0.0451)$ of deterministic model (1) in time average, which can be verified by using Figure 4. In addition, Figure 4 shows that the fluctuation increases with increase in σ^2.

Example 5. Take $\gamma_1 = 0.01$. Figure 5 plots the average in time of infected $(1/t)\int_0^t I(s)ds$ for different β in (a) and (b), respectively. From Figure 5, the smaller the β is, the smaller the number of infected cases is. In addition, when β tends to 0, the number of infected cases will tend to 0. This result can also be derived from Theorem 2.

Example 6. Take $\beta = 0.5$. Figure 6 plots the average in time of infected $(1/t)\int_0^t I(s)ds$ for different γ_1 in (a) and (b), respectively. Figure 6 shows that the larger the γ_1 is, the

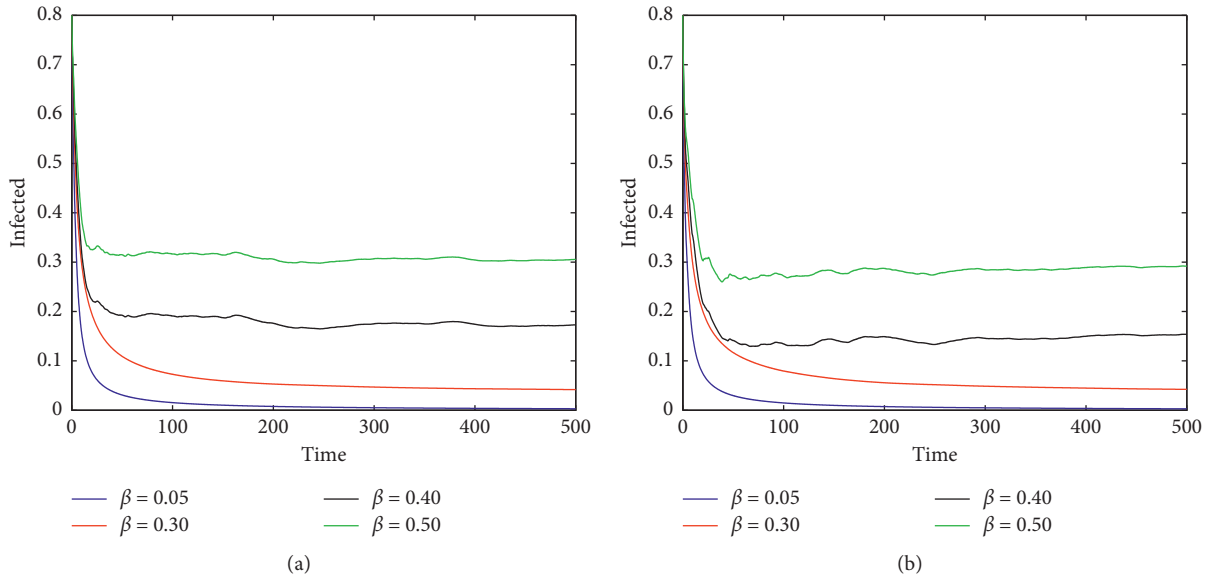

FIGURE 5: Trajectories of the average in time of infected $(1/t)\int_0^t I(s)ds$ for stochastic SIRS model (2) for different β with $\gamma_1 = 0.01$. (a) $\sigma^2 = 0.02$. (b) $\sigma^2 = 0.04$.

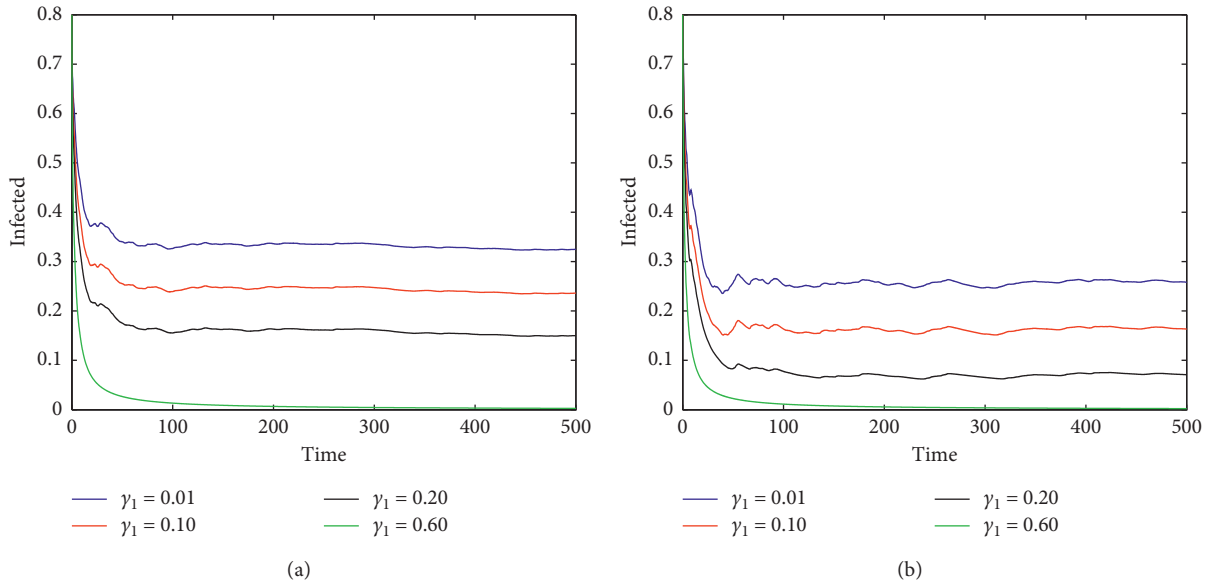

FIGURE 6: Trajectories of the average in time of infected $(1/t)\int_0^t I(s)ds$ for stochastic SIRS model (2) for different γ_1 with $\beta = 0.5$. (a) $\sigma^2 = 0.02$. (b) $\sigma^2 = 0.1$.

smaller the number of infected cases is. Furthermore, when γ_1 is sufficiently large, the number of infected cases tends to 0. This result can be derived from Remark 1 (iii).

Example 7. Take $\beta = 0.3$. Figure 7 plots the number of infected cases for different σ^2 in (a) and (b), where $\gamma_1 = 0.01$ and $\mathcal{R}_0 \approx 1.0613 > 1$ in (a) and $\gamma_1 = 0.02$ and $\mathcal{R}_0 \approx 1.0417 > 1$ in (b). From Corollary 2.3 in [15], endemic equilibrium of deterministic model (1) is globally asymptotically stable in $\mathbb{R}^3_+$. Figure 7 shows that σ^2 has a significant effect on both extinction and persistence of disease.

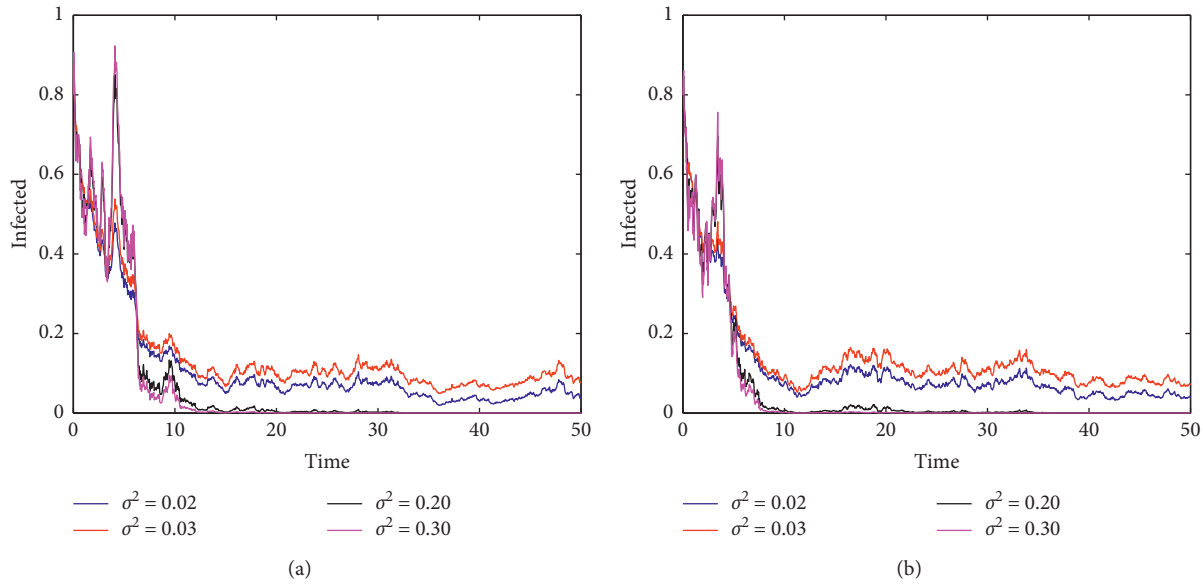

Figure 7: Trajectories of infected of stochastic SIRS model (2) for different σ^2 with $\beta = 0.3$. (a) $\gamma_1 = 0.01$. (b) $\gamma_1 = 0.02$.

6. Conclusions

Stability is one of the important topics encountered in applications. However, because of the complexity of stochastic dynamics, there are not many results on stability analysis of stochastic differential equations.

Based on this, we investigate stochastic stability of a stochastic SIRS model. To begin with, using stochastic stability theory, we study stochastic asymptotic stability of disease-free equilibrium of (2), which generalizes Theorem 2.1 in [15]. Moreover, if the transfer rate from infectious to susceptible is sufficiently large, disease goes extinct. Then, exponential stability of disease-free equilibrium is obtained. This result partially improves Theorem 2.1 in [15] and Theorem 2 in [26] and demonstrates that noises can result in extinction of the disease. Furthermore, by the Lyapunov method, we give conditions to ensure that solution of (2) fluctuates around endemic equilibrium of (1) in time average. This generalizes Corollary 2.3 in [15]. At last, numerical simulations are presented to confirm theoretical results and find new properties.

Figure 4 shows that if $\mathscr{R}_0 > 1$ and $\sigma^2 < \mu(a_3 + 1)/(a_2 I^*)$, then the solution of (2) fluctuates around endemic equilibrium of (1). Moreover, Figure 4 also shows that the fluctuation increases with increase in noise intensity. From Figure 5, the smaller the β is, the smaller the number of infected individuals will be. In addition, when β tends to 0, the number of infected individuals will tend to 0. This result can also be derived from Theorem 2. Figure 6 shows that the larger the γ_1 is, the smaller the number of infected will be. Furthermore, when γ_1 is sufficiently large, the number of infected tends to 0. This result can be derived from Remark 1 (iii). Figure 7 shows that noise intensity has a significant effect on both extinction and persistence of the disease. Hence, noises play a vital role in epidemic transmission.

For deterministic SIRS model (1), $\mathscr{R}_0$ is the basic reproduction number. However, for stochastic SIRS model (2), $\mathscr{R}_0$ is not a threshold parameter. From Theorem 2, no matter what the value of $\mathscr{R}_0$ is, the disease could go extinct. This can also be verified by the examples in this paper.

Although there are important findings revealed by the above investigation, the results still have some limitations. One may consider stochastic asymptotic stability in $\mathbb{R}^3_+$. In addition, our numerical simulation results show that the disease goes extinct as long as $\mathscr{R}_0 < 1$. Regrettably, our theoretical results do not lead to this conclusion.

Data Availability

No data were used to support this study.

Conflicts of Interest

The authors declare that they have no conflicts of interest.

Authors' Contributions

All the authors contributed equally and significantly in writing this paper. All authors read and approved the final manuscript.

Acknowledgments

This work was supported by the National Natural Science Foundation of China (No. 11971279).

References

[1] R. Liu and G. Liu, "Asymptotic behavior of a stochastict two species competition model under the effect of disease," *Complexity*, vol. 2018, Article ID 3127404, 15 pages, 2018.

[2] Q. Zhang, X. Wen, D. Jiang, and Z. Liu, "The stability of a predator-prey system with linear mass-action functional response perturbed by white noise," *Advances in Difference Equations*, vol. 2016, 2016.

[3] R. Liu and G. Liu, "Analysis on stochastic food-web model with intraguild predation and mixed functional responses," *Physica A*, vol. 531, Article ID 121782, 2019.

[4] C. C. McCluskey, "Complete global stability for an SIR epidemic model with delay-distributed or discrete," *Nonlinear Analysis: Real World Applications*, vol. 11, no. 1, pp. 55–59, 2010.

[5] A. Lahrouz, L. Omari, D. Kiouach, and A. Belmaâti, "Complete global stability for an SIRS epidemic model with generalized non-linear incidence and vaccination," *Applied Mathematics and Computation*, vol. 218, no. 11, pp. 6519–6525, 2012.

[6] M. Y. Li, J. R. Graef, L. Wang, and J. Karsai, "Global dynamics of a SEIR model with varying total population size," *Mathematical Biosciences*, vol. 160, no. 2, pp. 191–213, 1999.

[7] Y. Muroya, Y. Enatsu, and Y. Nakata, "Global stability of a delayed SIRS epidemic model with a non-monotonic incidence rate," *Journal of Mathematical Analysis and Applications*, vol. 377, no. 1, pp. 1–14, 2011.

[8] W. Ma, M. Song, and Y. Takeuchi, "Global stability of an SIR epidemicmodel with time delay," *Applied Mathematics Letters*, vol. 17, no. 10, pp. 1141–1145, 2004.

[9] Windarto, M. A. Khan, M. Altaf Khan, and A. Fatmawati, "Parameter estimation and fractional derivatives of dengue transmission model," *AIMS Mathematics*, vol. 5, no. 3, pp. 2758–2779, 2020.

[10] M. A. Khan and A. Atangana, "Modeling the dynamics of novel coronavirus (2019-nCov) with fractional derivative," *Alexandria Engineering Journal*, vol. 34, 2020.

[11] J. Li, Z. Ma, and Z. Ma, "Stability analysis for SIS epidemic models with vaccination and constant population size," *Discrete & Continuous Dynamical Systems-B*, vol. 4, no. 3, pp. 635–642, 2004.

[12] M. A. Khan, S. Ullah, S. Ullah, and M. Farhan, "Fractional order SEIR model with generalized incidence rate," *AIMS Mathematics*, vol. 5, pp. 2843–2857, 2020.

[13] A. Lahrouz, L. Omari, and D. Kiouach, "Global analysis of a deterministic and stochastic nonlinear SIRS epidemic model," *Nonlinear Analysis: Modelling and Control*, vol. 16, no. 1, pp. 59–76, 2011.

[14] Q. Liu and Q. Chen, "Analysis of the deterministic and stochastic SIRS epidemic models with nonlinear incidence," *Physica A: Statistical Mechanics and its Applications*, vol. 428, pp. 140–153, 2015.

[15] T. Li, F. Zhang, H. Liu, and Y. Chen, "Threshold dynamics of an SIRS model with nonlinear incidence rate and transfer from infectious to susceptible," *Applied Mathematics Letters*, vol. 70, pp. 52–57, 2017.

[16] Q. Liu, D. Jiang, N. Shi, T. Hayat, and A. Alsaedi, "Stationary distribution and extinction of a stochastic SIRS epidemic model with standard incidence," *Physica A: Statistical Mechanics and its Applications*, vol. 469, pp. 510–517, 2017.

[17] Z. Chang, X. Meng, and X. Lu, "Analysis of a novel stochastic SIRS epidemic model with two different saturated incidence rates," *Physica A: Statistical Mechanics and its Applications*, vol. 472, pp. 103–116, 2017.

[18] Y. Cai, Y. Kang, M. Banerjee, and W. Wang, "A stochastic SIRS epidemic model with infectious force under intervention strategies," *Journal of Differential Equations*, vol. 259, no. 12, pp. 7463–7502, 2015.

[19] H. Qi, L. Liu, and X. Meng, "Dynamics of a nonautonomous stochastic SIS epidemic model with double epidemic hypothesis," *Complexity*, vol. 2017, Article ID 4861391, 2017.

[20] Y. Lin and D. Jiang, "Threshold behavior in a stochastic SIS epidemic model with standard incidence," *Journal of Dynamics and Differential Equations*, vol. 26, no. 4, pp. 1079–1094, 2014.

[21] D. Jiang, J. Yu, C. Ji, and N. Shi, "Asymptotic behavior of global positive solution to a stochastic SIR model," *Mathematical and Computer Modelling*, vol. 54, no. 1–2, pp. 221–232, 2011.

[22] Y. Zhao and D. Jiang, "The threshold of a stochastic SIRS epidemic model with saturated incidence," *Applied Mathematics Letters*, vol. 34, pp. 90–93, 2014.

[23] A. Lahrouz and A. Settati, "Necessary and sufficient condition for extinction and persistence of SIRS system with random perturbation," *Applied Mathematics and Computation*, vol. 233, pp. 10–19, 2014.

[24] Q. Lu, "Stability of SIRS system with random perturbations," *Physica A: Statistical Mechanics and its Applications*, vol. 388, no. 18, pp. 3677–3686, 2009.

[25] M. EI Fatini, A. Lahrouz, R. Pettersson, A. Settati, and R. Taki, "Stochastic stability and instability of an epidemic model with relapse," *Applied Mathematics and Computation*, vol. 316, pp. 326–341, 2018.

[26] Y. Wang, G. Liu, and G. Liu, "Dynamics analysis of a stochastic SIRS epidemic model with nonlinear incidence rate and transfer from infectious to susceptible," *Mathematical Biosciences and Engineering*, vol. 16, no. 5, pp. 6047–6070, 2019.

[27] Q. Liu and Q. Chen, "Dynamics of a stochastic SIR epidemic model with saturated incidence," *Applied Mathematics and Computation*, vol. 282, pp. 155–166, 2016.

[28] X. Mao, *Stochsatic Differential Equations and Applications*, Horwood, Chichester, UK, 2007.

Hindawi
Complexity
Volume 2020, Article ID 8236060, 16 pages
https://doi.org/10.1155/2020/8236060

Research Article

Position Control of a Maglev System Fed by a DC/DC Buck Power Electronic Converter

Victor Manuel Hernández-Guzmán,[1] **Ramón Silva-Ortigoza**,[2] **and Magdalena Marciano-Melchor**[2]

[1]*Universidad Autónoma de Querétaro, Facultad de Ingeniería, Av. Hidalgo s/n, Centro Universitario, Cerro de Las Campanas, C.P. 76010, Querétaro, Mexico*
[2]*Instituto Politécnico Nacional, CIDETEC, Laboratorio de Mecatrónica & Energía Renovable, C.P. 07700, Ciudad de México, Mexico*

Correspondence should be addressed to Victor Manuel Hernández-Guzmán; vmhg@uaq.mx

Received 4 April 2020; Accepted 11 May 2020; Published 31 May 2020

Guest Editor: Alberto Luviano Juárez

Copyright © 2020 Victor Manuel Hernández-Guzmán et al. This is an open access article distributed under the Creative Commons Attribution License, which permits unrestricted use, distribution, and reproduction in any medium, provided the original work is properly cited.

In this paper, we solve the problem of position regulation in a magnetic levitation system that is fed by a DC/DC Buck power electronic converter as a power amplifier. We present a formal asymptotic stability proof. Although this result is local, the merit of our proposal relies on the fact that this is the first time that such a control problem is solved for a magnetic levitation system, a nonlinear electromechanical plant. In this respect, we stress that most works in the literature on control of electromechanical systems actuated by power electronic converters are devoted to control brushed DC motors which are well known to have a linear model. Furthermore, despite the plant that we control in the present paper is complex, our control law is simple. It is composed by four nested loops driven by one sliding mode controller, two proportional-integral controllers, and a nonlinear proportional-integral-derivative position controller. Each one of these loops is devoted to control each one of the subsystems that compose the plant: electric current through the converter inductor, voltage at the converter capacitor, electric current through the electromagnet, and position of the ball. Thus, our proposal is consistent with the simple and intuitive idea of controlling each subsystem of the plant in order to render robust the control scheme. We stress that such a solution is complicated to derive using other control approaches such as differential flatness or backstepping. In this respect, our proposal relies on a novel passivity-based approach which, by exploiting the natural energy exchange between the mechanical and electrical dynamics, renders possible the design of a control scheme with the above cited features.

1. Introduction

One common technique that is used to supply power to electromechanical systems is pulse width modulation (PWM). However, the hard commutation that is intrinsic to PWM stresses the electromechanical system inducing abrupt changes in its dynamics which are observed as sudden variations in voltages and electric currents [1]. One manner to avoid this situation is the employment of DC/DC power electronic converters. Since these devices have embedded capacitors and inductors, they provide smooth voltages and electric currents, diminishing the effects of hard commutation in PWM-based power amplifiers.

The mathematical models of some DC/DC power electronic converter-DC motor systems were proposed for the first time in [2]. Since then, many works have been reported on control of several DC/DC power electronic converter topologies and DC motors [3–12]. Among the proposed control techniques are differential flatness, proportional-integral (PI) control, generalized PI control, passivity, adaptive control, PI fuzzy control, LQR (linear-quadratic regulator) control, backstepping, and hierarchical control. The control problems that have been solved are unidirectional velocity regulation and tracking, velocity and torque control focusing on electrical transients, smooth velocity starters, and active disturbance rejection. In recent

works [13–15], the introduction of an inverter between the DC/DC power electronic converter and the DC motor has rendered possible the bidirectional control of velocity.

The approach in [16], to control the DC/DC Buck power electronic converter-DC motor system, was inspired in part by [17–19]. Control scheme in [16] has the advantage of including a PI loop to control voltage at converter capacitor, a PI loop to control motor armature's current, and an external PI loop to regulate motor velocity. Hence, the main components of the successful strategies employed in industry to control electromechanical systems are included in the proposal of [16]. Moreover, another internal loop is devoted to control electric current through converter inductance. This loop is driven by a sliding mode control, a common strategy for control of power electronic converters in practice. The approach is proven in experiments to be robust with respect to parametric uncertainties and external disturbances.

On the contrary, magnetic levitation systems are commonly used as benchmark problems to test novel control approaches. Among the proposed control techniques, the passivity-based approaches presented in [20–22] have been welcomed in the control community. In particular, the solution presented in [20] is interesting because it possesses a classical proportional-integral-derivative (PID) controller to cope with the mechanical part of the system. However, since the design is performed in terms of magnetic flux, instead of electric current, efforts are oriented to avoid the implementation of any internal loop to cope with the electrical dynamics. This is because of the complications arising from magnetic flux measurements. In this respect, we stress that experimental results have been reported in the literature showing that such internal loop is necessary to improve performance in practice, see [23], for instance.

The novel control technique known as immersion and invariance (I&I) has been employed in [24, 25] to control magnetic levitation systems. Novelty in those applications is that a (small) parasitic capacitance is considered to be present at terminals of the electromagnet. The main target to use I&I in such a control problem is to extend the application of any control law, say w, that has been designed when such a parasitic capacitor is not present. However, since this requires to feedback the time derivative of w, the online computation of an important number of additional complex terms are required.

In the present paper, we extend the work in [16] to control the ball position in a magnetic levitation system which is fed by a DC/DC Buck power electronic converter. This implies that additional inductance and capacitance with considerable values are included in the electrical circuitry of the magnetic levitation system. Since a magnetic levitation system only requires unipolar voltage, such a power converter topology is adequate and any inverter is not required. We stress that a magnetic levitation system is a complex and nonlinear system. Hence, controlling for the first time and from a theoretical point of view, a plant with these features when it is fed by a DC/DC Buck power electronic converter represents one important contribution of the present paper.

Despite the complex and nonlinear nature of the magnetic levitation system, our proposal is simple. It is composed by a PI loop to control voltage at the converter capacitor, a PI loop to control the electromagnet electric current, and an external PID loop to regulate the ball position. As in [16], an additional sliding modes' internal loop is employed to control electric current through the converter inductance. Formalizing this intuitively simple idea to control a complex plant is another important contribution of the present paper. The key for this is a novel passivity-based approach exploiting energy ideas, i.e., we take advantage from the natural energy exchange among the several subsystems to design the control law. This represents another contribution of the present paper.

This paper is organized as follows. In Section 2, we introduce the plant to be controlled and present its dynamical model. The passivity properties of the plant are described in Section 3 where we also give some insight on the rationale behind our approach. Our main result is presented in Section 4. In Section 5, we present a simulation study and, finally, some concluding remarks are given in Section 6.

2. Mathematical Model

The DC/DC Buck power electronic converter-Magnetic levitation system is depicted in Figure 1(a). The DC/DC Buck power converter is composed by a transistor Q, a diode D, an inductor L_c, a capacitor C, and a resistance R_c. Symbols i_c and v represent electric current through inductance L_c and voltage at capacitor terminals C, respectively, whereas E stands for voltage of the DC power supply. The system input is u which only takes the discrete values $\{0, +1\}$ representing the off and on states of transistor Q, see Figure 1(b).

The magnetic levitation system consists of an electromagnet, with inductance $L(y)$ and internal resistance R, and a ball with mass m, made in a ferromagnetic material, which receives an upwards magnetic force F from the electromagnet. This force must cancel the downwards ball weight mg in order to levitate the ball in space. Electromagnet is basically a ferromagnetic core with a conductor wire wound around it. The electric voltage v is applied at the electromagnet terminals which force an electric current i to flow through the electromagnet winding and this current produces the attractive magnetic force $F = (1/2)(\mathrm{d}L(y)/\mathrm{d}y)i^2$ on the ball. Symbol λ represents the magnetic flux produced by electric current i within the electromagnet core. Ball position, measured from the bottom of the electromagnet to the top of ball is represented by $y \geq 0$. We remark that inductance of electromagnet, $L(y) > 0$ for all $y \geq 0$, depends on the ball position y in the form shown in Figure 2. In order to understand this, recall that the magnetic flux is given as $\lambda = L(y)i$. Suppose that i remains constant and the ball approaches to electromagnet, i.e., y decreases. This reduces both the air gap and the reluctance. Hence, λ increases. Since $\lambda = L(y)i$ and i remains constant, this means that $L(y)$ must increase. Thus, $L(y)$ increases as y decreases. When $y \longrightarrow \infty$, it is obtained as the case when the ball is not

present, and in such a case, $L(y)$ reaches a minimum positive value. This also means that $\mathrm{d}L(y)/\mathrm{d}y < 0$.

We refer the reader to [23] for a detailed description of a magnetic levitation system as well as for precise instructions to construct one of them for experimental purposes. Furthermore, the complete procedure to obtain its dynamical model is presented and some experiments are provided to identify its parameters. Also, some controllers are designed and tested experimentally.

Using Kirchhoff's Laws (see Figure 1(b)), Faraday's Law, and Newton's Second Law, we find that the mathematical model of the DC/DC Buck power electronic converter-magnetic levitation system is given as follows [16, 23, 26, 27]:

$$L_c \frac{\mathrm{d}i_c}{\mathrm{d}t} = -v + Eu, \tag{1}$$

$$C\frac{\mathrm{d}v}{\mathrm{d}t} = i_c - i - \frac{v}{R_c}, \tag{2}$$

$$L(y)\frac{\mathrm{d}i}{\mathrm{d}t} = -\frac{\mathrm{d}L(y)}{\mathrm{d}y} i \frac{\mathrm{d}y}{\mathrm{d}t} - Ri + v, \tag{3}$$

$$m\ddot{y} = \frac{1}{2}\frac{\mathrm{d}L(y)}{\mathrm{d}y} i^2 + mg, \tag{4}$$

$$\frac{\mathrm{d}L(y)}{\mathrm{d}y} < 0, \quad \forall y \geq 0. \tag{5}$$

Important for our purposes is the following class of saturation functions.

Definition 1. Given positive constants L^* and M, with $L^* < M$, a function $\sigma: \mathscr{R} \longrightarrow \mathscr{R}: \varsigma \mapsto \sigma(\varsigma)$ is said to be a strictly increasing linear saturation for (L^*, M) if it is locally Lipschitz, strictly increasing, and satisfies [28]

$$\begin{aligned} &\sigma(\varsigma) = \varsigma, \quad \text{when } |\varsigma| \leq L^*, \\ &|\sigma(\varsigma)| < M, \quad \forall \varsigma \in \mathscr{R}. \end{aligned} \tag{6}$$

3. The Rationale behind Our Proposal

Consider the following slightly modified version of the mathematical model in (1)–(5):

$$\begin{aligned} C\frac{dv}{dt} &= i_c - i - \frac{v}{R_c}, \\ L(y)\frac{\mathrm{d}i}{\mathrm{d}t} &= -\frac{\mathrm{d}L(y)}{\mathrm{d}y} i\dot{y} - Ri + v, \\ m\ddot{y} &= \frac{1}{2}\frac{\mathrm{d}L(y)}{\mathrm{d}y} i^2 - G(y), \end{aligned} \tag{7}$$

where $G(y) = \mathrm{d}P(y)/\mathrm{d}y$ with $P(y)$ is a positive semidefinite scalar function. The total energy stored in the system is given as follows:

$$V_e(v, y, \dot{y}, i) = \frac{1}{2}Cv^2 + \frac{1}{2}L(y)i^2 + \frac{1}{2}m\dot{y}^2 + P(y), \tag{8}$$

where the first term stands for electric energy stored in the capacitor of the Buck power converter, whereas the last three terms stand for the magnetic, kinetic, and potential energies stored in the electrical and the mechanical subsystems, respectively, of the magnetic levitation system. The time derivative of V_e along the trajectories of system in (7) is given as follows:

$$\begin{aligned} \dot{V}_e &= vC\frac{\mathrm{d}v}{\mathrm{d}t} + \frac{1}{2}\frac{\mathrm{d}L(y)}{\mathrm{d}y}\dot{y}i^2 + iL(y)\frac{\mathrm{d}i}{\mathrm{d}t} + \dot{y}m\ddot{y} + \frac{\mathrm{d}P(y)}{\mathrm{d}y}\dot{y} \\ &= v\left[i_c - i - \frac{v}{R_c}\right] + \frac{1}{2}\frac{\mathrm{d}L(y)}{\mathrm{d}y}\dot{y}i^2 + i\left[-\frac{\mathrm{d}L(y)}{\mathrm{d}y}i\dot{y} - Ri + v\right] \\ &\quad + \dot{y}\left[\frac{1}{2}\frac{\mathrm{d}L(y)}{\mathrm{d}y}i^2 - G(y)\right] + G(y)\dot{y} \\ &= -\frac{v^2}{R_c} - Ri^2 + i_c v, \end{aligned} \tag{9}$$

Notice that the cancellation of terms

$$\begin{aligned} \frac{1}{2}\frac{\mathrm{d}L(y)}{\mathrm{d}y}\dot{y}i^2 - \frac{\mathrm{d}L(y)}{\mathrm{d}y}i^2\dot{y} + \frac{1}{2}\frac{\mathrm{d}L(y)}{\mathrm{d}y}\dot{y}i^2 &= 0, \\ iv - vi &= 0, \end{aligned} \tag{10}$$

represent (1) natural energy exchange between the electrical and the mechanical subsystems of the magnetic levitation system and (2) natural energy exchange between the capacitor and the electrical subsystem of the magnetic levitation system. Another cancellation of the terms involves $\pm G(y)\dot{y}$ which represents the exchange between kinetic and potential energies in the magnetic levitation system. Hence, if we define the input i_c and the output v, then

$$\dot{V}_e \leq -\frac{v^2}{R_c} + vi_c. \tag{11}$$

The expression in (11) proves that the model in (7) is output strictly passive [29], Definition 6.3.

In the present paper, we exploit these properties by proceeding as follows. First, we design u as a sliding mode controller to force i_c to reach a desired function i_c^d. Then, $i_c = i_c^d$ is employed as the control input for the sliding surface systems (2)–(4). In order to perform this step, we first obtain the error equation for this system by adding and subtracting some convenient terms (notice that these terms are not introduced using any control law), i.e.,

$$\begin{aligned} C\frac{\mathrm{d}\varepsilon}{\mathrm{d}t} &= i_c^d - \tilde{I} - i^d - \frac{\varepsilon}{R_c} - \frac{v^d}{R_c} - C\frac{\mathrm{d}v^d}{\mathrm{d}t}, \\ L(y)\frac{\mathrm{d}\tilde{I}}{\mathrm{d}t} &= -\frac{\mathrm{d}L(y)}{\mathrm{d}y}\tilde{I}\frac{\mathrm{d}y}{\mathrm{d}t} - \frac{\mathrm{d}L(y)}{\mathrm{d}y}i^d\frac{\mathrm{d}y}{\mathrm{d}t} - R\tilde{I} - Ri^d \\ &\quad + \varepsilon + v^d - L(y)\frac{\mathrm{d}i^d}{\mathrm{d}t}, \\ m\ddot{y} &= \frac{1}{2}\frac{\mathrm{d}L(y)}{\mathrm{d}y}\tilde{I}^2 + \frac{\mathrm{d}L(y)}{\mathrm{d}y}i^d\tilde{I} + \frac{1}{2}\frac{\mathrm{d}L(y)}{\mathrm{d}y}i^{d2} + mg, \end{aligned} \tag{12}$$

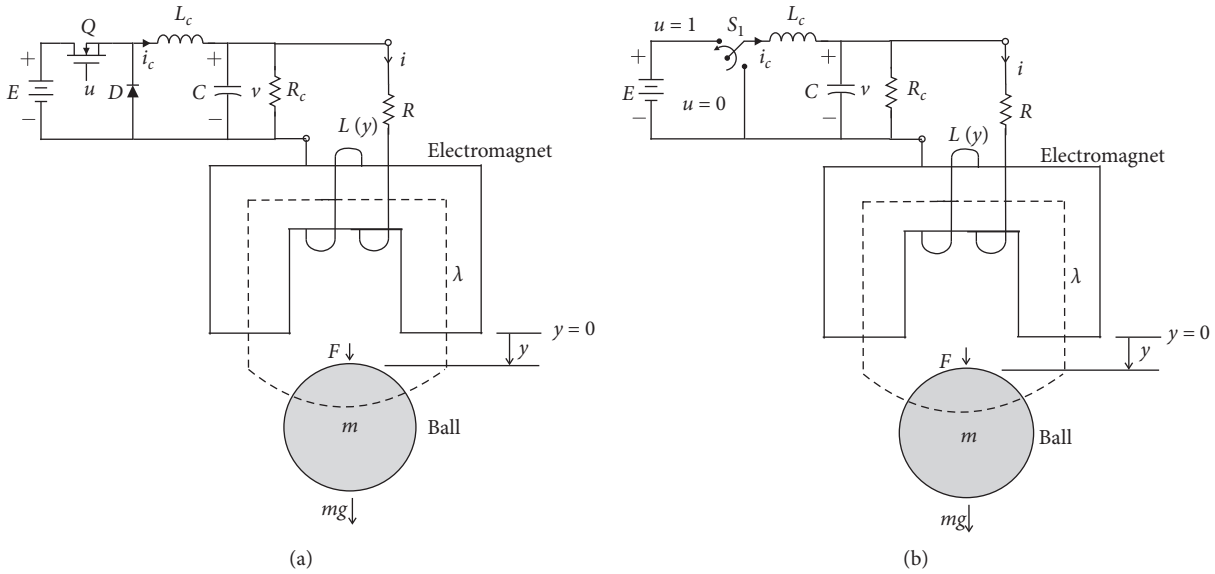

Figure 1: Electromechanical diagram of the DC/DC Buck power electronic converter-magnetic levitation system. (a) Implementation of the DC/DC Buck power electronic converter-magnetic levitation system using one diode and one transistor. (b) Ideal representation of the DC/DC Buck power electronic converter-magnetic levitation system using a switch S_1.

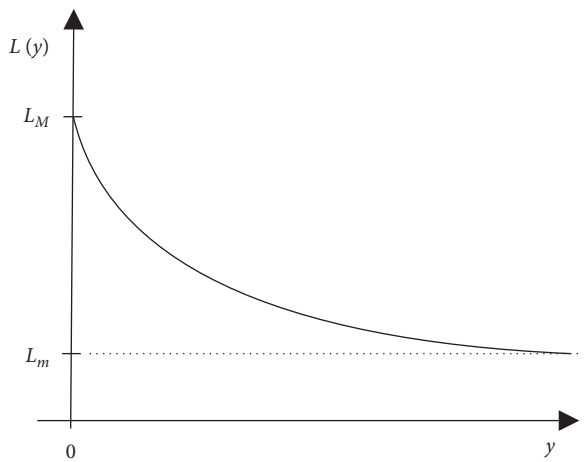

Figure 2: Inductance L as a function of the ball position y.

where $\varepsilon = v - v^d$ and $\tilde{I} = i - i^d$. The equivalence of these expressions and those in (2)–(4) can be verified by reducing the redundant terms in the three expressions in (12). Defining $V_{E1}(\varepsilon, \tilde{I}, \dot{y}) = (1/2)C\varepsilon^2 + (1/2)L(y)\tilde{I}^2 + (1/2)m\dot{y}^2$ and using the three expressions in (12), we have that

$$\begin{aligned}\dot{V}_{E1} = {} & \varepsilon\left[i_c^d - \tilde{I} - i^d - \frac{\varepsilon}{R_c} - \frac{v^d}{R_c} - C\frac{\mathrm{d}v^d}{\mathrm{d}t}\right] + \frac{1}{2}\frac{\mathrm{d}L(y)}{\mathrm{d}y}\dot{y}\tilde{I}^2 \\ & + \tilde{I}\left[-\frac{\mathrm{d}L(y)}{\mathrm{d}y}\tilde{I}\frac{\mathrm{d}y}{\mathrm{d}t} - \frac{\mathrm{d}L(y)}{\mathrm{d}y}i^d\frac{\mathrm{d}y}{\mathrm{d}t} - R\tilde{I} - Ri^d\right. \\ & \left. + \varepsilon + v^d - L(y)\frac{\mathrm{d}i^d}{\mathrm{d}t}\right] \\ & + \dot{y}\left[\frac{1}{2}\frac{\mathrm{d}L(y)}{\mathrm{d}y}\tilde{I}^2 + \frac{\mathrm{d}L(y)}{\mathrm{d}y}i^d\tilde{I} + \frac{1}{2}\frac{\mathrm{d}L(y)}{\mathrm{d}y}i^{d2} + mg\right].\end{aligned} \tag{13}$$

Hence, choosing $i_c^d = (v^d/R_c) + i_{cd}^d$, $i_{cd}^d = -k_1\varepsilon$, $v^d = -k_2\tilde{I}$, $i^d = \sqrt{2F^d/|(\mathrm{d}L(y)/\mathrm{d}y)|}$, $F^d = F_d + F_s$, and $F_d = k_3\dot{y}$ and taking advantage from several natural cancellations, as in (10), we have

$$\begin{aligned}\dot{V}_{E1} = {} & -\left(\frac{1}{R_c} + k_1\right)\varepsilon^2 + \varepsilon\left[-i^d - C\frac{\mathrm{d}v^d}{\mathrm{d}t}\right] - (R + k_2)\tilde{I}^2 \\ & + \tilde{I}\left[-Ri^d - L(y)\frac{\mathrm{d}i^d}{\mathrm{d}t}\right] - k_3\dot{y}^2 - \dot{y}F_s + \dot{y}[mg],\end{aligned} \tag{14}$$

where $(\mathrm{d}L(y)/\mathrm{d}y)/(|\mathrm{d}L(y)/\mathrm{d}y|) = -1$. Finally, if we choose $F_s = k_4(y - y^*) + mg$ and $V_E = V_{E1} + (1/2)k_4(y - y^*)^2$, we find

$$\begin{aligned}\dot{V}_E = {} & -\left(\frac{1}{R_c} + k_1\right)\varepsilon^2 + \varepsilon\left[-i^d - C\frac{\mathrm{d}v^d}{\mathrm{d}t}\right] - (R + k_2)\tilde{I}^2 \\ & + \tilde{I}\left[-Ri^d - L(y)\frac{\mathrm{d}i^d}{\mathrm{d}t}\right] - k_3\dot{y}^2.\end{aligned} \tag{15}$$

Thus, F_s suitably shapes the potential energy of the mechanical subsystem to have a unique minimum at $y = y^*$, whereas F_d, i_{cd}^d, and v^d, represent the damping injection terms, as usual in standard passivity-based control [20].

In Section 4, we will show that several cross terms arising from the rectangular brackets in (15) do not cancel naturally. This means that additional terms must be included in the control law if they are required to be cancelled. Hence, we prefer to dominate these terms instead of feeding back them in order to artificially cancel them. This allows us to design simpler control laws when compared to previous passivity-based approaches [20] where those terms must be online computed and fed back in order to be cancelled artificially.

In this respect, we stress that it is recognized in the literature that increasing the number of online computations deteriorates performance because this increases numerical errors and the effects of noise. Moreover, we will also show that including PI and PID controllers (instead of proportional controllers as above) is straightforward. Notice that this feature is important to render robust the control scheme. The features described in this paragraph render novel and advantageous our passivity-based approach with respect to that in [20] where the natural cancellations shown in (10) are not exploited.

4. Main Result

Our main result is stated in the following proposition.

Proposition 1. *Consider the mathematical model in (1)–(5) in a closed loop with the following controller:*

$$u = \frac{1}{2}\left[1 - \operatorname{sign}(s_c)\right], \quad s_c = i_c - i_c^*, \tag{16}$$

$$\begin{aligned} i_c^* = {} & \frac{\overline{v}}{R_c} - k_{p1}e - k_{i1}\int_0^t e(r)\mathrm{d}r \\ & - C\alpha_p\left(-\frac{\mathrm{d}L(y)}{\mathrm{d}y}i^*\dot{y} + v\right) - C\alpha_i\widetilde{i}, \quad e = v - \overline{v}, \end{aligned} \tag{17}$$

$$\overline{v} = -\alpha_p L(y)\widetilde{i} - \alpha_i\int_0^t \widetilde{i}(r)\mathrm{d}r, \quad \widetilde{i} = i - i^*, \tag{18}$$

$$\begin{aligned} & i^* = \sqrt{\frac{2}{\left|\mathrm{d}L(y)/\mathrm{d}y\right|}F^*}, \\ & F^* = k_p h(\widetilde{y}) + k_d\dot{y} + k_i\operatorname{sat}(z), \quad \widetilde{y} = y - y^*, \end{aligned} \tag{19}$$

$$z = \int_0^t\left[\alpha\left(1 + \frac{\beta k_p}{k_i}\right)h(\widetilde{y}) + \left(1 + \frac{\alpha\beta k_d}{k_i}\right)\dot{y}\right]\mathrm{d}s, \tag{20}$$

where $y^* > 0$ is a real constant standing for the desired position, $h(\widetilde{y}) = \sigma(\widetilde{y})$, and $\operatorname{sat}(z) = \sigma(z)$, where $\sigma(\cdot)$ is a strictly increasing linear saturation function for some (L^*, M) (see Definition 1). Furthermore, it is also required that function $\sigma(\cdot)$ be continuously differentiable such that

$$0 < \frac{\mathrm{d}\sigma(\varsigma)}{\mathrm{d}\varsigma} \le 1, \quad \forall\varsigma \in \mathscr{R}. \tag{21}$$

The closed-loop state evolution is assumed to be constrained to a subset $\mathscr{D} \subset \mathscr{R}^7$, where

$$\begin{aligned} & \left|\frac{\mathrm{d}L(y)}{\mathrm{d}y}\right| > \gamma_1, \\ & F^* > \gamma_2, \\ & |\widetilde{y}| \le L^*, \end{aligned} \tag{22}$$

for some $\gamma_1 > 0$ and $\gamma_2 > 0$. Under these conditions there always exist constant scalars $\alpha, \beta, k_{p1}, k_{i1}$, k_p, k_d, k_i, α_p, and α_i, such that the closed-loop system has a unique equilibrium point which is asymptotically stable as long as

$$0 < v + L_c\frac{\mathrm{d}i_c^*}{\mathrm{d}t} < E. \tag{23}$$

At this equilibrium point, $\widetilde{y} = 0$.

4.1. Reaching the Sliding Surface. The time derivative of the positive definite and radially unbounded scalar function $V_c(s_c) = (1/2)s_c^2$, along the trajectories of [1] is

$$\begin{aligned} \dot{V}_c = s_c\dot{s}_c &= s_c\left[\frac{\mathrm{d}i_c}{\mathrm{d}t} - \frac{\mathrm{d}i_c^*}{\mathrm{d}t}\right] \\ &\le \frac{\left|s_c\right|}{L_c}\left[\left|-v - L_c\frac{\mathrm{d}i_c^*}{\mathrm{d}t} + \frac{1}{2}E\right| - \frac{1}{2}E\right] < 0, \end{aligned} \tag{24}$$

where [15] has been used, if $|-v - L_c(\mathrm{d}i_c^*/\mathrm{d}t) + (1/2)E| - (1/2)E < 0$. By considering the two possibilities $-v - L_c(\mathrm{d}i_c^*/\mathrm{d}t) + (1/2)E > 0$ and $-v - L_c(\mathrm{d}i_c^*/\mathrm{d}t) + (1/2)E < 0$, it is not difficult to show that (24) implies (23). From the sliding condition $\dot{s}_c = 0$, [1, 22], we find that the equivalent control satisfies the following bound:

$$0 < u_{\mathrm{eq}} = \frac{1}{E}\left[v + L_c\frac{\mathrm{d}i_c^*}{\mathrm{d}t}\right] < 1, \tag{25}$$

which means that the sliding regime is possible. On the contrary, (24) ensure that the sliding surface $s_c = i_c - i_c^* = 0$ is reached, i.e., $i_c = i_c^*$ is reached. Thus, we only have to study the stability of dynamics (2)–(5) in closed loop with (17)–(20) when evaluated at $i_c = i_c^*$.

4.2. Closed-Loop Dynamics on the Sliding Surface. Using $i_c = i_c^*$, [16] in [2], and adding and subtracting the terms i^*, $(1 + C\alpha_p R)\sqrt{2mg/(\left|\mathrm{d}L(y^*)/\mathrm{d}y\right|)}$, $C\dot{\overline{v}}$, we find

$$\begin{aligned} C\dot{e} = {} & -\left(\frac{1}{R_c} + k_{p1}\right)e - \widetilde{i} - \left(1 + C\alpha_p R\right)\left[i^* - \sqrt{\frac{2mg}{\left|\mathrm{d}L(y^*)/\mathrm{d}y\right|}}\right] \\ & - k_{i1}\xi - C\alpha_p L(y)\frac{\mathrm{d}i^*}{\mathrm{d}t} - C\alpha_p R\widetilde{i}, \end{aligned} \tag{26}$$

$$\xi = \int_0^t e(r)\mathrm{d}r + \frac{1 + C\alpha_p R}{k_{i1}}\sqrt{\frac{2mg}{\left|\mathrm{d}L(y^*)/\mathrm{d}y\right|}}, \tag{27}$$

where

$$\frac{\mathrm{d}L(y^*)}{\mathrm{d}y} = \left.\frac{\mathrm{d}L(y)}{\mathrm{d}y}\right|_{y=y^*}. \tag{28}$$

On the other hand, adding and subtracting the terms i^*, $\overline{v}$, $L(y)(\mathrm{d}i^*/\mathrm{d}t)$, $R\sqrt{2mg/(\left|\mathrm{d}L(y^*)/\mathrm{d}y\right|)}$, $L(y)(\mathrm{d}i^*/\mathrm{d}t)$, and $(\mathrm{d}L(y)/\mathrm{d}y)i^*\dot{y}$, in [3], and replacing [17], we obtain

$$L(y)\frac{d\tilde{i}}{dt} = e - \left(R + \alpha_p L(y)\right)\tilde{i} - \alpha_i z_1 - R\left[i^* - \sqrt{\frac{2mg}{|dL(y^*)/dy|}}\right] - \frac{dL(y)}{dy}\tilde{i}\dot{y} - \frac{dL(y)}{dy}i^*\dot{y} - L(y)\frac{di^*}{dt}, \tag{29}$$

$$z_1 = \int_0^t \tilde{i}(r)dr + \frac{R}{\alpha_i}\sqrt{\frac{2mg}{|dL(y^*)/dy|}}, \tag{30}$$

where

$$\frac{di^*}{dt} = \left(\frac{2F^*}{|dL(y)/dy|}\right)^{-1/2} \times \left\{\left(\frac{d}{dy}\left|\frac{dL(y)}{dy}\right|^{-1}\right)\dot{y} \times \left[k_p h(\tilde{y}) + k_d\dot{y} + k_i s(z) + mg\right] + \left|\frac{dL(y)}{dy}\right|^{-1}\left[k_p\frac{dh(\tilde{y})}{d\tilde{y}}\dot{y} + k_d\ddot{y} + k_i\frac{d\,\mathrm{sat}(z)}{dz}\dot{z}\right]\right\}, \tag{31}$$

$$s(z) = \mathrm{sat}(z) - \frac{1}{k_i}mg. \tag{32}$$

Finally, adding and subtracting the terms $1/2\,(dL(y)/dy)i^*i$, $(1/2)(dL(y)/dy)i^*\tilde{i}$, and $(1/2)(dL(y)/dy)i^{*2}$, and replacing i^* and F^* from [18], the expression in [4] becomes

$$m\ddot{y} = \frac{1}{2}\frac{dL(y)}{dy}\tilde{i}^2 + \frac{dL(y)}{dy}\tilde{i}i^* - k_p h(\tilde{y}) - k_d\dot{y} - k_i s(z). \tag{33}$$

The closed-loop dynamics is given by (26)–(33) and (20). Equilibria of this dynamics are found as follows. From the state equation $\dot{\tilde{y}} = \dot{y} = 0$, it is concluded that $\dot{y} = 0$ at the equilibrium point. Using this result in $\dot{z} = 0$ (from (20)) yields $\tilde{y} = 0$. From $\dot{z}_1 = 0$ (see (30)), we find $\tilde{i} = 0$. Then, from $m\ddot{y} = 0$, in (33), we find $z = (1/k_i)mg$ if

$$L^* > \frac{1}{k_i}mg. \tag{34}$$

Using the above results in (19) yields $i^* = \sqrt{2mg/(|dL(y^*)/dy|)}$ and from $\dot{\xi} = 0$ in (27), we find that $e = 0$. From (31), we have that $di^*/dt = 0$. Using $\dot{e} = 0$ in (26), we have that $\xi = 0$ at the equilibrium point. Hence, from (29), we find that $z_1 = 0$.

This means that the only equilibrium point of the closed-loop dynamics is $\zeta = [\dot{y}, \tilde{y}, z - (1/k_i)mg, \tilde{i}, z_1, e, \xi]^T = [0, 0, 0, 0, 0, 0, 0]^T$. Notice that this closed-loop dynamics is autonomous because it can be written as $\dot{\zeta} = f(\zeta)$ for some nonlinear $f(\cdot) \in \mathcal{R}^7$.

4.3. Stability Analysis. The closed-loop dynamics (26)–(33) and (20) can be rewritten as follows:

$$C\dot{e} = \mathcal{I}_c - \tilde{i} - \left(\frac{1}{R_c} + k_{p1}\right)e, \tag{35}$$

$$L(y)\frac{d\tilde{i}}{dt} = -\left(R + \alpha_p L(y)\right)\tilde{i} - \frac{dL(y)}{dy}\tilde{i}\dot{y} + \Upsilon, \tag{36}$$

$$m\ddot{y} = \frac{1}{2}\frac{dL(y)}{dy}\tilde{i}^2 - \mathcal{G}, \tag{37}$$

$$\dot{z}_1 = \tilde{i}, \quad \dot{\xi} = e, \quad \dot{z} = \alpha\left(1 + \frac{\beta k_p}{k_i}\right)h(\tilde{y}) + \left(1 + \frac{\alpha\beta k_d}{k_i}\right)\dot{y}, \tag{38}$$

$$\mathcal{I}_c = -\left(1 + C\alpha_p R\right)\left[i^* - \sqrt{\frac{2mg}{|dL(y^*)/dy|}}\right] - k_{i1}\xi - C\alpha_p L(y)\frac{di^*}{dt} - C\alpha_p R\tilde{i},$$
$$\mathcal{G} = -\frac{dL(y)}{dy}\tilde{i}i^* + k_p h(\tilde{y}) + k_d\dot{y} + k_i s(z), \tag{39}$$
$$\Upsilon = e - R\left(i^* - \sqrt{\frac{2mg}{|dL(y^*)/dy|}}\right) - \frac{dL(y)}{dy}i^*\dot{y} - L(y)\frac{di^*}{dt} - \alpha_i z_1.$$

Notice that (35)–(38) are almost identical to the open-loop dynamics in (7) if we replace $y, \dot{y}, i, v, G, i_c$ by $\tilde{y}, \dot{y}, \tilde{i}, \Upsilon, \mathcal{G}, \mathcal{I}_c$. One important difference is that the resistances R_c and R in (7) have been enlarged to $(1/R_c) + k_{p1}$ and $R + \alpha_p L(y)$ in (35) and (36), respectively. Moreover, we can see that suitable damping can be introduced thanks to term $k_d\dot{y}$ in the definition of $\mathcal{G}$. Another important difference is the three new equations in (38) which represent the integral terms of the PI electric current controller, the PI controller of voltage at the capacitor, and the PID position controller, which are intended to compensate for the effects of the gravity term mg.

These observations motivate the use of the following "energy" storage function for the closed-loop dynamics:

$$W\left(\dot{y}, \tilde{y}, z - \frac{mg}{k_i}, \tilde{i}, z_1, e, \xi\right) = \frac{1}{2}Ce^2 + \frac{1}{2}k_{i1}\xi^2 + \frac{1}{2}L(y)\tilde{i}^2 + \frac{1}{2}\alpha_i z_1^2 + V_m\left(\dot{y}, \tilde{y}, z - \frac{mg}{k_i}\right), \tag{40}$$

where

$$V_m\left(\tilde{y}, \dot{y}, z - \frac{mg}{k_i}\right) = \frac{1}{2}m\dot{y}^2 + \alpha mh(\tilde{y})\dot{y} + \alpha k_d\int_0^{\tilde{y}} h(r)dr + k_p\int_0^{\tilde{y}} h(r)dr + k_i\int_{mg/k_i}^{z} s(r)dr + \alpha\beta ms(z)\dot{y}. \tag{41}$$

We stress that function $V_m(\dot{y}, \tilde{y}, z - mg/k_i)$ defined in (40) is very similar to the function $V(\tilde{q}, \dot{q}, z - (k_i')^{-1} g(q_d))$ analyzed in [30]. Thus, conditions to ensure that $V_m(\dot{y}, \tilde{y}, z - mg/k_i)$ is positive definite and radially unbounded are the same as those introduced in [30]. For the sake of completeness of this work, these conditions are presented in Appendix A as (A.1), (A.2), and (A.5) and $k_p > 0$, $\alpha > 0$, and $\beta > 0$. Thus, the function $W(\dot{y}, \tilde{y}, z - mg/k_i, \tilde{i}, z_1, e, \xi)$ qualifies as a Lyapunov function candidate because it is positive definite and radially unbounded if $k_{i1} > 0$ and $\alpha_i > 0$.

The first two terms in W represent the electric energy stored in the converter's capacitor and "energy" stored in the integral term of the PI voltage controller. The third and fourth terms represent the magnetic energy stored in the electrical system and the "energy" stored in the integral term of the PI electric current controller. On the other hand, function V_m includes the kinetic energy and the closed-loop "potential energy"

$$\mathscr{P}(\tilde{y}) = k_p \int_0^{\tilde{y}} h(r)\mathrm{d}r, \tag{42}$$

as well as the "energy" stored in the integral of position through an integral of $s(\cdot)$. The cross terms $\alpha m h(\tilde{y})\dot{y}$ and $\alpha\beta m s(z)\dot{y}$ are required to provide $\dot{W}$ with negative quadratic terms in both $h(\tilde{y})$ and $s(z)$. In this respect, it is easy to verify that

$$\frac{\mathrm{d}}{\mathrm{d}t}\left(\frac{1}{2}L(y)\tilde{i}^2 + \frac{1}{2}m\dot{y}^2 + \mathscr{P}(\tilde{y})\right) = -\left(R + \alpha_p L(y)\right)\tilde{i}^2 - k_d\dot{y}^2 + \tilde{i}\Upsilon + \frac{\mathrm{d}L(y)}{\mathrm{d}y}\dot{y}\tilde{i}i^* - k_i s(z)\dot{y}. \tag{43}$$

Since Υ depends on both $h(\tilde{y})$ and $s(z)$, negative quadratic terms on both $h(\tilde{y})$ and $s(z)$ are required to dominate some cross terms in both $h(\tilde{i})$ and $\tilde{i}$ and $s(z)$ and $\tilde{i}$. This is the reason for the cross terms $\alpha m h(\tilde{y})\dot{y}$ and $\alpha\beta m s(z)\dot{y}$ (the quadratic term $-(R + \alpha_p L(y))\tilde{i}^2$ already exists). The integral term $\alpha k_d \int_0^y h(r)\mathrm{d}r$ is intended to cancel an undesired cross term appearing in the time derivative of $\alpha m h(\tilde{y})\dot{y}$. Notice that term $\tilde{i}e$, arising from the product $\tilde{i}\Upsilon$ above, cancels with term $-e\tilde{i}$, arising from $(\mathrm{d}/\mathrm{d}t)(Ce^2/2)$. Moreover, some third order terms involving i^* appear from $\tilde{i}\Upsilon$. These terms can be dominated by quadratic negative terms in $\dot{y}$ and $\tilde{i}$ because $|h(\tilde{y})|$ and $|s(z)|$ are bounded by finite constants. This is the reason to employ a PID position controller with saturated proportional and integral actions.

After some straightforward natural cancellations (i.e., not requiring to use additional terms in the control law to achieve them), which include the closed-loop equivalents of (10) (see Remark 6), we find that the time derivative of W along the trajectories of the closed-loop systems (35)–(38) is given as follows:

$$\begin{aligned}\dot{W} = &-\left(\frac{1}{R_c} + k_{p1}\right)e^2 - \left(R + \alpha_p L(y) - \frac{\alpha}{2}\frac{\mathrm{d}L(y)}{\mathrm{d}y}h(\tilde{y}) - \frac{\alpha\beta}{2}\frac{\mathrm{d}L(y)}{\mathrm{d}y}s(z)\right)\tilde{i}^2 \\ &- \left[k_d - \alpha m\frac{\mathrm{d}h(\tilde{y})}{\mathrm{d}\tilde{y}} - \alpha\beta m\frac{\mathrm{d}s(z)}{\mathrm{d}z}\left(1 + \frac{\alpha\beta k_d}{k_i}\right)\right]\dot{y}^2 - \alpha k_p h^2(\tilde{y}) - \alpha\beta k_i s^2(z) \\ &- \left[e\left(1 + C\alpha_p R\right) + R\tilde{i}\right]\left(i^* - \sqrt{\frac{mg}{\left|\mathrm{d}L(y^*)/\mathrm{d}y\right|}}\right) + \alpha\frac{\mathrm{d}L(y)}{\mathrm{d}y}h(\tilde{y})\tilde{i}i^* + \alpha^2\beta m\frac{\mathrm{d}s(z)}{\mathrm{d}z}\left(1 + \frac{\beta k_p}{k_i}\right)h(\tilde{y})\dot{y} \\ &+ \alpha\beta\frac{\mathrm{d}L(y)}{\mathrm{d}y}s(z)\tilde{i}i^* - C\alpha_p \mathrm{R}e\tilde{i} - L(y)\tilde{i}\frac{\mathrm{d}i^*}{\mathrm{d}t} - C\alpha_p eL(y)\frac{\mathrm{d}i^*}{\mathrm{d}t}.\end{aligned} \tag{44}$$

Taking into account (19), (31), and Appendix B, it is found that $\dot{W}$ can be upper bounded as follows:

$$\begin{aligned}\dot{W} \le &-x^T Q x - \alpha_{p2}L(y)\tilde{i}^2 + \frac{1}{2m}k_{rr}k_d k_\sigma|\tilde{i}|^3 + \frac{C\alpha_p}{2m}k_{rr}k_d k_\sigma|e||\tilde{i}|^2 + \frac{C\alpha_p}{2m}k_{rr}k_d k_\sigma k_\delta|e||\tilde{i}||\dot{y}| \\ &- \alpha_{p4}L(y)\tilde{i}^2 - k_{p3}e^2 - k_{d4}\dot{y}^2 + \frac{1}{2m}k_{rr}k_d k_\sigma k_\delta\tilde{i}^2|\dot{y}| - \alpha_{p3}L(y)\tilde{i}^2 + \left[C\alpha_p k_r k_d + \left(1 + C\alpha_p R\right)k_t\right]|e|\dot{y}^2 - k_{d3}\dot{y}^2 \\ &+ \left(k_r k_d + Rk_t\right)||i|\dot{y}^2 - k_{d2}\dot{y}^2,\end{aligned} \tag{45}$$

$$x^T = [|\dot{y}|, |h(\tilde{y})|, |s(z)|, |\tilde{i}|, |e|],$$

where k_{d1}, k_{d2}, k_{d3}, k_{d4}, α_{p1}, α_{p2}, α_{p3}, α_{p4}, k_{p2}, and k_{p3} are positive constant scalars such that $k_{d1} + k_{d2} + k_{d3} + k_{d4} = k_d$, $\alpha_{p1} + \alpha_{p2} + \alpha_{p3} + \alpha_{p4} = \alpha_p$, and $k_{p2} + k_{p3} = k_{p1}$. The entries of matrix Q are defined as follows:

$$
\begin{aligned}
Q_{11} &= k_{d1} - \alpha m - \alpha\beta m\left(1 + \frac{\alpha\beta k_d}{k_i}\right),\\
Q_{22} &= \alpha k_p,\\
Q_{33} &= \alpha\beta k_i,\\
Q_{44} &= R + \alpha_{p1} L(y) - \frac{\alpha}{2} k_\sigma M - \alpha\beta k_\sigma M - \frac{1}{m} k_{rr} k_d k_\sigma I^*(0),\\
Q_{55} &= \frac{1}{R_c} + k_{p2},\\
Q_{12} &= Q_{21} = -\frac{\alpha^2\beta m}{2}\left(1 + \frac{\beta k_p}{k_i}\right),\\
Q_{31} &= Q_{13} = Q_{23} = Q_{32} = 0,\\
Q_{14} &= Q_{41} = -\frac{k_r k_p M}{2} - k_r k_i M - \frac{k_r m g}{2} - \frac{k_{rr} k_p}{2} - \frac{k_{rr} k_d^2}{2m} - \frac{Rk^*}{2}\\
&\quad - \frac{k_i k_{rr}}{2}\left(1 + \frac{\alpha\beta k_d}{k_i}\right) - \frac{\alpha k_\sigma k_\delta M}{2} - \alpha\beta M k_\delta k_\sigma - \frac{3Rk_t M}{2},\\
Q_{42} &= Q_{24} = -\frac{k_{rr} k_d k_p}{2m} - \frac{\alpha k_i k_{rr}}{2}\left(1 + \frac{\beta k_p}{k_i}\right) - \frac{\alpha k_\sigma I^*(0)}{2} - \frac{Rk^*}{2},\\
Q_{43} &= Q_{34} = -\frac{k_{rr} k_d k_i}{2m} - \frac{\alpha\beta k_\sigma I^*(0)}{2} - \frac{Rk^*}{2},\\
Q_{15} &= Q_{51} = -\frac{\left(1 + C\alpha_p R\right)k^*}{2} - \frac{3\left(1 + C\alpha_p R\right)k_t M}{2} - \frac{C\alpha_p k_r k_p M}{2}\\
&\quad - C\alpha_p k_r k_i M - C\alpha_p \frac{k_r m g}{2} - C\alpha_p \frac{k_{rr} k_p}{2} - C\alpha_p \frac{k_{rr} k_d^2}{2m} - C\alpha_p \frac{k_i k_{rr}}{2}\left(1 + \frac{\alpha\beta k_d}{k_i}\right),\\
Q_{52} &= Q_{25} = -\frac{\left(1 + C\alpha_p R\right)k^*}{2} - C\alpha_p \frac{k_{rr} k_d k_p}{2m} - C\alpha_p \frac{\alpha k_i k_{rr}}{2}\left(1 + \frac{\beta k_p}{k_i}\right),\\
Q_{53} &= Q_{35} = -\frac{\left(1 + C\alpha_p R\right)k^*}{2} - C\alpha_p \frac{k_{rr} k_d k_i}{2m},\\
Q_{45} &= Q_{54} = -\frac{1}{2} C\alpha_p R - \frac{C\alpha_p}{2m} k_{rr} k_d k_\sigma I^*(0),
\end{aligned}
\tag{46}
$$

where

$$
\begin{aligned}
k_r &= \max\left\{ L(y)\left(\frac{2F^*}{|\mathrm{d}L(y)/\mathrm{d}y|}\right)^{-1/2}\left|\frac{d}{dy}\left|\frac{\mathrm{d}L(y)}{\mathrm{d}y}\right|^{-1}\right|\right\},\\
k_{rr} &= \max\left\{ L(y)\left(\frac{2F^*}{|\mathrm{d}L(y)/\mathrm{d}y|}\right)^{-1/2}\left|\frac{\mathrm{d}L(y)}{\mathrm{d}y}\right|^{-1}\right\},
\end{aligned}
\tag{47}
$$

and constants $k_\sigma, k_\delta, k^*, k_t$, and $I^*(0)$ are defined in Appendix B.

Notice that the four leading principal minors of matrix Q can always be rendered positive definite by suitable selection of the controller gains k_{p1}, k_{d1}, k_p, k_i, and α_{p1}, and hence, $\lambda_{\min}(Q) > 0$. Furthermore, all of the expressions in the seven rows in (45) can be rendered negative, at least locally, using suitable gains $k_{d2}, k_{d3}, k_{d4}, \alpha_{p2}, \alpha_{p3}, \alpha_{p4}, k_{p2}$, and k_{p3}. Hence, it is concluded that $\dot{W} \leq 0$ for all $\zeta \in \mathscr{D}$, where $\mathscr{D}$ is a subset of $\mathscr{R}^7$ containing the origin. Thus, stability of the origin is concluded. Since the closed-loop system is autonomous, the LaSalle invariance principle is invoked to prove asymptotic stability. This completes the proof of Proposition 1.

Conditions for this stability result are summarized by (A.1), (A.2), and (A.5), in Appendix A, $k_p > 0$, $\alpha > 0$, $\beta > 0$, $k_{i1} > 0$, and $\alpha_i > 0$, (34), the four leading principal minors of matrix Q defined in (45) are positive, and $k_{d2}, k_{d3}, k_{d4}, \alpha_{p2}, \alpha_{p3}, \alpha_{p4}, k_{p2}$, and k_{p3} are chosen such that the seven rows in (45) are rendered negative. These stability conditions constitute explicit tuning guide lines.

Remark 1. Notice that the ith leading principal minor of matrix Q can be rendered positive by choosing large enough Q_{ii} entry of matrix Q and choosing small some constants such as $\alpha > 0$ and $\beta > 0$. In this respect, it is important to stress that each one of the Q_{ii} entries depend on a controller gain. Thus, once the ith leading principal minor is rendered positive by choosing a suitable controller gain, the $(i+1)$th leading principal minor can be rendered positive by suitably enlarging the entry $Q_{(i+1)(i+1)}$ of matrix Q and so on. Moreover, these ideas suggest that an intuitive try-and-error tuning procedure can also be derived; choose larger controller gains in the Q_{ii} entries as i is larger.

Remark 2. Notice that the system evolves by itself as long as the sliding surface is not reached. However, it is proven in standard books on sliding mode control that the system reaches the sliding surface in a finite time which depends on the initial conditions. Once the sliding surface is reached, the system evolves on the sliding surface starting from the state values that it has at the time where the sliding surface is reached. Thus, if initial conditions are close to the desired equilibrium point, then asymptotic convergence to the desired equilibrium point is ensured by Proposition 1.

On the other hand, limits in currents i_c and i are imposed by the circuit parameters and the applied voltage. With the problem at hand, limits on these currents are imposed by the DC power supply E which is manipulated through the variable u representing the on-off state of transistor Q. In Section 5, we explain how the variables u and E affect the system performance. Finally, saturation of the internal PI's only might occur if the state variables are allowed to take large values. Since our stability result is local, this prohibits the state to take such large values.

Remark 3. In Figure 3, we present a block diagram of the control scheme in control scheme in Proposition 1. Notice that this controller is made up of three main loops: (1) a PI controller for voltage at the DC/DC Buck power converter output (at the capacitor terminals), (2) a PI controller for electric current through the electromagnet, and (3) a nonlinear PID (NPID) controller for the ball position. Thus, our proposal contains the fundamental components in industrial applications and, hence, it is expected to be robust with respect to parametric uncertainties and external disturbances. Furthermore, another internal loop is provided to control electric current through the inductance of the DC/DC Buck power converter. This loop is driven by a sliding mode controller which constitutes one common technique to control power electronic devices in practice.

Remark 4. It is stressed that we introduce the factor $L(y)$ as a part of the proportional gain in (18) in order to ensure to be constant the term that is added to the integral term in (27). This is a necessary step for the integral action of the PI controller of voltage at the capacitor. In this respect, the last two terms in (17) are included in order to cancel some terms arising in (26) because of the fact that $-C\dot{\bar{v}}$ must be added and subtracted to complete (26).

Remark 5. Notice that the region where the result is valid can be enlarged by including the terms $-k_q\tilde{i}\dot{y}^2 - k_f\tilde{i}|\tilde{i}| - k_h\tilde{i}|e|$ in (18) and the terms $-k_m e\dot{y}^2 - k_n e|\tilde{i}|$ in (17), for some positive constants k_q, k_f, k_h, k_m, and k_n, to proceed as in [30] to dominate the positive terms in the five rows of (45). However, we have decided not to include the above cited terms because of several reasons. (1) The stability result would still remain to be local, as usual in magnetic levitation systems. (2) Including the above terms in (18) would result in additional complex terms that should be cancelled using the definition of i_c^* in (17). (3) In order to maintain the simple control law, we have decided not to proceed including the terms $-k_q\tilde{i}\dot{y}^2 - k_f\tilde{i}|\tilde{i}| - k_h\tilde{i}|e|$ in (18) which renders useless to include $-k_m e\dot{y}^2 - k_n e|\tilde{i}|$ in (17). Thus, proposing a simple and robust control law performing well is one important objective of our proposal.

Remark 6. The novel passivity-based approach that is employed in this paper has the following properties:

(i) Several terms cancel naturally. This means that they cancel without requiring to compute and feedback them. This property is a direct consequence of the fact that the closed-loop dynamics (35)–(38) is almost identical to the open-loop model in (6). Recall that the open-loop model was proven in Section 3 to be output strictly passive, and the existence of several natural cancellations is instrumental for this. This property is opposite to what happens in exact feedback linearization approaches where the plant undesired terms are online computed and fed back in order to force their cancellation.

The natural cancellation of terms that we refer to in this item is the same that is referred to before (44), which includes $(1/2)(dL(y)/dy)\tilde{i}^2\dot{y} - (dL(y)/dy)\tilde{i}^2\dot{y} - (dL(y)/dy)\tilde{i}i^*\dot{y}$ belonging to $(d/dt)((1/2)L(y)\tilde{i}^2)$ and $(1/2)(dL(y)/dy)\tilde{i}^2\dot{y} + (dL(y)/dy)\tilde{i}i^*\dot{y}$ belonging to $(d/dt)((1/2)m\dot{y}^2)$, as well as the

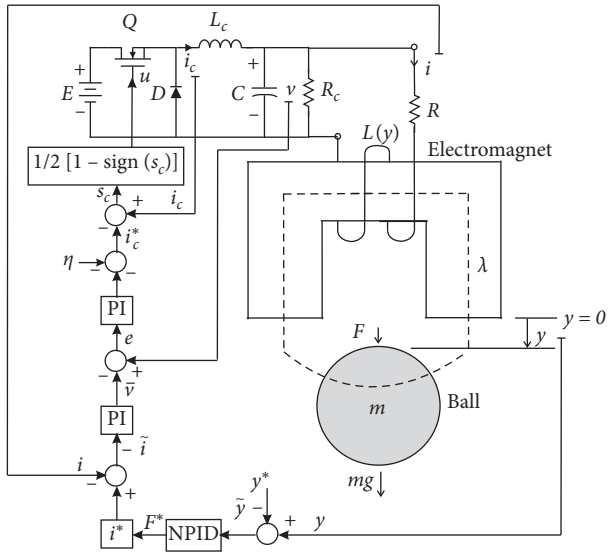

Figure 3: Control scheme in Proposition 1, where $\eta = -(\bar{v}/R_c) + C\alpha_p(-(dL(y)/dy)i^*\dot{y} + v) + C\alpha_i\tilde{i}$.

cancellation of $-e\tilde{i}$ belonging to $(d/dt)((1/2)Ce^2)$ and $e\tilde{i}$ belonging to $(d/dt)((1/2)L(y)\tilde{i}^2)$.

These natural term cancellations are very useful to obtain a simple control law. As stated above, other control approaches require to use additional terms in the control law in order to cancel these terms.

(ii) A nested-loop passivity-based control approach is exploited in [20]. This means that the electric current error is first proven to converge exponentially to zero, and this allows to use this variable as a vanishing perturbation for the mechanical subsystem. This, however, requires the online computation of either the time derivative of the desired force or the time derivative of the desired electric current. Instead of that we use an approach which is similar to what was called in [20] passivity-based control with total energy shaping. Although the latter approach has been disregarded in [20] by arguing that it results in more complex controllers, we prove the opposite in the present paper. This is one important novelty of our approach.

(iii) The previous features of our approach allow (1) to straightforwardly include PI internal loops and an external PID loop, which are important to improve the robustness properties of the control scheme and (2) to avoid the requirement on the exact knowledge of the electric resistance of the electromagnet, which is a parameter that changes during normal operation conditions.

Remark 7. The present work is inspired by [16] in the sense that some PI and PID loops are included for both the electrical and the mechanical dynamics of the electromechanical system, and a sliding mode controller is devoted to control electric current through the inductor of the DC/DC Buck converter, see Figure 4. However, the control scheme in [16] is designed for unidirectional control of velocity in a brushed DC motor, whereas the controller in the present work contains several refinements that extend work in [16] to control position in a magnetic levitation system, a highly nonlinear system. These refinements include (1) a clever selection of a nonlinear PID position controller, (2) a clever selection of internal PI controllers, and (3) proposing a suitable Lyapunov function for stability analysis. We stress that, aside from the sliding mode controller, the closed-loop system in [16] is linear, whereas both plant and controller are nonlinear in the present work.

5. Simulation Results

In this section, we present a numerical example to give some insight on the achievable performance when the controller in Proposition 1 is employed. To this aim, we use the numerical values of the magnetic levitation system that has been tested experimentally in [23]. In that work, the electromagnet inductance is modeled as follows:

$$L(y) = k_0 + \frac{k}{1 + (y/a)}, \tag{48}$$

where $k_0 = 36.3 \times 10^{-3}$ H, $k = 3.5 \times 10^{-3}$ H, and $a = 5.2 \times 10^{-3}$ m, and the remaining parameters are $R = 2.72$ Ohm, $m = 0.018$ kg, and $g = 9.81$ m/s^2. The practical range of input voltages is $[0, +12]$ V and the range of electric current through the electromagnet is $[0, +3]$ A. The Buck DC/DC power electronic system parameters were chosen as $L_c = 0.686$ H, $C = 114.4 \times 10^{-6}$ F, and $R_c = 28.5$ Ohm. We also use $E = 12$ V if $2\,\text{s} < t < 3\,\text{s}$ and $E = 50$ V, otherwise in order to study the response when disturbances appear in the DC power supply. These parameters are similar to the experimental values reported in [16].

The controller gains were chosen to be $k_p = 8$, $k_d = 1$, $k_i = 2$, $\alpha_p = 470$, $\alpha_i = 1000$, $\alpha = 64$, $\beta = 1$, $k_{p1} = 6000$, and $k_{i1} = 18000$. Inspired by [28], we used the saturation function:

$$\sigma(x) = \begin{cases} -L^* + (M - L^*)\tanh\left(\dfrac{x + L^*}{M - L^*}\right), & \text{if } x < -L^*, \\ x, & \text{if } |x| \le L^*, \\ L^* + (M - L^*)\tanh\left(\dfrac{x - L^*}{M - L^*}\right), & \text{if } x > L^*, \end{cases} \tag{49}$$

where $M = 0.51$ and $L^* = 0.5$. The initial conditions were set as follows $y(0) = 0.006$ m, $\dot{y}(0) = 0$, $i(0) = 1.56$ A, $v(0) = 4.2$ V, $i_c(0) = 1.65$ A, $\int_{-\infty}^{0} \tilde{i}dt = -4.24362 \times 10^{-3}$, $\int_{-\infty}^{0} edt = 0.022$, andn $z(0) = 0.0885$. The desired position y^*, in meters, was chosen as follows:

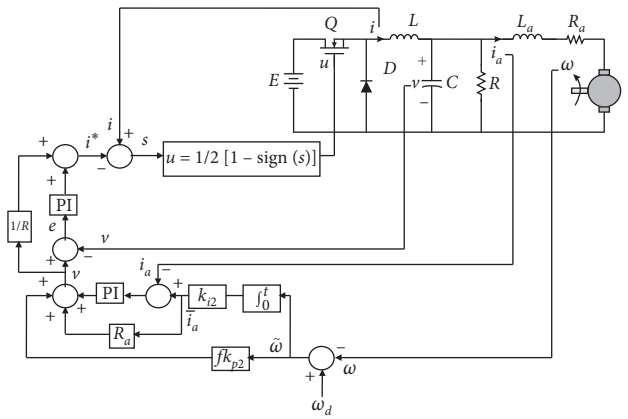

Figure 4: Block diagram of the controller in [16].

$$y^* = \begin{cases} 0.006, & 0 \le t < 1, \\ 0.008, & 1 \le t < 4, \\ 0.006, & 4 \le t < 5.5, \\ 0.004, & 5.5 \le t. \end{cases} \tag{50}$$

In Figure 5, we can see that the actual ball position y reaches its desired value y^* in the steady state. Notice that the settling time is about 0.5 s. We observe that the position response is very damped. In this respect, we have performed several additional simulations which make us to conclude that the term $(1 + \alpha\beta(k_d/k_i))\dot{y}$ appearing in (20) is responsible for such a damped response.

In Figures 6 and 7, we verify that electric current through the electromagnet i and voltage at the electromagnet terminals v remain within $[0, +3]$ A and $[0, +12]$ V, respectively, the actual ranges of values reported experimentally in [23].

In Figure 8, we present electric current through the converter inductor which also remains within the range $[0, +3]$ A. Finally, in Figure 9, we verify that evolution of all the above signals is achieved by applying, at the transistor input, a switching signal only taking the discrete values 1 or 0. Notice that, despite this hard switching signal, electric current through the electromagnet is smooth enough, see Figure 6. Moreover, this is achieved despite voltage at the electromagnet terminals has a small ripple, see Figure 7.

We also observe in Figure 5 that the step changes in the DC power supply, i.e., E, appearing at $t = 2$ s and $t = 3$ s have an almost imperceptible effect in the ball position. Moreover, the effects of these changes are more noticeable in Figures 7 and 8 as a simple change in ripple of both voltage at the electromagnet terminals and electric current through the converter inductor. The effects of these step changes are very small thanks to the employment of a sliding mode controller for electric current through the converter inductor and this is the reason why we employ sliding mode control in our approach.

Finally, we stress that the control signal u is constrained to only take the discrete values 0 or 1 and all of the system evolution must be controlled while u takes these discrete values. However, the designer has an additional degree-of-

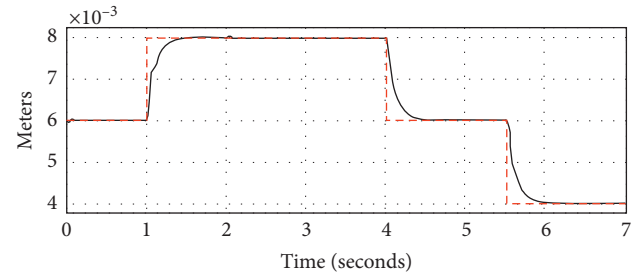

Figure 5: Continuous: actual ball position y. Dashed: desired ball position y^*.

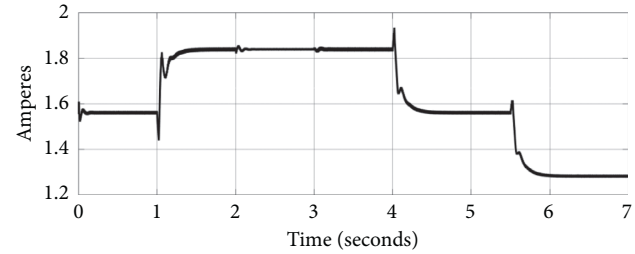

Figure 6: Electric current i through the electromagnet.

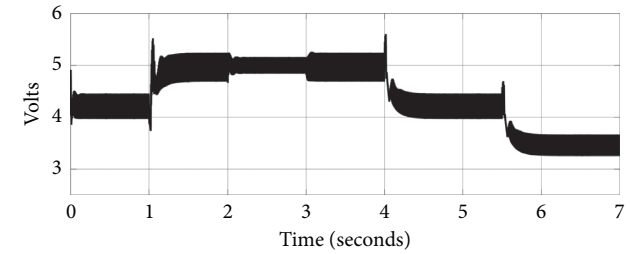

Figure 7: Voltage v at the electromagnet terminals.

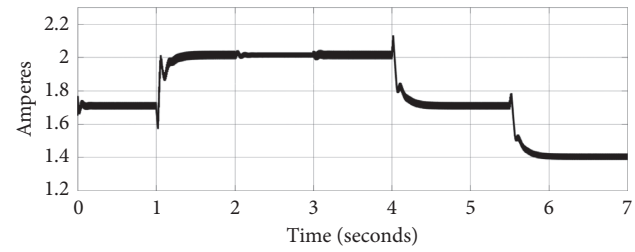

Figure 8: Electric current i_c through the converter inductor.

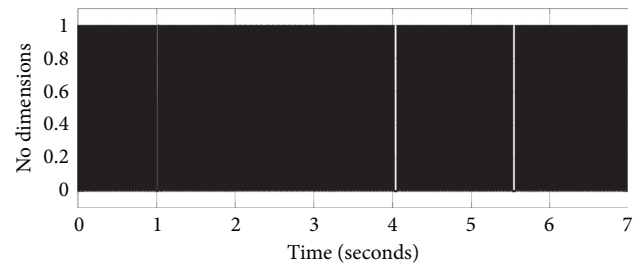

Figure 9: On-off signal u applied at the transistor input.

freedom in this respect; a larger value for E can be chosen if the system evolution requires more control effort. We have arrived to this conclusion during the simulations that we have performed. For instance, we can observe in Figure 9 three clear zones at $t = 1$ s, $t = 4$ s, and $t = 5.5$ s which are evidences that control effort saturates at its extremum values, i.e., either 1 or 0, when step changes in the desired position are commanded. We also have observed that the ball escapes if larger reference changes are commanded. This is the reason why we have used $E = 50$ V for most of the time in the above simulations.

Now, we present some simulation results when using the following classical control scheme:

$$v = k_{pi}(i^* - i) + k_{ii}\int_0^t (i^* - i)\mathrm{d}t, \tag{51}$$

$$i^* = k_p(y - y^*) + k_d\dot{y} + k_i\int_0^t (y - y^*)\mathrm{d}t. \tag{52}$$

It is assumed that the DC/DC Buck power electronic converter is not present and a static PWM-based power amplifier is employed. Notice that position error is given as $y - y^*$ for the classical PID controller. This is usual in control of magnetic levitation systems. A feature that is required because of the negative gain of the system which, in turn, is produced by the fact that $(\mathrm{d}L(y)/\mathrm{d}y) < 0$.

The controller gains were chosen to be $k_{pi} = 4.7$, $k_{ii} = 100$, $k_d = 0.0277$, $k_p = 0.866$, and $k_i = 1.082$. This results in two real dominant closed-loop poles located at $s = -21.5$ and $s = -2.11$. A third real closed-loop pole is at $s = -140$ and two very fast complex conjugate poles, due to the PI control of the electrical dynamics, located at $s = -19 \pm 500j$.

Our intention is not to compare results obtained with the controller in Proposition 1 and result with the classical control scheme since such a comparison would be unfair. We just want to point out on some features of the classical control scheme. The simulation results are shown in Figures 10–12. The desired position y^* is given, again, as in (50).

Notice that the position response has a very short rise time but a large settling time. This is produced by initial fast changes on both the applied voltage and the resulting electric current, which tend slowly to constant values afterwards. Notice that position response exhibits a large overshoot despite the dominant closed-loop poles being real. Recall that the fast complex conjugate poles due to the electrical dynamics cannot produce such a slow overshoot. As it is clearly explained in [31], reason for such a large overshoot is the open-loop unstable pole of the magnetic levitation system which is responsible of its open-loop instability. It is also demonstrated in [31] that this feature cannot be avoided when using the classical control scheme in (51) and (52).

Since classical control schemes rely on linear approximations of the plant to control, it is reasonable to wonder whether some advantages could be obtained when proposing control schemes that take into account more information of the plant nonlinear dynamical model. This is the intention of nonlinear control schemes as the one presented in

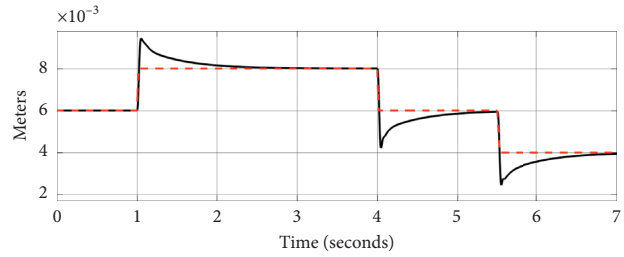

Figure 10: Classical control scheme. Continuous: actual ball position y. Dashed: desired ball position y^*.

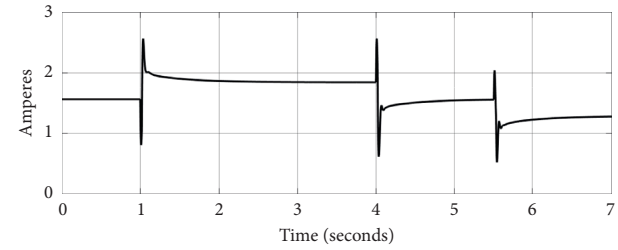

Figure 11: Classical control scheme. Electric current i through the electromagnet.

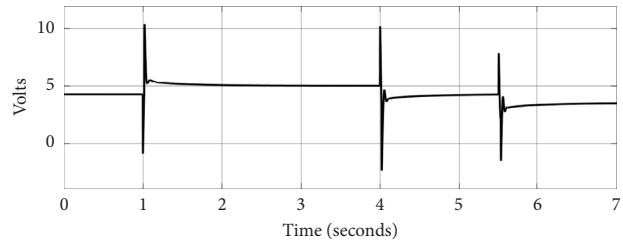

Figure 12: Classical control scheme. Voltage v at the electromagnet terminals.

Proposition 1 aside from taking into account some additional dynamics as that of the DC/DC Buck power electronic converter.

Notice that the expressions in (18)–(20) are the nonlinear versions of (51) and (52), i.e., they represent a PI electric current loop and a PID position loop. On the contrary, (16) and (17), represent a sliding mode control loop for electric current at the converter inductor and a nonlinear PI loop for voltage at the converter capacitor. This means that (16) and (17) are additional control loops that are included to cope with system components that are not present in standard magnetic levitation systems. This is what we mean when stating that the control scheme in Proposition 1 is simple if we take into account the complexity of the nonlinear model of the plant.

6. Conclusions

In this paper, we have solved the position regulation problem in a magnetic levitation system when it is fed by a DC/DC Buck power electronic converter as power amplifier.

Contrary to previous works in the literature, which are concerned with control of DC motors, we have solved this problem for the first time for a nonlinear electromechanical system.

This fact represents the merit of our proposal despite the local nature of the results. In this respect, we stress that the region of attraction might be enlarged by including additional nonlinear terms to the control law. However, we have decided not to do this because we are interested in presenting a simple control law in order to render it free of numerical errors and noise amplification.

Our proposal relies on a novel passivity-based approach which exploits the natural energy exchange existing among the mechanical and electrical subsystems that compose the plant. This allows several nonlinear terms to naturally cancel, i.e., without requiring to include additional terms in the control law, which renders simple the control law. Moreover, contrary to previous well known works in the literature, our approach does not rely on proving exponential convergence to zero of the electrical dynamics. This is good news since, otherwise, we would require to online compute and feedback both the time derivative of the desired electric current in the electromagnet and the time derivative of the desired voltage at the electromagnet terminals. Such online computations would render the control law complex and sensitive to numerical errors and noise amplification.

Finally, although the control law is simple, the stability proof may require much attention from the reader. This might be seen as a disadvantage of the approach but it is the authors' belief that it is the role of the control community to cope with mathematical analysis and other related theoretical complications. The important practical thing is that the resulting control scheme is intuitively simple to understand and to implement: a multiloop scheme driven by PI and PID controllers provided with explicit tuning guide lines. We must also say that our approach only considers the regulation task.

Appendix

A. Conditions for Positive Definiteness of $V_m(\dot{y}, \tilde{y}, z - mg/k_i)$, Defined in (40)

Choose

$$0 < L^* < M, \tag{A.1}$$

and $k_d > 0$ large enough such that

$$G(\tilde{y}) \geq \alpha^{*2} m H(\tilde{y}), \quad \forall \tilde{y} \in \mathscr{R}, \tag{A.2}$$

where $\alpha^* > \alpha > 0$ and

$$G(\tilde{y}) = \begin{cases} \dfrac{k_d}{2}\tilde{y}^2, & |\tilde{y}| \leq L^*, \\ \dfrac{k_d}{2}L^{*2} + k_d L^*(\tilde{y} - L^*), & \tilde{y} > L^*, \\ \dfrac{k_d}{2}L^{*2} - k_d L^*(\tilde{y} + L^*), & \tilde{y} < -L^*, \end{cases} \tag{A.3}$$

$$H(\tilde{y}) = \begin{cases} \tilde{y}^2, & |\tilde{y}| \leq M, \\ M^2, & |\tilde{y}| > M. \end{cases}$$

We stress that (A.2) can always be verified graphically. Define $d = mg/k_i$, $z' = z - d$, and

$$\Gamma(z') = \begin{cases} \dfrac{k_i}{2}(z')^2, & -L^* \leq z' + d \leq L^*, \\ \dfrac{k_i}{2}(L^* - d)^2 + k_i(z' + d - L^*)(L^* - d), & z' + d > L^*, \\ \dfrac{k_i}{2}(-L^* - d)^2 + k_i(z' + d + L^*)(-L^* - d), & z' + d < L^*, \end{cases} \tag{A.4}$$

$$F(z') = \begin{cases} z'^2, & -M \leq z' + d \leq M, \\ (M - d)^2, & z' + d > M, \\ (-M - d)^2, & z' + d < -M. \end{cases}$$

Choose a large enough $k_i > 0$ such that

$$\Gamma(z') \geq \alpha^{*2}\beta^{*2} m F(z'), \tag{A.5}$$

for some $\alpha^* > \alpha > 0$ and $\beta^* > \beta > 0$. Notice that (A.5) can always be verified graphically. Function $V_m(\dot{y}, \tilde{y}, z - mg/k_i)$ is positive definite and radially unbounded if $k_p > 0$, $\alpha > 0$,

and $\beta > 0$ and (A.1), (A.2), and (A.5) are satisfied. Proof of this result is presented in [30].

B. Some Algebraic Relations for Proof of Proposition 1

Notice the following:

$$\left|i^*\right| \leq \sqrt{\frac{2}{\left|\mathrm{d}L(y)/\mathrm{d}y\right|_{\min}}\left(k_p M + k_d|\dot{y}| + k_i M\right)} = I^*(|\dot{y}|), \tag{B.1}$$

where (19) has been employed. On the other hand, according to the Mean Value Theorem:

$$0 \leq I^*(|\dot{y}|) - I^*(0) = \left.\frac{\mathrm{d}I^*(|\dot{y}|)}{\mathrm{d}|\dot{y}|}\right|_{|\dot{y}|=\zeta}(|\dot{y}| - 0),$$

$$\left.\frac{\mathrm{d}I^*(|\dot{y}|)}{\mathrm{d}|\dot{y}|}\right|_{|\dot{y}|=\zeta} > 0, \quad \forall \zeta > 0, \tag{B.2}$$

i.e.,

$$I^*(|\dot{y}|) = \left.\frac{dI^*(|\dot{y}|)}{d|\dot{y}|}\right|_{|\dot{y}|t=n\zeta}|\dot{y}| + I^*(0), \tag{B.3}$$

for some $\zeta > 0$ belonging to the line joining the points $|\dot{y}|$ and 0. Hence, from (B.1) and (B.3), we find

$$\begin{aligned}\left|i^*\right| &\leq k_\delta|\dot{y}| + I^*(0),\\ k_\delta &= \max_{|\dot{y}|>0}\left\{\frac{\mathrm{d}I^*(|\dot{y}|)}{\mathrm{d}|\dot{y}|}\right\}.\end{aligned} \tag{B.4}$$

Notice that k_δ and $I^*(0)$ are positive and finite. This allows to write

$$\begin{aligned}&\left|\frac{\mathrm{d}L(y)}{\mathrm{d}y}\tilde{i}^2 i^*\right| \leq k_\sigma \tilde{i}^2\left(k_\delta|\dot{y}| + I^*(0)\right),\\ &\left|\alpha\frac{\mathrm{d}L(y)}{\mathrm{d}y}h(\tilde{y})\tilde{i}i^*\right| \leq \alpha k_\sigma k_\delta M|\tilde{i}||\dot{y}| + \alpha k_\sigma|\tilde{i}||h(\tilde{y})|I^*|0|,\\ &\left|\alpha\beta\frac{\mathrm{d}L(y)}{\mathrm{d}y}s(z)\tilde{i}i^*\right| \leq 2\alpha\beta M k_\sigma k_\delta|\tilde{i}||\dot{y}| + \alpha\beta k_\sigma|\tilde{i}||s(z)|I^*(0),\\ &k_\sigma = \max\left\{\left|\frac{\mathrm{d}L(y)}{\mathrm{d}y}\right|\right\}.\end{aligned} \tag{B.5}$$

We stress that $k_\sigma > 0$ is always finite, i.e., the maximal value of $|\mathrm{d}L(y)/\mathrm{d}y|$ appears when $y = 0$. On the contrary, we have that at the equilibrium point $i^* = i_e^*$, where

$$i_e^* = \sqrt{\frac{2mg}{\left|\mathrm{d}L(y^*)/\mathrm{d}y\right|}}. \tag{B.6}$$

Hence, if we assume that

$$\begin{aligned}i^* &= i^*(h(\tilde{y}), \dot{y}, s(z))\\ &= \sqrt{\frac{2}{|\mathrm{d}L(y)/\mathrm{d}y|}\left[k_p h(\tilde{y}) + k_d\dot{y} + k_i s(z) + mg\right]},\end{aligned} \tag{B.7}$$

then $i_e^* = i^*(0,0,0)$. Thus, according to the Mean Value Theorem

$$\begin{aligned}i^* - \sqrt{\frac{2mg}{\left|\mathrm{d}L(y^*)/\mathrm{d}y\right|}} &= i^*(h(\tilde{y}), \dot{y}, s(z)) - i^*(0,0,0)\\ &= \left.\frac{\partial i^*(x)}{\partial x}\right|_{x=p}\left((h(\tilde{y}), \dot{y}, s(z))^T - (0,0,0)^T\right),\end{aligned} \tag{B.8}$$

for some p belonging to the line joining the points $(h(\tilde{y}), \dot{y}, s(z))$ and $(0,0,0)$. Finally, recalling that $|v^T w| \leq \|v\|\|w\|$, for all $v, w \in \mathscr{R}^n$ and $\|x\| \leq \|x\|_1$, we can write

$$\left|i^* - \sqrt{\frac{2mg}{\left|\mathrm{d}L(y^*)/\mathrm{d}y\right|}}\right| \leq \left(k^* + k_t|\dot{y}|\right)[|h(\tilde{y})| + |\dot{y}| + |s(z)|], \tag{B.9}$$

where the constants k^* and k_t are defined from the norm of the following vector:

$$\begin{aligned}\frac{\partial i^*(x)}{\partial x} &= \left(\frac{2F^*}{|\mathrm{d}L(y)/dy|}\right)^{-1/2} \times \left\{[1,0,0]\left(\frac{\mathrm{d}}{\mathrm{d}y}\left|\frac{\mathrm{d}L(y)}{\mathrm{d}y}\right|^{-1}\right)\right.\\ &\quad \times \frac{\mathrm{d}(y^* + \tilde{y})}{\mathrm{d}\tilde{y}}\frac{\mathrm{d}\tilde{y}}{\mathrm{d}h(\tilde{y})}\left[k_p h(\tilde{y}) + k_i s(z) + mg\right]\\ &\quad \left. + \left|\frac{\mathrm{d}L(y)}{\mathrm{d}y}\right|^{-1}\left[k_p, k_d, k_i\right]\right\}\\ &\quad + \left(\frac{2F^*}{|\mathrm{d}L(y)/\mathrm{d}y|}\right)^{-1/2}[1,0,0]\left(\frac{\mathrm{d}}{\mathrm{d}y}\left|\frac{\mathrm{d}L(y)}{\mathrm{d}y}\right|^{-1}\right)\\ &\quad \times \frac{\mathrm{d}(y^* + \tilde{y})}{\mathrm{d}\tilde{y}}\frac{\mathrm{d}\tilde{y}}{\mathrm{d}h(\tilde{y})}k_d\dot{y},\end{aligned} \tag{B.10}$$

recalling that, according to (21), $\mathrm{d}\tilde{y}/\mathrm{d}h(\tilde{y})$ is bounded, $|\mathrm{d}L(y)/\mathrm{d}y| > 0$, $(2F^*/(|\mathrm{d}L(y)/\mathrm{d}y|))^{-1/2}$, and $\mathrm{d}/\mathrm{d}y|\mathrm{d}L(y)/\mathrm{d}y|^{-1}$ are bounded, and $|h(\tilde{y})| \leq M$ and $|s(z)| \leq 2M$. Thus, k^* and k_t are finite.

Data Availability

The data used to support the findings of this study are available from the corresponding author upon request.

Conflicts of Interest

The authors declare that there are no conflicts of interest regarding the publication of this article.

Acknowledgments

The processing charge of this article was generously supported by the Instituto Politécnico Nacional, México. The work of V. M. Hernández-Guzmán was supported by the SNI-México. The work of R. Silva-Ortigoza and M. Marciano-Melchor was supported by the SNI-México and IPN programs EDI and SIBE.

References

[1] F. Antritter, P. Maurer, and J. Reger, "Flatness based control of a buck-converter driven DC motor," in *Proceedings of the 4th IFAC Symposium on Mechatronic Systems*, Heidelberg, Germany, September 2006.

[2] S. E. Lyshevski, *Electromechanical Systems, Electric Machines, and Applied Mechatronics*, CRC Press, Boca Raton, FL, USA, 1999.

[3] I. Boldea and S. A. Nasar, *Electric Drives*, CRC Press LLC, Boca Raton, FL, USA, 1999.

[4] H. El Fadil and F. Giri, "Accounting of DC-DC power converter dynamics in DC motor velocity adaptive control," in *Proceedings of the IEEE International Conference on Control Applications*, pp. 3157–3162, Munich, Germany, October 2006.

[5] J. Linares-Flores and H. Sira-Ramírez, "A smooth starter for a DC machine: a flatness based approach," in *Proceedings of the 1st International Conference on Electrical and Electronics Engineering*, pp. 589–594, Acapulco, Mexico, September 2004.

[6] J. Linares-Flores and H. Sira-Ramírez, "Sliding mode-delta modulation GPI control of a DC motor through a buck converter," in *Proceedings of the 2nd IFAC Symposium on System*, pp. 405–409, Oaxaca, Mexico, December 2004.

[7] J. Linares-Flores and H. Sira-Ramírez, "DC motor velocity control through a DC-to-DC power converter," in *Proceedings of the 43rd IEEE Conference on Decision and Control*, vol. 5, pp. 5297–5302, Atlantis, The Bahamas, December 2004.

[8] R. Silva-Ortigoza, J. R. García-Sánchez, J. M. Alba-Martínez et al., "Two-stage control design of a buck converter/DC motor system without velocity measurements via aΣ−Δ-modulator," *Mathematical Problems in Engineering*, vol. 2013, Article ID 929316, 11 pages, 2013.

[9] R. Silva-Ortigoza, C. Márquez-Sánchez, F. Carrizosa-Corral, M. Antonio-Cruz, J. M. Alba-Martínez, and G. Saldaña-González, "Hierarchical velocity control based on differential flatness for a DC/DC Buck converter-DC motor system," *Mathematical Problems in Engineering*, vol. 2014, Article ID 912815, 12 pages, 2014.

[10] R. Silva-Ortigoza, V. M. Hernandez-Guzman, M. Antonio-Cruz, and D. Munoz-Carrillo, "DC/DC Buck power converter as a smooth starter for a DC motor based on a hierarchical control," *IEEE Transactions on Power Electronics*, vol. 30, no. 2, pp. 1076–1084, 2015.

[11] H. Sira-Ramirez and M. A. Oliver-Salazar, "On the robust control of buck-converter DC-motor combinations," *IEEE Transactions on Power Electronics*, vol. 28, no. 8, pp. 3912–3922, 2013.

[12] R. Sureshkumar and S. Ganeshkumar, "Comparative study of proportional integral and backstepping controller for buck converter," in *Proceedings of the International Conference on Emerging Trends in Electrical and Computer Technology*, pp. 375–379, Tamil Nadu, India, March 2011.

[13] E. Hernandez-Marquez, R. Silva-Ortigoza, J. R. Garcia-Sanchez, M. Marcelino-Aranda, and G. Saldana-Gonzalez, "A DC/DC buck-boost converter-inverter-DC motor system: sensorless passivity-based control," *IEEE Access*, vol. 6, pp. 31486–31492, 2018.

[14] E. Hernández-Márquez, J. R. García-Sánchez, R. Silva-Ortigoza et al., "Bidirectional tracking robust controls for a DC/DC buck converter-DC motor system," *Complexity*, vol. 2018, Article ID 1260743, 10 pages, 2018.

[15] R. Silva Ortigoza, J. N. Alba Juarez, J. R. Garcia Sanchez, M. Antonio Cruz, V. M. Hernandez Guzman, and H. Taud, "Modeling and experimental validation of a bidirectional DC/DC buck power electronic converter-DC motor system," *IEEE Latin America Transactions*, vol. 15, no. 6, pp. 1043–1051, 2017.

[16] V. M. Hernández-Guzmán, R. Silva-Ortigoza, and D. Muñoz-Carrillo, "Velocity control of a brushed DC-motor driven by a DC to DC buck power converter," *International Journal of Innovative Computing, Information and Control*, vol. 11, no. 2, pp. 509–521, 2015.

[17] Z. Chen, W. Gao, and X. Ye, "Frequency domain closed-loop analysis and sliding mode control of a nonminimum phase buck-boost converter," *Control and Intelligent Systems*, vol. 38, no. 4, pp. 245–255, 2010.

[18] Z. Chen, J. Hu, and W. Gao, "Closed-loop analysis and control of a non-inverting buck-boost converter," *International Journal of Control*, vol. 83, no. 11, pp. 2294–2307, 2010.

[19] Z. Chen, W. Gao, J. Hu, and X. Ye, "Closed-loop analysis and cascade control of a nonminimum phase boost converter," *IEEE Transactions on Power Electronics*, vol. 26, no. 4, pp. 1237–1252, 2011.

[20] R. Ortega, A. Loría, P. Nicklasson, and H. Sira-Ramírez, *Passivity-based Control of Euler-Lagrange Systems*, Springer, London, UK, 1998.

[21] R. Ortega, A. J. van der Schaft, I. Mareels, and B. Maschke, "Putting energy back in control," *IEEE Control Systems Magazine*, vol. 21, no. 2, pp. 18–33, 2001.

[22] H. Rodriguez, R. Ortega, and I. Mareels, "Nonlinear control of magnetic levitation systems via energy balancing," in *Proceedings of the American Control Conference*, Chicago, IL, USA, June 2000.

[23] V. M. Hernández-Guzmán and R. Silva-Ortigoza, *Automatic Control with Experiments*, Springer, Cham, Switzerland, 2019.

[24] A. Astolfi and R. Ortega, "Immersion and invariance: a new tool for stabilization and adaptive control of nonlinear systems," *IEEE Transactions on Automatic Control*, vol. 48, no. 4, pp. 590–606, 2003.

[25] A. Astolfi, D. Karagiannis, and R. Ortega, *Nonlinear and Adaptive Control with Applications*, Springer, Cham, Switzerland, 2008.

[26] R. S. Ortigoza, J. N. A. Juarez, J. R. G. Sanchez, V. M. H. Guzman, C. Y. S. Cervantes, and H. Taud, "A sensorless passivity-based control for the DC/DC buck converter-inverter-DC motor system," *IEEE Latin America Transactions*, vol. 14, no. 10, pp. 4227–4234, 2016.

[27] V. M. Hernández-Guzmán and R. Silva, "Current loops in a magnetic levitation system," *International Journal of Innovative Computing, Information and Control*, vol. 5, no. 5, pp. 1275–1283, 2009.

[28] A. Zavala-Rio and V. Santibanez, "A natural saturating extension of the PD-with-desired-gravity-compensation control law for robot manipulators with bounded inputs," *IEEE Transactions on Robotics*, vol. 23, no. 2, pp. 386–391, 2007.

[29] H. K. Khalil, *Nonlinear Systems*, Prentice-Hall, Upper Saddle River, NJ, USA, 3rd edition, 2002.

[30] V. M. Hernández-Guzmán and J. Orrante-Sakanassi, "Global PID control of robot manipulators equipped with PMSMs," *Asian Journal of Control*, vol. 20, no. 1, pp. 236–249, 2018.
[31] G. C. Goodwin, S. F. Graebe, and M. E. Salgado, *Control System Design*, Prentice-Hall, Upper-Saddle River, NJ, USA, 2001.

Hindawi
Complexity
Volume 2020, Article ID 9078471, 13 pages
https://doi.org/10.1155/2020/9078471

Research Article

Analysis of Stochastic Nicholson-Type Delay System under Markovian Switching on Patches

Xin Yi and Guirong Liu

School of Mathematical Sciences, Shanxi University, Taiyuan, Shanxi 030006, China

Correspondence should be addressed to Guirong Liu; lgr5791@sxu.edu.cn

Received 28 February 2020; Revised 15 April 2020; Accepted 24 April 2020; Published 23 May 2020

Guest Editor: Baltazar Aguirre Hernández

Copyright © 2020 Xin Yi and Guirong Liu. This is an open access article distributed under the Creative Commons Attribution License, which permits unrestricted use, distribution, and reproduction in any medium, provided the original work is properly cited.

Based on the influence of random environmental perturbations and the patch structure, we propose a stochastic Nicholson-type delay system under Markovian switching on patches. Existence of a global positive solution is studied. Then, we show ultimate boundedness and estimation of the sample Lyapunov exponent of the solution. Furthermore, sufficient conditions for extinction of species are established, which is the main new ingredient of this paper. Finally, some numerical examples are presented. Our results improve and generalize previous related results.

1. Introduction

In 1980, Gurney et al. [1] established Nicholson's blowflies equation according to experimental data of Nicholson [2]. In recent decades, there have been a large amount of results related to the dynamical behaviors for this model and its modification, see [3–13].

In ecosystems, the pattern of complex population dynamics is inevitably subject to some kind of environmental noises. As a matter of fact, the phenomenon of stochasticity plays a critical role in understanding the evolutionary dynamics and ecological characteristics of species. Particularly, May [14] has revealed that due to environmental fluctuations, the parameters in a system should be stochastic. Environmental noises are classified into two categories: the first is white noise, and the second one is coloured noise. Stochastic population models [15–20] are more realistic compared to deterministic population models. Wang et al. [21] first studied a scalar stochastic Nicholson's blowflies delayed equation

$$\mathrm{d}x(t) = \left[-\alpha x(t) + px(t-\tau)e^{-\gamma x(t-\tau)}\right]\mathrm{d}t + \sigma x(t)\mathrm{d}B(t). \quad (1)$$

Notice, however, that white noise is unable to depict the phenomena that the species may be invaded by the alien population [22] or suffer sudden catastrophic shocks [23]. And in recent years, some significant progress has been made in the theory of the stochastic population models with regime switching, see [24–27] and the references therein. In [28], Zhu et al. considered a stochastic equation with Markovian switching:

$$\mathrm{d}x(t) = \left[-\alpha_{r_t}x(t) + p_{r_t}x\left(t-\tau_{r_t}\right)e^{-\gamma_{r_t}x\left(t-\tau_{r_t}\right)}\right]\mathrm{d}t + \sigma_{r_t}x(t)\mathrm{d}B(t), \quad (2)$$

where continuous-time Markov chain $\{r_t\}_{t\geq 0}$ is defined on a state space $\mathbb{S} = \{1, 2, \ldots, m\}$.

On the contrary, migration is a ubiquitous phenomenon in the nature. Both continuous reaction-diffusion models and discrete patchy systems could incorporate and explain the phenomenology of spatial dispersion [29] in the literature of mathematical ecology. Objectively speaking, patch-structured models illustrate the spatial heterogeneity of species, depending on a lot of factors, such as ecological systems in different geographic types (e.g., nature reserves and other regions), various food-rich patches of habitats, and many other circumstances. Besides, models in the patchy environment include disease systems as well, such as the two-compartment model of the cancer cell population. In order to take the dispersal phenomenon into

consideration, Berezansky et al. [30] introduced the Nicholson-type delay system on patches as follows:

$$\begin{cases} x_1'(t) = -a_1 x_1(t) - b_2 x_1(t) + b_1 x_2(t) + p_1 x_1(t-\tau) e^{-\gamma_1 x_1(t-\tau)}, \\ x_2'(t) = -a_2 x_2(t) - b_1 x_2(t) + b_2 x_1(t) + p_2 x_2(t-\tau) e^{-\gamma_2 x_2(t-\tau)}, \end{cases} \tag{3}$$

which includes the novel two-compartment models of leukemia dynamics and the systems of marine protected areas.

In particular, considering that the parameters a_i of system (3) are affected by the white noise, Yi and Liu [31] formulated the stochastic diffusion system which consists of two patches:

$$\begin{cases} \mathrm{d}x_1(t) = \left[-a_1 x_1(t) - b_2 x_1(t) + b_1 x_2(t) + p_1 x_1(t-\tau) e^{-\gamma_1 x_1(t-\tau)}\right]\mathrm{d}t + \sigma_1 x_1(t)\mathrm{d}B_1(t), \\ \mathrm{d}x_2(t) = \left[-a_2 x_2(t) - b_1 x_2(t) + b_2 x_1(t) + p_2 x_2(t-\tau) e^{-\gamma_2 x_2(t-\tau)}\right]\mathrm{d}t + \sigma_2 x_2(t)\mathrm{d}B_2(t). \end{cases} \tag{4}$$

We can further model random shift in different regimes by a continuous-time Markov chain $\{\ell(t)\}_{t\geq 0}$ defined on a state space $\mathscr{M} = \{1, 2, \ldots, N\}$. Let $\{\ell(t)\}_{t\geq 0}$ be right-continuous and $\Gamma = (\rho_{ij})_{N\times N}$ be its generator of $\{\ell(t)\}_{t\geq 0}$, i.e.,

$$\mathbb{P}\{\ell(t+\delta) = j \mid \ell(t) = i\} = \begin{cases} \rho_{ij}\delta + o(\delta), & \text{if } j \neq i, \\ 1 + \rho_{ii}\delta + o(\delta), & \text{if } j = i, \end{cases} \tag{5}$$

where $\delta > 0$, $\rho_{ij} \geq 0$ for $i \neq j$, and $\sum_{j\in\mathscr{M}} \rho_{ij} = 0$, $i, j \in \mathscr{M}$. Suppose that $\{\ell(t)\}_{t\geq 0}$ is irreducible and has the unique stationary distribution $\pi = (\pi_1, \pi_2, \ldots, \pi_N)$. Hence, we obtain the stochastic Nicholson-type system under Markovian switching on the patch structure as follows:

$$\begin{cases} \mathrm{d}x_1(t) = \left[-a_1(\ell(t))x_1(t) - b_2(\ell(t))x_1(t) + b_1(\ell(t))x_2(t) + p_1(\ell(t))x_1(t-\tau(\ell(t)))e^{-\gamma_1(\ell(t))x_1(t-\tau(\ell(t)))}\right]\mathrm{d}t \\ \quad +\sigma_1(\ell(t))x_1(t)\mathrm{d}B_1(t), \\ \mathrm{d}x_2(t) = \left[-a_2(\ell(t))x_2(t) - b_1(\ell(t))x_2(t) + b_2(\ell(t))x_1(t) + p_2(\ell(t))x_2(t-\tau(\ell(t)))e^{-\gamma_2(\ell(t))x_2(t-\tau(\ell(t)))}\right]\mathrm{d}t \\ \quad +\sigma_2(\ell(t))x_2(t)\mathrm{d}B_2(t), \end{cases} \tag{6}$$

with initial conditions

$$x(t) = \varphi(t) = (\varphi_1(t), \varphi_2(t))^T, \quad t \in [-\tau, 0], \ell(0) = \ell_0 \in \mathscr{M}, \tag{7}$$

where $\varphi_h \in C([-\tau, 0]; [0, +\infty))$ and $\varphi_h(0) > 0$ for $h = 1, 2$ and $\tau = \max_{i\in\mathscr{M}}\{\tau(i)\}$.

We focus on the meaning of parameters with respect to fish population in marine protected area A_1 and fishing area A_2. $x_1(t)$ and $x_2(t)$ are the number of fish populations in A_1 and A_2, respectively; for $h = 1, 2$ and $i \in \mathscr{M}$, $a_1(i)$ and $a_2(i)$ are the mortality rate in A_1 and A_2, respectively; let $G(x_h(t - \tau(i))) = p_h(i)x_h(t-\tau(i))e^{-\gamma_h(i)x_h(t-\tau(i))}$ be the fish growth rates; $p_1(i)$ and $p_2(i)$ represent the maximum per adult yearly birth rate in A_1 and A_2, respectively; $\gamma_h(i) > 0$; $1/\gamma_1(i)$ and $1/\gamma_2(i)$ are the number at which the reproduction at their maximum birth rate in A_1 and A_2, respectively; $\tau(i)$ is the maturation time; $B_h(t)$ is the standard Brownian motion defined on the complete probability space $(\Omega, \mathscr{F}, \mathbb{P})$; and $\sigma_h(i) \geq 0$, for any $i \in \mathscr{M}$ and $h = 1, 2$. We assume $\{\ell(t)\}_{t\geqslant 0}$ is $\mathscr{F}_t$-adapted. Nevertheless, suppose $\{\ell(t)\}_{t\geq 0}$ and $B_h(t)$ are independent of each other, $h = 1, 2$.

Especially, system (6) can reduce to the model in [32] if $\tau(i) \equiv \tau$, $i \in \mathscr{M}$. By contrast, our work differs from and improves [32], which will be depicted further in detail.

In the field of ecology, it is important to use mathematics to study extinction of species, see [33, 34] and the references therein. However, no work has yet been done on the problem of extinction for scalar equation (1), not to mention the scalar equation with Markovian switching (2) and system (4). In order to prove the extinction of species, the conventional method is to construct a proper Lyapunov function or functional and then estimate the upper bound of the drift term of its Itô differential. Taking system (6) for example, $x_1(t)$ and $x_2(t)$ are likely to appear in the denominator of the expression of LV, and coefficients in front of them are positive, for a general Lyapunov function $V(x_1, x_2)$. Unfortunately, this leads to some difficulties in finding the upper bound of LV. So, based on this, we give a new method for investigating extinction of species.

Especially, system (6) reduces to (1), (2), (4), or the system in [32] when parameters of system (6) assume some special values. That is to say, we have derived extinction of the above systems at the same time.

In this paper, system (6) is more general than the model of [21, 28, 30–32]. In addition, our results improve and generalize the corresponding results in these literature studies.

The remainder of this paper is built up as follows. In Section 2, we show the global existence of almost surely positive solution. The asymptotic estimates for the solution, stochastically ultimate boundedness, and boundedness for the average in time of the θth moment of the solution are then constructed in Section 3. In Section 4, we discuss the pathwise properties of the solution. Sufficient conditions for extinction of species are obtained in Section 5. Numerical investigations are then given in Section 6. The last part is a conclusion.

2. Preliminary Results

To simplify, denote the solution of (6) with initial values (7):

$$x(t) \coloneqq x\left(t; \varphi, \ell_0\right), \tag{8}$$

where $x(t) = (x_1(t), x_2(t))^T$. Let

$$\begin{aligned} \beta_1(i) &= a_1(i) + b_2(i), \\ \beta_2(i) &= a_2(i) + b_1(i), \quad i \in \mathscr{M}. \end{aligned} \tag{9}$$

We denote $\mathbb{R}_+ = (0, +\infty)$, $\mathbb{R}_+^2 = \left\{(x_1, x_2)^T \in \mathbb{R}^2 : x_1 > 0, x_2 > 0\right\}$, and $\mathbb{R}_+^{2\times 2} = \left\{(w_{uv})_{2\times 2} \in \mathbb{R}^{2\times 2} : w_{uv} > 0,\ u, v = 1, 2\right\}$. For any $\Phi : \mathscr{M} \longrightarrow \mathbb{R}$, let $\hat{\Phi} = \min_{i\in\mathscr{M}} \Phi(i)$ and $\check{\Phi} = \max_{i\in\mathscr{M}} \Phi(i)$. Let $|\cdot|$ denote Euclidean norm in $\mathbb{R}^2$. Denote the trace norm $|A| = \sqrt{\operatorname{trace}(A^T A)}$ for matrix A.

Lemma 1. *Given any initial values (7), system (6) has a unique solution $x(t) \in R_+^2$ for all $t \in [-\tau, \infty)$ almost surely.*

Proof. We omit the proof since it is analogous to that of [31] by making use of the generalized Itô formula (see, e.g., Theorem 1.45 in [35]) to $\sum_{h=1}^2 (x_h - 1 - \log x_h)$. □

Remark 1. The delay stochastic Nicholson-type model under regime switching on patches (6) is a direct extension of the models in [21, 28, 30–32]. From Lemma 1, it is worthy to point out that priori conditions $\alpha > \sigma^2/2$ in [21] are unnecessary. Therefore, Lemma 1 improves and generalizes Lemma 2.2 in [21]. In addition, this lemma shows that both white noise and telegraph noise will not destroy a great property that the solution of (3) does not explode.

3. Boundedness

Because of resource constraints, asymptotic boundedness is the core of the research in ecosystems. And it is the main purpose of the present section. For simplicity, we use the following notations. For any $i \in \mathscr{M}$, denote

$$\begin{aligned} K_1(\theta, i) &\coloneqq a_1(i) - \frac{\theta - 1}{\theta}\left(b_1(i) - b_2(i)\right) - \frac{1}{2}(\theta - 1)\sigma_1^2(i) - (\theta - 1), \\ K_2(\theta, i) &\coloneqq a_2(i) - \frac{\theta - 1}{\theta}\left(b_2(i) - b_1(i)\right) - \frac{1}{2}(\theta - 1)\sigma_2^2(i) - (\theta - 1), \\ H_h(\theta, i) &\coloneqq \theta \cdot \sup_{x_h \in R^+}\left\{-K_h(\theta, i)x_h^\theta + \frac{p_h(i)}{\gamma_h(i)e}x_h^{\theta-1}\right\}, \\ \check{H}_h(\theta) &\coloneqq \max_{i\in\mathscr{M}} H_h(\theta, i), \\ A_1(\theta) &\coloneqq \frac{2^{\theta/2}}{\theta(\theta - 1)}\sum_{i\in\mathscr{M}} \pi_i\left[H_1(\theta, i) + H_2(\theta, i)\right], \\ A_2(\theta) &\coloneqq \frac{\sum_{h=1}^2 \check{H}_h(\theta)}{\theta(\theta - 1)}, \\ A_3(\theta) &\coloneqq 2^{\theta/2} \cdot \frac{\sum_{h=1}^2 \check{H}(\theta)}{\theta(\theta - 1)}, \quad h = 1, 2. \end{aligned} \tag{10}$$

Firstly, inspired by the work of Wang and Chen [32], we give this theorem.

Theorem 1. *Let $\theta > 1$ such that $K_h(\theta, i) > 0$, $h = 1, 2, i \in \mathscr{M}$. Given any initial values (7), solution $(x_1(t), x_2(t))$ of (6) satisfies*

$$\limsup_{t\longrightarrow\infty} \frac{1}{t}\int_0^t E\left|x_h(s)\right|^\theta \mathrm{d}s \le A_1(\theta), \quad h = 1, 2, \tag{11}$$

and

$$\limsup_{t\longrightarrow\infty} E\left(x_1^\theta(t) + x_2^\theta(t)\right) \le A_2(\theta). \tag{12}$$

In particular,

$$\limsup_{t\longrightarrow\infty} E|x(t)|^\theta \le A_3(\theta). \tag{13}$$

That is, system (6) is ultimately bounded.

Proof. Define

$$V_1(x_1, x_2) = x_1^\theta + x_2^\theta. \tag{14}$$

The generalized Itô formula, together with the fact $p_h(i)y_h e^{-\gamma_h(i)y_h} \le (p_h(i)/\gamma_h(i)e)$ and the elementary inequality $A^\varepsilon B^{1-\varepsilon} \le A\varepsilon + B(1 - \varepsilon)$ for any $A, B \ge 0$ and $\varepsilon \in [0, 1]$, yields

$$
\begin{aligned}
&LV_1(x_1,x_2,y_1,y_2,i)\\
&\quad=-\theta a_1(i)x_1^{\theta}-\theta b_2(i)x_1^{\theta}+\theta b_1(i)x_1^{\theta-1}x_2+\frac{1}{2}\theta(\theta-1)\sigma_1^2(i)x_1^{\theta}\\
&\quad-\theta a_2(i)x_2^{\theta}-\theta b_1(i)x_2^{\theta}+\theta b_2(i)x_1x_2^{\theta-1}+\frac{1}{2}\theta(\theta-1)\sigma_2^2(i)x_2^{\theta}\\
&\quad+\theta\sum_{h=1}^{2}p_h(i)x_h^{\theta-1}y_he^{-\gamma_h(i)y_h}\\
&\le\theta\Bigg(\left[-a_1(i)+\frac{\theta-1}{\theta}\left(b_1(i)-b_2(i)\right)+\frac{1}{2}(\theta-1)\sigma_1^2(i)+(\theta-1)\right]x_1^{\theta}\\
&\quad+\left[-a_2(i)+\frac{\theta-1}{\theta}\left(b_2(i)-b_1(i)\right)+\frac{1}{2}(\theta-1)\sigma_2^2(i)+(\theta-1)\right]x_2^{\theta}\\
&\quad+\sum_{h=1}^{2}\frac{p_h(i)}{\gamma_h(i)e}x_h^{\theta-1}\Bigg)-\theta(\theta-1)\left(x_1^{\theta}+x_2^{\theta}\right)\\
&\le\sum_{h=1}^{2}\theta\left[-K_h(\theta,i)x_h^{\theta}+\frac{p_h(i)}{\gamma_h(i)e}x_h^{\theta-1}\right]-\theta(\theta-1)V_1(x_1,x_2)\\
&\le\sum_{h=1}^{2}H_h(\theta,i)-\theta(\theta-1)V_1(x_1(t),x_2(t)).
\end{aligned}
\tag{15}
$$

Therefore, for $t>0$,

$$
\begin{aligned}
\mathrm{d}V_1(x_1(t),x_2(t))\le&\left[\sum_{h=1}^{2}H_h(\theta,\ell(t))-\theta(\theta-1)V_1\right.\\
&\left.\cdot(x_1(t),x_2(t))\right]\mathrm{d}t+\sum_{h=1}^{2}\theta\sigma_h(\ell(t))x_h^{\theta}(t)\mathrm{d}B_h(t).
\end{aligned}
\tag{16}
$$

Then, (16) implies

$$
\begin{aligned}
0\le E\left(V_1(x_1,x_2)\right)\le&\varphi_1^{\theta}(0)+\varphi_2^{\theta}(0)+\int_0^t\sum_{h=1}^{2}H_h(\theta,\ell(s))\mathrm{d}s\\
&-\theta(\theta-1)\int_0^t EV_1\left(x_1(s),x_2(s)\right)\mathrm{d}s.
\end{aligned}
\tag{17}
$$

Noting that the Markov chain $\ell(t)$ has an invariant distribution $\pi=(\pi_i.i\in\mathcal{M})$ and applying the ergodic property of the Markov chain, it yields

$$
\begin{aligned}
\limsup_{t\longrightarrow\infty}\frac{1}{t}\int_0^t EV_1\left(x_1(s),x_2(s)\right)\mathrm{d}s\le&\limsup_{t\longrightarrow\infty}\frac{1}{\theta(\theta-1)}\\
&\cdot\left(\frac{1}{t}V_1\left(\varphi_1(0),\varphi_2(0)\right)+\frac{1}{t}\int_0^t\sum_{h=1}^{2}H_h(\theta,\ell(s))\mathrm{d}s\right)\\
\le&\frac{1}{\theta(\theta-1)}\sum_{i\in\mathcal{M}}\pi_i\left[H_1(\theta,i)+H_2(\theta,i)\right],\ \text{a. s.}
\end{aligned}
\tag{18}
$$

Furthermore, we have

$$
\begin{aligned}
\mathrm{d}\left[e^{\theta(\theta-1)t}V_1\left(x_1(t),x_2(t)\right)\right]&\le e^{\theta(\theta-1)t}\sum_{h=1}^{2}H_h(\theta,\ell(t))\mathrm{d}t+e^{\theta(\theta-1)t}\sum_{h=1}^{2}\theta\sigma_h(\ell(t))x_h^{\theta}(t)\mathrm{d}B_h(t)\\
&\le\sum_{h=1}^{2}\check{H}_h(\theta)e^{\theta(\theta-1)t}\mathrm{d}t+e^{\theta(\theta-1)t}\sum_{h=1}^{2}\theta\sigma_h(\ell(t))x_h^{\theta}(t)\mathrm{d}B_h(t).
\end{aligned}
\tag{19}
$$

Hence,

$$
\begin{aligned}
e^{\theta(\theta-1)t}EV_1\left(x_1(t),x_2(t)\right)\le&V_1\left(\varphi_1(0),\varphi_2(0)\right)\\
&+\frac{\sum_{h=1}^{2}\check{H}_h(\theta)}{\theta(\theta-1)}e^{\theta(\theta-1)t}\\
&-\frac{\sum_{h=1}^{2}\check{H}_h(\theta)}{\theta(\theta-1)}.
\end{aligned}
\tag{20}
$$

Consequently, we infer immediately that (12) holds. On the contrary, according to (12), (18), and the fact that

$$
|x|^{\theta}\le2^{\theta/2}\max\left\{x_1^{\theta},x_2^{\theta}\right\}\le2^{\theta/2}V_1(x),
\tag{21}
$$

it follows that (11) and (13) hold. The proof is therefore complete. □

Remark 2. In Theorem 1, the parameter θ is greater than 1 in the result. Although ultimate boundedness in the θth moment was derived for θ restricted to the precondition $\theta>1$, θth moment of system (6) can be obtained when $\theta\le1$ by Hölder's equality.

Remark 3. Without regime switching or without migration and regime switching, Theorem 1 improves the corresponding results in [21, 31]. If $\tau(i)\equiv\tau$, system (6) is a direct extension of the model in [32]. Besides, no proof of ultimate boundedness in the pth moment is given in [32], which is

shown in Theorem 1. Therefore, this theorem extends and improves Theorem 3.1 in [21], Theorem 2.2 in [28], Theorem 3.3 in [31], and Theorem 3.2 in [32].

Theorem 2. *Given any initial values (7), solution* $(x_1(t), x_2(t))$ *of (6) satisfies*

$$\limsup_{t\longrightarrow\infty} E|x(t)| \le \limsup_{t\longrightarrow\infty} E\left[x_1(t)+x_2(t)\right] \le \frac{\widetilde{p}_1}{\widehat{\gamma}_1 e\lambda} + \frac{\widetilde{p}_2}{\widehat{\gamma}_2 e\lambda}, \tag{22}$$

where $\lambda = \min\{\widehat{a}_1, \widehat{a}_2\}$. *That is, (6) is ultimately bounded in mean.*

Proof. Let $\overline{V}_1(t, x_1, x_2) = e^{\lambda t}(x_1 + x_2)$. Then,

$$\begin{aligned} E\left(x_1(t)+x_2(t)\right) &\le e^{-\lambda t}\overline{V}_1(0, \varphi_1(0), \varphi_2(0)) \\ &\quad + \left(\frac{\check{p}_1}{\widehat{\gamma}_1 e} + \frac{\check{p}_2}{\widehat{\gamma}_2 e}\right)\int_0^t e^{(s-t)\lambda}\mathrm{d}s. \end{aligned} \tag{23}$$

Finally, (22) follows by letting $t \longrightarrow \infty$. The proof is therefore complete. □

Remark 4. Compared with Theorem 1, this theorem describes the case that $\theta = 1$, which does not require any conditions. If $\tau(i) \equiv \tau$, we get $(\check{p}_1/\widehat{\gamma}_1 e\lambda) + (\check{p}_2/\widehat{\gamma}_2 e\lambda) \le (c/a)$, where (c/a) is defined in [32]. So, this theorem improves and extends Theorem 3.1 in [21] and Theorem 3.1 in [32].

Theorem 3. *System (6) is stochastically ultimately bounded.*

Proof. By (22), we derive

$$\limsup_{t\longrightarrow\infty} E\left|x_h(t)\right| \le \frac{\check{p}_1}{\widehat{\gamma}_1 e\lambda} + \frac{\check{p}_2}{\widehat{\gamma}_2 e\lambda}, \quad h = 1, 2. \tag{24}$$

By the Chebyshev inequality, it yields, for any $\varepsilon \in (0, 1)$,

$$\limsup_{t\longrightarrow\infty} \mathbb{P}\{x_h(t) \ge H\} \le H^{-1}\left(\frac{\check{p}_1}{\widehat{\gamma}_1 e\lambda} + \frac{\check{p}_2}{\widehat{\gamma}_2 e\lambda}\right) = \varepsilon, \tag{25}$$

where $H = (1/\varepsilon)((\widetilde{p}_1/\widehat{\gamma}_1 e\lambda) + (\widetilde{p}_2/\widehat{\gamma}_2 e\lambda))$. The proof is therefore complete. □

Remark 5. Theorem 3 can be seen as the extension and improvement of [31, 32].

4. Asymptotic Pathwise Estimation

We shall estimate a sample Lyapunov exponent in what follows.

Lemma 2. *If* $a \in \mathbb{R}$ *and* $b \in \mathbb{R}_+$, *then* $(ax^2 + bx/1 + x^2) \le K(a)$ *for* $x \in \mathbb{R}$, *where* $K(a) = (a + \sqrt{a^2 + b^2}/2)$.

By the properties of quadratic functions, the proof of this lemma is easy and so is omitted. In the process of finding $K(a)$, we know that the precondition is $a - K(a) < 0$. In this case, we can choose $K(a)$ which satisfies $K(a) = (a + \sqrt{a^2 + b^2}/2)$. We have to mention that it has no relation with the sign of parameter a. If $a < 0$, we get $(a + \sqrt{a^2 + b^2}/2) < -(b^2/4a)$ by simple computation. So, this lemma is an improvement of Lemma 1.2 in [28] and Lemma 2.1 in [32].

Theorem 4. *Given any initial values (7), solution* $x(t)$ *of (6) satisfies*

$$\limsup_{t\longrightarrow\infty} \frac{1}{t}\log \quad x_h(t) \le \limsup_{t\longrightarrow\infty} \frac{1}{t}\log|x(t)| \le \frac{Q}{2}, \text{ a. s.} \tag{26}$$

where $h = 1, 2$, $Q = \max_{i\in\mathcal{M}}\left\{\min_{\varepsilon\in\mathbb{R}_+}[Q_1(i,\epsilon) + Q_2(i,\epsilon)]\right\}$ *with*

$$\begin{aligned} Q_1(i,\varepsilon) &= \frac{\sqrt{\left[2\beta_1(i) - \sigma_1^2(i) - \left(b_1(i)+b_2(i)\right)\epsilon\right]^2 + 4\left(p_1(i)/\gamma_1(i)e\right)^2} - \left[2\beta_1(i) - \sigma_1^2(i) - \left(b_1(i)+b_2(i)\right)\epsilon\right]}{2}, \\ Q_2(i,\varepsilon) &= \frac{\sqrt{\left(2\beta_2(i) - \sigma_2^2(i) - b_1(i) + b_2(i)/\varepsilon\right)^2 + 4\left(p_2(i)/\gamma_2(i)e\right)^2} - \left(2\beta_2(i) - \sigma_2^2(i) - \left(b_1(i)+b_2(i)\right)/\varepsilon\right)}{2}, \end{aligned} \tag{27}$$

for any positive constant ε.

Proof. The generalized Itô formula, together with Lemma 2 and the Cauchy–Schwarz inequality, yields

$$\begin{aligned}\log\left(1+x_1^2(t)+x_2^2(t)\right) &\le \log\left(1+x_1^2(0)+x_2^2(0)\right)\\ &+\int_0^t \frac{-\left[2\beta_1(\ell(s))-\sigma_1^2(\ell(s))-\left(b_1(\ell(s))+b_2(\ell(s))\right)\epsilon\right]x_1^2(s)+\left(2p_1(\ell(s))/\gamma_1(\ell(s))e\right)x_1(s)}{1+x_1^2(s)+x_2^2(s)}\,\mathrm{d}s\\ &+\int_0^t \frac{-\left[2\beta_2(\ell(s))-\sigma_2^2(\ell(s))-\left(b_1(\ell(s))+b_2(\ell(s))/\epsilon\right)\right]x_2^2(s)+\left(2p_1(\ell(s))/\gamma_1(\ell(s))e\right)x_2(s)}{1+x_1^2(s)+x_2^2(s)}\,\mathrm{d}s\\ &-2\sum_{h=1}^{2}\sigma_h^2(\ell(s))\int_0^t\frac{x_h^4(s)}{\left(1+x_1^2(s)+x_2^2(s)\right)^2}\,\mathrm{d}s+M_1(t)+M_2(t)\\ &\le \log\left(1+x_1^2(0)+x_2^2(0)\right)+Qt-2\sum_{h=1}^{2}\int_0^t\frac{\sigma_h^2(\ell(s))x_h^4(s)}{\left(1+x_1^2(s)+x_2^2(s)\right)^2}\,\mathrm{d}s+M_1(t)+M_2(t),\end{aligned} \tag{28}$$

where for any $h\in\{1,2\}$,

$$M_h(t)=2\int_0^t\frac{\sigma_h(\ell(s))x_h^2(s)}{1+x_1^2(s)+x_2^2(s)}\mathrm{d}B_h(s), \tag{29}$$

with the quadratic variation

$$\langle M_h(t),M_h(t)\rangle=4\int_0^t\frac{\sigma_h^2(\ell(s))x_h^4(s)}{\left(1+x_1^2(s)+x_2^2(s)\right)^2}\mathrm{d}s. \tag{30}$$

According to the exponential martingale inequality (see, e.g., [36]), for any integer $m>0$, we have

$$\begin{aligned}&\mathbb{P}\left\{\sup_{0\le t\le m}\left\{M_h(t)-2\int_0^t\frac{\sigma_h^2(\ell(s))x_h^4(s)}{\left(1+x_1^2(s)+x_2^2(s)\right)^2}\mathrm{d}s\right\}\right.\\ &\left.>2\log m\right\}\le\frac{1}{m^2},\quad h=1,2.\end{aligned} \tag{31}$$

Since $\sum_{m=1}^{\infty}1/m^2<\infty$ and Borel–Cantelli's lemma (see, e.g., [36]), there exist $\Omega_0\in\mathcal{F}$ with $\mathbb{P}(\Omega_0)=1$ and an integer $m_0=m_0(\omega)$ such that

$$\begin{aligned}M_h(t)\le 2\int_0^t\frac{\sigma_h^2(\ell(s))x_h^4(s)}{\left(1+x_1^2(s)+x_2^2(s)\right)^2}\mathrm{d}s+2\log m,\\ h=1,2,\end{aligned} \tag{32}$$

for all $\omega\in\Omega_0$, $0\le t\le m$. Substituting the above inequality into (28), for any $\omega\in\Omega_0$, $m\ge m_0$, $0\le t\le m$, we have

$$\begin{aligned}\log\left(1+x_1^2(t)+x_2^2(t)\right)&\le\log\left(1+x_1^2(0)+x_2^2(0)\right)\\ &+Qt+4\log m,\end{aligned} \tag{33}$$

which yields

$$\begin{aligned}\frac{1}{t}\log\left(1+x_1^2(t)+x_2^2(t)\right)&\le\frac{1}{m-1}\left[\log\left(1+x_1^2(0)+x_2^2(0)\right)\right.\\ &\left.+Qm+4\log m\right],\end{aligned} \tag{34}$$

for all $\omega\in\Omega_0$, $0\le m-1\le t\le m$, $m\ge m_0$. Letting $m\longrightarrow\infty$ and using the inequality $y\le(1/2)(1+y^2)$ for any $y\in(-\infty,+\infty)$, we obtain

$$\begin{aligned}\limsup_{t\longrightarrow\infty}\frac{1}{t}\log x_h(t)&\le\limsup_{t\longrightarrow\infty}\frac{1}{2(m-1)}\left[\log\left(1+x^2(0)\right)\right.\\ &\left.+Qm+4\log m\right]=\frac{Q}{2},\ \text{a. s.}\end{aligned} \tag{35}$$

The proof is therefore complete. □

Remark 6. Without migrations, we get $Q_1(i)=(\sqrt{[2\beta_1(i)-\sigma_1^2(i)]^2+4(p_1(i)/\gamma_1(i)e)^2}-[2\beta_1(i)-\sigma_1^2(i)]/2)$. By comparison, we find that $Q_1(i)\le C_i$, where C_i is defined in [28]. In addition, without migration and regime switching, we can get Q in Theorem 4 is less than K, where K is defined in [21]. Furthermore, the condition $2\alpha_1-\sigma_1^2-(b_1+b_2)\epsilon>0$, $2\alpha_2-\sigma_2^2-(b_1+b_2)/\epsilon>0$ in [31] means that the parameter ϵ needs to be satisfied: $(b_1+b_2)/2\alpha_2-\sigma_2^2<\varepsilon<2\alpha_1-\sigma_1^2/(b_1+b_2)$. However, we know that this condition is unnecessary from the above theorem. Despite all this, if we let the parameter ε satisfy $\varepsilon\in(((b_1+b_2)/2\alpha_2-\sigma_2),(2\alpha_1^2-\sigma_1^2/(b_1+b_2)))$, we compute that Q in Theorem 4 is less than Q in [31]. Therefore, the above work is a promotion of Theorem 4.1 in [21], Theorem 2.2 in [28], and Theorem 4.1 in [31].

5. Extinction

Sufficient conditions for extinction are the subject of this section. Unless otherwise stated, we hypothesize $\tau(i) \equiv \tau, \quad i \in \mathcal{M}$ in this section. We first rewrite (6) as follows:

$$dx(t) = f_1(x(t), x(t-\tau), \ell(t))dt + f_2(x(t), \ell(t))dB(t), \tag{36}$$

where the operator $f_1: \mathbb{R}_+^2 \times \mathbb{R}_+^2 \times \mathcal{M} \longrightarrow \mathbb{R}_+^2$ is defined as

$$f_1(x, y, i) = \begin{pmatrix} -\beta_1(i)x_1 + b_1(i)x_2 + p_1(i)y_1 e^{-\gamma_1(i)y_1} \\ -\beta_2(i)x_2 + b_2(i)x_1 + p_2(i)y_2 e^{-\gamma_2(i)y_2} \end{pmatrix}, \tag{37}$$

the operator $f_2: \mathbb{R}_+^2 \times \mathcal{M} \longrightarrow \mathbb{R}_+^{2\times 2}$ is defined as $f_2(x, i) = \begin{pmatrix} \sigma_1(i)x_1 & 0 \\ 0 & \sigma_2(i)x_2 \end{pmatrix}$, and $dB(t) = \begin{pmatrix} dB_1(t) \\ dB_2(t) \end{pmatrix}$. We first note that

$$\begin{aligned} f_1(0, 0, i) &\equiv 0, \\ f_2(0, i) &\equiv 0, \end{aligned} \tag{38}$$

for $i \in \mathcal{M}$, whence (6) admits a trivial solution corresponding to $\varphi(0) = 0$.

Before our result, we give a lemma.

Lemma 3. *For system (36), the terms $f_1(x, y, i)$ and $f_2(x, i)$ are locally bounded in (x, y) while uniformly bounded in i. That is, for any $m > 0$, there is $K_m > 0$ satisfying*

$$\left|f_1(x, y, i)\right| \vee \left|f_2(x, i)\right| \le K_m, \tag{39}$$

for all $i \in \mathcal{M}$, $x, y \in \mathbb{R}_+^2$ with $|x| \vee |y| \le m$.

The proof is not particularly difficult, so we omit the proof.

Theorem 5. *Assume that*

$$\begin{aligned} 2\widehat{\beta}_1 &> \breve{\sigma}_1^2 + \breve{b}_1 + (1+\sqrt{2})\breve{b}_2 + \left(2 + \frac{1}{\sqrt{2}}\right)\breve{p}_1 + (1+\sqrt{2})\breve{p}_2, \\ 2\widehat{\beta}_2 &> \breve{\sigma}_2^2 + (1+\sqrt{2})\breve{b}_1 + \breve{b}_2 + (1+\sqrt{2})\breve{p}_1 + \left(2 + \frac{1}{\sqrt{2}}\right)\breve{p}_2. \end{aligned} \tag{40}$$

Then, the solution of (36) satisfies $\lim_{t\longrightarrow\infty} x(t) = 0$, a.s., for any initial values (7). That is, all populations in system (36) go to extinction with probability one.

Proof

Step 1: let

$$V_2(x_1, x_2) = x^T \begin{pmatrix} 1 & \frac{1}{\sqrt{2}} \\ \frac{1}{\sqrt{2}} & 1 \end{pmatrix} x = x_1^2 + \sqrt{2}x_1x_2 + x_2^2. \tag{41}$$

Obviously, V_2 is positive-definite and radially unbounded. That is,

$$\lim_{|x|\longrightarrow\infty} V_2(x_1, x_2) = \infty. \tag{42}$$

The generalized Itô formula yields

$$\begin{aligned} V_2(x_1(t), x_2(t)) = V_2(\varphi_1(0), \varphi_2(0)) &+ \int_0^t LV_2(x(s), x \\ &\cdot (s - \tau(\ell(s))), \ell(s))ds \\ &+ \int_0^t \left[\frac{\partial}{\partial x} V_2(x_1(s), x_2(s))\right] f_2(x(s), \ell \\ &\cdot (s))dB(s). \end{aligned} \tag{43}$$

By computation, we know

$$\begin{aligned} LV_2(x, y, i) \le &-\left[2\beta_1(i) - \sigma_1^2(i) - b_1(i) - (1+\sqrt{2})b_2(i) - p_1(i) - \frac{1}{\sqrt{2}}p_2(i)\right]x_1^2 \\ &-\left[2\beta_2(i) - \sigma_2^2(i) - (1+\sqrt{2})b_1(i) - b_2(i) - \frac{1}{\sqrt{2}}p_1(i) - p_2(i)\right]x_2^2 \\ &+\left(1 + \frac{1}{\sqrt{2}}\right)p_1(i)y_1^2 + \left(1 + \frac{1}{\sqrt{2}}\right)p_2(i)y_2^2 \\ \le &-\lambda_1 x_1^2 - \lambda_2 x_2^2 + \left(1 + \frac{1}{\sqrt{2}}\right)\breve{p}_1 y_1^2 + \left(1 + \frac{1}{\sqrt{2}}\right)\breve{p}_2 y_2^2, \end{aligned} \tag{44}$$

where $\lambda_1 = 2\widehat{\beta}_1 - \check{\sigma}_1^2 - \check{b}_1 - (1+\sqrt{2})\check{b}_2 - \check{p}_1 - (1/\sqrt{2})\check{p}_2$ and $\lambda_2 = 2\widehat{\beta}_2 - \check{\sigma}_2^2 - (1+\sqrt{2})\check{b}_1 - \check{b}_2 - (1/\sqrt{2})\check{p}_1 - \check{p}_2$.

It is straightforward to see from (40) that $\lambda_h > 0$, $h = 1, 2$. For simplicity, we let

$$\begin{aligned} F_1(x) &= \min\{\lambda_1, \lambda_2\}|x|^2, \\ F_2(x) &= \left(1 + \frac{1}{\sqrt{2}}\right)\max\{\check{p}_1, \check{p}_2\}|x|^2. \end{aligned} \tag{45}$$

By condition (40) again, we obtain that

$$\begin{aligned} F(x) &:= F_1(x) - F_2(x) \\ &= \left[\min\{\lambda_1, \lambda_2\} - \left(1 + \frac{1}{\sqrt{2}}\right)\max\{\check{p}_1, \check{p}_2\}\right]|x|^2 > 0, \quad x \neq 0. \end{aligned} \tag{46}$$

Applying (44) and (46), we derive

$$\begin{aligned} &\int_0^t LV_2(x(s), x(s - \tau(\ell(s))), \ell(s))\mathrm{d}s \\ &\quad \leq \int_{-\tau}^0 F_2(x(s))\mathrm{d}s - \int_0^t F(x(s))\mathrm{d}s. \end{aligned} \tag{47}$$

Substituting the preceding equality into (43), it yields

$$\begin{aligned} V_2(x_1(t), x_2(t)) \leq V_2(\varphi_1(0), \varphi_2(0)) &+ \int_{-\tau}^0 F_2(x(s))\mathrm{d}s \\ &- \int_0^t F(x(s))\mathrm{d}s \\ &+ \int_0^t \left[\frac{\partial}{\partial x}V_2(x_1(s), x_2(s))\right] f_2(x(s), \ell \\ &\cdot (s))\mathrm{d}B(s). \end{aligned} \tag{48}$$

Then, the nonnegative semimartingale convergence theorem (see, e.g., [37]) implies

$$\limsup_{t \longrightarrow \infty} V_2(x_1(t), x_2(t)) < \infty \quad \text{a. s.} \tag{49}$$

Moreover, we obtain from (48) that

$$E\int_0^t F(x(s))\mathrm{d}s \leq V_2(\varphi_1(0), \varphi_2(0)) + \int_{-\tau}^0 F_2(x(s))\mathrm{d}s. \tag{50}$$

Then, letting $t \longrightarrow \infty$, together with the Fubini theorem, we have

$$E\int_0^\infty F(x(t))\mathrm{d}t < \infty. \tag{51}$$

Let $A_k = \left\{\omega | Y(\omega) = \int_0^\infty F(x(s, \omega))\mathrm{d}s > 2^k\right\}$, where $k = 1, 2, \ldots$. Obviously, $\{A_k\}^{\{A_{k+1}\}}$. Combining Chebyshev's inequality and (51), we see that $\sum_{k=1}^\infty \mathbb{P}(A_k) < \infty$. By Borel–Cantelli's lemma, one can show that $\mathbb{P}(\lim_{k \longrightarrow \infty} A_k) = \mathbb{P}\{\omega | Y(\omega) = \infty\} = 0$, that is,

$$\int_0^\infty F(x(t))\mathrm{d}t < \infty \quad \text{a. s.} \tag{52}$$

Step 2: from (52), we observe

$$\liminf_{t \longrightarrow \infty} F(x(t)) = 0, \quad \text{a. s.} \tag{53}$$

One now needs to consider

$$\lim_{t \longrightarrow \infty} F(x(t)) = 0 \quad \text{a. s.} \tag{54}$$

If the above conclusion would not hold, then $\mathbb{P}\{\limsup_{t \longrightarrow \infty} F(x(t)) > 0\} > 0$. So, there is $\varepsilon \in (0, (1/3))$ satisfying

$$\mathbb{P}(\Omega_1) \geq 3\varepsilon, \tag{55}$$

where

$$\Omega_1 = \left\{\limsup_{t \longrightarrow \infty} F(x(t)) > 2\varepsilon\right\}. \tag{56}$$

Noting that Lyapunov function $V_2(x(t))$ and the solution $x(t)$ of (6) are all continuous, together with (49), it yields

$$\sup_{-\tau \leq t < \infty} V_2(x(t)) < \infty, \quad \text{a.s.} \tag{57}$$

Define

$$\nu(r) = \inf_{|x| \geq k} V_2(x), \quad \text{for } k > 0. \tag{58}$$

Clearly,

$$\sup_{-\tau\le t<\infty} \nu(|x(t)|) \le \sup_{-\tau\le t<\infty} V_2(x(t)) < \infty, \quad \text{a. s.} \tag{59}$$

In addition, by (42), we get

$$\lim_{k\longrightarrow\infty} \nu(k) = \infty. \tag{60}$$

So,

$$\sup_{-\tau\le t<\infty} |x(t)| < \infty, \quad \text{a. s.} \tag{61}$$

Recalling (7), we know that the initial values satisfy $\varphi_h \in C([-\tau, 0]; [0, +\infty))$ for $h = 1, 2$. We therefore could find an integer $m > 0$, depending on ε, sufficiently large for $|\varphi(s)| < m$ for $s \in [-\tau, 0]$ almost surely, while

$$\mathbb{P}(\Omega_2) \ge 1 - \varepsilon, \tag{62}$$

where $\Omega_2 = \{\sup_{-\tau\le t<\infty}|x(t)| < m\}$. By (55) and (62), one implies

$$\mathbb{P}(\Omega_1 \cap \Omega_2) \ge \mathbb{P}(\Omega_1) - \mathbb{P}(\Omega_2^c) \ge 2\varepsilon, \tag{63}$$

where Ω_2^c is the complement of Ω_2. Let

$$\begin{aligned}
\rho_1 &= \inf\{t \ge 0\colon F(x(t)) \ge 2\varepsilon\},\\
\rho_{2j} &= \inf\left\{t \ge \rho_{2j-1}\colon F(x(t)) \le \varepsilon\right\}, \quad j = 1, 2, \ldots,\\
\rho_{2j+1} &= \inf\left\{t \ge \rho_{2j}\colon F(x(t)) \ge 2\varepsilon\right\}, \quad j = 1, 2, \ldots,\\
\sigma_m &= \inf\{t \ge 0\colon |x(t)| \ge m\}.
\end{aligned} \tag{64}$$

From (53) and the definitions of Ω_1 and Ω_2, we have

$$\{\Omega_1 \cap \Omega_2\} \subset \left\{\{\sigma_m = \infty\} \cap \left(\bigcap_{j=1}^{\infty}\{\rho_j < \infty\}\right)\right\}. \tag{65}$$

Hence, we define $\{\zeta(t)\} = \{x(t \wedge \sigma_m)\}$ for $t > -\tau$, and its differential is

$$\mathrm{d}\zeta(t) = \widetilde{f}_1(t)\mathrm{d}t + \widetilde{f}_2(t)\mathrm{d}B(t), \tag{66}$$

where

$$\begin{aligned}
\widetilde{f}_1(t) &= f_1(x(t), x(t-\tau), \ell(t))I_{[0,\sigma_m)}(t),\\
\widetilde{f}_2(t) &= f_2(x(t), \ell(t))I_{[0,\sigma_m)}(t).
\end{aligned} \tag{67}$$

Here, I_A is the indicator function of A. Recalling Lemma 3, we know

$$\left|\widetilde{f}_1(t)\right| \vee \left|\widetilde{f}_2(t)\right| \le K_m, \quad \text{a. s,} \tag{68}$$

for any $t \ge -\tau$, $\ell(t) \in \mathscr{M}$, and $|x(t)| \vee |x(t-\tau)| \le m$. Moreover, the definition of yields $|\zeta(t)| \le m$, $t \ge 0$. We also note that, for all $\omega \in \Omega_1 \cap \Omega_2$ and $j \ge 1$,

$$\begin{aligned}
F\left(\zeta\left(\rho_{2j-1}\right)\right) - F\left(\zeta\left(\rho_{2j}\right)\right) &= \varepsilon,\\
F(\zeta(t)) \ge \varepsilon, \quad t &\in \left[\rho_{2j-1}, \rho_{2j}\right].
\end{aligned} \tag{69}$$

In the close ball $\overline{S}_m = \{x \in \mathbb{R}^2\colon |x| \le m\}$, $F(\cdot)$ is uniformly continuous. Therefore, there exists $\xi = \xi(\varepsilon) > 0$ small sufficiently such that

$$|F(\zeta) - F(\overline{\zeta})| < \varepsilon, \quad \zeta, \overline{\zeta} \in \overline{S}_m \text{ with } |\zeta - \overline{\zeta}| < \xi. \tag{70}$$

For $\omega \in \Omega_1 \cap \Omega_2$, we emphasize that if $|\zeta(\rho_{2j-1} + t) - \zeta(\rho_{2j-1})| < \xi$ for some $T > 0$ and $t \in [0, T]$, then $\rho_{2j} - \rho_{2j-1} \ge T$. Furthermore, let the number $T = T(\varepsilon, \xi, m) > 0$ be small enough such that

$$2K_m^2 T(T+4) \le \varepsilon\xi^2. \tag{71}$$

By (63) and (65), we can obtain that

$$\mathbb{P}\left(\rho_{2j} < \infty\right) \ge 2\varepsilon. \tag{72}$$

In particular, if $\rho_{2j} < \infty$, then $|\zeta(\rho_{2j})| < m$. Hence, the definition of $\zeta(t)$ implies $\rho_{2j} < \sigma_m$. So,

$$\zeta(t, \omega) = x(t, \omega), \tag{73}$$

for all $0 \le t \le \rho_{2j}$, $\omega \in \left\{\rho_{2j} < \infty\right\}$. Then, from the Hölder inequality and the Burkholder–Davis–Gundy inequality, it follows that

$$
\begin{aligned}
&E\left[I_{\{\rho_{2j-1}<\infty\}}\sup_{0\le t\le T}\left|\zeta\left(\rho_{2j-1}+t\right)-\zeta\left(\rho_{2j-1}\right)\right|^2\right]\\
&\quad\le E\left[I_{\{\rho_{2j-1}<\infty\}}\sup_{0\le t\le T}\left|\int_{\rho_{2j-1}}^{\rho_{2j-1}+t}\mathrm{d}\zeta(s)\right|^2\right]\\
&\quad= E\left[I_{\{\rho_{2j-1}<\infty\}}\sup_{0\le t\le T}\left|\int_{\rho_{2j-1}}^{\rho_{2j-1}+t}\widetilde{f}_1(s)\mathrm{d}s+\int_{\rho_{2j-1}}^{\rho_{2j-1}+t}\widetilde{f}_2(s)\mathrm{d}B(s)\right|^2\right]\\
&\quad\le 2E\left[I_{\{\rho_{2j-1}<\infty\}}\sup_{0\le t\le T}\left(\left|\int_{\rho_{2j-1}}^{\rho_{2j-1}+t}\widetilde{f}_1(s)\mathrm{d}s\right|^2+\left|\int_{\rho_{2j-1}}^{\rho_{2j-1}+t}\widetilde{f}_2(s)\mathrm{d}B(s)\right|^2\right)\right]\\
&\quad\le 2TE\left[I_{\{\rho_{2j-1}<\infty\}}\sup_{0\le t\le T}\int_{\rho_{2j-1}}^{\rho_{2j-1}+t}\left|\widetilde{f}_1(s)\right|^2\mathrm{d}s\right]+8E\left[I_{\{\rho_{2j-1}<\infty\}}\sup_{0\le t\le T}\int_{\rho_{2j-1}}^{\rho_{2j-1}+t}\left|\widetilde{f}_2(s)\right|^2\mathrm{d}B(s)\right]\\
&\quad\le 2K_m^2T(T+4),
\end{aligned}
\tag{74}
$$

which together with (71) and the Chebyshev inequality, imply easily that

$$
\mathbb{P}\left(\left\{\rho_{2j-1}<\infty\right\}\cap\left\{\sup_{0\le t\le T}\left|\zeta\left(\rho_{2j-1}+t\right)-\zeta\left(\rho_{2j-1}\right)\right|\ge\xi\right\}\right)\le\varepsilon.
\tag{75}
$$

Obviously, we observe that $\rho_{2j-1}<\infty$ if $\rho_{2j}<\infty$. Hence, by (72) and (75), we can derive that

$$
\begin{aligned}
&\mathbb{P}\left(\left\{\rho_{2j}<\infty\right\}\cap\left\{\sup_{0\le t\le T}\left|\zeta\left(\rho_{2j-1}+t\right)-\zeta\left(\rho_{2j-1}\right)\right|<\xi\right\}\right)\\
&\quad=\mathbb{P}\left(\rho_{2j}<\infty\right)-\mathbb{P}\left(\left\{\rho_{2j}<\infty\right\}\cap\left\{\sup_{0\le t\le T}\left|\zeta\left(\rho_{2j-1}+t\right)\right.\right.\right.\\
&\qquad\left.\left.\left.-\zeta\left(\rho_{2j-1}\right)\right|\ge\xi\right\}\right)\\
&\quad\ge\varepsilon.
\end{aligned}
\tag{76}
$$

This, together with (70), we can get that

$$
\mathbb{P}\left(\left\{\rho_{2j}<\infty\right\}\cap\left\{\rho_{2j}-\rho_{2j-1}\ge T\right\}\right)\ge\varepsilon.
\tag{77}
$$

Recalling (51), (69), and (77), for all $\omega\in\Omega_1\cap\Omega_2$ and $j\ge1$, we compute

$$
\begin{aligned}
\infty&>E\int_0^\infty F(x(t))\mathrm{d}t\\
&\ge\sum_{j=1}^\infty E\left[I_{\{\rho_{2j}<\infty\}}\int_{\rho_{2j-1}}^{\rho_{2j}}F(\zeta(t))\mathrm{d}t\right]\\
&\ge\varepsilon\sum_{j=1}^\infty E\left[I_{\{\rho_{2j}<\infty\}}\left(\rho_{2j}-\rho_{2j-1}\right)\right]\\
&\ge\varepsilon T\sum_{j=1}^\infty\varepsilon=\infty,
\end{aligned}
\tag{78}
$$

which is a contradiction. Consequently, we infer (54).

Step 3: by (46) and (54), we now derive $\lim_{t\longrightarrow\infty}x(t)=0$, a. s. The proof is therefore complete. □

Corollary 1. *Assume that are nonnegative constants,* $\tau_{r_t}\equiv\tau\ge0$, *and*

$$
2\min_{r_t\in\mathbb{S}}\left\{\alpha_{r_t}\right\}>\max_{r_t\in\mathbb{S}}\left\{\sigma_{r_t}\right\}^2+\left(3+\frac{3\sqrt{2}}{2}\right)\max_{r_t\in\mathbb{S}}\left\{p_{r_t}\right\}.
\tag{79}
$$

Then, solution $x(t)$ of (2) obeys

$$
\lim_{t\longrightarrow\infty}x(t)=0,\ \text{a. s.},
\tag{80}
$$

for any initial value $x(t)=\phi(t),t\in[-\tau,0]$, $\phi(0)>0,\phi\in C([-\tau,0];[0,+\infty))$. That is, all populations in equation (2) go to extinction with probability one.

Corollary 2. *Assume that* a_h, b_h, p_h, γ_h, σ_h,τ *are nonnegative constants,* $h=1,2$, *and*

$$
\begin{aligned}
2a_1&>\sigma_1^2+b_1+(\sqrt{2}-1)b_2+\left(2+\frac{1}{\sqrt{2}}\right)p_1+(1+\sqrt{2})p_2,\\
2a_2&>\sigma_2^2+(\sqrt{2}-1)b_1+b_2+(1+\sqrt{2})p_1+\left(2+\frac{1}{\sqrt{2}}\right)p_2.
\end{aligned}
\tag{81}
$$

Then, solution $x(t)$ of (4) obeys

$$
\lim_{t\longrightarrow\infty}x(t)=0,\quad\text{a. s.},
\tag{82}
$$

for any initial value $x_h(t)=\phi_h(t),t\in[-\tau,0],\phi_h(0)>0,\phi_h\in C([-\tau,0];[0,+\infty))$. That is, all populations in model (4) go to extinction with probability one.

Remark 7. This theorem reveals that the solutions of (6) will all tend to the origin asymptotically with probability one when the intensities of noises and the parameters satisfy condition (40). However, [21, 28, 31, 32] do not study extinction of populations. Besides, this method can be extended to research extinction in the above literature studies.

Corollaries 1 and 2 give the conditions of extinction of (2) and (4), respectively. Therefore, our work is the extension of [21, 28, 31, 32].

6. Numerical Simulations

Based on [38], we show numerical simulations in the present section.

Here, we consider model (6) with the same initial data $\varphi_1(0) = 1$, $\varphi_2(0) = 0.5$ and the same $\{\ell(t)\}_{t\geq 0}$ on $\mathcal{M} = \{1, 2, 3\}$ with

$$\Gamma = \begin{pmatrix} -10 & 4 & 6 \\ 2 & -3 & 1 \\ 3 & 5 & -8 \end{pmatrix}. \tag{83}$$

Then, we know the Markov chain $\ell(t)_{t\geq 0}$ is irreducible and has a unique stationary distribution $\pi = (0.1845, 0.6019, 0.2136)$.

In Figure 1, we give a simulation of the sample path of $\ell(t)_{t\geq 0}$ with $\ell(0) = 3$.

In Figure 2, we can choose $a_1 = [1, 2, 3]$; $b_1 = [0.12, 0.23, 0.22]$; $p_1 = [4, 5, 6]$; $\gamma_1 = [0.4, 0.5, 0.6]$; $\sigma_1 = [1.2, 1.1, 2]$; $a_2 = [3, 1, 2]$; $b_2 = [0.23, 0.16, 0.12]$; $p_2 = [7, 4, 3]$; $\gamma_2 = [0.3, 0.4, 0.5]$; $\sigma_2 = [0.45, 1.5, 0.25]$; $\tau = [1, 2, 3]$. It is easy to see that $1 = a_{22} < (\sigma_{22}^2/2) = 1.125$ when $\xi(t) = 2$. There is a good agreement between Lemma 1 and Figure 2. By Theorem 2, we know $(\check{p}_1/\widehat{\gamma}_1 e\lambda) + (\check{p}_2/\widehat{\gamma}_2 e\lambda) = 14.1020$. Furthermore, we get $Q = \max\{9.5553, 6.3244, 3.8081\}$ by calculation. Therefore, conditions of Theorem 4 have been checked. So, $\limsup_{t\longrightarrow\infty}(1/t)\ln x_h(t) \leq 4.7777$, a. s.

In Figure 3, we can choose $a_1 = [2.1, 2.2, 2]$; $b_1 = [0.11, 0.13, 0.12]$; $p_1 = [3.2, 3, 3.5]$; $\gamma_1 = [0.83, 0.85, 0.86]$; $\sigma_1 = [0.62, 0.61, 0.63]$; $a_2 = [2, 2.1, 2.2]$; $b_2 = [0.11, 0.13, 0.12]$; $p_2 = [3.1, 3.3, 3.2]$; $\gamma_2 = [0.81, 0.8, 0.83]$; $\sigma_2 = [0.71, 0.75, 0.71]$. Let $\theta = 2$. Then, conditions of Theorem 1 could be checked. By calculation, we get $\limsup_{t\longrightarrow\infty}(1/t)\int_0^t E|x_h(s)|^\theta ds \leq 31.9797$, $\limsup_{t\longrightarrow\infty} E(x_1^\theta(t) + x_2^\theta(t)) \leq 19.3208$, $\limsup_{t\longrightarrow\infty} E|x(t)|^\theta \leq 38.6416$. Figure 3 clearly supports this result.

In Figure 4, we can choose $a_1 = [17, 18, 19]$; $b_1 = [0.14, 0.35, 0.15]$; $p_1 = [4.55, 6, 5.43]$; $\gamma_1 = [0.8, 0.5, 0.6]$; $\sigma_1 = [0.5, 0.45, 0.12]$; $a_2 = [16.5, 16.9, 17.5]$; $b_2 = [0.5, 0.13, 0.22]$; $p_2 = [3.23, 4.67, 6]$; $\gamma_2 = [0.3, 0.4, 0.8]$; $\sigma_2 = [0.49, 1, 0.65]$; $\tau = [3, 3, 3]$. By calculation, we get $\tau(1) = \tau(2) = \tau(3) = 3$, $35 = 2\widehat{\beta}_1 > \check{\sigma}_1^2 + \check{b}_1 + (1 + \sqrt{2})\check{b}_2 + (2 + (1/\sqrt{2}) =)\check{p}_1 + (1 + \sqrt{2})\check{p}_2 \approx 32.5350$, and $33.28 = 2\widehat{\beta}_2 > \check{\sigma}_2^2 + (1 + \sqrt{2})\check{b}_1 + \check{b}_2 + (1 + \sqrt{2})\check{p}_1 + (2 + (1/\sqrt{2}))\check{p}_2 \approx 33.0729$.

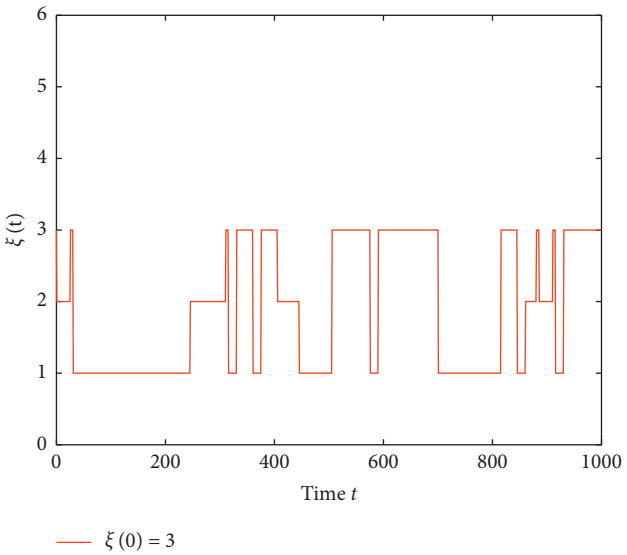

Figure 1: Sample path of $\{\ell(t)\}_{t\geq 0}$ with $\ell(0) = 3$.

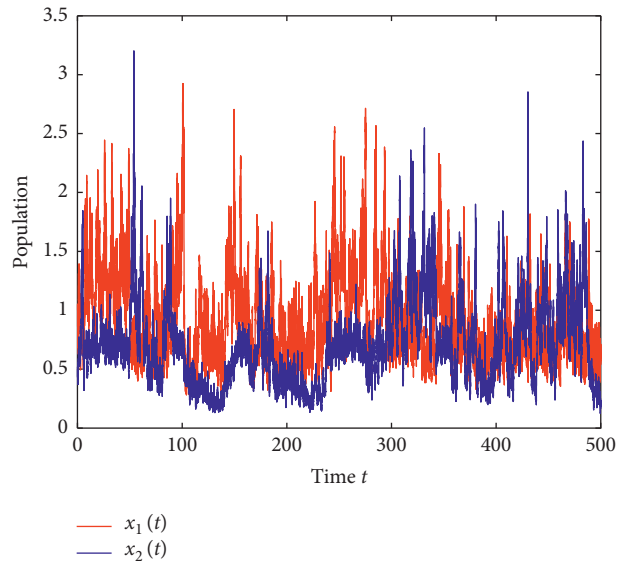

Figure 2: Numerical solutions of (6) with $a_1 = [1, 2, 3]$; $b_1 = [0.12, 0.23, 0.22]$; $p_1 = [4, 5, 6]$; $\gamma_1 = [0.4, 0.5, 0.6]$; $\sigma_1 = [1.2, 1.1, 2]$; $a_2 = [3, 1, 2]$; $b_2 = [0.23, 0.16, 0.12]$; $p_2 = [7, 4, 3]$; $\gamma_2 = [0.3, 0.4, 0.5]$; $\sigma_2 = [0.45, 1.5, 0.25]$; and $\tau = [1, 2, 3]$.

Therefore, conditions of Theorem 5 have been checked. Thus, from Theorem 5, all species become extinct. Figure 4 clearly supports this result.

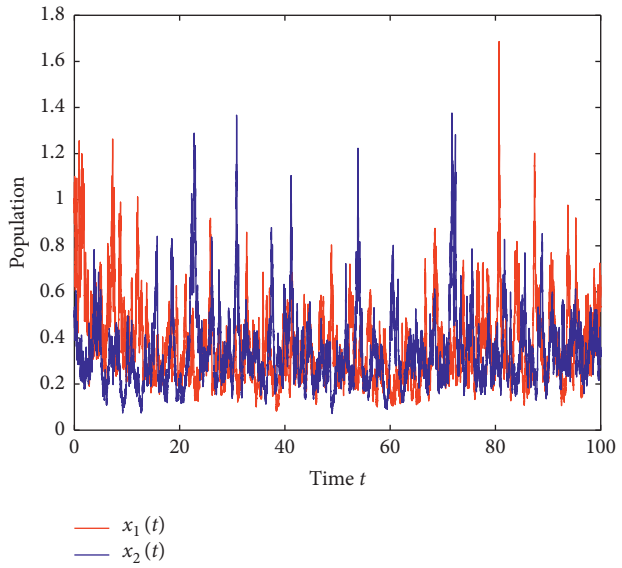

Figure 3: Numerical solutions of (6) with $a_1 = [2.1, 2.2, 2]$; $b_1 = [0.11, 0.13, 0.12]$; $p_1 = [3.2, 3, 3.5]$; $\gamma_1 = [0.83, 0.85, 0.86]$; $\sigma_1 = [0.62, 0.61, 0.63]$; $a_2 = [2, 2.1, 2.2]$; $b_2 = [0.11, 0.13, 0.12]$; $p_2 = [3.1, 3.3, 3.2]$; $\gamma_2 = [0.81, 0.8, 0.83]$; $\sigma_2 = [0.71, 0.75, 0.71]$; $\tau = [1, 2, 3]$.

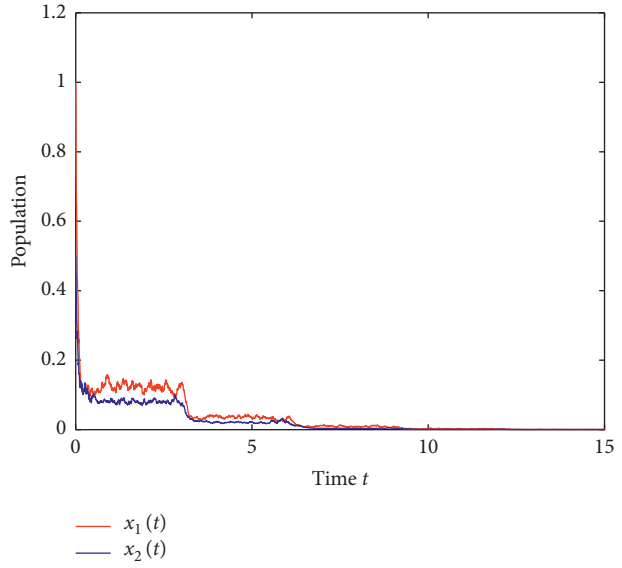

Figure 4: Numerical solutions of (6). The parameters of model (5) are $a_1 = [17, 18, 19]$; $b_1 = [0.14, 0.35, 0.15]$; $p_1 = [4.55, 6, 5.43]$; $\gamma_1 = [0.8, 0.5, 0.6]$; $\sigma_1 = [0.5, 0.45, 0.12]$; $a_2 = [16.5, 16.9, 17.5]$; $b_2 = [0.5, 0.13, 0.22]$; $p_2 = [3.23, 4.67, 6]$; $\gamma_2 = [0.3, 0.4, 0.8]$; $\sigma_2 = [0.49, 1, 0.65]$; and $\tau = [3, 3, 3]$.

7. Conclusions

By the conclusion of Lemma 1, it is worthy to point out that the Brownian noise and colored noise will not destroy a great property that the solution of (6) may not explode. Especially, system (6) reduces to (1)–(4) or the model in [32] when parameters of system (6) take some special values. From Lemma 1, the condition $\alpha > (\sigma^2/2)$ in [21] is too strict and unnecessary. In Theorem 1, we comprehensively analyze ultimate boundedness in the θth moment and boundedness for the average in time of the θth moment of solution, which is the improvement of Theorem 3.1 in [21], Theorem 2.2 in [28], Theorem 3.3 in [31], and Theorem 3.2 in [32]. In Theorem 4, we find an upper bound $Q/2$ of the sample Lyapunov exponent. When parameters of system (6) take some special values, we compute that the upper bound $Q/2$ is less than the corresponding upper bound in [21, 28]. Furthermore, we find that the condition $2\alpha_1 - \sigma_1^2 - (b_1 + b_2)\epsilon > 0$, $2\alpha_2 - \sigma_2^2 - b_1 + b_2/\epsilon > 0$ in [31] is not necessary. Despite all this, if we let parameter ϵ satisfy the above conditions, we compute that $Q/2$ is less than the upper bound in [31]. One point should be stressed is that the method for extinction in Theorem 5 can be used successfully for the models in [21, 28, 31, 32]. And then, Corollaries 1 and 2 give the conditions of extinction of (2) and (4), respectively. From Remarks 1–7, our work is a generalization and promotion of the corresponding work in [21, 28, 30–32]. To some extent, our proposed approaches are both more robust and more efficient than the existing methods.

Data Availability

No data were used to support this study.

Conflicts of Interest

The authors declare that they have no conflicts of interest.

Authors' Contributions

All the authors contributed equally and significantly to writing this paper. All authors read and approved the final manuscript.

Acknowledgments

This work was supported by the National Natural Science Foundation of China (no. 11971279).

References

[1] W. S. C. Gurney, S. P. Blythe, and R. M. Nisbet, "Nicholson's blowflies revisited," *Nature*, vol. 287, no. 5777, pp. 17–21, 1980.

[2] A. Nicholson, "An outline of the dynamics of animal populations," *Australian Journal of Zoology*, vol. 2, no. 1, pp. 9–65, 1954.

[3] W. Chen and B. Liu, "Positive almost periodic solution for a class of Nicholson's blowflies model with multiple time-varying delays," *Journal of Computational and Applied Mathematics*, vol. 235, no. 8, pp. 2090–2097, 2011.

[4] M. Yang, "Exponential convergence for a class of Nicholson's blowflies model with multiple time-varying delays," *Nonlinear Analysis: Real World Applications*, vol. 12, no. 4, pp. 2245–2251, 2011.

[5] L. Berezansky, E. Braverman, and L. Idels, "Nicholson's blowflies differential equations revisited: main results and open problems," *Applied Mathematical Modelling*, vol. 34, no. 6, pp. 1405–1417, 2010.

[6] T. Faria and G. Röst, "Persistence, permanence and global stability for an *n*-dimensional Nicholson system," *Journal of Dynamics and Differential Equations*, vol. 26, no. 3, pp. 723–744, 2014.

[7] C. Huang, X. Yang, and J. Cao, "Stability analysis of Nicholson's blowflies equation with two different delays," *Mathematics and Computers in Simulation*, vol. 171, pp. 201–206, 2020.

[8] X. Long and S. Gong, "New results on stability of Nicholson's blowflies equation with multiple pairs of time-varying delays," *Applied Mathematics Letters*, vol. 100, Article ID 106027, 2020.

[9] J. Zhang and C. Huang, "Dynamics analysis on a class of delayed neural networks involving inertial terms," *Advances in Difference Equations*, vol. 2020, p. 120, 2020.

[10] C. Qian and Y. Hu, "Novel stability criteria on nonlinear density-dependent mortality Nicholson's blowflies systems in asymptotically almost periodic environments," *Journal of Inequalities and Applications*, vol. 2020, p. 13, 2020.

[11] W. Wang, F. Liu, and W. Chen, "Exponential stability of pseudo almost periodic delayed Nicholson-type system with patch structure," *Mathematical Methods in the Applied Sciences*, vol. 42, no. 2, pp. 592–604, 2019.

[12] C. Huang, X. Long, L. Huang, and S. Fu, "Stability of almost periodic Nicholson's blowflies model with involoving patch structure and mortality terms," *Canadian Mathematical Bulletin*, vol. 63, no. 2, pp. 405–422, 2019.

[13] C. Huang, H. Zhang, and L. Huang, "Almost periodicity analysis for a delayed Nicholson's blowflies model with nonlinear density-dependent mortality term," *Communications on Pure & Applied Analysis*, vol. 18, no. 6, pp. 3337–3349, 2019.

[14] R. M. May, *Stability and Complexity in Model Ecosystems*, Princeton University Press, Princeton, NJ, USA, 1973.

[15] R. Liu and G. Liu, "Asymptotic behavior of a stochastic two-species competition model under the effect of disease," *Complexity*, vol. 2018, Article ID 3127404, 15 pages, 2018.

[16] W. Wang, C. Shi, and W. Chen, "Stochastic Nicholson-type delay differential system," *International Journal of Control*, 2019, In press.

[17] W. Wang and W. Chen, "Stochastic delay differential neoclassical growth model," *Advances in Difference Equations*, vol. 2019, p. 355, 2019.

[18] X. Mao, "Stationary distribution of stochastic population systems," *Systems & Control Letters*, vol. 60, no. 6, pp. 398–405, 2011.

[19] G. Liu, X. Wang, X. Meng, and S. Gao, "Extinction and persistence in mean of a novel delay impulsive stochastic infected predator-prey system with jumps," *Complexity*, vol. 2017, Article ID 1950907, 15 pages, 2017.

[20] F. Bian, W. Zhao, Y. Song, and R. Yue, "Dynamical analysis of a class of prey-predator model with Beddington-DeAngelis functional response, stochastic perturbation, and impulsive toxicant input," *Complexity*, vol. 2017, Article ID 3742197, 18 pages, 2017.

[21] W. Wang, L. Wang, and W. Chen, "Stochastic Nicholson's blowflies delayed differential equations," *Applied Mathematics Letters*, vol. 87, pp. 20–26, 2019.

[22] J. M. Drake, "Allee effects and the risk of biological invasion," *Risk Analysis*, vol. 24, no. 4, pp. 795–802, 2004.

[23] M. Assaf, A. Kamenev, and B. Meerson, "Population extinction risk in the aftermath of a catastrophic event," *Physical Review E*, vol. 79, no. 1, Article ID 011127, 2009.

[24] X. Mao, "Stability of stochastic differential equations with Markovian switching," *Stochastic Processes and Their Applications*, vol. 79, no. 1, pp. 45–67, 1999.

[25] Q. Luo and X. Mao, "Stochastic population dynamics under regime switching II," *Mathematical Analysis and Applications*, vol. 355, no. 2, pp. 577–593, 2007.

[26] T. K. Siu, "Bond pricing under a Markovian regime-switching jump-augmented Vasicek model via stochastic flows," *Applied Mathematics and Computation*, vol. 216, no. 11, pp. 3184–3190, 2010.

[27] A. Settati and A. Lahrouz, "Stationary distribution of stochastic population systems under regime switching," *Applied Mathematics and Computation*, vol. 244, pp. 235–243, 2014.

[28] Y. Zhu, K. Wang, Y. Ren, and Y. Zhuang, "Stochastic Nicholson's blowflies delay differential equation with regime switching," *Applied Mathematics Letters*, vol. 94, pp. 187–195, 2019.

[29] L. J. S. Allen, "Persistence, extinction, and critical patch number for island populations," *Journal of Mathematical Biology*, vol. 24, no. 6, pp. 617–625, 1987.

[30] L. Berezansky, L. Idels, and L. Troib, "Global dynamics of Nicholson-type delay systems with applications," *Nonlinear Analysis: Real World Applications*, vol. 12, no. 1, pp. 436–445, 2011.

[31] X. Yi and G. Liu, "Analysis of stochastic Nicholson-type delay system with patch structure," *Applied Mathematics Letters*, vol. 96, pp. 223–229, 2019.

[32] W. Wang and W. Chen, "Stochastic Nicholson-type delay system with regime switching," *Systems & Control Letters*, vol. 136, p. 104603, 2020.

[33] A. Lahrouz and A. Settati, "Necessary and sufficient condition for extinction and persistence of SIRS system with random perturbation," *Applied Mathematics and Computation*, vol. 233, pp. 10–19, 2014.

[34] A. Settati, S. Hamdoune, A. Imlahi, and A. Akharif, "Extinction and persistence of a stochastic Gilpin-Ayala model under regime switching on patches," *Applied Mathematics Letters*, vol. 90, pp. 110–117, 2019.

[35] X. Mao, Ren, and C. Yuan, *Stochastic Differential Equations with Markovian Switching*, Imperical College Press, London, UK, 2006.

[36] X. Mao, *Stochsatic Differential Equations and Applications*, Horwood, Chichester, UK, 2007.

[37] R. S. Liptser and A. N. Shiryayev, *Theory of Martingales*, Kluwei Academic Publisherm, Dordrecht, Netherlands, 1989.

[38] D. J. Higham., "An algorithmic introduction to numerical simulation of stochastic differential equations," *SIAM Review*, vol. 43, no. 3, pp. 525–546, 2001.